THE UNIVERSITY
of EDINBURGH

Reduction and functionalisation of binuclear uranium-oxo complexes

Guy M. Jones

University of Edinburgh

Submitted for the degree of Doctor of Philosophy

28th March 2013

Declaration

The work described in this thesis is entirely my own, except where I have either acknowledged help from a named person or given reference to a published source. Text taken from another source will be enclosed in quotation marks and a reference given. This thesis has not been submitted, in whole or in part, for any other degree.

Signature: Date:

Acknowledgements

I would first like to thank Prof. Polly Arnold and Dr. Jason Love for their constant provision of ideas and enthusiasm throughout my Ph.D. Their support in matters both in and out of the lab has been invaluable.

I am hugely grateful for the practical assistance given by the following people: Prof. Georg Schreckenbach, Dr. Qing-Jiang Pan and Dr. Samuel Odoh for theoretical calculations; Dr. Ross Inglis and Dr. Alessandro Prescimone for performing the SQIUD measurements; Dr. Nicola Magnani for modelling the SQUID data; Prof. Simon Parsons, Dr. Fraser White and Dr. Gary Nichol for help with difficult crystal structures; Juraj Bella, Dr. Marika McCremoux and Dr. Lorna Murray for letting me near the NMR machines; Dr. Logan Mackay, Alan Taylor and Harriet Cole for mass spectrometry (sorry for consistently turning your instruments brown); Stephen Boyer and Analytische Laboratorien for elemental analyses (even the ones that failed); Dr. Daniel Meyer, Dr. Caroline Gene and the staff at the CEA Marcoule for letting get near, and away from, Neptunium chemistry and all the support staff at the School of Chemistry in Edinburgh for putting out the fires.

The EPSRC and ACTINET-I3 are gratefully acknowledged for provision of funding.

Special thanks must be given to those who showed me the ropes: Dr. Stephen Mansell, Dr. Emmalina Hollis, Dr. Natalie Potter, Dr. Zoë Turner, Dr. Aline Devoille, Dr. James Leeland, Dr. Anne-Frédérique Pecharman, Dr. Anne Germeroth and Dr. John Hart without whom I would have undoubtedly made much more of a mess. I also wish to thank the members of Lab 34; Nicola, Aaron, Colin, Isobel, Rebecca, Andrew, Charlotte, Markus and those who joined after for their help, donations of free food, enunciation, funny ears, well-groomed beards, racial tolerance, *n*-butyl ammonium impressions, and huge support over the course of my Ph.D. Additional commendation is deservedly given to Maxwell Reinhardt for his sympathetic handling of mess, early morning noise and flatmate absenteeism over my Ph.D years.

Finally I would like to thank my family, hopefully one day I will be able to explain it to you.

Abbreviations

General

Ac	acetate
Ad	adamantyl
An	actinide
Ar	generic aryl group
9-BBN	9-borabicyclo[3.3.1]nonane
BM, μ_B	Bohr Magneton
CCI	Cation-Cation Interaction
Cp	cyclopentadienyl, C_5H_5
Cp*	pentamethyl cyclopentadienyl, C_5Me_5
Cy	cyclohexyl
dme	dimethoxyethane
DMF	dimethyl foramide
DFT	Density Functional Theory
Dtbp	2,6-di-*tert*-butyl phenyl
HMPA	hexamethylphosphoramide
HOMO	Highest Occupied Molecular Orbital
ITI	Inverse Trans Influence
LDA	lithium diisopropyl amide
Ln	lanthanide
LUMO	Lowest Unoccupied Molecular Orbital
MBO	Mayer Bond Order
μ_{eff}	effective magnetic moment
MS	Mass Spectrometry
NBO	Natural Bond Order
NIR	near infrared
py	pyridine
rt	room temperature
SHE	Standard Hydrogen Electrode
SQUID	Superconducting Quantum Interference Device
tacn	1,4,7-triazacyclonane
TEMPO	(2,2,6,6-tetramethylpiperidin-1-yl)oxyl
TFA	trifluoroacectic acid

THF	tetrahydrofuran
TGA	thermogravimetric analysis
tmeda	tetramethyldiamine
TMP	2,2,6,6-tetramethylpiperidine
UV-vis	ultraviolet-visible

Nuclear Magnetic Resonance spectroscopic data

$^{13}C\{^{1}H\}$	proton decoupled ^{13}C NMR experiment
δ	chemical shift in ppm
br.	broad
COSY	^{1}H-^{1}H 2D correlation spectroscopy
DOSY	diffusion ordered NMR spectroscopy
d	doublet
dd	doublet of doublets
J	coupling constant
Hz	Hertz
m	multiplet
MHz	Megahertz
NMR	Nuclear Magnetic Resonance
ppm	parts per million
s	singlet
t	triplet

Mass spectroscopic data

amu	atomic mass unit
ESI	electrospray ionisation
LDI	laser desorption ionisation
MALDI	matrix-assisted laser desorption ionisation
QTOF	quadrupole injection time of flight

Infrared spectroscopic data

br	broad
FTIR	Fourier-transform infrared
m	medium
s	strong
w	weak

Abstract

Chapter one introduces uranium oxo chemistry with a focus on the structure, oxo-group reactivity and single electron reduction of the uranyl(VI) dication. In this context, the previous work in our group on the use of Schiff-base Pacman complexes for the reductive functionalisation of uranyl will be discussed.

Chapter two details the synthesis of binuclear uranium(V) oxo complexes $[(RMe_2SiOUO)_2(L)]$ (R = Me, Ph) by oxo group rearrangement and reductive silylation of uranyl(VI) silylamido precursors. The electronic structure and magnetic behaviour of the complexes are presented as well as insights into the mechanism of formation and stability.

Chapter three describes the reduction and desilylation reactions of $[(Me_3SiOUO)_2(L)]$. It begins with the one- and two-electron reductions of $[(Me_3SiOUO)_2(L)]$ and continues with the reactivity of the resultant mixed-valence complex $K[(Me_3SiOUO)_2(L)]$. The reactivity of the $U^{IV}U^{IV}$ complex $K_2[(Me_3SiOUO)_2(L)]$ with water is detailed and the products, $K[(OU^{V}O)(OU^{IV}OSiMe_3)(L)]$ and a $U_{12}O_{24}L_6$ supramolecular wheel are reported. The oxidation of $K_2[(Me_3SiOUO)_2(L)]$ with pyridine-*N*-oxide is demonstrated as a route to metalated $K_2[(OUO)_2(L)]$ complexes, and the synthesis of $Li_2[(OUO)_2(L)]$ and the mixed lithiated/silylated complex $Li[(OUO)(OUOSiMe_3)(L)]$ are presented as direct routes to $M_x[(OUO)_2(L)]$ complexes.

Chapter four discusses the reactivity of $M_2[(OUO)_2(L)]$ (M = K, Li) towards oxidation and oxo-functionalisation. The oxo- and peroxo-bridged binuclear uranyl(VI) complexes $K_2[(UO_2)_2(\mu\text{-}X)(L)]$ ($X = O^{2-}$, O_2^{2-}) are reported from the reaction of $K_2[(OUO)_2(L)]$ with different oxo-oxidising agents and the new, Group 14-functionalised oxo complexes $[(ROUO)_2(L)]$ (R = stannyl or alkyl group) are described showing similar structures, bonding and stabilities to the silylated complexes.

Chapter five describes the uranyl(VI) complexes of other polypyrrolic ligands. The uranyl(VI) chemistry of the anthracenyl- and fluorenyl-substituted Pacman ligands L^F and L^A is demonstrated as a means of using macrocyclic control to govern the nature of the complexes formed. Uranyl(VI) complexes of the polypyrrolic, tripodal ligand H_3L^T are shown to form either molecular species or supramolecular gels depending on the solvent used.

Chapter six concludes the work presented in this Thesis.

Chapter seven outlines all experimental details.

Table of contents

Chapter Two: Binuclear uranium-oxo complexes from uranyl oxo rearrangement and reductive silylation

Chapter Three: Group one metal salts of binuclear uranium-oxo complexes

Chapter Five: Uranyl(VI) complexes of alternative polypyrrolic ligands

Introduction

1.1 Forward

Uranium is the heaviest naturally occurring element, with an abundance of 2.4 ppm in the Earth's crust. The usage of uranium compounds as colourants for ceramics and glass has been documented since Roman times however the element was not recognised it its pure form until the 1840s when Péligot succeeded in preparing metallic uranium by reduction of UCl_4 with potassium. The crucial importance of uranium to mankind was not established until 1939 upon the discovery of the nuclear fission of the element by Hahn and Strassman. Since then, the chemistry of uranium has occupied a central position in the field of nuclear energy, studied alongside the materials science and physics of the element with the primary aim of improving the safety and effectiveness of the many nuclear process in which uranium is now employed.[1]

The chemistry of both uranium and the other early-actinides (Th-Np) present a number of properties that are unique in f-block elements. The early actinides display a much greater range of oxidation states than both the lanthanides and late actinides with all the valence electrons available for bonding up to and including neptunium. In addition, the contributions to bonding from the 5f and 6d orbitals is much greater than in the rest of the f-block, a feature in part due to the single radial node in the 5f atomic orbitals limiting penetration into the core orbitals and in part due to the 5f orbital relativistic expansion. The covalent contribution to the bonding in compounds of the early f-elements is greater than that of the lanthanides and late actinides. For all these reasons, the early actinides are amongst the most synthetically attractive elements at the frontier of the periodic table, with uranium being the most readily available, easiest to manipulate and perhaps of greatest relevance to nuclear science.

In its compounds, uranium exhibits the oxidation states III, IV, V and VI, with IV and VI being by far the most predominant. For compounds of uranium in these two oxidation states, uranium oxides are ubiquitous in both the natural environment and the nuclear fuel cycle and it is for this reason that the physiochemical properties of such compounds have been studied in great detail.[2] In this chapter, the coordination chemistry of uranium with oxo ligands is detailed, with particular focus on the structure and reactivity of the most common motif in uranium chemistry; the uranyl dication $[UO_2]^{n+}$ (n = 1, 2).

1.2 The uranyl dication

The uranyl dication, formally $[UO_2]^{2+}$, is the most common form of uranium in the environment and is present in the majority of high oxidation state uranium complexes.[2]

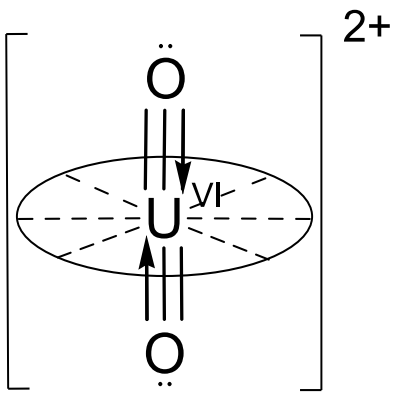

Figure 1: A schematic uranyl(VI) dication showing the axial U–O triple bonds in a valence bond representation and the equatorial coordination sphere.

The species is composed of a uranyl centre bound to two *trans* dioxo ligands of which the uranium-oxygen bonds are extremely short, strong and exclusively conlinear. The cation is chemically robust, with a mean U–O bond enthalpy for dissociation of 604 kJ mol^{-1} comparable to many transition-metal dioxides.[3] In addition to the axially-bound oxo ligands, the uranyl dication typically binds 3–6 equatorial ligands in the equatorial plane, forming pyramidal coordination geometries in which the equatorial ligands are weakly bound and labile.[4]

1.2.1 Electronic structure and bonding

The U–O bonds in uranyl have notional bond orders of three, with a valence bond model of the species describing a double covalent bond with an additional dative contribution (Figure 1). For clarity, the dative contribution is usually not included in the chemical formula of the species, with the multiple bonds in uranyl(VI) represented as O=U=O and U–O bonds of lower multiplicity depicted as single or partial-double bonds. Such representations are used throughout this thesis.

The U–O triple bonds are constructed by combination of the uranium 5f and 6d orbitals with linear combinations of the two sets of three oxygen 2p orbitals. Using a basic MO treatment, all six of the linearly combined oxygen 2p orbital sets (σ_u, σ_g, $2 \times \pi_u$, $2 \times \pi_g$) have symmetry allowed bonding combinations with the metal orbitals, resulting in six bonding orbitals from which to construct the U–O triple bonds.

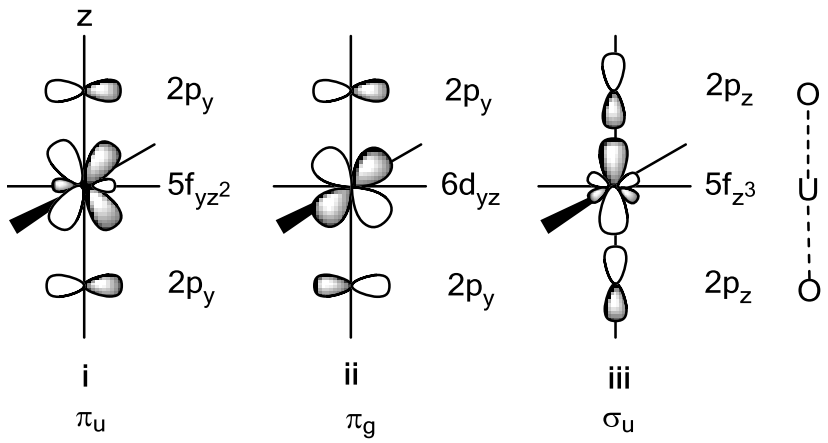

Figure 2: Examples of U-O bonding combinations in the uranyl dication.

From these 6 MOs, several important bonding combinations can be identified; principally a π_u symmetry combination of the O(p_y) and U(f_{yz^2}) orbitals and an orbital arising from overlap between the π_g O(p_y) combination and U(d_{yz}) (Figure 2 i, ii). It is noteworthy that the former contribution could not be constructed using metal d-orbitals due to their gerade symmetry, a feature that in part contributes to the rarity of *trans* MO_2^{n+} geometries in transition metal complexes. The ordering of the six bonding molecular orbitals cannot be inferred by simple MO theory but has been established using a variety of spectroscopic and theoretical techniques. Perhaps the most unusual conclusion of such analysis is that the σ-bonding molecular orbitals are of higher energy than the π. One explanation for this is that the σ_u combination between the O(p_z) and the U(f_z^3) contains a destructive component as a result of overlap with the equatorial lobes of the latter orbital (Figure 2, iii). The remaining 5f orbitals of δ and ϕ symmetry remain non-bonding and unoccupied in uranyl(VI) but form the valence orbitals for reduced uranyl complexes as well as in the heavier actinyls $[NpO_2]^{2+}$, $[PuO_2]^{2+}$ and $[AmO_2]^{2+}$, classified as $5f_1$, $5f_2$ and $5f_3$ species respectively.[2]

1.2.2 The inverse *trans* influence

Although a simple MO description of uranyl bonding can be used to partially rationalise the strength of the U-O multiple bonds, the more complex facets of the species behaviour can only be accounted for using higher level theory. The inverse *trans* influence (ITI) is an experimentally observed feature in early actinide chemistry that describes the mutual strengthening of an M–L bond to a π-donor ligand by an opposing π-donor ligand. The phenomenon operates predominantly, but not exclusively, in the chemistry of high oxidation state actinyl and mono-oxo complexes and is evidenced by shorter-than-average bond distances between a metal centre and its *trans* ligand. One of the simplest examples of an ITI species is $[UOCl_5]^+$,with the U–Cl bond *trans* to the oxo group being 0.103 Å shorter

than U–Cl bonds *cis* to it (see section 1.7.2).[5] The first theoretical description of the ITI was provided in 1992 by Denning in which the term was first coined.[6] In this and one later contribution,[7] the ITI was rationalised qualitatively by consideration of the polarisation across the M–O bond, the nature of which is dependent of on the relative parity of the metal-based HOMO and LUMO. It was proposed that if these two sets of orbitals have opposite parity, such as in the early transition metals where the valence orbitals are p and d, the polarisation is predominantly dipolar, leading to a build-up of negative charge in the *trans* position resulting in greater M–L_{trans} repulsion. In complexes such as $[UOCl_5]^+$ the valence orbitals are p and f, resulting in predominantly quadrupolar polarisation and a build-up of negative charge in the *cis* position. Later work by the Kaltsoyannis group modelled the ITI using DFT calculations, reporting that the ligand interactions with the 5f shell are crucial to the formation of the interaction in addition to significant contributions from the pseudo core 6p orbitals.[8] The latter conclusion in particular highlights that bonding in uranium oxo species such as the uranyl dication cannot simply be rationalised by consideration of the valence 5f and 6d orbitals, with the latest accounts of the electronic structure of $[UO_2]^{2+}$ invoking the 5f, 6d, 6p and even 7s orbitals in the MO diagram. The often similar energies between the aforementioned orbitals is also routinely used to induce 5f/6d/6p hybridisation, further complicating the description of the bonding in a deceptively simple-looking species.[9]

1.2.3 Comparison with transition metal dioxo complexes

In contrast to transition metal dioxo species in which there are examples of both *cis* (bent) and *trans* (linear) O-M-O configurations,[10] the presence of the ITI results in actinyl ions $[AnO_2]^{2+}$ (An = U, Np, Pu) being exclusively *trans*, with no reported examples of *cis*-uranyl complexes at the time of writing.[11] The reactivities of actinyl cations starkly contrast those of transition metal dioxo compounds, which are strong Lewis bases and can readily activate organic substrates.

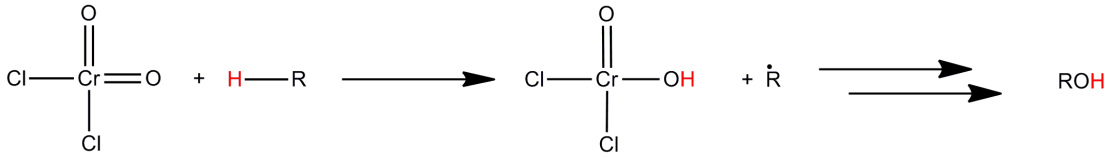

Scheme 1: The Etard reaction, an example of transition metal dioxo reactivity.

Perhaps the most famous example of such reactivity is the Etard reaction, discovered over 100 years ago and details the homolytic cleavage of sp^3 C–H bonds by $[Cr^{VI}O_2Cl_2]$ forming the reduced $[Cr^{VI}O(OH)Cl_2]$ species and an organic radical (Scheme 1).[12] In contrast, the uranyl dication will not oxidise organic substrates and oxo-group Lewis-adducts

are only observed in the presence of very strong Lewis acids (see section 1.4.2). The thermodynamic stability of $[UO_2]^{2+}$ in comparison to transition metal dioxos is due to the aforementioned strength of the U-O triple bonds and the subsequent diminished availability of the oxygen lone pairs to take part in further bonding. A further difference between actinide and transition metal dioxos is the aforementioned ITI, with early transition metal complexes exhibiting the regular *trans* influence whereby ligands positioned *trans* to a strong donor ligand can display lengthened M–L bonding (the *trans* influence) and subsequent kinetic lability (the *trans* effect).[13]

1.3 Actinyl redox chemistry and the environment

The aqueous chemistry of high oxidation state actinide compounds is dominated by actinyl cations. Neptunyl and plutonyl are stable in the An^{VI} ($[AnO_2]^{2+}$) and An^{V} ($[AnO_2]^{+}$) forms in aqueous media whereas uranyl(V) ($[UO_2]^{+}$) is highly unstable in water with respect to disproportionation (Scheme 2).[2]

$$2\,[UO_2]^{+} + 4H^{+} \longrightarrow [UO_2]^{2+} + U^{4+} + 2H_2O$$

Scheme 2: Aqueous disproportionation of uranyl(V).

The disproportionation of uranyl(V) has important environmental consequences as the resultant $[U^{VI}O_2]^{2+}$ and U^{IV} phases display different aqueous solubilities. Uranyl(VI) ions are water soluble and environmentally mobile whereas U^{IV} phases are insoluble except in highly acidic solutions. Reduction of uranyl(VI) compounds by both bacterial and mineral species has been shown to occur in nature, although whether this occurs by single-electron reduction and uranyl(V) disproportionation or by a direct two-electron transfer has yet to be determined. It has been suggested that such routes may be employed for reductive precipitation of uranyl from aqueous phases, allowing potential remediation of contaminated groundwater sources.[14-16]

Throughout the literature the terms "hexavalent" and "pentavalent" are used to described uranyl(VI) and uranyl(V) respectively however the terms will not be used in this thesis due to the ambiguity surrounding definition of "valence" when applied to metal oxidation states.[17]

1.4 Uranyl(VI) complexes

In contrast to the chemically inert behaviour of the axial uranyl oxo ligands, ligands bound in the uranyl equatorial plane are labile. The facility of ligand exchange has enabled the synthesis of an enormous number of uranyl(VI) complexes of a diverse range of ligands.[18] Unlike the U=O bonds, which are strongly covalent, equatorial uranyl-bonds are

predominantly electrostatic, with complexes featuring hard-type oxygen, nitrogen, and light-halide donor ligands being the most stable. For this reason, such ligands form the mainstay of extractants used in nuclear waste reprocessing, with the former two types often being preferred due to their relative ease of combustion (the so-called "CHON" principle). Ligands that are highly selective for the uranyl ion are of interest for sequestering applications where the concentration of the metal ion in solution is very low. Such conditions can be found in seawater (3 ppb uranium), which could be viewed as a possible uranium resource, or in contaminated drinking water supplies that may require purification.

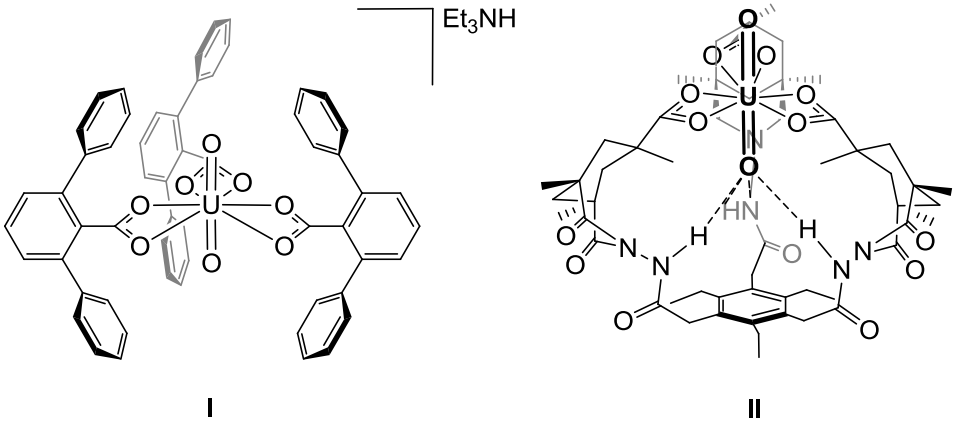

Figure 3 Uranyl(VI) extractant complexes synthesised by Rebek and co-workers.

Two recent publications by the Rebek group have demonstrated the ability of carboxylate ligands to bind uranyl by self-assembly. In the first they showed that the $[Et_3NH]^+$ salt of 2,6-terphenyl carboxylate (TPC) ligand can precipitate crystals of $[Et_3NH][UO_2(TPC)_3]$ upon addition to aqueous solutions of uranyl nitrate (Figure 3, **I**).[19] The second paper reported the coordination chemistry of a tripodal receptor bearing three carboxylate groups tethered to a triethylbenzene core.[20] This ligand was shown to be capable of extracting uranyl at concentrations as low as 400 ppm and in the presence of seawater-level concentrations of numerous ions. Structural characterisation of the extracting complex revealed a six-coordinate uranyl cation in the equatorial plane bonding to the three bidentate carboxylate donors. The amine hydrogen atoms were shown to provide secondary stabilising interactions with three long hydrogen bonds to the uranyl oxo group that are directed toward the inside of the ligand capsule (Figure 3, **II**).Both **I** and **II** are examples of hard-donor-type uranyl(VI) complexes with, for example, the equatorial U–O bonds in the former complex (2.445(6) – 2.518(6) Å) being characteristically longer than the extremely short axial U=O bonds within the cation itself (1.724(6) – 1.737(6) Å).

1.4.1 Uranyl(VI) complexes of non-classical ligands

While uranyl(VI) complexes of hard-donor ligands are extremely common those featuring softer donor ligands are comparatively rare. Such a difference is exemplified in uranyl halide complexes, with 106 examples of uranyl-chloride complexes in the Cambridge Structural Database, 53 examples featuring fluoride ligands, 26 examples featuring bromide yet only 6 featuring iodide.[21-24] The first example of the latter class of complexes was the thermally unstable $[UO_2I_2(H_2O)_2]$, a deceptively simple species that was not isolated until 2003 (Figure 4, **III**).[21]

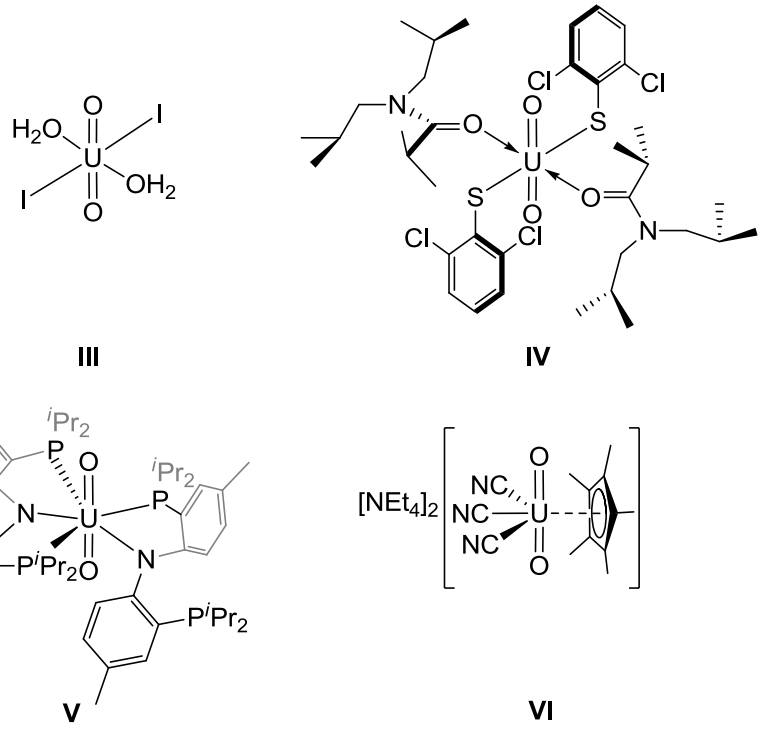

Figure 4: Uranyl(VI) complexes featuring iodide (**III**), sulfur (**IV**), phosphorus (**V**) and cyclopentadienyl (**VI**) ligands.

The U–I bonds in **III** are 2.939(2) Å in length comparable only to those found in other uranyl iodide complexes and to complexes of $[UO_2]^{2+}$ with other soft-donor ligands such as phosphine and sulfide. Although there are comparatively more examples of uranyl-sulfur compounds (over 30) the U–S bonds in such complexes are almost invariably supported within multidentate ligands with their proximity to the uranium centre facilitated by uranyl-coordination by stronger donors. The uranyl 2,6-dichlorothiophenolate complex $[UO_2(S\text{-}2,6\text{-}Cl_2C_6H_3)_2(DIBIPA)_2$ (DIBIPA = N,N-diisobutylisopropylamide) is the only exception, exhibiting unsupported uranyl–sulphur bonds of 2.7143(7) and 2.7325(8) Å from two unidentate ligands (Figure 4, **IV**).[25] There is only one structurally characterised example

of a uranyl complex featuring a phosphine donor; the complex $[UO_2(PNP)_2]$ (PNP = bis{2-(diisopropylphosphino)-4-methylphenyl} amide)) (Figure 4, **V**).[26] The complex was synthesised by oxidation of the U^{IV} precursor $[U(PNP)_4]$ with pyridine-*N*-oxide and contains four supported uranyl-phosphine interactions with long U–P bond distances of 3.017(3) and 2.984(3) Å. The lack of other uranyl-phosphine complexes contrasts the commonplace of phosphine complexes of transition metal chemistry and further highlights the preference of the $[UO_2]^{2+}$ dication for harder donors. An even more common class of ligands almost entirely absent from uranyl chemistry is cyclopentadienyl (Cp) with the only structurally characterised example of a uranyl-Cp complex being $[NEt_4]_2[UO_2(C_5Me_5)(CN)_3]$, synthesised by Berthet and co-workers in 2007 (Figure 4, **VI**).[27] In analogy with the uranyl-phosphine complex, **VI** was also prepared by oxidation of a uranium(IV) precursor with pyridine-*N*-oxide. In this case the complex was $[NEt_4]_3[U(C_5Me_5)_2(CN)_5]$, itself a rare example of an An–CN complex.[28]

In contrast to the formation of uranyl phosphine complexes, which is unfavourable due to the weak binding of such soft ligands to hard U^{VI} centres, the instability of uranyl Cp complexes is instead derived from the reducing nature of the ligand.[27] The reducing ability of strongly basic hydrocarbyl and amide ligands is well documented and is often purported to explain the instabilities of their uranyl complexes towards reductive decomposition (see Chapter Two, section 2.8 for a full discussion).

1.4.2 Oxo-group reactivity of uranyl(VI) complexes

In the vast majority of cases, the U–O bonding in $[UO_2]^{2+}$ is unaffected by equatorial coordination, with very little variation in U–O bond distances observed across a diverse range of complexes. In certain scenarios however, oxo-group reactivity can be promoted by the use of strongly electron-donating ligands. It is thought that such ligands act to partially quench the positive charge on the uranium, reducing the amount of electron density withdrawn from the axial oxygen atoms and therefore promoting increased Lewis basicity.

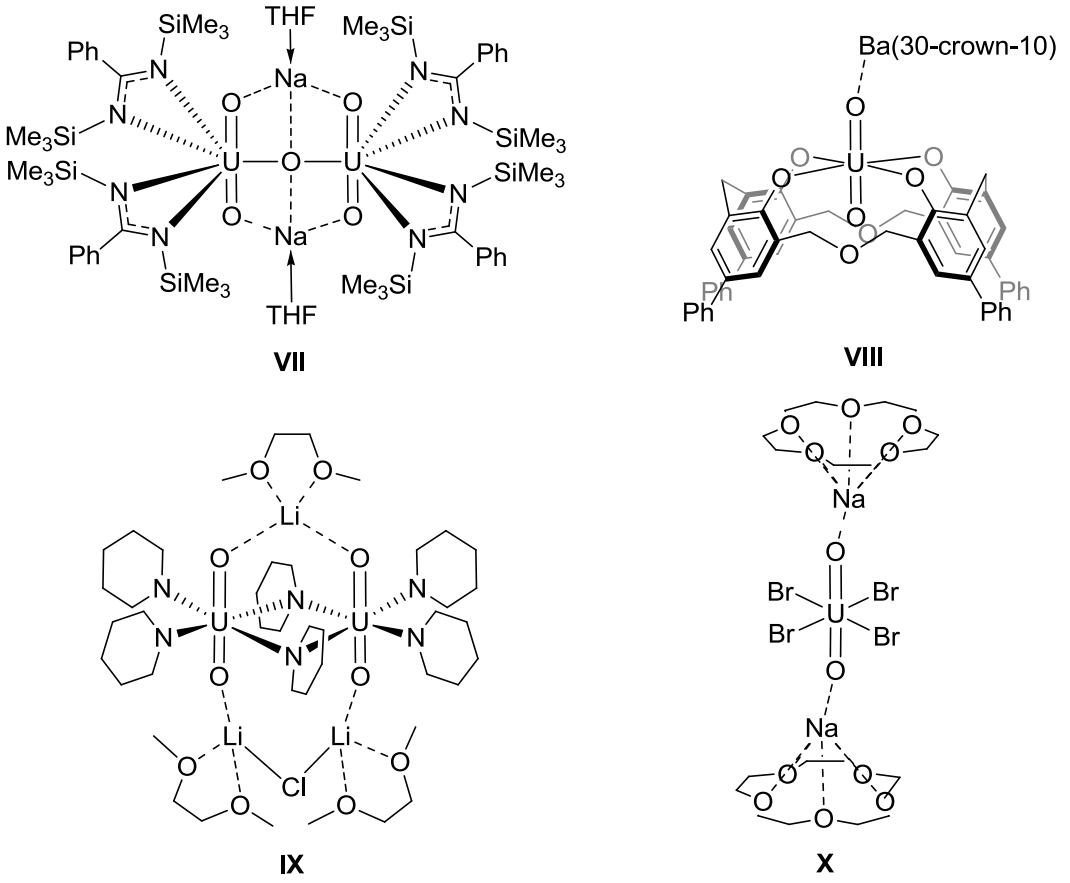

Figure 5: Examples of uranyl(VI) adducts of Groups 1 and 2

A number of uranyl(VI) adducts have been synthesised using this rational, most commonly by coordination of the uranyl oxo groups to Group 1 metals, of which there are over 50 structurally characterised examples currently in the Cambridge Structural Database. The binuclear oxo-bridged uranyl complex $[\{Na(THF)UO_2(\{Me_3SiN\}_2CPh)_2\}_2(\mu\text{-}O)]$, synthesised by Sarsfield and co-workers in 2004,[29] exhibits two uranyl dications coordinated by separate NCN ligands bridged by a single oxygen atom (Figure 5, **VII**). Two sodium cations lie in-between the uranyl oxo groups forming two sets of OUO-Na-OUO motifs with each cation also coordinated by the bridging oxo group lying at the centre of a hexagonal $U_2O_4Na_2$ plane. The uranyl bond distances in **VII** are within the range 1.80–1.82 Å, longer than those expected for a uranyl(VI) complex (1.76–1.78 Å) and therefore indicative of partial U–O bond activation. The O–Na bond lengths between uranyl oxo groups and the Na atom are between 2.21–2.30 Å demonstrating the presence of a Lewis pair. Thuéry and Masci have prepared two rare examples of a uranyl adducts with Group 2 metals using macrocyclic calixarene ligands. One of which, $[UO_2(calix)][Ba(30\text{-}crown\text{–}10)]$ (calix = p-Ph-[3.1.3.1]homooxacalixarene) is shown in Figure 5 (**VIII**).[30] The U–O bond elongation in **VIII** is slightly lower than that of **VII,** with an average U–O bond distance of 1.80 Å perhaps

due to the weaker Lewis acidity of the Ba^{2+} cation in comparison to the smaller Na^{+}. This difference is also reflected in the longer OUO–Ba bond length of 2.885(6) Å in comparison to the analogous O–Na bond distances in **VII**. The use of the even smaller lithium cation to form OUO–M interactions results in even longer U–O bonds, with the complex $[\{Li(DME)_2\}_2Cl][Li(DME)][UO_2(NC_5H_{10})_3]_2$ synthesised by Hayton and co-workers exhibiting O–Li bond lengths in the range 1.89–1.93 Å (Figure 5, **IX**).[31] As in the complexes **VII** and **VIII**, the formation of OUO–M Lewis pairs is facilitated by the use of strong σ-donors ligands on uranyl such as the piperidide ligands in **IX**. There are rare examples however of $OU^{VI}O$–M complexes which feature weak uranyl equatorial donor ligands. The uranyl bromide salt $[Na(15\text{-crown-}5)]_2[UO_2Br_4]$ features a single $[UO_2]^{2+}$ dication from which each oxo group is coordinated to a sodium centre (Figure 5, **X**).[32] Two short and symmetric U–O bond distances, each of 1.780(3) Å, are within the normal range for uranyl(VI) with the lack of uranyl bond activation perhaps expected for such a weak equatorial ligand field. The O–Na bond lengths in **X** are significantly longer than those in **VII** (2.387(3) *vs* 2.21–2.30 Å) with the latter complex being comprised of the more strongly donating NCN ligands promoting greater U=O Lewis basicity.

The O=U=O–M bonding motifs in complexes **VII**–**X** are examples of actinyl "cation-cation interactions" or CCIs. Such interactions are relatively uncommon in uranyl(VI) chemistry due to the poor Lewis basicity of the $[UO_2]^{2+}$ dication but are more prevalent in the chemistry of the heavier actinyls, with those of $[NpO_2]^{n+}$ (n = 1, 2) being the most studied.[33-38] Upon reduction of uranyl(VI) to uranyl(V), the Lewis basicity of the oxo group increases, greater promoting the formation of CCI complexes (see section 1.5).

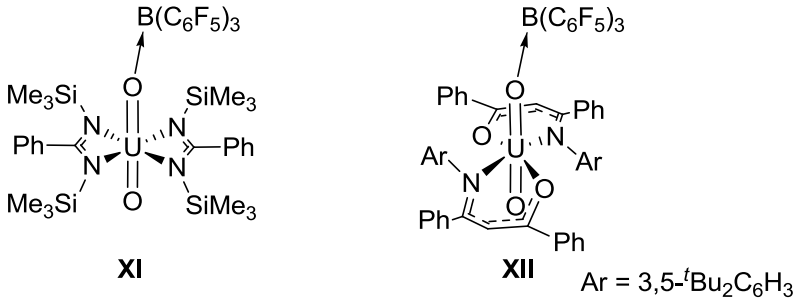

Figure 6: Uranyl(VI)-tris(pentaflurophenyl)borane adducts.

Uranyl(VI) complexes functionalised with non-metal Lewis acids are restricted to two adducts of the strong Lewis acid $B(C_6F_5)_3$ (Figure 6). The first example was synthesised by Sarsfield and co-workers in 2004 and utilises the same strongly-donating benzaminato ligand (NCN) as used in the preparation of **VII**. The borane-functionalised complex, $[\{(C_6F_5)_3B\}OUO(NCN)_2]$ **XI** features a long $B(C_6F_5)_3$-coordinated U=O bond of 1.898(3) Å that is

elongated significantly in comparison to the uncoordinated precursor complex $[UO_2(NCN)_2]$ (1.770(3) Å).[39] The second example of such a complex was synthesised by Hayton and Wu by treatment of $[UO_2(acnac)_2]$ (acnac = (3,5-^{t}Bu$_2$C$_6$H$_3$)NC(Ph)CHC(Ph)O) with $B(C_6F_5)_3$ to form $[\{(C_6F_5)_3B\}OUO(acnac)_2]$ **XII**. The complex features a comparatively elongated U=O{$B(C_6F_5)_3$} bond of 1.890(4) Å to that of **XI,**[40] with the use of the strongly-donating, bidentate σ-donor ligands in **XI** and **XII** again postulated to promote their greater uranyl Lewis basicity.

1.5 Uranyl(V) complexes

Of all the oxidation states of uranium (III, IV, V and VI), complexes of uranium(V) have, historically, received the least attention. The aforementioned affinity of uranyl(V) to undergo disproportionation is often highlighted as a reason for this, with complexes of the species regularly found to be highly sensitive towards oxygen and water.[1-2] In light of this, the majority of U^V complexes known are non-oxo complexes of uran*ium*, rather than uran*yl*, with the classical halide species UOX_5^{2-}, UX_5 and UX_6^- known since the pre-1950s.[41] Despite the chemistry of uranium(V) still being underdeveloped in comparison to the other oxidation states, the modern development of handling techniques for air-sensitive compounds has facilitated the preparation of numerous alkoxide, amide, and organometallic U^V complexes in recent decades.[42] In contrast, well-characterised uran*yl*(V) complexes remained elusive until the 2000s, with previous knowledge into the nature of the species gained almost exclusively from its transient electrochemical generation.

1.5.1 Electrochemical generation of $[UO_2]^+$

The first direct evidence of uranyl(V) formation in solution was by electrolytic reduction in of $[UO_2]^{2+}$ in DMF solution. Miyake and co-workers used electron paramagnetic resonance (EPR) and UV-vis-NIR spectroscopies to monitor the products of photo- and electrolytic reduction of $[UO_2(DMF)(ClO_4)_2]$, with the resulting spectra indicating the formation of a 5*f*^{1} cation.[43] Since this initial discovery, the group of Ikeda and co-workers have used electrochemical methods to reduce a wide range of aqueous uranyl(VI) complexes featuring ligands such as carbonate ($U^{VI}O_2(CO_3)_3^{4-}$), acetylacetonate ($U^{VI}O_2$ $(acac)_2(DMSO)$) and salen (N,N''-disalicylidenethylenediaminate) ($U^{VI}O_2(salen)_2(DMSO)$ (N,N''-disalicylidenethylenediaminate) amongst others.[44-46] The formation of these $[U^VO_2]^+$ complexes from $[U^{VI}O_2]^{2+}$ precursors was typically observed from a quasi-reversible single electron reduction, with the disproportionation of the resultant species slow enough within pH 2–4 to be spectroscopically characterised. Quantitative information about the structure of reduced uranyl complexes in solution has been gained by Livens and co-workers who

utilised EXAFS spectroscopy to study the electrochemically generated species. It was reported that the U=O bond distances of uranyl carbonate solutions increased from 1.80 to 1.90 Å upon reduction, indicative of a lowering of the U=O bond order upon population of the non-bonding uranium 5f orbitals.

None of the electrochemically generated uranyl(V) complexes were ever isolated from solution nor were they independently synthesised. However, the insights gained into the structure and redox potentials of the $[U^{V}O_2]^+$ cation were later corroborated upon the crystallisation of the first uranyl(V) complex by Berthet and co-workers in 2003. Crystals of $[UO_2(OPPh_3)_4][OTf]$ **XIII** were isolated serendipitously from a mixture of $[UO_2(OTf)_2]$ and triphenylphosphine oxide however attempts to access the molecule by a formal synthetic route were unsuccessful.[47] The U=O bond lengths in the structure are 1.817(6) and 1.821(6) Å, slightly longer than those in the analogous uranyl(VI) complex $[UO_2(OPPh_3)_4][OTf]_2$ (mean bond length 1.76 Å), again indicative of reduction-induced U–O bond weakening.

1.5.2 Oligomeric uranyl(V) complexes

The isolation of the uranyl(V) polymer $[\{UO_2(py)_5\}\{KI_2(py)_2\}]_n$ **XIV** by Mazzanti and co-workers in 2006 provided the first reproducible preparation of an isolated $[UO_2]^+$ species (Scheme 3).[48]

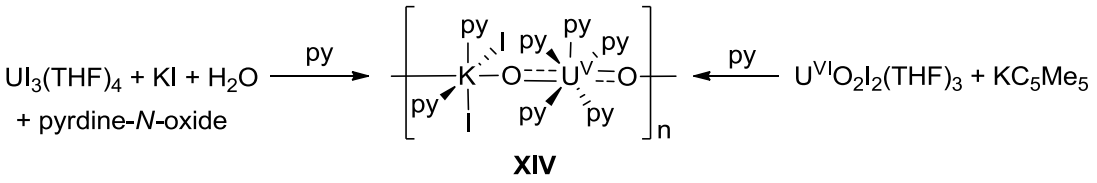

XIV

Scheme 3: Oxidative and reductive routes to the uranyl(V) coordination polymer **XIV**.

The complex was synthesised by the two-electron oxidation of $UI_3(THF)_4$ using pyridine-*N*-oxide in the presence of water and has a structure consisting of an infinite 1-D chain of trigonal bypyramidal $[UO_2(py)_5]$ units linked via oxo-potassium cation-cation interactions. Such extended CCI formation in comparison to the uranyl(VI) complexes **VII-XII** demonstrates the greater Lewis basicity of the uranyl(V) oxo groups and is facilitated by quenching of the uranium positive charge by the $5f^1$ electron. The uranium-oxygen bond order reduction is again represented by long U–O bonds of 1.836(2) and 1.834(2) Å which are slightly longer than those in the mononuclear uranyl(V) complex **XIII** perhaps due to the formation of the CCIs. Evidence for the weakening of the U–O bonds in **XIV** is also evident in the FTIR spectrum with the asymmetric $[UO_2]^+$ stretch at 797 cm^{-1} occurring at significantly lower energy than that of the corresponding uranyl(VI) complex $[UO_2I_2(py)_3]$

(927 cm^{-1}). The group of Berthet reported a alternative synthesis of **XIV** in the same year, accessing the polymer by reduction of $[UO_2I_2(THF)_2]$ with either KCp* or TlCp* (Cp* = pentamethylcyclopentadiene) in pyridine solvent.[49] The complex **XIV** was later used by the Mazzanti group as a versatile precursor to a number of other oligomeric CCI complexes by the reactions of the complex with K(DBM) (DBM = dibenzoylmethoate) under various conditions (Scheme 4).

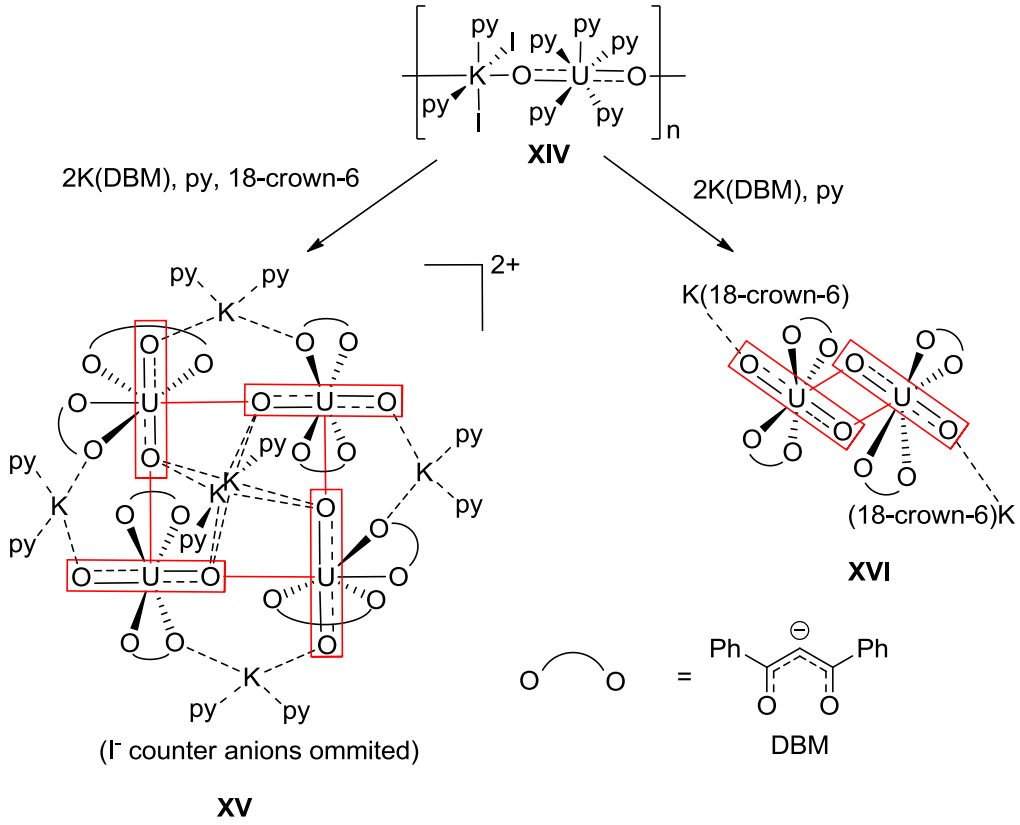

Scheme 4: Deaggregation of $[\{UO_2(py)_5\}\{KI_2(py)_2\}]_n$ to form $[U^VO_2]^+$/ $[U^VO_2]^+$ CCI complexes.

The reaction of **XIV** with two equivalents of K(DBM) in pyridine was reported to result in the complete dissolution of the polymeric precursor and formation of tetrameric uranyl(V) CCI complex $[\{UO_2(DBM)_2\}_4\{K_6py_{10}\}I_2]$ **XV** (Scheme 4).[50] The complex consists of a centrosymmetric tetramer of four $[U^VO_2]^+$ units, each linked by monodentate cation-cation interactions with two neighbours. The complex provided the first crystallographic example of a uranyl(V)/uranyl(V) CCI, with each $[UO_2]^+$ species acting as both a Lewis base through its oxo groups and Lewis acid by the metal centre. In addition to these so-called "T-shaped" CCIs (Scheme 4, left, boxes) the structure shows multiple CCIs between the $[UO_2]^+$ units and μ_2- and μ_8-bridging potassium cations. Due to symmetry, there are only two crystallographically distinct $[UO_2]^+$ units in the structure, with the U–O bonds involved in interactions between the uranyl(V) cations exhibiting long bond lengths of 1.923(10) and

1.934(8) Å. The other U–O bonds coordinated to the potassium cations show more limited elongation (1.828(10) and 1.811(9) Å) and are more comparable to those found the $[UO_2]^+$/K coordination polymer **XIV**. Evidence of weakening of the U–O bonds in **XV** is found in the FTIR spectrum, which exhibits an absorption at 782 cm^{-1} similar to that shown by **XIV** (797 cm^{-1}). Studies on the structure of **XV** in solution were undertaken using ^1H NMR spectroscopy and revealed the presence of a C_{4h} symmetric species indicating that the tetrameric structure was retained in solution. Dissolution of **XV** in DMSO results in simpler ^1H NMR spectrum consistent with the disruption of the cation–cation interactions and the formation of a monomeric species.

Performing the synthesis of **XV** in the presence of 18-crown-6 prevents potassium bridging and results in the formation of the dimeric complex [K(18-crown-6)]$_2$[{UO_2(DBM)$_2$}$_2$] (Scheme 4, **XVI)**.[51] The solid state structure of the complex shows it contains monodentate O=U=O–K interactions in addition to the dimeric or "diamond-shaped" uranyl/uranyl CCIs of the central U_2O_4 core (Scheme 4, right, boxes). Diamond-shaped CCIs had been previously observed in solid state complexes of neptunyl(V) however **XVI** was the first example of a uranyl complex containing the same motif. The greater stability of heavier actinyl(V) cations towards disproportionation has led to suggestions that $[NpO_2]_2^+$ and $[PuO_2]_2^+$ CCI dimers might be more stable in solution that their uranyl analogues. [52-53] Both **XV** and **XVI** were shown to be stable in a pyridine solution and found to de-aggregate to monomeric species in the presence of strong donor solvents such as triphenylphosphine oxide or DMSO. Decomposition was observed in the presence of water and which was demonstrated to occur faster for the CCI complexes than for the monomeric products of their deaggregation. Such an observation complements theoretical studies, which suggest CCI formation may be implicit in the disproportionation of UO_2^+ in aqueous phases.[54]

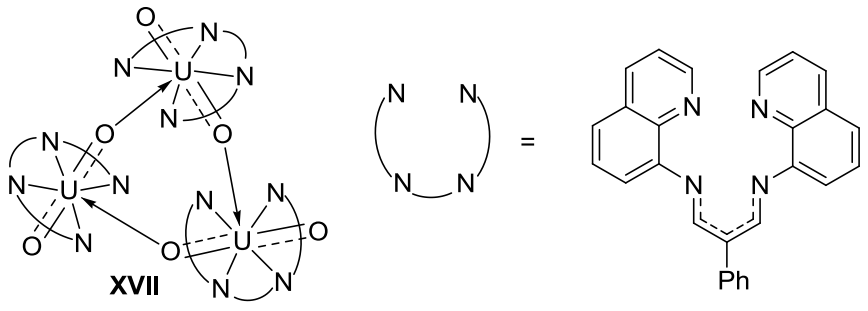

Figure 7: The trimeric uranyl(V) CCI complex **XVII**.

The first homometallic uranyl(V) CCI complex was synthesised by the Mazzanti group in 2012 by treatment of the polymeric uranyl(V) precursor **XIV** with one equivalent of

K(TQD) (TQD = 2-(4-Tolyl)-1,3-bis(quinolyl)malondiiminate) forming one third of an equivalent of the trimetallic complex [{UO_2(TQD)}$_3$] (Figure 7, **XVII**). By utilisation of the monoanionic TDQ, the charge-balancing potassium cations present in complexes such as **XVI** are not required, with elimination of the potassium iodide by-product upon complexation of the multidentate ligand. The three $[UO_2]^+$ cations in **XVII** aggregate by $[UO_2]^+/[UO_2]^+$ CCIs forming an approximate equilateral triangle with a pseudo three-fold symmetry axis at the centre; The first example of a trimeric uranyl(V) CCI complex. The U–O bond lengths in **XVII** are similar to those in **XV** and **XVI** with longer bonds observed for the U-coordinated U–O_{endo} bonds (average 1.91 Å) than for the uncoordinated U–O_{exo} bonds (average 1.84 Å). In analogy with **XV** and **XVI** the complex was found to retain its trimeric structure in pyridine solution, further demonstrating the stability of $[UO_2]^+/[UO_2]^+$ CCI complexes towards deaggregation.

1.5.3 Uranyl(V) disproportionation

Despite the well-documented affinity of uranyl(V) complexes to undergo disproportionation in protic media there have been very few studies in which full characterisation of the resultant uranyl(VI) and U^{IV} materials produced has been achieved. Such a lack of information is surprising considering the relevance of uranyl(V) disproportionation for the speciation of uranium in the environment, spent nuclear fuel disposal and the development of waste remediation strategies.[14, 55-56]

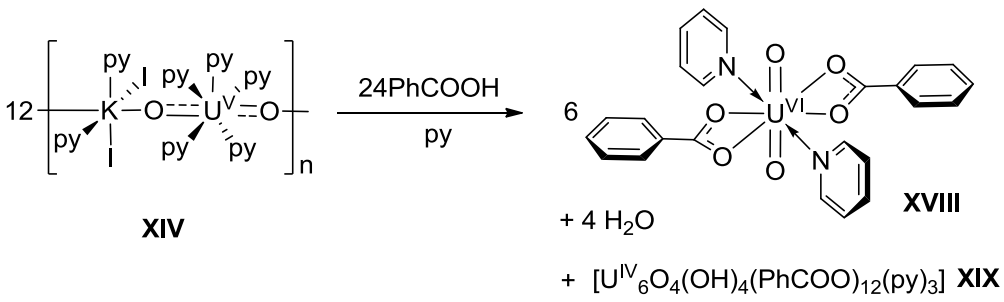

XIV

Scheme 5: Disproportionation of **XIV** using benzoic acid.

One synthetic study of uranyl(V) disproportionation was undertaken by the Mazzanti group, demonstrating that the treatment of 12 equivalents the uranyl(V) polymer [{UO_2(py)$_5$}{KI_2(py)$_2$}]$_n$ **XIV** with two equivalents of benzoic acid in pyridine resulted in the immediate formation of 6 equivalents of the uranyl(VI) complex [UO_2(C_6H_5COO)$_2$(py)$_2$] **XVIII**, one equivalent of the uranium(IV) cluster [U_6O_4(OH)$_4$(C_6H_5COO)$_{12}$(py) **XIX**, and 4 equivalents of water (Scheme 5).[57] Both **XVIII** and **XIX** were characterised spectroscopically and in the solid state, with the X-ray crystal structure of the uranyl(VI) complex displaying a hexagonal bypyramidal U centre with a linear O-U-O geometry (bond

angle 180˚) and two short and symmetric U=O bond lengths (1.769(5) Å). In contrast, the structure of the U^{IV} complex **XIX** exhibits six uranium cations arranged at in an octahedron, with each of the resulting triangular faces capped by a μ_3-bridging oxygen atom forming a U_6O_8 cluster. Four of the capping ligands are hydroxides, evidenced by long U–O bond lengths between 2.419(2) and 2.455(15) Å, and four are oxides, with much shorter U-O distances within the range 2.229(20)–2.271(13) Å. Each uranium cation is additionally coordinated by two bidentate benzoate ligands that bridge between adjacent metal centres. DOSY NMR spectroscopy was used to show that the solid state structures of both **XVIII** and **XIX** were maintained in solution with the diffusion coefficient observed for the latter complex being expectedly larger. Although no direct studies were made on the mechanism of the disproportionation of **XIV** it was proposed that the process involves the initial protonation of the uranyl(V) oxo groups of a CCI complex intermediate before inner sphere electron transfer and complex dissociation to form the uranyl(VI) and uranium(IV) oxo/hydroxo products **XVIII** and **XIX**.

1.5.4 Mononuclear uranyl(V) complexes

The studies into aggregated uranyl(V) CCI complexes and the growing evidence that such motifs may facilitate uranyl(V) disproportionation has led to the development of mononuclear uranyl(V) complexes by greater emphasis on ligand design.

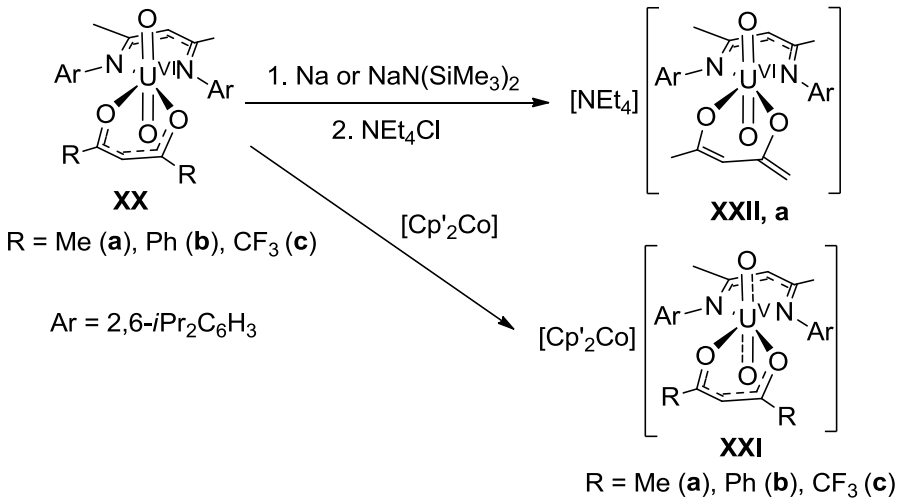

Scheme 6: The contrasting reactivity of the uranyl(VI) precursor **XX** with Cp_2*Co or Na reducing agents to form uranyl(V) or deprotonated complexes respectively.

Hayton and co-workers postulated that bulky chelating ligands can stabilise $[UO_2]^+$ by both preventing CCI formation and providing steric protection of the two uranyl oxo groups toward protonation. In 2008 they demonstrated the single electron reduction of the uranyl acac/nacnac complexes $[UO_2(Ar_2nacnac)(RC(O)CHC(O)R]$ **XX** (Ar_2nacnac = (2,6-

$^{i}Pr_2$-C_6H_3)NC(Me)CHC(Me)N(2,6-$^{i}Pr_2$-C_6H_3, R = Me **a**, Ph **b,** CF_3 **c**) both electrochemically and by formal chemical reduction (Scheme 6).[58] It was reported that the reduction potential of **XX** decreases for more electron-withdrawing β-diketonate ligands, with E_{red} values of –1.82, –1.59 and –1.39 for **XXa**, **b** and **c** respectively. All three complexes could be reduced chemically using decamethyl cobaltacene (Cp_2*Co), forming the respective monomeric uranyl(V) complexes [Cp*Co][UO_2(Ar_2nacnac)(RC(O)CHC(O)R] **XIX** (Scheme 6). The phenyl-substituted β-diketonate complex, **XXIb**, was characterised in the solid state and was found to consist of a discrete cation/anion pair containing a mononuclear [$U^{V}O_2$(Ar_2nacnac)(PhC(O)CHC(O)Ph]$^{-}$ anion that does not form CCIs. The U–O bond lengths in **XXIb** are only marginally elongated in comparison to **XXb**, with distances of 1.79(1) and 1.81(1) Å observed in the former complex and 1.780(4) and 1.790(4) Å in the latter. Such minimal extension of the uranium-oxygen bonds upon reduction is perhaps due to the inability of the **XXIb** to engage in adduct formation, with the U–O bond lengths in the uranyl(V) CCI complexes **XIV**-**XVI** all being longer than those in the monomeric complexes **XIII** and **XXIb**.

The shorter U–O bond lengths in **XIXb** suggests that the reduction in the U–O bond order upon reduction to uranyl(V) may perhaps be more dependent on the more favourable formation of Lewis adducts than on reduction alone, a theory corroborated by the observation that CCI complexes of stronger Lewis acids, such as the other $[UO_2]^{+}$ cations in **XV** and **XVI**, exhibit greater U–O bond elongations than those of weaker Lewis acids such as the potassium cations in complexes such as **XIV**. This postulate is further supported by the observation that the U–O bonds in the uranyl(VI)/$B(C_6F_5)_3$ complexes **XI** and **XII** are much greater than those in **XIII** and **XXIb** despite the U^{VI} oxidation states of the former complexes.

In contrast to the reductions of **XX** with Cp^*_2Co, the reaction of the complex **XXa** with sodium metal followed by cation exchange with [NEt_3]Cl was shown to result in the formation of the uranyl(VI) complex [NEt_3][UO_2(Ar_2nacnac)(H_2C=C(O)CH(O)Me] **XXII**. The formation of **XXII** results from the formal loss of H· from the methyl group of the acac ligand and can be alternatively synthesised by the deprotonation reaction with $NaN(SiMe_3)_2$.

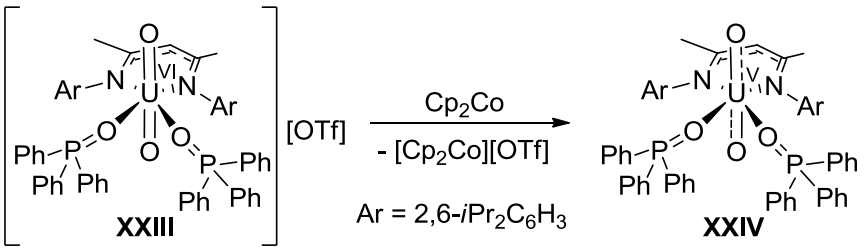

Scheme 7: Synthesis of **XXIV** by the reduction of **XXIII** with Cp_2Co.

The group of Hayton and co-workers also reported the single electron reduction of the uranyl triflate salt $[UO_2(Ar_2nacnac)(Ph_2MePO)_2][OTf]$ **XXIII** with cobaltocene.[59] In contrast to the reduction of **XX,** the reduction of the mono-β-diketiminate salt proceeds with elimination of $[Cp_2Co]OTf]$ to produce a rare example of a neutral, mononuclear uranyl(V) complex $[UO_2(Ar_2nacnac)(Ph_2MePO)_2]$ **XXIY** (Scheme 7). In analogy with **XXI,** it was postulated that the steric bulk provided by 2,6-diisopropyl-phenyl groups on the Ar_2nacnac ligand prevented CCI formation by either dimerisation or coordination to the $[Cp_2Co]^+$ cation. The U–O bond lengths of 1.810(4) and 1.828(4) Å in **XXIV** are again shorter than those present in CCI complexes such as **XVII**. Although the use of the Ar_2nanac protects **XXIV** against dimerisation, the proposed greater stability of the mononuclear uranyl(V) complex towards aqueous disproportionation was not tested, preventing comparison with aggregated CCI complexes such as **XIV**.

1.5.5 Functionalised uranyl(V) complexes

A subject of perhaps the greatest interest in uranyl(VI) reduction chemistry is that of oxo group functionalisation. It was demonstrated in the previous sections that the $[UO_2]^{2+}$ dication can coordinate to strong Lewis bases and that the prevalence and stability of these so-called CCI complexes increases upon reduction to uranyl(V). The natural advancement beyond these Lewis adducts has been the preparation of complexes with formal UO-R covalent bonds, a process that occurs concomitantly with U-O bond activation by reduction to uranyl(V). The first examples of such complexes were prepared by our groups in 2008 and are discussed in section 1.6 however Hayton and co-workers have subsequently synthesised a number of other functionalised uranyl(V) complexes of the ^{Ar}acnac (ArNC(Ph)CHC(Ph)O, Ar = 3,5-^{t}Bu$_2$C$_6$H$_3$) ligand.

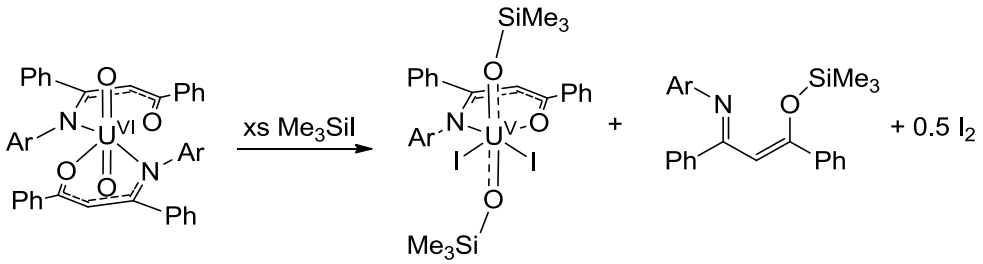

XXV **XXVI**

Scheme 8: Reduction and oxo-group silylation of a uranyl(VI) β-ketoiminate.

In the simplest example, the uranyl(VI) complex $[UO_2(^{Ar}acnac)_2]$ **XXV** was treated with excess Me_3SiI resulting in the formation of the $SiMe_3$-functionalised uranyl(V) complex $[U(OSiMe_3)_2I_2(^{Ar}acnac)]$ **XXVI** (Scheme 8).[60] The uranyl(V) complex **XXVI** displays two trimethyl silylated axial oxo groups with a single β-ketoiminate ligand and two iodide ligands coordinated in the equatorial plane. The fate of the second β-ketoiminate ligand of **XXV** was determined by ^1H NMR spectroscopy being found to dissociate by Me_3Si^+ abstraction during the formation of **XXVI** to form the silylated organic compound ArNC(Ph)CHC(Ph)OSiMe. The formation of I· during the synthesis of **XXVI** was confirmed by addition of Ph_3P to the reaction mixture, with the resultant production of Ph_3PI_2 monitored by ^1H NMR and UV-vis spectroscopies. The reaction was proposed to proceed by initial coordination of Me_3Si^+ to the uranyl oxo group, lowering the $[UO_2]^{2+}$ reduction potential to enable its reduction by the weakly-reducing iodide. Previous studies undertaken by the same group found that the reduction potential of the uranyl(VI) precursor **XXV** was reduced from –1.35 to –0.78 V upon coordination of the strong Lewis acid $B(C_6F_5)_3$ to form **XII**. The U–O bond lengths in **XXVI** are 1.996(5) and 1.986(5) Å, longer than any of the aforementioned uranyl(V) complexes and consistent with the greater Lewis acidity of, and covalent-bond formation to, Me_3Si^+.

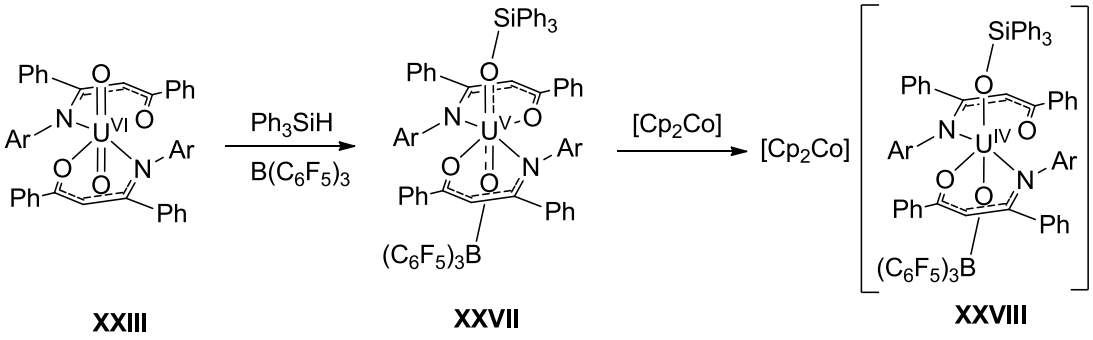

XXIII **XXVII** **XXVIII**

Scheme 9: Reductive silylation of a uranyl(VI) complex mediated by $B(C_6F_5)_3$.

The greater oxidising ability of $[UO_2]^{2+}$ upon oxo-coordination was later demonstrated more conclusively by reductive silylation of the *in-situ* generated OUO-$B(C_6F_5)_3$ complex **XII** with Ph_3SiH to form the triphenylsilylated complex $[U(OSiPh_3)(OB\{C_6F_5\}_3)(^{Ar}acnac)_2]$ **XXVII** (Scheme 9).[61] The fact that the reductive silylation of **XXV** *via* **XII** can be achieved using the much weaker reducing agent Ph_3SiH compliments the aforementioned cyclic voltammetry evidence for the lower reduction potential of **XII**. The U–O bond lengths of the $B(C_6F_5)_3$ and Ph_3Si-functionalised oxo groups in **XXVII** are 1.941(8) and 2.034(9) Å respectively, with the latter being longer still than any of the aforementioned uranyl(V) complexes. The double oxo-group functionalisation present in **XXVII** was purported also to lower the reduction potential of that complex, with a value of –0.72 V for the U^V/U^{IV} couple being 0.63 V higher than the analogous, unsilylated uranyl(V) complex $[Cp^*_2Co][U(OB\{C_6F_5\}_3)_2(^{Ar}acnac)_2]$.[62] The reduced uranium(IV) complex $[Cp_2Co][U(OSiPh_3)(OB\{C_6F_5\}_3)(^{Ar}acnac)_2]$ **XXVIII** was prepared by treatment of **XXV** with Cp_2Co, a weaker reducing agent than Cp^*_2Co. The latter reducing agent was required to reduce the unsilylated uranyl(V) analogue $[Cp^*_2Co][U(OB\{C_6F_5\}_3)_2(^{Ar}acnac)_2]$ to its respective uranium(IV) salt $[Cp^*_2Co]_2[U^{IV}(OB\{C_6F_5\}_3)_2(^{Ar}acnac)_2]$ again demonstrating the more facile reduction potential of **XXV**.[62] The bond lengths in the U^{IV} complex **XXVIII** are longer still than those of **XXVII** and **XXV**, with the U–O(borane) and U–O(siloxide) bonds being 2.056(8) and 2.173(8) Å respectively and consistent with further reduction of the U–O bond order and the formation of the larger U^{4+} cation. The complex **XXVIII** presents a rare example of a uranium(IV) oxo complex which retains the UO_2 motif, with the aforementioned isolation of the doubly-borylated complex $[Cp^*_2Co]_2[U^{IV}(OB\{C_6F_5\}_3)_2(^{Ar}acnac)_2]$ being the only other example.[62]

1.6 Pacman complexes

The chemistry of a number of polypyrrolic, potentially dinucleating Schiff-base macrocylic ligands has been studied within our groups over the last decade. First reported

independently by both Love and Sessler in 2003,[63-64] the ligands contain two distinct N_4 donor compartments, each formed from diiminodiyrrolmethane subunits, that can be deprotoned to form complexes that mimic the structures of co-facial, or Pacman, diporphyrins (Figure 8).[65] The latter class of complexes, composed of two porphyrins arranged cofacially by the use of a rigid spacer group, have been employed to form a number of binuclear transition metal complexes which exhibit reactivities towards multielectron redox processes such as dioxygen reduction.[65] The single-pillared, dibenzoxanthene bridged diporphyrin ligand DPX is one such example of a Pacman dipporphyrin, the binuclear iron complex of which, [Fe_2(DPX)] **XXX**, has been shown to facilitate dioxygen reduction and subsequent oxygen atom transfer catalysis (Figure 8).[66] The Schiff-base macrocylic ligands used by our groups exhibit D_{2h} symmetry in their protonated states but fold to form cofacial C_{2v} symmetric complexes upon deprotonation and metal complexation mimicking the structure of complexes such as **XXX**. The simplest and first prepared example of these non-porphyrin Pacman ligands was the tetramethylated macrocycle H_4L^{tet} (Figure 8).

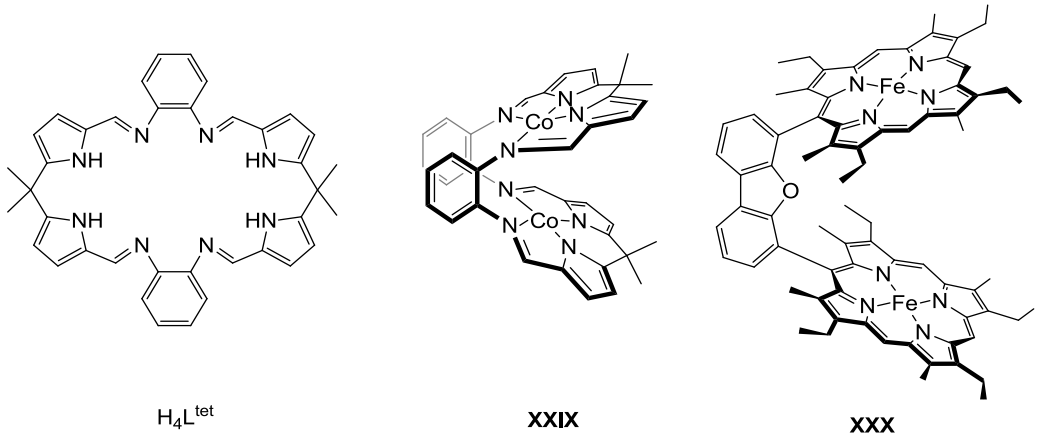

H_4L^{tet} **XXIX** **XXX**

Figure 8: The tetramethylated Pacman ligand H_4L^{tet}, a binuclear cobalt complex of L^{tet} **XXIX** and a Pacman cofacial diporphyrin complex **XXX**.

In addition to mimicking the structures of Pacman dipporphyrin complexes the transition complexes of Pacman ligands can also mimic some of their reactivity, with the binuclear cobalt complex of the L^{tet} ligand, [$Co_2(L^{tet})$] (Figure 8, **XXIX**) having been shown to act as dioxygen reduction catalyst.[67] The main advantages of Pacman ligands over their porphyrin analogues is their ease of synthesis, with a simple acid/base condensation reaction between a diformyldipyrromethane unit and a diamine spacer being utilised to form a variety of ligands in high yields. Since their initial discovery, Schiff-base Pacman macrocycles have been used to prepare a large number of binuclear transition metal complexes for the purposes of small molecule activation and multi-electron redox catalysis.[68]

1.6.1 Mononuclear pacman complexes

Monometallic complexes of Pacman ligands are much rarer than their binuclear counterparts owing to the symmetrical ligand environment providing no clear selectivity for the incorporation of one or two metals. However, both the $[UO_2]^{2+}$ and $[SnMe_2]^{2+}$ dications have been shown to react with Pacman ligands to form monometallic complexes selectively.[69-71] In these specific cases, the two axial ligands present in each species block the adjacent N_4-donor pocket and prevent the complexation of a second trinuclear cation.

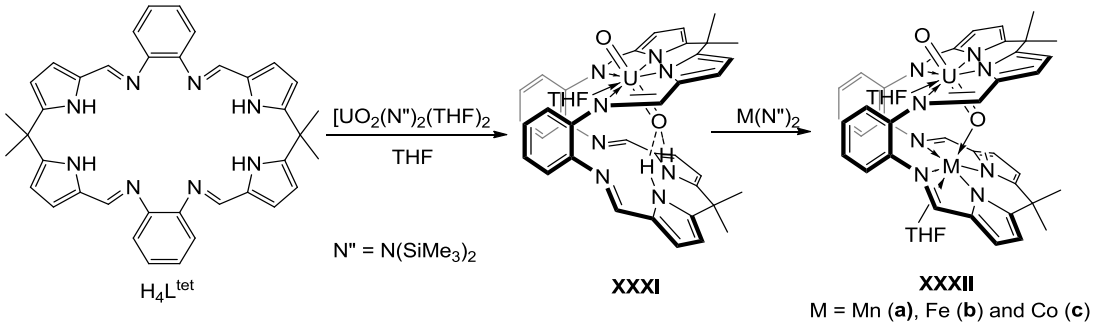

Scheme 10: Synthesis of monometallic and heterobimetallic uranyl(VI) Pacman complexes.

The uranyl(VI) complex of the L^{tet} ligand, $[UO_2(THF)(H_2L^{tet})]$ **XXXI**, is one example of a mononuclear Pacman complex, synthesised by the addition of one equivalent of the uranyl(VI) bis(silylamido) base $[UO_2(N")_2(THF)_2]$ (N" = $N(SiMe_3)_2$) to the free ligand H_4L^{tet} in THF (Scheme 10).[69] The solid state structure of **XXXI** displays a folded macrocyclic ligand containing an approximately pentagonal bipyramidal uranium metal centre complexed equatorially by four nitrogen donors and one molecule of THF. The U=O bond lengths of 1.790(4) and 1.766(4) Å are typical of a uranyl(VI) complex, with the $[UO_2]^{2+}$ dication desymmetrised in comparison to the starting material by the formation of *endo* and *exo* uranium-bound oxygen atom environments. The *endo* oxo group forms an intramolecular hydrogen bond between itself and the pyrrolic protons of the vacant N_4-donor pocket, with relevant O···N bond distances of 3.111(7) and 3.146(7) Å describing the interaction.

The reactions of **XXXI** with the transition metal silylamide complexes $[M(N(SiMe_3)_2]$ (M = Mn, Fe, Co) were later shown to yield the heterobimetallic uranyl-transition metal complexes $[UO_2(THF)(L^{tet})M(THF)]$ **XXXIIa,b** and **c**; The first examples of uranyl/transition metal CCI complexes.[72] Desymmetrisation of the uranyl dication was evidenced by the elongation of the metal-coordinated *endo* U–O bond in **XXXIIa** (1.808(4) Å) in comparison to the *exo* (1.790(4) Å), with the degree of lengthening of the former bond comparable with those observed in the uranyl(VI) CCI complexes described in section 1.4.2.

Interestingly, no U-O_{endo} bond elongation was observed in cobalt complex **XXXIIc** which exhibits a bond length of 1.784(6) Å that is shorter than that in **XXXIIa**, a result perhaps due the lower Lewis acidity of the Group 9 M^{II} cation in comparison to Group 7 as per the Irving-Williams series.[73] Crucially however, the U-O_{endo} bond elongation in **XXXIIa** is not significant enough to be indicative of a formal uranyl reduction, a postulate confirmed by SQUID magnetometry measurements which suggested $U^{VI}M^{II}$ oxidation states for all the $[UO_2(THF)(L^{tet})M(THF)]$ complexes.

1.6.2 Reductive functionalisation of uranyl Pacman complexes

In 2008 Arnold, Love and co-workers further exploited the reactivity of uranyl Pacman complexes to achieve, for the first time, the reduction and selective oxo group silylation of the uranyl dication (Scheme 11).[74]

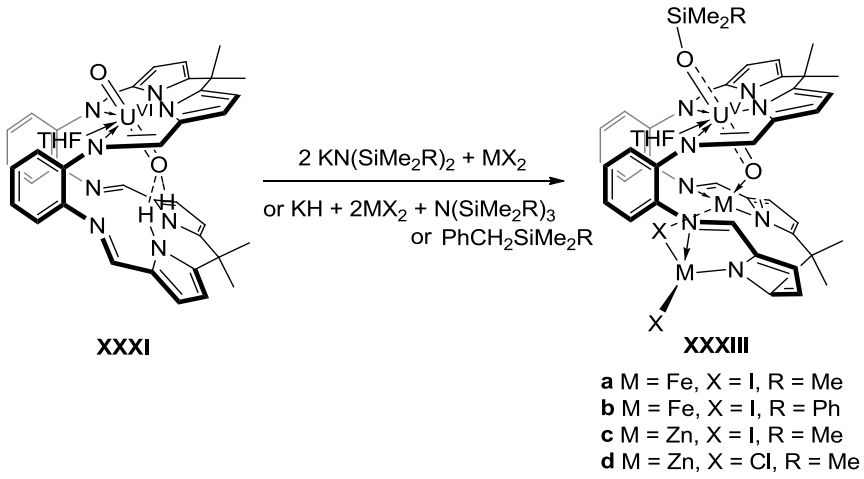

Scheme 11: Single-electron reduction and oxo-group silylation of the uranyl(VI) dication.

The one pot reaction between $[UO_2(THF)(H_2L^{tet})]$, two equivalents of $KN(SiMe_3)_2$ and two equivalents of FeI_2 in THF resulted in the formation of $[(Me_3SiOUO)(THF)(Fe_2(\mu\text{-}I)(I)(L^{tet})]$ **XXXIIIa**. Both the *endo* and *exo* U-O bond distances in **XXXIIIa** show appreciable lengthening (1.870(4) and 1.993(4) Å respectively) with the latter being appreciably longer than the former. While the *endo* bond length lies within the known range of bond lengths observed for uranyl(V) complexes, the *exo* bond was reported as being significantly longer than any in present the literature at the time and has since being shown to be comparable with the silylated uranyl(V) complexes synthesised by Hayton and co-workers (Section 1.5.5). A more general route to the complex **XXXIIIa** was reported in the same paper by the one-pot reaction between $[UO_2(THF)(H_2L^{tet})]$, KH and FeI_2 in the presence of either $N(SiMe_3)_3$ or $PhCH_2SiMe_3$. The analogous zinc complexes were also obtained by this route by substitution of the iron halide salt for ZnI_2 or $ZnCl_2$ forming the

complexes $[(Me_3SiOUO)(THF)(Zn_2(\mu\text{-}X)(X)(L^{tet})]$ (X = I, Cl, **XXXIII c, d)**. Oxo-functionalisation with different organosilyl compounds was achieved by variation of the substrate, with the dimethylphenylsilated complex $[(PhMe_2SiOUO)(THF)(Zn_2(\mu\text{-}I)(I)(L^{tet})$ **XXXIIIb** synthesised directly from $[UO_2(THF)(H_2L^{tet})]$, $KN(SiMe_2Ph)$ and ZnI_2.

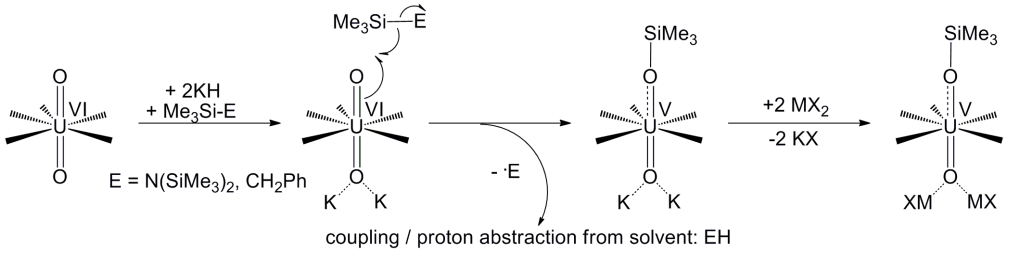

Scheme 12: Proposed mechanism of uranyl reductive silylation.

Although the mechanism of reductive functionalisation has yet to be defined the isolation of the complexes **XXXIII** from two different routes allowed certain conclusions to be drawn. The formation of the heterobimetallic uranyl(VI) complexes **XXXII** in the absence of a potassium bases suggested that transition metals were not able to act as reductants, a postulate further indicated by the isolation of the zinc complexes **c** and **d**. DFT calculations support the postulate that $[UO_2K_2(L)]$ is the reactive intermediate, with the inclusion of potassium cations in the vacant cleft thought to activate uranyl towards reductive C–Si or N–Si bond cleavage, forming the silylated uranyl(V)/potassium intermediates $[(RMe_2SiOUO)(THF)(K_2L^{tet})]$.[75] The transition metal complexes **XXXIII** were proposed to form after the reductive silylation, with transmetalation between the potassium cation and metal halide forming the isolated complexes and a KX by-product (Scheme 12).

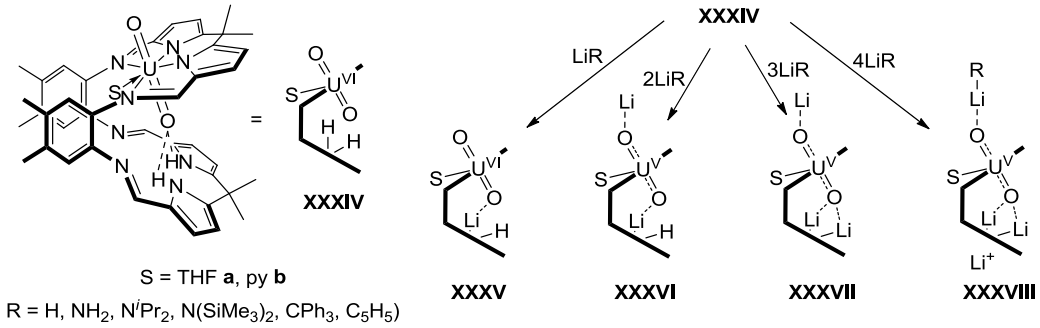

Scheme 13: Mono-uranyl(VI) complexes $[UO_2(S)(H_2L)]$ (S = THF, py) **XXXIV** of the octamethylated Pacman ligand L and their reactivity towards lithium bases.

In subsequent work, the same groups demonstrated that the reactions of lithium, rather than potassium, bases with the analogous mono-uranyl(VI) complex of the octamethylated Pacman ligand L ($[UO_2(S)(H_2L)]$ S = THF, py), could be used to form reductively lithiated, rather than reductively silylated complexes (Scheme 13).[76] The reaction

of the THF-solvated uranyl(VI) Pacman complex **XXXIVa** with one equivalent of LiN" in THF was shown to form the mono-lithiated complex [(OUO)(LiHL)] **XXXIVa**, an intramolcular $OU^{VI}O\cdots Li$ CCI complex. The U=O bond lengths in the solid state structure of **XXXIVa** of 1.794(3) and 1.767(3) Å were consistent with the retention of the uranyl(VI) oxidation state with no evidence for reductive silylation observed. The reaction between the pyridine-solvated uranyl(VI) complex **XXXIVb** and two equivalents of LiN" did result in the formation of a uranyl(V) complex, with the sole formation of the oxo-lithiated complex $[(py)_3LiOU^{V}O(py)Li(py)(HL)]$ **XXXVIb** observed when the reaction was undertaken in the presence of dihydroanthracene (DHA). From the crystal structure of **XXXVIb** it was determined that the complex is the reductively lithiated analogue of **XXXV**, with the same incorporation of a single lithium cation in the bottom N_4-donor pocket accompanied by a second lithium cation bound to the *exo* uranyl(V) oxo group. The $U\text{-}O_{endo}$ and $U\text{–}O_{exo}$ bond lengths in the structure of were found to be 1.834(4) and 1.879(5) Å respectively, consistent with the lowering of the uranium-oxygen bond order and the formation of $[U^{V}O_2]^{+}$. The complex **XXXVIb** was also prepared from **XXXIVb** and two equivalents of $LiN^{i}Pr_2$, LiC_5H_5, $LiCPh_3$, $LiNH_2$, or LiH in the absence of DHA, with the first reagent found to yield the complex the most cleanly. The reactions of **XXXIV** with 3 or 4 equivalents of LiN" were found to produce the triply- and quadruply-lithiated complexes $[(py)_3LiOU^{V}O)(Li_2L)]$ **XXXVII** and $[R_2NLi][(LiOU^{V}O)Li_2L]$ **XXXVIII** ($R = SiMe_3$) respectively. Both complexes are derived from the incorporation of a second lithium cation into the bottom N_4-donor cleft by deprotonation of the second pyrrolic NH group with the formation of latter complex resulting from the neutral incorporation of an $LiN(SiMe_3)_2$ molecule. The complexes **XXXVI-XXXVIII** are the only examples of reductively lithiated uranyl complexes adding to the family of uranyl(V) complex functionalised with potassium (**XIV-XVII**) and trialkyl silyl groups (**XXVI**, **XXVII**, **XXXIII**).

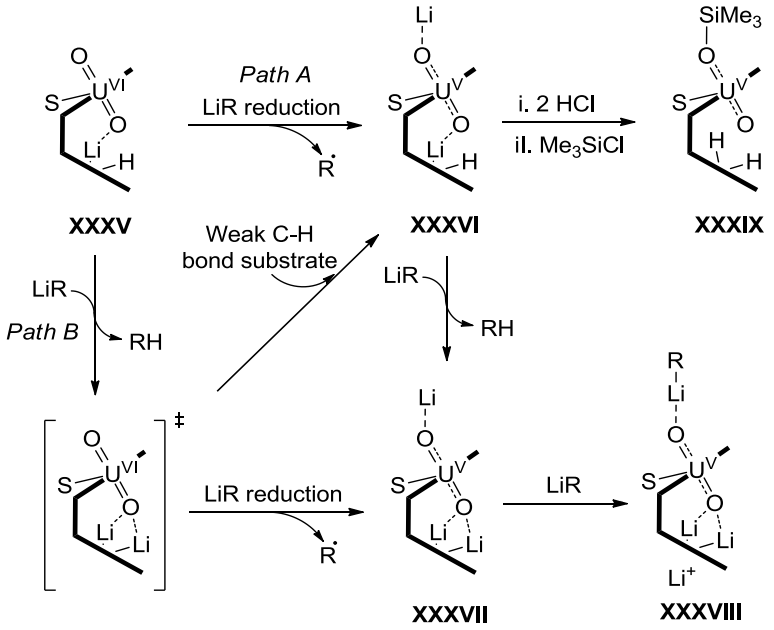

Scheme 14: Proposed mechanisms for the reductive lithiation of uranyl(VI) Pacman complexes and the synthesis of the silylated complex **XXXIV.**

Several plausible mechanisms to account for the formation of the complexes **XXXVI** and **XXXVII** were proposed, with the lithium reagent acting either as a reductant (Path A) or a base (Path B) (Scheme 14). The U^{V}/U^{VI} reduction potential of the mono-lithiated complex **XXXV** was found to be –1.18 V (in THF *vs* Fc/Fc^{+}) suggesting that only strongly reducing lithium reagents such as lithium alkyls and hydrides should reduce the complex. The aforementioned work by Hayton and co-workers however showed that Lewis acid oxo-coordination to uranyl(VI) can reduce the reduction potential to more positive potentials. It was therefore proposed that both the singly lithiated U^{VI} complex **XXXV** and the postulated doubly deprotonated uranyl(VI) intermediate $[UO_2(Li_2L)]$ were easier to reduce than the mono uranyl(VI) precursor **XXXIV** due to the respective single- and double-coordination of one or two lithium cations by the uranyl oxo groups. The proposed lowering of the uranyl(VI) reduction potential and evidence that the formation of **XXXVI** proceeds more cleanly in the presence of DHA lead to speculation that hydrocarbyl species, rather than LiR reagents, may as the reducing agent of $[UO_2(Li_2L)]$, with the single electron required for the reaction instead coming from homolytic cleavage of the C–H bonds of DHA or the solvent (THF or py). In this mechanism, the formation of the doubly-deprotonated $[U^{VI}O_2(Li_2L)]$ intermediate by Path B is proceeded by H-atom abstraction, forming the reductively protonated intermediate $[(HOU^{V}O)Li_2L)]$ which undergoes Li/H exchange to form **XXXVI**. Although full understanding of the reaction mechanism has not yet been achieved it was clear that a number of different processes may be occurring in tandem, with

formation of radicals during the processes demonstrated by the formation of radical-derived products upon addition of DHA, a bonded radical scavenger containing weak C–H bonds. The contrasting chemistry of Li and K potassium bases in forming either reductively lithiated or reductively silylated products suggested that the nature of the metals incorporated within the vacant macrocyclic cleft is crucial in determining which process ensued.

Although reductive silylation was not observed upon treatment of **XXXV** with lithium bases, treatment of the reductively lithiated product **XXXVI** with two equivalents HCl in Et_2O followed by addition of excess Me_3SiCl allowed the isolation of the mononuclear, silylated uranyl(V) complex $[(Me_3OUO)(H_2L)]$ **XXXIX** (Scheme 14).[77] The reaction proceeds by an initial acid/base reaction to form the oxo-protonated intermediate $[(HOUO)(H_2L)]$ before functionalisation of that complex with the silylating agent. The complex **XXXIX** was fully characterised, with the solid state structure exhibiting similar U–O_{endo} (1.854(4) Å) and U–O_{exo} (2.034(4) Å) bond lengths to those observed in the complex **XXXIIIa** (1.870(4) and 1.993(4) Å respectively).

The reductive metalation of **XXXIV** with rare earth cations was achieved in 2011, with the reaction of the complex with $[Sm(THF)_2(N")_2]$ shown to form the dimeric uranyl(V) CCI complex $[UO_2Sm(py)_2(L)]_2$ **XLa** and two equivalents of HN" (Scheme 15).[78]

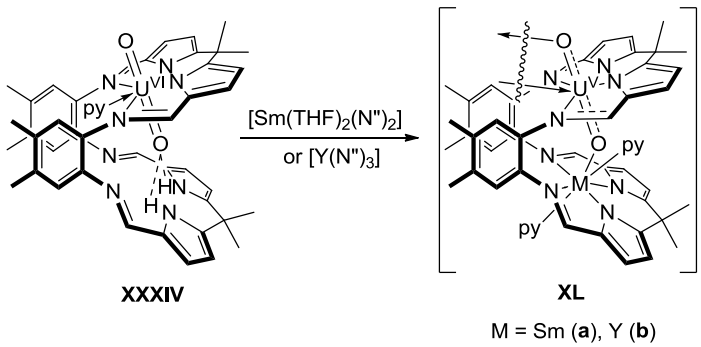

Scheme 15: The syntheses of the uranyl(V)/rare earth complexes **XLa** and **b**.

The complex displays a similar structure to those of the uranyl(VI)/transition metal complexes **XXXIIa-c**, with the incorporation of a single metal cation into the vacant N_4-donor pocket of the macrocycle and the formation of an intramolecular O=U=O–M CCI. In contrast to the formation of **XXXII**, in which uranyl reduction was not observed, the incorporation of Sm^{II} into the vacant pocket of uranyl(VI) Pacman complex was accompanied by an intramolecular redox reaction to form a $[U^{V}O_2]^+$ cation and an oxidised Sm^{III} centre. The Sm–O bond length of 2.238(5) Å in **XLa** was consistent with a Sm(III) oxidation state and the U–O bonds of 1.890(5) and 1.941(5) Å confirmed the formation of uranyl(V). The reaction to form **XLa** proceeds with dimerisation of the complex, with the

loss of the uranyl-bound pyridine molecule in the starting material facilitating the formation of a diamond-shaped $[UO_2]^+$/ $[UO_2]^+$ CCI complex. The *exo* bound oxygen atom from one uranyl cation in **XLa** coordinates in the fifth equatorial donor position of a second uranium centre in a similar motif to that observed in **XVI**.

The reduction of **XXXIV** with Sm^{II} is the only synthesis of a uranyl(V) Pacman complex that results from the use of a classical reducing agent, with the aforementioned syntheses of **XXXIII** and **XXXVI-XXXVIII** thought to proceed by bond homolysis. Perhaps of greater interest is the synthesis of the yttrium analogue $[UO_2Y(py)_2(L)]_2$ **XLb** from the reaction of **XXXIV** and one equivalent of $Y(N'')_3$ (Scheme 15).[78] The reduction of uranyl(VI) using a redox-inactive metal precursor mimics the syntheses of the lithium complexes **XXXVI-XXXVIII**. It was proposed that the reaction proceeds by the initial complexation of $Y(N'')_3$ into the vacant macrocyclic cleft by deprotonation of the two pyrrolic amine groups forming the uranyl(VI) mono-amido intermediate $[U^VO_2(py)Y(N'')_2(L)]_2$. The sterically induced reduction (SIR) of this intermediate by homolysis of the pendent Y–N'' bond was thought to provide the reducing electron, forming **XLb** and an aminyl ·N'' radical. The reaction may be considered the intermolecular equivalent of the reduction of $[UO_2(py)(H_2L)]$ by lithium bases, a comparison supported by the observation that the C–H bonds in an added DHA substrate can be cleaved during the reaction to form **XLb**, indicating the formation of a radical by-product.

The complexes **XXXIII**, and **XXXV-XL** demonstrate that the reductive functionalisation of uranyl(VI) may be facilitated by its encapsulation within the Pacman macrocycle L, allowing isolation of the first silylated,[74] lithiated,[76] protonated,[77] and rare-earth metalated[78] uranyl(V) complexes. In this thesis, the chemistry of binuclear uranyl Pacman complexes will be explored, investigating whether the activation of mononuclear uranyl Pacman complexes with electropositive metal cations can be extended by incorporation of a second uranyl dication into the vacant N_4-donor cleft.

1.7 Terminal oxo complexes

Another important class of compounds in molecular uranium-oxide chemistry are the terminal oxides. Comprised of a uranium(IV), V or VI centre with a single multiply bonded oxygen atom, study into the electronic structure and reactivity of U=O complexes is important due to their similarity with the uranyl dication. In contrast to complexes of uranyl, there are only a handful of fully characterised uranium terminal oxo complexes.

1.7.1 Uranium(IV) terminal oxo complexes

The most common class of uranium(IV) terminal oxide complexes are metallocene complexes, with the first isolated example being the U^{IV} carbene oxide complex $[Cp^*_2UO\{C(NMeCMe)_2\}]$ ($Cp^* = \eta^5$-C_5Me_5) **XLI** (Figure 9), crystallised serendipitously by Evans and co-workers from the reaction of $[U^{III}(Cp^*)_3]$ and $C(NMeCMe)_2$.[79]

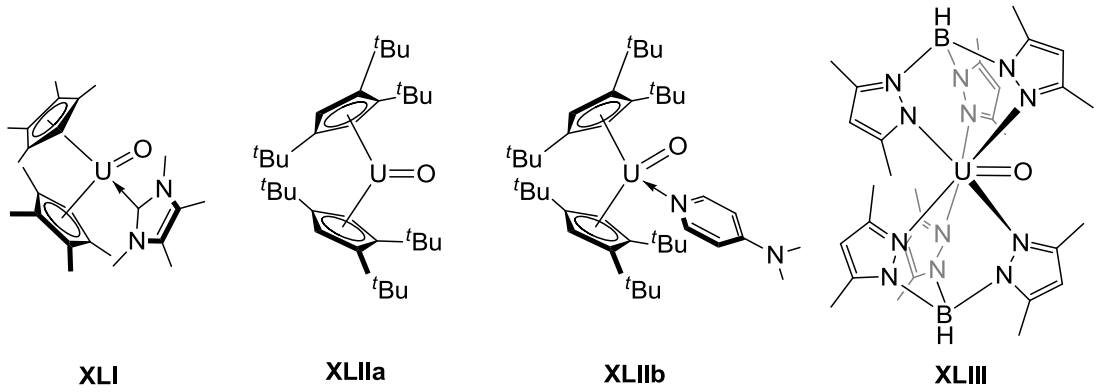

Figure 9: Uranium(IV) terminal oxo complexes.

The complex was the first structurally characterised example of a both a uranium(IV) terminal oxide and a uranium(IV) carbene complex and exhibits a short U–O bond length of 1.916(6) Å. The first repeatable syntheses of metallocene UO complexes were reported by Andersen and co-workers, with the complex $[Cp'_2UO]$ ($Cp' = \eta^5$-1,2,4-$^t Bu_3C_5H_2$) **XLIIa** and its various solvates synthesised by treatment of $[Cp'_2U(bipy)]$ with pyridine-*N*-oxide.[80] Although the unsolvated complex could not be characterised in the solid state, the dimethylaminopyridine (DMAP) solvated complex $[Cp'_2U(O)(DMAP)]$ **XLIIb** was successfully crystallised and was shown to have a U–O bond length of 1.860(3) Å (Figure 9). The only other fully-characterised example of a uranium(IV) terminal oxide complex is the non-metallocene complex $[Tp^*_2UO]$ (Tp* = hydrotris(3,5-dimethylpyrazolyl)borate) **XLIII** which was again synthesised by oxidation of a uranium(IV) bipyridide precursor, in this case $[Tp^*_2U(bipy)]$, with pyridine-*N*-oxide (Figure 9).[81] The complex **XLIII** is the only structurally characterised example of a donor-solvent-free terminal uranium(IV) oxide complex and has an identical U–O bond length, within error, to that of **XXLIIb** (1.863(4) Å). Such a lack of variation in the U–O bond distances between **XLI**-**XLIII** suggests that the presence or absence of strongly donating ligands such as DMAP does not significantly affect the strength of the U=O bonds. The only documented oxo-group reactivity a uranium(IV) terminal oxide complex is that of **XLIIa** which was shown to react with one or two equivalents of Me_3SiX (X = halide or pseudohalide) to yield the oxo functionalised and oxo-abstracted complexes $[Cp'_2U(OSiMe_3)X]$ and $[Cp'_2UX_2]$ respectively.[80]

1.7.2 Uranium(V) and VI terminal oxo complexes

The first ever structurally characterised example of a uranium terminal mono-oxo complex in any oxidation state was the pentachloro uranium oxide salt $[Ph_4P][UOCl_5]$ **XLIV** prepared by de Wet and du Preez in 1978 (Figure 10).[5]

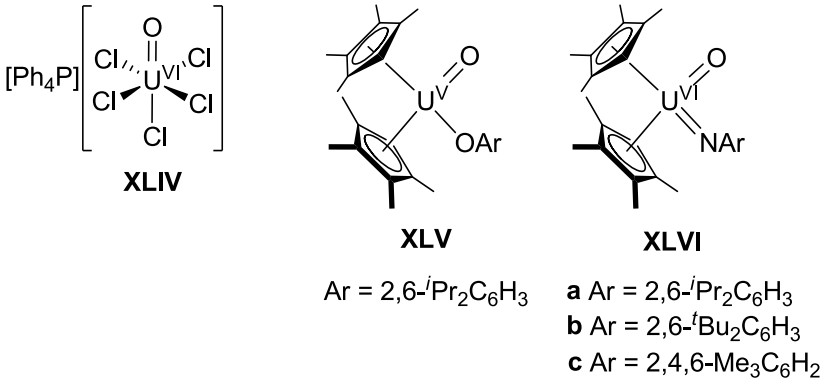

Figure 10: The first uranium(V) and uranium(VI) terminal oxo complexes **XLV** and **XLVI**.

The complex consists of an approximately octahedral anion featuring a perfectly square planar UCl_4 unit with axially bound O and Cl ligands. As described in section 1.2.2, the complex was the first reported example of a compound exhibiting the inverse *trans* influence (ITI). The short U–O bond of 1.76(1) Å in **XLIV** is mutually *trans* to an axial U–Cl bond of 2.433(4) Å and mutually *cis* to four identical U–Cl bonds in the equatorial plane exhibiting longer U–Cl bond lengths of 2.536(2) Å. The authors described the bonding using a predominantly ionic model, proposing greater electronic repulsion between the four mono-anionic *cis* chlorides and the dianionic oxo atom than between the *trans* choride and its four *cis* chloride neighbours. This description was not expanded until the work of Denning in 1992, who developed a covalent model for U^{IV}=O bonding that better explained the observed ITI (see section 1.2).[6, 9] The complex **XLIV** still provides the clearest demonstration of the ITI, with the perfectly *trans* O-U-Cl angle of 180˚ and the shortest U-O bond length of 1.76(1) Å not replicated in any other terminal oxo complex since.

The second examples of uranium terminal oxo complexes were synthesised by Arney and Burns in 1993.[82] The neutral U^V and U^{VI} complexes $[(C_5Me_5)_2U(E\text{-}2,6\text{-}^iPr_2\text{-}C_6H_3)(O)]$ (E = O **XLV**, N **XLVIa,** Figure 10) were synthesised by the respective oxidations of the uranium(III) and IV metallocene complexes $[(C_5Me_5)_2U(E\text{-}2,6\text{-}^iPr_2\text{-}C_6H_3)]$ with pyridine-*N*-oxide. Both **XLV** and **XLVI** exhibit similar U–O bond distances, with only a slightly shorter bond observed for the aryloxide complex (1.844(4 Å) over the imido complex (1.859(6) Å) despite the higher oxidation state of the latter. Both bond lengths are longer than those seen in unfunctionalised uranyl(V) and uranyl(VI) complexes, perhaps

indicative of lower U–O bond orders in the terminal oxo complexes resulting from a lack of *trans* π-donor ligand and subsequent ITI. In later work by the same group, the IR stretching frequencies of both $[(C_5Me_5)_2U(N\text{-}2,6\text{-}^iPr_2\text{-}C_6H_3)(O)]$ **XLVIa** and the related complexes $[(C_5Me_5)_2U(N\text{-}2,6\text{-}^tBu_2\text{-}C_6H_3)(O)]$ **XLVIb** and $[(C_5Me_5)_2U(N\text{-}2,4,6\text{-}Me_3C_6H_2)(O)]$ **XLVIc** were all found to be 755 cm^{-1}, with the stretching frequencies for the ^{18}O-labelled derivatives being 715 cm^{-1}.[83] Both these values are significantly lower than the uranyl(VI) symmetric (υ_{symm} = 860 cm^{-1}) and asymmetric (υ_{asymm} = 930 cm^{-1}) stretches, an observation attributed to both columbic repulsion between the mutually *cis* oxo and imido ligands and the competition for empty metal-based orbitals between the more strongly π-donating NAr ligands and the oxo group. It could again be postulated however that the lack of the stabilising effect of *trans* π-donor ligand may also contribute to the weaker U^{VI}–O bonding in **XLVI** in comparison to **XLIV**.

The synthesis of the $[\{(^RArO)_3tacn\}U(O)]$ (tacn = triazacyclononane, R = ^{t}Bu **XLVIIIa**, Ad **XLVIIIb**) complexes by Meyer and co-workers were the first examples of non-oxidative preparations of uranium(V) terminal oxo complexes.[84] In contrast to complexes **XLV** and **XLVI**, which were synthesised from the two-electron oxidation of low-valent uranium precursors, **XLVIIa** and **XLVIIb** were prepared by multiple bond metathesis between the respective uranium(V) imido precursors $[\{(^RArO)_3tacn\}U(N\text{-}2,4,6\text{-}Me_3C_6H_2)]$ **XLVIIa,b** and CO_2, forming the uranium(V) terminal monooxo complexes alongside single equivalents of the respective mesityl isocyantates ArN=C=O (Scheme 16).

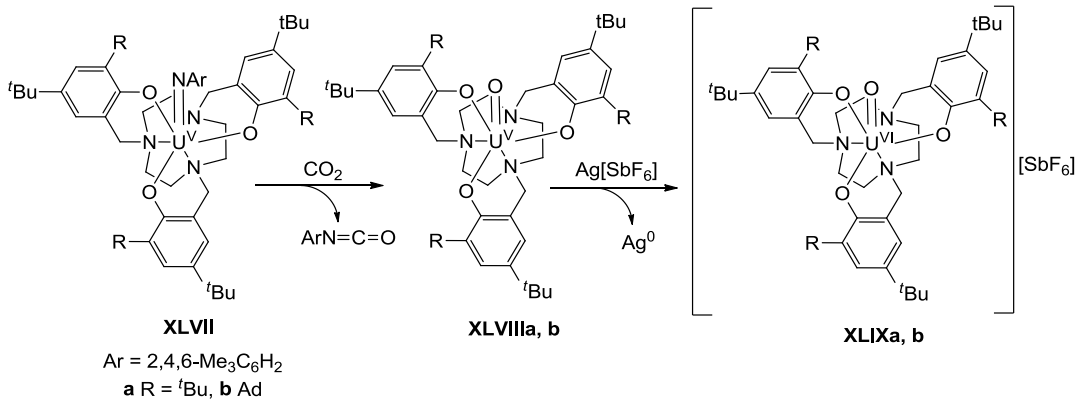

Scheme 16: Synthesis of the uranium V and VI terminal oxo complexes **XLVIII** and **XLIX**.

Both **XLVIIIa** and **XLVIIIb** display identical U–O bond lengths of 1.848(8) and 1.848(8) Å respectively which were comparable to the U–O bond length of **XLV**, the only other structurally characterised uranium(V) complex present in the literature at the time. In later work, both **XLVIIIa** and **XLVIIIb** were oxidised to their uranium(VI) analogues using $Ag[SbF_6]$, forming the salts $[\{(^RArO)_3tacn\}U(O)][SbF_6]$ **XLIX** (**a** = ^{t}Bu, **b** = Ad).[85] The U–O

bond length in **XLIX a** was observed to contract to upon oxidation to 1.836(6) Å, with migration of the uranium oxo group to a position *trans* to an aryloxide O-donor group evidenced in both the solid state and solution. This migration was facilitated by an unusual rearrangement of the $(^{tBu}ArO)_3tacn^{3-}$ ligand that had not been observed in any previous complexes and was proposed to be driven by the greater propensity of uranium(VI) to adopt an ITI.

Another set of uranium terminal oxo complexes shown to support both the +V and +VI oxidation states were the oxo metallacycle complexes $[Ph_3PCH_3][U^V(O)(CH_2SiMe_2NSiMe_3)\{N(SiMe_3)_2\}_2]$ **LI** and $[U^{VI}(O)(CH_2SiMe_2NSiMe_3)\{N(SiMe_3)_2\}_2]$ **LII** synthesised by Hayton and co-workers in 2011.[86]

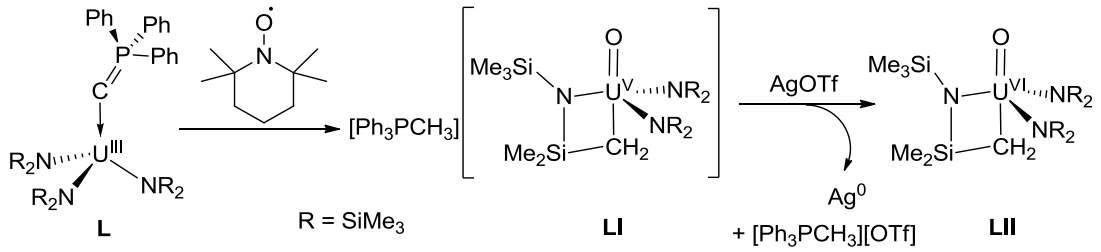

Scheme 17: Synthesis of the U^V and U^{VI} terminal oxo complexes **LI** and **LII.**

The former complex was prepared by treatment of the uranium(III) phosphonium ylide adduct $[U(CH_2PPh_3)\{N(SiMe_3)_2\}_3]$ **L** with TEMPO with oxidation to the neutral uranium(VI) complex **LII** accomplished by subsequent addition of AgOTf (Scheme 17). The initial oxidation reaction to form **LI** is perhaps surprising as it does not form the neutral uranium(V) complex $[U(O)\{N(SiMe_3)_2\}_3]$ **LIII** and instead proceeds with deprotonation of an Me_3Si group by the Ph_3PCH_2 donor forming the metallocylic salt complex **LI**. The U–O bond length of 1.847(2) Å in **LI** is comparable to the other uranium(V) terminal oxo complexes **XLV** and **XLVIII** and was shown to significantly contract to 1.800(2) Å upon oxidation to form **LII**. The U–O bond length in the U^{IV} complex is the second shortest terminal U-O bond in literature after that of **XLIV**, a feature perhaps due to the presence of the strongly-donating methylenide ligand *trans* to the U–O bond (C–U–O angle 167(1)˚) exerting a strong ITI. Later work by the same group demonstrated that the non-cyclised uranium(V) complex **LIII** could be synthesised treatment of $[U\{N(SiMe_3)_2\}_3]$ with pyridine-*N*-oxide with the resultant complex found to exhibit a short U=O bond length 1.817(1) Å.[87]

1.8 E=U=O Complexes

A class of compounds related to both uranyl (O=U=O) and terminal oxo (U=O) complexes are the complexes E=U=O, were E is a non-oxo, doubly-anionic π-donor ligand. These complexes are important as they provide further insights into both the nature of uranium-oxygen multiple bonds and the ITI.

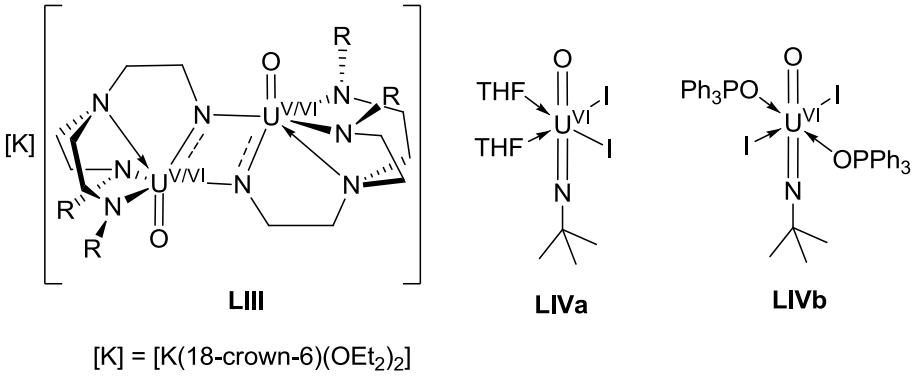

Figure 11: Examples of uranium *trans* oxo/imido (RN=U=O) complexes.

The first example of an E=U=O complex was isolated by Burns and Clark from attempts to study the uranyl(VI) chemistry of the triamidoamine ligand $[N(CH_2CH_2NSi^tBuMe_2)_3]^{3-}$. The reaction of the lithium salt of the ligand with $[K(18\text{-crown-}6)]_2[UO_2Cl_4]$ yielded single crystals of the binuclear mixed valence $U^{V/VI}$ oxo/imido complex $[K(18\text{-crown-}6)(Et_2O)][UO(\mu\text{-}NCH_2CH_2N(CH_2CH_2NSi^tBuMe_2)_2)]_2$ (Figure 11, **LIII**).[88] The reaction to form **LIII** proceeds by reduction of the average uranium oxidation state by 0.5, abstraction of a single oxo group from each uranyl cation, cleavage of a ligand N–Si bond and dimerisation to form a binuclear complex, none of which were rationalised by the authors. The complex was characterised in the solid state, with both the U–O (1.838(5) Å) and U–NR (2.097(6) Å) bonds were found to be consistent with U–L multiple bonding and the O-U-N bond angle of 161.2(2)˚ representative of a uranyl-like geometry.

A more convincing synthesis of an oxo/imido complex was later reported by Boncella and co-workers by exchange of a single imido group in the *trans* imido precursor $[U(N^tBu)_2I_2(THF)_2]$ with one equivalent of $H_2O{\cdot}B(C_6F_5)_3$, forming $[OU(N^tBu)I_2(THF)_2]$ in high yield (Figure 11, **LIVa**).[89] Although single crystals of the THF solvate **LIVa** were found to exhibit extensive structural disorder, the crystal structure of the alternative solvate $[U(N^tBu)I_2(OPPh_3)_2]$ **LIVb** allowed determination of the $[OU(N^tBu)]^{2+}$ bond lengths. As perhaps expected, both the U–O (1.781(4) Å) and U–NR (1.823(4) Å) bonds were shorter than those found in the $U^{V/VI}$ complex **LIII**, being closely comparable to the respective U–O

and U–NR bonds in the symmetric uranyl(VI) and U^{IV} bis-imido analogues $[UO_2I_2(OPPh_3)_2]$ and $[U(N^tBu)I_2(OPPh_3)_2]$ (1.758(8) and 1.839(3)–1.840(3 Å respectively).[24, 90]

It is perhaps interesting to note that, although terminal oxo complexes can be synthesised by the reactions between uranium imido complexes single equivalents of H_2O (as in **LIV**) or CO_2 (as in **XLVIII**) the reaction between $[U(N^tBu)I_2(OPPh_3)_2]$ **LV** and an ArN=C=O (Ar = Ph, Mes) did not result in the formation of **LIV**.[91] Instead, the imido-exchanged complexes $[U(N^tBu)(NAr)I_2(OPPh_3)_2]$ **LVIa** (Ar = Ph) and **b** (Ar = 2,4,6-$Me_3C_6H_3$) were observed to form *via* a proposed [2 + 2] cycloaddition of the aryl isocyanate OC=NAr bond across the U=N imido bond to form An *N*,*N*-bound ureato intermediates. The breakdown of such intermediates by bond-metathesis formed the complexes **LVI** and ^{t}BuN=C=O, with the reaction of either complex with a second equivalent of ArNCO resulting in the formation of the symmetric bis-imido complexes $[U(NAr)I_2(OPPh_3)_2]$ **LVIIa, b**.

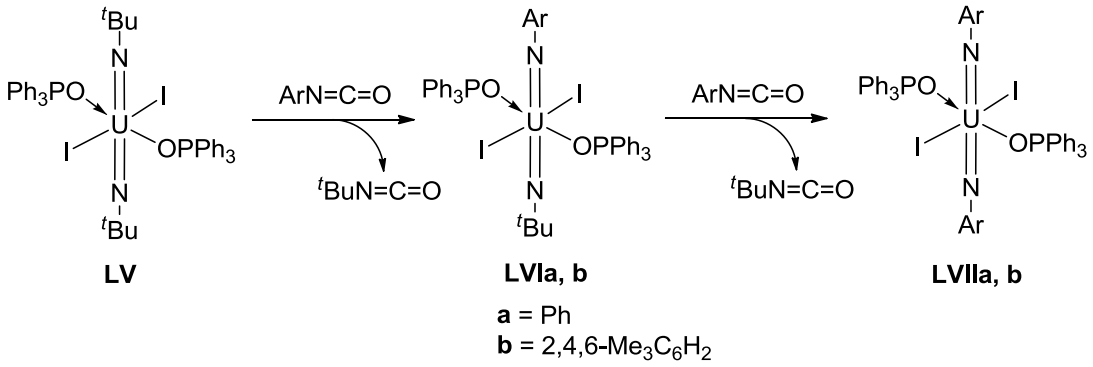

Scheme 18: Imido exchange in bis(imido) uranium(VI) complexes with aryl isocyanates.

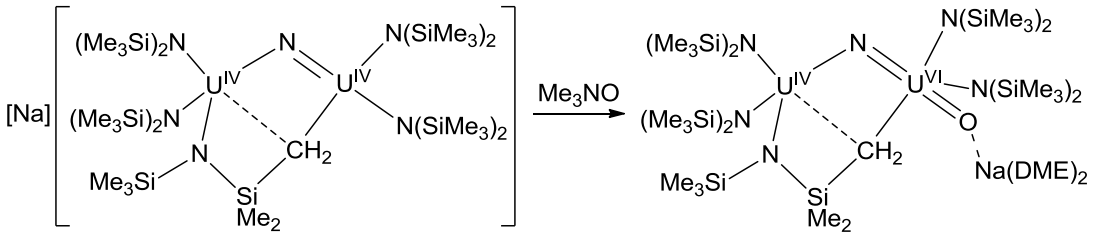

LVIII **LVIX**

[Na] = $[Na(DME)_2(TMEDA)]$

Scheme 19: Synthesis of the uranium *trans* oxo-nitride complex **LIX.**

The single example of a structurally-characterised uranium *trans* oxo-nitride (O=U=N) complex was synthesised by the Hayton group in 2010.[92] The complex $[Na(DME)_2][\{N(SiMe_3)_2\}_2(O)U(\mu\text{-}N)(CH_2SiMe_2NSiMe_3)U\{N(SiMe_3)_2\}_2]$ **LVIX** was prepared by oxidation of the nitride-bridged binuclear uranium(IV) complex $[Na(DME)_2(TMEDA)][\{N(SiMe_3)_2\}_2U(\mu\text{-}N)(CH_2SiMe_2NSiMe_3)U\{N(SiMe_3)_2\}_2]$ **LVIII** with Me_3NO (Scheme 19). The complex **LVIX** is formally described as exhibiting mixed valence $U^{IV/VI}$ oxidation states, with the alternative $U^{V/V}$ interpretation rejected on the grounds of the asymmetric bonding displayed by each uranium cation. Whereas the bonding in the nominally uranium(IV) centre is virtually unchanged upon the oxidation of **LVIII** to **LVIX**, the opposing uranium(VI) cation displays short $U–N_{nitride}$ and U-O bonds of 1.818(9) and 1.797(7) Å respectively which are comparable to the U–O and U–NR bonds of the uranium(VI) imido complex **LIVb**. The oxidation state assignment of **LVIX** is also supported by SQUID magnetometry, with data consistent with the presence of a single $5f^2$ centre. The formation of the $[OUN]^+$ ion proceeds with retention of both the geometry of the opposing uranium(IV) centre and the bridging nitrido motif however it was noted that slight elongation of the $U^{IV}–N_{nitride}$ bond from 2.212(1) to 2.284(8) Å occurred upon oxidation of **LVIII**, a feature consistent with formation of stronger $U^{V}–N_{nitride}$ multiple bonding and the concomitant weakening of the opposing U–N bond.

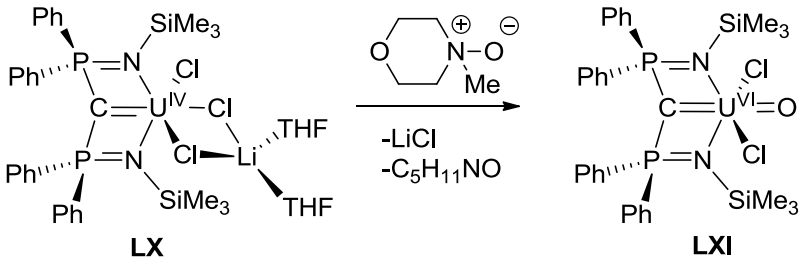

Scheme 20: Synthesis of the $[R_2C{=}U{=}O]^{2+}$ complex **LVIII**.

In addition to the nitride and imide complexes, the recent synthesis of an uranium(VI) t*rans*-oxide carbene complex by Liddle and co-workers represents the first synthesis of a $[R_2C{=}U{=}O]^{2+}$ complex.[93] It was found that the two-electron oxidation of the uranium(IV) carbene complex $[(BIPM)UCl_3Li(THF)_2]$ **LX**, (BIPM = $C(PPh_2NSiMe_3)_2$)) with 4-morpholine-*N*-oxide yielded the U^{VI} oxo-carbene complex $[(BIPM)U(O)Cl_2]$ **LXI** (Scheme 20). The complex was purported to be first uranium(VI) carbene although in light of the previous isolation of a two uranyl(VI) carbene,[94] and one uranyl(VI) NHC complexes,[95] **LXI** is perhaps better described as the first non-uranyl uranium(VI)-carbene complex. Analysis of the solid state structure of **LXI** reveals the presence a *trans* $[R_2C{=}U{=}O]^{2+}$ unit, with a C−U−O angle of 175.54(15)°. The U–O bond distance of 1.841(4) Å is longer than expected in light of the presence of the *trans* carbene ligand, a result perhaps indicative of the ligand being a weaker π-donor than the imido and nitrido ligands in complexes **LIII**, **LIV** and **LIX** resulting in a weaker ITI. This postulate was supported by DFT calculations which suggested a strengthening of the carbene σ-donation contribution and weakening of the π-donor contribution upon oxidation of the complex from U^{IV} to U^{VI}. The strong σ-donating ability of the ligand is represented by **LXI** exhibiting the shortest-reported U-C bond length of 2.184(3) Å.

1.9 Binuclear uranium oxo complexes

This thesis describes the synthesis of binuclear uranium oxo complexes of the octamethylated Schiff-base "Pacman" macrocycle L. The previous activation of mononuclear uranyl(VI) Pacman complexes towards reductive functionalisation using electropositive metals will be extended to include activation of the molecule by uranyl itself, forming a range of binuclear uranium complexes exhibiting a range of oxidation states and alternatively functionalised oxo-groups.

1.10 References

1 I. Grenthe, J. Drożdżyński, T. Fujino, E. C. Buck, T. E. Albrecht-Schmitt, S. F. Wolf, in *The chemistry of the actinide and transactinide elements, Vol. 1*, 3rd ed. (Eds.: L. R. Morss, N. M. Edelstein, J. Fuger, J. J. Katz), Springer,, **2006**.

2 N. Kaltsoyannis, P. Scott, *The f elements*, Oxford University Press, **1999**.

3 J. K. Gibson, R. G. Haire, M. Santos, J. Marçalo, A. Pires de Matos, *J. Phys. Chem. A* **2005**, *109*, 2768-2781.

4 F. A. Cotton, G. Wilkinson, *Advanced Inorganic Chemistry*, Wiley, **1988**.

5 J. F. de Wet, J. G. H. du Preez, *J. Chem. Soc., Dalton Trans.* **1978**, 592-597.

6 R. Denning, in *Complexes, Clusters and Crystal Chemistry, Vol. 79*, Springer Berlin / Heidelberg, **1992**, pp. 215-276.

7 J. M. Bartleet, R. G. Denning, I. D. Morrison, *Mol. Phys.* **1992**, *75*, 601-612.

8 E. O'Grady, N. Kaltsoyannis, *J. Chem. Soc., Dalton Trans.* **2002**, 1233-1239.

9 R. G. Denning, *J. Phys. Chem. A* **2007**, *111*, 4125-4143.

10 W. A. Nugent, J. M. Mayer, *Metal-Ligand Muliple Bonds*, Wiley, **1988**.

11 C. Villiers, P. Thuéry, M. Ephritikhine, *Angew. Chem., Int. Ed. Engl.* **2008**, *47*, 5892-5893.

12 J. M. Mayer, *Acc. Chem. Res.* **1998**, *31*, 441-450.

13 C. E. Housecroft, A. G. Sharpe, *Inorganic Chemistry*, Prentice Hall, Harlow, **2001**.

14 D. R. Lovley, E. J. P. Phillips, Y. A. Gorby, E. R. Landa, *Nature* **1991**, *350*, 413-416.

15 Y. Suzuki, S. D. Kelly, K. M. Kemner, J. F. Banfield, *Nature* **2002**, *419*, 134-134.

16 E. J. O'Loughlin, S. D. Kelly, R. E. Cook, R. Csencsits, K. M. Kemner, *Environ. Sci. Technol.* **2003**, *37*, 721-727.

17 P. Muller, *Pure Appl. Chem.* **1994**, *66*, 1077-1194.

18 M. B. Jones, A. J. Gaunt, *Chem. Rev.* **2012**.

19 S. Beer, O. B. Berryman, D. Ajami, J. Rebek Jr, *Chem. Sci.* **2010**, *1*, 43-47.

20 A. C. Sather, O. B. Berryman, J. Rebek, *J. Am. Chem. Soc.* **2010**, *132*, 13572-13574.

21 M.-J. Crawford, A. Ellern, H. Nöth, M. Suter, *J. Am. Chem. Soc.* **2003**, *125*, 11778-11779.

22 J.-C. Berthet, M. Nierlich, M. Ephritikhine, *Chem. Commun.* **2004**, 870-871.

23 M.-J. Crawford, P. Mayer, *Inorg. Chem.* **2005**, *44*, 5547-5549.

24 M.-J. Crawford, A. Ellern, K. Karaghiosoff, P. Mayer, H. Nöth, M. Suter, *Inorg. Chem.* **2004**, *43*, 7120-7126.

25 S. Kannan, C. L. Barnes, P. B. Duval, *Inorg. Chem.* **2005**, *44*, 9137-9139.

26 T. Cantat, C. R. Graves, B. L. Scott, J. L. Kiplinger, *Angew. Chem., Int. Ed. Engl.* **2009**, *48*, 3681-3684.

27 J. Maynadie, J.-C. Berthet, P. Thuery, M. Ephritikhine, *Chem. Commun.* **2007**, 486-488.

28 J.-C. Berthet, P. Thuery, M. Ephritikhine, *Chem. Commun.* **2007**, *0*, 604-606.

29 M. J. Sarsfield, M. Helliwell, J. Raftery, *Inorg. Chem.* **2004**, *43*, 3170-3179.

30 B. Masci, P. Thuery, *CrystEngComm* **2007**, *9*, 582-590.

31 L. A. Seaman, D. D. Schnaars, G. Wu, T. W. Hayton, *Dalton Trans.* **2010**, *39*, 6635-6637.

32 J. A. Danis, M. R. Lin, B. L. Scott, B. W. Eichhorn, W. H. Runde, *Inorg. Chem.* **2001**, *40*, 3389-3394.

33 N. N. Krot, M. S. Grigoriev, *Russ. Chem. Rev.* **2004**, *73*, 89-100.

34 I. Charushnikova, E. Bossé, D. Guillaumont, P. Moisy, *Inorg. Chem.* **2010**, *49*, 2077-2082.

35 S. Skanthakumar, M. R. Antonio, L. Soderholm, *Inorg. Chem.* **2008**, *47*, 4591-4595.

36 R. Copping, V. Mougel, S. Petit, C. D. Auwer, P. Moisy, M. Mazzanti, *Chem. Commun.* **2011**, *47*, 5497-5499.

37 G. B. Jin, S. Skanthakumar, L. Soderholm, *Inorg. Chem.* **2011**, *50*, 5203-5214.

38 S. Wang, J. Diwu, E. V. Alekseev, L. J. Jouffret, W. Depmeier, T. E. Albrecht-Schmitt, *Inorg. Chem.* **2012**, *51*, 7016-7018.

39 M. J. Sarsfield, M. Helliwell, *J. Am. Chem. Soc.* **2004**, *126*, 1036-1037.

40 T. W. Hayton, G. Wu, *Inorg. Chem.* **2009**, *48*, 3065-3072.

41 J. Selbin, J. D. Ortego, *Chem. Rev.* **1969**, *69*, 657-671.

42 C. R. Graves, J. L. Kiplinger, *Chem. Commun.* **2009**, 3831-3853.

43 C. Miyake, Y. Yamana, S. Imoto, H. Ohya-Nishiguchi, *Inorg. Chim. Acta* **1984**, *95*, 17-21.

44 K. Mizuguchi, Y.-Y. Park, H. Tomiyasu, Y. Ikeda, *J. Nucl. Sci. Technol.* **1993**, *30*, 542-548.

45 S.-H. Lee, K. Mizuguchi, H. Tomiyasu, Y. Ikeda, *J. Nucl. Sci. Technol.* **1996**, *33*, 190-192.

46 S.-Y. Kim, T. Asakura, Y. Morita, G. Uchiyama, Y. Ikeda, *Radiochim. Acta* **2005**, *93*, 75-81.

47 J.-C. Berthet, M. Nierlich, M. Ephritikhine, *Angew. Chem., Int. Ed. Engl.* **2003**, *42*, 1952-1954.

48 L. Natrajan, F. Burdet, J. Pécaut, M. Mazzanti, *J. Am. Chem. Soc.* **2006**, *128*, 7152-7153.

49 J.-C. Berthet, G. Siffredi, P. Thuery, M. Ephritikhine, *Chem. Commun.* **2006**, 3184-3186.

50 F. Burdet, J. Pécaut, M. Mazzanti, *J. Am. Chem. Soc.* **2006**, *128*, 16512-16513.

51 G. g. Nocton, P. Horeglad, J. Pécaut, M. Mazzanti, *J. Am. Chem. Soc.* **2008**, *130*, 16633-16645.

52 A. Cousson, S. Dabos, H. Abazli, F. Nectoux, J. Jové, M. Pagès, *Inorg. Chim. Acta* **1984**, *94*, 99-100.

53 M. S. Grigoriev, N. N. Krot, A. A. Bessonov, K. Y. Suponitsky, *Acta Crystallographica Section E* **2007**, *63*, m561-m562.

54 H. Steele, R. J. Taylor, *Inorg. Chem.* **2007**, *46*, 6311-6318.

55 A. J. Francis, C. J. Dodge, *Environ. Sci. Technol.* **2008**, *42*, 8277-8282.

56 J. C. Renshaw, L. J. C. Butchins, F. R. Livens, I. May, J. M. Charnock, J. R. Lloyd, *Environ. Sci. Technol.* **2005**, *39*, 5657-5660.

57 V. Mougel, B. Biswas, J. Pecaut, M. Mazzanti, *Chem. Commun.* **2010**, *46*, 8648-8650.

58 T. W. Hayton, G. Wu, *Inorg. Chem.* **2008**, *47*, 7415-7423.

59 T. W. Hayton, G. Wu, *J. Am. Chem. Soc.* **2008**, *130*, 2005-2014.

60 J. L. Brown, G. Wu, T. W. Hayton, *J. Am. Chem. Soc.* **2010**, *132*, 7248-7249.

61 D. D. Schnaars, G. Wu, T. W. Hayton, *Inorg. Chem.* **2011**, *50*, 4695-4697.

62 D. D. Schnaars, G. Wu, T. W. Hayton, *J. Am. Chem. Soc.* **2009**, *131*, 17532-17533.

63 G. Givaja, A. J. Blake, C. Wilson, M. Schroder, J. B. Love, *Chem. Commun.* **2003**, 2508-2509.

64 J. L. Sessler, W.-S. Cho, S. P. Dudek, L. Hicks, V. M. Lynch, M. T. Huggins, *J. Porphyrins Phthalocyanines* **2003**, *07*, 97-104.

65 J. P. Collman, P. S. Wagenknecht, J. E. Hutchison, *Angew. Chem., Int. Ed. Engl.* **1994**, *33*, 1537-1554.

66 B. J. Pistorio, C. J. Chang, D. G. Nocera, *J. Am. Chem. Soc.* **2002**, *124*, 7884-7885.

67 G. Givaja, M. Volpe, M. A. Edwards, A. J. Blake, C. Wilson, M. Schröder, J. B. Love, *Angew. Chem., Int. Ed. Engl.* **2007**, *46*, 584-586.

68 J. B. Love, *Chem. Commun.* **2009**, 3154-3165.

69 P. L. Arnold, A. J. Blake, C. Wilson, J. B. Love, *Inorg. Chem.* **2004**, *43*, 8206-8208.

70 J. W. Leeland, A. M. Z. Slawin, J. B. Love, *Organometallics* **2010**, *29*, 714-716.

71 P. L. Arnold, D. Patel, A.-F. Pecharman, C. Wilson, J. B. Love, *Dalton Trans.* **2010**, *39*, 3501-3508.

72 P. L. Arnold, D. Patel, A. J. Blake, C. Wilson, J. B. Love, *J. Am. Chem. Soc.* **2006**, *128*, 9610-9611.

73 H. Irving, R. J. P. Williams, *J. Chem. Soc.* **1953**, 3192-3210.

74 P. L. Arnold, D. Patel, C. Wilson, J. B. Love, *Nature* **2008**, *451*, 315-317.

75 A. Yahia, P. L. Arnold, J. B. Love, L. Maron, *Chem. Commun.* **2009**, 2402-2404.

76 P. L. Arnold, A.-F. Pécharman, E. Hollis, A. Yahia, L. Maron, S. Parsons, J. B. Love, *Nature Chem.* **2010**, *2*, 1056-1061.

77 P. L. Arnold, A.-F. Pécharman, J. B. Love, *Angew. Chem., Int. Ed. Engl.* **2011**, *50*, 9456-9458.

78 P. L. Arnold, E. Hollis, F. J. White, N. Magnani, R. Caciuffo, J. B. Love, *Angew. Chem., Int. Ed. Engl.* **2011**, *50*, 887-890.

79 W. J. Evans, S. A. Kozimor, J. W. Ziller, *Polyhedron* **2004**, *23*, 2689-2694.

80 G. Zi, L. Jia, E. L. Werkema, M. D. Walter, J. P. Gottfriedsen, R. A. Andersen, *Organometallics* **2005**, *24*, 4251-4264.

81 S. J. Kraft, J. Walensky, P. E. Fanwick, M. B. Hall, S. C. Bart, *Inorg. Chem.* **2010**, *49*, 7620-7622.

82 D. S. J. Arney, C. J. Burns, *J. Am. Chem. Soc.* **1993**, *115*, 9840-9841.

83 D. S. J. Arney, C. J. Burns, *J. Am. Chem. Soc.* **1995**, *117*, 9448-9460.

84 S. C. Bart, C. Anthon, F. W. Heinemann, E. Bill, N. M. Edelstein, K. Meyer, *J. Am. Chem. Soc.* **2008**, *130*, 12536-12546.

85 B. Kosog, H. S. La Pierre, F. W. Heinemann, S. T. Liddle, K. Meyer, *J. Am. Chem. Soc.* **2012**, *134*, 5284-5289.

86 S. Fortier, N. Kaltsoyannis, G. Wu, T. W. Hayton, *J. Am. Chem. Soc.* **2011**, *133*, 14224-14227.

87 S. Fortier, J. L. Brown, N. Kaltsoyannis, G. Wu, T. W. Hayton, *Inorg. Chem.* **2012**, *51*, 1625-1633.

88 P. B. Duval, C. J. Burns, W. E. Buschmann, D. L. Clark, D. E. Morris, B. L. Scott, *Inorg. Chem.* **2001**, *40*, 5491-5496.

89 T. W. Hayton, J. M. Boncella, B. L. Scott, E. R. Batista, *J. Am. Chem. Soc.* **2006**, *128*, 12622-12623.

90 T. W. Hayton, J. M. Boncella, B. L. Scott, E. R. Batista, P. J. Hay, *J. Am. Chem. Soc.* **2006**, *128*, 10549-10559.

91 L. P. Spencer, P. Yang, B. L. Scott, E. R. Batista, J. M. Boncella, *J. Am. Chem. Soc.* **2008**, *130*, 2930-2931.

92 S. Fortier, G. Wu, T. W. Hayton, *J. Am. Chem. Soc.* **2010**, *132*, 6888-6889.

93 D. P. Mills, O. J. Cooper, F. Tuna, E. J. L. McInnes, E. S. Davies, J. McMaster, F. Moro, W. Lewis, A. J. Blake, S. T. Liddle, *J. Am. Chem. Soc.* **2012**, *134*, 10047-10054.

94 J.-C. Tourneux, J.-C. Berthet, T. Cantat, P. Thuéry, N. Mézailles, M. Ephritikhine, *J. Am. Chem. Soc.* **2011**, *133*, 6162-6165.

95 S. A. Mungur, S. T. Liddle, C. Wilson, M. J. Sarsfield, P. L. Arnold, *Chem. Commun.* **2004**, 2738-2739.

Binuclear uranium-oxo complexes from uranyl oxo rearrangement and reductive silylation

2.1 Introduction

In light of the remarkable reactivity of $[UO_2(sol)(H_2L)]$ (L = octamethylated Pacman macrocycle, sol = THF, py) towards group one,[1-2] and rare-earth silylamides[3] studies were undertaken to investigate the action of other electropositive metal amides upon mononuclear uranyl Pacman complexes. This chapter describes the reactivity of $[UO_2(sol)(H_2L)]$ towards the uranyl silylamides $[UO_2\{N(SiMe_2R)_2\}_2(py)_2]$ (R = Me and Ph) to form binuclear uranium(V) oxo complexes from uranyl oxo-group rearrangement and reductive silylation.

2.2 Synthesis and characterisation of pyridine-solvated uranyl silylamides

In the previous study of the reaction of $[UO_2(THF)(H_2L)]$ with $[UO_2\{N(SiMe_3)_2\}_2(THF)_2]$ THF was employed as the solvent with no reaction observed between the two species at room or elevated temperatures.[4] It was shown later by our groups that $[UO_2(THF)(H_2L)]$ and $[UO_2(py)(H_2L)]$ form different products when treated with the same lithium silylamide base in their respective parent solvents.[2] Upon this observation, the reactivity of mono uranyl Pacman complexes with uranyl silylamide was reinvestigated in pyridine, requiring the synthesis of alternative, pyridine-solvated uranyl silylamide precursors.

The THF-solvated uranyl silylamide complex $[UO_2(N'')_2(THF)_2]$ (N'' = $N(SiMe_3)_2$) was first prepared by Anderson and co-workers by reaction of anhydrous $[UO_2Cl_2]$ with two equivalents of NaN''.[5] The preparation was later adapted by Burns and Clark, who treated $[UO_2Cl_2(THF)_2]$ with two equivalent of KN'' to achieve greater product purity.[6] Structural characterisation of the molecule was undertaken by our groups in 2006 showing that the complex contains a uranyl dication with two axial oxo groups and two sets of mutually *trans* THF and N'' ligands bound in the equatorial plane.[7]

2.2.1 Synthesis of $[UO_2\{N(SiMe_3)_2\}_2(py)_2]$

Recrystallisation of $[UO_2(N'')_2(THF)_2]$ from pyridine solvent resulted in the formation of the orange, pyridine-solvated analogue $[UO_2(N'')_2(py)_2]$ in high yield.

$$[UO_2Cl_2(THF)_2] + 2KN(SiMe_2R)_2 \xrightarrow{py} [UO_2\{N(SiMe_2R)_2\}_2(py)_2] + 2\ KCl + 2\ THF$$

$N(SiMe_2R)_2$ = N" (R= Me) or N* (R = Ph)

Scheme 1: Synthesis of uranyl bis(silylamides).

The complex may also be synthesised in the same manner as the THF-adduct; by a salt elimination reaction between $[UO_2Cl_2(THF)_2]$ and two equivalents of KN" in pyridine. For the latter preparation, work up in toluene allowed removal of the KCl by-product and isolation of the product in 58 % yield on a 15 g scale (Scheme 1).

The ^{1}H NMR spectrum of $[UO_2(N")_2(py)_2]$ in C_6D_6 exhibits three broad resonances at 9.31, 6.91 and 6.78 ppm with a total integration of 10 protons attributed to the coordinated pyridine solvent molecules. In addition, resonances assigned to the four $SiMe_3$ resonances from the two uranyl-bound $N(SiMe_3)_2$ groups are present at 0.62 (9 protons) and 0.46 ppm (27 protons). Both the asymmetry and broadness of the N" resonances are indicative of fluxional processes occurring in benzene in solution, behaviour that contrasts that observed in d_5-pyridine in which a single methyl resonance is observed at 0.30 ppm. The presence of the uranyl dication is confirmed by FTIR spectroscopy, with the characteristic asymmetric U–O stretch occurring at 935 cm^{-1}.

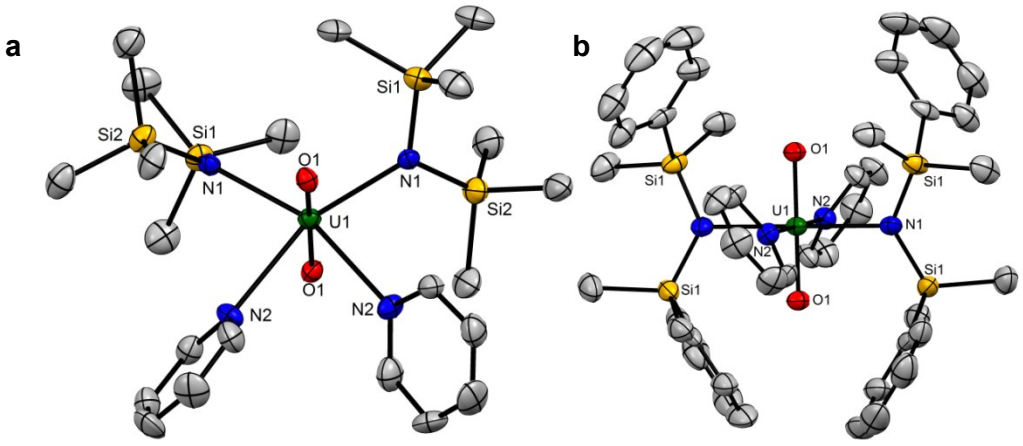

Figure 1: Displacement ellipsoid plot (50 %) of $[UO_2(N")_2(py)_2]$ (**a**) and $[UO_2(N^*)_2(py)_2]$ (**b**). H atoms omitted for clarity.

Analysis of the solid state structure of the complex reveals a single uranium centre with two mutually-*trans* axial oxo ligands that are equivalent by X-ray crystallography (Figure 1, a). The short U1–O1 bond length of 1.779(3) Å is characteristic of the uranium-oxygen multiple bonds present in uranyl(VI). The U1–N1 and U1–N2 bonds of the equatorially bound $^-N(SiMe_3)_2$ and pyridine ligands are comparatively longer at 2.314(4) and 2.590(5) Å respectively, a result of much weaker, predominantly electrostatic bonding. Both

the U–O and U–N(SiMe$_3$)$_2$ bonds are comparable to those observed in the THF adduct (1.784(2) and 2.319(1) Å respectively)[7] however the arrangement of equatorial ligands in each complex differs. The pyridine solvated analogue displays mutually *cis* sets of pyridine and N" ligands contrasting the mutually *trans* sets of the analogous ligands in [UO$_2$(N")$_2$(THF)$_2$]. Although the size of the bis(trimethylsilylamide) ligand would predicate a preference for the latter geometry, the low equatorial coordination number of the [UO$_2$]$^{2+}$ unit in the complexes (four) minimises the steric clash between mutually *cis* ligands. This is addition to the electrostatic nature of the equatorial bonding and subsequent lability of the bound ligands implies the differences in geometry between [UO$_2$(N")$_2$(py)$_2$] and [UO$_2$(N")$_2$(THF)$_2$] are more likely determined by solvent and crystal packing effects than the donor ability of the coordinated ligand.

2.2.2 Synthesis of [UO$_2${N(SiMe$_2$Ph)$_2$}$_2$(py)$_2$]

In an analogous preparation to that of [UO$_2$(N")$_2$(py)$_2$], the uranyl bis(silylamido) complex [UO$_2$(N*)$_2$(py)$_2$] (N* = N(SiMe$_2$Ph)$_2$) was synthesised by the reaction of [UO$_2$Cl$_2$(THF)$_2$] and two equivalents of [KN*] in pyridine (Scheme 1). Extraction of the product into boiling hexane allowed separation from the KCl by-product and subsequent isolation of the orange complex in 70 % yield. In contrast to the trimethylsilylamine complex, the ^{1}H NMR spectrum of [UO$_2$(N*)$_2$(py)$_2$] exhibits a single set of sharp resonances at 7.50, 7.12 and 0.54 ppm corresponding to the silylamide ligand, in addition to those of the two pyridine donor solvent molecules at 8.52, 6.95 and 6.72 ppm. This well resolved ^{1}H NMR spectrum contrasts that of [UO$_2$(N")$_2$(py)$_2$] and is suggestive of a comparative lack of fluxionally of the ligands in [UO$_2$(N*)$_2$(py)$_2$] in benzene solvent.

Single crystals of [UO$_2$(N*)$_2$(py)$_2$] were grown from pyridine solution allowing an X-ray diffraction study of be undertaken showing the expected structure of a [UO$_2$]$^{2+}$ *trans* dioxo cation bound to two anionic N(SiMe$_2$Ph)$_2$ ligands and two pyridine donor solvent molecules (Figure 1, b). The U–O1, U–N1 and U–N2 bond lengths (1.782(3), 2.346(4), and 2.531 Å respectively) are almost identical in length to those observed in the THF- and pyridine-solvated *bis*-N(SiMe$_3$)$_2$ complexes. The complex differs in comparison to [UO$_2$(N")$_2$(py)$_2$] as it contains mutually *trans* silylamide ligands, with an N1–U1–N1 bond angle of 180° with the difference perhaps attributed to the greater size of the SiMe$_2$Ph group in comparison to SiMe$_3$.

[UO$_2$(N*)$_2$(py)$_2$] is the third structurally characterised example of an f-block complex of the N(SiMe$_2$Ph) ligand following the lanthanum complex [(C$_5$Me$_5$)$_2$La(N*)]

synthesised by Evans and co-workers in 2006[8] and the homoleptic uranium(III) complex $[U(N^*)_3]$ prepared by the Arnold group in 2010.[9]

2.3 Synthesis of reductively silylated binuclear uranium oxo complexes

2.3.1 Synthesis of $[(Me_3SiOUO)_2(L)]$

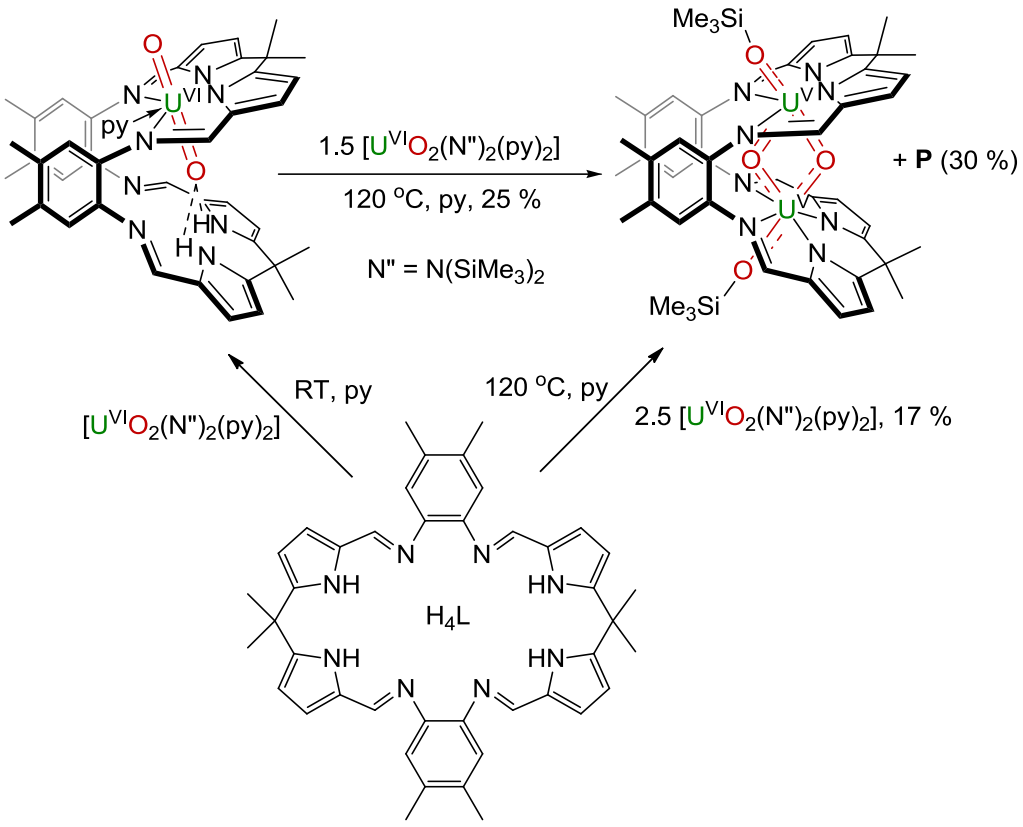

Scheme 2: Synthesis of $[(Me_3SiOUO)_2(L)]$.

The reaction between a pyridine solution of the pyridine-solvated mono(uranyl) Pacman complex $[UO_2(py)(H_2L)]$ and 1.5 molar equivalents of $[UO_2(N")_2(py)_2]$ at 120 °C for 12 h afforded the brown, diethyl-ether soluble, paramagnetic binuclear uranium(V) complex $[(Me_3SiOUO)_2(L)]$ in 25 % yield (Scheme 2). The same complex may also be synthesised from H_4L and 2.5 molar equivalents of $[UO_2(N")_2(py)_2]$ under the same conditions, forming the mononuclear uranyl(VI) complex *in situ* prior to the formation of the binuclear product.

The ^1H NMR spectrum of $[(Me_3SiOUO)_2(L)]$ displays 8 resonances between +15 and –11 ppm, seven of which are attributable to the Pacman ligand, corresponding to an increase ligand symmetry in comparison to the mono(uranyl) Pacman starting material (15 resonances). The greater ligand symmetry supports the formation of a binuclear complex, with the retention of the folded "Pacman" geometry evidenced by the presence of two

separate resonances at –4.38 and 11.08 ppm for the *meso*-methyl groups, which lie *endo* or *exo* to the interfacial cavity. The 5 other ligand resonances correspond to the imine, α-pyrrole, β-pyrrole, aryl and aryl-methyl groups, with a single resonance for each suggestive of symmetric occupation of the two N_4-donor pockets to form a molecule with C_{2v} symmetry. The final resonance at 14.8 ppm is assigned to the $SiMe_3$ group, the presence of which is further supported by ^{29}Si NMR spectroscopy, the spectrum of which shows a single resonance at 160 ppm. The high paramagnetic shifts of both the ^{1}H and ^{29}Si NMR resonances support the assignment of uranium(V) oxidation states, with FTIR bands at 862 and 802 cm^{-1} suggestive of weakened and desymmetrised uranium-oxygen bonding in comparison to $[UO_2(py)(H_2L)]$ (U=O stretch at 908 cm^{-1}). Further evidence for reduced uranium oxidation states arises from the absorption spectrum, with the complex displaying five features between 1000–1665 nm in the near-infrared (NIR) region arising from *f-f* transitions resulting from the occupation of the valence 5*f* orbitals.

Single crystals of $[(Me_3SiOUO)_2(L)]$ were grown from toluene solution allowing an X-ray diffraction study to be undertaken.

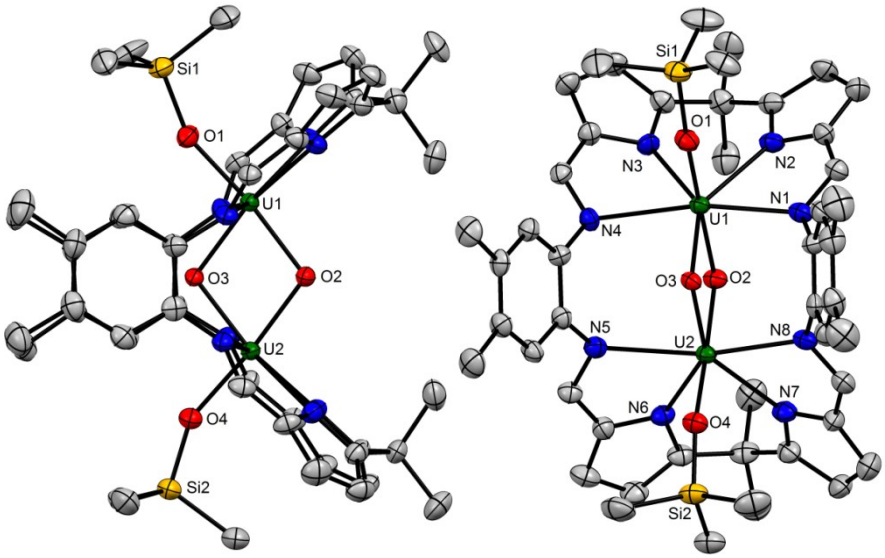

Figure 2: Solid state structure of $[(Me_3SiOUO)_2(L)]$ shown side-on (left) and rear-on (right). Ellipsoids are drawn at 50 % probability, H-atoms and solvent molecules omitted for clarity.

The solid state structure shows the macrocyclic ligand in a wedge-shaped "Pacman" geometry exhibiting symmetric occupation of the upper and lower binding pockets with uranium cations (Figure 2). The presence of $SiMe_3$ groups in the molecule is confirmed by the presence of two (trimethyl)silylated *exo* oxo groups, each bound to a separate uranium centre. Within the macrocyclic cleft exists a diamond-shaped U_2O_2 bonding core, with two shared oxo groups bridging between the uranium centres in mutually *cis* and *trans* positions

to the *exo*-bound oxo groups. The approximate pentagonal bypramidal geometries of the uranyl(VI) precursors are retained in the complex, with axial *exo*-silyloxide and *endo*-bridging oxide ligands lying perpendicular to the four nitrogen donors of the macrocylic cleft. The fifth equatorial site, which was previously occupied by a pyridine solvent molecule in the mononuclear precursor $[UO_2(py)(H_2L)]$, is occupied by the *endo*-bound, *cis*-bridging oxo-group. The geometry of $[(Me_3SiOUO)_2(L)]$ occurs as a result of the loss of the robust, *trans* dioxo bonding contained within the two discrete uranyl dications of the starting materials, with the formation of the binuclear complex proceeding with coupling of these two $[UO_2]^{2+}$ groups and migration of one oxygen atom to the *cis* position. Although the majority of single-reduced uranyl complexes show interactions of one or both oxo groups with another metal cation, the complex $[(Me_3SiOUO)_2(L)]$ presents the first case in which the same uranyl-derived oxo groups are shared by two uranium centres and occupy both mutually *trans* and *cis* positions. While mutually *trans* π-donor ligands present a common motif in actinide chemistry, a complex exhibiting mutually *cis* oxo ligands has never been observed, being thermodynamically unfavourable in comparison to the former geometry due to the inverse trans influence (ITI) that operates in actinyl chemistry.

Analysis of the uranium-oxygen bond lengths in the structure confirm the presence of uranium(V) oxidation states, with an average U–O bond distance of 2.075 Å indicative of partial retention of uranium-oxygen multiple bonding. The average bond distance in the central diamond-shaped U_2O_2 core is 2.094 Å (range of 0.012 Å) and is much shorter than that expected for a bridging hydroxide ligand (range 2.27–2.51 Å), confirming that the atoms are not protonated and further asserting, by total charge-balance, the assignment of the oxidation states. The bond distances between the uranium centres and the silylated *exo*-oxygen atoms U1–O1 and U2–O4 are shorter at 2.034(4) and 2.040(4) Å, respectively, than those of the U_2O_2 core. This asymmetry is suggestive of greater bond multiplicity in the uranium-oxygen bonds of the *exo*-bound oxo groups than the central *endo*-bridging oxos.

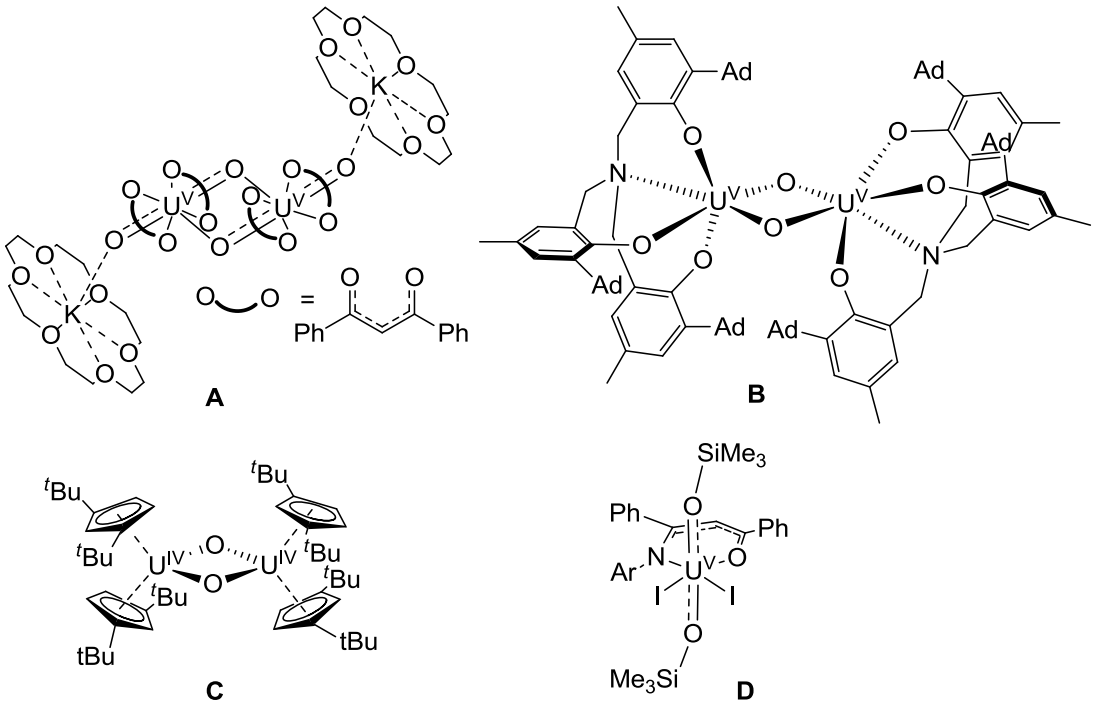

Figure 3: Uranium complexes that exhibit the diamond-shaped U_2O_2 bonding motif (**A**-**D**), or silyated oxo ligands (D).

The diamond-shaped U_2O_2 core has precedence in a number of other lower-oxidation-state uranium complexes, notably in the diamond-shaped $[U^VO_2]^+/[U^VO_2]^+$ CCI complexes, such as $[(K\{18\text{-crown-}6\})(OUO\{acac\}_2)]_2$, (Figure 3, **A**),[3, 10] introduced in Chapter One. While these molecules exhibit the same connectivity as the bis-silylated Pacman molecules, the bridging oxo groups in **A** remain predominantly associated with a single uranium atom by a U–O multiple bond, with the interaction with the second uranium maintained by a dative covalent interaction. The binuclear, oxo-bridged complex $[\{((^{Ad}ArO)_3N)U\}_2(\mu\text{–}O)_2]$, synthesised by Meyer and co-workers, is the only non uranyl example of a uranium(V) complex featuring a U_2O_2 motif (Figure 3, **B**).[11] The complex displays similarly asymmetric bonding as that exhibited by the CCI complexes, with two sets of two parallel bonds that are either short (1.971(4) and 2.057(4) Å) or long (2.174(4) and 2.325(5) Å) with the molecule described as two datively-interacting terminal oxo species (U=O), the mono-oxo equivalent of a uranyl(V) CCI complex. Complexes that exhibit symmetric U_2O_2 bonding are restricted to those of uranium(IV), with three examples of symmetric U^{IV}/U^{IV} molecules of the type $[(X_2U)_2(\mu\text{-}O)_2]$ (X = a monoanionic ligand)[12-14] in addition to the mixed valence U^{IV}/U^V complex $[(Ph_2N)_3U)_2(\mu\text{-}O)_2][Li(OEt)]$.[15] Of these four examples, the complex $[\{(Cp^‡)_2U\}_2(\mu\text{-}O)_2]$ ($Cp^‡ = C_5H_3{}^tBu_2$) is the only example that is fully

characterised, and exhibits a similar U–O bond distance of 2.096(6) Å to those observed in the U_2O_2 core of $[(Me_3SiOUO)_2(L)]$ (Figure 3, **C**).

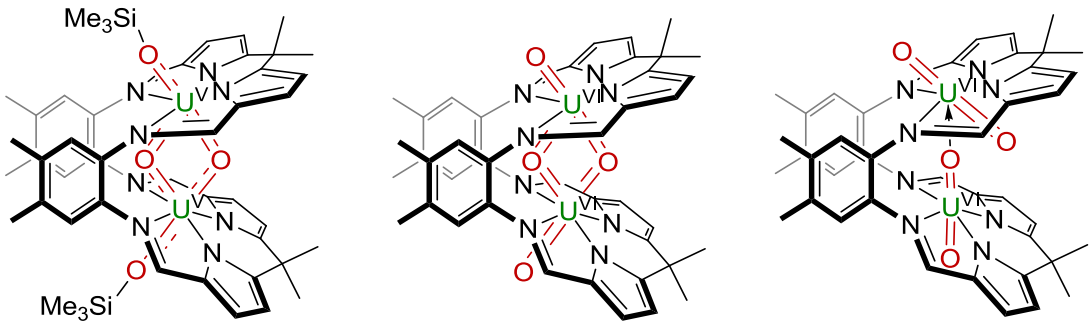

Figure 4: $[(Me_3SiOU^{V}O)_2(L)]$, the theoretical unsilylated U^{VI} butterfly $[(OU^{VI}O)_2L]$ (**i**) and the bis-uranyl CCI $[(U^{VI}O_2)_2(L)]$ (**ii**) complexes.

Despite these 7 previous examples of complexes exhibiting the U_2O_2 core, the full $OU(\mu\text{-}O)_2UO$ "butterfly" shape has not been previously observed in uranium or uranyl chemistry and presents a new structural type in the oxo chemistry of the metal. Interestingly, the unsilylated $U^{VI}U^{VI}$ analogue $[(OU(\mu\text{-}O)_2UO(L)]$ was predicted in a recent computational study by Schreckenbach and co-workers to be an energetically accessible arrangement for two $U^{VI}O_2$ groups in the Pacman macrocycle (Figure 4, **i**), being 12.4 kcal mol^{-1} lower in energy than the alternative bis-uranyl(VI) Pacman $[(UO_2)_2(L)]$ arrangement containing a T-shaped intramolecular cation-cation interaction (CCI) (Figure 4, **ii**).[16]

In addition to exhibiting a novel uranium oxygen bonding arrangement, a notable feature of $[(Me_3SiOUO)_2(L)]$ is that it forms as a result of spontaneous reductive silylation of uranyl oxo groups. First reported by our groups in 2008, the functionalisation of the uranyl dication with silyl groups is a process which occurs concomitant with the single electron reduction of uranyl(VI) to uranyl(V).[17] Hayton and co-workers have recently prepared a number of new examples of silylated uranyl complexes, such as the mononuclear, doubly oxo-silylated complex $[U(OSiMe_3)_2I_2(^{Ar}acnac)]$ ($^{Ar}acnac$ = OC(Ph)CHC(Ph)N(2,6-$^{t}Bu_2C_6H_3$)) (Figure 3, **D**),[18] which displays slightly shorter U–O bond distances of 1.996(5) and 1.986(5) Å than those of $[(Me_3SiOUO)_2(L)]$.

2.3.2 Synthesis of [(PhMe$_2$SiOUO)$_2$(L)]

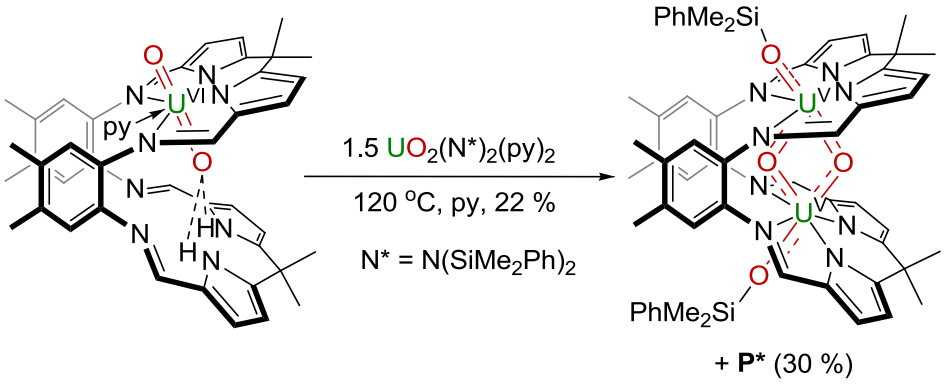

Scheme 3: Synthesis of [(PhMe$_2$SiOUO)$_2$(L)].

In an analogous preparation to that of [(Me$_3$SiOUO)$_2$(L)], the dimethylphenyl derivative was prepared by the reaction of [UO$_2$(py)(H$_2$L)] and 1.5 molar equivalents of [UO$_2$(N*)$_2$(py)$_2$] in pyridine at 120 °C for 12 h. The resulting brown solid [(PhMe$_2$SiOUO)$_2$(L)] was the only soluble complex formed and was separated from the insoluble by-product by extraction into toluene allowing isolation in 22 % yield (Scheme 3).

The ^{1}H NMR spectrum of [(PhMe$_2$SiOUO)$_2$(L)] shows strong similarity to that of [(Me$_3$SiOUO)$_2$(L)], with the 7 resonances attributable to the Pacman ligand lying between +13 and –11 ppm being present at almost the same chemical shifts those of the trimethyl analogue. The resonance at 17.35 ppm (integral of 12 H) is assigned to the silicon-bound methyl groups indicative of the incorporation of the SiMe$_2$Ph group. Additional resonances at 14.67, 13.09 and 8.48 ppm are attributed to the silicon-bound phenyl groups, with respective integrations of 4, 4 and 2 protons. A notable feature of these phenyl resonances is that they exhibit multiplicities due to proton-proton couplings despite the line-broadening effects typically observed in paramagnetic complexes. The ^{29}Si NMR spectrum of [(PhMe$_2$SiOUO)$_2$(L)] shows a single peak at 152 ppm, comparable to that observed for [(Me$_3$SiOUO)$_2$(L)] (160 ppm) and again suggestive of silyl-group incorporation.

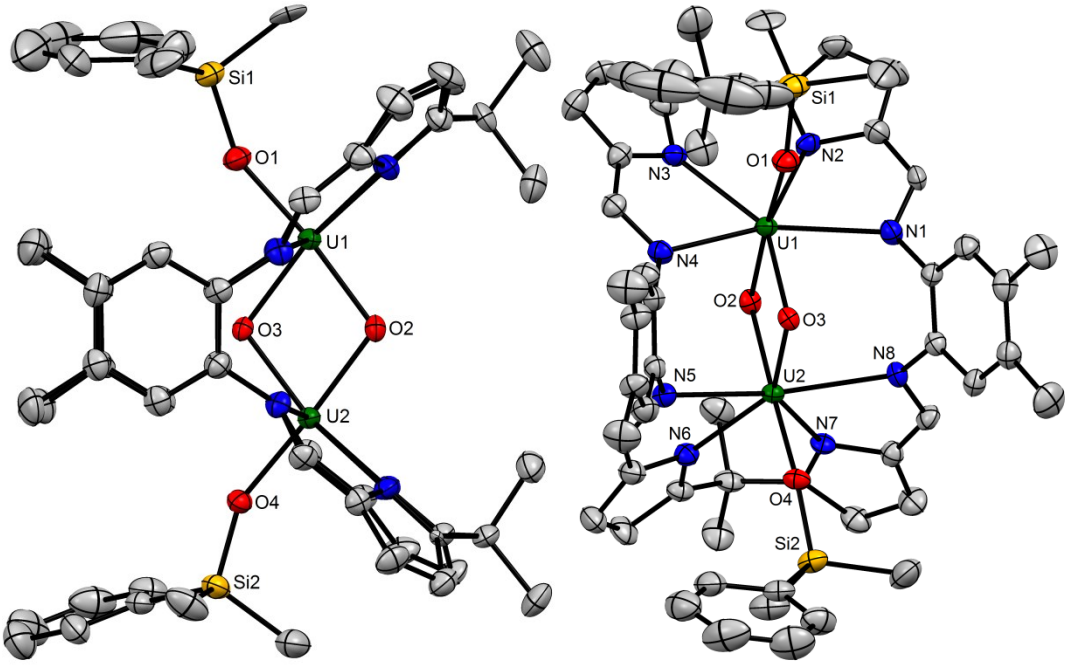

Figure 5: Displacement ellipsoid plot (50 %) of $[(PhMe_2SiOUO)_2(L)]$ shown side-on (left) and rear-on (right). H-atoms and solvent molecules omitted for clarity.

The solid state structure of $[(PhMe_2SiOUO)_2(L)]$ reveals a similar atom connectivity to that of the trimethyl analogue, containing the same wedge-shaped Pacman macrocycle incorporating the $OU(\mu\text{-}O)_2UO$ motif (Figure 5). The bond distances in the U_2O_2 core lie in the range 2.081–2.097 Å, comparable to those of $[(Me_3SiOUO)_2(L)]$ and being similarly longer than the bonds between the uranium centres of the exo-silylated oxo atoms O1 and O4 (2.030(5) and 2.038(5) Å respectively). As indicated by the ^{1}H NMR spectrum, the exo-bound oxygen atoms O1 and O4 are functionalised with $SiMe_2Ph$ groups, with silicon-oxygen bond distances of 1.664(5) and 1.665(5) Å within the normal range.

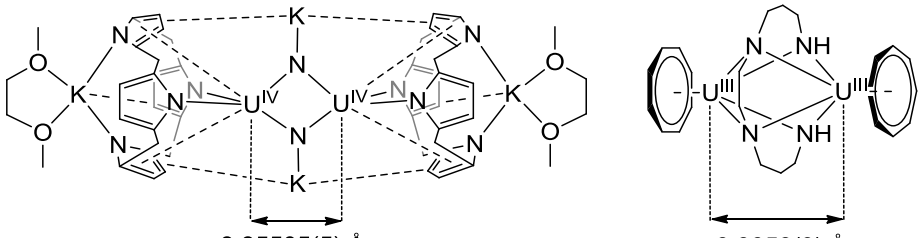

Figure 6: Uranium complexes that display the short U···U separations.

An interesting of property of both $[(PhMe_2SiOUO)_2(L)]$ and $[(Me_3SiOUO)_2(L)]$ is that they exhibit very short U···U separations of 3.3562(4) and 3.3557(5) Å respectively, with only two other reported complexes exhibiting distances of 3.36 Å or less. The binuclear

$U^{IV}U^{IV}$ complex $[K(dme)_4][\{(\mu_3\text{-}N)K(dme)_2U\}_2(\mu_4\text{-}\eta_5{:}\eta_3{:}\eta_2\text{-octamethylcalix(4)pyrrole})]_2$, synthesised by Gambarotta and co-workers and featuring two μ_3-bridging nitrido ligands,[19] (Figure 6, **E**) has a U···U separation of 3.35505(5) Å while and the $U^{III}U^{III}$ amido-bridged complex $[((\eta\text{-}C_8H_8)]_2[\mu\text{-}\kappa^4{:}\kappa^4\text{-}HN(CH_2)_3N(CH_2)_2N(CH_2)_3NH]$ (Figure 6, **F**) prepared by the Ephritikhine group has the shortest reported U···U distance of 3.3058(9) Å.[20]

2.4 Electronic structure of $[(Me_3SiOUO)_2(L)]$

Analysis of the bonding in the U_2O_4 butterfly motif of $[(Me_3SiOUO)_2(L)]$ was undertaken by Dr. Samuel Odoh and Dr. Georg Schreckenbach of the University of Manitoba using density functional theory (DFT) and natural bond order (NBO) calculations. Single point calculations in pyridine solvent continuum were carried out on a molecule of $[(Me_3SiOUO)_2(L)]$ that had optimised in the gas phase using the B3LYP functional with relativistic pseudopotentials. Three possible arrangements of the two uranium(V) single *f*-electrons were considered: a ferromagnetically coupled triplet (*fαfα*), an antiferromagnetic unrestricted broken-symmetry singlet (*fαfβ* independently localised orbitals) and a restricted singlet (*fαfβ* single delocalised orbital over both uranium centres). The unrestricted broken-symmetry state was calculated to be the most stable, being of marginally lower energy than the triplet state (–1.4 kcal mol^{-1}) and significantly more stable than the restricted singlet state (–42.7 kcal mol^{-1}). This was also the case when larger basis sets were employed.

For the unrestricted singlet state of $[(Me_3SiOUO)_2(L)]$ the $U–O_{endo}$ bond lengths, limited to two unique distances due to C_{2v} symmetry, were calculated to be 2.092 and 2.099 Å, close to the experimental range of 2.854–2.993 Å. The $U–O_{exo}$ bond, limited to one unique value by symmetry, was predicted to be 2.053 Å, slightly greater than the two experimental bond distances of 2.034(5) and 2.040(4) Å. The calculated Mayer bond orders for the O_{exo}–Si, $U–O_{exo}$ and two $U–O_{endo}$ bonds were calculated as 1.04, 1.27, 1.20 and 1.19 respectively allowing the bonds in the U_2O_4 core to be considered as single bonds with partial double-bond character. The $U–O_{exo}$ bonds were found to be slightly stronger, a result in agreement with the bond distances found in the crystal structure, with the similar results obtained for the alternative triplet and unrestricted singlet electronic states.

Although there has been no comparative computational study into the bonding of the only other uranium(V) bridging-oxo complex $[\{((^{Ad}ArO)_3N)U\}_2(\mu\text{-}O)_2]$ (Figure 3, **B**),[11] the calculated Mayer bond orders of the U-O($SiMe_3$) bonds in $[(Me_3SiOUO)_2(L)]$ can be compared with the calculated U–OAr bond orders in the U^{VI} oxo/aryloxide complex $[((^{tBu}ArO)_3tacn)U^{VI}(O)][SbF_6]$ (see Chapter One, section 1.7.2).[21] The bond orders in the U^{VI} complex (1.28–1.42) were predicted to be slightly larger than those of of $[(Me_3SiOU^{V}O)_2(L)]$

(1.27), suggesting a greater π-contribution to the U–OAr bond in the former complex than that of the U–$OSiMe_3$ in bond the latter. The trend is the opposite of what would be expected from structural analysis, with the average U–OAr bond length of 2.09 Å in $[(({}^{t\text{Bu}}ArO)_3tacn)U^{VI}(O)][SbF_6]$ being slightly greater than the average U–$OSiMe_3$ bond length of 2.04 Å in $[(Me_3SiOU^{V}O)_2(L)]$.

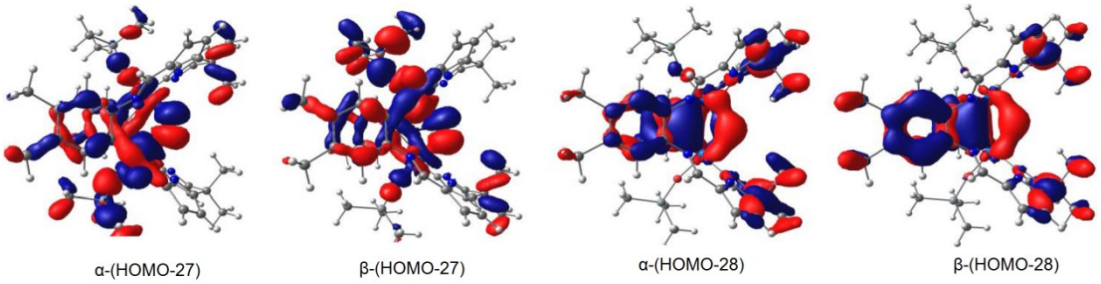

Figure 7: Molecular orbitals of primarily σ and π character in the unrestricted singlet state of $[(Me_3SiOUO)_2(L)]$, isocontours at 0.02.

The α-(HOMO–27) and β-(HOMO–27) orbitals for the unrestricted singlet state are present at –0.333 a.u. and describe the primary σ-bonding interaction across the U_2O_4 core (Figure 7). The contributions to these two orbitals from the *trans*-*endo*-oxo atom (27 and 25 % for α and β respectively) are significantly larger than those of the *cis*-oxo atom (13 and 11 % respectively). Below these (predominantly) σ-bonding orbitals lie the π-type α-(HOMO–28) and β-(HOMO–28) orbitals at -0.334 a.u. with more dominant contributions from the 2p-orbital of the *cis*-oxo group (34 % and 37 % respectively) and diminished contributions from the *endo*-bridging oxygen 2p-orbital orbital (9 % for α and β). These results show that the *cis*-oxo group contributions are the only remnants of the prominent and stable π-interactions that were predicted to be present in the non-silylated, uranium(VI) analogue $[(OUO)_2L]$ (Figure 4, **i**). In addition to exhibiting different oxo-group contributions, the degenerate pairs of σ and π-type orbitals also differ with respect to which uranium atomic orbitals provide their major contributions, with the former being composed mainly of the U-5f (13 % for α and β) and the latter exhibiting shared contributions from both the U-5f and U-6d atomic orbitals (α is comprised of 5 and 6 % respectably, β is comprised of 5 % of both).

The combined structural and computational data show that the butterfly $U_2O_4Si_2$ motif can be formulated as predominantly σ-bonded uranium *trans*-*endo*-oxo and *exo*-siloxide groups combined with a significant π-bonding contribution from the *cis*-*endo*-oxo group. This has resulted from the formal rearrangement of two linear uranyl dications to form a new bonding mode with shared *trans* and *cis* oxo groups. The fact that the latter ligand retains some π-donor character upon *cis*-migration is important as it allows the

tentative classification of $[(Me_3SiOUO)_2(L)]$ as a *cis*-uranyl containing species. The ubiquitous *trans* arrangement of oxo groups in all other uranyl species is thought to derive from the inverse trans influence (ITI) that operates in actinyl chemistry in which mutually *trans*-π-donor ligands act to mutually stabilise one another.[22] The synthesis of the alternative *cis* isomer has remained elusive,[23-24] with the species proposed to play a role as an intermediate in oxo-group exchange process between uranyl centres in aqueous uranyl hydroxide complexes prevalent in high-pH nuclear wastes.[25-27] Uranium lies directly below the group 6 transition metals, the dioxo complexes of which can adopt *cis* or *trans* geometries and have widespread use as oxidising agents.

Within group 6 chemistry, the $OM(\mu\text{-}O)_2MO$ species is a commonly observed motif, with complexes often found to exhibit metal-metal bonds. In one example by Nocera and co-workers, oxidation reactions of the quadruple-bonded Mo(II) acetate dimer gave $OMo^{V}(\mu\text{-}O)_2Mo^{V}O$ complexes that have single Mo-Mo bonds.[28] It is tempting therefore to look for metal-metal interactions in $[(Me_3SiOUO)_2(L)]$ as no f-block metal-metal bonded complex has been reported. The U···U separation of 3.3557(5) Å is the third smallest found in the literature (see Section 2.3 .2) and is much shorter than twice the covalent radius of the uranium atom (3.92 Å).[29] The calculated Mayer bond order between the two uranium centres in the butterfly complex has a non-trival value of 0.34 Å, comparable to those calculated for the equatorial U-N bonds in the complex (0.38 – 0.55 Å).

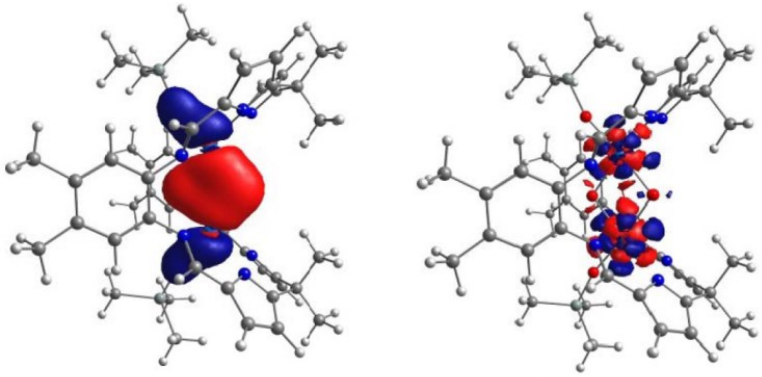

Figure 8: Bonding and antibonding orbitals between the two U atoms, isocontour value 0.02.

NBO analysis allows the identification of a core bonding orbital (HOMO-145 at -1.094 a.u.) and a corresponding antibonding orbital formed almost exclusively from 5*f*-orbital overlap (Figure 8). The complex $[(Me_3SiOUO)_2(L)]$ is however clearly paramagnetic at room temperature, with a paramagnetically shifted ^{1}H NMR spectrum in addition to an approximate solution μ_{eff} (by Evan's method) of 2.1 μ_B per uranium centre. Although there

are no reported examples of molecular bonds between *f*-elements, a quintuple bond in the hypothetical U_2 diatomic has been predicted by theory.[30]

2.5 Variable temperature magnetic study of [(Me$_3$SiOUO)$_2$(L)]

A variable temperature magnetic study on solid [(Me$_3$SiOUO)$_2$(L)] shows a room temperature magnetic moment of 1.53 μ_B/U atom with Curie-Weiss behaviour (C = 0.297 e.m.u. K mol^{-1}, Θ = –16.8 K, per U atom) down to 25 K. This paramagnetic behaviour demonstrates that the single $5f^1$ electrons on each uranium centre remain non-interacting over the majority of the temperature range.

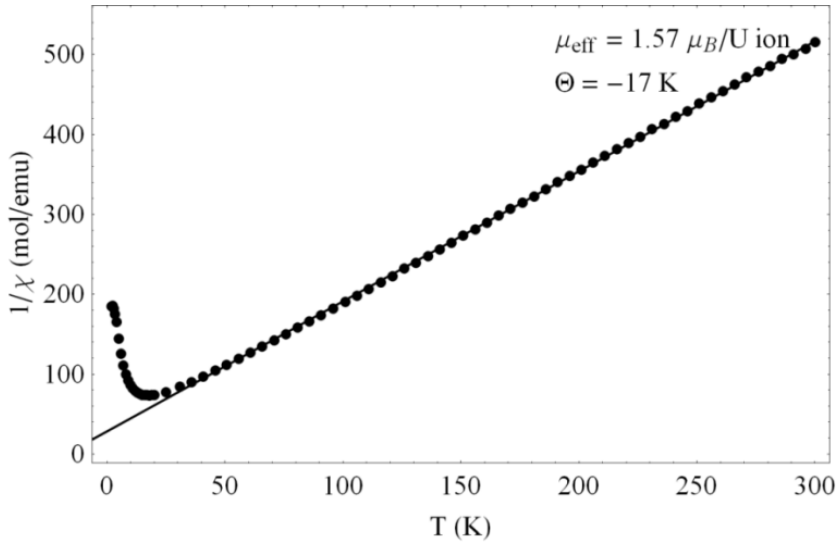

Figure 9: Temperature-dependent inverse magnetic susceptibility of [(Me$_3$SiOUO)$_2$(L)] in the range 2–300 K measured at 50000 Oe with zero-field cooling. Points are experimentally measured and the line is a fit of the high-temperature data to a Curie-Weiss law.

A linear fit of the 1/χ plot to the Curie-Weiss law ($1/\chi = (T-\Theta)/(8\mu_{eff}^2)$ or $\mu_{eff} = \sqrt{(C8)}$) over the range 45 to 300 K gives an effective moment of 1.57 μ_B/U atom (Figure 9), lower than what would be expected for a single for a single U f^1 ion in the L-S coupling scheme (μ_{eff} = 2.54 μ_B/U). Such a reduction cannot be attributed to antiferromagnetic coupling, as any low-temperature interaction cannot significantly affect the linear part of the 1/ χ curve, with the value of μ_{eff} extracted from the plot (1.57 μ_B/U atom) almost identical to that observed at room temperature (1.57 μ_B/U atom). One reason for the difference could be that μ_{eff} is lowered due to an orbital contribution from metal-ligand covalency, with siphoning of spin density from the metal to the ligand causing a reduction in the orbital magnetism. This theory, originally proposed to explain the lower-than-expected magnetic moments of mononuclear U^V complexes,[31] has since however been disputed by Kiplinger and co-workers who reported a positive correlation between the qualitative M-L covalency

and μ_{eff} for uranium(V)-imido halide complexes.[32] In light of these considerations, the reduction in μ_{eff} is instead ascribed to the strong ligand field that arises from a uranyl-type geometry, with an axial ligand-field model, recently proposed by Mazzanti and co-workers for pentavalent monomeric uranyl-type complexes,[33] used to model the Hamiltonian (Figure 10 and below).

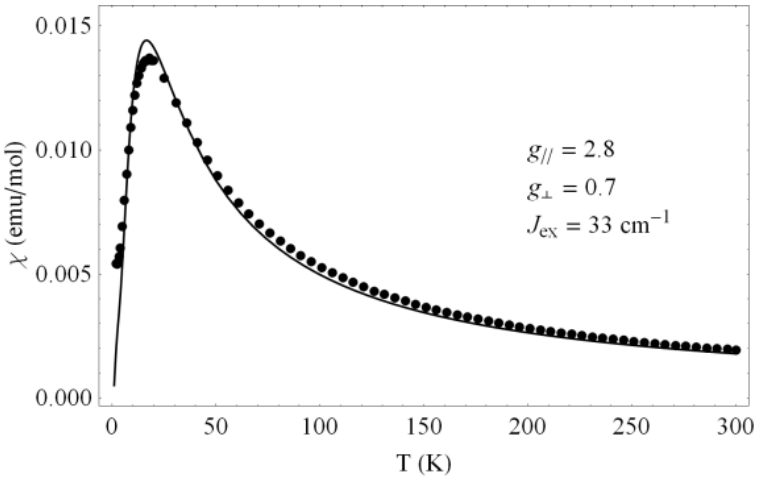

Figure 10: Temperature-dependent magnetic susceptibility of $[(Me_3SiOUO)_2(L)]$ in the range 2–300 K measured at 50000 Oe with zero-field cooling. Points are experimentally measured and the line is a fit of the data based on superexchange across the two bridging oxo groups.

Below 25 K a clear signature of antiferromagnetic coupling between the two f^1 centres occurs, with a maximum in the χ(T) curve at a Néel temperature of 17 K (Figure 10). The value is much higher than that exhibited by other doubly-oxo-bridged uranium complexes, with the previous largest Néel temperature being 5 K,[10] but comparable to that of 20 K measured for the singly-oxo-bridged uranium(IV) complex $[\{(^{Ad}ArO)_3\text{-}TACN\}U)_2(\mu\text{-}O)]$ (TACN = triazacyclononane).[11] For the latter example, it was postulated that it was the geometry of the oxo-group interaction, rather than the U···U proximity, that was the primary mediator of the magnetic superexchange.

In order to quantify the magnitude of the observed magnetic coupling the SQUID data was modelled by Dr. Nicola Magnani at The Lawrence Berkeley National Laboratory. The coupling due to superexchange across the two oxo groups was simulated by a spin Hamiltonian, containing one Zeeman term for each magnetic site, modelled using the strong ligand field model described above, and the exchange interaction. The best fit was obtained with $g_{//} = 2.8$, $g_{\perp} = 0.7$, and $J_{ex} = -33\ cm^{-1}$, with the latter exchange coupling being particularly large with respect to other *f*-electron complexes (Figure 10).[34] Fundamental understanding of the factors that govern the exchange interactions and electron delocalisation are poorly understood, a factor exacerbated by the rarity of $5f^1$ dimers, which are easiest to

study.[34] It is still tempting, however, to speculate that the strong antiferromagnetic exchange exhibited by $[(Me_3SiOUO)_2(L)]$ at low temperatures may be attributed to the proximity of uranium centres or to partial electron delocalisation around the U_2O_2 core, the latter of which may be facilitated by the large contribution of the *endo-cis*-oxo atom to the π- bonding in the molecule inferred by theoretical calculations.

2.6 Reactivity of $[(Me_3SiOUO)_2(L)]$

Almost all of the recently isolated $[U^VO_2]^+$ complexes are relatively unstable towards redox-induced decomposition so it is remarkable that, on exposure to air for 48 h, a wet benzene solution of $[(Me_3SiOUO)_2(L)]$ showed no change in its ^{1}H NMR spectrum. Furthermore, only 20 % consumption of the complex to form 0.2 equivalents of H_4L by ^{1}H NMR spectroscopy and trace amounts of insoluble precipitate was observed after five days. Solution-phase cyclic voltammetry experiments display no oxidation processes within the window afforded by THF (+0.5 to –3 V vs Fc/Fc^+) and the complex is similarly difficult to oxidise chemically, with no reaction observed with the oxidising agents $[Cp_2Fe][OTf]$, $[Ce(OTf)_4]$, $[AgBPh_4]$, $[AgSbF_6]$, Ph_3CCl, pyridine-*N*-oxide or iodine. In addition, no reactivity was exhibited towards either silyl group exchange with Ph_2SiHCl or silyl/uranyl exchange by treatment with additional equivalents of $[UO_2(N'')_2(py)_2]$. Attempts to abstract the $OSiMe_3$ group completely using excess Me_3SiI or B-bromocatecholborane were also unsuccessful. The only reactivity that could be elicited from the $[(Me_3SiOUO)_2(L)]$ was towards reduction, a topic that is discussed in Chapter three.

2.7 Mechanistic insights into the formation of $[(Me_3SiOUO)_2(L)]$

In contrast to the insights gained into the structure and bonding of $[(Me_3SiOUO)_2(L)]$ the mechanism by which it forms is not immediately obvious. Monitoring the reaction at 120 °C by ^{1}H NMR spectroscopy revealed no intermediates between the consumption of $[UO_2(py)(H_2L)]$ and the formation of the product, with $HN(SiMe_3)_2$ being the only other soluble species forming during the reaction. The low yields of both the $[(Me_3SiOUO)_2(L)]$ and $[(PhMe_2SiOUO)_2(L)]$ products derive from the concomitant formation of significant amounts of pyridine-intractable material which occurs regardless of the presence of light and in the absence of oxygen or moisture. The use of the alternative solvents resulted in either no reaction or decomposition, with the latter result also observed when using greater than 1.5 equivalents of $[UO_2\{N(SiMe_2R)_2(py)_2]$ (R = Me or Ph). The use of fewer than 1.5 equivalents of the uranyl silylamide precursor left unreacted $[UO_2(py)(H_2L)]$ remaining. With these variables accounted for, variation of both the silyl

starting materials and the reaction temperature were carried out in order to elicit more information.

2.7.1 Investigations into the origin of reductive silylation

As detailed in Chapter One, the only previous examples of reductive silylation of the uranyl dication by silylamido reagents were the formations of the heterobimetallic, mono-silylated-uranyl Pacman complexes [$Me_3SiOUO(THF)\{M_2(\mu\text{-}X)(X)L)$] (R = alkyl group, M = Fe, Zn, X = I, Cl) by our groups in 2008.[1] In that study, [$UO_2(THF)(H_2L)$] was treated with two equivalents of [$KN(SiMe_3)_2$] at –78 °C forming the highly reactive potassium/uranyl(VI) intermediate [$OUO(THF)(K_2L)$]. This readily undergoes reductive silylation upon warming to room temperature by reaction with the liberated $HN(SiMe_3)_2$ to form a silylated uranyl(V) complex [$Me_3SiOUO(THF)(K_2L)$] from which transmetalation upon addition of a transition metal halide affords the isolated product. It was proposed in the study that the oxo-group silylation occurred by homolytic cleavage of an N–Si bond of HN", with the amine providing both an $SiMe_3$ group and single electron required for reductive silylation.

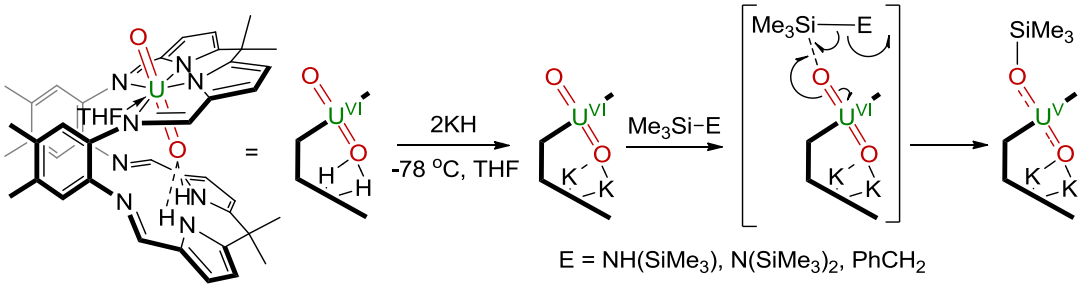

Scheme 4: General synthesis of oxo-silylated mono-urany(V) Pacman complexes.

The original synthetic route was extended to employ the non-silyl base KH to form the reactive [$OUO(THF)(K_2L)$] complex, to which was added $N(SiMe_3)_3$ or $PhCH_2SiMe_3$ as the silylating agent, the use of latter reagent being demonstrative of the additional capacity of [$OUO(THF)(K_2L)$] to cleave C–Si, in addition to N–Si, bonds (Scheme 4). The mechanism, by which the uranyl oxo group acts as a single-electron oxidant, produces either aminyl or hydrocarbyl radicals as the by-products and is supported by theoretical calculations.[35]

Undertaking the synthesis of [$(Me_3SiOUO)_2L$] from [$UO_2(py)(H_2L)$] and [$UO_2(N'')_2(py)_2$] in the presence of the hydrocarbyl silanes $Ph_2CH_2SiMe_3$ or 1,1-dimethylsiletane gave no evidence of C–Si bond cleavage and reactions were instead carried in the presence of alternative silylamines.

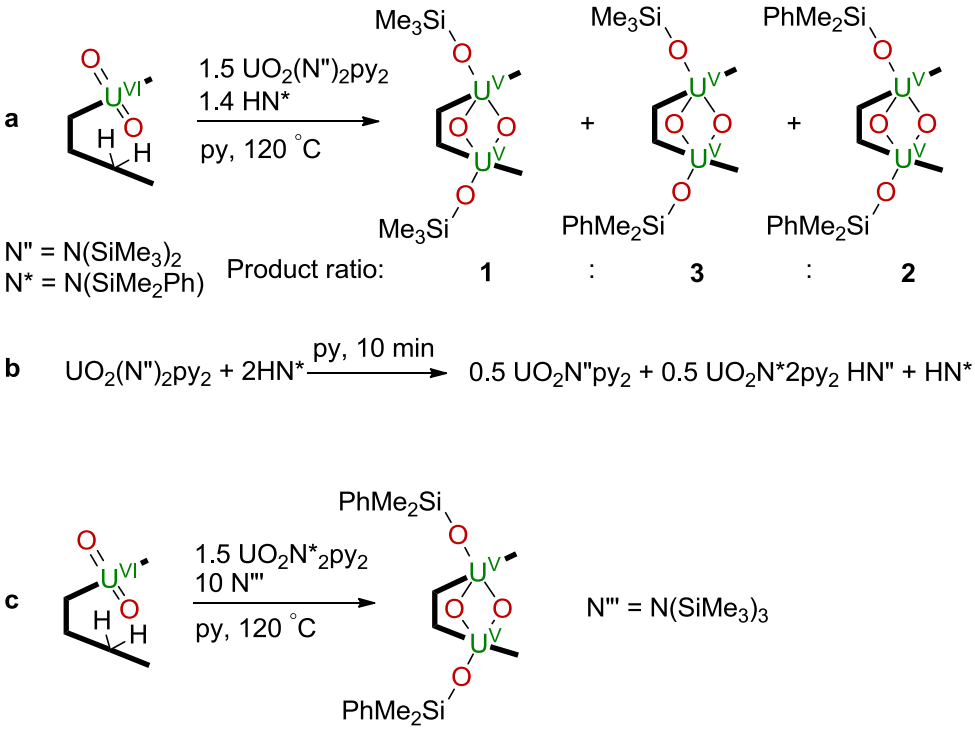

Scheme 5: Reactions to determine the source of the silyl group: **a.** Effect of an added secondary amine. **b.** Amine/amide scrambling. **c.** The effect of an added tertiary amine.

The reaction of $[UO_2(py)(H_2L)]$ and 1.5 equivalents of $[UO_2(N")_2(py)_2]$ in the presence of the HN* produced a mixture of the symmetrically silylated butterfly complexes $[(Me_3SiOUO)_2L]$ and $[(PhMe_2SiOUO)_2L]$ in addition to the asymmetrically silylated complex $[(PhMe_2SiOUO)L(OUOSiMe_3]$ (Scheme 5, a). Although it is clear that formation of the latter two products occurs as a result of the added HN*, it cannot be attributed directly to silylation by the secondary amine. This is because $[UO_2(N")_2(py)_2]$ readily undergoes transamination with HN* under the reaction conditions, producing a mixture of both N" and N* amides (Scheme 5, b). To test which reagent was responsible for the silylation, the synthesis of $[(PhMe_2SiOUO)_2L]$ was attempted in the presence of a large excess of $N(SiMe_3)_3$ (N'''), a comparably reducing tertiary silylamine reagent that cannot undergo transaminative exchange with the uranyl amide (Scheme 5, c). In this case, no evidence for a trimethyl-silylated product was observed, leading to the conclusion that it is the uranyl silylamide reagent, and not the silylamine by-product, that is the reagent responsible for oxo-group silylation.

2.7.2 Synthesis of polymeric butterfly material P

Investigations of the reaction to form $[(Me_3SiOUO)_2(L)]$ at lower temperatures led to the discovery of a competing reaction involving reductive metalation, rather than reductive silylation, of the uranyl oxo groups.

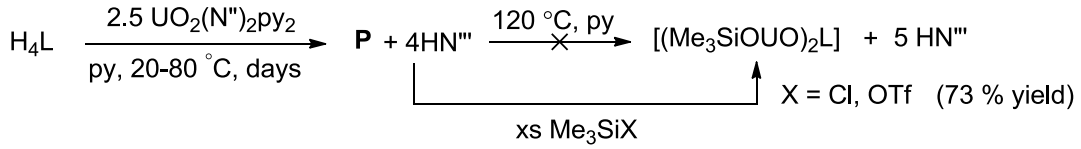

Scheme 6: Synthesis of the insoluble product **P** and its conversion to $[(Me_3SiOUO)_2(L)]$.

Reaction of H_4L with 2.5 equivalents of $[UO_2(N'')_2(py)_2]$ for two weeks at 20 °C formed an insoluble paramagnetic compound **P** and four equivalents of HN", with the amine being the only species observable by ^{1}H NMR spectroscopy after the reaction period (Scheme 6). Undertaking the same reaction with a greater or lower amount of $[UO_2(N'')_2(py)_2]$ resulted in the retention of unreacted $[UO_2(N'')_2(py)_2]$ or $[UO_2(py)(H_2L)]$ respectively while at 70 °C the reaction period was lowered to 4 days. At temperatures greater than 80 °C, both **P** and $[(Me_3SiOUO)_2(L)]$ are formed in addition to other intractable materials. Significantly, **P** was found to react with Me_3SiCl or Me_3SiOTf to form $[(Me_3SiOUO)_2(L)]$ in greater yields than the previous synthesis, generating the silylated product in 73 % yield from a two-step, *in-situ* reaction (Scheme 6).

Despite being formed under similar conditions, **P** is not an intermediate in the high temperature synthesis of $[(Me_3SiOUO)_2(L)]$, with no conversion to the silylated product observed upon heating the material at 120 °C (Scheme 6). The insolubility of the material in all common organic solvents inhibited analysis by ^{1}H NMR spectroscopy and made the growth of single crystals for X-ray diffraction studies extremely difficult. Attempts to crystallise the product directly from the reaction mixture or by vapour deposition were unsuccessful. The high insolubility of the material is suggestive of a polymeric structure, with its facile conversion into $[(Me_3SiOUO)_2(L)]$ indicative of it being composed of $[(OUO)_2(L)]$ butterfly units, symmetric monomers linked by bridged oxo groups. Despite readily undergoing silylation, the polymeric structure of **P** cannot be disaggregated to form other soluble molecular compounds, with addition of Lewis acids, Lewis bases or chelating ligands resulting in no dissolution even at elevated temperatures. Attempts to utilise alternative reaction conditions that avoid aggregation were also unsuccessful, with little or no reaction observed between $[UO_2(N'')_2(py)_2]$ and $[UO_2(py)(H_2L)]$ in THF (as observed

previously by our groups)[4] and decomposition observed in benzene. Carrying out the synthesis in pyridine at –30 °C was found to halt the reduction reaction completely allowing isolation of crystalline $[UO_2(py)(H_2L)]$ in stoichiometric yields.

Calibrated NMR-scale reactions show that 4 equivalents of the by-product HN" are liberated on formation of **P** from 2.5 equivalents of $[UO_2(N")_2(py)_2]$ and that a further 1 equivalent is formed upon addition of Me_3SiCl (Scheme 6). While it is evident four equivalents of the amine may result from the tetra-deprotonation of the macrocyclic ligand, the formation of HN" from TMSCl is suggestive of the presence of a $HN(SiMe_3)$ (HN') amide in the material **P**. Mass balance, and the assumption the **P** contains the butterfly motif, are suggestive of an empirical formula of $[(Me_3SiNH)(OUO)_{2.5}(L)\}]$, which is supported by elemental analysis. The FTIR spectrum of **P** exhibits a weak stretch at 912 cm^{-1} corresponding to the asymmetric stretching mode of the uranyl(VI) dication and is suggestive of $[U^{VI}O_2]^{2+}$ incorporation within the material.

The empirical formula, reaction stoichiometry, and FTIR spectroscopy of **P** suggest that each $[(OU^{V}O)_2(L)]^{2-}$ unit contains with an average of 0.5 uranyl(VI) groups which presumably bound to the *exo*-oxo groups and suggestive that half an equivalent of $[UO_2(py)_2Cl_2]$ would be formed as by-product of treatment of **P** with R_3SiCl reagents. Unfortunately however, the exact nature of the intractable yellow by-product produced from such a reaction reaction could not be discerned by FTIR spectroscopy or elemental analysis due to contamination of the material with trace amounts of the free ligand H_4L. The use of R_3SiOTf as the silylating agent allowed the reaction to be followed by ^{19}F NMR spectroscopy however attempts to identify $[UO_2(py)_2(OTf)_2]$ as the uranyl(VI) by-product of this reaction were also unsuccessful due to the broadness of the ^{19}F NMR spectrum resulting from fluxional ^{-}OTf exchange processes.

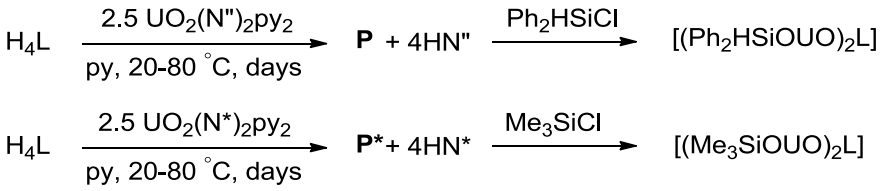

Scheme 7: Silylation of **P** and **P*** to form $[(R_3SiOUO)_2(L)]$ complexes.

The reaction of **P** with Ph_2HSiCl results in the formation of $[(Ph_2HSiOUO)_2(L)]$ as the only butterfly-containing product in the reaction, indicating that the oxo groups in **P** are predominantly unsilylated and the polymeric material can be used as a reagent from which to synthesise any $[(R_3SiOUO)_2(L)]$ silyl-butterfly complex. The reaction of H_4L with 2.5 equivalents of $[UO_2(N^*)_2(py)_2]$ at 70 °C for four days allows the quantitative formation of

P* (Scheme 7), a brown material of comparable insolubility to **P**, with both materials failing to dissolve in pyridine, THF, toluene, benzene, ^{t}BuOH, hexane and Et_2O. In analogy with **P**, such insolubility prohibited analysis by ^{1}H NMR spectroscopy as well the growth of single crystals and no suitable ionisation technique was found to allow its analysis by mass spectrometry. Treatment of **P*** with Me_3SiCl did however result in the formation of $[(Me_3SiOUO)_2(L)]$ as the only product in solution suggesting that the **P*** has a similar, predominantly unsilylated structure to that of **P**. Attempts to characterise the silylamine by-products resulting from either of the reactions shown in Scheme 7 were unsuccessful by ^{1}H NMR spectroscopy owing to the complexity of the mixture of those products with the added R_3SiCl reagents and *in-situ* generated $HN(SiR_3)$ by-products. Analyses of the mixtures by ESI mass spectrometry or FTIR spectrometry were similarly unsuccessful.

As mentioned above, the reaction between H_4L and 2.5 equivalents $[UO_2(N'')_2(py)_2]$ at temperatures greater than 80 °C results in the simultaneous formation of **P** and $[(Me_3SiOUO)_2(L)]$. This observation can partly explain the low isolated yields of the $[(RMe_2SiOUO)_2(L)]$ complexes (R = Ph, Me) (less than 30 %) and the formation of significant quantities of pyridine-insoluble materials from the "heating-only" synthetic route. Addition of TMSCl to the crude reaction mixture to form $[(Me_3SiOUO)_2(L)]$ at 120 °C increases the isolated yield to 60 % indicating that **P** and the silylated product form in an equimolar ratio at this temperature however it is worth noting that approximately 30 % of the material remains intractable after Me_3SiCl addition suggesting that other decomposition reactions occur at higher temperatures.

2.7.3 Hydrolysis of P to form $[\{(Me_3SiOUO)(UO_2)(L)UO_2(THF)_2(\mu\text{-}OH)\}_2]$

Although crystalline samples of **P** could not be produced, information regarding the structure of the material was gained by accidental exposure of the material to water.

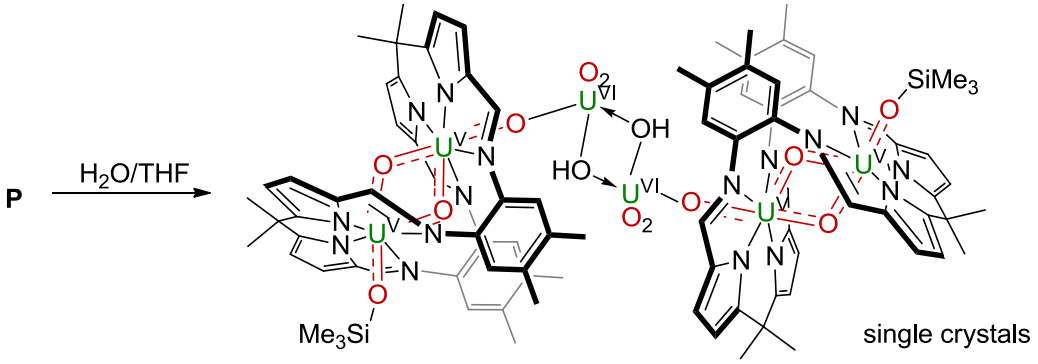

Scheme 8: Crystallisation of $[\{(Me_3SiOUO)(UO_2)(L)UO_2(THF)_2(\mu\text{-}OH)\}_2]$.

A solution of the crude equimolar mixture of $[(Me_3SiOUO)_2(L)]$ and **P**, synthesised from H_4L and 2.5 equivalents $[UO_2(N'')_2(py)_2]$ at 120 °C, was suspended in wet THF, resulting in the precipitation of red crystals of the mixed uranyl/silyl butterfly complex $[\{(Me_3SiOUO)(UO_2)(L)UO_2(THF)_2(\mu\text{-}OH)\}_2]$ after one week (Scheme 8).

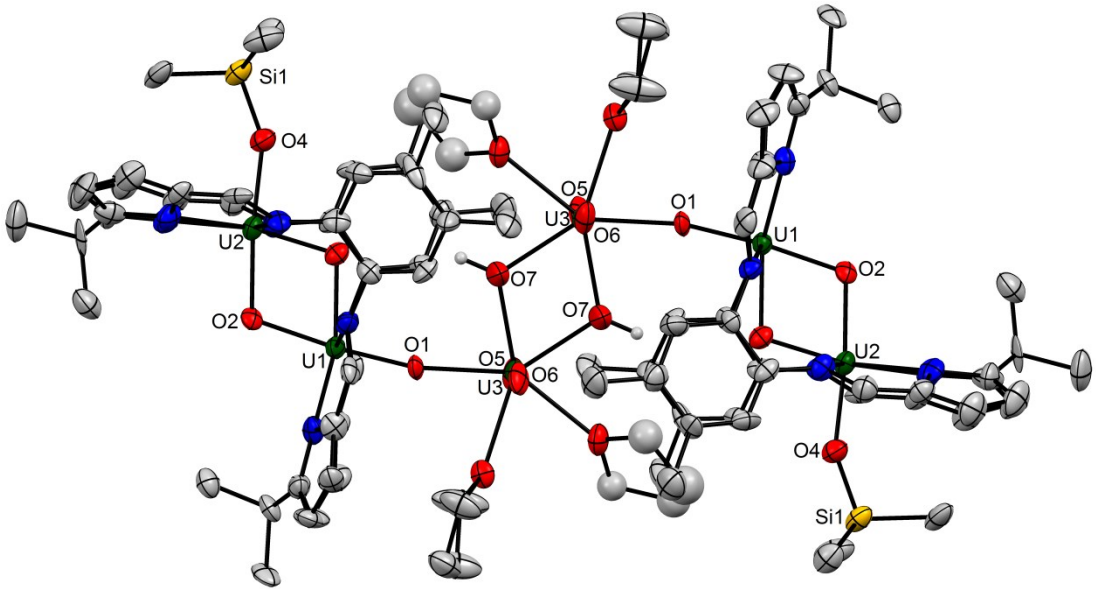

Figure 11: Displacement ellipsoid plot (50 %) of $[\{(Me_3SiOUO)(OUO)(L)UO_2(THF)_2(\mu\text{-}OH)\}_2]$, solvent molecules and all carbon-bound hydrogen atoms are omitted for clarity.

Analysis of the crystals by X-ray diffraction showed a structure containing two Pacman macrocycles, each incorporating the oxo-bridged, binuclear uranium(V) butterfly motif seen in $[(Me_3SiOUO)_2(L)]$ (Figure 11). In contrast to the other $U^V{}_2O_4$ complexes discussed so far, the butterfly units in $[\{(Me_3SiOUO)(OUO)(L)UO_2(THF)_2(\mu\text{-}OH)\}_2]$ are asymmetrically functionalised, with one *exo* oxo group bonded to an $SiMe_3$ group and the other to the uranyl(VI) monohydroxide motif $U^{VI}O_2(OH)$. The two Pacman molecules are linked by these uranyl-bound bridging hydroxides, forming a crystallographic dimer, with the oxo-bound uranyl(VI) dications each exhibiting two *trans* dioxo groups, arranged perpendicular to the planes of the $U^V{}_2O_4$ units. Each U(VI) cation has a pentagonal bypyramidal geometry with the equatorial coordination sphere of each metal containing a butterfly oxo group, two bridging hydroxides, and two THF solvent molecules. Each half of the dimer is crystallographically equivalent, related by an inversion centre in the centre of the $\{U^{VI}O_2(OH)\}_2$ diamond.

Analysis of the bond distances in the structure reveals asymmetric U–O bonding across the U_2O_4 motif. The bond distance between the uranium cation U2 and the *exo*-bound, silylated oxo group O4 is 2.05(1) Å, slightly longer than those observed in the

symmetrically-silylated complexes. In contrast however, the distance between the opposite uranium cation U1 and the uranyl(VI)-bound *exo*-oxo group is 1.910(8) Å, significantly shorter than the U–O bonds in the bis-silylated butterfly molecules and representative of a greater degree of U–O multiple bonding that is similar to that observed in uranyl(V) complexes.[36] The four bonds between the uranium centres and the *cis*- and *trans-endo*-bridging oxygen atoms (O2 and O3 respectively) also show greater asymmetry than those observed in the $[(RMe_2SiOUO)_2(L)]$ (R = Me, Ph) complexes, with the parallel U1-O2 (2.051(8) Å) and U2–O3 (2.033(8) Å) bonds shorter than their analogues in the bis-silyl complexes while the U1–O3 bond is significantly longer (2.170(9) Å). The U2–O2 bond distance of 2.099(9) Å is comparable to those in $[(RMe_2SiOUO)_2(L)]$ however the overall structure of the U_2O_2 core is more representative of localised U–O multiple bonds separated by weaker, more dative interactions. The $U^{(VI)}$3–O5 and $U^{(VI)}$3–O6 bond lengths of 1.757(8) and 1.761(7) Å respectively are expectedly shorter than those in the bis-silylated butterfly complexes and are instead comparable to those in the uranyl(VI) bis(silylamides) $[UO_2(N'')_2(py)_2]$ and $[UO_2(N^*)_2(py)_2]$ endorsing the assignment of a uranyl(VI) oxidation states.

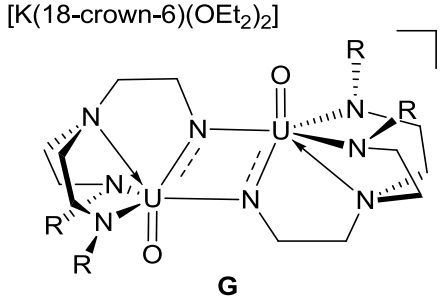

G

Figure 12: The only other example of a mixed valence U^{VI}/U^{V} complex **G**.

To date, the structure is the only example of a mixed valence uranyl(VI)/uranium(V) complex to have been structurally characterised with the oxo/imido complex $[K(18\text{-crown-}6)(Et_2O)][UO\{\mu_2\text{-}NCH_2CH_2N(CH_2CH_2NSi^tBuMe_2)_2\}]_2$, synthesised by Burns and co-workers being the only other example of a mixed valence uranium(V/VI) complex (Figure 12, **G** and Chapter one, Section 1.8).

The structure of $[\{(Me_3SiOUO)(UO_2)(L)UO_2(THF)_2(\mu\text{-}OH)\}_2]$, although not representative of the bulk material, still alludes to the structure of the polymeric material **P** containing linked uranyl(VI)-functionalised butterfly units. In light of the empirical formula described above, it is tempting to attribute the structure of the complex to hydrolysis of an oxo-bound $(U^{VI}O_2)$–$N(H)SiMe_3$ group, affirming the concept of a butterfly polymer featuring metalated oxo groups. The source of the opposing $SiMe_3$ group is more difficult to define

however as it is possible that at temperatures above 80 °C, the onset of formation of the bis-silylated complex, the material **P** contains a proportion of silylated end groups. This postulate was confirmed by treatment of **P*** that had been isolated as the by-product from the reaction to form [($PhMe_2SiOUO$)(L)] at 120 °C with Me_3SiCl, a repeat of the experiment shown in Scheme 7 at a higher temperature. In contrast to the previous reaction, both [(Me_3SiOUO)$_2$(L)] (75 %) and [($PhMe_2SiOUO$)(L)($OUOSiMe_3$] (25 %) were formed, a result suggestive of partial silylation of **P** at higher temperatures. Treatment of either this high-temperature derived material or the unsilylated material **P** with water did not provide a repeatable synthesis of [{(Me_3SiOUO)(UO_2)(L)UO_2(THF)$_2$(μ-OH)}$_2$] however its origin as a hydrolysis product of **P**, rather than [(Me_3SiOUO)$_2$(L)], is presumed based on the lack of reactivity of the latter product to either hydrolysis or silyl/uranyl exchange (see Section 2.6).

2.7.4 Oxidation of P to form crystals of [{(UO_2)$_2$(μ-O)(L)}(UO_2)]

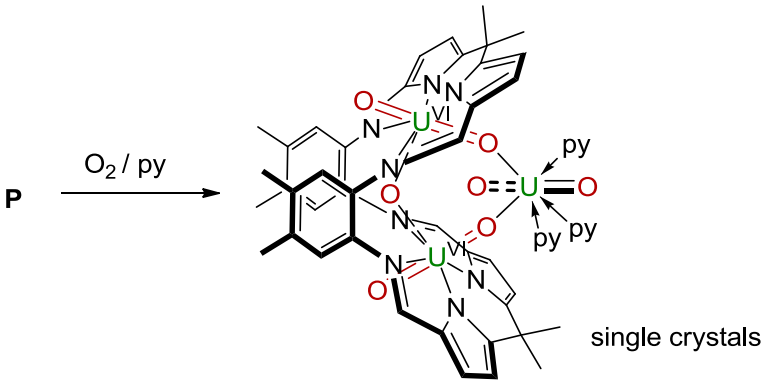

Scheme 9: Crystallisation of [{(UO_2)$_2$(μ-O)(L)}(UO_2)].

A second decomposition product of **P** was also isolated from unsuccessful attempts to dissolve the material in organic solvents. Leakage of air into a Schlenk tube containing a suspension of **P** (synthesised at room temperature) resulted in partial dissolution of the more soluble oxidation product [{(UO_2)$_2$(μ-O)(L)}(UO_2)] and the precipitation of brown crystals after one month (Scheme 9).

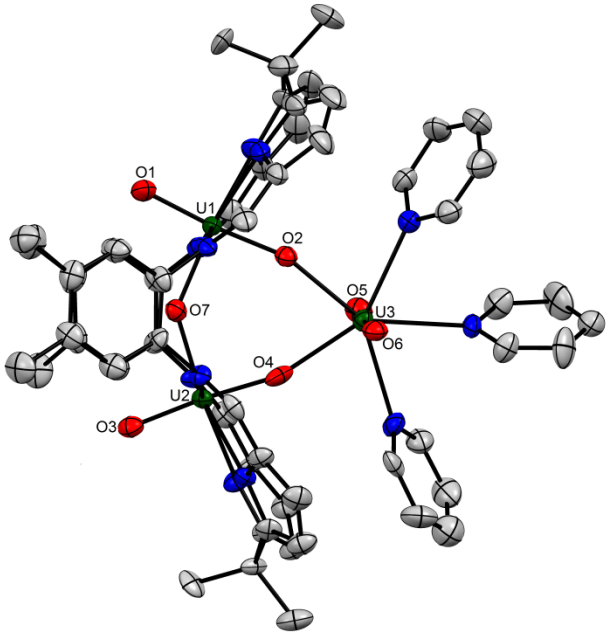

Figure 13: Displacement ellipsoid plot (50 %) of [{$(UO_2)_2$(μ-O)(L)}(UO_2)], solvent molecules and hydrogen atoms are omitted for clarity.

In contrast to the hydrolysis product described above, the solid state structure of [{$(UO_2)_2$(μ-O)(L)}(UO_2)] contains no uranium(V) centres and instead exhibits a wedge-shaped, Pacman macrocycle incorporating single uranyl(VI) dications into each of the two N_4-donor pockets forming a binuclear complex (Figure 13). Each uranyl(VI) centre is pentagonal bypryramidal, with the two axial oxo groups situated perpendicular to the four nitrogen-donors of the macrocyclic cleft. The fifth equatorial coordination sites of each $[UO_2]^{2+}$ cation are mutually fulfilled by a bridging oxo-group, situated between the two aryl rings of the macrocycle backbone forming a doubly-anionic, binuclear assembly $[(UO_2)_2(\mu\text{-}O)(L)]^{2-}$. To maintain charge-balance in the complex, the oxo-bridged binuclear anion acts as a chelating metaloligand, with the *endo* oxo groups of each of the two L-bound uranyl dications coordinating to a third uranyl(VI) dication encapsulated within the macrocylic cavity. This third uranyl dication also exhibits a pentagonal bipyramidal geometry, with the linear $[UO_2]^{2+}$ motif aligned perpendicular to the plane of the two Pacman-bound uranyl species, complexed in the equatorial plane by the two oxo donors and three pyridine solvent molecules.

All the uranium-oxygen bond distances in [{$(UO_2)_2$(μ-O)(L)}(UO_2)] are consistent with uranyl(VI) oxidation states, with an average across all 6 bonds of 1.79 Å. Slightly longer bonds are exhibited between the Pacman-coordinated uranium centres U1 and U2 and their respective *endo*-bound, uranyl-coordinating oxo groups O2 and O3 (both 1.845(9) Å)

than between the metals and their respective *exo*-oxo ligands U1–O1 (1.777(9) Å) and U2–O3 (1.775(7) Å). The third $[UO_2]^{2+}$ species in the complex does not coordinate to another metal and exhibits two almost identical, extremely short U–O bond lengths of 1.760(8) and 1.761(6) Å characteristic of an unperturbed uranyl(VI) dication. There are significant differences between the U–O bond distances between the metal centres and their respective equatorially-donating oxo ligands, with shorter distances of 2.122(8) and 2.1211(8) Å exhibited for the U1–O7 and U2–O7 distances from μ-oxo ligand than those between the third, uranyl-bound $[UO_2]^{2+}$ group and its uranyl donors (2.3125(7) and 2.331(9) Å).

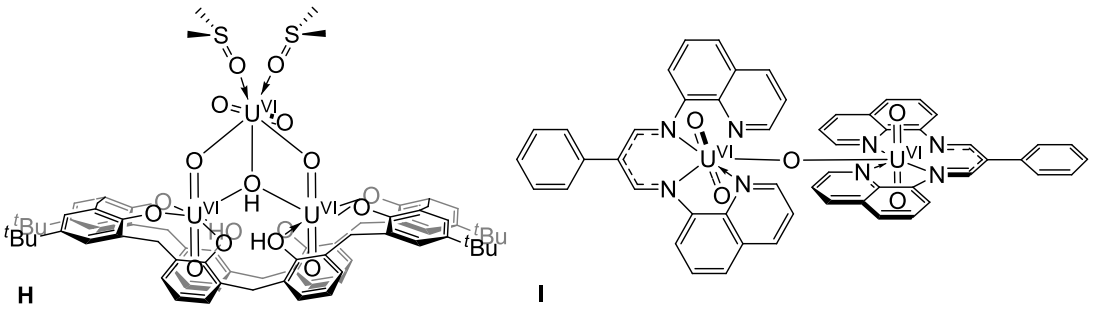

Figure 14: Complexes exhibiting $[U^{VI}O_2]^{2+}$/$[U^{VI}O_2]^{2+}$ CCIs (**H**, anion only) or a mono-oxo bridging ligand (**I**).

Another complex that features bidentate CCI coordination between a binuclear uranyl complex and a third uranyl dication is $[NMe_4][\{(UO_2)_2(calix[8]\text{-}2H)\}(UO_2)(\mu\text{-}OH)_3]$ Å (calix[8]-8H = *p*-^{t}Bu-calix[8]arene) synthesised by Ogden and co-workers. The molecule features similarly elongated U^{VI}=O bond lengths of 1.840(6) and 1.847(6) Å between the two macrocycle-bound uranium atoms and the donated yl atoms as observed in $[\{(UO_2)_2(\mu\text{-}O)(L)\}(UO_2)]$ (Figure 14 **H**).[37] The complex $[\{UO_2(TQD)\}_2(\mu\text{-}O)]$ (TQD = 2-(4-Tolyl)-1,3-bis(quinolyl)malondiiminate) by the Mazzanti group exhibits uranyl dications bound to separate equatorially-chelating ligands and bridged with a single oxygen atom (Figure 14, **I**).[38] In analogy with the complex above, **I** was prepared by the reaction of dioxygen with a uranyl(V) precursor, in this case the trimeric CCI complex $[\{U^{V}O_2(TQD)\}]$. Comparable bond distances between the bridging ligand and the two uranium atoms to those observed in $[\{(UO_2)_2(\mu\text{-}O)(L)\}(UO_2)]$ are observed in **I** (2.19(1) Å each) although the U–O–U bond angle is contrastingly linear (177.2(7)°) in comparison to the bent angle of 140.3(4)° exhibited by $[\{(UO_2)_2(\mu\text{-}O)(L)\}(UO_2)]$.

2.7.5 Analysis of P by laser desorption ionisation mass spectrometry

In order to gain greater insight into the composition of **P** efforts were made to analyse the material by mass spectrometry. Electron ionisation (EI) mass spectrometry

studies did not provide meaningful results due to extensive compound fragmentation and solution-phase mass spectrometry techniques such as electrospray ionisation (ESI) and quadrupole injection time of flight (QTOF) were hindered by poor dissolution of the analyte. Matrix-assisted laser desorption ionisation (MALDI) mass spectroscopy is a soft ionisation technique that allows analysis of materials in the solid state, with the analyte supported on a laser-absorbing matrix that helps induce ablation. For the analysis of **P,** the use of a matrix, typically a conjugated organic molecule such as α-cyano-4-hydroxycinnamic acid, was negated by the aromaticity of the Pacman macrocycle, meaning samples could be analysed quickly and without prior preparation in order to minimise oxidative decomposition.

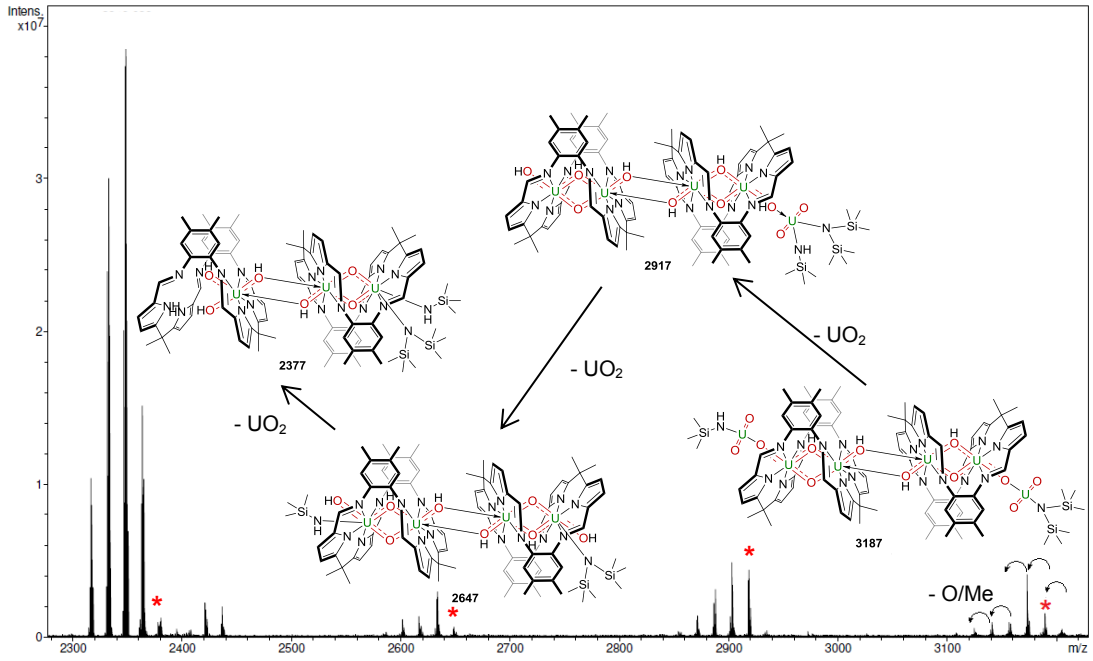

Figure 15: LDI mass spectrum of **P** with selected fragments related by loss of $[UO_2]^{2+}$(*).

The LDI mass spectrum of **P** displays a fragmentation pattern indicative of an oligomeric material (Figure 15). The highest ion visible is at 3187 amu and is assigned to a dimer of two butterfly Pacman complexes, with either $SiMe_3$, $U^{VI}O_2N(SiMe_3)H$, or H as the *exo*-oxo bound groups. Upon binding to an oxygen atom, the latter two groups are capable of bridging between the uranium centres of separate butterfly complexes whereas the former would act as a chain-terminating end group. Four equally-spaced peaks lie at lower masses of 3171, 3156, 3140 and 3124 amu, three of which of have resolvable fragmentation patterns. The five peaks form a distinct cluster, with peaks separations corresponding to the loss of oxygen (16 amu) or methyl (15 amu) from the largest ion. A smaller cluster is found at lower mass, comprised of a set of four well-resolved fragment peaks at 2933, 2918, 2902 and 2886 amu which are again separated by the loss of oxygen or methyl groups. Peaks in

this lighter cluster are separated from those in the heavier set by approximately 270 amu (2886/3156, 2902/3171, 2918/3187, 2933/3203) corresponding to the loss of a UO_2 group between the two clusters. A third cluster of four peaks at 2647–2601 amu arises from the loss of a second $[UO_2]^{2+}$ group, with the small inter-peak separations of 15 or 16 amu again indicative of the loss of methyl of oxygen atoms. The pattern continues until a fourth cluster of 5 peaks at 2378–2317 amu of much greater intensity, containing sets of overlapped fragmentations (2378/2379, 2363/2363, 2348/2347 amu, etc) that were modelled by twin sets of bis-Pacman compounds resulting from the loss of either oxygen (16 amu) or methyl (15 amu) from the next corresponding fragment. Two peaks at 2435 and 2421 amu lie outside of the fourth cluster, being 88 and 89 amu greater than the compound peaks at 2348/2347 and 2332 amu respectively. These out-of-pattern fragments represent the loss of the $HN(SiMe_3)$ (89 amu) from the uranyl(VI) group bound to the *exo* oxo groups of the butterfly units. Clusters corresponding to dimeric, bis-Pacman structures are visible until 1239 amu, after which point the oligomeric units have fragmented sufficiently enough to form bi- and mono-nuclear complexes of single Pacman ligands. Such fragments observed include $[(Me_3SiOUO)(L)(UOH)]$ (1239 amu), $[(UO_2)_2(L)]$ (1197 amu), and $[(OUOUO)(L)]$ (1181 amu) with the lightest uranyl-Pacman fragments observed being [UO(HL)] (913 amu) and [UO(L)] (912 amu). No fragments containing uranium were present below 912 amu with ion peaks resulting from fragmentation of the Pacman ligand (660 amu) not modelled.

2.7.6 Structure of P

Although the exact structure of the material **P** could not be determined it is clear from the available data that is has an oligomeric structure, composed of interlinked U^VU^V $[(OUO)(L)]^{2-}$ units functionalised at their *exo* oxo groups with uranyl(VI) dications. Upon these criteria, assignment of the $[\{(OU^VO)(L)\}\{U^{VI}O_2\}]_n$ structure, whereby every butterfly unit is functionalised by a single $[UO_2]^{2+}$ group and the oligomeric structure is maintained by O_{exo}-$U^{VI}O_2$–O_{exo} bridges, would seem fitting. Such a model contrasts however with the 2.5:1 (rather than 3:1) $[UO_2]^{n+}$:L stoichiometry, the empirical formula derived from element analysis, and the ^1H NMR evidence of incorporation of $HN(SiMe_3)$ groups. In order to satisfy both these criteria and the LDI mass spectral data, functionalisation of certain *exo* groups with protons is proposed, with the oligerisation of the butterfly units arising from bridging hydroxide groups.

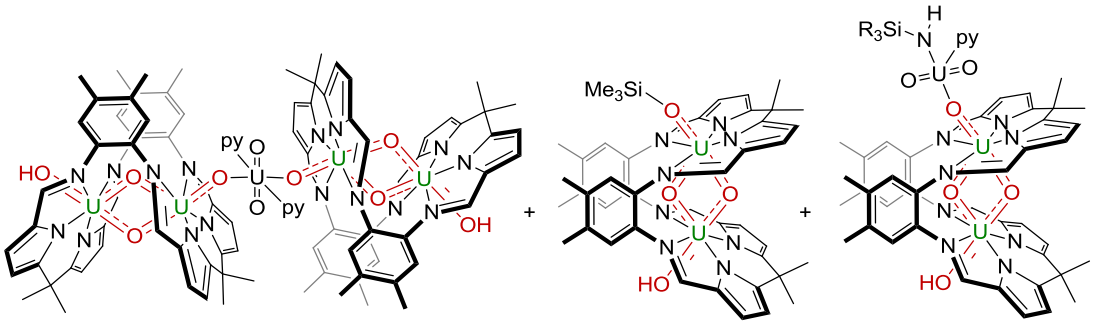

Figure 16: Proposed composition of **P** as an oligomeric aggregate of three components

Functionalisation of the *exo*-oxo groups with $[UO_2]^{2+}$ and $[UO_2\{N(SiMe_3)H\}]^+$ is also included in the model, resulting in an aggregate of a number of components all of which can oligomerise to form the final material (Figure 16). Both the protonated and metalated oxo groups can be removed upon treatment with R_3SiCl reagents to form the two O–SiR_3 bonds present in the $[(R_3SiOUO)_2(L)]$ complexes.

2.7.7 Mechanistic discussion

The characterisation of two different butterfly products, the oligomeric **P** and the molecular, oxo-silylated complex $[(Me_3SiOUO)_2(L)]$, from the same reaction suggests that two competing reductive pathways occur, in greater or lesser amounts depending on the temperature. In both cases, the reducing agent is $[UO_2(N'')_2py_2]$ which, by lacking valence electrons, must undergo homolytic cleavage of one or more valence bonds in order to reductively silylate, metalate or protonate the uranyl(VI) dication. Previous work involving the reactions of $[UO_2(py)(H_2L)]$ with lithium bases to form reductively lithiated uranyl(V) Pacman complexes has invoked homolytic cleavage of Li–R (R = H, NH_2, CPh_3, Cp, N^iPr_2) bonds in the reaction mechanism, as well as some evidence for solvent C–H bond homolysis forming OU^VO–H intermediates.[2] The reduction of $[UO_2(py)(H_2L)]$ with the trivalent rare earth silylamides $Y(N'')_3$ and $Sm(N'')_3$ has also been postulated to proceed by M–N'' bond cleavage, in those cases promoted by the formation of heterobimetallic $[U^{VI}O_2(py)(LM^{III}N'')]$ intermediates followed by intramolecular homolytic M–N'' cleavage to form $[U^VO_2(py)(LM^{III})]$.[3] Both O_2U–N'' and solvent C–H bond homolysis could be employed to explain the formation of **P** however the mechanism by which the silylated product $[(Me_3OUO)_2(L)]$ forms is still unclear. In the absence of any other source of silyl group, the cleavage of N–$SiMe_3$ bonds must be invoked to provide the oxo-bound group however there is no data to confirm whether this occurs by N–Si bond homolysis, in a so-called "reductive silylation" mechanism or whether the silylation occurs after a "reductive-metalation" by a proceeding heterolytic N–Si bond cleavage. Although it is strongly implied by the lack of a

formal reducing agent, direct evidence for any radical formation as a result of bond homolysis was not found. The addition of dihydroanthracene (DHA), a reagent containing weak C–H bonds with low C–H bond dissociation energies (DBE), has been employed to prove that the reduction of $[UO_2(py)(H_2L)]$ by both lithium and rare-earth silylamides proceeds with radical formation.[2-3] In the presence of single-electron oxidation agents, the homolytic cleavage of the C–H bonds in DHA results in the formation of either anthracene (upon double C–H bond homolysis) or a radically-coupled product (upon single C–H bond homolysis and coupling) however neither was observed upon addition of DHA the reactions to form **P** or $[(Me_3OUO)_2(L)]$ under a range of reaction conditions

2.7.8 Thermal decomposition of $[UO_2(N'')_2(py)_2]$

The identification of $[UO_2(N'')_2py_2]$ as the reducing agent in the formation of **P** and $[(Me_3SiOUO)_2(L)]$ led to investigations regarding the stability of the uranyl(VI) precursor under the reaction conditions. Heating an orange solution of $[UO_2(N'')_2(py)_2]$ in pyridine at 120 °C for 12 h resulted in the formation of an insoluble black solid in addition to the quantitative formation of two equivalents of HN" as evidenced by calibrated ^{1}H NMR spectroscopy experiments. Undertaking the same reaction in the presence of DHA resulted in 0.33 equivalents of the substrate being converted into the oxidised product anthracene, confirming the presence of radical formation as evidenced by C–H bond homolysis. $[UO_2(N'')_2(py)_2]$ is indefinitely stable in pyridine solutions up to 50 °C, after which temperature the slow decomposition starts to occur, with rates increasing up to the boiling point of the solvent. No such decomposition was observed in THF or benzene, perhaps explaining the lack of U^V-product formation in these solvents. In contrast to $[UO_2(N'')_2(py)_2]$ mono-uranyl(VI) Pacman complex $[U^{VI}O_2(py)(H_2L)]$, an intermediate to the formation of $[(Me_3OUO)_2(L)]$ and **P** from H_4L and 2.5 equivalents of $[UO_2(N'')_2py_2]$, is stable in solutions of boiling pyridine for over four days.

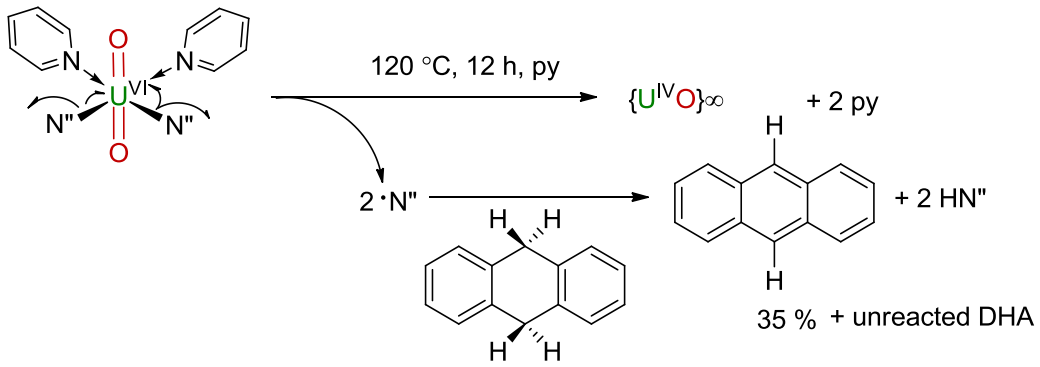

Scheme 10: Postulated mechanism of thermally-induced reduction of $[UO_2(N'')_2(py)_2]$.

In consideration of these observations, it is postulated that $[UO_2(N'')_2(py)_2]$ decomposes by homolytic U–N bond cleavage, with the formation of the aminyl ·N" radical inducing a subsequent H-atom abstraction from the pyridine solvent or DHA (Scheme 10). The formation of two whole equivalents of HN" is indicative of the double reduction of the uranyl(VI) dication to uranium(IV), resulting in a weakening of the discrete multiple bonds in $[UO_2]^{2+}$ in favour of bridging oxide bonds to form black uranium(IV) oxide that is characteristically insoluble in the pyridine solvent.

The facile reduction of $[UO_2(N'')_2py_2]$ in boiling pyridine confirms the source of the reducing electron in the formation of **P** and $[(Me_3SiOUO)_2(L)]$ and also explains the low yields and formation of intractable materials in the formation of the latter complex at 120 °C. It is likely that, at these temperatures, the decomposition of the uranyl(VI) silylamide precursor occurs in tandem with butterfly formation, with the use of greater amounts of the radical-producing $[UO_2(N'')_2py_2]$ in the reaction resulting in total decomposition of all starting materials.

2.8 Attempted syntheses of other $[UO_2R_2]$ reagents

In a final effort to discern more about uranyl reduction by U^{VI}–N" bond homolysis the use of alternative uranyl(VI) starting materials was explored in order to attempt to inhibit the complicating factors of uranyl silylation and/or metalation. To date, uranyl silylamides are the only class of neutral, homoleptic uranyl(VI) reagents featuring monodentate amide ligands, with no other reported examples of uranyl alkyls or organometallics. In light of this, attempts were made to prepare a selection of such complexes featuring strongly basic amide or hydrocarbyl ligands. Although there are a wide variety of neutral homoleptic uranyl(VI) complexes featuring monodentate halide, pseudohalide, alkoxide and aryloxide ligands these are not deemed basic enough to deprotonate the pyrrolic N*H* groups upon uranyl

complexation. Unfortunately, attempts to prepare neutral uranyl complexes of the anionic ligands $^{-}$HNDipp, imidazolide, $^{-}$TMP, $^{-}N^{i}Pr_2$ and $^{-}HC(SiMe_3)_2$ were all unsuccessful from either protonolysis reactions of $[UO_2(N")_2py_2]$ and the respective amines or salt elimination reactions from $[UO_2Cl_2THF_2]$ and the respective group one metal salts. It was found repeatedly that black, intractable solids were formed upon reagent mixing, suggestive of similar reduction processes forming uranium(IV) oxide as observed in the thermal decomposition of $[UO_2(N")_2py_2]$. The same results were obtaining in THF solvents and at 0 °C. In addition to these efforts, the difficulties in forming alternative $[UO_2R_2]$ reagents are well documented in the literature, with the same formation of uranium(IV) oxide precipitates observed during the attempted syntheses of uranyl bis(piperiridide) $[UO_2(NC_5H_{10})_2]$,[39] $[UO_2(C_5Me_5)_2]$[40] and $[UO_2(CH_2SiMe_3)_2]$.[40]

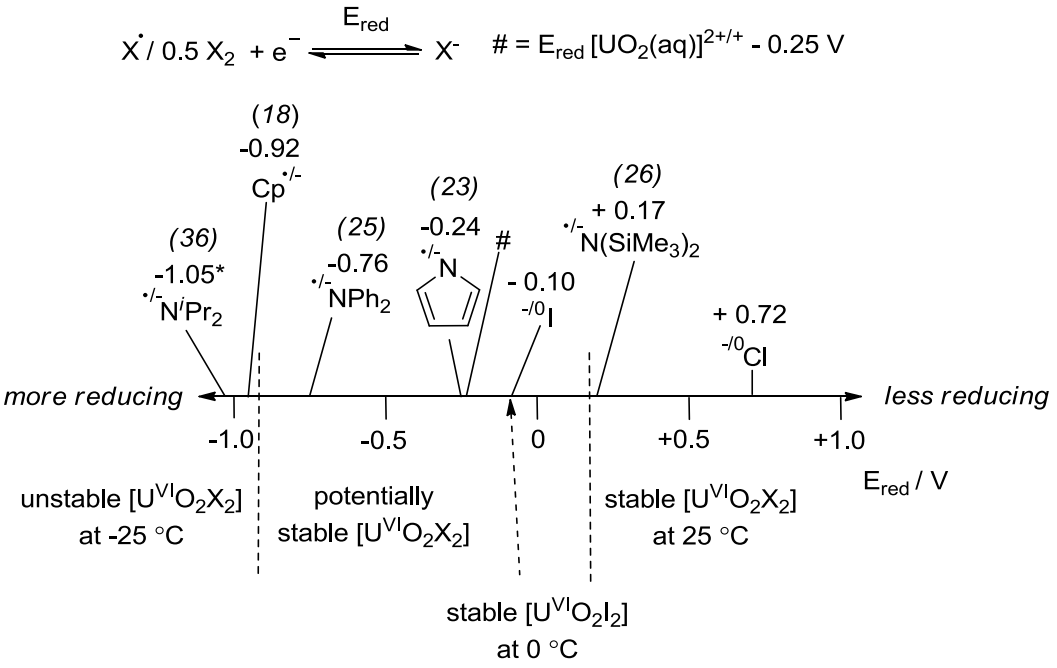

Figure 17: Reduction potentials of anionic X^{-} ligands versus Fc/Fc^{+}, all data recorded at room temperature apart from *(–12 °C). pKa values for HX given in bracketed italics. Standard reduction potential for aqueous uranyl(VI) shown for comparison (#).[41]

It is known that, for a given class of anionic ligands such as alkyls or amides, the reducing ability of anion is proportional to the pKa of the conjugate acid as the greater instability of the R^{-} species increases the propensity its oxidation.[42-43] The stability of the product, the neutral R· radical, is related to the R–H bond dissociation energy, which remains relatively unchanged for a given class of ligands.[42-43] The reduction potential for ·N", formally the reduction potential across the ·N"/$^{-}$N" couple, is +0.17 V (from the cyclic voltammogram of LiN" at 33 °C versus Fc/Fc^{+} in THF/HMPA),[44] with the pKa of the

conjugate acid HN" being 26 (in THF).[45] In comparison, the pKa of the structurally related HN^iPr_2 is 36,[43] with $\cdot N^iPr_2$ exhibiting a much more negative reduction potential of –1.05 V (from the cyclic voltammogram of $[Li^iNPr_2]$ at –12 °C versus Fc/Fc^+ in THF/HMPA).[44] The more negative reduction potential of $^iNPr_2$ perhaps explains why its corresponding uranyl(VI) complex is unstable with respect to reductive decomposition, with the reduction potentials of hydrocarbyl ligands, such as Cp (E_{red} $^{\cdot/-}$Cp –0.92 V versus Fc/Fc^+) also useful in rationalising the aforementioned instabilities of their respective complexes.

Although exact reduction potentials of uranyl(VI) complexes have not been measured in pyridine, upper and lower bounds for the species reduction by amide ligands at room temperature are given by the reduction potentials described above (Figure 17). It is worth noting that uranyl(VI) -ate complexes of the type $[M_2\{UO_2R_4\}]$ (M = group one metal) have been stabilised using piperidide despite the respective neutral complex being unstable.[39] In this case, the stability of the resultant complex was attributed to an increase in the reduction potential of the uranyl(VI) centre by loading it with electron density by multiple π-donors. The recent synthesis of the uranyl(VI) alkyl –ate complex $[Li(DME)_{1.5}]_2[U^{VI}O_2(CH_2SiMe_3)_4]$ provides further affirmation that such –ate complexes are more stable than their neutral analogues,[46] with the aforementioned neutral $[U^{VI}O_2(CH_2SiMe_3)_2]$ complex remaining elusive.[40] Such examples demonstrate the competing effects of increasing ligand donor strength of the redox stability of UO_2X_2 complexes, with more strongly donating ligands *decreasing* the ease at which the U^{VI} centre can be reduced but being themselves more *reducing*.

In consideration of the limits shown in Figure 17, attempts were made to source alternative, non-silyl amides which will not reduce $[UO_2]^{2+}$ at room temperature. For those ligands for which data is available, none are less reducing than $^-$N" however both pyrrolide and $^-NPh_2$ were identified as having relatively low ^-NR_x reduction potentials (–0.24 and –0.76 V respectively, versus Fc/Fc^+ in DMSO at 25 °C) while remaining sufficiently basic (HNR_x pKs of 23 and 25 respectively), the latter factor being a requirement for a uranyl amide precursor to deprotonate the H_4L macrocycle.[43]

The transamination reactions between $[UO_2(N'')_2py_2]$ and two equivalents of $HNPh_2$ resulted in the clean formation of $[UO_2\{NPh_2\}_2py_x]$ and two equivalents of HN" by ^{1}H NMR spectroscopy (Scheme 11).

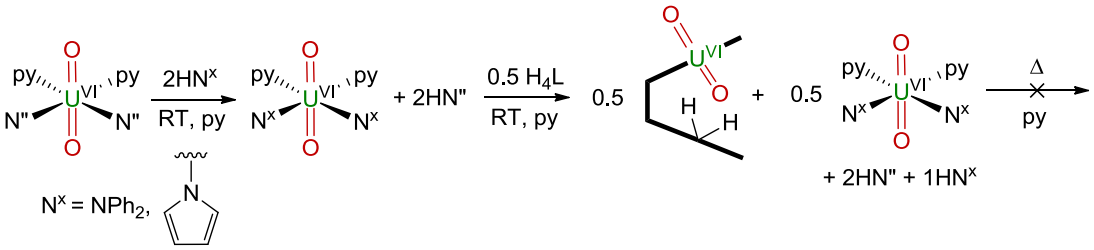

Scheme 11: Synthesis of two stable uranyl amides and their reactivities towards H_4L.

The complex exhibits three aromatic resonances in the ^{1}H NMR spectrum at 7.39, 6.93 and 6.62 ppm which are shifted in comparison to free $HNPh_2$. The analogous reaction between $[UO_2(N'')_2py_2]$ and two equivalents of pyrrole resulted in the formation of the uranyl pyrrolide complex $[UO_2\{NC_4H_5\}_2py_x]$ and two equivalents of HN", with the latter exhibiting two resonances in the ^{1}H NMR spectrum at 8.17 and 6.34 ppm which are also shifted in comparison to C_4H_4NH. Attempts to synthesise either complex on a preparative scale resulted in decomposition to black uranium(IV) oxide and the respective amine however the *in situ* synthesis of both reagents allowed assessment of their reactivity towards the Pacman macrocycle. The reaction of two equivalents of either uranyl amide complex, formed *in situ* alongside two equivalents of HN" which does not partake in further reaction, with the free Pacman ligand H_4L resulted in the clean, quantitative (referenced against HN") formation of the mono-uranyl Pacman complex $[UO_2(py)(H_2L)]$ and liberation of two equivalents of the respective free amines C_4H_4NH or $HNPh_2$. No further reaction was observed between the mono-uranyl Pacman complex and the second equivalent of the uranyl amides, with heating either reaction resulting only in the reductive decomposition of the amide starting materials to form two further equivalents of C_4H_4NH or $HNPh_2$.

2.9 Summary

In conclusion, two new, pyridine-solvated uranyl(VI) silylamides $[UO_2\{N(SiMe_2R)_2\}_2(py)_2]$ (R = Me, Ph) have been synthesised from $[UO_2Cl_2(THF)_2]$ and two equivalents of $[KN(SiMe_2R)_2]$ in pyridine. The complexes display contrasting *cis* (R – Me) or *trans* (R = Ph) arrangements of silylamide ligands bound in the $[UO_2]^{2+}$ equatorial plane with the different geometries likely occurring as a result of the larger size of the latter ligand.

Synthesis of the binuclear uranium(V) oxo complexes $[(RMe_2SiOUO)_2(L)]$ was achieved by heating 2.5 equivalents of $[UO_2\{N(SiMe_2R)_2\}_2(py)_2]$ with H_4L in pyridine solution. The complexes form from a combination of single-electron uranyl(VI) reduction and oxo-group silylation and exhibit novel *cis*/*trans* arrangements of axial oxo ligands and extremely short U···U separations. In addition, the complexes were shown to be highly inert towards oxidation or hydrolysis making them amongst the most stable uranium(V) complexes currently known.

Investigations into the electronic structure of the U_2O_4 "butterfly" core of $[(Me_3SiOUO)_2(L)]$ were undertaken with DFT calculations. It was revealed that the complex exhibits partial U–O multiple bonding with the mutually *trans* bridging *endo* oxo ligand contributing a greater amount to the σ-bonding and the mutually *cis* bridging oxo contributing predominantly to the π-bonding. Core molecular orbitals formed from direct 5*f*-5*f* orbital overlap between the uranium(V) centres were also found despite the paramagnetic nature of the complex.

The temperature-dependent magnetism of $[(Me_3SiOUO)_2(L)]$ demonstrated strong antiferromagnetic coupling between the two uranium centres below 25 K which is maximised at 17 K. Modelling the magnetic data with a Hamiltonian allowed an estimation of the exchange coupling of $J_{ex} = -33$ cm^{-1} to be made.

The preparation of a polymeric, butterfly-containing material **P** from H_4L and 2.5 equivalents of $[UO_2\{N(SiMe_3)_2\}_2(py)_2]$ at low temperature was achieved. The material is also formed in competition with $[(Me_3SiOUO)_2(L)]$ at high temperature but can be converted into the bis-silyl complex by treatment with excess Me_3SiCl. The structure of **P** was partially elucidated by ^{1}H NMR studies, elemental analysis, LDI mass spectrometry and structural analysis of its oxidation and hydrolysis products. It is proposed that the material is an oligomeric aggregate of a number of primarily unsilylated butterfly units, with either uranyl silylamide groups or protons bound to the *exo*-oxo groups.

The mechanisms to form **P** and $[(Me_3SiOUO)_2(L)]$ were not fully elucidated but both the reducing and silyating agent in either case was identified as $[UO_2\{N(SiMe_3)_2\}_2(py)_2]$. The complex which was found to undergo U–N bond homolysis upon heating in pyridine solution to form uranium(IV) oxide, with a similar process proposed to explain the reduction of uranyl(VI) to form the butterfly complex under similar analogues.

Finally, the synthesis of a number of alternative uranyl(VI) amides was unsuccessful due to reductive decomposition. The regents $[UO_2\{NPh_2\}_2(py)_2]$ and $[UO_2\{NC_4H_5\}_2(py)_2]$

were however prepared in solution after consideration of the basicity and reduction potentials of their respective ligands. Both complexes were used to synthesise the mono-uranyl Pacman complex $[UO_2(py)(H_2L)]$ but no formation of binuclear complexes was achieved.

2.10 References

1 P. L. Arnold, D. Patel, C. Wilson, J. B. Love, *Nature* **2008**, *451*, 315-317.

2 P. L. Arnold, A.-F. Pécharman, E. Hollis, A. Yahia, L. Maron, S. Parsons, J. B. Love, *Nature Chem.* **2010**, *2*, 1056-1061.

3 P. L. Arnold, E. Hollis, F. J. White, N. Magnani, R. Caciuffo, J. B. Love, *Angew. Chem., Int. Ed. Engl.* **2011**, *50*, 887-890.

4 P. L. Arnold, A. J. Blake, C. Wilson, J. B. Love, *Inorg. Chem.* **2004**, *43*, 8206-8208.

5 R. A. Andersen, *Inorg. Chem.* **1979**, *18*, 209-209.

6 D. M. Barnhart, C. J. Burns, N. N. Sauer, J. G. Watkin, *Inorg. Chem.* **1995**, *34*, 4079-4084.

7 P. L. Arnold, D. Patel, A. J. Blake, C. Wilson, J. B. Love, *J. Am. Chem. Soc.* **2006**, *128*, 9610-9611.

8 W. J. Evans, D. B. Rego, J. W. Ziller, *Inorg. Chem.* **2006**, *45*, 3437-3443.

9 S. M. Mansell, B. F. Perandones, P. L. Arnold, *J. Organomet. Chem.* **2010**, *695*, 2814-2821.

10 G. Nocton, P. Horeglad, J. Pécaut, M. Mazzanti, *J. Am. Chem. Soc.* **2008**, *130*, 16633-16645.

11 O. P. Lam, F. W. Heinemann, K. Meyer, *Chem. Sci.* **2011**, *2*, 1538-1547.

12 A. Zalkin, S. M. Beshouri, *Acta Crystallogr., Sect. C: Cryst. Struct. Commun.* **1988**, *44*, 1826-1827.

13 W. W. Lukens, P. G. Allen, J. J. Bucher, N. M. Edelstein, E. A. Hudson, D. K. Shuh, T. Reich, R. A. Andersen, *Organometallics* **1999**, *18*, 1253-1258.

14 T. Le Borgne, P. Thuery, M. Ephritikhine, *Acta Crystallogr., Sect. C: Cryst. Struct. Commun.* **2002**, *58*, m8-m9.

15 J. G. Reynolds, A. Zalkin, D. H. Templeton, N. M. Edelstein, *Inorg. Chem.* **1977**, *16*, 1090-1096.

16 Q.-J. Pan, G. A. Shamov, G. Schreckenbach, *Chem. Eur. J.* **2010**, *16*, 2282-2290.

17 S. Fortier, T. W. Hayton, *Coord. Chem. Rev.* **2010**, *254*, 197-214.

18 J. L. Brown, G. Wu, T. W. Hayton, *J. Am. Chem. Soc.* **2010**, *132*, 7248-7249.

19 I. Korobkov, S. Gambarotta, G. P. A. Yap, *Angew. Chem., Int. Ed. Engl.* **2002**, *41*, 3433-3436.

20 T. Le Borgne, M. Lance, M. Nierlich, M. Ephritikhine, *J. Organomet. Chem.* **2000**, *598*, 313-317.

21 B. Kosog, H. S. La Pierre, F. W. Heinemann, S. T. Liddle, K. Meyer, *J. Am. Chem. Soc.* **2012**, *134*, 5284-5289.

22 R. G. Denning, *J. Phys. Chem. A* **2007**, *111*, 4125-4143.

23 C. Villiers, P. Thuéry, M. Ephritikhine, *Angew. Chem., Int. Ed. Engl.* **2008**, *47*, 5892-5893.

24 G. Schreckenbach, P. J. Hay, R. L. Martin, *Inorg. Chem.* **1998**, *37*, 4442-4451.

25 D. L. Clark, S. D. Conradson, R. J. Donohoe, D. W. Keogh, D. E. Morris, P. D. Palmer, R. D. Rogers, C. D. Tait, *Inorg. Chem.* **1999**, *38*, 1456-1466.

26 G. A. Shamov, G. Schreckenbach, *J. Am. Chem. Soc.* **2008**, *130*, 13735-13744.

27 M. Bühl, G. Schreckenbach, *Inorg. Chem.* **2010**, *49*, 3821-3827.

28 J. I. Dulebohn, T. C. Stamatakos, D. L. Ward, D. G. Nocera, *Polyhedron* **1991**, *10*, 2813-2820.

29 B. Cordero, V. Gomez, A. E. Platero-Prats, M. Reves, J. Echeverria, E. Cremades, F. Barragan, S. Alvarez, *Dalton Trans.* **2008**, 2832-2838.

30 L. Gagliardi, B. O. Roos, *Nature* **2005**, *433*, 848-851.

31 N. M. Edelstein, G. H. Lander, in *The Chemistry of the Actinide and Transactinide Elements, Vol. 4*, 3 ed. (Eds.: L. R. Morss, N. M. Edelstein, J. Fuger), Springer, **2006**, pp. 2241-2247.

32 C. R. Graves, P. Yang, S. A. Kozimor, A. E. Vaughn, D. L. Clark, S. D. Conradson, E. J. Schelter, B. L. Scott, J. D. Thompson, P. J. Hay, D. E. Morris, J. L. Kiplinger, *J. Am. Chem. Soc.* **2008**, *130*, 5272-5285.

33 G. Nocton, P. Horeglad, V. Vetere, J. Pécaut, L. Dubois, P. Maldivi, N. M. Edelstein, M. Mazzanti, *J. Am. Chem. Soc.* **2009**, *132*, 495-508.

34 J. D. Rinehart, T. D. Harris, S. A. Kozimor, B. M. Bartlett, J. R. Long, *Inorg. Chem.* **2009**, *48*, 3382-3395.

35 A. Yahia, P. L. Arnold, J. B. Love, L. Maron, *Chem. Commun.* **2009**, 2402-2404.

36 P. L. Arnold, J. B. Love, D. Patel, *Coord. Chem. Rev.* **2009**, *253*, 1973-1978.

37 J. M. Harrowfield, M. I. Ogden, B. W. Skelton, A. H. White, *Dalton Trans.* **2010**, *39*, 8313-8318.

38 L. Chatelain, V. Mougel, J. Pecaut, M. Mazzanti, *Chem. Sci.* **2012**, *3*, 1075-1079.

39 L. A. Seaman, D. D. Schnaars, G. Wu, T. W. Hayton, *Dalton Trans.* **2010**, *39*, 6635-6637.

40 J.-C. Berthet, G. Siffredi, P. Thuery, M. Ephritikhine, *Dalton Trans.* **2009**, 3478-3494.

41 D. E. Morris, *Inorg. Chem.* **2002**, *41*, 3542-3547.

42 F. G. Bordwell, J. A. Harrelson, A. V. Satish, *J. Org. Chem.* **1989**, *54*, 3101-3105.

43 F. G. Bordwell, X. Zhang, J. P. Cheng, *J. Org. Chem.* **1991**, *56*, 3216-3219.

44 P. Renaud, M. A. Fox, *J. Am. Chem. Soc.* **1988**, *110*, 5702-5705.

45 R. R. Fraser, T. S. Mansour, S. Savard, *J. Org. Chem.* **1985**, *50*, 3232-3234.

46 L. A. Seaman, P. Hrobárik, M. F. Schettini, S. Fortier, M. Kaupp, T. W. Hayton, *Angew. Chem., Int. Ed. Engl.* **2013**, DOI: 10.1002/anie.201301041.

Group one metal salts of binuclear uranium-oxo complexes

3.1 Introduction

In the previous chapter, the binuclear uranium(V) oxo complex $[(Me_3SiOUO)_2L]$ was presented, with detailed discussion of its *cis*/*trans* oxo arrangement of ligands, proximate uranium $5f_1$ centres and magnetic properties. Of particular interest was the chemical inertness of the molecule towards oxidation, hydrolysis or oxo-group exchange, a surprising feature considering its typically unstable uranium(V) oxidation states. In this chapter, the reduction chemistry of $[(Me_3SiOUO)_2L]$ is reported as a means of unlocking the reactivity of the silylated U_2O_4 "butterfly" core towards hydrolysis, oxidation and desilylation chemistry.

3.2 1 and 2e⁻ reductions of $[(Me_3SiOUO)_2(L)]$

3.2.1 Synthesis of $K[(Me_3SiOUO)_2(L)]$

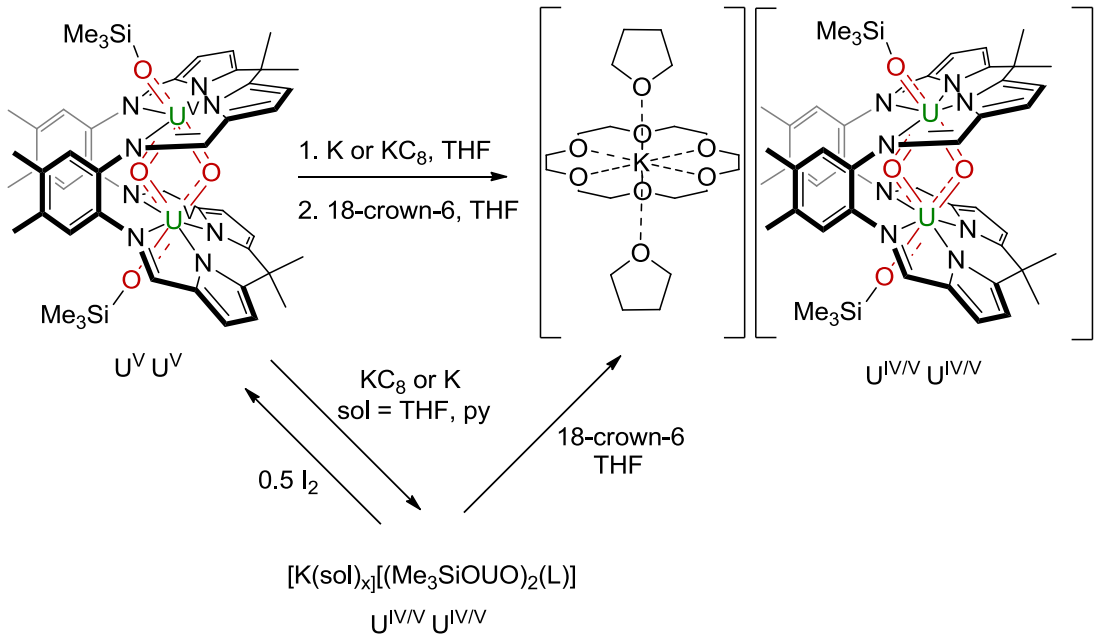

Scheme 1: Single-electron reduction of $[(Me_3SiOUO)_2(L)]$ with potassium to form $K[(Me_3SiOUO)_2(L)]$ complexes.

The reaction between the bimetallic uranium oxo complex $[(Me_3SiOUO)_2(L)]$ and a single equivalent of potassium graphite (KC_8) in THF formed immediately a brown solution of the singly reduced, anionic, mixed-valence U^{IV}/U^{V} salt $K[(Me_3SiOUO)_2(L)]$ (Scheme 1).

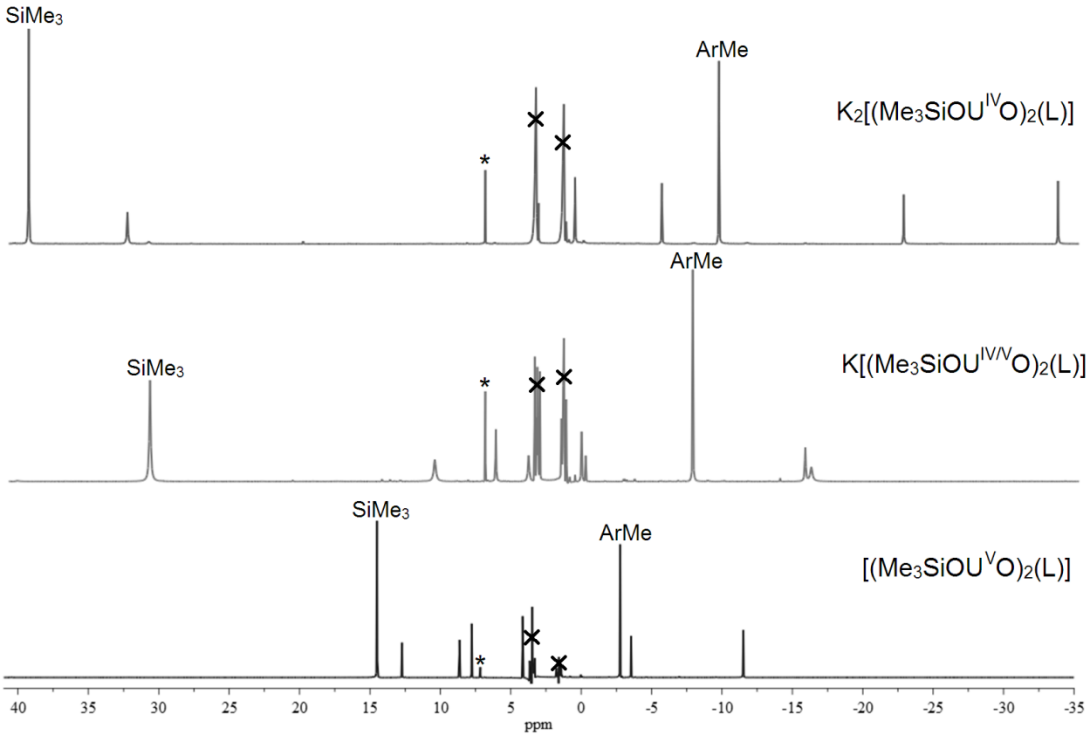

Figure 1: ^{1}H NMR spectra of [(Me$_3$SiOUO)$_2$(L)], K[(Me$_3$SiOUO)$_2$(L)] and K$_2$[(Me$_3$SiOUO)$_2$(L)] in 1:1 C$_6$D$_6$(*)-THF(x). Selected resonances highlighted.

The complex is visibly paramagnetic in the ^{1}H NMR spectrum which contains eight resonances between +31 and −16 ppm (Figure 1). Seven resonances are attributable to the macrocylic Pacman ligand, exactly the same number as is observed for [(Me$_3$SiOUO)$_2$(L)], which is consistent with the outer-sphere reduction of the parent complex proceeding with the complete retention of C_{2v} symmetry. In addition, the resonance at 31.0 ppm, which has an integral of 18 protons, confirms the *exo*-oxo bound SiMe$_3$ groups present in the parent complex are retained upon reduction. Although K[(Me$_3$SiOUO)$_2$(L)] is stable indefinitely in solution under anaerobic conditions, all attempts to isolate it in the solid state led to its decomposition. It was however further characterised in solution by UV-vis-NIR spectroscopy, with the spectrum exhibiting a series of new bands at 924, 1023, 1161, 1220, 1382 and 1676 nm that are significantly shifted in comparison to those of [(Me$_3$SiOUO)$_2$(L)]. In addition to the THF solvate, the K[(Me$_3$SiOUO)$_2$(L)] salt can also be prepared in pyridine, as well as from addition of one equivalent of potassium metal to boiling pyridine or THF solutions of [(Me$_3$SiOUO)$_2$(L)]. Furthermore, the reduction is completely reversible, with addition of 0.5 equivalents of I$_2$ to solutions of K[(Me$_3$SiOUO)$_2$(L)] reforming the U$^{V/V}$ complex alongside potassium iodide.

3.2.2 Synthesis of [K(18-crown-6)(THF)$_2$][(Me$_3$SiOUO)$_2$(L)]

The complex K[(Me$_3$SiOUO)$_2$(L)] was precipitated from solution by addition of one equivalent of 18-crown-6 to a THF solution of the product affording brown crystals of [K(18-crown-6)(THF)$_2$][(Me$_3$SiOUO)$_2$(L)] in 79 % yield.

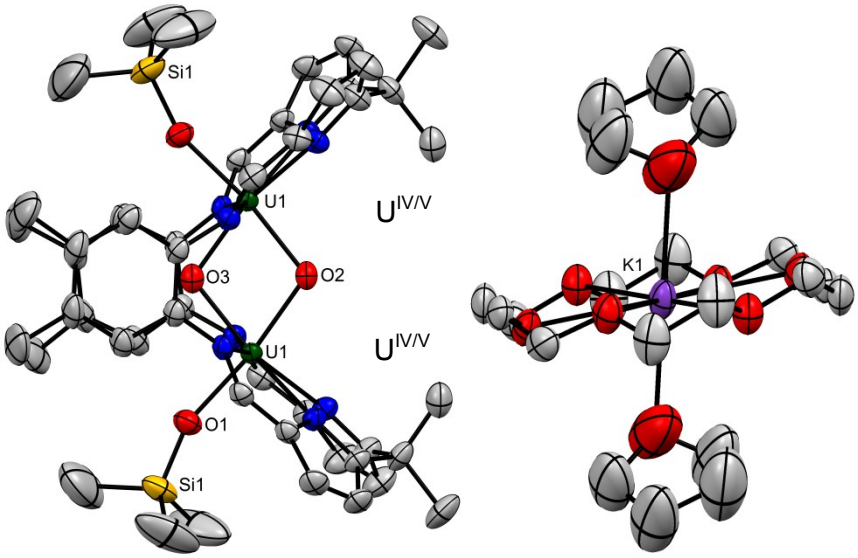

Figure 2: Solid state structure of [K(18-crown-6)(THF)$_2$][(Me$_3$SiOUO)$_2$(L)]. Ellipsoids are drawn at 50 % probability, H-atoms and solvent molecules omitted for clarity.

The solid state structure of the complex depicts the coordination of pentagonal bipyramidal uranium cations in each of the two N$_4$-donor pockets of the wedge-shaped macrocycle. Each uranium centre has a silylated oxo group (O1) perpendicular to the N$_4$-donor plane, exogenous to the macrocyclic cleft. In addition, two *endo*-bound oxo groups (O2 and O3) bridge the uranium centres forming the *cis/trans* oxo U$_2$O$_4$ "butterfly" geometry (Figure 2). The U1–O1, U1–O2 and U1–O3 bond lengths are similar (2.106(4), 2.117(3), and 2.123(3) Å respectively) and are elongated moderately with respect to those in the U^V/U^V parent complex [(Me$_3$SiOUO)$_2$(L)], which has an average U–O bond length of 2.09 Å. Lengthening of the uranium-oxygen bond distances is indicative of a lowering of U–O bond order, consistent with the reduction of the average uranium oxidation state. A further result of this bond elongation is an increase in the U1···U1' separation from 3.3557(4) Å in [(Me$_3$SiOUO)$_2$(L)] to 3.3932(1) Å in the singly reduced complex and a widening of the inter-cleft "bite" angle, defined as the angle subtended by the two N$_4$ donor planes of the Pacman macrocycle, from 77.4° in A to 79.7° upon reduction. The two uranium centres in [K(18-crown-6)(THF)$_2$][(Me$_3$SiOUO)$_2$(L)] are equivalent crystallographically, and cannot be assigned specific U^{IV} or U^V oxidation states. Further discussion regarding the extent of oxidation state mixing in the complex is made in section 3.5.

The magnetic susceptibility and computational studies on the parent $U^{V/V}$ complex $[(Me_3SiOUO)_2(L)]$ showed that strong antiferromagnetic coupling of the uranium f_1 centres occurs up to 17 K, facilitated by an exchange pathway through the endo-bridged U–O bonds.

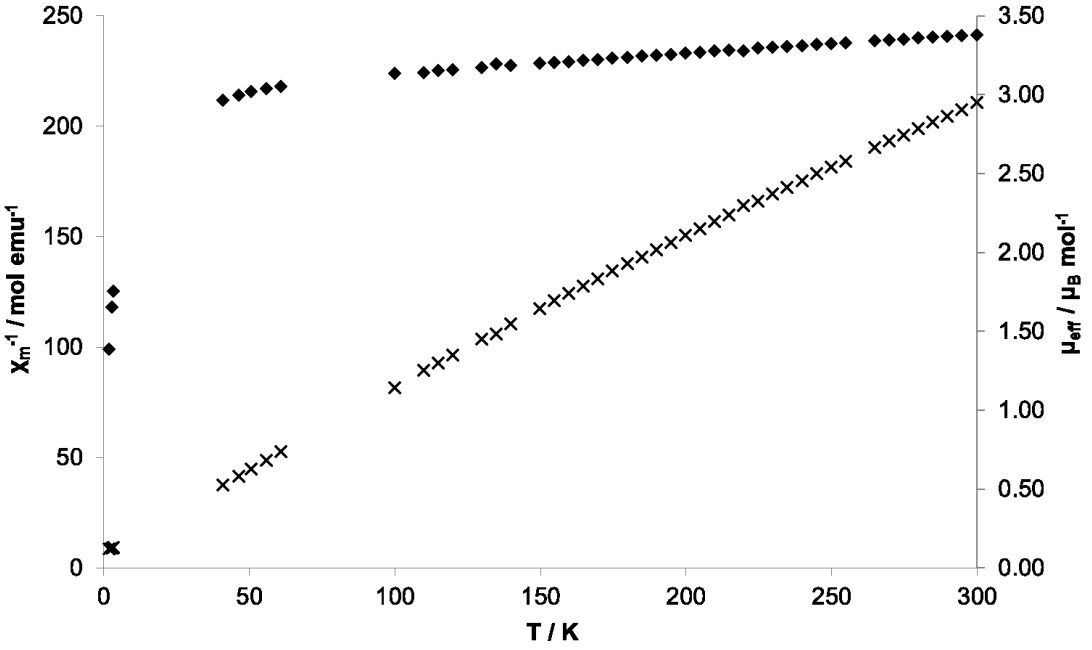

Figure 3: Temperature-dependent inverse magnetic susceptibility (crosses) and magnetic moment (diamonds) of $[K(18\text{-crown-6})(THF)_2][(Me_3SiOUO)_2(L)]$ in the range 2–300 K measured at 50000 Oe with field cooling.

In contrast to the $U^{V/V}$ complex however, magnetic susceptibility measurements of $[K(18\text{-crown-6})(THF)_2][(Me_3SiOUO)_2(L)]$ display no coupling as low as 2 K, an observation perhaps explained by the increased U··U separation coupled with an overall lowering of the uranium-oxygen bond order upon reduction (Figure 3). The size of the room temperature magnetic moment μ_{eff} is increased upon reduction from 1.57 to 2.94 B.M per U atom, fitted from the inverse magnetic susceptibility using Curie-Weis Law, indicative of the complex being a stronger paramagnet as is also suggested by the widening of the paramagnetic sweep width of the ^{1}H NMR spectrum from 27 (+15/–12) to 47 (+31/–16) ppm.

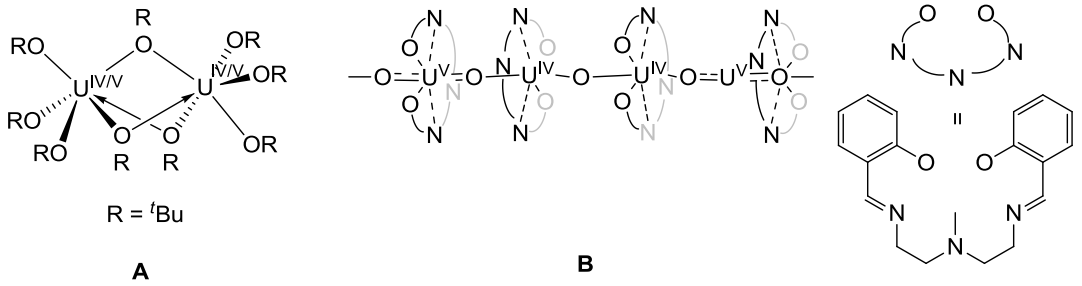

Figure 4: Other mixed valence uranium(IV/V) complexes.

Several other mixed-valence U^{IV}/U^{V} complexes of alkoxide,[1-2] calixpyrrole, [3] and Schiff-base ligands have been reported.[4] In addition, Mazzanti and co-workers have synthesized a number of poly-oxo clusters that also incorporate a mixture of uranium(IV) and uranium(V) centres.[5] Of all these examples, the only complex exhibiting identical coordination environments at each two uranium centre is the calixpyrrole complex $[K(dme)_4][\{(\mu_3\text{-}N)K(dme)_2U\}_2(\mu_4\text{-}\eta_5{:}\eta_3{:}\eta_2\text{-octamethylcalix(4)pyrrole})]_2$ (see Chapter Two, section 2.3.2). Others, such as $[\{U(O^tBu)_3\}_2(\mu\text{-}O^tBu)_3]$ (Figure 4, **A**), synthesised by Cotton and co-workers, contain uranium centres with the same connectivity but with asymmetric U-O bond lengths, suggestive of distinct uranium(IV) and uranium(V) centres.[1] The only complex showing yl-type U–O multiple bonding is the uranium(IV)/uranyl(V) coordination polymer $[\{UO_2(Mesaldien)\text{-}\{U(Mesaldien)\}_2(\mu\text{-}O)]$ (Figure 4, **B**). The complex, synthesised by Mazzanti and co-workers, is composed of chains of $[U^{V}O_2]^{+}$ cations linked by $U^{IV}(\mu\text{-}O)U^{IV}$ units, with the U–O bond distances in the uranyl species being considerably shorter (1.816 and 2.003 Å) than those for the uranium(IV)-bound oxo groups (2.198 and 2.085 Å).

3.2.3 Synthesis of $K_2[(Me_3SiOUO)_2(L)]$ complexes

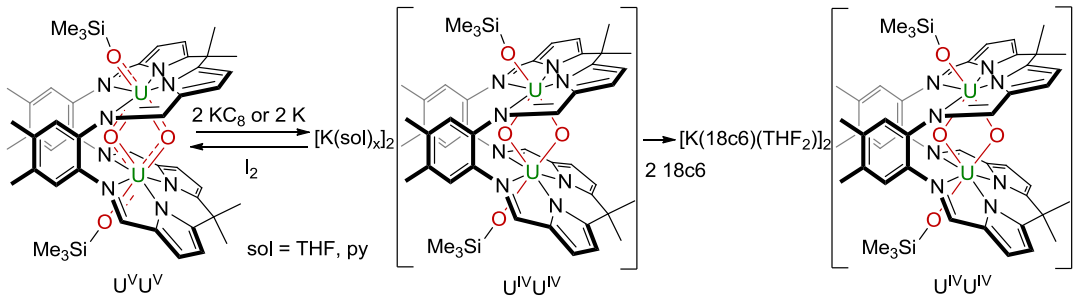

Scheme 2: Two-electron reduction of $[(Me_3SiOUO)_2(L)]$ with potassium to form $K_2[(Me_3SiOUO)_2(L)]$ complexes.

The reaction between $[(Me_3SiOUO)_2(L)]$ and two equivalents of potassium graphite or potassium metal in THF or pyridine cleanly generated the U^{IV}/U^{IV} salt $K_2[(Me_3SiOUO)_2(L)]$ in solution (Scheme 2). By analogy with mixed-valence species

$K[(Me_3SiOUO)_2(L)]$, the brown $U^{IV}U^{IV}$ complex retains its C_{2v} symmetry upon reduction, with seven ligand resonances displayed between the wider sweep width of +35 and −35 ppm in the ^1H NMR spectrum indicative of the formation of a more paramagnetic complex (Figure 1). The eighth resonance at 39.6 ppm, integrating to 18 protons, demonstrates that both of the $SiMe_3$ groups are retained upon reduction of both uranium centres. In analogy with the mixed-valence complex $K[(Me_3SiOUO)_2(L)]$, $K_2[(Me_3SiOUO)_2(L)]$ can be isolated in the solid state by treating a solution of the THF-solvate with two equivalents of 18-crown-6, yielding $[K(THF)_2(18\text{-crown-}6)]_2[(Me_3SiOUO)_2(L)]$ in 60 % yield. In contrast however, the growth of single crystals suitable for X-ray diffraction was not possible due to the extreme insolubility of the material, although its composition is supported by ^1H NMR and elemental analysis. The UV-vis-NIR spectrum of $K_2[(Me_3SiOUO)_2(L)]$ in THF shows several unique bands between 785–1677 nm that are shifted in comparison to both the $U^{V/V}$ and $U^{IV/V}$ complexes and is suggestive of the formation of a new complex. Like $K[(Me_3SiOUO)_2(L)]$, the binuclear uranium(IV) complexes can be re-oxidised back to the $[(Me_3SiOUO)_2(L)]$ parent complex by treatment with one equivalent of I_2, liberating potassium iodide.

3.3 Hydrolytic reactivity of $K[(Me_3SiOUO)_2(L)]$

In marked contrast to the U^V/U^V complex $[(Me_3SiOUO)_2(L)]$, which is extremely stable towards hydrolysis, the singly-reduced complex $K[(Me_3SiOUO)_2(L)]$ reacts readily with H_2O to form singly desilylated $U^{IV}U^V$ complexes without disproportionation.

3.3.1 Synthesis of $K[(Me_3SiO)U(\mu\text{-}OH)(OUO)(L)]$ complexes

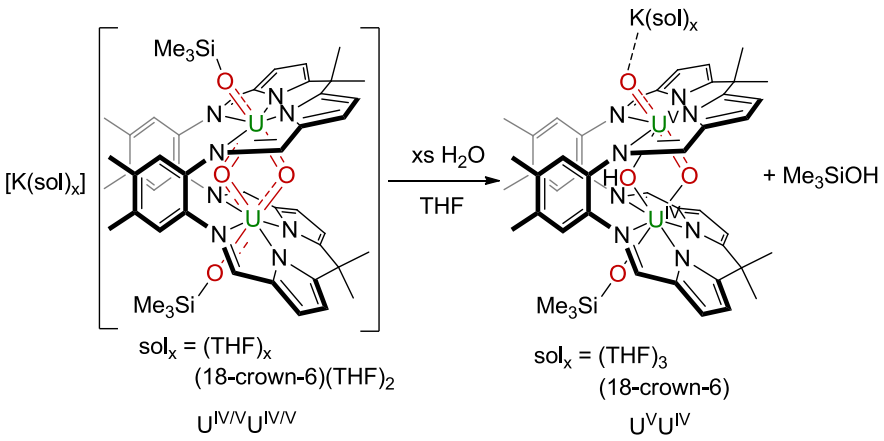

Scheme 3: Synthesis of $[K(sol)_x][(Me_3SiOU)(\mu\text{-}OH)(OUO)(L)]$ complexes.

The addition of excess H_2O (ca. 40 equivalents) to THF solutions of the $U^{IV/V}$ complexes $[K(THF)_x][(Me_3SiOUO)_2(L)]$ or $[K(18\text{-crown})(THF)_2][(Me_3SiOUO)_2(L)]$ results

in the clean formation a red solution of the mono-silylated, mono-hydroxyl compounds $[K(sol)_x][(Me_3SiOU)(\mu\text{-}OH)(OUO)(L)]$ (sol = 2 x THF or 18-crown-6) (Scheme 3). Significantly, no precipitation of material is observed on hydrolysis, a feature that is typically associated with uranyl(V) disproportionation reactions. Work-up of the products from THF or benzene solutions allows the isolation of the pure THF or 18-crown-6 solvates in 44 and 66 % yields respectively. Both compounds display almost identical ^{1}H NMR spectra, containing 15 resonances between +56 and −40 ppm, 14 of which are attributed to the Pacman ligand, and double the number observed for $K[(Me_3SiOUO)_2(L)]$, $K_2[(Me_3SiOUO)_2(L)]$ and $[(Me_3SiOUO)_2(L)]$. Such an increase in the number of resonances is indicative of a reduction of molecular symmetry from C_{2v} to C_s and is attributed to an asymmetric occupation of the two N_4 donor compartments. The presence of a single $SiMe_3$ resonance at ca. 55.1 ppm, with integrals equating to nine protons, confirms the loss of one oxo-bound $SiMe_3$ group upon hydrolysis. Monitoring either reaction by ^{1}H NMR spectroscopy reveals that the complexes $K[(Me_3SiOU)(\mu\text{-}OH)(OUO)(L)]$ are the only uranium-containing products and the occurrence of a single additional resonance at ca. 0 ppm integrating to nine protons, supports the formation of trimethylsilanol as the sole by-product.

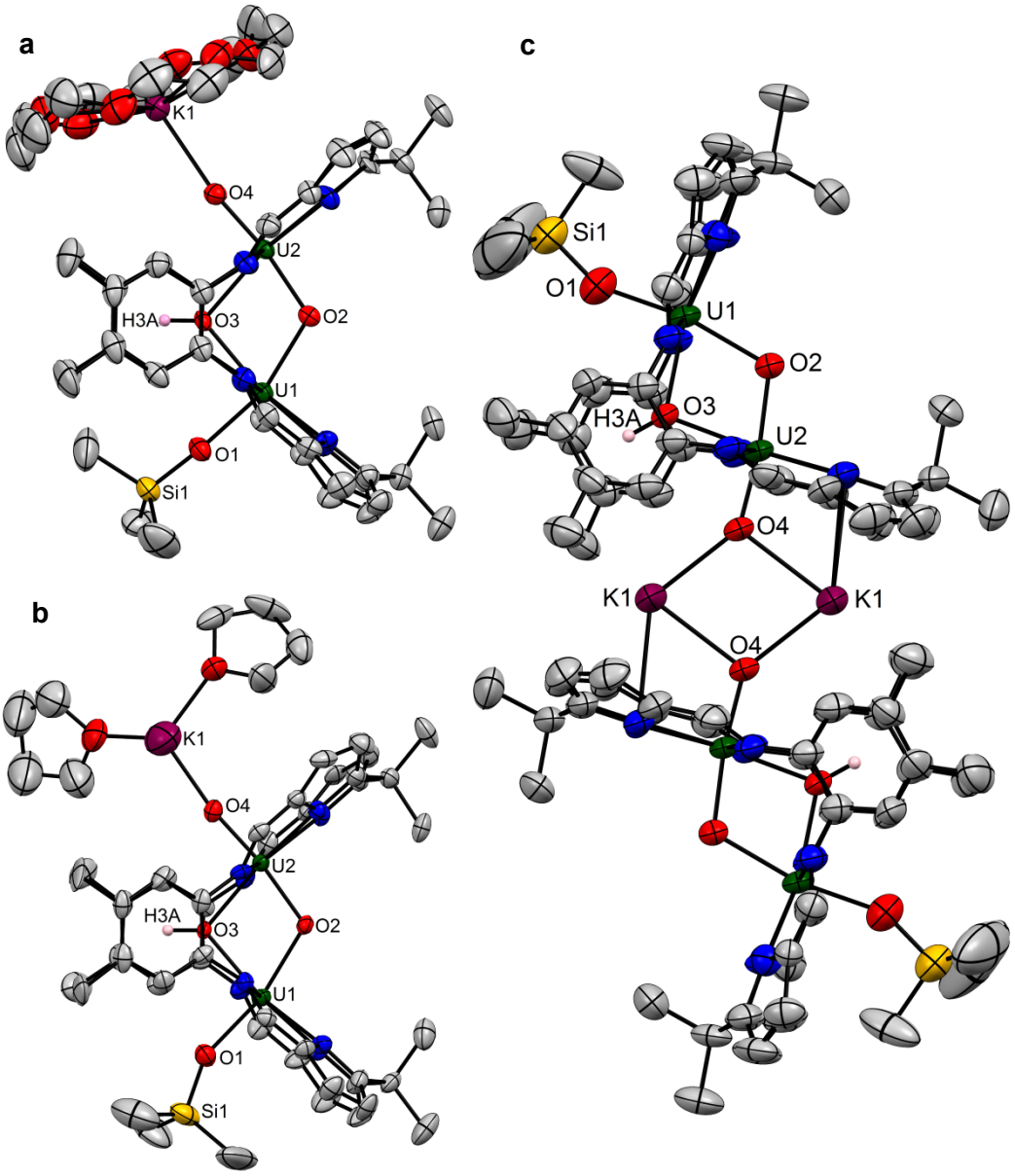

Figure 5: Solid state structures of three alternative K[(Me_3SiOU)(μ-OH)(OUO)(L)] solvates: **a** 18-crown-6 adduct, **b** monomeric THF-adduct and **c** dimeric THF-adduct. Ellipsoids are drawn at 50 % probability, and all free solvent molecules and selected H-atoms are omitted for clarity.

The solid-state structure of [K(18-crown-6)][(Me_3SiOU)(μ-OH)(OUO)(L)] was determined by single-crystal X-ray diffraction and depicts an asymmetric Pacman molecule with a single $SiMe_3$ group bound to an axial, exogenous oxo group with a Si1-O1 bond length of 1.628(4) Å (Figure 5, a). The potassium cation now forms a tight ion pair with the exo oxo group, with the K1–O4 bond distance of 2.683(4) Å. Analysis of the uranium-oxo bond distances allows the assignment of localized U^{IV} and U^{V} oxidation states, with the U2 dioxo group best classified as a singly reduced uranyl, $[UO_2]^+$. The sum of the six U–O bond

lengths of [K(18-crown-6)][(Me_3SiOU)(μ-OH)(OUO)(L)] confirms that no change in the average oxidation state has occurred, with the value lying within 0.1 Å of the sum for the $U(+4.5)_2$ complex [K(18-crown)$(THF)_2$][$(Me_3SiOUO)_2$(L)]. In contrast, however, to the symmetric $U^{IV/V}$ precursor, the U–O distances in the hydrolysed product have much greater variation. The U2–O4 (1.836(4) Å) and U2-O2 (1.993(4) Å) bonds are significantly shorter than the U1–O1 (2.106(4) Å) and U1–O2 (2.213(4) Å) distances in the parent $U^{IV/V}$ complex and are similar to those observed in the samarium-functionalized, dimeric uranyl (V) Pacman complex [$\{UO_2Sm(py)_2(L)\}_2$] (U–O distances of 1.890(5)and (1.941(5) Å)).[6]

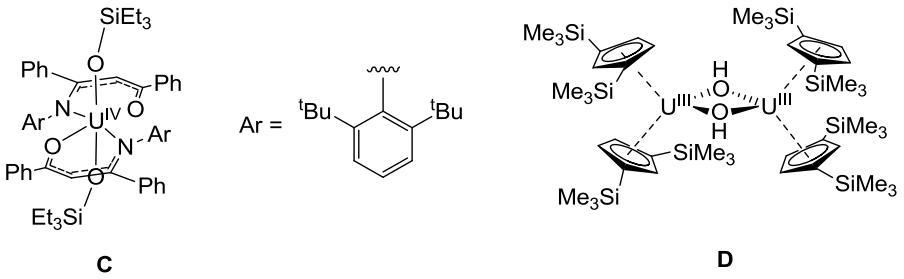

Figure 6: A uranium(IV) with silylated oxo groups (**C**) and a binuclear uranium complex containing hydroxide bridging groups (**D**).

The U^{IV} cation U1 in [K(18-crown-6)][(Me_3SiOU)(μ-OH)(OUO)(L)] has a U1-O1 bond length of 2.106(4), which is similar to that of 2.129(2) Å in the U^{IV} siloxide complex [$U(OSiEt_3)_2(^{Ar}acnac)_2$] (^{Ar}acnac = (3,5-$tBu_2C_6H_3$)NC(Ph)CHC(Ph)O)) (Figure 6, **C**).[7] As in [$(Me_3SiOUO)_2$(L)] and K[$(Me_3SiOUO)_2$(L)], the *trans-endo* oxo O2 bridges the two uranium centres, but no longer in a symmetrical fashion, while the *cis-endo* oxygen O3, is now protonated as a bridging hydroxide. Protonation of O3 is evident as the U1–O3 bond length of 2.316(4) Å is significantly longer than the U2–O2 bond length of 2.213(4) Å, and is similar to that seen in other U^{IV} hydroxide complexes, for example 2.295(3) and 2.299(3) Å for the two U–O bond lengths in the U^{IV}/U^{IV} metallocene hydroxide [$Cp"_2U(\mu\text{-}OH)]_2$ (Cp" = 1,3-$(Me_3Si)_2C_5H_3$) (Figure 6, **D**).[8] This unambiguous structural assignment of individual uranium oxidation states contrasts with [$(Me_3SiOUO)_2$(L)] and [K(18-crown-6)$(THF)_2$][$(Me_3SiOUO)_2$(L)] which both exhibit symmetric "butterfly" structures with much lower variation in U-O bond lengths.

The solid state structure of the THF-solvated analogue [$K(THF)_2$][(Me_3SiOU)(μ-OH)(OUO)(L)] was also determined by X-ray crystallography and was found to be almost identical to the 18-crown-6 solvate, displaying exactly the same [(Me_3SiOU)(μ-OH)(OUO)(L)]$^-$ anion weakly associated to a potassium cation which is alternatively solvated by two THF molecules (Figure 5, b). The potassium coordination sphere is

completed by intermolecular π-interactions between the cation and the η^2-donating pyrrole of an adjacent Pacman molecule. The THF-complex was also crystallised in an alternative, dimeric form $\{[K(THF)][(Me_3SiOU)(\mu\text{-}OH)(OUO)(L)]\}_2$ from different crystallisation conditions, with the now singly-THF-solvated potassium cation bridging between two uranyl(V) oxo groups (Figure 5, c). In this alternative structure, the O1-K1 bond distances are again extremely long (2.55(1) and 2.685(9) Å), indicative of electrostatic bonding between the uranyl oxo groups and the potassium cation. The weak O-K bonding indicates that the oligomeric structure is not maintained in solution, perhaps explaining the high solubility of the $K[(Me_3SiOU)(\mu\text{-}OH)(OUO)(L)]$ complexes.

Both the THF and 18-crown-6 solvates of $K[(Me_3SiOU)(\mu\text{-}OH)(OUO)(L)]$ display similar bands in their infrared spectra at 841 and 837 cm^{-1} respectively, assigned as the asymmetric uranyl stretching mode and characteristically weakened in comparison to uranyl (VI) (912 cm^{-1}).[9]

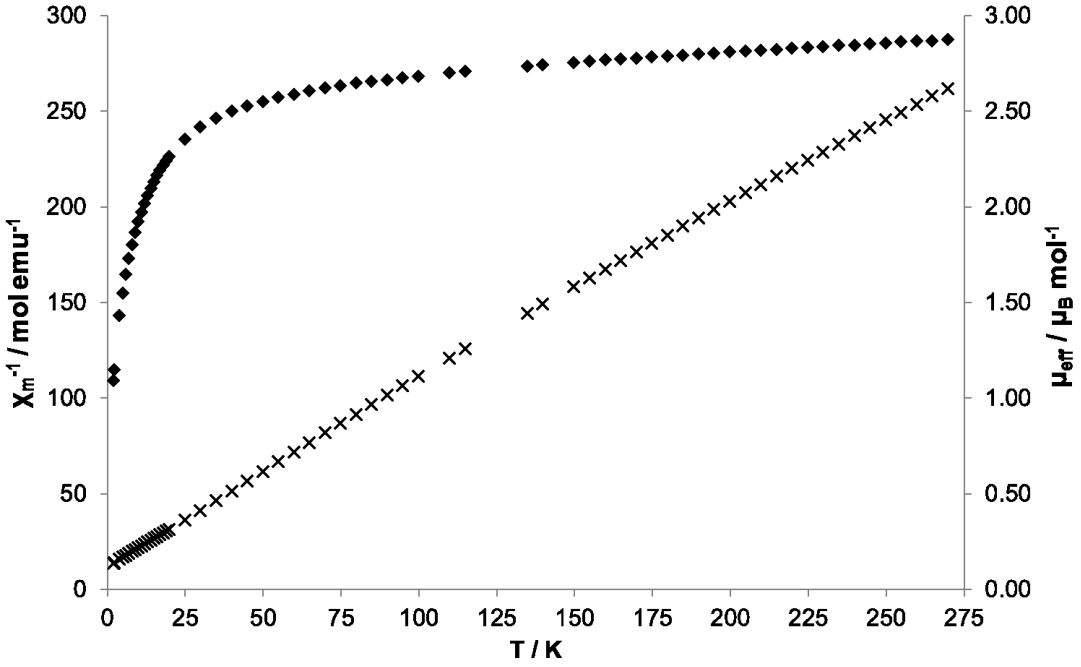

Figure 7: Temperature-dependent inverse magnetic susceptibility (crosses) and magnetic moment (diamonds) of $[K(18\text{-crown-6})][(Me_3SiOU)(\mu\text{-}OH)(OUO)(L)]$ in the range 2–275 K measured at 50000 Oe with field cooling.

Magnetic susceptibility measurements of $[K(18\text{-crown-6})][(Me_3SiOU)(\mu\text{-}OH)(OUO)(L)]$ display no coupling as low as 2 K, analogous behaviour to that of the precursor $[K(18\text{-crown-6})][(Me_3SiOUO)_2(L)]$ (Figure 7). The size of the room temperature magnetic moment of $[K(18\text{-crown-6})][(Me_3SiOU)(\mu\text{-}OH)(OUO)(L)]$ is also comparable to

that of the previous complex with a μ_{eff} value of 2.03 B.M per U atom in comparison to 2.94 B.M in the latter complex.

3.3.2 Synthesis of $[C_5H_5NH][(Me_3SiOUO)_2(L)]$

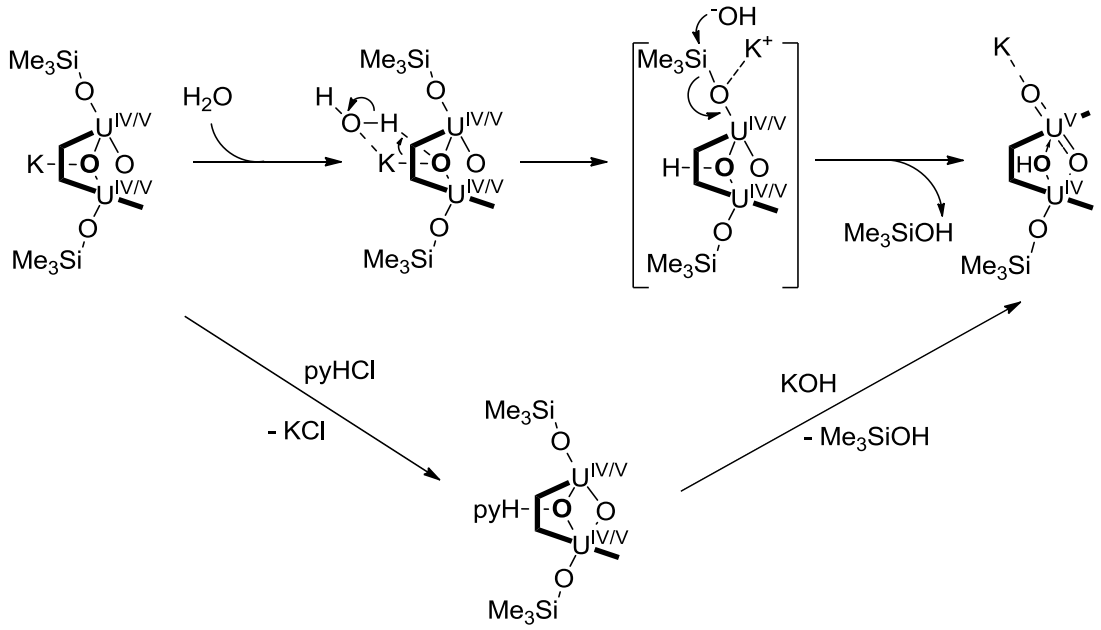

Scheme 4: Synthesis of $[C_5H_5NH][(Me_3SiOUO)_2(L)]$ as a possible intermediate to the formation of K[(Me$_3$SiOU)(μ-OH)(OUO)(L)]. Atom O3 is highlighted in bold.

The facile desilylation of $K[(Me_3SiOUO)_2(L)]$ upon reaction with water prompted further investigation into its reactivity towards other Brønsted acids. While the reaction of either the THF or 18-crown-6 adducts of the complex with stoichiometric HCl in diethyl ether lead only to the formation of intractable materials, the addition of one equivalent of pyridinium chloride to a pyridine solution of $[K(py)_x][(Me_3SiOUO)_2(L)]$ resulted in the instant precipitation a red solid; the cation-exchanged, mixed valence, $U^{IV/V}$ pyridinium salt $[C_5H_5NH][(Me_3SiOUO)_2(L)]$ in high yield (Scheme 4). Heating the mixture to 120 °C caused full dissolution of all solids allowing spectroscopic characterisation and crystallisation. The ^{1}H NMR spectrum of $[C_5H_5NH][(Me_3SiOUO)_2(L)]$ displays eight resonances between +32 to −17 ppm shifted slightly in comparison to those of $K[(Me_3SiOUO)_2(L)]$ providing strong evidence that the $(Me_3SiOUO)_2$ motif is retained.

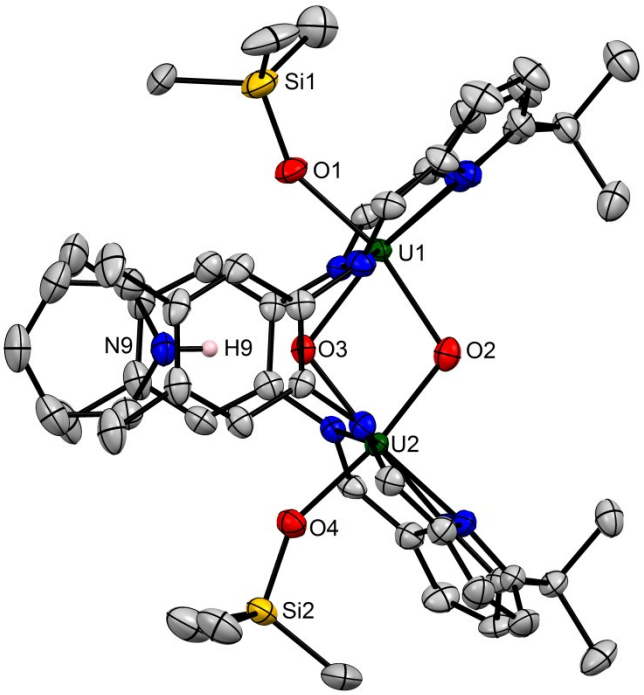

Figure 8: Solid state structure of $[C_5H_5NH][(Me_3SiOUO)_2(L)]$. Ellipsoids are drawn at 50 % probability, selected H-atoms and all free solvent molecules omitted for clarity.

The solid state structure of the complex confirms the presence of the $[(Me_3SiOUO)_2(L)]^-$ anion, which adopts the same wedge-shaped, diuranium, oxo-bridged butterfly structure seen in $[K(18\text{-crown-6})(THF)_2][(Me_3SiOUO)_2(L)]$ and $[(Me_3SiOUO)_2(L)]$ (Figure 8). The average U–O bond distance of 2.13 Å is almost identical to that observed in the potassium salt precursor (2.12 Å) and supports the assignment of an average uranium oxidation state of +4.5. In contrast to $[K(18\text{-crown-6})(THF)_2][(Me_3SiOUO)_2(L)]$ however, the charge balance in $[C_5H_5NH][(Me_3SiOUO)_2(L)]$ is maintained by the presence of a pyridinium cation which is located between the two aryl spacers of the macrocyclic framework with the nitrogen atom of the pyridine ring (N9) lying 2.53 Å away from the *cis*-bound bridging oxygen atom O3. Examination of the difference Fourier map reveals electron density consistent with a hydrogen situated along the hydrogen-bonding vector, 0.87 Å from N9 and 1.68 Å from O3, i.e. formally localised on the pyridine rather than the bridging oxygen, and validating the assignment of the complex as a pyridinium salt of $[(Me_3SiOUO)_2(L)]^-$ rather than a neutral, protonated complex with a hydrogen-bonded, proximal pyridine. In addition to these data, the IR spectrum of $[C_5H_5NH][(Me_3SiOUO)_2(L)]$ is almost identical to that of the potassium salt**,** with bands at 835, 764, 727 and 625 cm^{-1} all characteristic of the singly reduced $[(Me_3SiOUO)_2(L)]^-$ anion.

3.3.3 Mechanism of K[(Me$_3$SiOUO)$_2$(L)] hydrolysis

Although the mechanism of hydrolysis of K[(Me$_3$SiOUO)$_2$(L)] to form K[(Me$_3$SiOU)(μ-OH)(OUO)(L)] was not probed directly, the oxo-protonated complex [C$_5$H$_5$NH][(Me$_3$SiOUO)$_2$(L)] may be considered as an intermediate of the transformation (Scheme 5). The reaction of a suspension of [C$_5$H$_5$NH][(Me$_3$SiOUO)$_2$(L)] with one equivalent of KOH in pyridine yields the pyridine solvate of K[(Me$_3$SiOU)(μ-OH)(OUO)(L)] and trimethylsilanol as the only products observable by ^{1}H NMR spectroscopy after 10 min. It is possible that a similar reaction occurs upon direct hydrolysis of K[(Me$_3$SiOUO)$_2$(L)], with protonation of the rear-bridging oxo-group and formation of potassium hydroxide followed by a nucleophilic substitution by hydroxide on the oxo-bound silyl substituent and reformation of a uranyl(V) cation (Scheme 4). Such a mechanism could be used to explain why it is not possible to form a doubly desilylated complex by addition of excess water, as a second hydrolysis step would require protonation of the uranyl oxo atom O3, presumed to be a much weaker base due to its engagement in a stable Lewis pair with the potassium cation K1.

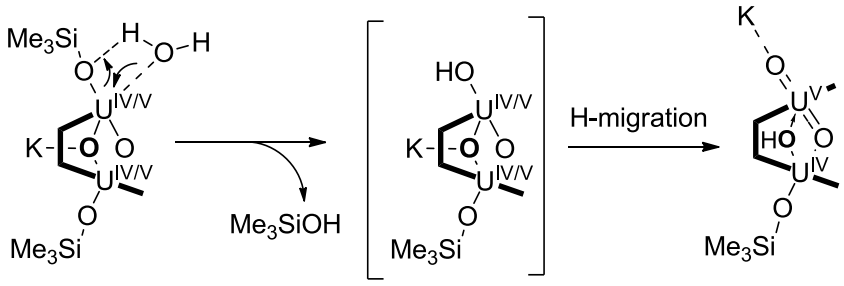

Scheme 5: Alternative mechanism for the hydrolytic abstraction of SiMe$_3$. O3 is highlighted.

An alternative mechanism is also proposed, whereby the pyridinium cation is simply deprotonated by KOH, forming H$_2$O and a K[(Me$_3$SiOUO)$_2$(L)] salt as the starting materials required for the one-step hydrolysis reaction. For this case, the subsequent desilylation reaction would occur by direct attack on the oxo-bound silyl group group by water, either by protonolysis of the U–O or O–SiMe bonds, resulting in an axially-bound OH group which migrates to the bridging *cis*-position to form K[(Me$_3$SiOU)(μ-OH)(OUO)(L)] (Scheme 5). Although no evidence in support of either mechanism has been found, the former mechanism is perhaps more favourable due to both the greater nucleophilicty of KOH than H$_2$O and the presumed lower stability of the axially-bound [OU^{V}OH] *vs* a μ-OH complex towards proton-induced uranyl(V) disproportionation.

3.3.4 KX-induced disproportionation of $[(Me_3SiOUO)_2(L)]$

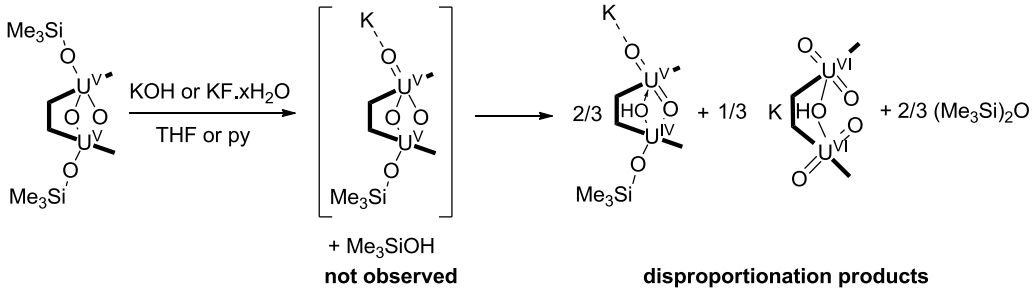

Scheme 6: Desilylation of $[(Me_3SiOUO)_2(L)]$ with KOH inducing disproportionation.

The postulate that *in situ* generated potassium hydroxide, rather than water, acts as the desilylating reagent in forming $K[(Me_3SiOU)(\mu\text{-}OH)(OUO)(L)]$ from $[(Me_3SiOUO)_2(L)]$ lead to investigation as to whether the neutral uranium(V) precursor $[(Me_3SiOUO)_2L]$, which does not react with water, could be desilylated using the same reagent. The reaction of $[(Me_3SiOUO)_2L]$ with one equivalent of potassium hydroxide does not however result in the anticipated formation a mono-silylated bis-uranium(V) complex, with the expected product instead undergoing a proton-induced disproportionation to the U^{IV}/U^{V} product $K[(Me_3SiOU)(\mu\text{-}OH)(OUO)(L)]$ and a bimetallic uranyl(VI) complex (Scheme 6).

The 7 resonances in the ^{1}H NMR spectrum corresponding to the new product lie between 1–9 ppm, suggestive of formation of a diamagnetic bis-uranium(VI) Pacman complex with C_{2v} symmetry, with integrations revealing a 2:1 ratio between the $U^{IV}U^{V}$ and $U^{VI}U^{VI}$ products. Summation of the integrals of the $SiMe_3$ resonances of $[K(THF)_2][(Me_3SiOU)(\mu\text{-}OH)(OUO)(L)]$ and $(Me_3Si)_2O$, present in a 1:2 ratio, reveal all the silyl groups from the starting material are accounted for, with the balanced equation indicating a $[KOH][(UO_2)_2(L)]$ formula for the unidentified product. Although no further purification of the mixture was achieved, a number of binuclear uranyl(VI) complexes have been characterised with various bridging ligands (see Chapters two, four and five), with the complex $K_2[(UO_2)_2(\mu\text{-}\kappa^2\text{-}\kappa^2\text{-}O_2)(L)]$ exhibiting an almost identical ^{1}H-NMR spectrum to that of the unidentified product, allowing tentative assignment of the structure of the uranium(VI) product as the hydroxide-bridged, binuclear uranyl(VI) complex $K[(UO_2)_2(\mu\text{-}OH)(L)]$.

The same disproportionation reaction was induced by boiling a mixture of $[(Me_3SiOUO)_2(L)]$ and wet KF in pyridine for 4 days which, upon subsequent addition of 18-crown-6, produced a mixture of $[K(THF)_2(18\text{-crown-}6)][(Me_3SiOU)(\mu\text{-}OH)(OUO)(L)]$ and a binuclear uranyl(VI) product tentatively assigned as $K[(UO_2)_2(\mu\text{-}F)(L)]$ by ^{1}H NMR spectroscopy. Further evidence for the formation of the $U^{IV}U^{V}$ complex was achieved by X-ray analysis of single crystals of the product precipitating out of the crude mixture after one

week. Repetition of the reaction using KF that had been dried rigorously at 275 °C at 10^{-6} Torr resulted in no reaction, suggesting both water and K^+ are both required to induce the disproportionation.

Attempts to use ^{t}BuOH as an alternative protonolysis regent to prepare either K[(Me_3SiOU)(μ-OH)(OUO)(L)] or the hypothetical alkoxide-bridged complex K[(Me_3SiOU)(μ-O^{t}Bu)(OUO)(L)] were unsuccessful.

3.4 Reactivity of K_2[($Me_3SiOUO)_2$(L)]

The contrasting transformations of K[($Me_3SiOUO)_2$(L)] to either K[(Me_3SiOU)(μ-OH)(OUO)(L)] or [C_5H_5NH][($Me_3SiOUO)_2$(L)] depending on the nature of Brønsted acid represent the first formation of uranyl(V) species by protonolysis of a uranium oxo precursor which occurs without any net redox or disproportionation chemistry taking place. The mixed-valence complexes K[(Me_3SiOU)(μ-OH)(OUO)(L)] fail to undergo any further reaction with water, even at elevated temperatures, despite the well-documented instability of uranyl (V) complexes in aqueous disproportionation processes. [10-11] Although a number of stable complexes have been isolated previously from the hydrolysis of isolated uranyl (V) compounds, these result exclusively from disproportionation rather than being the products of ligand exchange alone.[4, 12] In light of the comparative stability of the U^V unit in K[(Me_3SiOU)(μ-OH)(OUO)(L)], and the reactivity of the U^{IV} centre in K[($Me_3SiOUO)_2$(L)] towards desilylation and protonolysis, the chemistry of the doubly-reduced $U^{IV/IV}$ complex K_2[($Me_3SiOUO)_2$(L)] was investigated.

3.4.1 Synthesis of [$K(THF)_2$][($Me_3SiOU)_2$(μ-O)(μ-OH)]

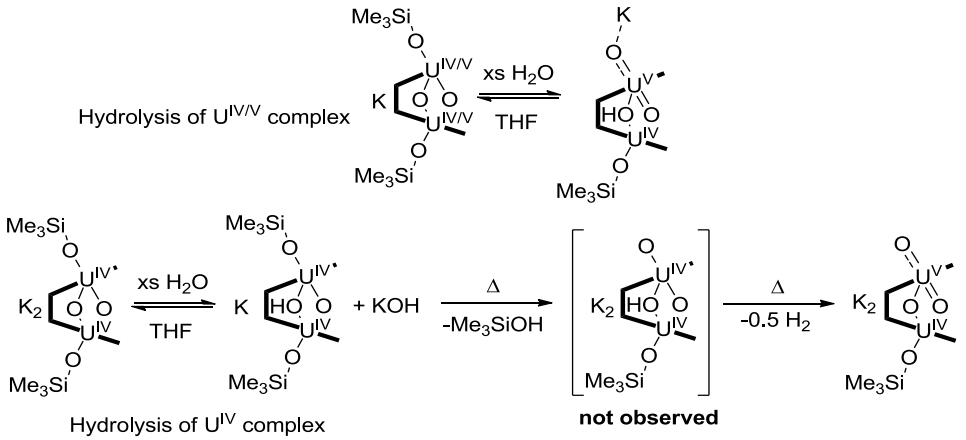

Scheme 7: Protonation of K_2[($Me_3SiOU^{IV}O)_2$(L)] oxo groups to form [$K(THF)_2$][(Me_3SiOU^{IV})$_2$(μ-O)(μ-OH)] and KOH and its thermally-induced oxidation to K_2[(Me_3SiOUO)(OUO)(L)]. Hydrolysis of K[($Me_3SiOU^{IV/V}O)_2$(L)] shown for comparison.

In contrast to the reactivity shown by $K[(Me_3SiOU^{IV/V}O)_2(L)]$, reaction of $K_2[(Me_3SiOU^{IV}O)_2(L)]$ with an excess of water in THF did not result in desilylation at room temperature, with the reaction mixture virtually unchanged after 6 h. Boiling the reaction mixture for 24 h resulted in the formation of the brown protonated complex $[K(THF)_2][(Me_3SiOU^{IV})_2(\mu\text{-}O)(\mu\text{-}OH)]$ in 60 % yield and a grey precipitate from which it was isolated by filtration (Scheme 7).

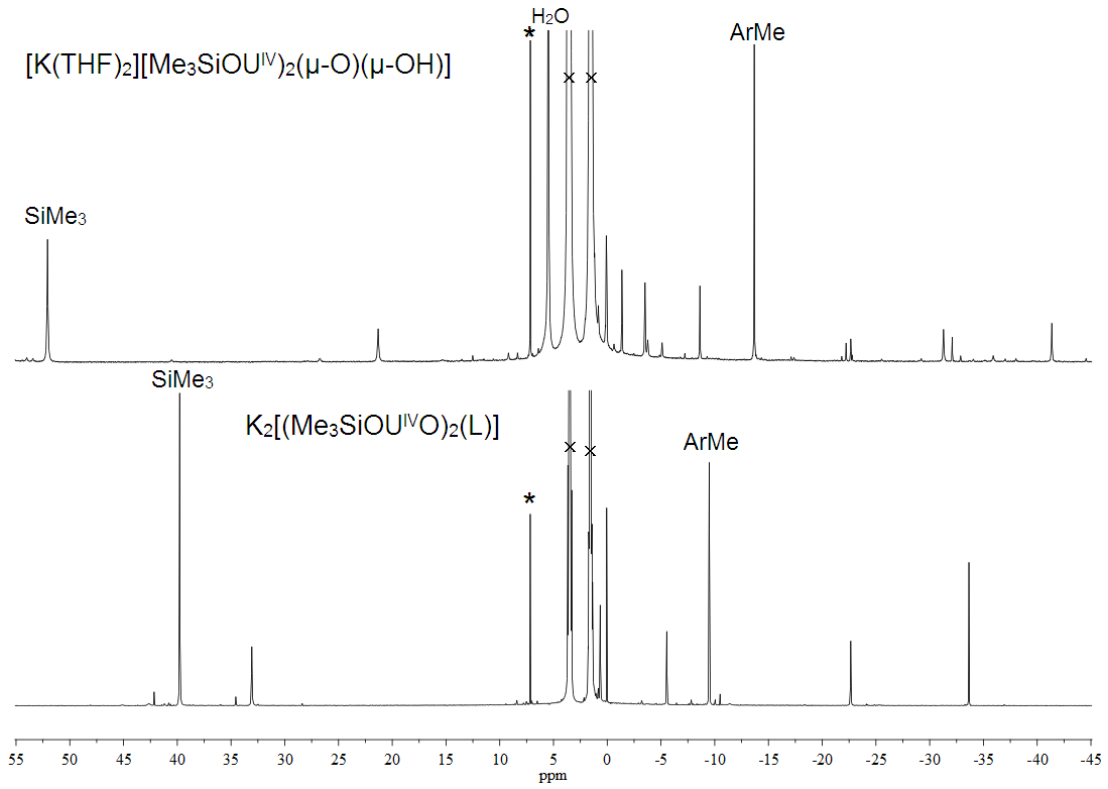

Figure 9: ^{1}H NMR spectra showing the conversion of $K_2[(Me_3SiOUO)_2(L)]$ (bottom) to $K[(Me_3SiOU)_2(\mu\text{-}O)(\mu\text{-}OH)]$ (top) in 1:1 C_6D_6(*)-THF(x). Selected resonances highlighted.

The complex exhibits the same 8 resonances in the ^{1}H NMR spectrum as $K_2[(Me_3SiOUO)_2(L)]$ between 52 and -41 ppm, with the wide sweep width suggestive of preservation of the uranium(IV) oxidation states (Figure 9). Evidence for the retention of the two oxo-bound $SiMe_3$ groups is given by the resonance at 52 ppm, which has an integral of 18 protons that is equal to that in the starting material. From these data, it is evident that the core $[(Me_3SiOUO)_2(L)]^{2-}$ unit is retained, with the formation of the precipitate, presumed to be potassium hydroxide, evidence that protonation of the basic μ-oxo groups has occurred. Although no crystals of $[K(THF)_2][(Me_3SiOU)_2(\mu\text{-}O)(\mu\text{-}OH)]$ suitable for X-ray diffraction could be grown, its composition is supported by ^{1}H NMR spectroscopy and elemental analysis.

3.4.2 Synthesis of $K_2[(Me_3SiOUO)(OUO)(L)]$

Boiling a solution of $K_2[(Me_3SiOUO)_2(L)]$ and a single equivalent of water for an extended period (72 h) resulted in the clean formation of the mono-silylated U^{IV}/U^{V} complex $K_2[(Me_3SiOUO)(OUO)(L)]$ as an insoluble, red crystalline solid in 52 % yield (Scheme 7). Although poorly soluble in its parent solvent, the complex dissolves readily in d_5-pyridine, and exhibits 15 resonances in the ^{1}H NMR spectrum between 27 and -24 ppm, the same number observed for the mono-silylated products $K[(Me_3SiOU)(\mu\text{-}OH)(OUO)(L)]$ and is indicative of the formation of a C_s symmetric product with non-symmetric upper and lower N_4-binding pockets. Additionally, the resonance at 27.0 ppm, attributed to the oxo-bound $SiMe_3$ group, has an integral of 9, rather than 18 protons, further supporting the assignment of the product as a mono-silylated complex. The formation of Me_3SiOH as a by-product of the formation of $K_2[(Me_3SiOUO)(OUO)(L)]$, evidenced by ^{1}H NMR spectroscopy, further validates the postulate that desilylation of $K_2[(Me_3SiOUO)_2(L)]$ upon addition of water has occurred, albeit requiring much more forcing conditions than the analogous desilylation of $K[(Me_3SiOUO)_2(L)]$. In contrast to $K[(Me_3SiOU)(\mu\text{-}OH)(OUO)(L)]$ however, no OH stretch is present in the infrared spectrum.

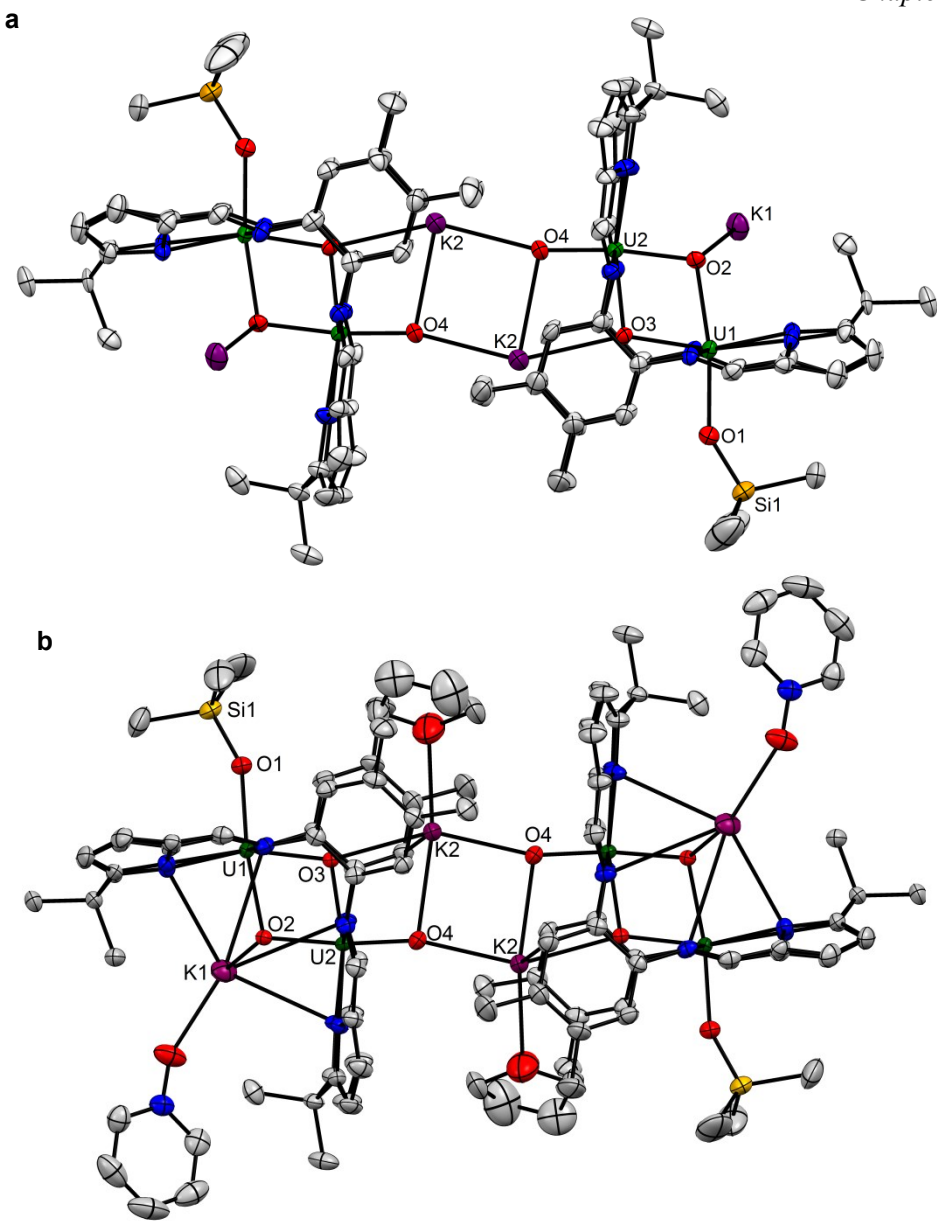

Figure 10: The X-ray crystal structures of $[K(sol)]_2[(Me_3SiOUO)(OUO)(L)\}]$. **a** THF solvate, donor solvates omitted for clarity. **b** THF/pyridine-*N*-oxide solvate. All hydrogen atoms and free solvent molecules are omitted for clarity; ellipsoids are drawn at 50 % probability.

Analysis of the solid state structure of $K_2[(Me_3SiOUO)(OUO)(L)]$ reveals there to be a very similar U_2O_4 core to that observed in $K[(Me_3SiOU)(\mu\text{-}OH)(OUO)(L)]$ with an average U-O bond length of 2.10 Å indicative of an average uranium oxidation state of 4.5 (Figure 10, a). In addition, these data reveal oxidation state localisation similar to that in protonated complexes, with the oxo-silylated U1, displaying long U–O bonds of 2.142(6), 2.246(5) and 2.144(4) Å that are representative of a U^{IV} oxidation state and the un-functionalized U2 depicting two shorter U–O bonds to the mutually *trans* oxygen atoms O2 (2.020(4) Å) and O4 (1.875(5) Å) with a longer bond of 2.146(5) Å to the *cis* bridging O3.

The much shorter U–O bonds to O3 than observed in K[(Me_3SiOU)(μ-OH)(OUO)(L)], as well as the absence of a proximal hydrogen bond donor, endorses the NMR and IR evidence that O3 is an oxo, rather than hydroxyl, bridge. The average uranium oxidation state of 4.5 in K_2[(Me_3SiOUO)(OUO)(L)] is maintained by the presence of two potassium cations instead of one potassium cation and one proton in the previous complexes. In analogy with K[(Me_3SiOU)(μ-OH)(OUO)(L)], the structure of K_2[(Me_3SiOUO)(OUO)(L)] contains one *exo*-potassium K2, which bridges between the *exo* oxo O4 and the *endo*-*cis* oxo O3. The structure forms a metal-polyoxo ladder, with the U_2O_2 diamond present in each Pacman molecule linked by a central K_2O_2 unit with six successive M–O rungs. The structure is maintained by each K2 atom binding the *exo* oxo atom O4' from an adjacent molecule, resulting in a crystallographic dimer maintained by each μ_3-bridging potassium cation.

The second potassium cation, K1, does not participate in the ladder structure, being bound to the *endo* oxo O2, further emphasising the enhanced Lewis base character of the uranyl(V) O4–U2–O2 unit. The presence of a uranyl (V) cation in K_2[(Me_3SiOUO)(OUO)(L)] is additionally supported by the characteristic stretching frequency at 837 cm^{-1} in the IR spectrum and similar to those seen for K[(Me_3SiOU)(μ-OH)(OUO)(L)].

Although a number of polyoxometalate uranium structures are present in the literature, the majority of these feature bridging hydroxide, rather than oxide ligands, such as uranium(IV) polyhydroxide clusters resulting from uranyl(V) disproportionation.[12] Those featuring purely oxide ligands limited to a few examples,[5, 13-15] such as the uranium(IV) oxide cluster [$U^{IV}O_8I_8(py)_{10}$] **E** synthesised by Berthet and co-workers from the redox reaction between two equivalents of [$U^{IV}(COT)_2$] and four equivalents of [$U^{VI}O_2I_2(THF)_3$].[14]

3.5 Absorption spectra of mixed valence complexes

Despite the variation in structure, the three classes of mixed valence $U^{IV/V}$ complexes K[($Me_3SiOUO)_2$(L)], K[(Me_3SiOU)(μ-OH)(OUO)(L)] and K_2[(Me_3SiOUO)(OUO)(L)] exhibit similar UV-vis-NIR absorption spectra allowing a characteristic set of absorptions specific to the mixed-valence Pacman complexes to be identified (Figure 11).

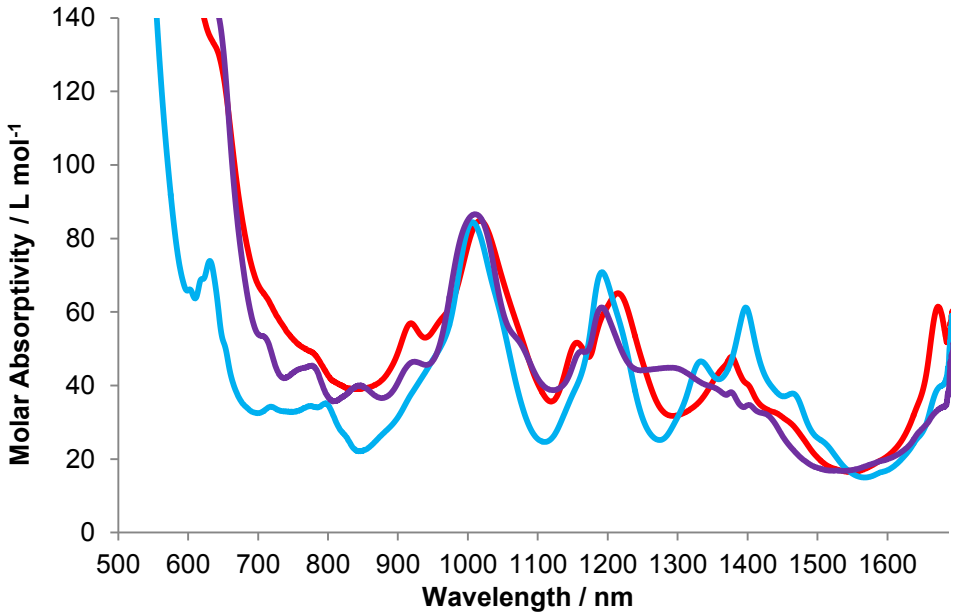

Figure 11: UV-vis-NIR absorption sprectra of K[$(Me_3SiOUO)_2$(L)], (red)) K[(Me_3SiOU)(μ-OH)(OUO)(L)] (blue) and K_2[(Me_3SiOUO)(OUO)(L)] (purple).

The absorptions at 1002–1023, 1197–1206 and 1380–1400 nm provide a fingerprint for this class of compounds and allow some insight into nature of the oxidation state mixing in the complexes. The Robin-Day Classification is used to describe the extent of such mixing,[16] with complexes exhibiting "trapped" or localised oxidation states which do not readily interconvert categorised as Class I. Class III complexes exhibit the opposite behaviour, with oxidation states that are not distinguishable by spectroscopic methods as the valence electrons are completely delocalised. Mixed-valence complexes that demonstrate intermediate behaviour are defined as Class II, with partial localisation of distinct oxidation states but a low activation energy for their interconversion.

The complex [K(18-crown-6)$(THF)_2$][$(Me_3SiOUO)_2$(L)], which exhibits two crystallographically identical uranium environments in the solid state, could be described, based on its structure, as Robin-Day Type III mixed valence complex, with indistinguishable uranium "4.5" oxidation states. Crystallographic disorder of the bridging-oxo ligands can, however, exaggerate the true symmetry of the molecule, meaning Robin-Day classification of mixed valence complexes cannot rely on structure alone.[17] The fact that the *f-f* transitions in the NIR region of the absorption spectrum of the complex occur in almost identical positions to those of the structurally localised uranyl(V)/uranium(IV) complexes suggests that the degree of spin localisation in each complex is similar, with no additional intervalence charge transfer (IVCT) band present in the spectrum of K[$(Me_3SiOUO)_2$(L)]. Although the wavelength at which such an $U^{IV/V}$ IVCT band would occur is still unclear, due

to the lack of unambiguous Type II or III uranium(4.5) complexes in the literature (see 3.2.2), the almost identical absorption spectra of $K[(Me_3SiOUO)_2(L)]$ and $K[(Me_3SiOU)(\mu\text{-}OH)(OUO)(L)]$ and the fact that the latter complex can be described as an unambiguous Type I complex, suggest that an IVCT band is also not present in the former spectrum. In addition to the UV/vis/NIR data, both $[K(18\text{-crown-}6)(THF)_2][(Me_3SiOUO)_2(L)]$ and $[K(THF)_2][(Me_3SiOU)(\mu\text{-}OH)(OUO)(L)]$ exhibit paramagnetic behaviour down to 2 K (Figures 3 and 7), further indication that no exchange is facilitated by the bridging oxo groups of either complex. In light of these observations, $K[(Me_3SiOUO)_2(L)]$ would be more accurately described as a Type I complex despite being unable to locate specifically the U^{IV} and U^{V} oxidation states in the same manner as $K[(Me_3SiOU)(\mu\text{-}OH)(OUO)(L)]$ and $K_2[(Me_3SiOUO)(OUO)(L)]$.

3.5.1 Alternative routes to $K_2[(Me_3SiOUO)(OUO)(L)]$

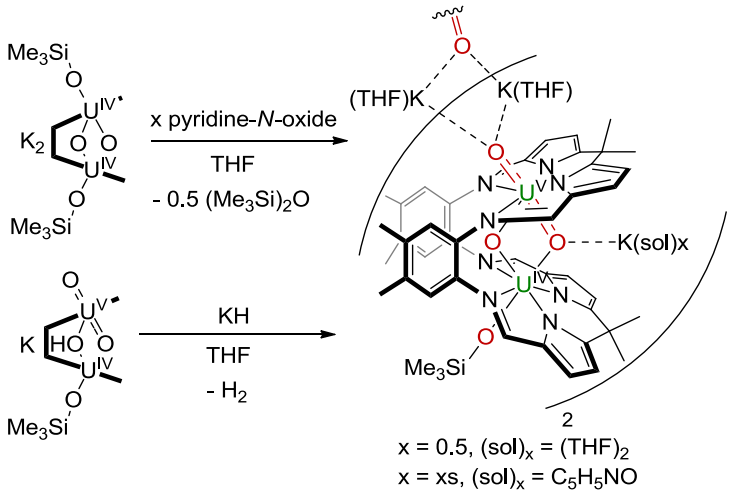

Scheme 8: Alternative routes to $K_2[(Me_3SiOUO)(OUO)(L)]$.

The structural relationship of $K[(Me_3SiOU)(\mu\text{-}OH)(OUO)(L)]$ to the mono-silylated uranyl(V) complex $K_2[(Me_3SiOUO)(OUO)(L)]$ means it may be considered as the potassium salt of the latter complex. This postulate is confirmed by the fact that the hydroxyl group in $K[(Me_3SiOU)(\mu\text{-}OH)(OUO)(L)]$ may be straightforwardly deprotonated in THF by one equivalent of potassium hydride to form $K[(Me_3SiOUO)(OUO)(L)]$ as the only product observed by ^1H NMR spectroscopy (Scheme 8).

Overall, the reaction to form $K_2[(Me_3SiOUO)(OUO)(L)]$ from the binuclear U^{IV} salt $K_2[(Me_3SiOUO)_2(L)]$ by the addition of half an equivalent of water proceeds with desilylation of one oxo group and retention of the two potassium cations, forming a product similar to the mixed valence U(4.5) complex $K[(Me_3SiOU)(\mu\text{-}OH)(OUO)(L)]$ formed from $K[(Me_3SiOUO)_2(L)]$. However, the desilylation of $U^{IV}U^{IV}$ $K_2[(Me_3SiOUO)_2(L)]$ is less

simple, as the removal of one oxo-bound $SiMe_3$ is now also associated with an oxidation. In light of this observation, an analogous reaction of $K_2[(Me_3SiOUO)_2(L)]$ with half an equivalent of the aprotic oxidizing agent pyridine-*N*-oxide was carried out and found to yield cleanly $K_2[(Me_3SiOUO)(OUO)(L)]$ in 60 % yield after 36 h in boiling THF, confirming that the formation of complex occurs with oxidation. In contrast, the single-electron oxidation of $K_2[(Me_3SiOUO)_2(L)]$ with half an equivalent of iodine yields the expected mixed valence U(4.5) complex $K[(Me_3SiOUO)_2(L)]$ as the only product by ^{1}H NMR spectroscopy. This contrasting reactivity offered by oxygen and non-oxygen containing oxidising agents is presumably driven by the greater affinity of the former towards O–Si bond formation and is analogous to the aforementioned reactivity of the $U_2(4.5)$ complex $K_2[(Me_3SiOUO)_2(L)]$ towards O-containing Brønsted acids.

Attempts to oxidatively desilylate $K_2[(Me_3SiOUO)(OUO)(L)]$ were unsuccessful, presumably due to the insolubility of the dimeric THF adduct. The reaction between $K_2[(Me_3SiOUO)_2(L)]$ and 3 equivalents of pyridine-*N*-oxide in boiling THF yielded crystals of the analogous pyridine-*N*-oxide salt of $K_2[(Me_3SiOUO)(OUO)(L)]$, $[K(THF)_2]_2[\{K(ONC_5H_5\}\{(Me_3SiOUO)_2(L)\}]_2$ (Figure 10, b). The solid state structure of the complex depicts the same $[(Me_3SiOUO)(OUO)(L)]^{2-}$ dianions arranged in an identical ladder motif as the THF-adduct, with the only difference being the replacement of the two THF molecules bound to the *endo*-bound potassium cation K1 with a single coordinating pyridine-*N*-oxide molecule.

3.5.2 Crystal structure of the $U_{12}O_{24}L_6$ supramolecular wheel

The double desilylation of $K_2[(Me_3SiOUO)_2(L)]$ was achieved accidentally by ingress of air into a vessel containing a THF solution of the complex and excess water over one month. The result was the precipitation of red crystals of $\{K_3[\{(OU)(\mu\text{-}O)(\mu\text{-}OH)U(L)\}_2(\mu\text{-}O)(\mu\text{-}OH)]\}_3$, a $U_{12}O_{24}L_6$ supramolecular wheel.

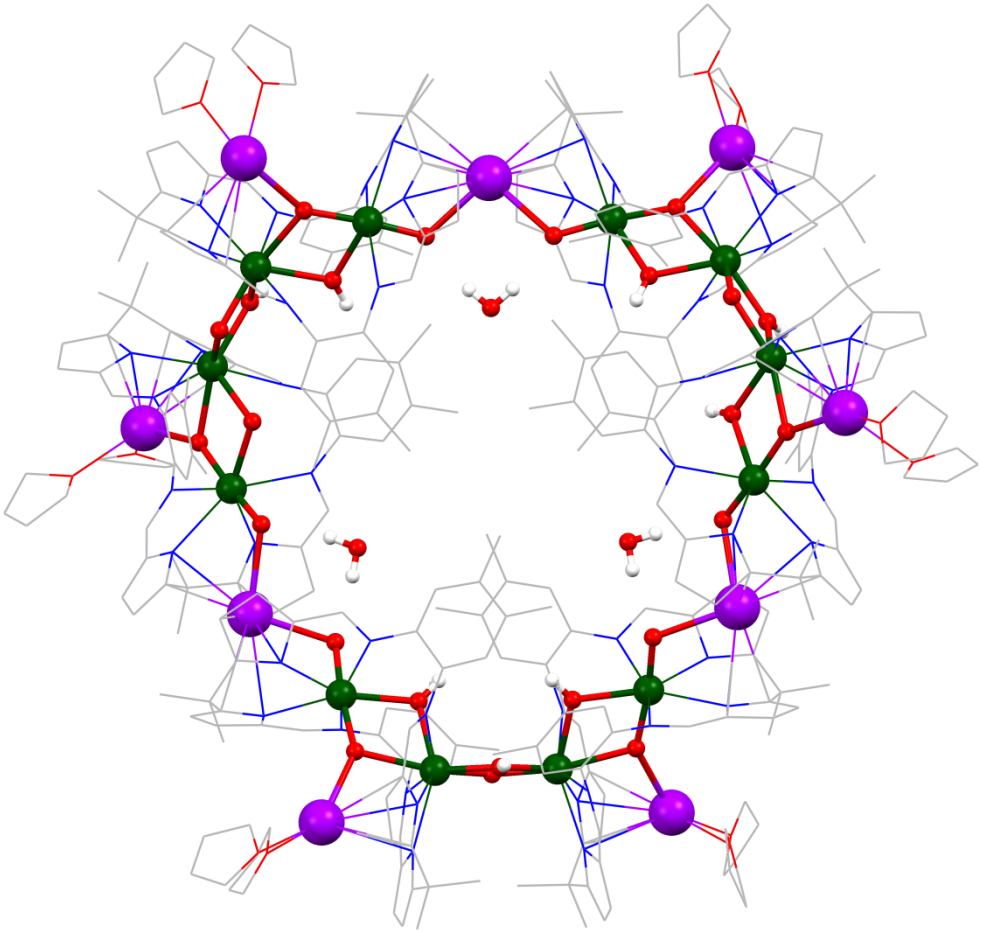

Figure 12: Solid state structure of $[K_9(U^{V}O_2)_6U^{IV}{}_6O_6(OH)_6(L)_6(THF)_{12}]\cdot 3H_2O$ supramolecular wheel. Pacman ligands and coordinated THF molecules are shown as a wireframe. Uranium (green), potassium (purple) and oxygen (red) atoms are depicted as balls and sticks. All free solvent molecules apart from the central water molecules were removed using the PLATON SQUEEZE algorithm.[18] Carbon-bound H atoms are omitted for clarity.

Analysis of the structure by single-crystal X-ray diffraction revealed a large unit cell volume of 18697 Å containing a single molecular wheel in the asymmetric unit, composed of six interlocking binuclear uranium Pacman molecules each exhibiting the same diamond shaped U_2O_4 oxo-ligand connectivity observed in the other $U^{IV/V}$ and $U^{V/V}$ complexes (Figure 12).

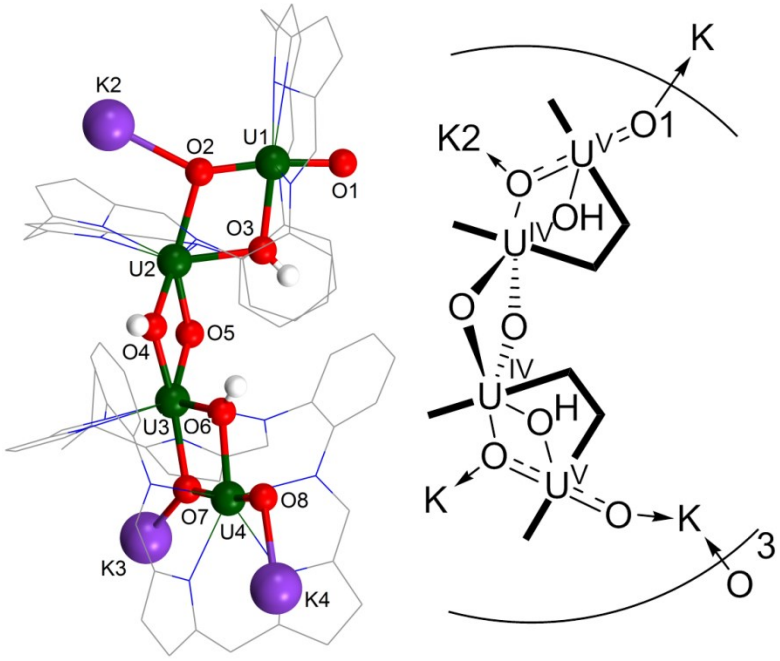

Figure 13: Dimeric repeat unit of the supramolecular wheel complex, methyl groups and carbon-bound H atoms are omitted for clarity.

The repeat unit of the structure may be described as two binuclear uranyl(V)/uranium(IV)-containing Pacman molecules linked between the two U^{IV} centres by single μ-O and μ-OH bridging ligands, with three such $\{[K]_3[\{(OU)(\mu\text{-}O)(\mu\text{-}OH)U(L)\}_2(\mu\text{-}O)(\mu\text{-}OH)]\}$ units linked by three $[UO_2]^+\cdots K\cdots[UO_2]^+$ CCI interactions to form a $U_{12}O_{24}L_6$ wheel (Figure 13). Each of the six *endo*-bound potassium cations are solvated by two THF molecules and three free water molecules are present within the wheel cavity, located in positions from which to form hydrogen bonds between the uranyl(V) exo *oxo* groups.

Of the 12 uranium atoms in the structure, six exhibit the characteristics of uranyl(V), with six $[UO_2]^+$ *trans* dioxo units displaying one short $U–O_{endo}$ and one shorter $U–O_{exo}$ bond with ranges between 1.92(2) –1.975(9) and 1.81(2) –1.87(2) Å respectively. Each uranyl(V) cation lies adjacent to a second around the U_{12} ring, with each set of two $[UO_2]^+$ units separated by two non-uranyl uranium atoms in a U^V12, U^V1, $U^{IV}2$, $U^{IV}3$, U^V4, U^V5, $U^{IV}6$, $U^{IV}7$ (etc) arrangement. These adjacent uranyl(V) centres are linked by single potassium cations, which form bridging CCI interactions between the *exo* oxo groups, such as U12–O24···K6···O1–U1, that form three of the six linking motifs that connect the six Pacman molecules together. Six other potassium cations bind to the trans-*endo* bridging uranyl(V) oxo groups as in $K_2[(Me_3SiOUO)(OUO)(L)]$ and do not assist supramolecular aggregation. The six *cis*-, or rear-bridging endo oxygen atoms within each Pacman molecule are protonated, evidenced by the presence of much longer uranium-oxygen bond lengths

(2.29(2) – 2.34(2) Å) that are only observed for bridging hydroxyl groups (range 2.27–2.51 Å). The U–O bond lengths displayed by the six non-uranyl uranium atoms range between 2.13(2) – 2.455(9) Å suggestive of the metals being in the uranium(IV) oxidation state. No silyl groups remain,, with each $[U^{V}U^{IV}O_4(L)]$ unit requiring three cations for charge balance with 18 cations required across the entire wheel. Nine potassium cations (3 *exo*- and 6 *trans-endo*-bound) and six protonated *cis-endo*-oxo groups are easily identified, leaving a deficit of 3 that must be fulfilled by three protons. These are placed on three of the six μ-O_{exo} atoms bridge between the uranium(IV) atoms of adjacent Pacman molecules and maintain the wheel structure. Of the 12 U–O bonds involved in such bridge-bonding, six are longer (2.20(2) – 2.31(2) Å) than the others (2.13(3) –2.18(3) Å), allowing for three of the six U^{IV}-bridging oxygen atoms (O5, O12 and O20) to be identified as hydroxides.

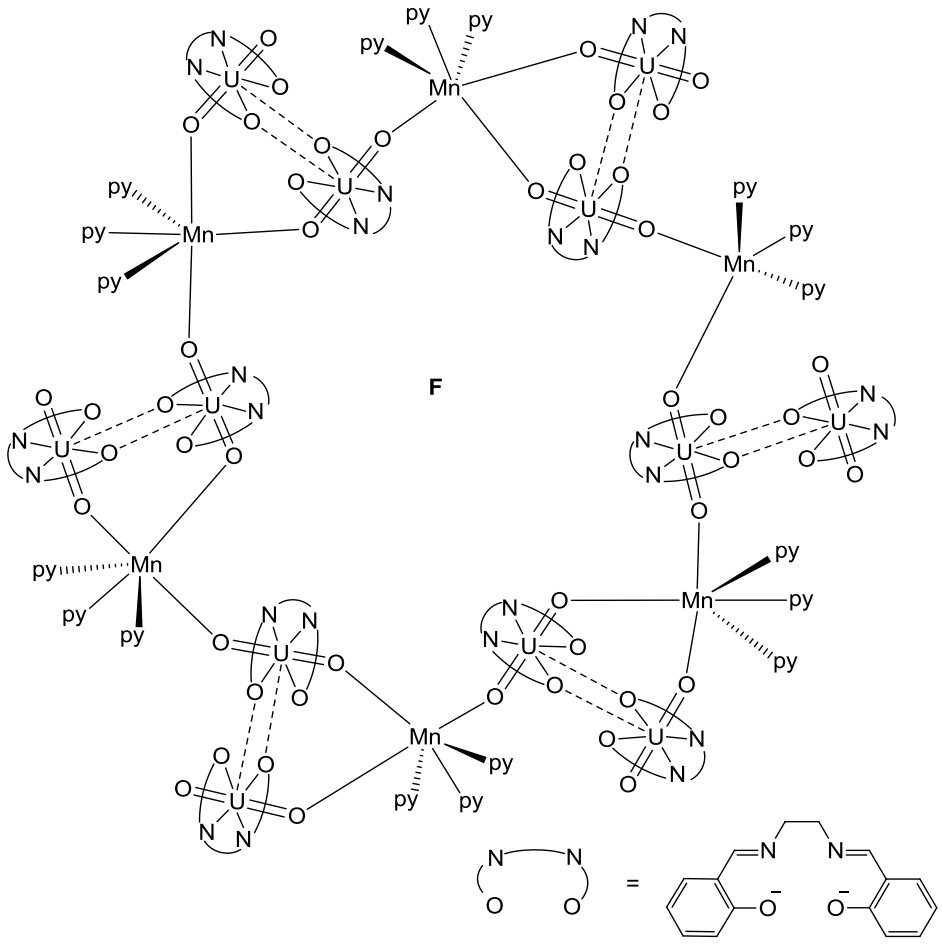

Figure 14: The $[\{(UO_2)(salen)\}_{12}\{Mn(py)_3\}_6]$ wheel **F** by Mazzanti and co-workers.

There are a number of other polynuclear uranium oxide clusters in the literature which are also maintained by either uranyl(V)/potassium CCI interactions,[19-23] or oxo/hydroxo bridges between uranium(IV) centres.[4-5, 12, 14, 24] Recently, the heterobimetallic

polynuclear uranyl(V) molecular wheel $[\{(UO_2)(salen)\}_{12}\{Mn(py)_3\}_6]$ has been published by Mazzanti and co-workers (Figure 14, **F**).[25] It features six dimeric $[\{(UO_2)(salen)\}_2]$ units arranged in a ring linked by uranyl(V)/manganese CCIs and displays magnetic hysteresis below 4 K, evidence of retention of the clusters magnetic spin state after the external field is removed, with a high barrier to its relaxation.

3.5.3 Attempted syntheses of the supramolecular wheel

The crystallisation of the supramolecular wheel indicated that complete desilylation of $K_2[(Me_3SiOUO)_2(L)]$ was possible and can result in the formation of polyoxo structures maintained by supramolecular interactions.

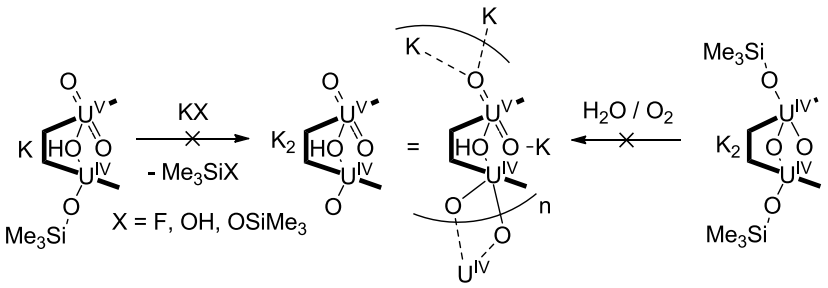

Scheme 9: Attempted syntheses of polynuclear wheel complexes

In light of this, efforts were made to devise a more formal synthesis of polynuclear clusters by desilylation of the uranyl(V)/uranium(IV) precursor $K[(Me_3SiOU)(\mu\text{-}OH)(OUO)(L)]$ (Scheme 9). Despite extensive efforts however, no route was found and attempts to repeat the wheel structure by controlled exposure of $K_2[(Me_3SiOUO)_2(L)]$ to oxygen and water were also unsuccessful.

3.5.4 Oxidative desilylation

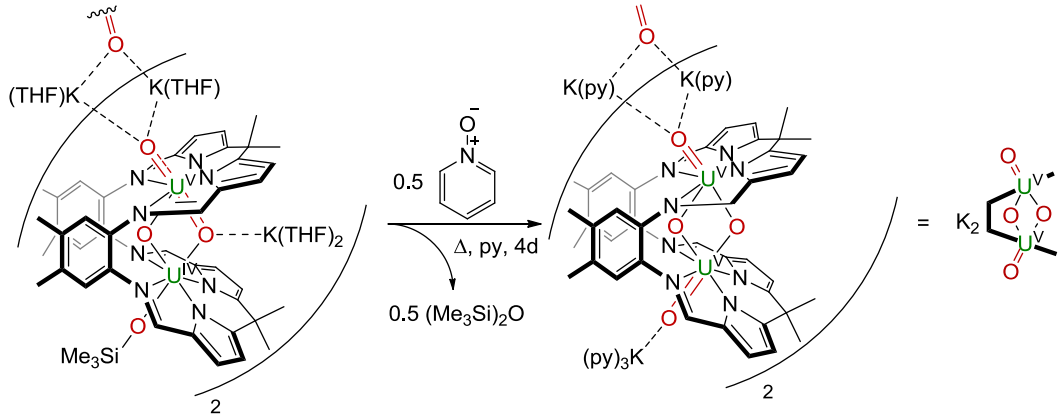

Scheme 10: Synthesis of the dimeric pyridine solvate of $K_2[(OUO)_2(L)]$.

A repeatable route to doubly desilylated butterfly complexes was eventually achieved by oxidative desilylation of $K_2[(Me_3SiOUO)(OUO)(L)]$. The reaction between the $U^{IV}U^{V}$ complex and half an equivalent of pyridine-*N*-oxide in pyridine resulted in the formation of the red-brown, oxidativly desilylated, binuclear U^{V} compound $K_2[(OUO)_2(L)]$ and half an equivalent of $(Me_3Si)_2O$ as the only products observable by ^1H NMR spectroscopy after boiling for 4 days (Scheme 10).

The ^1H NMR spectrum of $K_2[(OUO)_2(L)]$ is very similar to $[(Me_3SiOUO)_2(L)]$, albeit with the notable absence of a $SiMe_3$ resonance at 15 ppm, with the seven resonances from the symmetrically-occupied Pacman ligand occurring in almost identical positions to those of $[(Me_3SiOUO)_2(L)]$. Isolation of the pyridine solvate of $K_2[(OUO)_2(L)]$ in the bulk was achieved using a one-pot strategy in which $[(Me_3SiOUO)_2(L)]$ was reduced to the $U^{IV}U^{IV}$ salt $K_2[(Me_3SiOUO)_2(L)]$ and then re-oxidised by the addition of one equivalent of pyridine-*N*-oxide; boiling the resulting mixture for 6 days results in the precipitation of the crystalline product in 69 % yield.

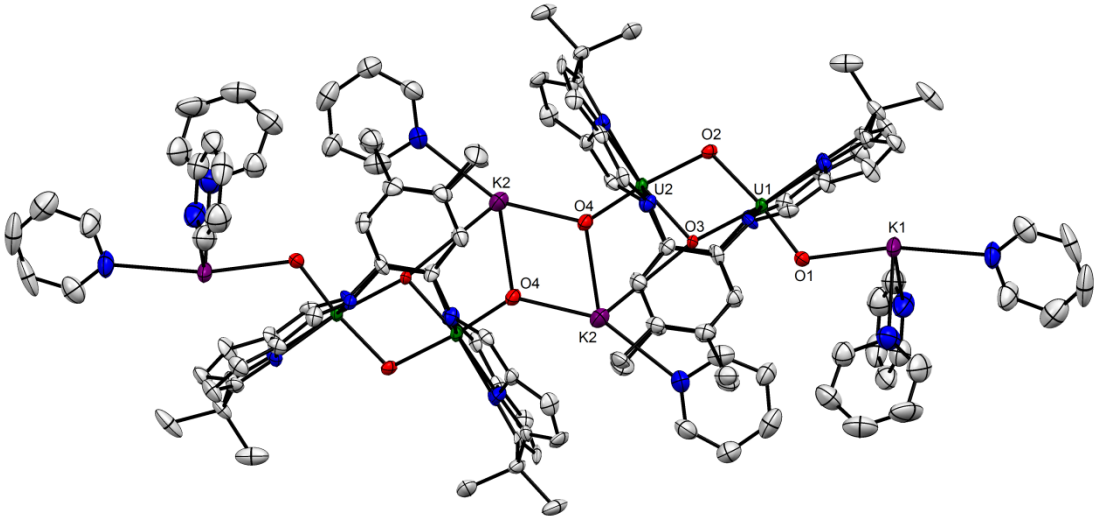

Figure 15: X-ray crystal structure of the pyridine-solvate of $K_2[(OUO)_2(L)]$. All H-atoms and free solvent molecules are omitted for clarity; ellipsoids are drawn at 50 % probability.

Analysis of the crystal structure of the pyridine adduct of $K_2[(OUO)_2(L)]$ confirmed the absence of the silyl substituents and the presence of U^{V} oxidation states in which the average U–O bond length of 2.03 Å is comparable to that seen in $[(Me_3SiOUO)_2(L)]$ (2.09 Å) (Figure 15). In contrast to the silylated analogue, which exhibits six, almost identical U–O bond distances between 2.03 to 2.10 Å, those in the di potassium complex show significant variation between the four $U–O_{endo}$ bonds (2.090(6), 2.101(5), 2.105(6) and 2.168(5) Å) and the two $U–O_{exo}$ bonds (1.871(5) and 1.851(6) Å), with the latter being much

more indicative of 'yl-type U–O multiple bonding. The U1···U2 separation of 3.3795(5) Å is short but elongated slightly compared to that of 3.3557(5) Å seen in $[(Me_3SiOUO)_2(L)]$. The contrast in bonding in $K_2[(OUO)_2(L)]$ to its silylated analogue is further represented in the UV-vis-NIR spectra, with the potassium salt displaying absorptions at 897, 1142, 1191, 1300, and 1684 nm at completely different wavelengths to $[(Me_3SiOUO)_2(L)]$ (1018, 1040, 1163, 1592 and 1665 nm) despite their common oxidation states (Figure 21).

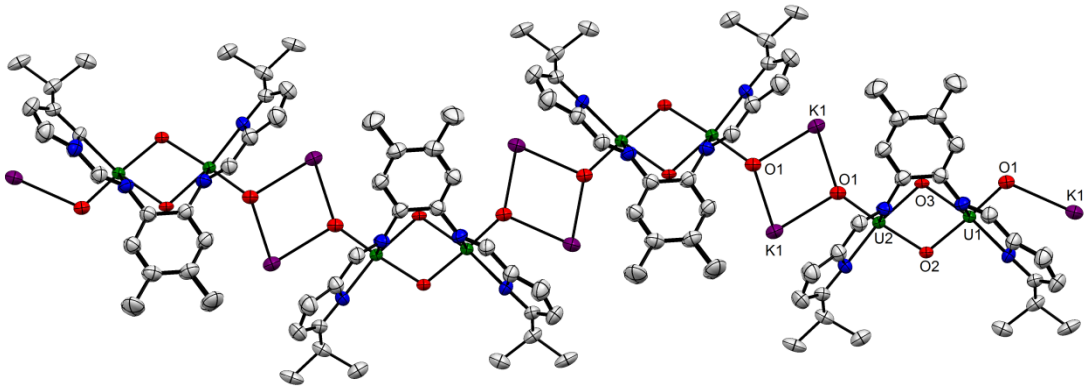

Figure 16: X-ray crystal structure of the unsolvated $K_2[(OUO)_2(L)]$ polymer. All H-atoms and free solvent molecules are omitted for clarity; ellipsoids are drawn at 50 % probability.

The alternative, unsolvated analogue $[(KOUO)_2(L)]$ was synthesised by direct exposure of a THF solution of $K_2[(Me_3SiOUO)_2(L)]$ to air, resulting in the immediate precipitation of crystals of $[(KOUO)_2(L)]$ along with other intractable materials. Analysis of the X-ray crystal structure of the complex revealed a contrasting structure to that of $[K(py)_x]_2[(OUO)_2(L)]$, in which pyridine solvation of the external potassium cations truncates the structure as a crystallographic dimer (Figure 16). $[(KOUO)_2(L)]$ exhibits a polymeric structure in which each potassium bridges two Pacman molecules in a K_2O_2 diamond motif.

These desilylated compounds are best described as displaying bimetallic *endo*-oxo-bridged U^V motifs with terminal *exo*-oxo groups. Although the former presents a very common bonding motif in uranium chemistry, U^V complexes exhibiting terminal oxo groups are still rare.[26]

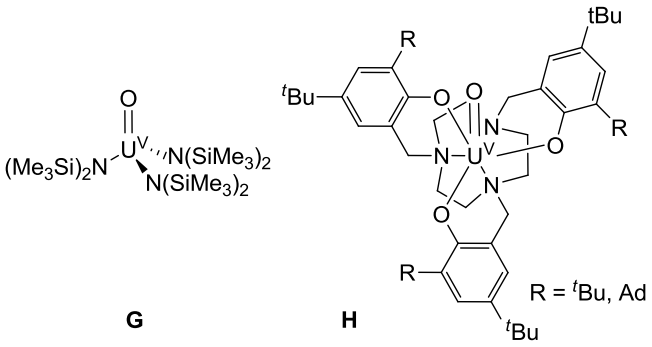

Figure 17: Uranium(V) terminal oxo complexes **G** and **H**.

One recent example is $[U(O)\{N(SiMe_3)_2\}_3]$ (Figure 17, **G**), synthesised by treatment of $[U\{N(SiMe_3)_2\}_3]$ with pyridine-*N*-oxide, which displays a similar U=O bond length (1.817(1) Å) to those in $[K(py)_x]_2[(OUO)_2(L)]$.[27] In addition, the terminal U^V oxo complexes $[\{(RArO)_3tacn\}U(O)]$ (R = Bu^t or 1-adamantyl, tacn = 1,4,7-triazacyclononane)[28] (Figure 17, **H)** are unique examples of complexes that can be oxidised to U^{VI} terminal oxo compounds (see Chapter One, section 1.7.2).[29]

3.5.5 Attempted desilylation

$[(Me_3SiOUO)_2(L)]$ cannot be directly desilylated to form $[(OUO)_2(L)]^{2-}$ salts using common desilylation reagents such as KF, KOH, $KOSiMe_3$, $[nBu_4N][F]$ or $[nBu_4N][Ph_3SiF_2]$ nor can it be oxidatively desilylated to a uranium(VI) complex such as $[(OUO)_2(L)]$ using benzoquinone, TEMPO or ^{t}BuOO^{t}Bu. In addition, the latter three reagents cannot be employed to oxidise $K_2[(Me_3SiOUO)_2(L)]$ or $K_2[(Me_3SiOUO)(OUO)(L)]$ with pyridine-*N*-oxide being the only reagent found to result in reaction.

3.6 Direct synthesis of oxo-lithiated binuclear uranium(V) complexes

The synthesis of $K_2[(OUO)_2(L)]$ is a multi-step process requiring: (a) The synthesis of the bis-silylated complex $[(Me_3SiOUO)_2(L)]$ by reaction of the macrocycle H_4L and 2.5 equivalents of uranyl silylamide; (b) The reduction of $[(Me_3SiOUO)_2(L)]$ to $K_2[(Me_3SiOUO)_2(L)]$ with two equivalents of potassium metal and (c) Subsequent re-oxidation with pyridine-*N*-oxide to form the metalated complex. The laborious nature of this synthesis encouraged investigation into an alternative method.

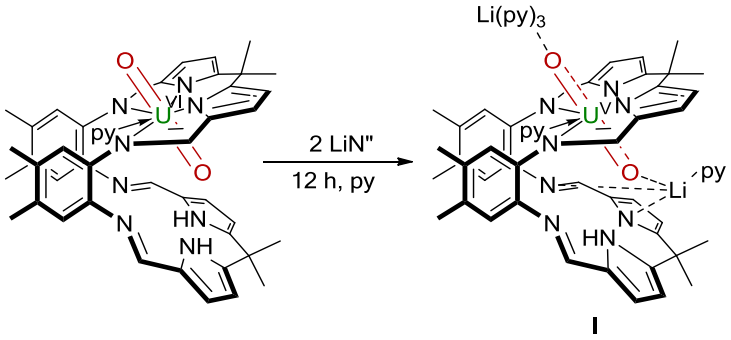

I

Scheme 11: Previously reported reductive lithiation of $[UO_2(py)(H_2L)]$.[30]

The reaction between $[UO_2(py)(H_2L)]$ and 2 equivalents of LiN" (N" = $N(SiMe_3)_2$), reported by Arnold and Love in 2010, led to single electron reduction and concomitant oxo-group lithiation of the uranyl centre to form the uranyl(V) complex $[(py)_3LiOUO(py)Li(py)(HL)]$ **I** (Scheme 11).[30] In was postulated therefore that the addition of LiN" to the reaction mixture used to synthesise $[(Me_3SiOUO)_2(L)]$ could yield oxo-lithiated, rather than oxo- silylated complexes.

3.6.1 Synthesis of $[Li(py)_2][UO_2(N")_3]$

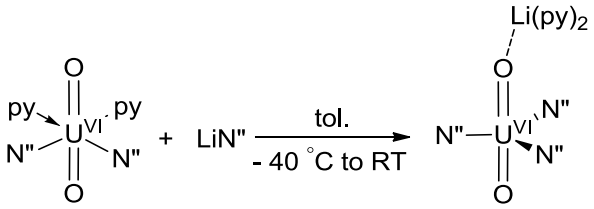

Scheme 12: Synthesis of $[Li(py)_2][(OUO)(N")_3]$.

In order to attempt the synthesis of a lithium solvate, the speciation of a 1:1 mixture of LiN" and $[UO_2(N")_2(py)_2]$ was first assessed by reaction between the two reagents at −40 °C in toluene, resulting in the formation of the red lithium "-ate" complex $[Li(py)_2][(OUO)(N")_3]$ upon warming to room temperature in 58 % yield (Scheme 12). The complex exhibits a single (methyl) resonance in the d_5-pyridine ^1H NMR spectrum at 0.78 ppm that is shifted in comparison to both silylamide precursors. In C_6D_6, complex sets of broad singlets are present in the both the aromatic and alkyl regions of the spectra, with total integrations of 10 and 54 protons respectively. Such a complex pattern is suggestive of fluxional ligand exchange processes between the pyridine and N" that are not observed in the corresponding NMR spectrum measured in d_5-pyrdine. A single resonance in the $^7Li\{^1H\}$ NMR spectrum is present at 3.45 ppm, shifted in comparison to LiN" and confirming incorporation of lithium within the complex.

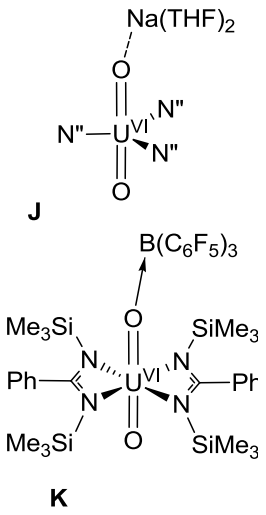

Figure 18: Other uranyl(VI) CCI complexes.

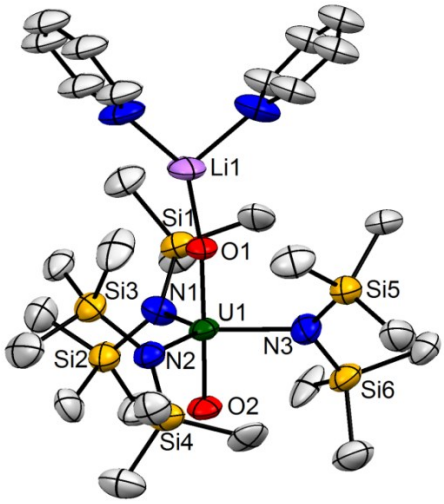

Figure 19: Displacement ellipsoid plot (50 %) of $[Li(py)_2][(OUO)(N")_3]$, H atoms omitted for clarity.

Analysis of the solid state structure $[Li(py)_2][(OUO)(N")_3]$ of reveals it to be isostructural to the Na analogue $[Na(THF)_2](OUO)(N")_3]$,[31] featuring a trigonal bipyramidal $[UO_2(N")_3]^-$ anion, resulting from a linear $[UO_2]^{2+}$ dication with three $N(SiMe_3)_2$ ligands in the equatorial plane (Figure 19). The bond lengths U1–O1 and U1–O2 of 1.88(1) and 1.81(1) Å respectively are elongated in comparison to free uranyl(VI) (1.76 – 1.78 Å) and are comparable to the analogous "donated" and "free" U–O bond distances in other uranyl(VI) CCI complexes $[Na(THF)_2](OUO)(N")_3]$ (1.810(5) and 1.781(5) Å) and $[\{(C_6F_5)_3BOUO\}(NCN)_2]$ (NCN = $\{(Me_3SiN)_2CPh\}$) (1.898(3) and 1.770(3) Å) (Figure 18, **J** and **K**).[31-32]

3.6.2 Synthesis of $[\{(py)_3LiOUO\}_2(L)]$

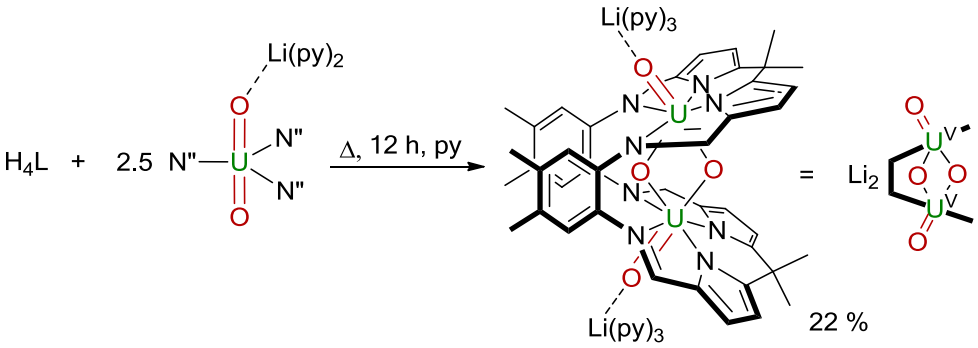

Scheme 13: Synthesis of $[\{(py)_3LiOUO\}_2(L)]$.

The reaction of 2.5 equivalents of $[Li(py)_2][(OUO)(N")_3]$ with H_4L in boiling pyridine over 12 h was carried out resulting in the formation of the brown, oxo-lithiated,

binuclear uranium(V) complex [{(py)$_3$LiOUO}$_2$(L)] and HN" as the only soluble products, as well as intractable brown solids; pure [{(py)$_3$LiOUO}$_2$(L)] was isolated in 21 % yield by filtration and recrystallisation from pyridine (Scheme 13). The ^{1}H NMR spectrum of [{(py)$_3$LiOUO}$_2$(L)] is almost identical to that of the potassium analogue K$_2$[(OUO)$_2$(L)], with seven resonances between 12 and −12 ppm indicative of the formation of a bimetallic uranium(V) Pacman complex with C_{2v}-symmetry. In addition, the UV-vis-NIR spectrum of the complex shows striking similarity to the potassium salt, with broad absorptions at 913, 1152, 1190, 1320 and 1684 nm closely matching those present in the spectrum of K$_2$[(OUO)$_2$(L)] (897, 1142, 1191, 1300 and 1684 nm (see Figure 21).

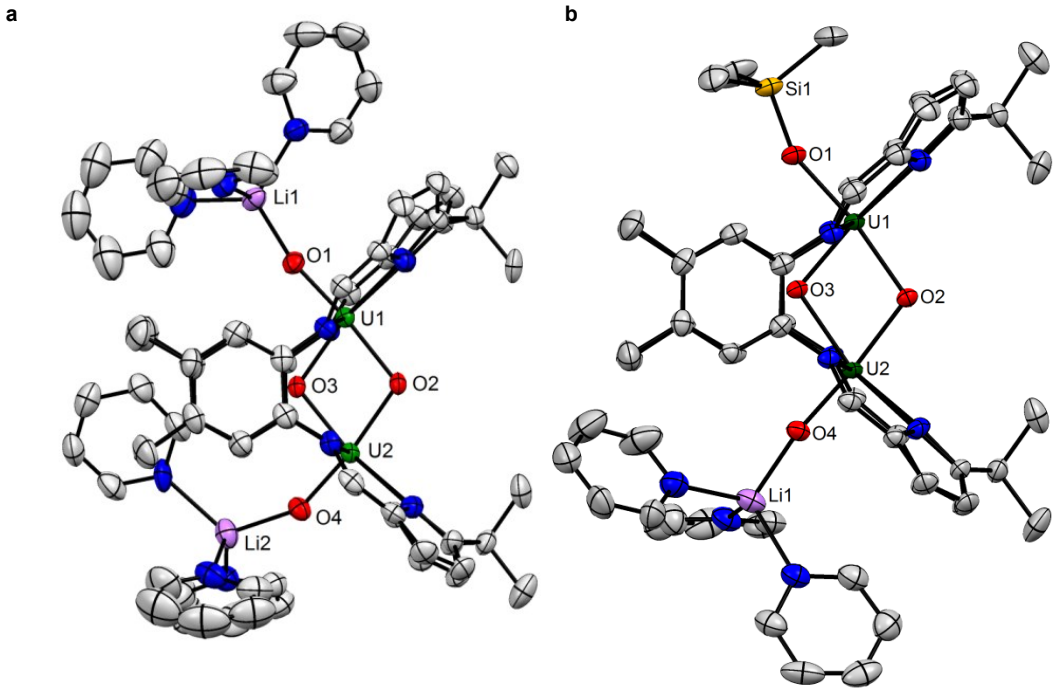

Figure 20: Displacement ellipsoid plots (50 %) of [{(py)$_3$LiOUO}$_2$(L)] (**a**) and [{Li(py)$_3$OUO}(OUOSiMe$_3$)(L)] (**b**), H atoms and free solvent molecules omitted for clarity.

Analysis of the solid state structure of [{(py)$_3$LiOUO}$_2$(L)] reveals the presence of the [(OUO)$_2$(L)]$^{2-}$ dianion, with the wedge-shaped, binucleating Pacman macrocycle holding the two uranium centres proximate (U1···U2 3.3793(4) Å) (Figure 20, a). Each uranium atom has an Li-bound *exo*-oxo group, with the U–O bond lengths of 1.877(4) (U1–O1) and 1.883(4) Å (U2-O4) very similar to those in [K(py)$_2$]$_2$[(OUO)$_2$(L)] (1.851(6) and 1.871(5) Å). The two *endo*- oxo atoms bridge the uranium centres in mutually *cis* and *trans* positions forming the diamond-shaped, U_2O_2 core observed in both [(Me$_3$SiOUO)$_2$(L)] and K$_2$[(OUO)$_2$(L)]. These four *endo* U–O bonds are lengthened and correspond to uranium-oxygen single bonds. In contrast to [K(py)$_2$]$_2$[(OUO)$_2$(L)] which exists as a crystallographic

dimer, the smaller size and greater electronegativity of the lithium cation means that [{(py)$_3$LiOUO}$_2$(L)] does not aggregate in the solid state, with much shorter O–Li bonds (1.87(1) and 1.93(1) Å) as compared to the O–K bonds in [K(py)$_2$]$_2$[(OUO)$_2$(L)] (2.658(6) - 2.765(6) Å). These O–Li bond distances are similar to those seen in other lithiated uranyl(V) complexes such as [(py)$_3$LiOUO(py)Li(py)(HL)] **H** (O–Li = 1.927(13) –1. 94(2) Å).[30]

The lack of aggregation of [{(py)$_3$LiOUO}$_2$(L)] in the solid state likely contributes to its greater solubility and its synthesis provides a more convenient route to salts of [(OUO)$_2$(L)]$^{2-}$ dianion. Although the mechanism of formation of the complex from H$_4$L and [Li(py)$_2$][(OUO)(N")$_3$] has yet to be elucidated, it is possible that it proceeds by a similar route to the formation of [(Me$_3$SiOUO)$_2$(L)], resulting in the same pyridine-insoluble by-product **P** formed in both cases which is proposed to be an aggregate of a [(OUO)$_2$(L)]$^{2-}$ units linked through coordination of the *exo* oxo groups to uranyl(VI) dications (see Chapter one).

Trace amounts of [{(py)$_3$LiOUO}$_2$(L)] may also be prepared by boiling a mixture of the polymeric material **P** (see Chapter One) with excess LiN" in pyridine for four days forming the lithium complex and two equivalents of HN" as the only soluble products. The reaction is the second example of the disaggregation of **P** to form a stable molecular complex in addition to its silylation to form [(Me$_3$SiOUO)$_2$(L)].

3.6.3 Synthesis of [{(py)$_3$LiOUO}(OUOSiMe$_3$)(L)]

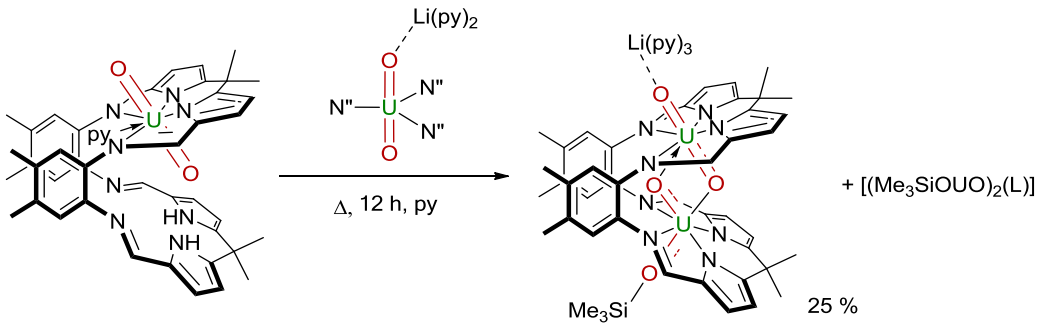

Scheme 14: Synthesis of [{(py)$_3$LiOUO}(OUOSiMe$_3$)(L)] and [(Me$_3$SiOUO)$_2$(L)].

The reaction between [UO$_2$(py)(H$_2$L)] and one equivalent of [Li(py)$_2$][(OUO)(N")$_3$] in boiling pyridine yields the brown, asymmetric, mono-lithiated, mono-silylated, complex [{(py)$_3$LiOUO}(OUOSiMe$_3$)(L)], half an equivalent of [(Me$_3$SiOUO)$_2$(L)] and excess HN" as the only products by ^{1}H NMR spectroscopy (Scheme 13). A toluene wash successfully separates [{(py)$_3$LiOUO}(OUOSiMe$_3$)(L)] from [(Me$_3$SiOUO)$_2$(L)] and HN" allowing its isolation in 25 % yield. The ^{1}H NMR spectrum of the complex shows 14 resonances between 14 and −12 ppm for L, double the number observed for the complexes [(Me$_3$SiOUO)$_2$(L)],

[{(py)$_3$LiOUO}$_2$(L)] and K$_2$[(OUO)$_2$(L)] so indicating asymmetric occupation of each of the N$_4$-donor pockets of the Pacman macrocycle. No resonances consistent with N–H protons are seen and the resonance at 12.19 ppm, integrating to 9 protons, is symptomatic with the silylation of a single oxo-group. This, coupled with the presence of a single, paramagnetically-shifted resonance at 33.16 ppm in the ^{1}H-decoupled ^{7}Li NMR spectrum, suggests unequal functionalisation of the uranium(V) oxo groups.

The growth of single crystals of [{(py)$_3$LiOUO}(OUOSiMe$_3$)(L)] allowed the solid state structure of the complex to be determined which shows the wedge-shaped, Pacman macrocycle accommodating two uranium centres, each with an *exo*-bound oxygen atom, bridged by mutually *cis*- and *trans*-oxo groups, all features of which are present in complexes [(Me$_3$SiOUO)$_2$(L)], K$_2$[(OUO)$_2$(L)] and [{(py)$_3$LiOUO}$_2$(L)] (Figure 20, b). The average U–O bond length in the complex is 2.06 Å and is consistent with two uranium(V) oxidation states and close that displayed in complexes [(Me$_3$SiOUO)$_2$(L)] (2.07 Å), [K(py)$_2$]$_2$[(OUO)$_2$(L)] (2.03 Å) and [{(py)$_3$LiOUO}$_2$(L)] (2.03 Å). In contrast to these complexes however, significant asymmetry is present across all six of the uranium-oxygen bonds in [{(py)$_3$LiOUO}(OUOSiMe$_3$)(L)]. The U1–O1 bond length is comparable to those of [(Me$_3$SiOUO)$_2$(L)] (2.056(2) *vs.* 2.034(5) and 2.085(4) Å), while the opposing, lithium-bound *exo* oxo group displays a much a shorter U–O bond length of 1.857(3) Å, analogous to the terminal oxo-uranium bonds exhibited in the dilithiated complex [{(py)$_3$LiOUO}$_2$(L)] (1.87(1) and 1.93(1) Å). The four uranium-oxygen bonds between each of two uranium centres and the two *endo* bridging oxygen atoms exhibit much greater variability in bond length than in any of the symmetric complexes, with the U1–O3 and U2–O2 bond lengths of 2.024(3) and 2.077(2) Å respectively similar to those in [(Me$_3$SiOUO)$_2$(L)] (2.040(0)–2.099(3) Å) which was found by computational analysis to have bond orders of 1.4 (see Chapter One). The other two U–O bonds in the molecule, U1–O2 and U2–O3, have bond lengths of 2.113(2) and 2.238(2) Å respectively and are too long for uranium-oxygen multiple bonding and closer in length to the predominantly ionic bonding between discrete uranyl cations $[UO_2]^{n+}$ (n = 1, 2) and their equatorially-bound ligands such as in uranyl(VI) poly oxo clusters.[33] In light of these assessments, the bonding in [{(py)$_3$LiOUO}(OUOSiMe$_3$)(L)] may be considered closer to that of two discrete uranyl cations, one *trans* and lithiated (O4–U2–O2) the other *cis* and silylated (O1–U1–O3), with each of the multiply-bonded $[UO_2]^+$ cations linked by weaker bonds (U1–O2 and U2–O3) of lower bond order.

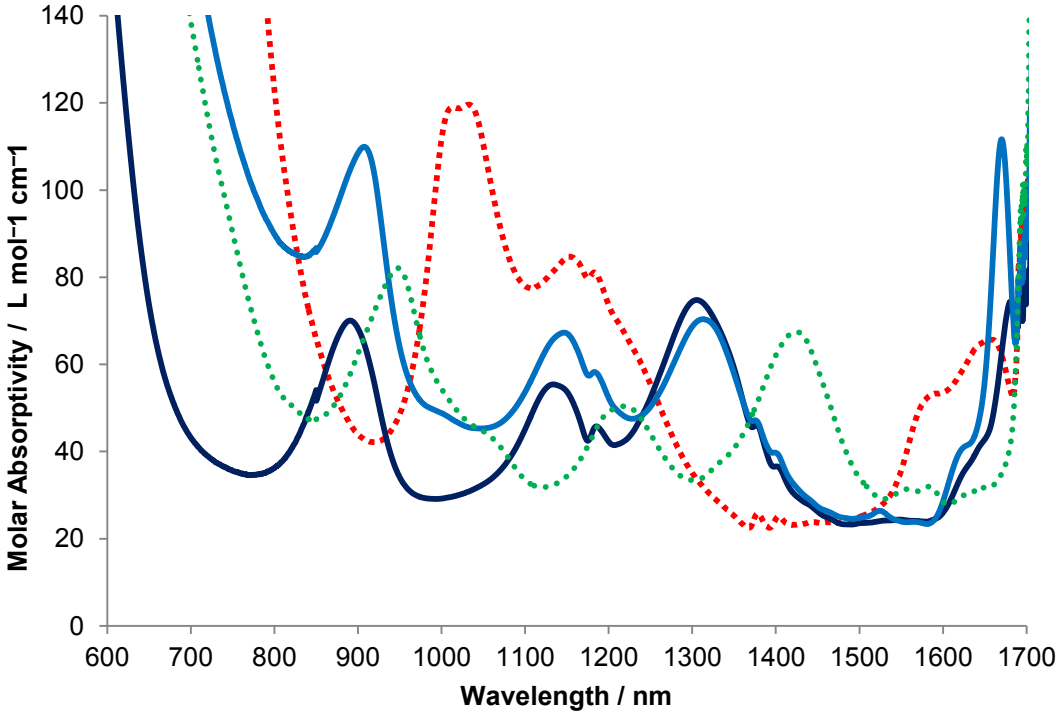

Figure 21: UV-vis-NIR absorption spectra of $[(Me_3SiOUO)_2(L)]$ (red dashes), $Li[OUO\}(OUOSiMe_3)(L)]$ (green dots), $Li_2[(OUO)_2(L)]$ (light blue bold) and $K_2[(OUO)_2(L)]$ (dark blue bold) in THF.

This alternate bonding motif is reflected in the UV/vis/NIR spectrum of $[\{(py)_3LiOUO\}(OUOSiMe_3)(L)]$, which does not feature the absorptions characteristic of either the fully silylated complex or the Group 1 metal salts of the $[(OUO)_2L]^{2-}$ with features at 954, 1063, 1225 and 1430 nm lying intermediate to the corresponding absorptions of $[(Me_3SiOUO)_2(L)]$ and $[\{(py)_3LiOUO\}_2(L)]$ (Figure 21).

Neither $K_2[(OUO)_2(L)]$ or $K[(OUO)(OUOSiMe_3)(L)]$ may be prepared from the analogous reactions of $[K(py)_2][(OUO)(N'')_3]$. Attempts were made to prepare the potassium analogue of the $[(OUO)(OUOSiMe_3)(L)]^-$ anion by oxidation of the uranyl(V)/uranium(IV) complex $K_2[(Me_3SiOUO)(OUO)(L)]$ with 0.5 equivalents of iodine however the reaction resulted only in ligand redistribution to form an equimolar solution $[(Me_3SiOUO)_2(L)]$ and $K_2[(OUO)_2(L)]$.

3.7 Discussion of reactivity of $M_2[(OUO)_2L]$ complexes

The differences in structure and bonding between oxo-silylated $[(Me_3SiOUO)_2(L)]$ and oxo-unfunctionalised $K_2[(OUO)_2(L)]$ and $[\{(py)_3LiOUO\}_2(L)]$ complexes are mirrored by differences in their stability towards disproportionation. Solutions of both $[(OUO)_2(L)]^{2-}$ complexes were found to react instantly with two equivalents of water or pyridinium

chloride in the absence of air to generate the mono-uranyl(VI) Pacman complex $[UO_2(py)(H_2L)]$ and an insoluble precipitate, presumed to contain uranium (IV). In addition, solutions of $K_2[(OUO)_2(L)]$ in pyridine can be readily oxidised to form bis-uranyl(VI) complexes and can undergo salt elimination reactions to form alternatively-functionalised oxo complexes (see Chapter Three). The potassium and lithium salt complexes can both be cleanly transformed back to their silylated analogue $[(Me_3SiOUO)_2(L)]$ by treatment with two equivalents of chlorotrimethylsilane, upon which its stability towards oxidation and functional-group exchange is restored, suggesting that the oxo-bound SiR_3 groups in $[(Me_3SiOUO)_2(L)]$ are responsible for its redox stability. As such, the trialkylsilyl group may be viewed as an effective protecting group for the uranyl oxo and therefore analogous to the well-documented silyl-group protection of functional groups in organic synthesis.

Table 1: U–O bond lengths (Å) in binuclear uranium(V) oxo complexes

	U1-O1	U1-O2	U1-O3	U2-O2	U2-O3	U2-O4	U-O_{av}
$[(Me_3SiOU^{V}O)_2(L)]$	2.034(5)	2.099(3)	2.098(3)	2.085(4)	2.095(3)	2.040(4)	2.075
$K[(Me_3SiOU^{IV/V}O)_2(L)]$	2.106(4)	2.117(3)	2.123(3)	n/a	n/a	n/a	2.115
$[C_5H_5NH][(Me_3SiOU^{IV/V}O)_2(L)]$	2.111(4)	2.218(4)	2.227(4)	2.042(4)	2.134(4)	2.076(4)	2.135
$K[(Me_3SiOU^{IV})(\mu\text{-}OH)(OU^{V}O)(L)]$	2.105(8)	2.217(7)	2.312(7)	1.994(7)	2.302(7)	1.843(8)	2.129
$K_2[(Me_3SiOU^{IV}O)(OU^{V}O)(L)]$	2.142(6)	2.246(5)	2.144(4)	2.020(4)	2.146(5)	1.875(5)	2.096
$K_2[(OU^{V}O)_2(L)]\cdot py_4$	1.851(6)	2.090(6)	2.168(5)	2.101(5)	2.105(6)	1.871(5)	2.031
$Li_2[(OU^{V}O)_2(L)]\cdot py_6$	1.877(4)	2.1103(2)	2.1097(2)	2.1005(2)	2.1155(2)	1.883(4)	2.033

The differences in reactivity between all the $U^{IV}U^{IV}$, $U^{IV}U^{V}$ and $U^{V}U^{V}$ complexes synthesised in this chapter are related to the different U–O bonding motifs in each complex. For comparison, the U–O bond lengths of all the complexes reported in this chapter are tabulated above (Table 1). As described previously, elongation of the average U–O bond length in the complexes is visible upon a reduction of the oxidation states from U^{V}/U^{V} to U^{V}/U^{IV} and is indicative of a lowering of the U–O bond order resulting in greater reactivity towards Brønsted acids. Although the average U–O bond lengths in the silylated and metalated U^{V}/U^{V} complexes are comparable, structural asymmetry between the U–O_{endo} and

$U–O_{exo}$ bonds upon desilylation promotes oxidation and functionalization chemistry, a topic discussed more extensively in Chapter four.

3.8 Summary

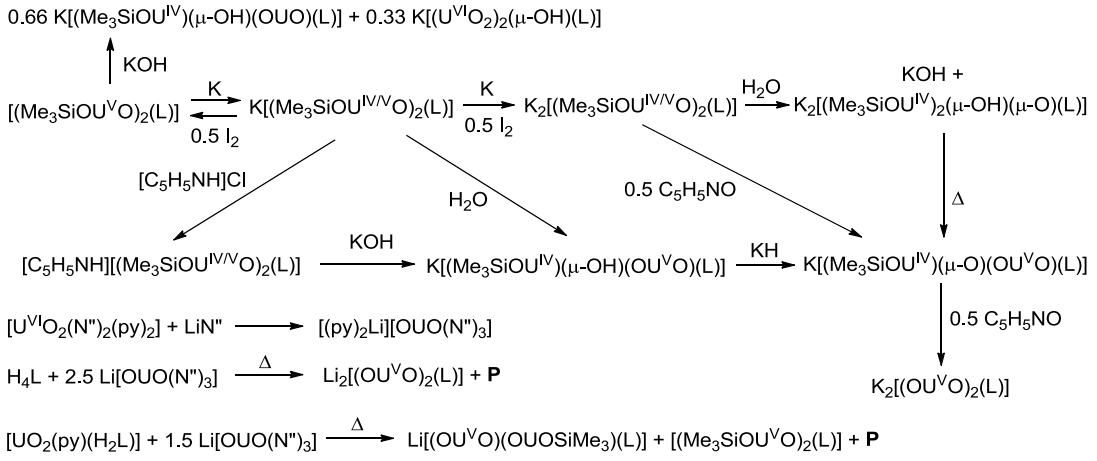

Scheme 15: Summary of Chapter Three.

The $U^{IV/V}$ and $U^{IV/IV}$ species $K[(Me_3SiOUO)_2(L)]$ and $K_2[(Me_3SiOUO)_2(L)]$ were synthesised in THF or pyridine solution by reduction of $[(Me_3SiOUO)_2(L)]$ with one or two equivalents of potassium or KC_8. Both salts were isolated in the solid state by 18-crown-6-induced crystallisation from THF solutions and were found to easily re-oxidise to the parent complex upon addition of iodine.

The THF and 18-crown-6 adducts of $K[(Me_3SiOUO)_2(L)]$ react cleanly with water to form two $K[(Me_3SiOU)(\mu\text{-}OH)(OUO)(L)]$ solvates. The complexes exhibit localised uranyl(V)/uranium(IV) oxidation states and the reaction proceeds with desilylation of the parent complex. The mechanism or hydrolytic desilylation was examined by isolation of the potential protonated intermediate $[C_5H_5NH][(Me_3SiOUO)_2(L)]$ by cation exchange of $K[(Me_3SiOUO)_2(L)]$ with pyridinium chloride. The complex can be converted to $K[(Me_3SiOU)(\mu\text{-}OH)(OUO)(L)]$ by addition of KOH. Further studies revealed that $K[(Me_3SiOU)(\mu\text{-}OH)(OUO)(L)]$ complexes could be synthesised directly by desilylation of $[(Me_3SiOUO)_2(L)]$ with KOH and subsequent disproportionation to form the $U^{IV/V}$ complex and $K[(U^{VI}O_2)_2(\mu\text{-}OH)(L)$ although the products could not be separated.

The doubly-reduced complex $K_2[(Me_3SiOUO)_2(L)]$ was found to form the protonated $U^{IV/IV}$ complex $[K(THF)_2][(Me_3SiOU)_2(\mu\text{-}O)(\mu\text{-}OH)]$ and KOH upon boiling in excess water for 24 h. Continued boiling of the same mixture for 3 days resulted in oxidative desilylation to form the aprotic uranyl(V)/uranium(IV) ladder complex $K_2[(Me_3SiOUO)(OUO)(L)]$, which was also prepared by oxidation of $K_2[(Me_3SiOUO)_2(L)]$

with pyridine oxide or deprotonation of $K[(Me_3SiOU)(\mu\text{-}OH)(OUO)(L)]$ with KH. Double oxidative desilylation was not achieved in THF due to insolubility of this $U^{IV}U^{V}$ complex.

The crystal structure of the $[K_9(U^{V}O_2)_6U^{IV}{}_6O_6(OH)_6(L)_6(THF)_{12}]\cdot 3H_2O$ supramolecular wheel was obtained accidentally from slow oxidation and hydrolysis of $K_2[(Me_3SiOUO)_2(L)]$. Full structural analysis was achieved but no repeatable synthesis was found.

A fully desilylated butterfly complex $K_2[(OUO)_2(L)]$ was prepared reproducibly by oxidative desilylation of $K_2[(Me_3SiOUO)_2(L)]$ in pyridine with pyridine-N-oxide. The complex was found to be highly reactive towards hydrolysis, disproportionation, oxidation and oxo-group functionalisation. Treatment of the complex with TMSCl formed the silylated complex $[(Me_3SiOUO)_2(L)]$ upon which stability was restored leading to the postulate that oxo-group silylation may be used as an effective strategy for protecting highly reactive U^{V} centres and that reactivity may be switched on by protecting group removal.

Preparation of the lithium-salt of the $[(OUO)_2(L)]^{2-}$ anion was achieved in low yields directly from the Pacman macrocycle and the new uranyl(VI) –ate complex precursor $[Li(py)_2][(UO_2)\{N(SiMe_3)_2\}_3]$. In addition the mono-silylated, mono-lithio $U^{V/V}$ complex $[\{(py)_3LiOUO\}(OUOSiMe_3)(L)]$ was synthesised by treatment of $[Li(py)_2][(UO_2)\{N(SiMe_3)_2\}_3]$ with the mono-uranyl Pacman complex $[(UO_2)(py)(H_2L)]$.

3.9 References

1 F. A. Cotton, D. O. Marler, W. Schwotzer, *Inorg. Chem.* **1984**, *23*, 4211-4215.

2 A. J. Zozulin, D. C. Moody, R. R. Ryan, *Inorg. Chem.* **1982**, *21*, 3083-3086.

3 I. Korobkov, S. Gambarotta, G. P. A. Yap, *Angew. Chem.* **2002**, *114*, 3583-3586.

4 V. Mougel, J. Pecaut, M. Mazzanti, *Chem. Commun.* **2012**, *48*, 868-870.

5 G. Nocton, F. Burdet, J. Pécaut, M. Mazzanti, *Angew. Chem., Int. Ed. Engl.* **2007**, *46*, 7574-7578.

6 P. L. Arnold, E. Hollis, F. J. White, N. Magnani, R. Caciuffo, J. B. Love, *Angew. Chem., Int. Ed. Engl.* **2011**, *50*, 887-890.

7 D. D. Schnaars, G. Wu, T. W. Hayton, *Inorg. Chem.* **2011**, *50*, 9642-9649.

8 W. W. Lukens, S. M. Beshouri, L. L. Blosch, R. A. Andersen, *J. Am. Chem. Soc.* **1996**, *118*, 901-902.

9 L. H. Jones, R. A. Penneman, *J. Chem. Phys.* **1953**, *21*, 542-544.

10 A. Ikeda, C. Hennig, S. Tsushima, K. Takao, Y. Ikeda, A. C. Scheinost, G. Bernhard, *Inorg. Chem.* **2007**, *46*, 4212-4219.

11 K. Mizuoka, S. Tsushima, M. Hasegawa, T. Hoshi, Y. Ikeda, *Inorg. Chem.* **2005**, *44*, 6211-6218.

12 V. Mougel, B. Biswas, J. Pecaut, M. Mazzanti, *Chem. Commun.* **2010**, *46*, 8648-8650.

13 L. Salmon, P. Thuéry, M. Ephritikhine, *Polyhedron* **2004**, *23*, 623-627.

14 J.-C. Berthet, P. Thuéry, M. Ephritikhine, *Inorg. Chem.* **2010**, *49*, 8173-8177.

15 J.-C. Berthet, P. Thuery, M. Ephritikhine, *Chem. Commun.* **2005**, 3415-3417.

16 M. B. Robin, P. Day, in *Advances in Inorganic Chemistry and Radiochemistry, Vol. Volume 10* (Eds.: H. J. Emeléus, A. G. Sharpe), Academic Press, **1968**, pp. 247-422.

17 P. Roussel, P. B. Hitchcock, N. Tinker, P. Scott, *Chem. Commun.* **1996**, 2053-2054.

18 A. Spek, *J. Appl. Crystallogr.* **2003**, *36*, 7-13.

19 J.-C. Berthet, G. Siffredi, P. Thuéry, M. Ephritikhine, *Chem. Commun.* **2006**, 3184-3186.

20 L. Natrajan, F. Burdet, J. Pécaut, M. Mazzanti, *J. Am. Chem. Soc.* **2006**, *128*, 7152-7153.

21 G. Nocton, P. Horeglad, J. Pécaut, M. Mazzanti, *J. Am. Chem. Soc.* **2008**, *130*, 16633-16645.

22 V. Mougel, P. Horeglad, G. Nocton, J. Pécaut, M. Mazzanti, *Angew. Chem., Int. Ed. Engl.* **2009**, *48*, 8477-8480.

23 G. Nocton, P. Horeglad, V. Vetere, J. Pécaut, L. Dubois, P. Maldivi, N. M. Edelstein, M. Mazzanti, *J. Am. Chem. Soc.* **2009**, *132*, 495-508.

24 B. Biswas, V. Mougel, J. Pécaut, M. Mazzanti, *Angew. Chem., Int. Ed. Engl.* **2011**, *50*, 5745-5748.

25 V. Mougel, L. Chatelain, J. Pécaut, R. Caciuffo, E. Colineau, J.-C. Griveau, M. Mazzanti, *Nature Chem.* **2012**, *4*, 1011-1017.

26 D. S. J. Arney, C. J. Burns, *J. Am. Chem. Soc.* **1993**, *115*, 9840-9841.

27 S. Fortier, J. L. Brown, N. Kaltsoyannis, G. Wu, T. W. Hayton, *Inorg. Chem.* **2012**, *51*, 1625-1633.

28 S. C. Bart, C. Anthon, F. W. Heinemann, E. Bill, N. M. Edelstein, K. Meyer, *J. Am. Chem. Soc.* **2008**, *130*, 12536-12546.

29 B. Kosog, H. S. La Pierre, F. W. Heinemann, S. T. Liddle, K. Meyer, *J. Am. Chem. Soc.* **2012**, *134*, 5284-5289.

30 P. L. Arnold, A.-F. Pécharman, E. Hollis, A. Yahia, L. Maron, S. Parsons, J. B. Love, *Nature Chem.* **2010**, *2*, 1056-1061.

31 C. J. Burns, D. L. Clark, R. J. Donohoe, P. B. Duval, B. L. Scott, C. D. Tait, *Inorg. Chem.* **2000**, *39*, 5464-5468.

32 M. J. Sarsfield, M. Helliwell, *J. Am. Chem. Soc.* **2004**, *126*, 1036-1037.

33 J. Ling, J. Qiu, G. E. Sigmon, M. Ward, J. E. S. Szymanowski, P. C. Burns, *J. Am. Chem. Soc.* **2010**, *132*, 13395-13402.

Reactivity of unfunctionalised binuclear uranium-oxo complexes

4.1 Introduction

The binuclear uranium(V) complexes $M_2[(OUO)_2L]$ presented in Chapter Three were prepared by either redox-induced desilylation of $[(Me_3SiOUO)_2L]$ (from M = K) or directly from H_4L and $[Li(py)_2][(UO_2)(N'')_3]$ (M = Li). In this chapter, the reactions of $M_2[(OUO)_2L]$ complexes towards oxidation are presented, highlighting the contrasting reactivity between the inert, protected $[(Me_3SiOUO)_2L]$ complex and its desilylated analogues. In addition, the Group one salts $M_2[(OUO)_2L]$ are employed as precursors for new functionalised $[(ROUO)_2L]$ complexes, demonstrating how the bonding and stability of the silylated complex can be extended to other group 14 elements.

4.2 Oxidation of $K_2[(OUO)_2L]$

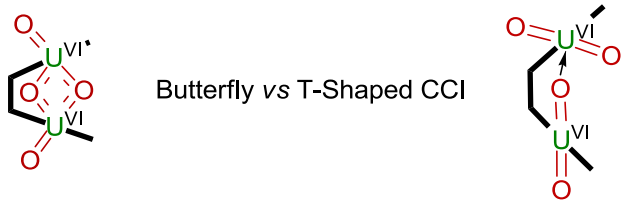

Figure 1: Possible geometries of $[(OU^{VI}O)_2(L)]$

Oxidation of the $M_2[(OU^{V}O)_2L]$ complexes were the first reactions to be studied with the hope of preparing the neutral uranium(VI) complexes $[(OU^{VI}O)_2(L)]$. The most attractive synthetic target was the complex $[(O_{exo}U)_2(\mu\text{-}O_{cis})(\mu\text{-}O_{trans})(L)]$, the uranium(VI) analogue of the butterfly molecule, which was predicted computationally by the Schreckenbach group in 2010 (Figure 1).[1] The reduced and silylated uranium(V) complex $[(Me_3SiOUO)_2L]$ (Chapter One) was the first uranium(V) complex to display both *cis* and *trans* arrangements of oxo ligands and was found to exhibit partial U–O bond multiplicity by both computational and magnetic analysis. The unsilylated uranium(VI) analogue was predicted to exhibit greater U–O bond multiplicities implying uranyl-, rather than uranium-μ-oxo-type bonding and therefore would be much closer to the elusive *cis*-uranyl geometry. An alternative geometry of $[(OU^{VI}O)_2(L)]$ is the bis-uranyl, composed of separate $[UO_2]^{2+}$ dications which may partake in intramolecular cation-cation interactions. In the original publication by Schreckenbach and co-workers, one such geometry exhibiting perpendicular or T-shaped CCIs was found to be 12.44 kcal mol^{-1} higher than the butterfly geometry,

suggesting that the complexes $M_2[(OU^VO)_2L]$ (M = Li, K) may retain their μ-oxo ligand arrangements upon oxidation.

4.2.1 Synthesis of $K_2[(\mu\text{-}\kappa^2\text{-}\kappa^2\text{-}O_2)(UO_2)_2(L)]$

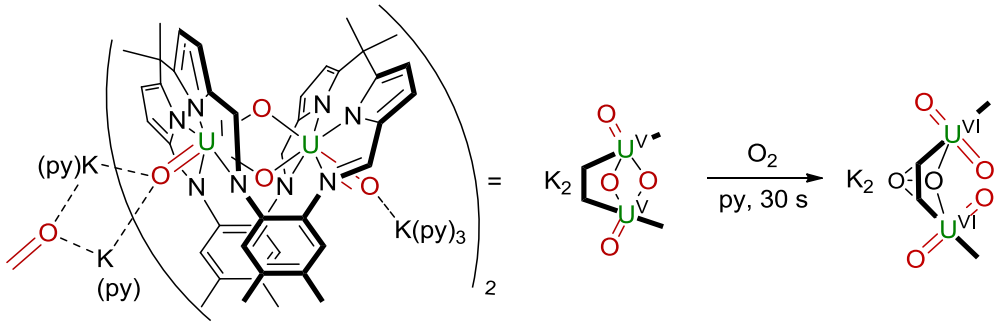

Scheme 1: Synthesis of $K_2[(\mu\text{-}\kappa^2\text{-}\kappa^2\text{-}O_2)(UO_2)_2(L)]$.

The differences in structure and bonding between oxo-silylated complex $[(Me_3SiOUO)_2L]$ and the oxo-metalated salt $K_2[(OUO)_2L]$ are mirrored by differences in their stability towards oxidation. While boiling solutions of $[(Me_3SiOUO)_2L]$ are stable indefinitely under an atmosphere of dry dioxygen, the exposure of a THF or pyridine solution of $K_2[(OUO)_2L]$ to dioxygen results in instantaneous oxidation and the sole formation of the binuclear U^{VI} peroxide $K_2[(UO_2)_2(\mu\text{-}\kappa^2\text{-}\kappa^2\text{-}O_2)(L)]$, isolated in 55 % yield as a red crystalline solid (Scheme 1).

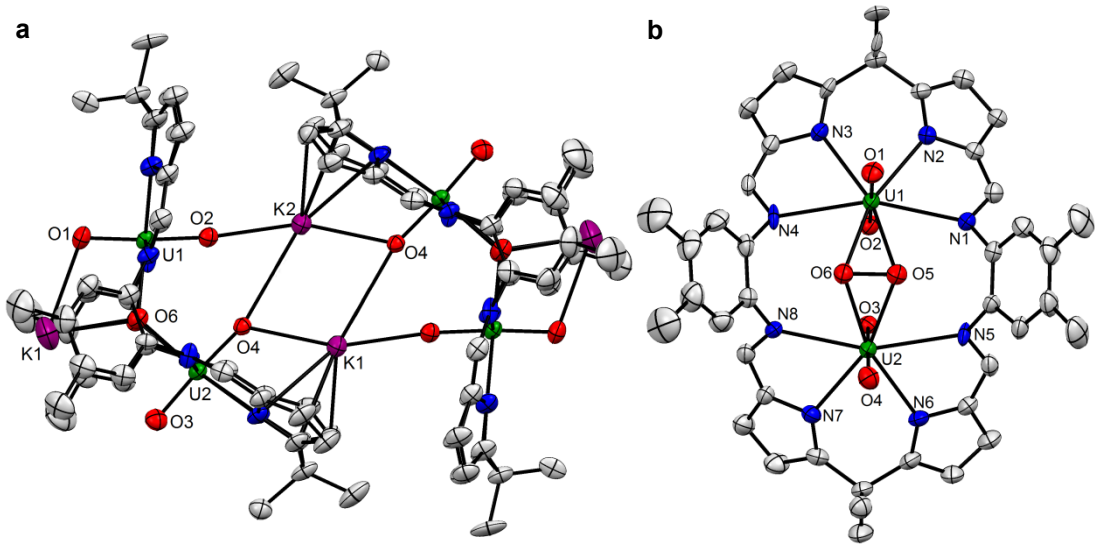

Figure 2 Displacement ellipsoid plot (50 %) of $K_2[(UO_2)_2(\mu\text{-}\kappa^2\text{-}\kappa^2\text{-}O_2)(L)]$ (**a**) Side-on, K-coordinated pyridine molecules omitted. (**b**) End-on, anion only. All free solvent molecules and H atoms omitted for clarity.

The solid state structure of $K_2[(UO_2)_2(\mu\text{-}\kappa^2\text{-}\kappa^2\text{-}O_2)(L)]$ depicts a wedge-shaped, Pacman macrocycle, with symmetric occupation of each of the N_4-donor pockets by uranyl dications (Figure 2). The $OU(\mu\text{-}O)_2UO$ cis/trans oxo-group bonding motif seen in $[(Me_3SiOUO)_2L]$ is replaced by two discrete, linear $[UO_2]^{2+}$ units in which the four U–O bond distances (1.781(6) to 1.788(6) Å) are characteristic of uranyl(VI). The accommodation of both $[UO_2]^{2+}$ dications by the macrocycle is facilitated by significant structural distortion away from the usual Pacman geometry, with opening of the mouth resulting in an inter-cleft bite angle of 90.1˚ for $K_2[(UO_2)_2(\mu\text{-}\kappa^2\text{-}\kappa^2\text{-}O_2)(L)]$ compared to 61.3˚ and 65.1˚ for $[(Me_3SiOUO)_2L]$ and the pyridine adduct of $K_2[(OUO)_2L]$, respectively; this widening of the cleft presumably prevents clashing of the *endo* oxo groups. In $K_2[(UO_2)_2(\mu\text{-}\kappa^2\text{-}\kappa^2\text{-}O_2)(L)]$, each uranium centre has approximate hexagonal bipyramidal geometry, with the two axially-bound oxo ligands sited perpendicular to the four equatorial nitrogen donors of the Pacman macrocycle. The fifth and sixth equatorial donors to each metal centre are provided by the bridging peroxide ligand, which lies sandwiched between the two aryl spacers of the wedge-shaped ligand in a $\mu\text{-}\kappa^2\text{-}\kappa^2$ motif. The O5–O6 bond length is 1.433(7) Å and is characteristic of peroxide; charge balance is maintained by retention of the two potassium cations which coordinate to the exo uranyl oxo atom O1, the bridging peroxide atoms O5 and O6, and the O2 and O4 atoms of separate Pacman molecules.

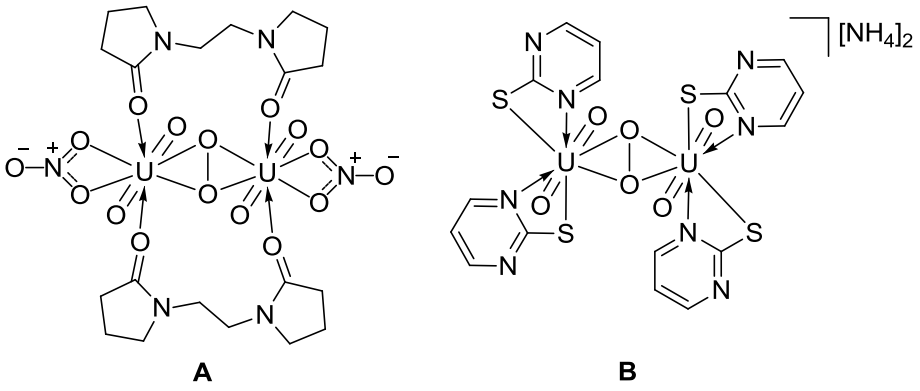

Figure 3: Other binuclear uranyl(VI) peroxide complexes

Although numerous uranyl peroxide complexes are known, they are formed exclusively by ligand exchange between uranyl(VI) precursors.[2-13] Of these examples, most are binuclear, such as the uranyl nitrate compound $[\{(UO_2(NO_3)(ebpyrr)\}_2(\mu\text{-}\kappa^2\text{-}\kappa^2\text{-}O_2)]$ (ebpyrr = *N*,*N*-ethylenebis(2-pyrrolidone)), which exhibits a slightly longer O-O bond distance than $K_2[(UO_2)_2(\mu\text{-}\kappa^2\text{-}\kappa^2\text{-}O_2)(L)]$ of 1.469(13) Å (Figure 3, **A**).[11] The uranyl(VI) thiopyramidine complex $[\{(UO_2(SC_4H_3N_2)\}_2(\mu\text{-}\kappa^2\text{-}\kappa^2\text{-}O_2)]$ is another example, displaying an O-O bond distance of 1.46(3) Å and a rare example of sulfur atom coordination of a

uranyl(VI) dication (Figure 3, **B**).[12] In contrast to these examples, $K_2[(UO_2)_2(\mu\text{-}\kappa^2\text{-}\kappa^2\text{-}O_2)(L)]$ represents the first uranyl peroxide complex formed by a redox reaction, adding to the wealth of small molecule activation chemistry known for uranium complexes.[14] The aforementioned uranyl(V) complex $[\{UO_2(TQD)\}_3]$ (see Chapter Two), recently prepared by Mazzanti and co-workers, was also shown to react with dioxygen but in that case formed an oxo-bridged uranyl(VI) complex $[\{UO_2(TQD)\}_2(\mu\text{-}O)]$.[15]

4.2.2 Synthesis of $K_2[(UO_2)_2(\mu\text{-}O)(L)]$

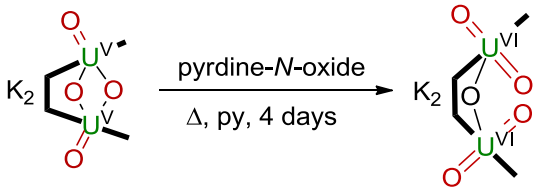

Scheme 2: Synthesis of $K_2[(UO_2)_2(\mu\text{-}O)(L)]$.

Oxidation of the U^V complex $K_2[(OUO)_2L]$ in pyridine with pyridine-*N*-oxide instead of dioxygen yields the red mono-oxo-bridged complex $K_2[(UO_2)_2(\mu\text{-}O)(L)]$ in moderate yield (Scheme 2). Unlike the reaction with oxygen, which occurs in seconds at room temperature, the synthesis of the oxo complex requires boiling of the reagents in pyridine for 4 days, perhaps as a result of the weaker oxidising power of pyridine-*N*-oxide. The ^{1}H NMR spectrum of $K_2[(UO_2)_2(\mu\text{-}O)(L)]$ displays 14 resonances for the Pacman ligand, double the number observed for the peroxide complex, and perhaps indicative of asymmetric uranyl(VI) coordination to potassium in solution. All the resonances lie in the range 1–10 ppm, the same as is observed for $K_2[(UO_2)_2(\mu\text{-}\kappa^2\text{-}\kappa^2\text{-}O_2)(L)]$ and in agreement with the formation of uranium(VI) oxidation states.

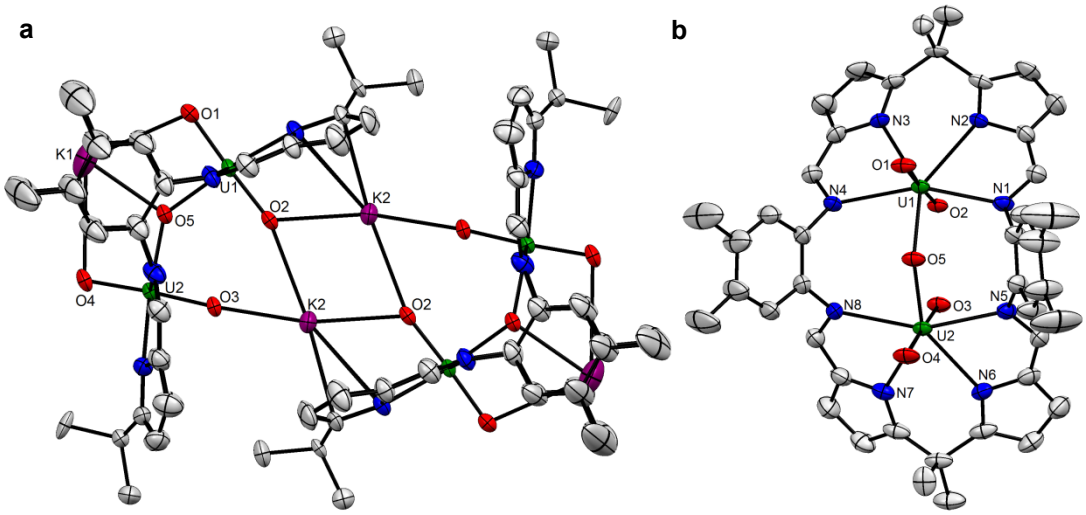

Figure 4: Displacement ellipsoid plot (50 %) of $K_2[(UO_2)_2(\mu\text{-}O)(L)]$ (**a**) Side-on, coordinated pyridine molecules omitted. (**b**) End-on, anion only. Free solvent molecules were removed by the PLATON SQUEEZE algorithm[16] and H atoms are omitted for clarity.

The solid state structure of $K_2[(UO_2)_2(\mu\text{-}O)(L)]$ is similar to that of $K_2[(UO_2)_2(\mu\text{-}\kappa^2\text{-}\kappa^2\text{-}O_2)(L)]$, with occupation of the Pacman ligand by two uranyl(VI) dications in adjacent N_4-donor pockets (Figure 4). In contrast to the peroxide complex however, the single oxide ligand O5, rather than peroxide, bridges U1 and U2 at an obtuse U1–O5–U2 angle of 136.4(3)°, resulting in pentagonal bipyramidal uranium geometries. The U–O bond distances in each uranyl(VI) dication (1.781(6) –1.788(6) Å) are almost identical to those in the peroxide complex. In further analogy with $K_2[(\mu\text{-}\kappa^2\text{-}\kappa^2\text{-}O_2)(UO_2)_2(L)]$, the mono-oxo structure exists as a crystallographic dimer maintained by uranyl/potassium CCIs.

The preparation of $K_2[(UO_2)_2(\mu\text{-}O)(L)]$ by oxidation of $K_2[(OUO)_2L]$ provides a repeatable route to salts of the $[(UO_2)_2(\mu\text{-}O)(L)]^{2-}$ anion, the uranyl complex of which, $[(UO_2)\{(UO_2)_2(\mu\text{-}O)(L)\}]$, was serendipitously isolated as a rogue crystal from aerial oxidation of the polymeric uranium(V) Pacman material **P** (see section 2.7.4). In contrast to the uranyl complex, $K_2[(UO_2)_2(\mu\text{-}O)(L)]$ does not exhibit the same U–O bond elongation of the metal-coordinated oxo groups O2 and O3 suggesting that the $[UO_2]^{2+}$/K CCI interactions in the potassium salt are weaker than those in $[(UO_2)\{(UO_2)_2(\mu\text{-}O)(L)\}]$. This is perhaps unsurprising considering the greater Lewis acidity of uranyl(VI) *vs* potassium, with uranium(VI)-oxygen bond lengths greater than 1.82 Å observed only in the rare examples of uranyl coordination complexes with stronger Lewis acids, such as $B(C_6F_5)_3$, or where the Lewis basicity of the uranyl oxo groups has been increased by strong equatorial donors such as in $[Li(py)_2][(OUO)(N'')_3]$ (see section 3.6.1 for both).[17]

4.2.3 Synthesis of $[(UO_2)\{(UO_2)_2(\mu\text{-}O)(L)\}]$

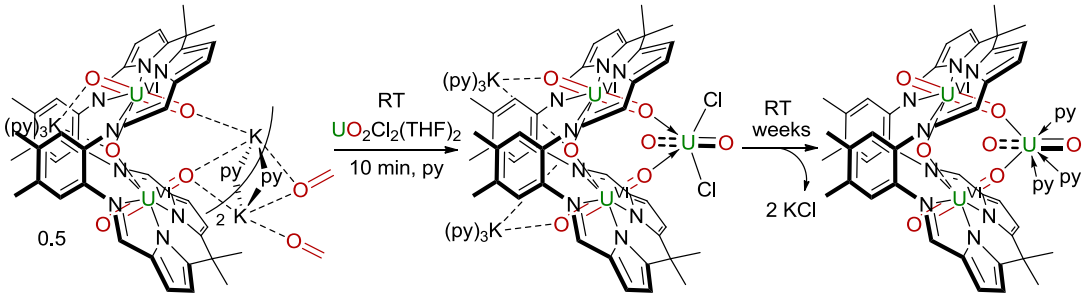

Scheme 3: Uranyl(VI) complexation by $K_2[(UO_2)_2(\mu\text{-}O)(L)]$ and subsequent salt elimination to form $[(UO_2)\{(UO_2)_2(\mu\text{-}O)(L)\}]$ via the proposed intermediate $K_2[(UO_2)_2(\mu\text{-}O)(L)\}\{UO_2Cl_2]$.

The $K_2[(UO_2)_2(\mu\text{-}O)(L)]$ complex may be converted into $[(UO_2)\{(UO_2)_2(\mu\text{-}O)(L)\}]$ by addition of one equivalent of $[UO_2Cl_2(THF)_2]$ to a pyridine solution and leaving to stand for four weeks, providing a repeatable synthesis of the serendipitously crystallised complex (Scheme 3).

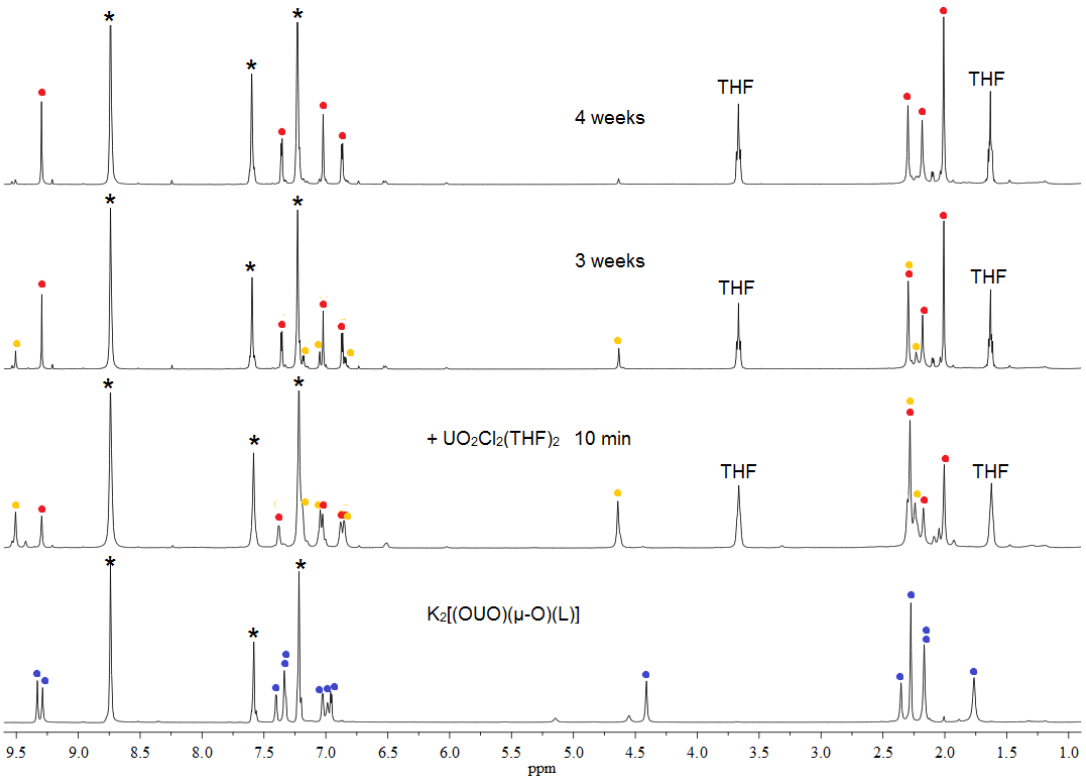

Figure 5: ^{1}H NMR spectra showing the formation of $[(UO_2)\{(UO_2)_2(\mu\text{-}O)(L)\}]$ (red) from $K_2[(UO_2)_2(\mu\text{-}O)(L)]$ (blue) and $[UO_2Cl_2(THF)_2]$ via the proposed intermediate $K_2[(UO_2)_2(\mu\text{-}O)(L)\}\{UO_2Cl_2]$ (yellow).

The brown complex exhibits seven resonances in the ^{1}H NMR spectrum within 0–10 ppm all of which are assignable to the macrocycle L and indicative of a symmetrically

occupied Pacman complex (Figure 5). The presence of two separate *endo* and *exo meso*-methyl resonances at 2.30 and 2.18 ppm indicates that the ligand folding observed in all other binuclear uranium complexes in retained. The symmetry of the complex is C_{2V}, the same as that of $K_2[(\mu\text{-}\kappa^2\text{-}\kappa^2\text{-}O_2)(UO_2)_2(L)]$ but greater than that of the starting material $K_2[(UO_2)_2(\mu\text{-}O)(L)]$ perhaps resulting from the loss of the dimeric structure in solution. Monitoring the formation of $[(UO_2)\{(UO_2)_2(\mu\text{-}O)(L)\}]$ with time by ^{1}H NMR spectroscopy reveals that disaggregation of $K_2[(UO_2)_2(\mu\text{-}O)(L)]$ in solution occurs within 10 min of addition of $[UO_2Cl_2(THF)_2]$ as evidenced by the reduction in the number of resonances from 14 to 7 and suggestive of the formation of an intermediate such as $K_2[\{(UO_2)_2(\mu\text{-}O)(L)\}\{UO_2Cl_2\}]$ (Figure 5). Over four weeks, the seven resonances assigned to the intermediate diminish concurrently with the formation of $[(UO_2)\{(UO_2)_2(\mu\text{-}O)(L)\}]$ and the precipitation of KCl. Integration of the product resonances against the two molecules of THF liberated upon dissolution of $[UO_2Cl_2(THF)_2]$ reveals that conversion to the product is quantitative.

4.2.4 Attempted syntheses of $[(OUO)_2L]$

The formation of the oxo- and peroxo-bridged complexes $K_2[(UO_2)_2(\mu\text{-}X)(L)]$ ($X = O^{2-}, O_2^{2-}$) rather than the uranium(VI) butterfly complex $[(OU)_2(\mu\text{-}O)_2(L)]$ from the oxidation of $K_2[(OUO)_2L]$ prompted investigation into the oxidation of the complex with non-oxo-containing oxidising agents. Unfortunately however, the reactions of either $K_2[(OUO)_2L]$ or $Li_2[(OUO)_2L]$ with $AgBPh_4$, iodine, Ph_3CCl or CO_2 were not successful, with the formation or intractable or unidentifiable mixtures in each case. This leads to the postulate that the oxo-bridged, binuclear uranyl(VI) compounds are significantly more stable than the hypothetical U^{VI} butterfly however no computational analysis of the former complexes has been performed to confirm this. In addition, the attempted syntheses of mixed $U^{V/VI}$ complexes by the single-electron oxidation of $[Li(py)_3][(OUO)(OUOSiMe_3)(L)]$ with half and equivalent of iodine were also unsuccessful.

4.3 Group 14 analogues of $[(Me_3SiOUO)_2L]$

It was proposed in Chapter Three that oxo-group silylation of uranium(V) oxo groups protects the highly reactive uranium(V) centres from decomposition, leading to speculation whether oxo-group functionalisation by other elements can be used to achieve the same stability. The next section illustrates how the "unprotected" group one salts $M_2[(OUO)_2L]$ (M = Li, K) can be used as precursors for new carbon- and tin-functionalised uranium(V) butterfly complexes of the type $[(ROUO)_2L]$, and how such alternative Group 14 complexes exhibit similar structures and bonding to $[(Me_3SiOUO)_2L]$.

4.3.1 Synthesis of $[(R_3SnOUO)_2L]$ complexes

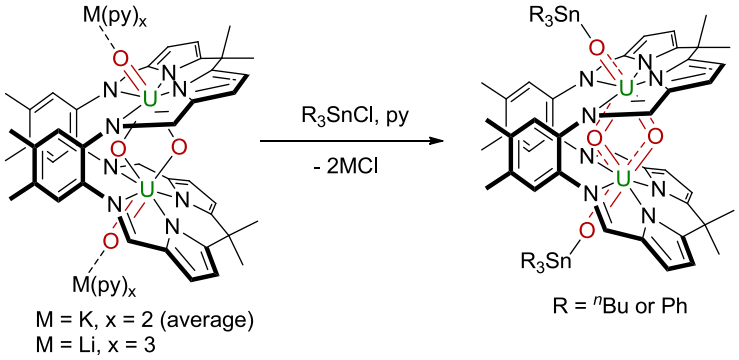

Scheme 4: Syntheses of $[(R_3Sn)OUO\}_2(L)]$

The reaction between either $Li_2[(OUO)_2L]$ or $K_2[(OUO)_2L]$ with two equivalents of $^nBu_3SnCl$ was carried out in pyridine solvent and found to yield the doubly stannylated complex $[\{(^nBu_3Sn)OUO\}_2(L)]$ (Scheme 4) as a dark red solid. The hexane-solubility of the resultant molecule facilitated its separation from the MCl (M = Li, K) by-product allowing the complex to be isolated in 70 % yield. The ^1H NMR spectrum of $[\{(^nBu_3Sn)OUO\}_2(L)]$ contains eleven paramagnetically shifted resonances between 13 and −12 ppm, seven of which are attributed to the symmetrically occupied, folded Pacman macrocycle, being situated in almost identical positions to those of $[(Me_3SiOUO)_2(L)]$, $K_2[(OUO)_2L]$ and $Li_2[(OUO)_2L]$. The remaining four resonances at 12.57, 7.96, 4.82 and 2.46 ppm are assigned to the three methylene and one methyl group of each of the six identical *n*-butyl chains and are subject to a greater paramagnetic shift the closer they are sited to the uranium centre.

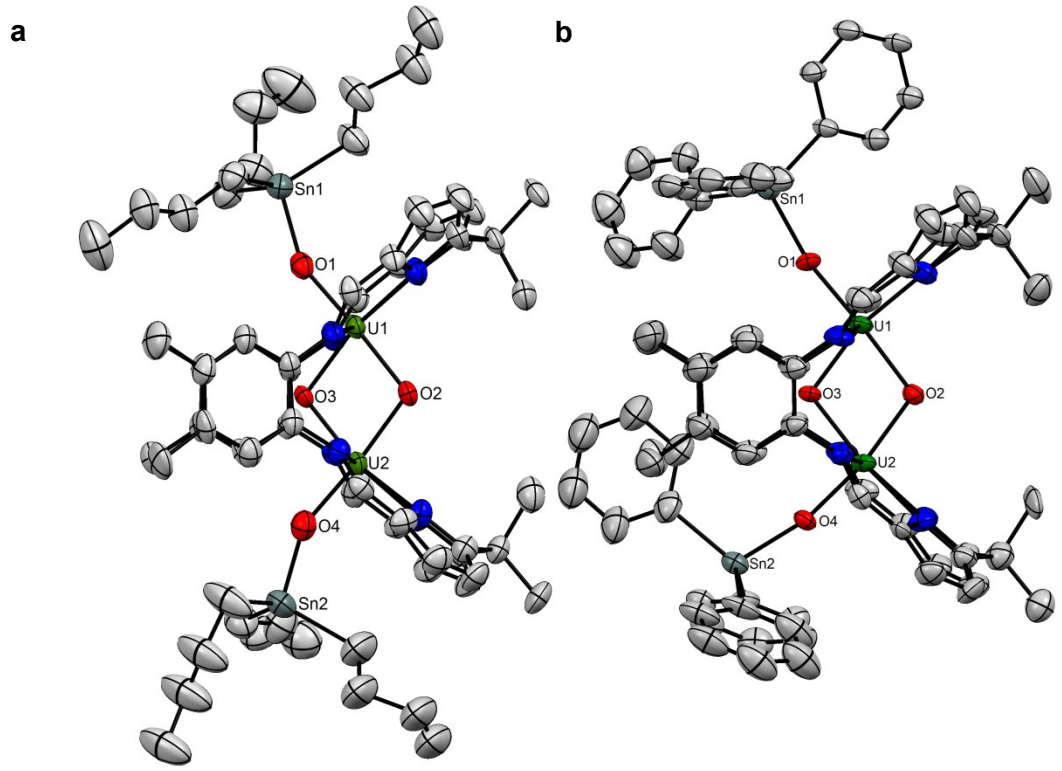

Figure 6: Displacement ellipsoid plot (50 %) of: a [($^{n}Bu_3SnOUO)_2(L)$], one of two molecules from the asymmetric unit, only one set of disordered *n*-butyl chain parts shown and solvent molecules omitted. b [$(Ph_3SnOUO)_2(L)$] one of two molecules from the asymmetric unit and solvent molecules removed by SQUEEZE. H atoms omitted for clarity.

The crystal structure of [{($^{n}Bu_3Sn$)OUO}$_2$(L)] shows that the complex adopts a similar motif to that of [$(Me_3SiOUO)_2(L)$], a binuclear uranium(V) complex with two *endo*-bound oxygen ligands bound within the intramolecular cleft in a diamond-shaped U_2O_2 arrangement, with the *exo*-bound oxygen ligands bound to the tributyl tin unit (Figure 6, a). Analysis of the bond lengths in the structure was not performed due to the weak diffraction of the crystal which presumably results from poor crystal packing between the highly flexible alkyl chains which show extensive disorder of the n-butyl groups, resulting in a high overall R-factor. A new preparation using triphenyl, rather than tributyl tin chloride as the stannylation agent was therefore performed to produce a complex with improved crystallinity. From the resulting reaction, the red complex [$(Ph_3SnOUO)_2(L)$] was produced, from which it was possible to grow higher quality crystals and therefore analyse the U–O bonding motif.

The complex [$(Ph_3SnOUO)_2(L)$] displays a similar ^{1}H NMR spectrum to [{($^{n}Bu_3Sn$)OUO}$_2$(L)], with seven ligand resonances present in all other C_{2V} symmetric $U^{V}_2O_4(L)$ complexes. Three additional resonances are attributed to the tin-bound phenyl

groups, occurring at 15.39 (12 protons), 8.95 (12 protons) and 8.34 (6 protons) and corresponding to the ortho, meta and para protons, respectively, with the ortho proton displaying the greatest paramagnetic shift. In analogy with [{(^{n}Bu$_3$Sn)OUO}$_2$(L)] and the [(RMe$_2$SiOUO)$_2$(L)] (R = Me, Ph) complexes, oxo group functionalisation facilitates high solubility allowing separation from the KCl by-product by extraction, in this case into toluene. [(Ph$_3$SnOUO)$_2$(L)**]** is isostructural with both [(RMe$_2$SiOUO)$_2$(L)] (R = Me, Ph) and [{(^{n}Bu$_3$Sn)OUO}$_2$(L)] in the solid state (Figure 6, b). The U–O bond lengths in [(Ph$_3$SnOUO)$_2$(L)**]** range between 1.987(8)–2.13(1) Å and are close to those of [(Me$_3$SiOUO)$_2$(L)], with shorter U–O bonds to the exo-stannylated oxygen atoms O1 (1.987(8) Å) and O4 (2.00(1) Å), and longer U–O bonds to the endo-bridging oxygen atoms O2 and O3 (2.057(8)–2.13(1) Å).

The smaller variation of the uranium-oxygen bond lengths in comparison to the partially- or fully-metalated compounds K$_2$[(OUO)$_2$(L)], Li$_2$[(OUO)$_2$(L)] and Li[(OUO)(OUOSiMe$_3$)(L)] is indicative of more delocalised uranium-oxygen bonding as a result of significant π-bonding interactions across the OU(O)$_2$UO network. Both [{(^{n}Bu$_3$Sn)OUO}$_2$(L)] and [(Ph$_3$SnOUO)$_2$(L)] are inert towards oxidation, remaining unchanged upon boiling benzene solutions of either complex under an oxygen atmosphere for several days. This lack of oxidation chemistry contrasts that shown by non-functionalised complexes such as K$_2$[(OUO)$_2$(L)] which readily undergoes reactions with oxygen to form the di-uranyl(VI) Pacman complex K$_2$[(μ-κ^2-κ^2-O$_2$)(UO$_2$)$_2$(L)]. The stability of [{(^{n}Bu$_3$Sn)OUO}$_2$(L)] and [(Ph$_3$SnOUO)$_2$(L)] towards oxidation suggests that R$_3$Sn groups may act similarly to R$_3$Si groups as protecting groups for U(V) oxos.

Despite the facile syntheses of the [(R$_3$SnOUO)$_2$(L)] complexes from K$_2$[(OUO)$_2$(L)], stannylated butterfly complexes cannot be prepared by treatment of the polymeric material **P** (see Chapter One) with stannyl chlorides despite the fact that **P** may be converted into silylated [(R$_3$SiOUO)$_2$(L)] complexes by reaction with chlorotrialkyl silanes. The contrasting reactivity between K$_2$[(OUO)$_2$(L)] and **P** perhaps occurs as a result of the weaker nature of the oxo-potassium electrostatic bonds in the former complex in comparison to those of the oxo-uranyl interactions assumed to be present in **P**. In addition to proving unreactive towards stannylation, **P** cannot be converted into alkylated or protonated [(ROUO)$_2$(L)] complexes by combination with of two equivalents of MeI, MeOTf, HCl, TfOH or ^{t}BuOH.

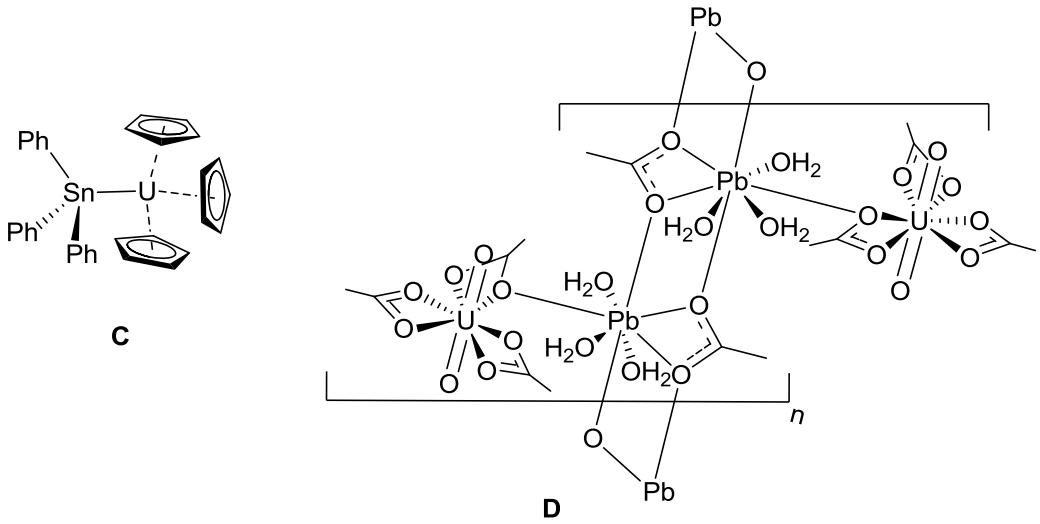

Figure 7: Other uranium complexes incorporating heavier group 14 metals.

No stannylated uranyl complex has been previously characterised. In addition, the two $[\{(R_3Sn)OUO\}_2(L)]$ complexes provide only the second and third structurally characterised examples of heterobimetallic uranium-tin complexes, the first being the complex $[(C_5H_5)_3USnPh_3]$ that contains the first actinide-metal bond (Figure 7, **C**).[18] Despite thousands of heteronuclear uranium-carbon complexes and hundreds of uranium complexes containing silicon, structurally characterised uranium complexes containing heavier group 14 complexes are extremely rare. In addition to the aforementioned example of a U–Sn complex there are three uranium materials incorporating lead, all of which are heterobimetallic uranyl(VI)/Pb coordination polymers.[19] The simplest of these materials is the uranyl-lead acetate material $[\{UO_2(OAc)_3\}\{Pb(OAc)(H_2O)_3\}]_n$ (Figure 7 **D**).[20] There are no heterobimetallic uranium-germanium complexes that have been characterised in the solid state.

The ease with which the salts of the $[(OUO)_2(L)]^{2-}$ anion can be functionalised with silicon and tin alkyl groups prompted investigation of their reactivity with transition metal halides as a number of complexes have been synthesised recently featuring oxo-group coordination of uranyl cations to transition metals.[14, 21-28] The commercially available $Ti(O^iPr)_3Cl$ was selected initially due to its high affinity for oxygen ligands and single exchangeable halide ligand.

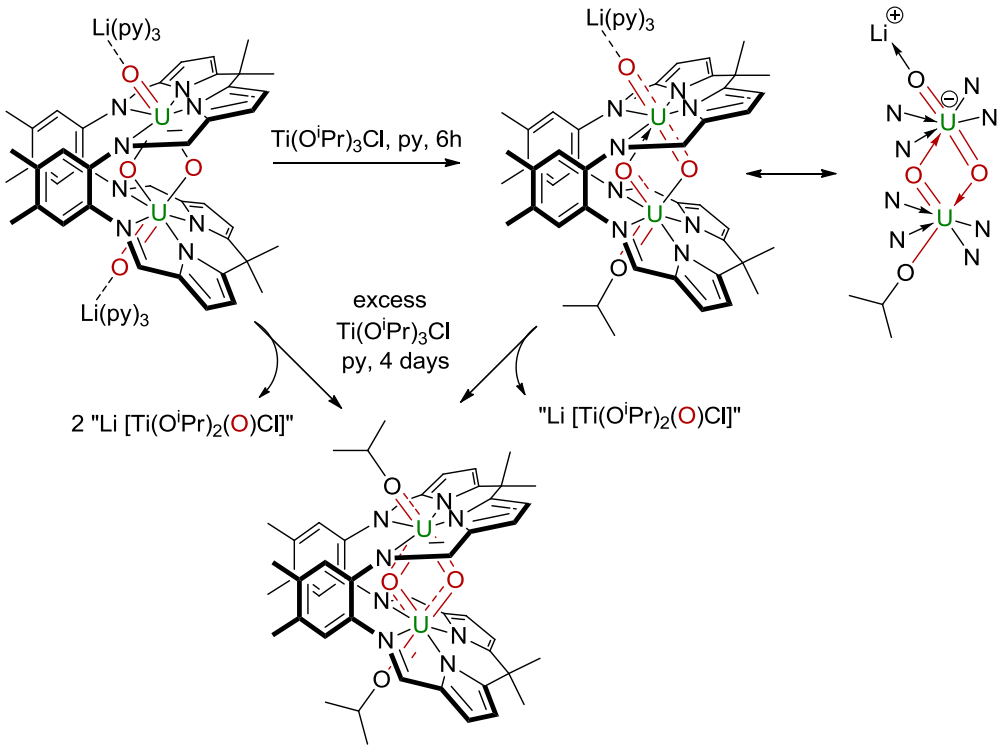

Scheme 5: Synthesis of the binuclear uranium(V) isopropoxide complexes $[Li(py)_3][(OUO)(OUO^iPr)(L)]$ and $[(^iPrOUO)_2(L)]$ by oxo-group exchange with titanium(IV).

Surprisingly, the reaction between $Li_2[(OUO)_2(L)]$ and two equivalents of $Ti(O^iPr)_3Cl$ did not generate the expected titanium-functionalised U^V–O–$Ti(O^iPr)_3$ complex but instead formed the mixed lithium/isopropyl binuclear uranium complex $[Li(py)_3][(OUO)(OUO^iPr)(L)]$ as the only product visible by ^1H NMR spectroscopy after 6 h (Scheme 5). The brown complex $[Li(py)_3][(OUO)(OUO^iPr)(L)]$ displays sixteen resonances in its ^1H NMR spectrum, fourteen of which are attributable to the Pacman ligand and occur at very similar chemical shifts to those observed for asymmetrically functionalised $[\{Li(py)_3OUO\}(OUOSiMe_3)(L)]$ (see Chapter Three). The two remaining, highly paramagnetically shifted resonances at 16.0 (6H) and 42.8 ppm (1H) are mutually coupled, as evidenced in a ^1H-^1H COSY NMR spectrum, and support the presence of a single isopropoxide group proximate to U^V.

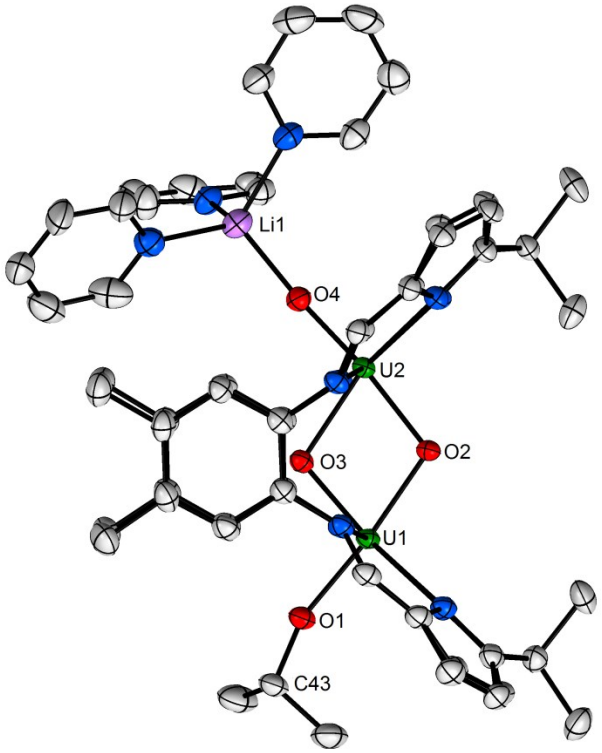

Figure 8: Crystal structure of $[Li(py)_3][(OUO)(L)(OUO^iPr)]$. All hydrogen atoms and solvent of crystallisation are omitted for clarity (displacement ellipsoids are drawn at 50 % probability).

This is further supported by analysis of the solid state structure of $[Li(py)_3][(OUO)(OUO^iPr)(L)]$ by X-ray diffraction which shows the same $OU(O)_2O$ core as present in the starting material, incorporated within the Pacman macrocycle and with the *exo*-bound oxygen atoms bound to either an isopropyl group (O1) or a lithium cation (O4) (Figure 8). The most paramagnetically shifted proton in the ^1H NMR spectrum is the methine proton of the isopropyl group and is situated one bond closer to the uranium(V) centre than both its neighbouring methyl group and the $Si(CH_3)_3$ and $Sn(CH_2)$ protons of $[(Me_3SiOUO)_2(L)]$ and $[\{(^nBu_3Sn)OUO\}_2(L)]$, perhaps explaining the extreme paramagnetic shift of that resonance in comparison to the other protons. The U1–O1 distance of 2.034(2) Å is consistent with a uranium(V) centre bound to a covalently functionalised oxo group, and is comparable to those in $[(Me_3SiOUO)_2(L)]$ (2.034(5) and 2.040(4) Å), $[\{Li(py)_3OUO\}(OUOSiMe_3)(L)]$ (2.056(2) Å), and $[(Ph_3SnOUO)_2(L)]$ (1.987(8) and 2.00(1) Å). The opposing *endo* oxo group, O4, remains bound to a lithium cation resulting in a much shorter U2–O4 multiple bond of 1.865(2) Å. As indicated by the comparable ^1H NMR spectra, $[Li(py)_3][(OUO)(OUO^iPr)(L)]$ is isostructural with the mixed lithium/silyl complex $[\{Li(py)_3OUO\}(OUOSiMe_3)(L)]$, with the complexes displaying similar bonding between the uranium(V) centres and their *endo* bridging oxygen ligands. As seen in $[\{Li(py)_3OUO\}(OUOSiMe_3)(L)]$, the mixed lithium/isopropoxide complex is composed of

mutually-planar sets of two shorter and two longer bonds between the four atoms of the U_2O_2 diamond, with U1–O3 and U2–O2 bonds of 2.013(2) and 2.076(2) Å respectively contracted in comparison to those of U1–O2 (2.111(2) Å) and U2–O3 (2.221(2) Å). The disparity between the four bonds defines O1–U1–O3 and O2–U2–O4 as discrete uranyl(V)-like cations with respective *cis* and *trans* arrangements of oxo ligands, a description that contrasts to the more symmetric arrangements of U–O bonds in $[(Me_3SiOUO)_2(L)]$, $K_2[(OUO)_2(L)]$, $Li_2[(OUO)_2(L)]$, and $[(Ph_3SnOUO)_2(L)]$.

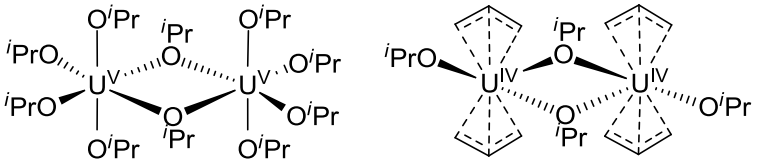

E F

Figure 9: Other uranium isopropoxide complexes.

Similar U–O bond distances to those displayed by $[Li(py)_3][(OUO)(OUO^iPr)(L)]$ are present in $[U_2(O^iPr)_{10}]$ (e.g. 2.03(1) Å), the only other structurally characterised uranium(V) isoproxide complex known (Figure 9, **E**),[29] with U^{IV}–O^{i}Pr complexes such as $[\{(^iPrO)(C_3H_5)U\}_2(\mu\text{-}O^iPr)_2]$ exhibiting larger average uranium-oxygen bond lengths (2.25 Å).[30]

The surprising tendency of only one of the *exo* oxo groups to react with $Ti(O^iPr)_3Cl$ over the reaction period prompted repetition of the reaction with a single equivalent of $Ti(O^iPr)_3Cl$ which produced $[Li(py)_3][(OUO)(L)(OUO^iPr)]$ as the only major product in pyridine solution. Despite the stability of the complex in pyridine and the ability to grow low yield batches of crystals of the complex from the crude reaction mixture, its isolation in the bulk was not achieved, with attempts to separate the complex from the lithium- and titanium-containing by-products by extraction into toluene resulting in ligand redistribution to form 0.5 equivalents of the doubly lithiated salt $Li_2[(OUO)_2(L)]$ and half an equivalent of the bis-isopropoxide-uranium(V) complex $[(^iPrOUO)_2(L)]$. The ^{1}H NMR spectrum of $[(^iPrOUO)_2(L)]$ exhibits seven resonances assigned to the Pacman ligand between 14 and −12 ppm which are found in almost identical positions to those for the symmetric bis-silyl and bis-stannyl complexes. The remaining resonances in the spectrum of $[(^iPrOUO)_2(L)]$ are the strongly paramagnetically shifted isopropyl resonances at 53.28 (2H) and 21.76 ppm (12H). Attempts to produce $[(^iPrOUO)_2(L)]$ in a more efficient manner, by the reaction of $Li_2[(OUO)_2(L)]$ with two equivalents of $Ti(^iOPr)_3Cl$ in pyridine, were inhibited by the slow rate of reaction, with just 25 % completion to $[(^iPrOUO)_2(L)]$ after 4 days. The use of either

$K_2[(OUO)_2(L)]$ as an alternative starting material or non-coordinating solvents resulted in diminished solubility of the reactants, slowing the rate of reaction even further. Attempts to accelerate the conversion using elevated temperatures resulted in decomposition. Both the slow rate of reaction to form $[(^i PrOUO)_2(L)]$ and the aforementioned tendency of the intermediate complex $[Li(py)_3][(OUO)(L)(OUO^iPr)]$ to rearrange to $Li_2[(OUO)_2(L)]$ and $[(^i PrOUO)_2(L)]$ suggested the presence of an equilibrium between the two complexes. As a result, the reaction to form $[(^i PrOUO)_2(L)]$ was attempted with a five-equivalent excess of $Ti(^i OPr)_3Cl$, resulting in the full conversion of the starting material to the desired product in four days. Removal of the excess $Ti(iOPr)_3Cl$ by vacuum distillation followed by extraction and crystallisation from Et_2O allowed pure $[(^i PrOUO)_2(L)]$ to be isolated in 85 % yield as a brown solid (Scheme 5).

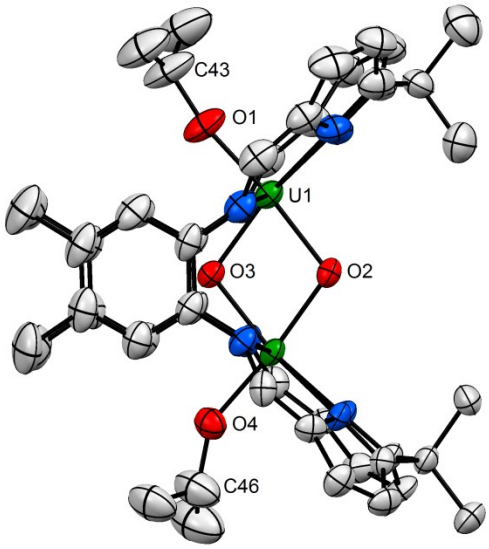

Figure 10: Solid state structure of $[(^i PrOUO)_2(L)]$. Isopropoxide group starting C43 is disordered over two sites, only one is shown. For clarity, all hydrogen atoms and solvent of crystallization are omitted (displacement ellipsoids are drawn at 50 % probability).

The growth of single crystals of $[(^i PrOUO)_2(L)]$ permitted elucidation of the solid state structure which contains isopropyl groups bound to each of the *exo*-bound oxo groups of the uranium(V) centres (Figure 10). The U1–O1 and U2–O4 bond lengths between the metal centres and the isopropoxide-functionalised oxo groups are 2.0135(1) and 2.0109(1) Å respectively and are slightly shorter than the analogous bond in $[Li(py)_3][(OUO)(L)(OUO^iPr)]$ (2.034(2) Å). In comparison with the other covalently-functionalised uranium(V) oxo compounds $[(Me_3SiOUO)_2(L)]$ and $[(Ph_3SnOUO)_2(L)]$, all the U–O bond lengths in $[(^i PrOUO)_2(L)]$ show less variation than those which are oxo-

metalated, with the range of 2.0109(1)–2.1157(1) Å suggestive of a delocalised U_2O_4 bonding environment.

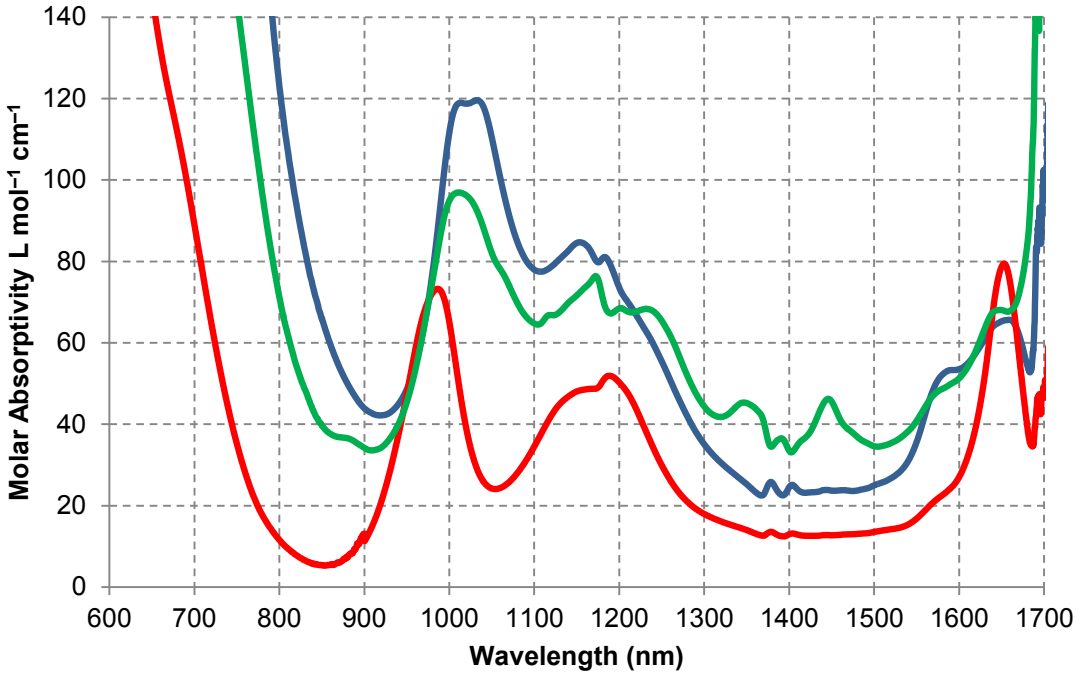

Figure 11: Absorption spectra of $[(Me_3SiOUO)_2(L)]$ (blue), $[\{(^nBu_3Sn)OUO\}_2(L)]$ (red) and $[(^iPrOUO)_2L]$ (green) in THF.

The complex $[(^iPrOUO)_2(L)]$ may be considered an alkylated analogue of the doubly silylated or stannylated uranium(V) oxo complexes $[(Me_3SiOUO)_2(L)]$, $[\{(^nBu_3Sn)OUO\}_2(L)]$, and $[Ph_3SnOUO\}_2(L)]$, and exhibits similar inertness towards oxidation. Furthermore, the similarity between the UV-vis-NIR absorption spectra of the symmetric bis-alkyl, silyl, and stannyl complexes supports further the assertion that they contain similar U–O bonding (Figure 11).

A comparative table of U–O bond lengths for the $[(ROUO)_2(L)]$, $M_2[(OUO)_2(L)]$ and M $[(OUO)(OUOR)(L)]$ complexes is shown in Table 1.

Table 1: U-O bond lengths (Å) in binuclear uranium(V) oxo complexes.

R1 / R4	U1–O1	U1–O2	U1–O3	U2–O2	U2–O3	U2–O4	$U–O_{av}$
Me_3Si	2.034(5)	2.099(3)	2.098(3)	2.085(4)	2.095(3)	2.040(4)	2.075
Ph_3Sn	1.988(8)	2.058(8)	2.126(8)	2.114(8)	2.088(8)	1.997(8)	2.062
^{i}Pr	2.014(6)	2.106(5)	2.095(6)	2.081(6)	2.116(5)	2.011(6)	2.086
Li	1.876(4)	2.110(4)	2.110(4)	2.101(4)	2.116(4)	1.883(4)	2.033
K	1.851(6)	2.090(6)	2.168(5)	2.101(5)	2.105(6)	1.871(5)	2.031
Me_3Si / Li	2.056(2)	2.113(2)	2.024(2)	2.077(2)	2.238(2)	1.857(2)	2.061
^{i}Pr / Li	2.034(2)	2.111(2)	2.013(2)	2.076(2)	2.221(2)	1.865(2)	2.053

Key: Top = symmetrically functionalised complexes, middle = symmetrically metalated complexes, bottom = asymmetric mono-metalated/mono-functionalised complexes. Atom labelling: O1 and O4 = *exo*, O2 = *cis*-bridging *endo*, O3 = *trans*-bridging *endo*. Rn = substiuent bound to On.

4.3.2 Mechanism of oxo group exchange

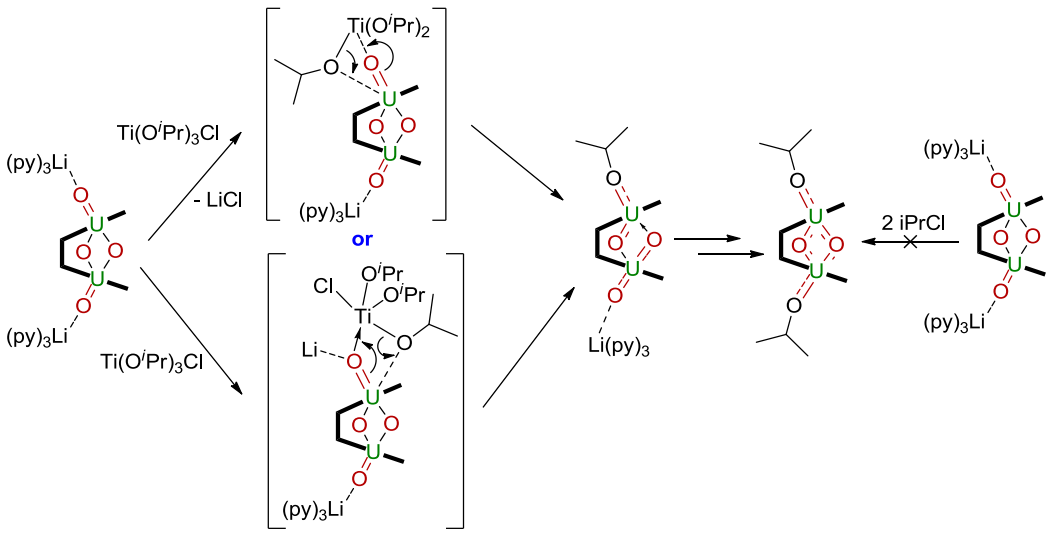

Scheme 6: Potential mechanisms of oxo/isopropoxide exchange through intra- or inter-molecular processes.

The isolation of the isoproxide complexes $[Li(py)_3][(OUO)(L)(OUO^iPr)]$ and $[(^iPrOUO)_2(L)]$ is unexpected considering that the attempted salt elimination reactions between $Li_2[(OUO)_2(L)]$ or $K_2[(OUO)_2(L)]$ and ^iPrCl did not result in formation of either product, instead yielding intractable mixtures (Scheme 6). The formation of $[Li(py)_3][(OUO)(L)(OUO^iPr)]$ and $[(^iPrOUO)_2(L)]$ from a titanium isoproxide precursor indicates that a ligand exchange reaction between the uranium(V) and titanium(IV) metal centres occurs, this is perhaps due to the greater oxophilicity of the smaller Group IV metal than uranium although the exact nature of the Ti- and Li- containing oxo by-product(s) could not be determined. It is possible that the reaction proceeds by the initial formation of the titanium-functionalised complex $[\{(^iPrO)_3Ti\}OUO)_2(L)]$ by salt elimination, followed by an intramolecular oxo-isopropoxide exchange between the Ti and U metal centres yielding the isoproxide butterfly complexes and a $\{Ti(O^iPr)_2O\}_n$ by-product (Scheme 6). A second possibility is the exchange occurs directly from $Ti(O^iPr)_3Cl$ by an single-step, intermolecular process, with the elimination of a $Li[Ti(O^iPr)_2(O)Cl]$ –ate complex as the by-product.

Efforts to elucidate the nature of the by-product by NMR spectroscopy and ESI-MS were unsuccessful, perhaps unsurprisingly, considering the speciation of titainium-oxide-alkoxide compounds is extremely complex, with four structurally characterised examples of such clusters ranging from Ti_{11}-Ti_{17} in size and each exhibiting different $Ti_x(O^iPr)_y(O)_z$ stoichiometries.[31-35]

The exchange of oxo-groups in $K_2[(OUO)_2(L)]$ and $Li_2[(OUO)_2(L)]$ with titanium-bound isoproxide ligands is only the second known example of the complete removal of a multiply-bound oxo ligand from a high-valent uranium complex, the first being the reductive abstraction of the oxo ligands in UO_2I_2 with Me_3SiX (X = Cl, Br, I) to form the U(IV) halides, UX_4 and two equivalents of $(Me_3Si)_2O$.[36] Attempts to produce an analogous $[(ClUO)_2(L)]$ complex from oxo/halide exchange between $Li_2[(OUO)_2(L)]$ and $TiCl_4$ were unsuccessful, resulting in only in starting material decomposition. Such contrasting reactivity is perhaps due to the weaker nature of the U^V–Cl in the target complex bond in comparison to the U^V–OR bonds formed in $[(^iPrOUO)_2(L)]$ or due to a complicating $Ti^{III/IV}$ redox reaction.

4.4 Attempted syntheses of other oxo-functionalised complexes

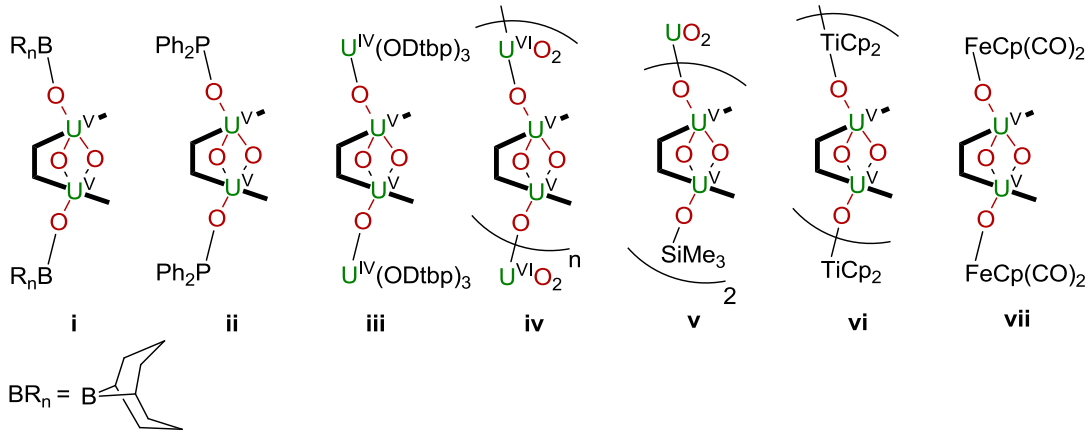

Figure 12: Target binuclear uranium(V) oxo complexes which could not be synthesised

The simple preparations of the uranium(V)/group 14 complexes led to attempts to extend the oxo-group functionalisation of the $[(OU^{V}O)_2(L)]$ species to other elements. Efforts to synthesise covalently-functionalised $[(ROU^{V}O)_2(L)]$ complexes containing O–B or O–P bonds were however unsuccessful from reactions of either $Li_2[(OUO)_2(L)]$ or $K_2[(OUO)_2(L)]$ with two equivalents of 9-BBN-I (9-BBN = 9-borabicyclo[3.3.1]nonane) or Ph_2PCl (Figure 12, i+ii). In all cases, either insoluble precipitates or complex mixtures of unidentified products were observed to form, a result perhaps due to the greater oxophillicity of boron and phosphorus resulting in unwanted oxo-abstraction processes and subsequent decomposition. The attempted transmetalation of $Li_2[(OUO)_2(L)]$ with $U(ODtbp)_3I$ to form the uranium(IV) functionalised complex $[\{(U\{ODtbp\}_3)OUO\}_2(L)]$ was also attempted with the aim to studying the magnetic properties of the resulting mixed valence complex. The precipitation of intractable materials was again however observed to occur upon reagent combination (Figure 12, iii). The synthesis of dimeric or polymeric materials of similar composition to the polyatomic uranium(V)/uranyl(VI) material **P** were also attempted by the reaction of single or half equivalents of $UO_2Cl_2(THF)_2$ with $Li_2[(OUO)_2(L)]$ or $Li[(OUO)(OUOSiMe_3)(L)]$ respectively (Figure 12, iv, v). Again, only intractable materials were produced, the further characterisation of which was not possible. Finally, attempts to synthesise similar transition metal functionalised complexes using $TiCp_2Cl_2$ or $[\{CpFe(CO_2)I\}_2]$ as precursors were also unsuccessful (Figure 12, target molecules vi, vii).

4.5 Summary

The desilylated complex $K_2[(OUO)_2(L)]$ is highly reactive towards oxidation, facilitating the formation of the oxo and peroxo-bridged compounds $K_2[(UO_2)_2(\mu\text{-}\kappa^2\text{-}\kappa^2\text{-}O_2)(L)]$ and $K_2[(UO_2)_2(\mu\text{-}O)(L)]$ from addition of oxygen and pyridine-*N*-oxide respectively.

Both complexes contain two discrete uranyl dications, and not the elusive uranium(VI) butterfly species {$OU(\mu\text{-}O)_2UO$} which contains both *cis*- and *trans*-uranyl cations fused in a diamond-shaped motif. Attempts to synthesise the uranium(VI) butterfly complex from oxidation of either $K_2[(OUO)_2(L)]$ or $Li_2[(OUO)_2(L)]$ with non-oxygen containing oxidising agents were similarly unsuccessful.

The complexes $[\{(^nBu_3Sn)OUO\}_2(L)]$, $[(PhSnOUO)_2(L)]$ and $[(^iPrOUO)_2(L)]$ add to the family of binuclear oxo uranium(V) complexes featuring the $(ROUO)_2$ motif, with alkyl, silyl, and stannyl derivatives all displaying a cis/trans arrangement of the oxo ligands and extending the covalent functionalization of uranium oxo groups to tin and carbon. Furthermore, the high stabilities of these compounds against oxidative decomposition provide further evidence that highly reactive uranium(V) centres can be 'protected' by functionalisation of their oxo ligands with Group 14 elements. No other $[(ROUO)_2(L)]$ complexes could be synthesised using reagents containing elements outside of group 14 despite a number of attempted reactions.

4.6 References

1 Q.-J. Pan, G. Schreckenbach, *Inorg. Chem.* **2010**, *49*, 6509-6517.

2 I. M. Aladzheva, O. V. Bykhovskaya, Y. V. Nelyubina, Z. S. Klemenkova, P. V. Petrovskii, I. L. Odinets, *Inorg. Chim. Acta* **2011**, *373*, 130-136.

3 R. Haegele, J. C. A. Boeyens, *J. Chem. Soc., Dalton Trans.* **1977**, 648-650.

4 P. Thuéry, M. Nierlich, B. W. Baldwin, N. Komatsuzaki, T. Hirose, *J. Chem. Soc., Dalton Trans.* **1999**, 1047-1048.

5 G. E. Sigmon, J. Ling, D. K. Unruh, L. Moore-Shay, M. Ward, B. Weaver, P. C. Burns, *J. Am. Chem. Soc.* **2009**, *131*, 16648-16649.

6 G. H. John, I. May, M. J. Sarsfield, H. M. Steele, D. Collison, M. Helliwell, J. D. McKinney, *Dalton Trans.* **2004**, 734-740.

7 A. R. de Aquino, P. C. Isolani, J. Zukerman-Schpector, L. B. Zinner, G. Vicentini, *J. Alloys Compd.* **2001**, *323–324*, 18-21.

8 B. Masci, P. Thuéry, *Polyhedron* **2005**, *24*, 229-237.

9 J. Ling, J. Qiu, G. E. Sigmon, M. Ward, J. E. S. Szymanowski, P. C. Burns, *J. Am. Chem. Soc.* **2010**, *132*, 13395-13402.

10 J. Ling, C. M. Wallace, J. E. S. Szymanowski, P. C. Burns, *Angew. Chem., Int. Ed. Engl.* **2010**, *49*, 7271-7273.

11 G. A. Doyle, D. M. L. Goodgame, A. Sinden, D. J. Williams, *J. Chem. Soc., Chem. Commun.* **1993**, 1170-1172.

12 D. Rose, Y.-D. Chang, Q. Chen, J. Zubieta, *Inorg. Chem.* **1994**, *33*, 5167-5168.

13 P. Thuéry, B. Masci, *Supramol. Chem.* **2003**, *15*, 95-99.

14 P. L. Arnold, *Chem. Commun.* **2011**, *47*, 9005-9010.

15 L. Chatelain, V. Mougel, J. Pecaut, M. Mazzanti, *Chem. Sci.* **2012**, *3*, 1075-1079.

16 A. Spek, *J. Appl. Crystallogr.* **2003**, *36*, 7-13.

17 M. J. Sarsfield, M. Helliwell, *J. Am. Chem. Soc.* **2004**, *126*, 1036-1037.

18 M. Porchia, U. Casellato, F. Ossola, G. Rossetto, P. Zanella, R. Graziani, *J. Chem. Soc., Chem. Commun.* **1986**, 1034-1035.

19 M. Frisch, C. L. Cahill, *Dalton Trans.* **2006**, *0*, 4679-4690.

20 L. B. Serezhkina, A. V. Vologzhanina, V. V. Klepov, V. N. Serezhkin, *Kristallografiya* **2011**, *56*, 138-141.

21 P. L. Arnold, D. Patel, A. J. Blake, C. Wilson, J. B. Love, *J. Am. Chem. Soc.* **2006**, *128*, 9610-9611.

22 P. L. Arnold, D. Patel, C. Wilson, J. B. Love, *Nature* **2008**, *451*, 315-317.

23 C. L. Cahill, D. T. de Lill, M. Frisch, *CrystEngComm* **2007**, *9*, 15-26.

24 A. N. Alsobrook, B. G. Hauser, J. T. Hupp, E. V. Alekseev, W. Depmeier, T. E. Albrecht-Schmitt, *Chem. Commun.* **2010**, *46*, 9167-9169.

25 Y. Yu, W. Zhan, T. E. Albrecht-Schmitt, *Inorg. Chem.* **2007**, *46*, 10214-10220.

26 S. Wu, J. Ling, S. Wang, S. Skanthakumar, L. Soderholm, T. E. Albrecht-Schmitt, E. V. Alekseev, S. V. Krivovichev, W. Depmeier, *Eur. J. Inorg. Chem.* **2009**, *2009*, 4039-4042.

27 A. N. Alsobrook, E. V. Alekseev, W. Depmeier, T. E. Albrecht-Schmitt, *Cryst. Growth Des.* **2011**, *11*, 2358-2367.

28 P. Thuéry, *Inorg. Chem. Commun.* **2009**, *12*, 800-803.

29 F. A. Cotton, D. O. Marler, W. Schwotzer, *Inorg. Chem.* **1984**, *23*, 4211-4215.

30 M. Brunelli, G. Perego, G. Lugli, A. Mazzei, *J. Chem. Soc., Dalton Trans.* **1979**, *0*, 861-868.

31 N. Steunou, F. Ribot, K. Boubekeur, J. Maquet, C. Sanchez, *New J. Chem.* **1999**, *23*, 1079-1086.

32 A. Senouci, M. Yaakoub, C. Huguenard, M. Henry, *J. Mater. Chem.* **2004**, *14*, 3215-3230.

33 N. Steunou, F. Robert, K. Boubekeur, F. Ribot, C. Sanchez, *Inorg. Chim. Acta* **1998**, *279*, 144-151.

34 N. Steunou, G. Kickelbick, K. Boubekeur, C. Sanchez, *J. Chem. Soc., Dalton Trans.* **1999**, *0*, 3653-3655.

35 V. W. Day, T. A. Eberspacher, W. G. Klemperer, C. W. Park, *J. Am. Chem. Soc.* **1993**, *115*, 8469-8470.

36 J.-C. Berthet, G. Siffredi, P. Thuéry, M. Ephritikhine, *Eur. J. Inorg. Chem.* **2007**, *2007*, 4017-4020.

Uranyl(VI) complexes of alternative polypyrrolic ligands

5.1 Introduction

In the previous chapters, the octamethylated polypyrrolic Schiff base macrocycle L was used to prepare a number of binuclear uranium oxo complexes of various bonding types and oxidation states. In this chapter, the uranyl chemistry of other polypyrrolic ligands is presented, demonstrating how modification of the macrocyclic environment can be used to synthesise complexes of alternative structures to those derived from L.

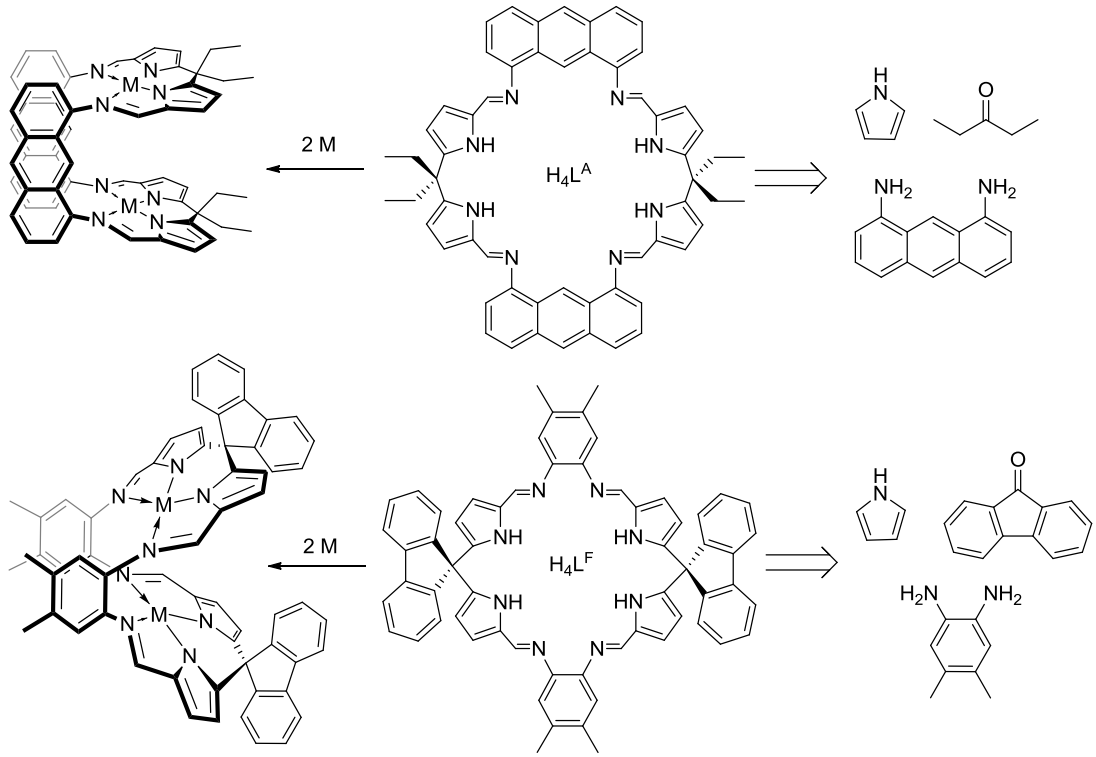

Figure 1: Structures of the Pacman ligands H_4L^A (top) and H_4L^F (bottom), the reagents used for their preparation and their ensuing structures upon metal coordination.

Structural modification of L is relatively straightforward due to the ligands simple three-step synthesis from pyrrole, acetone and 1,2-diamino 4,5-dimethyl benzene,[1] with substitution of either of the latter two reagents for alternative ketones or aryl diamines allowing the formation of alternatively substituted Pacman ligands.[2] Two new macrocycles, H_4L^A and H_4L^F, have been recently prepared by our group using this methodology, with both molecules being used as ligands for transition metal complexes. [3] In both cases, structural modifications were made to L for the specific purpose of allowing greater metal-metal

separations in the ensuing complexes, resulting in both ligands being attractive candidates for the synthesis of binuclear uranyl complexes. In exploring the uranyl chemistry of both H_4L^A and H_4L^F it was hoped that altering the M···M spacing would induce other bonding motifs than those observed in the $U_2O_4(L)$ "butterfly" complexes.

The first of the two ligands, H_4L^A, is an anthracenyl-substituted Pacman macrocycle synthesised using 1,8 diaminoanthracene in place of the 1,2-diamino 4,5-dimethyl benzene used in the synthesis of H_4L. Upon metal binding to L^A and subsequent macrocylic folding, the elongated aromatic fragment is observed to force the two N_4-donor pockets apart resulting in increased metal-metal separation that is enforced by the rigidity of the anthracenyl backbone (Figure 1).[3] The second ligand, H_4L^F is fluorenyl-substituted, with retention of the phenylene spacer present in L but exchange of *meso*-methyl groups for bulky aromatic groups by the replacement of acetone with fluorenone in the macrocycle synthesis (Figure 1). It was previously observed by our group that the use of more sterically hindering *meso*-substitutents promotes a lateral twist between the upper and lower macrocyclic binding pockets and therefore "opens the mouth" of the cleft upon metal-induced ligand folding, resulting in increased M···M separations in comparison with L.[3]

5.2 Uranyl(VI) complexes of H_4L^A

The mono-uranyl, octamethyl-Pacman, complexes $[UO_2(sol)(H_2L)]$ (sol = THF, pyridine) are synthesised in high yields by transamination reactions between $[UO_2(N")_2(THF)_2]$ and H_4L in THF or pyridine.[4-5] As such, a similar method was used to synthesise uranyl complexes of H_4L^A, with pyridine selected as the solvent due to poor solubility of the macrocycle in THF.

5.2.1 Synthesis of the mononuclear complex $[UO_2(py)(H_2L^A)]$

The reaction between the anthracenyl macrocycle H_4L^A and one equivalent of $[UO_2(N")_2(py)_2]$ in pyridine was not as straightforward as the analogous reaction of H_4L, affording a mixture of the mono- and binuclear complexes $[UO_2(py)(H_2L^A)]$ and $[\{UO_2(py)\}_2(L^A)]$ respectively, in addition to HN" and unreacted H_4L^A in a 70:15:200:15 ratio (Figure 2). Attempts to thermally comproportionate the mixture by extensive boiling had no effect while the use of sub-stoichiometric amounts of the uranyl silyamido base also resulted in the formation of mixtures.

$H_4L^A + [UO_2(N'')_2(py)_2] \longrightarrow 0.7\ [UO_2(py)(H_2L^A)] + 0.15\ [\{UO_2(py)\}_2(L^A)] + 0.15\ H_4L^A + 2\ HN''$

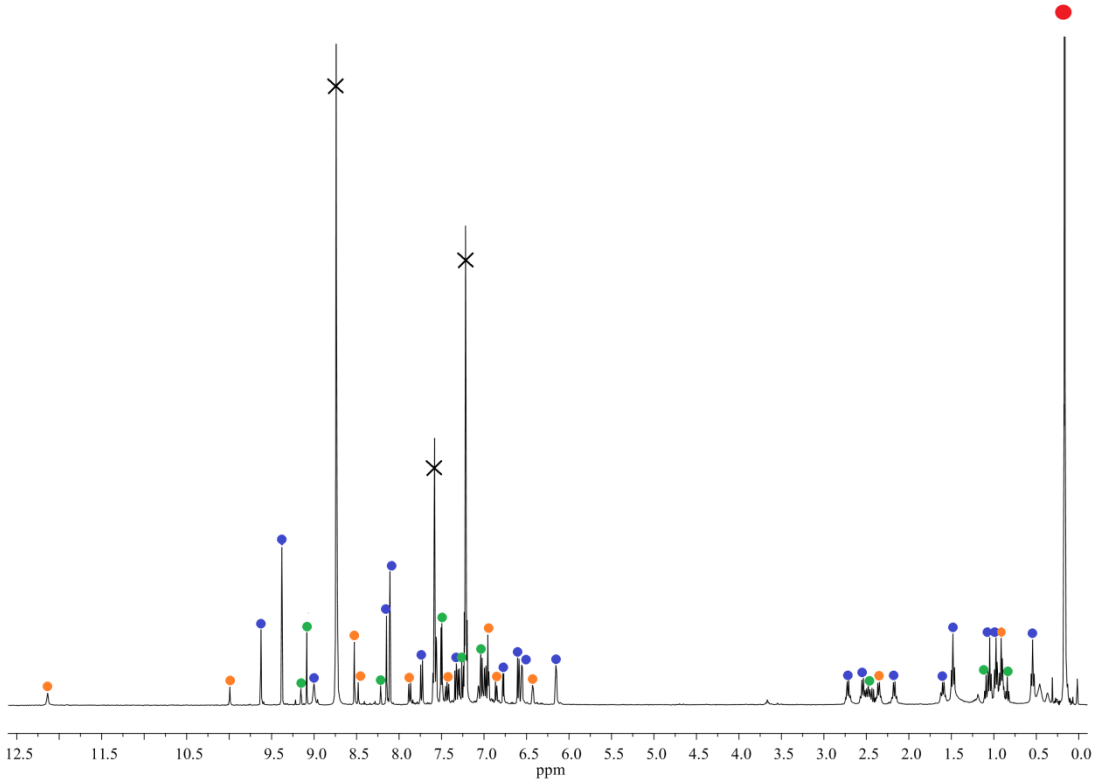

Figure 2: ^{1}H NMR spectrum of the mixture of $[UO_2(py)(H_2L^A)]$ (blue markers), $[\{UO_2(py)\}_2(L^A)]$ (green markers), HN'' (red marker) and unreacted H_4L^A (orange markers).

The ^{1}H NMR spectrum of the mixture contains 23 resonances attributable to $[UO_2(py)(H_2L^A)]$ all of which are assigned to the ligand L^A and are indicative of asymmetric occupation of the two N_4-donor pockets as evidenced by twin sets of imine, α- and β-pyrrole resonances, as well as 8 resonances arising from the anthracene backbone. Further evidence for mono-uranyl incorporation is given by a single resonance at 9.01 ppm for two protons, assigned to the NH groups of the unoccupied donor pockets. Evidence of ligand folding is derived from the two sets of four resonances each for the CH_2 (2.71, 2.54, 2.17 and 1.60 ppm) and CH_3 protons (1.47, 1.05, 0.97 and 0.54 ppm) of the ethyl *meso* groups with magnetic non-equivalence between the two sets the result of distinct inner- (*endo*) and outer-cleft (*exo*) ethyl groups.

The compounds $[\{UO_2(py)\}_2(L^A)]$, $[UO_2(py)(H_2L^A)]$ and H_4L^A all exhibit similar solubilities, being insoluble in non-polar organic solvents and poorly soluble in pyridine, a property which causes undesired precipitation of products over the course of the reaction. Separation of the products from the 1:1 reaction between H_4L^A and $[UO_2(N'')_2(py)_2]$ was

therefore not possible although the structure of the mono-uranyl complex was further verified by analysis of the crude mixture by MALDI mass spectrometry (Figure 3).

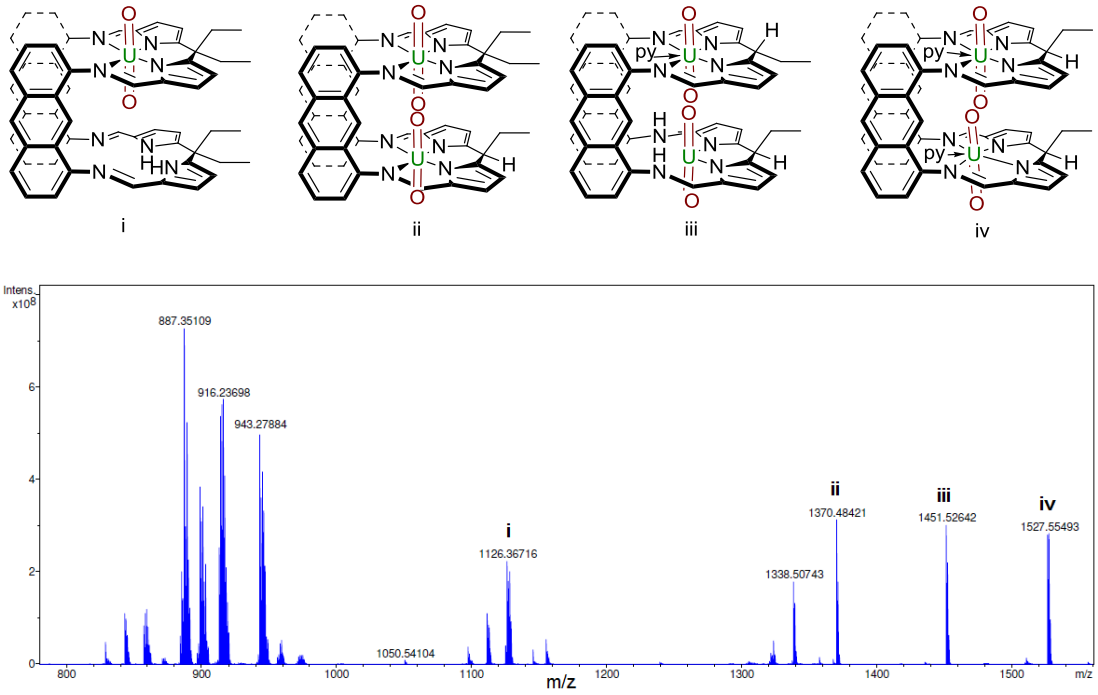

Figure 3: MALDI mass spectrum of a mixture of $[\{UO_2(py)\}_2(L^A)]$, $[\{UO_2(py)\}_2(L^A)]$ and H_4L^A.

The mass spectrum of the mixture shows multiple fragments attributable to the Pacman products, with the ion at 1128 amu attributed to $[UO_2(H_2L^A)]^+$, a fragment resulting from the desolvation of $[UO_2(py)(H_2L^A)]$ upon ionisation. The ion at 1527 amu results from the fragmentation of $[\{UO_2(py)\}_2(L^A)]$ by loss of two of the *meso*-ethyl groups and is followed by fragments at 1452 and 1370 which form by the additional loss of one or two bound pyridine solvent molecules respectively. Despite the evidence for the formation of $[UO_2(py)(H_2L^A)]$ pure samples of the complex were never obtained and efforts were instead focused on characterisation of the binuclear complex $[\{UO_2(py)\}_2(L^A)]$.

5.2.2 Synthesis of the binuclear complex [{UO_2(py)}$_2$(L^A)]

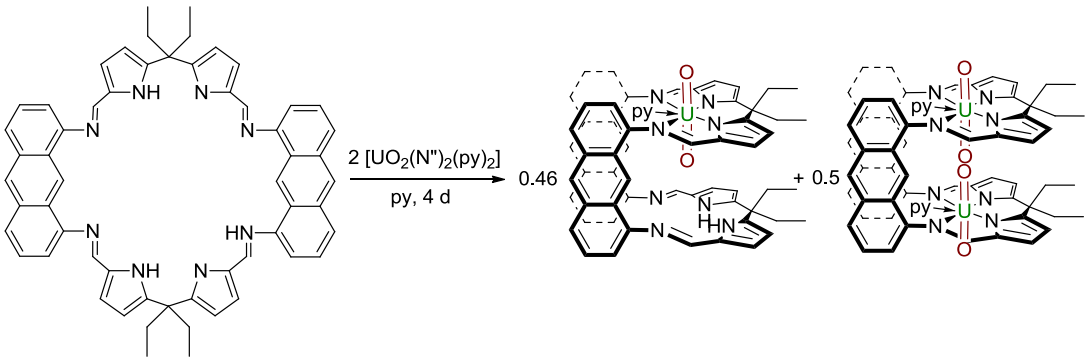

Scheme 1: Synthesis of [{UO_2(py)}$_2$(L^A)] and [{UO_2(py)}$_2$(L^A)].

The reaction between H_4L^A and two equivalents of [UO_2(N")$_2$(py)$_2$] in pyridine also yielded a mixture of [UO_2(py)(H_2L^A)] and [{UO_2(py)}$_2$(L^A).] However, the latter complex was formed in the greater yield of 50 % along with 46 % of the mono-uranyl complex (Scheme 1). Despite their similar solubilities, fractional crystallisation of the crude mixture allowed isolation of pure samples of [{UO_2(py)}$_2$(L^A)] in 28 % yield. Despite extensive efforts, complete removal of [{UO_2(py)}$_2$(L^A)] from [UO_2(py)(H_2L^A)] was not achieved, with the highest purity of the mononuclear complex that could be attained being 70 %.

The ^{1}H NMR spectrum of pure [{UO_2(py)}$_2$(L^A)] contains 12 resonances, all of which are assigned to a symmetrically occupied L^A ligand. Single resonances are observed for each of the imine, α-pyrrole and β-pyrrole protons and 5 resonances are assignable to the anthracene backbone. No NH resonance is observed in the spectrum, complicit with the full deprotonation of the macrocycle by two equivalents of the uranyl bis(silylamide) base, with ligand-folding upon complexation to form the "Pacman" motif evidenced by two sets of two resonances for the respective *endo* and *exo* CH_2 (2.46 ppm, overlapped) and CH_3 (1.09 and 0.90 ppm) protons. The FTIR spectrum of [{UO_2(py)}$_2$(L^A)] shows a weak band at 912 cm^{-1}, consistent with the asymmetric stretch of the $[UO_2]^{2+}$ dication.

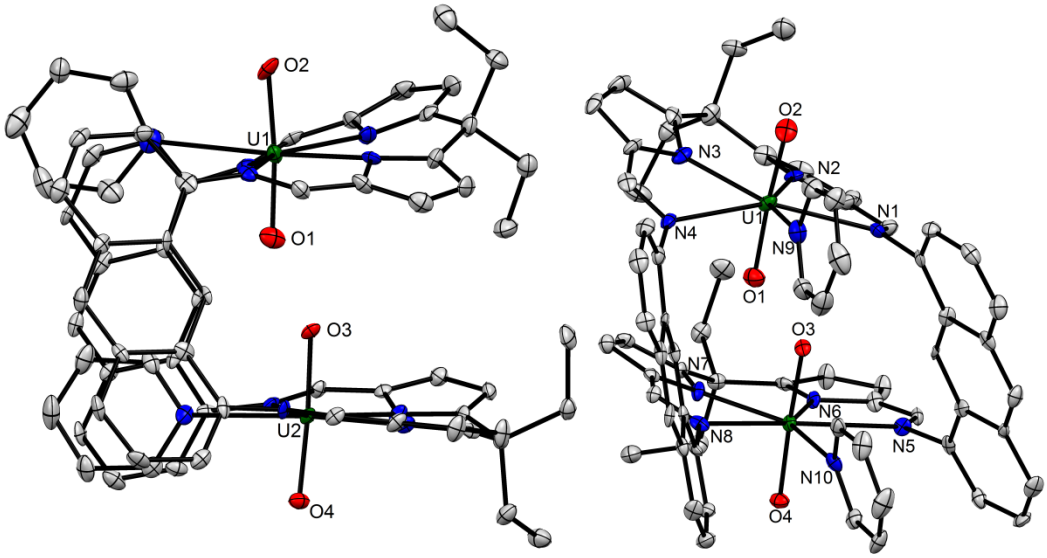

Figure 4: X-ray crystal structure of $[\{UO_2(py)\}_2(L^A)]$ shown side-on (left) and rear-on (right).

Single crystals of $[\{UO_2(py)\}_2(L^A)]$ suitable for an X-ray diffraction study were grown from pyridine solution. The solid state structure displays the anthracenyl macrocycle L^A folded into the Pacman geometry, with symmetric incorporation of both N_4-binding pockets with $[UO_2]^{2+}$ dications forming a binuclear complex (Figure 4). Both uranium atoms display pentagonal bypryramidal geometries with the macrocylic N_4-donor set comprising four of the equatorial ligands, the fifth being occupied by a pyridine solvent molecule. The two oxo atoms, which are mutually trans with O-U–O angles of 174.0(2) and 176.0(2)°, comprise the axial ligands, with short U–O bond distances within the range 1.747(4) – 1.779(4) Å supporting the assignment of uranyl(VI) oxidation states.

The most notable feature of the structure is the short separation of 2.709(6) Å between the two *endo* oxo groups O1 and O3 within the molecular cleft. The two uranyl-coordinated N_4-donor sets are approximately co-planar, subtending an angle of 16.8° due to steric constraints of the *meso* ethyl groups. Each set is slipped laterally relative to the *meso*-ethyl groups by rotation of all four N-C anthracenyl bonds, with the perpendicular distance between U1 and the plane described by U2, O3, O4 and N10 being 1.957 Å. This lateral twist allows favourable π-stacking interactions between the equatorially-bound pyridine molecules and the anthracenyl hinge groups, contrasting the complexes of the octamethylated ligand L in which lateral twisting is not facilitated by the smaller phenylene spacer group.

A number of other $[M_2(L^A)]$ complexes (M = Zn, Pd, Co) have been prepared using salt elimination routes by the initial deprotonation of H_4L^A with four equivalents of an alkali metal base followed by addition of two equivalents of the respective metal halide.[3, 6] In light

of this, attempts were made to synthesise $[\{UO_2(py)\}_2(L^A)]$ using a similar strategy, by addition of two equivalents of $[UO_2Cl_2(THF)_2]$ to K_4L^A, prepared *in-situ* by deprotonation of H_4L with $KN\{SiMe_3\}_2$. Unfortunately however, this route did not allow selective formation of the binuclear complex, but resulted in a similar mixture of $[UO_2(py)(H_2L^A)]$ and $[\{UO_2(py)\}_2(L^A)]$ being observed by ^1H NMR spectroscopy.

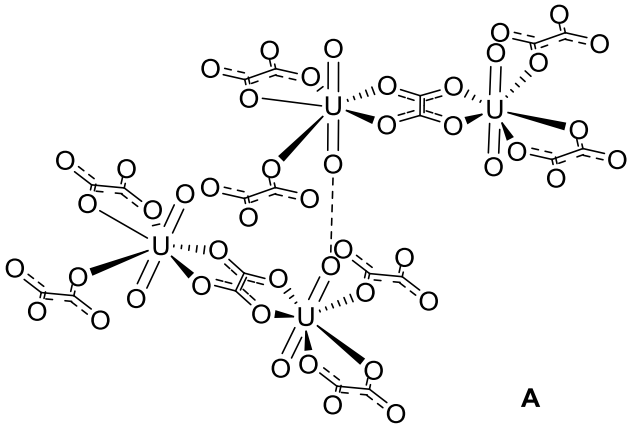

Figure 5: Partial structure of $[NH_4][(U^{VI}O_2)_2(\mu_4\text{-}C_2O_4)_3]_n$ **A** which exhibits proximal OUO···OUO groups.

Examples of complexes which contain similarly close uranyl oxo contacts in the solid state are rare. The uranyl oxalates $[NH_4]_2[(U^{VI}O_2)_2(\mu_4\text{-}C_2O_4)_3]$ (Figure 4, **A**),[7] $[Rb]_2[(U^{VI}O_2)_2(\mu_4\text{-}C_2O_4)_3]$,[8] and $[\text{alkyl-imidazolium}]_2[(U^{VI}O_2)_2(\mu_4\text{-}C_2O_4)_3]$[9] have similarly short oxo-oxo distances of 2.434, 2.702 and 2.703 Å respectively; all other O···O separations are >2.8 Å and result from crystal packing in the solid state (39 examples up to 3.0 Å). The intermolecular nature of such close contacts means their persistence is unlikely in solution whereas it is assumed the *endo* oxo atoms in $[\{UO_2(py)\}_2(L^A)]$ remain proximal due to enforcement of the geometry of the complex by the folded macrocycle.

5.2.3 Reduction of [{UO_2(py)}$_2$(L^A)]

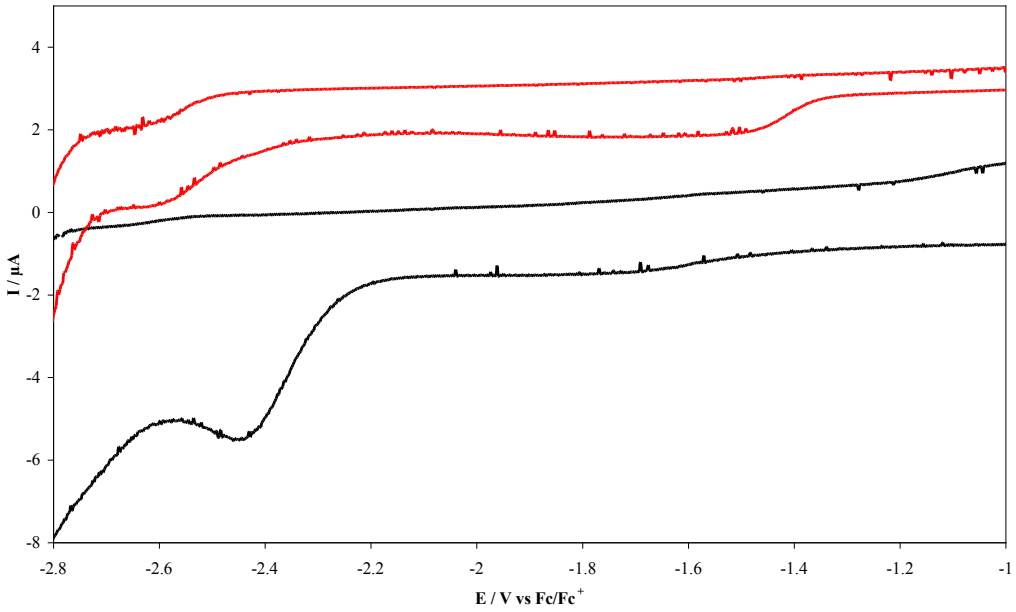

Figure 6: Cyclic voltammograms of [{UO_2(py)}$_2$(L^A)] (black line) and a 70:30 mixture of [{UO_2(py)}(H_2L^A)] and [{UO_2(py)}$_2$(L^A)] (red line, current adjusted for clarity) in THF.

A cyclic voltammetry experiment on [{UO_2(py)}$_2$(L^A)] in THF (0.2 M Bu_4BF_4, Fc^+/Fc) displayed a single, irreversible reduction at –2.46 V, provisionally assigned to the reduction of two non-communicating uranyl(VI) centres to uranyl(V) (Figure 6). The feature represents a much more difficult reduction than that of the mononuclear uranyl Pacman complex [UO_2(THF)(H_2L)] which shows a clear, quasi-reversible $U^{V/VI}$ couple at –1.17 V and an irreversible reduction to uranium(IV) at –2.88 V.[10]

It is proposed that the reason for the large disparity between the two complexes, which contain the same N_5 equatorial donor set, is due to the proximity of the two uranyl cations in [{UO_2(py)}$_2$(L^A)] which may be a destabilising factor on reduction to uranyl(V). The Lewis basicity of the uranyl oxo group is known to increase considerably on reduction, with uranyl(V) species stabilised by the formation of Lewis adduct CCI complexes. The parallel orientation of the two [UO_2^{2+}] dications in [{UO_2(py)}$_2$(L^A)] disfavours the formation of both T- and diamond-shaped CCIs removing any stabilising effect upon reduction. The CV study of the crude mixture of [{UO_2(py)}$_2$(L^A)] and [{UO_2(py)}$_2$(L^A)] exhibits additional reductions at Ep^c –1.45 and –2.6 V suggesting that the redox behaviour of the mononuclear L^A complex is closer to that of [UO_2(THF)(H_2L)] (Figure 6).

In analogy with its electrochemical behaviour, attempts to formally reduce [{UO_2(py)}$_2$(L^A)] proved as difficult. The reaction of the binuclear complex with [$CoCp_2$],

$[UI_3(THF)_4]$ or KC_8 resulted in either no reaction in the first case or the formation of intractable solids in the second and third. The lack of stable uranium complexes of L^A in lower oxidation states contrasts the behaviour of complexes of H_4L, which was observed to preferentially form binuclear uranium(V) oxo complexes on treatment with two equivalents of $[UO_2(N'')_2(py)_2]$. Such contrasting reactivity between L and L^A highlights the significance of size of the macrocyclic cleft upon on the structure and oxidation state of the binuclear uranium complexes formed upon uranyl coordination.

5.3 Mononuclear uranyl complexes of H_4L^F

In contrast to the anthracene ligand H_4L^A, the *meso*-substituted fluorenyl macrocycle H_4L^F can be used to synthesise both mono- and binuclear uranyl(VI) complexes depending on the conditions used.

5.3.1 Synthesis of the $[UO_2(py)(H_2L^F)]$

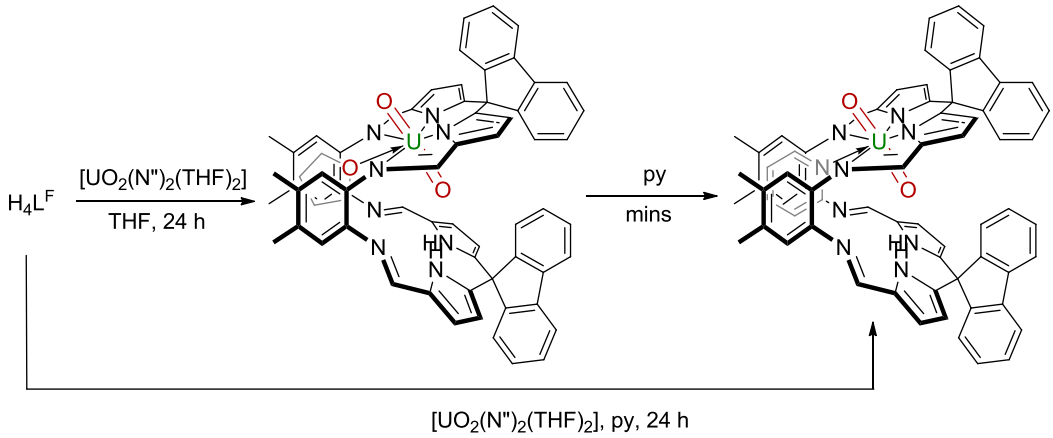

Scheme 2: Synthesis of $[UO_2(THF)(H_2L^F)]$ and $[UO_2(py)(H_2L^F)]$.

The 1:1 reaction between H_4L^F and $[UO_2(N'')_2(THF)_2]$ in THF formed a brown suspension after 24 h, with the insolubility of the product in pyridine comparable to that of the free ligand (Scheme 2). The mononuclear complex $[UO_2(THF)(H_2L^F)]$ was isolated in 63 % yield by filtration and was found also to be insoluble in benzene, dichloromethane and chloroform. Dissolution of $[UO_2(THF)(H_2L^F)]$ in pyridine resulted in instant conversion to the pyridine adduct $[UO_2(py)(H_2L^F)]$ with the concomitant release of one equivalent of THF. The pyridine solvate may also be synthesised directly from H_4L^F and $[UO_2(N'')_2(THF)_2]$ in pyridine, resulting in the complete dissolution of all solids over 24 h with pure $[UO_2(py)(H_2L^F)]$ isolated in 72 % yield by hexane-precipitation (Scheme 2).

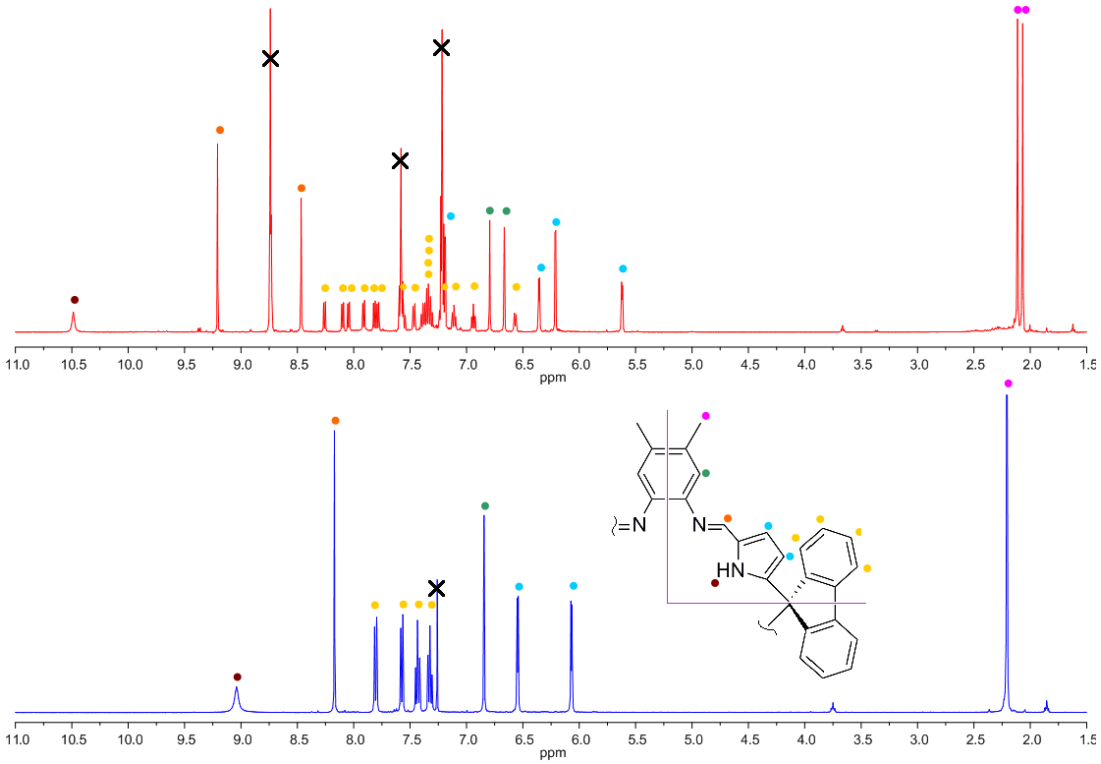

Figure 7: ^{1}H NMR spectra of H_4L^F (blue) and $[UO_2(py)(H_2L^F)]$ (red).

The ^{1}H NMR spectrum of the free ligand H_4L^F contains 10 resonances, consistent with a molecule of D_{2h} symmetry, with single resonances observed for each of the four NH, imine, α-pyrrole, β-pyrrole, aryl and methyl resonances (Figure 7). Four resonances are also observed for each of the four non-equivalent protons of the fluorenyl rings, with two doublets and two triplets each with integrals of four protons each. The ^{1}H NMR spectrum of the mononuclear uranyl complex $[UO_2(py)(H_2L^F)]$ displays a greater number of resonances in accordance with the ligand adopting a lower symmetry (Figure 7, ii). Mononuclear uranyl coordination is evidenced by the splitting of the imine, α- and β-pyrrole, aryl and methyl resonances into twin sets, corresponding to the metalated and metal-free pockets of the macrocycle. The retention of a pyrrolic NH proton (10.46 ppm) and the reduction of its integral to 2H are further indicative of the incorporation of a single species into one of the N_4-donor pockets of the macrocycle. The number of *meso*-fluorenyl resonances increases from 4 to 16 upon uranyl complexation indicative not only of mononuclear metal incorporation, which would result in splitting to 8 resonances, but also ligand folding, resulting in a C_s-symmetric molecule in which each fluorenyl proton is chemically distinct.

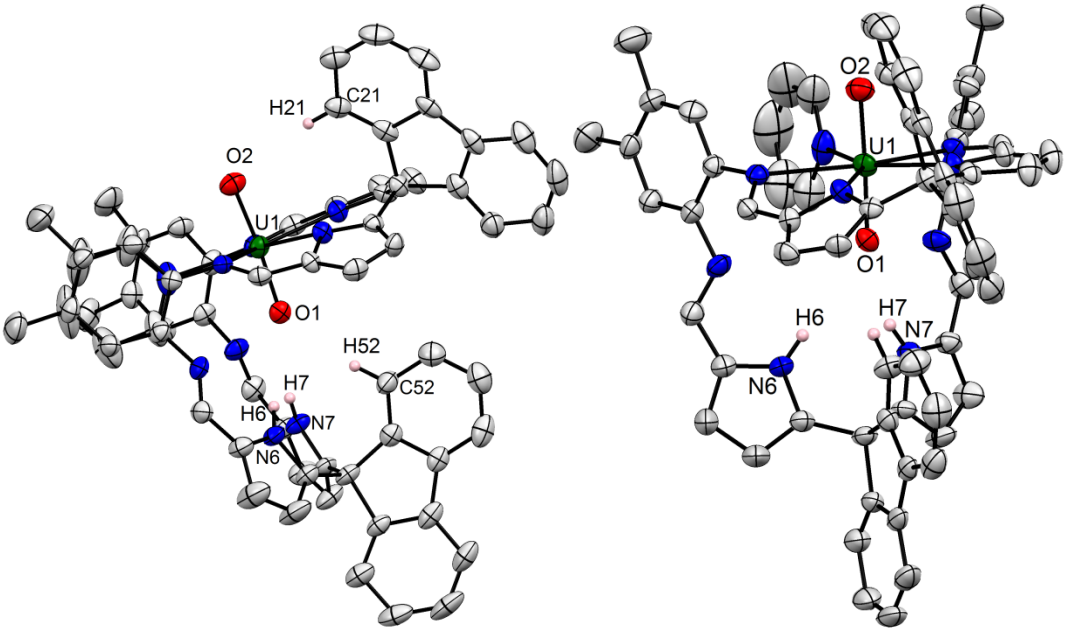

Figure 8: Displacement ellipsoid plot (50 %) of $[UO_2(py)(H_2L^F)]$ shown side-on (left) and front-on (right). All free solvent molecule and selected H atoms are omitted for clarity.

The X-ray crystal structure of $[UO_2(py)(H_2L^F)]$ confirms that the ligand is as folded and that a single $[UO_2]^{2+}$ dication has been bound, resulting in the formation of a mononuclear Pacman complex. The uranyl O-U–O bond angle of 174.9° demonstrates that the uranyl oxo groups maintain the *trans* arrangement upon complexation, with five nitrogen donors in the equatorial plane resulting in a metal centre with a pentagonal bypyramidal geometry. The U1-O1 and U1-O2 bond lengths of 1.798(2) and 1.783(6) Å respectively, fall within the expected range for uranyl(VI) and compare favourably with the analogous bond lengths in $[UO_2(THF)(H_2L)]$ (1.787(3) and 1.771(4) Å respectively).[4]

There are several weak, non-covalent interactions in the structure, including two hydrogen bonding interactions between the pyrrole protons and the *endo* uranyl oxo group as evidenced by O1···N6 and O1···N7 distances of 3.621(5) and 3.265(4) Å, respectively. Such distances are longer and more asymmetric than those observed for $[UO_2(THF)(H_2L)]$ (3.139(5) and 3.098(5) respectively) and are suggestive of a diminished NH···OUO interaction in comparison to the octhamethylated Pacman complex that is perhaps due to the bulky fluorenyl fragments preventing the jaws of the complex from closing efficiently. However, significant twisting of the upper fluroenyl group in comparison to the lower by 21° is present providing some indication that the structure seeks to minimise this steric effect and maximise the intramolecular NH···OUO interactions. The bite angle between the upper and lower jaws of the Pacman macrocycle is 64° and appreciably larger than that of 58° observed in $[UO_2(THF)(H_2L)]$.[4] Such a difference could again be attributed to the bulkier *meso* groups

in $[UO_2(py)(H_2L^F)]$, although it is noteworthy that the bite angles in the dipalladium and dicobalt fluorenyl-Pacman complexes $[Pd_2(L^F)]$ and $[Co_2(L^F)]$ are smaller than $[UO_2(py)(H_2L^F)]$, being 56.4 and 54.7° respectively (Figure 9, **B** and **C**). [3] In these complexes however, the lower bite angle is afforded by a significant offset of the two jaws, with twist angles of 27.8 and 34.2° allowing partial overlap of the fluroenyl fragments and relief from any steric clash. No such offset is present in $[UO_2(py)(H_2L^F)]$, with the adoption of such a less favourable geometry perhaps an additional result of the NH···OUO hydrogen bonding interaction.

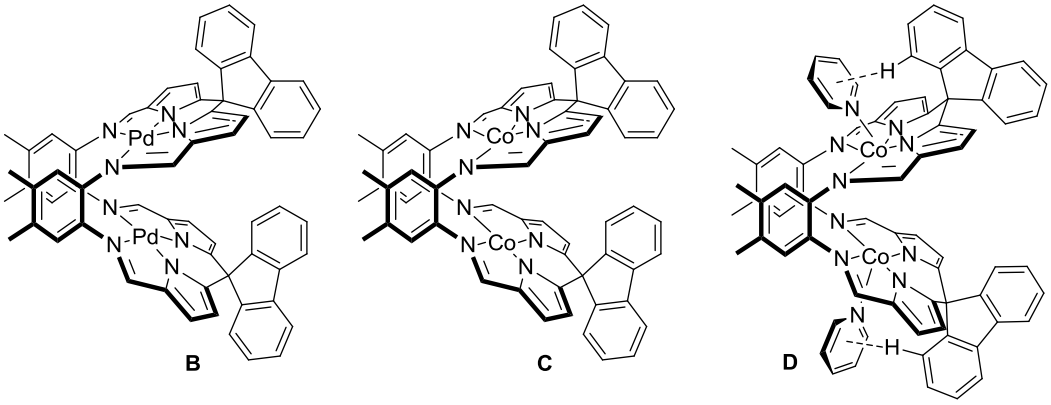

Figure 9: Other complexes of the L^F ligand.

Weaker hydrogen bonding interactions may be present between the uranyl oxo groups and the fluorenyl protons as evidenced by O2···C21 and O1···C52 distances of 3.624(7) and 3.417(7) Å respectively. There is some indication again that the molecule seeks to maximise these interactions through structural distortion, with both fluorenyl groups rotated upwards to perhaps facilitate greater proximity between the donor C-H groups and the uranyl oxo groups. The complexes $[Pd_2(L^F)]$ and $[Co_2(L^F)]$ contain no such interactions and therefore show no such distortion. However, fluorenyl group twisting is observed in the pyridine solvated complex $[\{Co(py)\}_2(L^F)]$ which exhibits CH···π interactions between the fluroenyl protons and the cobalt-bound pyridine donor solvent molecule (Figure 9, **D**).[3]

5.4 Binuclear uranyl complexes of H_4L^F

5.4.1 Synthesis of $K_2[(UO_2)_2(\mu\text{-}O)(L^F)]$

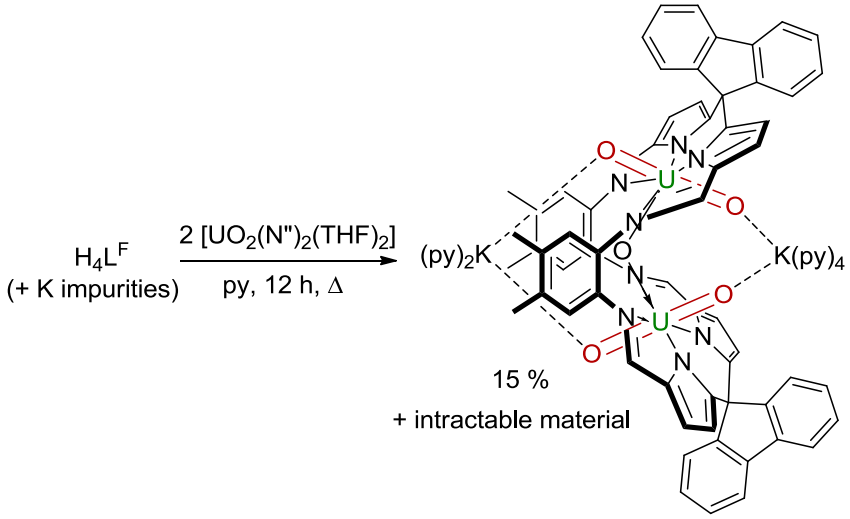

Scheme 3: Synthesis of $K_2[(UO_2)_2(\mu\text{-}O)(L^F)]$.

After the successful isolation of $[UO_2(py)(H_2L^F)]$, the binuclear uranyl(VI) chemistry of H_4L^F was investigated, with the reaction of the free ligand with two equivalents of $[UO_2(N")_2(py)_2]$ in boiling pyridine resulting, after 12 h, in the formation of the binuclear uranyl(VI) oxo complex $K_2[(UO_2)_2(\mu\text{-}O)(L^F)]$ in low yield (Scheme 3). The complex was isolated as the only pyridine-soluble material from the reaction mixture alongside a significant amount of insoluble material which could not be characterised.

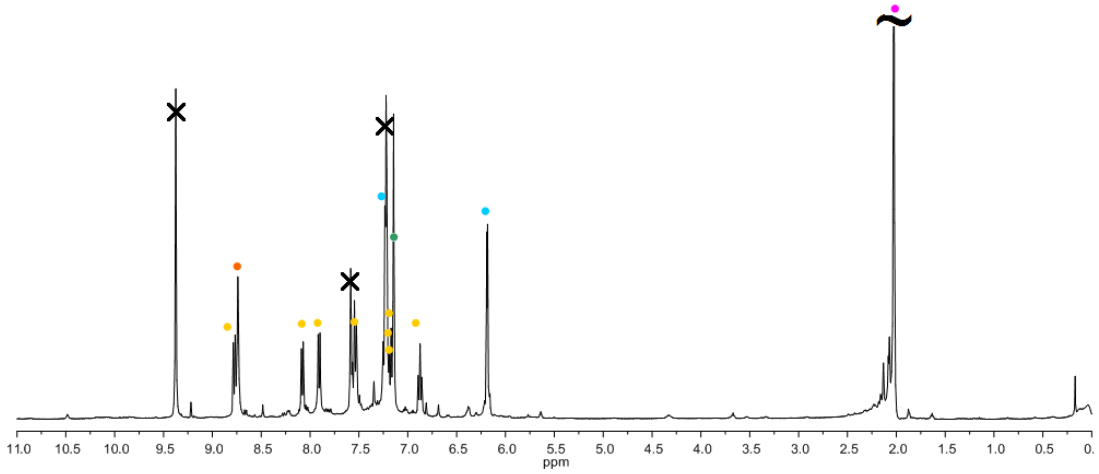

Figure 10: ^{1}H NMR spectrum of $K_2[(UO_2)_2(\mu\text{-}O)(L^F)]$ (methyl resonance truncated).

The ^{1}H NMR spectrum of $K_2[(UO_2)_2(\mu\text{-}O)(L^F)]$ contains 13 resonances, with single resonances observed for the imine, α-pyrrole, β-pyrrole, aryl and methyl groups in a similar pattern that is observed for H_4L^F (Figure 10). No NH resonances are present, indicating that

the complex contains two identically occupied N_4-donor pockets. The presence of 8 resonances attributed for the *meso*-fluorenyl fragments shows that the molecule adopts the folded Pacman structure, with two sets of four *endo* and *exo* protons indicative of a complex with C_{2V} symmetry. The presence of the uranyl dication is indicated by FTIR spectroscopy with shows the characteristic $[UO_2]^{2+}$ asymmetric stretch at 922 cm^{-1}.

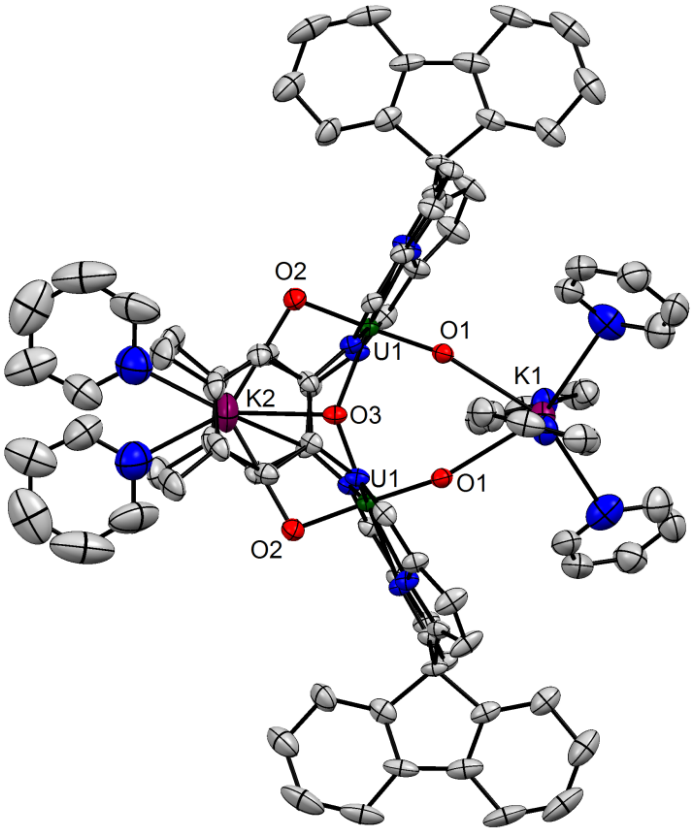

Figure 11: Displacement ellipsoid plot (50 %) of $K_2[(UO_2)_2(\mu\text{-}O)(L^F)]$. For clarity, all free solvent molecules and selected H atoms omitted.

The growth of single crystals of $K_2[(UO_2)_2(\mu\text{-}O)(L^F)]$ allowed its solid state structure to be determined which displays a wedge-shaped L^F macrocycle folded into the Pacman geometry exhibiting symmetric incorporation of each N_4-donor cleft with a uranyl cation (Figure 11). As in all other uranyl Pacman complexes, the uranium centres in $K_2[(UO_2)_2(\mu\text{-}O)(L^F)]$ are pentagonal bipyramidal, with two axial oxo ligands and four equatorial nitrogen donors, that latter being provided by the Pacman ligand. The fifth equatorial coordination sites of both uranium centres are mutually filled by a bridging oxo group, resulting in the same $(UO_2)_2(\mu\text{-}O)$ motif as is observed in the octamethylated ligand complex $K_2[(UO_2)_2(\mu\text{-}O)(L)]$. In contrast to $K_2[(UO_2)_2(\mu\text{-}O)(L)]$, which crystallises as a dimer maintained by intermolecular uranyl/potassium CCIs (see Chapter Four), $K_2[(UO_2)_2(\mu\text{-}O)(L^F)]$ is monomeric in the solid state, with half a molecule in the asymmetric unit mapping to the full

structure by a 2-fold symmetry axis. The U1-O1 and U1-O2 bond lengths of 1.798(4) and 1.810(4) Å are comparable to those observed in $K_2[(UO_2)_2(\mu\text{-}O)(L)]$ (1.781(6)–1.788(6) Å) and suggest the retention of uranium(VI) oxidation states. The U1-O3 distance between the uranyl centres and the bridging oxo group of 2.138(2) Å is also similarly close to those observed in $K_2[(UO_2)_2(\mu\text{-}O)(L)]$ (2.143(6) and 2.139(6) Å). The most striking feature of the crystal structure of $K_2[(UO_2)_2(\mu\text{-}O)(L^F)]$ is the extreme inter-cleft bite angle of 79° which is significantly larger than that observed for $[UO_2(py)(H_2L^F)]$ (64°) and close to that exhibited by $K_2[(UO_2)_2(\mu\text{-}O)(L)]$ (83°). Such comparative structures between $K_2[(UO_2)_2(\mu\text{-}O)(L^F)]$ and $K_2[(UO_2)_2(\mu\text{-}O)(L)]$ suggests that the *meso*-methyl and -fluorenyl macrocyles are equally capable of incorporating two uranyl dications within the macrocyclic cleft by jaw-widening, and that the bulky *meso*-substituents of L^F do not exert significant influence on the structures of the resulting complexes. The isolation of $K_2[(UO_2)_2(\mu\text{-}O)(L^F)]$ therefore discounts the proposal that *meso*-substitution can be used to influence the size of the inter-cleft bite angle leading to the postulate that it is actually the fulfilment of the fifth uranyl equatorial-coordination sites that is more important in determining the structure of binuclear uranyl Pacman complexes. This theory is further validated by the fact that no doubly pyridine-solvated complex of the type $[\{UO_2(py)\}_2(L)]$ has ever been isolated using a phenylene substituted macrocycle, with all structurally-characterised examples of such complexes containing bridging oxo groups.

In contrast to the synthesis of $K_2[(UO_2)_2(\mu\text{-}O)(L)]$ which proceeds by addition of pyridine-*N*-oxide to the binuclear uranium(V) complex $K_2[(OUO)_2(L)]$, the source of both the potassium cations and bridging oxide groups in $K_2[(UO_2)_2(\mu\text{-}O)(L^F)]$ are unknown. Furthermore, the low 15 % yield of the complex as well the concomitant formation of large amounts of intractable material suggests that $K_2[(UO_2)_2(\mu\text{-}O)(L^F)]$ is a minor, soluble product from the reaction and results instead from a potassium impurity in the starting material. The final step in the synthesis of H_4L^F involves neutralisation of the [2 + 2] acid salt $[H_8L^F][CF_3CO_2]_4$ with KOH.[3] It is presumed that, despite extensive washing, the latter regent remains incorporated within the macrocycle post-synthesis, providing the potassium required for the formation of $K_2[(UO_2)_2(\mu\text{-}O)(L^F)]$. This postulate was confirmed upon repetition of the macrocycle synthesis using NEt_3 as the base in an analogous preparation to that of H_4L and H_4L^A,[1] allowing potassium-free H_4L^F to be isolated from which alternative binuclear uranium products could be formed.

5.4.2 Attempted syntheses of $[(UO_2)_2(\mu\text{-}X)(L/L^F)]$ complexes

The synthesis of $K_2[(UO_2)_2(\mu\text{-}O)(L^F)]$ was not repeatable upon modification of the synthesis of H_4L^F, although the small batch of material from the original experiment was fully characterised by NMR, FTIR spectroscopy, X-Ray crystallography and elemental analysis. In spite of this, the isolation of $K_2[(UO_2)_2(\mu\text{-}O)(L^F)]$, as well as the successful syntheses of $K_2[(UO_2)_2(\mu\text{-}O)(L)]$ and $K_2[(UO_2)_2(\mu\text{-}k^2\text{-}k^2\text{-}O_2)(L)]$, demonstrate the inherent stability of binuclear uranyl complexes with bridging ligands. In light of this, investigation into a direct synthesis of these complexes was performed, with a proposed two-step synthesis involving the initial binding of an anionic ligand by addition of KX (X = OH, Cl, F) to either $[UO_2(py)(L/L^F)]$ complex before the addition of second equivalent of $[UO_2(N'')_2(py)_2]$ to form the binuclear complex (Scheme 4).

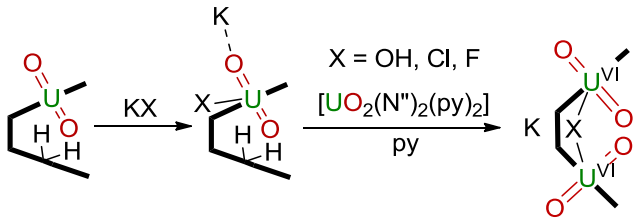

Scheme 4: Attempted syntheses of $K[(UO_2)_2(\mu\text{-}X)(L^x)]$

Incorporation of KOH into $[UO_2(THF)(L)]$ has been reported, with equatorial binding of the anion resulting in displacement of the coordinated THF molecule to form $K[UO_2(OH)(L)]$ as a molecular or dimeric CCI complex depending on the conditions used.[4] Despite this, no binuclear $K[(UO_2)_2(\mu\text{-}OH)(L/L^F)]$ complex could be synthesised, with the formation of insoluble precipitates resulting upon addition of $[UO_2(N'')_2(py)_2]$ to solutions of the *in-situ* generated $K[UO_2(OH)(L)]$ or $K[UO_2(OH)(L^F)]$. The use of KF or KCl as a source of the bridging ligand did not allow the formation of $K[(UO_2)_2(\mu\text{-}X)(L/L^F)]$, resulting in the formation of either intractable products or unreacted starting materials. In view of these attempts, a formal synthesis of $K_2[(UO_2)_2(\mu\text{-}X)(L^F)]$ complexes was not found and the preparations of $K_2[(UO_2)_2(\mu\text{-}O)(L)]$ and $K_2[(UO_2)_2(\mu\text{-}k^2\text{-}k^2\text{-}O_2)(L)]$ remains restricted to oxidation of the binuclear uranium(V) oxo complex $K_2[(OUO)_2(L)]$.

5.4.3 Synthesis of $[(UO_2)_2\{\mu\text{-}O(CH_2)_4NC_5H_5\}(L^F)]$

A surprising feature of the KOH-contaminated H_4L^F is the difference in reactivity of this material towards alternatively solvated uranyl silylamide precursors.

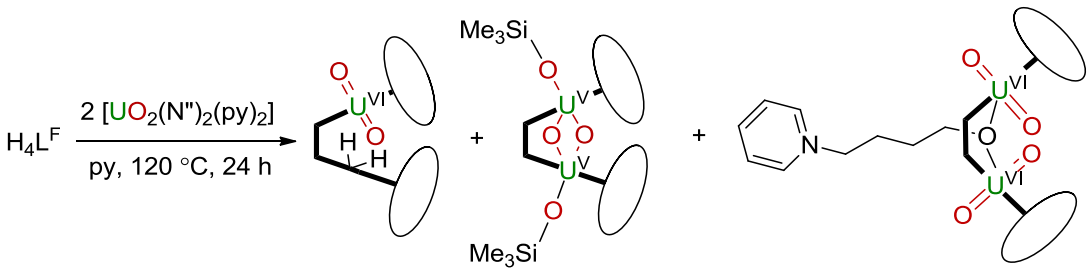

Scheme 5: Synthesis of $[UO_2(py)(H_2L^F)]$, $[(Me_3SiOUO)_2(L^F)]$ and $[(UO_2)_2\{\mu\text{-}(O\{CH_2\}_4)NC_5H_5\}(L^F)]$ from H_4L^F and $[UO_2(N'')_2(THF)_2]$.

Whereas the boiling reaction between the free ligand and two equivalents of the pyridine-solvate of uranyl bis(trimethylsilylamide) was found to yield $K_2[(UO_2)_2(\mu\text{-}O)(L^F)]$ in low yields, a similar reaction between H_4L^F and two equivalents of $[UO_2(N'')_2(THF)_2]$ resulted in the precipitation of a crude mixture of $[UO_2(py)(H_2L^F)]$, $[(Me_3SiOUO)_2(L^F)]$ and the binuclear uranyl(VI) complex $[(UO_2)_2\{\mu\text{-}(O\{CH_2\}_4)NC_5H_5\}(L^F)]$ after 24 h (Scheme 5). From this crude mixture the latter product was obtained by layering of the pyridine supernatant with hexanes, resulting in precipitation of single crystals of $[(UO_2)_2\{\mu\text{-}(O\{CH_2\}_4)NC_5H_5\}(L^F)]$ in 9 % yield.

The ^{1}H NMR spectrum of $[(UO_2)_2\{\mu\text{-}O(CH_2)_4NC_5H_5\}(L^F)]$ is broadly similar to that of $K_2[(UO_2)_2(\mu\text{-}O)(L^F)]$, with 13 ligand resonances between 10 and 2 ppm suggestive of a C_{2V} symmetric complex. The single imine (9.34 ppm), α- and β-pyrrole (7.23 and 6.20 ppm), methyl (2.01 ppm) resonances (the aryl resonance is obscured by the pyridine solvent) are present in similar positions to the respective resonances of $K_2[(UO_2)_2(\mu\text{-}O)(L^F)]$ (9.37, 6.17, 7.13 and 2.01 ppm). In contrast to the ox-bridged complex however, there are four additional resonances at 2.12, 2.09, 2.03 and 2.01 ppm corresponding to the butyl chain of the $\{O(CH_2)_4\}NC_5H_5$ group.

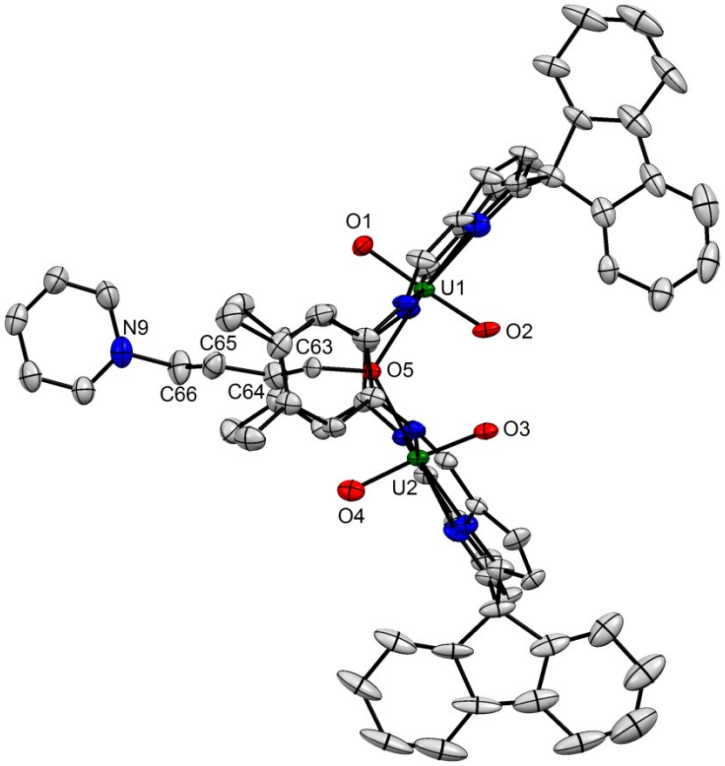

Figure 12: Displacement ellipsoid plot (50 %) of $[(UO_2)_2\{\mu\text{-}O(CH_2)_4NC_5H_5\}(L^F)]$. All free solvent molecules and selected H atoms omitted for clarity.

From the solid state structure of $[(UO_2)_2\{\mu\text{-}O(CH_2)_4NC_5H_5\}(L^F)]$ it can be discerned that the same binuclear uranyl(VI)-incorporated L^F ligand is present as is observed in $K_2[(UO_2)_2(\mu\text{-}O)(L)]$ (Figure 12). The U1-O1, U1-O2, U2-O3 and U2-O4 are within the range 1.758(7) – 1.809(7) Å, consistent with uranium(VI) oxidation states, and similar to those of $K_2[(UO_2)_2(\mu\text{-}O)(L)]$ (1.798(4) and 1.810(4) Å). In contrast to $K_2[(UO_2)_2(\mu\text{-}O)(L)]$, the complex contains no potassium cations, with a zwitterionic pyridinium *n*-butoxide ligand instead bridging between each of the uranyl centres by its terminal alkoxide head group which is linked by a butyl chain to a cationic pyridinium tail group resulting in an overall neutral species. As expected, the U1-O5 and U2-O5 bond distances of 2.334(5) and 2.350(5) Å between the uranyl centres and the alkoxide bridging atom are much longer than those between the uranyl centres and the bridging oxide group of $K_2[(UO_2)_2(\mu\text{-}O)(L^F)]$ (2.138(2) Å). Instead, the U–O5 bond distances in $[(UO_2)_2\{\mu\text{-}O(CH_2)_4NC_5H_5\}(L^F)]$ are more comparable to those seen in the aryloxide-bridged binuclear uranyl(VI) complex $[\{UO_2(salen)\}_2]$ (Figure 13, **E**).[11]

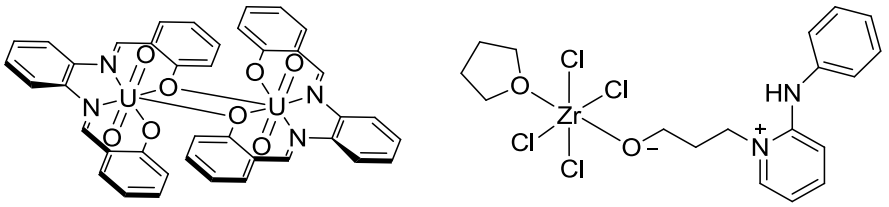

E **F**

Figure 13: [{UO_2(salen)}$_2$] **E**, another binuclear uranyl(VI) complex with a bridging alkoxide and **F**, a zirconium complex featuring a zwitterionic pyridinium butoxide ligand.

Although the exact mechanism of formation of [$(UO_2)_2${μ-$O(CH_2)_4NC_5H_5$}(L^F)] could not be deduced, it is clear that the zwitterionic pyrdinium alkoxide bridging group results from ring-opening of the uranyl-bound THF solvent molecule by pyridine. Ring-opening of THF is a common occurrence in the chemistry of more Lewis acidic metals, but there are no documented examples of Lewis acid-catalysed THF ring-opening by uranyl or potassium. It is more likely therefore that the butoxide motif found in [$(UO_2)_2${μ-$O(CH_2)_4NC_5H_5$}(L^F)] is formed by a radically-induced process as a by-product of a reduction reaction such as the formation of [$(Me_3SiOUO)_2(L^F)$]. In Chapter Two, the synthesis of [$(Me_3SiOUO)_2$(L)] was reported, with the reduction of uranyl(VI) to uranium(V) postulated to occur by thermally induced radical decomposition of [$UO_2(N'')_2(py)_2$] in pyridine solvent. Attempts to trap the radical by-products during [$(Me_3SiOUO)_2$(L)] formation were unsuccessful, but it is possible that radicals resulting from the synthesis of [$(Me_3SiOUO)_2(L^F)$] may have induced ring-opening of the uranyl-bound THF solvent and given rise to the complex [$(UO_2)_2${μ-$O(CH_2)_4NC_5H_5$}(L^F)]. It is worth noting that in the absence of the trace KOH-impurities in H_4L^F no ring-opening of THF is observed, suggesting that the presence of an additional Lewis acid may also be required for the ring-opening process to occur. Other metal complexes featuring pyridium *n*-butoxide ligands are extremely rare with only one other structurally characterised example, the $ZrCl_4$ adduct [$ZrCl_4$(THF){($O\{CH_2\}_4$)NC_5H_4(2-(H)NPh) formed by THF ring-opening occurring upon heating $ZrCl_4$ and 2-(phenylamino)pyridine in THF (Figure 13, **F**).[12] This complex exhibits a similar motif to [$(UO_2)_2${μ-$O(CH_2)_4NC_5H_5$}(L^F)], with the cationic pyridinium fragment connected to the metal centre by a THF-derived *n*-butoxide chain.

5.1.1 Syntheses of $[(Me_3SiOUO)_2(L^F)]$ and $[(PhMe_2SiOUO)_2(L^F)]$

In the absence of a salt impurity, the addition of 2 equivalents of $[UO_2(N'')_2(py)_2]$ to a pyridine solution of H_4L^F at room temperature results in the slow consumption of both starting materials to form an insoluble precipitate after one week. Although no further characterisation of the insoluble product was achieved, the similarity of the phenylene substituted macrocycles H_4L and H_4L^F leads to the postulate that the material may be similar to **P,** the polymeric uranium(V) oxo product resulting from the analogous reaction of H_4L and excess $[UO_2(N'')_2(py)_2]$ at room temperature.

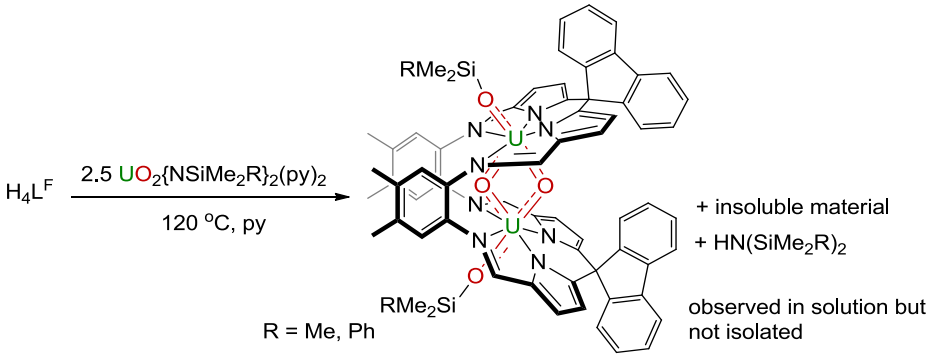

Scheme 6: Synthesis of $[(Me_3SiOUO)_2(L^F)]$ and $[(PhMe_2SiOUO)_2(L^F)]$

In further analogy with the chemistry of H_4L, the NMR-scale reaction between H_4L^F and 2.5 equivalents of $[UO_2(N'')_2(py)_2]$ in boiling pyridine was found to form the binuclear uranium(V) butterfly complex $[(Me_3SiOUO)_2(L^F)]$ as the major product after 12 h (Scheme 6).

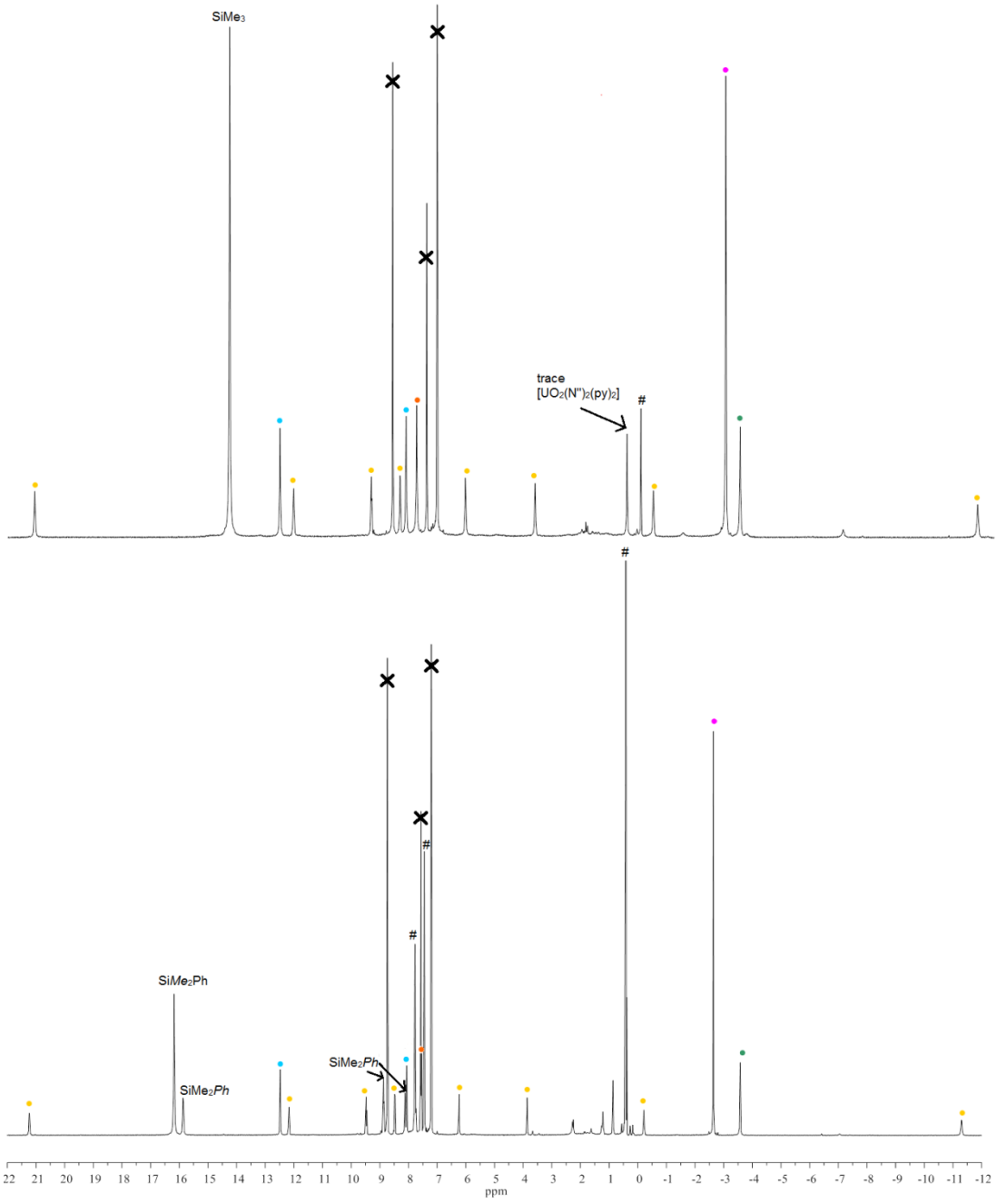

Figure 14: ^{1}H NMR spectra of [$(Me_3SiOUO)_2(L^F)$] (top) and [$(PhMe_2SiOUO)_2(L^F)$] (bottom). Resonance labelling is analogous to Figure 7, # = residual $HN(SiMe_2R)_2$.

The ^{1}H NMR spectrum of [$(Me_3SiOUO)_2(L^F)$] contains 14 paramagnetically-shifted resonances between 22 and –12 ppm, 13 of which are attributable to the L^F ligand (Figure 14). This is exactly the same number as is observed for the complex $K_2[(UO_2)_2(\mu\text{-}O)(L^F)]$ and is indicative of the formation of a binuclear uranium(V) Pacman complex of C_{2V} symmetry (Figure 14). The pyrrole (12.63 and 8.28 ppm), imine (7.92 ppm), methyl (2.75 ppm) and aryl (–3.24 ppm) resonances all lie in similar positions to those of

$[(Me_3SiOUO)_2(L)]$ (13.17, 9.13, 8.56, –2.87 and –3.32 ppm respectively) with the single resonance at 14.36 ppm, which has an integral of 18 protons, demonstrating exo-oxo silylation.

The alternatively silylated complex $[(PhMe_2SiOUO)_2(L^F)]$ can be prepared in solution by the nmr-scale reaction between $[UO_2(py)(H_2L^F)]$ and 1.5 equivalents of $[UO_2(N^*)_2(py)_2]$ in boiling pyridine, forming the dimethyl-phenylsilylated complex as the major product observed by ^{1}H NMR spectroscopy after 12 h (Scheme 6). The ^{1}H NMR spectrum of $[(PhMe_2SiOUO)_2(L^F)]$ contains an almost identical set of L^F resonances as observed for $[(Me_3SiOUO)_2(L^F)]$, being 13 in number and occurring between 22 and –12 ppm (Figure 14). In contrast to the trimethylsilylated complex however, $[(PhMe_2SiOUO)_2(L^F)]$ contains three resonances that are not attributable to L^F at 16.18, 15.87 and 8.87 and 8.12 corresponding to the methyl, ortho-phenyl, meta-phenyl and para-phenyl resonances of the oxo-bound $SiMe_2Ph$ groups which are present in similar positions to those in $[(PhMe_2SiOUO)_2(L)]$ (17.23, 15,57, 8.88 and 8.15 ppm respectively).

Neither $[(Me_3SiOUO)_2(L^F)]$ or $[(PhMe_2SiOUO)_2(L^F)]$ were isolated in the solid state as, in contrast to $[(Me_3SiOUO)_2(L)]$ and $[(PhMe_2SiOUO)_2(L^F)]$, poor solubility prohibited their extraction into non-donor solvents meaning separation from the polymeric by-products could not be achieved. Both complexes were characterised in solution, providing further evidence that performing *meso*-substitution of phenylene-derived Pacman macrocycles does not significantly affect the nature of the binuclear uranium products formed upon treatment with excess uranyl silyamides.

5.2 Uranyl(VI) chemistry of the tris(pyrrolide) tripod ligand L^T

The chemistry of tris(pyrrolide) ligands has received significant attention in recent years due to their ability to stabilise low-coordinate transition metal complexes that exhibit a range of reactivity, including small molecule activation, the formation supramolecular interactions, or molecular magnetism.[13-22]

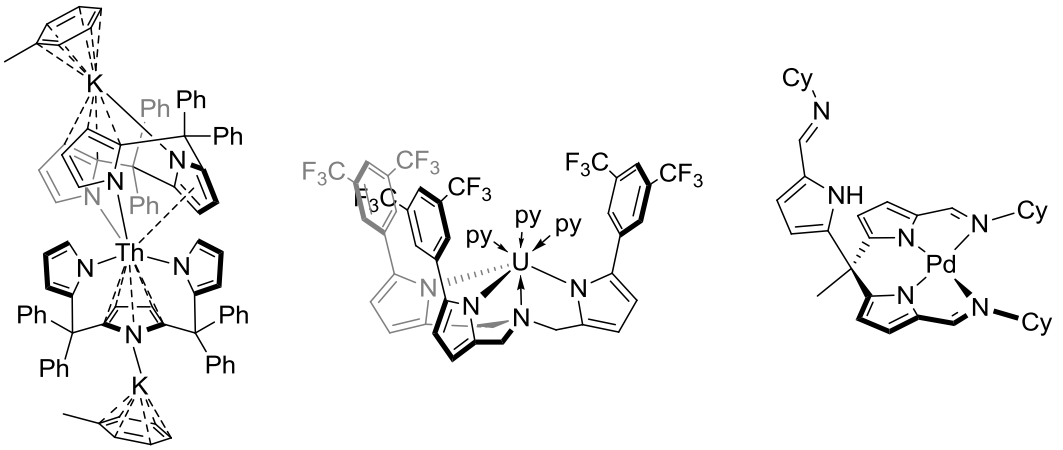

G **H** **I**

Figure 15: Tris(pyrrolide) complexes of thorium (**G**) and uranium (**H**) and a square planar palladium complex of the tripodal iminopyrrole ligand L^T (**I**).

There are fewer examples of f-block tris(pyrrolide) complexes, with the dimeric thorium(IV) complex $K_2[\{2,5\text{-}(C_4H_3N)CPh_2\}_2C_4H_2N\}_2Th]$ **G** prepared by Gambarotta and co-workers and the recently synthesis uranium(III) pyrrolylamine complex $[U(Ar^F{}_3TPA)(py)_3]$ **H** (Ar^F = 3,5-bis(trifluoromethyl)phenyl; TPA = tris(pyrrolyl-α-methylamine)) by the Schelter group being the only structurally characterised examples of actinide complexes (Figure 15).[23-24] In addition, there are two examples of lanthanide complexes of tris(pyrrolide) ligands; $[Sm(TPA)(THF)_3]$ and $[Dy(TPA)(THF)_3]$ (TPA = tris(pyrrolyl-α-methyl)amine.[25] Our group has recently employed the tripodal iminopyrrole ligand H_3L^T, originally prepared by Beer and co-workers,[26] in the synthesis of Group one and transition metal complexes that exhibit unusual structures and supramolecular interactions.[27] The ligand can act as either a traditional, fully-encapsulating tridentate ligand or a bidentate ligand, with complexes such as $[Pd(HL^T)]$ formed when two ligand arms coordinate in an N_4 square planar fashion with the third arm pendent and partaking in hydrogen bonding interactions (Figure 15, **I**).[28]

5.2.1 Synthesis of $[UO_2(HL^T)]$

The isolation of $[Pd(HL^T)]$ prompted investigation into the chemistry of the L^T ligand with uranyl, another dicationic species with a strong preference for co-planar ligand binding.

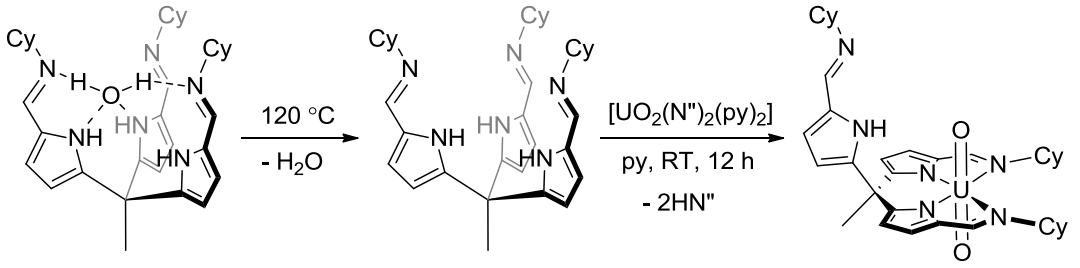

Scheme 7: Synthesis of $[UO_2(py)(HL^T)]$

The reaction of H_3L^T with one equivalent of $[UO_2(N")_2(py)_2]$ in pyridine resulted in the formation of $[UO_2(HL^T)]$ and two equivalents of HN" as the only species present by ^1H NMR spectroscopy after 12 h (Scheme 7). Prior to the reaction being carried out, the free ligand was dried under vacuum at 120 °C for 12 h during which the white solid $H_3L^T \cdot H_2O$ melted to form a red oil which solidified upon cooling to form a glassy pale pink solid. Previous studies of the reactivity of H_3L^T do not report any thermal dehydration the ligand prior to use, with treatment with an excess of an alkali metal base instead used to remove the encapsulated H_2O. This strategy was not employed for the synthesis of $[UO_2(HL^T)]$ as it would require excess $[UO_2(N")_2(py)_2]$. Attempts to dry H_3L^T at lower temperatures did not result in the melting of the species but also did not remove the water, with the resulting syntheses of $[UO_2(HL^T)]$ from this material requiring the unfavourable excesses of the uranyl base.

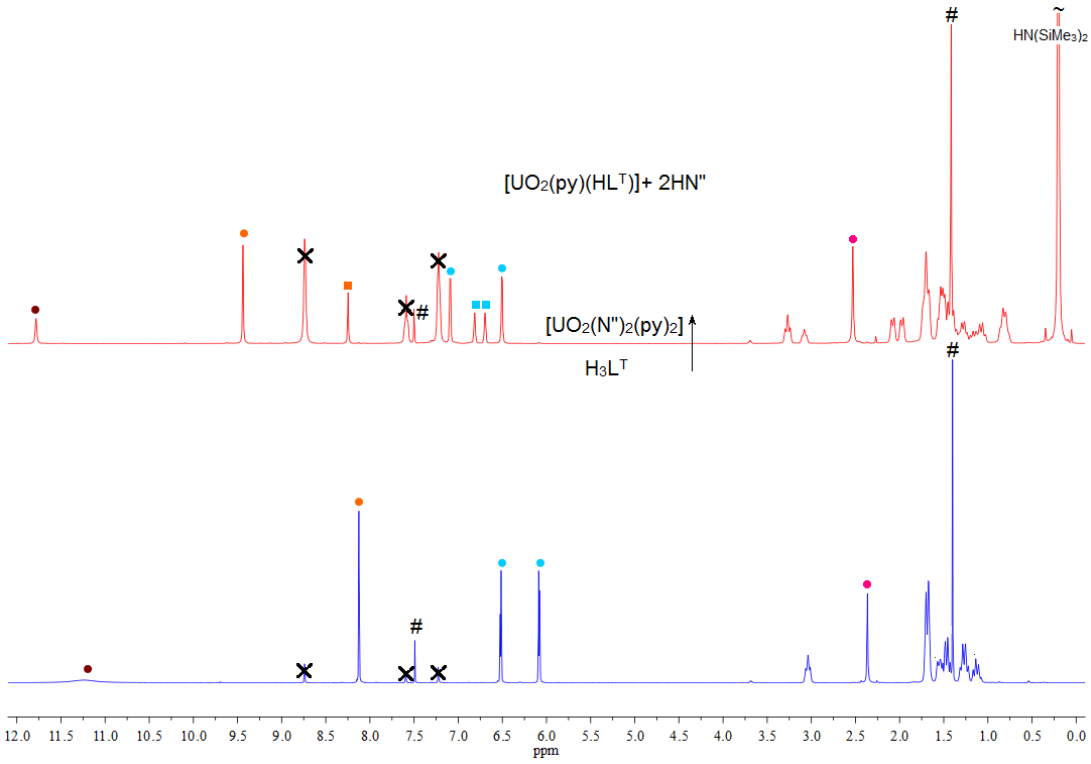

Figure 16: ^{1}H NMR spectrum showing the formation of $[UO_2(py)(HL^T)]$ and 2 HN" (top) from H_3L^T (bottom) and $[UO_2(N")_2(py)_2]$.

The ^{1}H NMR spectrum of $[UO_2(HL^T)]$ contains two sets of resonances in a 2:1 ratio corresponding to the free and complexed iminopyrrole ligand arms (Figure 16). In each set, single resonances are observed for each of the imine, α-pyrrole, and β-pyrrole resonances as well as complex set of multiplets for the cyclohexyl group(s). The set corresponding to the uncomplexed arm of the tripodal ligand contains an additional resonance at 11.8 ppm which has an integral of 1H and is attributed to the pyrrole NH group. No resonance is present for the NH groups of the two other pyrrole groups due to their removal upon uranyl complexation. Two similar sets of resonances in a 2:1 ratio are observed in the ^{1}H NMR spectrum of $[Pd(HL^T)]$ as well as a single resonance for the apical methyl group which is also present in the spectrum of $[UO_2(py)(HL^T)]$ at 2.53 ppm.

Single crystals of $[UO_2(HL^T)]$ could not be obtained from pyridine or THF solvents as the addition or suspension of the material in all common non-donor solvents resulted in gelation (see 5.52). The composition of the complex is however supported by elemental analysis, which confirms that there is no pyridine solvent molecule in the fifth equatorial position. This is further supported by ^{1}H NMR spectroscopy, with dissolution of the complex in $CDCl_3$ displaying no resonances attributed to pyridine. The metalation of the tris(pyrrolide) tripod ligand by uranyl is supported by FTIR spectroscopy, which displays a

stretch at 916 cm^{-1} characteristic of the $[UO_2]^{2+}$ asymmetric stretch. The FTIR data also supports the assignment of an N_4-coordinated ligand with a pendent ligand arm, with a two separate C=N stretches corresponding to both the uranyl-coordinated and uranyl-free-imine groups at 1603 and 1634 cm^{-1} respectively, with the double degeneracy of the former stretch highlighted in its larger transmission.

5.2.2 Synthesis of the $[UO_2(HL^T)]$ gel

Attempts to work up solutions of $[UO_2(HL^T)]$ by removal of the pyridine solvent and dissolution in benzene resulted in the formation of an immobile gel phase with a high viscosity. The solid $[UO_2(HL^T)]$ complex gelates at a concentration of 40 mg ml^{-1} without forming a free-flowing solution with the material only forming a solid phase upon removal of the non-polar solvent under vacuum. Samples of the gel in benzene can by melted to form a free-flowing solution by heating the material to 67 °C, with the solution returning to a gel phase upon cooling. The gel can also be formed *in-situ* by direct combination of equimolar solutions of H_3L^T and $[UO_2(N'')_2(py)_2]$ in benzene, with the initial formation of brown solution followed by gelation upon shaking for 10 s. Immediate removal of the solvent under vacuum and dissolution of the resultant residue in THF, pyridine or chloroform resulted in the formation of $[UO_2(HL^T)]$ and trace amounts of H_3L^T, suggesting that reaction to form $[UO_2(HL^T)]$ is accelerated by gel formation, with the reaction normally taking 12 h in pyridine. Although the rate is increased however, the trace amounts of free ligand present after dissolution of material is perhaps indicative of poorer reagent mixing in the immobile phase resulting in less than 100 % reaction completion. Gel formation can also be induced by addition of non-polar solvents to solutions of $[UO_2(HL^T)]$ in THF or pyridine with layering of either solution with an equal volume hexane or benzene resulting in the formation of the brown gel material suspended in an almost colourless solution of the solvent mixture.

The starkly differing behaviour of $[UO_2(HL^T)]$ in donor or non-donor solvents leads to speculation as to the origin of the gelation in the latter medium. Although the solid state structure of the complex could not be inferred it is proposed, based on the available data, that it has a broadly similar structure to the square planar palladium complex $[Pd(HL^T)]$. In the latter complex, the free or "hanging" ligand arm that does not partake in metal coordination was observed to participate in hydrogen-bonding with the arm of an adjacent molecule to form a dimer in the solid state, with the pyrrole NH and imine groups acting as respective hydrogen-bond donors and acceptors. Although such an interaction could be used to explain gelation of $[UO_2(HL^T)]$ it is not anticipated that dimerisation alone would be sufficient enough to significantly change the solution properties of the complex, especially considering

that [Pd(HL^T)] is soluble in a range of organic solvents. It is more likely, therefore, that the gelation of [UO_2(HL^T)] results from the formation of continuous supramolecular network, with such a structure of significant rigidity and porosity of encapsulate large quantities of the benzene solvent. Such a continuous hydrogen bonding network could only result from asymmetric hydrogen-bonding interactions whereby the hanging arm of one molecule binds to another H-bond donor/acceptor unit of a second leaving the free arm of the second complex to bind to the next unit.

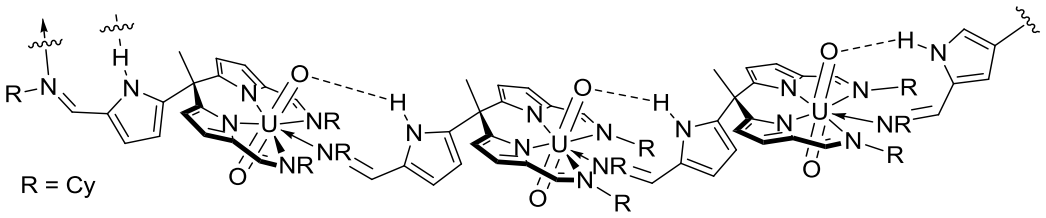

Figure 17: Proposed structure of the [UO_2(HL^T)] gel.

It is proposed therefore that the uranyl dication acts as the second supramoleular synthon to which the hanging arm binds, being capable of acting as both a Lewis acid and base to form interactions with the imine donor and the acidic NH bond respectively (Figure 17). The complicit nature of the $[UO_2]^{2+}$ species proposed to explain the gelation of [UO_2(HL^T)] perhaps explains why supramolecular aggregation is not observed in any other metal complexes of the L^T ligand. In order to facilitate aggregation, the fifth equatorial coordination site of the uranyl dication must be free to accept the imine donor of an adjacent complex, a postulate supported by the spectroscopic data. While exact nature of the fifth-donor in molecular [UO_2(HL^T)] is unclear, it may be that partial aggregation by imine/uranyl interactions also occurs in pyridine solution, albeit to a lower degree than in non-polar solvents, retaining the solubility of the complex.

5.2.3 Attempted disaggregation of the [UO_2(HL^T)] gel

The reversibility of the [UO_2(HL^T)] gel formation upon solvent exchange led to investigations as to whether donor species could be used to deaggregate the gel to form soluble adduct in benzene solution (Scheme 8). The greater aim of such investigation was to crystallise any soluble adducts, allowing structural characterisation.

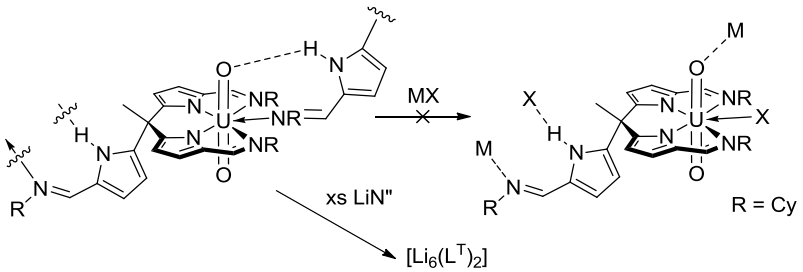

Scheme 8: Synthesis of $[UO_2(py)(HL^T)]$

To this end, a number of salts were added to samples of the $[UO_2(HL^T)]$ gel in the hope that they would disrupt the non-covalent interactions that maintain the supramolecular structure. Although it was found that addition of solid $[Me_4N][Cl]$ or KX salts (X = F, Cl) resulted in the rapid dissolution of the gel to form a benzene-soluble phases, analysis of the resultant solutions by ^{1}H NMR spectroscopy suggested that deaggregation was facilitated by degredation of the $[UO_2(HL^T)]$ complex rather than the formation of a molecular adduct. The same results were obtained by addition of the strong donors pyridine-*N*-oxide and Ph_3PO with neither reagent allowing the formation of a stable molecular species. The addition excess amounts of the strong lithium base $LiN(SiMe_3)_2$ to the $[UO_2(HL^T)]$ gel in benzene also resulted in complex degradation, in this case inducing a transmetalation reaction between the $[UO_2]^{2+}$ and Li cations precipitating single crystals of the lithium salt complex $[Li_6(L^T)_2]$ after one week.

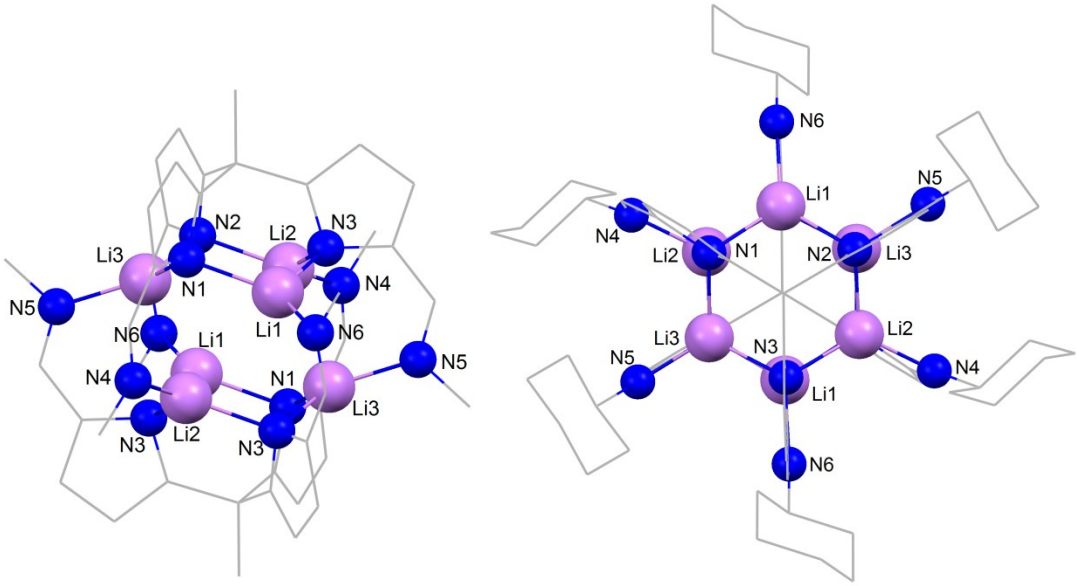

Figure 18: Solid state structure of $[Li_6(L^T)_2]$ shown side-on (left, cyclohexyl groups omitted for clarity) and top-down (right). Carbon atoms are shown in wireframe and other atoms are depicted as balls-and-sticks. Solvent molecules and H-atoms are omitted for clarity.

The X-ray crystal structure of $[Li_6(L^T)_2]$ shows two interlocking L^T molecules in tripodal conformations, each coordinating to three lithium cations through the pyrrolide N-donor atoms (Figure 18). The imine donors of each L^T ligand bind to a lithium cation of the opposing Li_3L^T unit, forming a dimeric cage structure in which two cofacial Li_3N_3 rings, each in an approximate chair conformation, lie staggered above each other, with the imine donors from the opposing Li_3L^T unit bound to the Li cation of the next in a position equatorial to the hexagonal Li_3N_3 ring.

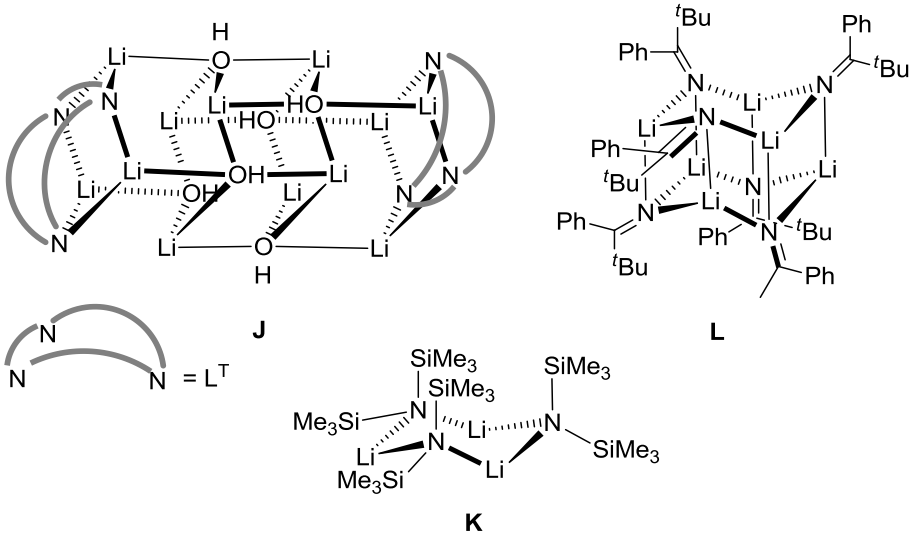

Figure 19: The previously reported LiOH-incorporated Li_3L^T complex (**J**), a discrete Li_3N_3-complex (**K**) and a dimeric Li_6N_6 complex (**L**).

One previous crystal structure of the lithium salt of L^T has been reported, derived from addition of excess $LiN(SiMe_3)_2$ to improperly-dried H_3L^T and resulting in the crystallisation of the LiOH incorporated structure $[Li_3(THF)_3(L^T)(LiOH)_3]_2$ (Figure 19, **J**).[27] The hexagonal Li_3N_3 units in $[Li_6(L^T)_2]$ are a common motif in lithium amide chemistry and are often observed to oligomerise through secondary lithium-nitrogen bonds to form extended structures through so-called "ring-laddering", in contrast to lithium alkyls which typically aggregate to form by "ring-stacked" structures.[29] The complex $[Li_6(L^T)_2]$ presents an unusual case of Li_3N_3-ring aggregation that is facilitated by ligand bridging groups, with the more usual aggregation by inter-ring Li-N interaction prohibited by the size L^T ligands. The crystal structure of $LiN(SiMe_3)_2$, the precursor to $[Li_6(L^T)_2]$, provides one of the simplest examples of a Li_3N_3 ring, with laddering in this case also prevented by the large size of the amide ligand (Figure 18, **K**).[30] In the case of smaller ligands, such as the lithium imide complex [LiNC(Ph)^{t}Bu], dimerisation of the Li_3N_3 rings to form a ring-laddered cage is seen.[31]

5.2.4 Attempted salt elimination reactions from M_3L^T complexes

Upon the successful isolation of anhydrous Li_3L^T, efforts were undertaken to use it as a precursor to other f-block complexes of the L^T ligand. The reaction of $[Li_6(L^T)_2]$ with half equivalents of either $[UO_2Cl_2(THF)_2]$, $[UI_3(THF)_4]$ or $[UI_4(OEt_2)_4]$ did not however result in the formation of the target uranium complexes $Li[UO_2(L^T)]$, $[U(L^T)]$ or $[UI(L^T)]$ respectively, with either reagent decomposition or no reaction observed in all cases. The analogous reactions from anhydrous potassium salt K_3L^T, a completely insoluble solid prepared *in-situ* by addition of three equivalents of KN" to the free ligand, were similarly unsuccessful.

5.3 Attempted synthesis of dileptic uranyl(VI) complexes

The final polypyrrolic ligand studied in this chapter was the dipyrrolic macrocycle H_2L^M, a heterocalixarene first synthesised by Sessler and co-workers which features two pyrrole groups bridged by meta-substituted dimethylene-phenyl rings.[32]

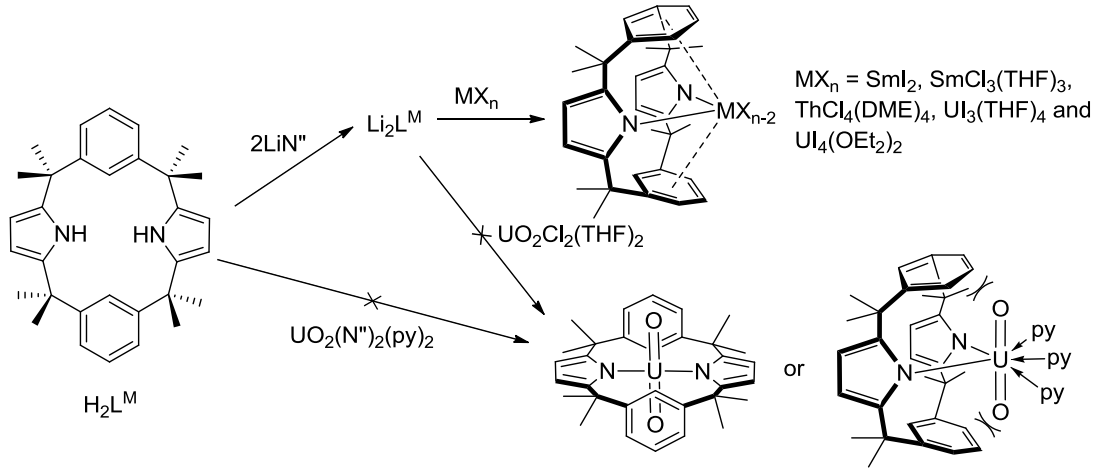

Scheme 9: Structure and reactivity of H_2L^M towards f-block metalation.[33]

More recently, the ligand has been used by ourselves and the Gardiner group to synthesise a number of f-block complexes of samarium, thorium and low-valent uranium (Scheme 7).[33] A common feature of all the complexes is that they exhibit both M-N bonds between the pyrrolide groups and the respective metals, and cation-π interactions, the latter derived from π-donation from the ligand phenyl groups to the cationic centres. Attempts to synthesise a uranyl complex of the L^M ligand were however unsuccessful from either direct deprotonation of the macrocycle with $[UO_2(N")_2(py)_2]$ or from salt elimination reactions between the lithium salt Li_2L^M and uranyl chloride, with no reaction observed in either case in benzene solution (Scheme 7).

Such a lack of reactivity towards uranyl complexation is perhaps due to unfavourable square planar geometry of the target compound $[UO_2(L^M)]$, with the absence of neutral donor ligands on the L^M macrocycle being unable to fulfil the equatorial coordination requirements of the uranyl cation. The attempted synthesis of a donor-solvated $[UO_2(py)_x(L^M)]$ complex were also unsuccessful, suggesting that the folding of the macrocycle that would be required to allow metal protrusion and subsequent coordination of donor solvents is also not favourable, perhaps due to an envisaged electronic repulsion between the rigorously axial uranyl oxo groups and the π-system of the proximal phenyl groups.

5.4 Alternative syntheses of mononuclear uranyl Pacman complexes

As discussed previously, the syntheses of the mono uranyl Pacman complexes $[UO_2(sol)(H_2L)]$ (sol = THF or pyridine) are typically carried out by transmetalation reactions between the free ligand H_4L and one equivalent of a uranyl bis(silylamide) base.[4-5] While this synthetic route is relatively simple, the synthesis of the uranyl precursor $[UO_2(N'')_2(THF)_2]$ from $[UO_2Cl_2(THF)_2]$ and KN" is difficult and time-consuming requiring multiple extractions and filtrations of the reaction mixture to remove the KCl by-product.

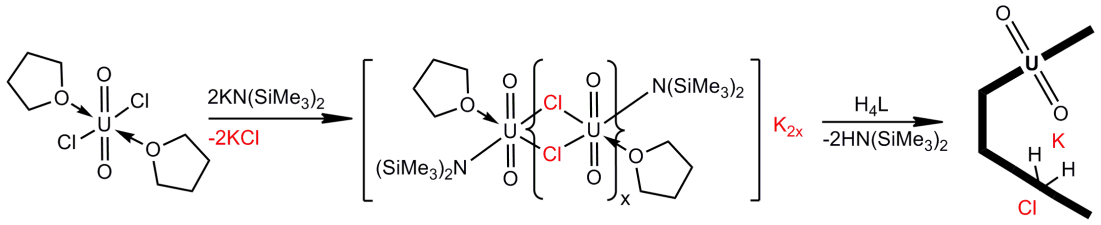

Scheme 10: Potassium chloride incorporation in $[UO_2(sol)(H_2L)]$

Previous studies using silylamide-derived $[UO_2(THF)(H_2L)]$ have shown that, despite the best efforts of the synthetic chemist, chloride contaminants from $[UO_2(N'')_2(THF)_2]$ can be incorporated into the vacant N_4-donor pocket of the macrocycle and can often be carried forward upon subsequent reaction (Scheme 10).[34] Removal of the KCl by-product from the pyridine-solvated precursor $[UO_2(N'')_2(py)_2]$ is relatively straightforward (see Chapter One) however this although precursor cannot be used to obtain the THF-solvate $[UO_2(THF)(H_2L)]$. In light of this, new routes to $[UO_2(sol)(H_2L)]$ complexes were sought that did not employ $[UO_2(N'')_2(THF)_2]$ as a precursor.

5.4.1 Uranyl carboxylates as precursors to $[UO_2(sol)(H_2L)]$

The conjugate amine of $[UO_2(N'')_2(THF)_2]$, HN", has as pK_a 26.1 whereas the likely pK_a of the pyrrolic amine protons of H_4L are approximately 23 with the difference between

the values explaining the facile deprotonation of H_4L with the uranyl base.[35-36] It has been observed previously in the syntheses of bimetallic palladium Pacman complexes however that less basic acetate ligands can directly deprotonate H_4L despite the much lower pK_a of 15 for the conjugate acetic acid.[37] It has been suggested for this case that the metal may act to reduce the pK_a of the pyrrole NH groups by neutral coordination in the N_4-donor cavity and subsequent "pre-complex" formation, a process that occurs in tandem with the macrocylic effect to facilitate complex formation.[38] In light of this, uranyl acetate was explored as a potential starting material for the synthesis of $[UO_2(THF)(H_2L)]$.

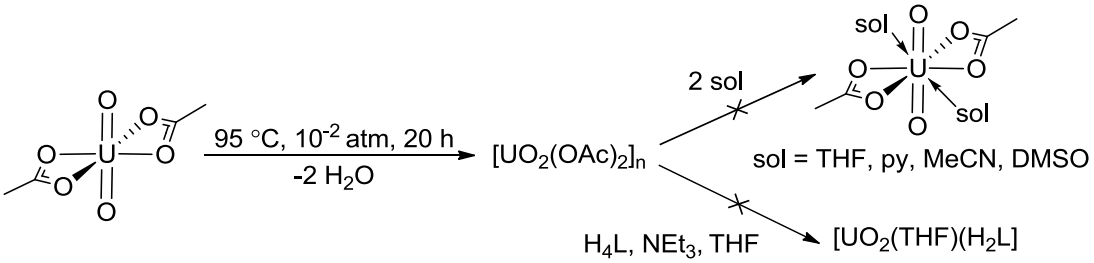

Scheme 11: Dehydration and aggregation of uranyl acetate

In light of the moisture sensitivity of $[UO_2(THF)(H_2L)]$, attempts were made to dehydrate the readily available $[UO_2(OAc)_2(H_2O)_2]$ before assessing it's reactivity. A number of groups have demonstrated by TGA (thermogravimetric analysis) that heating hydrated uranyl acetate at 100–160 °C under air or 90 °C under vacuum yields anhydrous material,[39-40] with dehydration at 95°C under vacuum for 20 h producing $[UO_2(OAc)_2]$ in quantitative yield, confirmed by the mass loss of water (Scheme 11).

Hydrated uranyl acetate is insoluble in organic solvents but partially soluble in water, with increasing aqueous solubility at lower pH. In contrast, the anhydrous material produced by thermal dehydration is completely insoluble even in acidic solutions. One explanation for this is that the material aggregates upon loss of water, with uranyl cations linking together to form an oligomeric species by bridging acetate ligands. Attempts to disrupt such oligomerisation using strong donors proved unsuccessful and perhaps unsurprisingly, no reaction was observed between anhydrous uranyl acetate and H_4L even at elevated temperatures.

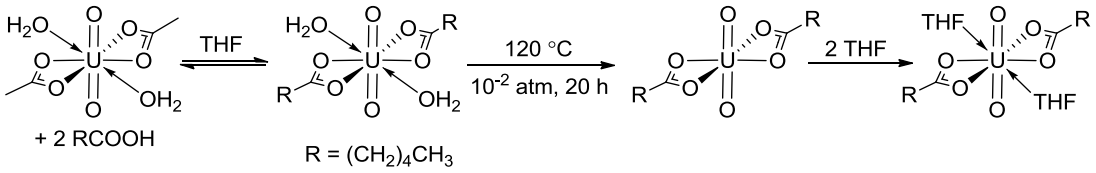

Scheme 12: Synthesis of uranyl hexanoate

In an attempt to prevent aggregation, hydrous uranyl acetate was converted into uranyl hexanoate in a carboxylate exchange reaction (Scheme 11). Addition of two equivalents of hexanoic acid to a suspension of hydrous uranyl acetate in THF resulted in the complete dissolution of the solids. Removal of the solvent under vacuum before dehydration of the remaining solid resulted in the sole formation of $[UO_2\{O_2C(CH_2)_4CH_3\}_2]$ in almost quantitative yield. Unlike uranyl acetate, uranyl hexanoate demonstrated partial solubility in C_6D_6 allowing a ^1H NMR spectrum to be recorded. The spectrum displays five separate resonances corresponding to the hexanoate ligands which are broadened and shifted in comparison with the hexanoic acid starting material. Resonances attributable to either starting material are not present and there is no evidence for the presence water or THF indicating that the complex remains unsolvated. The FTIR spectrum of the complex contains a band 945 cm^{-1} attributable to the $[U^{VI}O_2]^{2+}$ asymmetric stretching mode and the composition of the material was verified by elemental analysis. In contrast to $[UO_2(OAc)_2]$, dissolution of the complex in THF to form the solvate analogue $[UO_2\{O_2C(CH_2)_4CH_3\}_2(THF)_x]$ is extremely facile at room temperature.

The reaction of $[UO_2\{O_2C(CH_2)_4CH_3\}_2]$ with one equivalent of H_4L was carried out in THF in the presence of triethylamine, the latter being required to neutralise any hexanoic acid released upon uranyl complexation. However, the reaction did not proceed to completion at room temperature or upon boiling, with resonances attributable to uranyl hexanoate and the free ligand H_4L remaining present in the ^1H NMR spectrum after 24 h. Although $[UO_2(THF)(H_2L)]$ was formed in residual quantities, no evidence for the formation of NEt_3-neutralised hexanoic acid was observed.

In contrast, performing the same reaction in pyridine was found to produce $[UO_2(py)(H_2L)]$ in much greater abundance. An additional base was not used initially in the hope that the more basic solvent may itself neutralise any hexanoic acid.

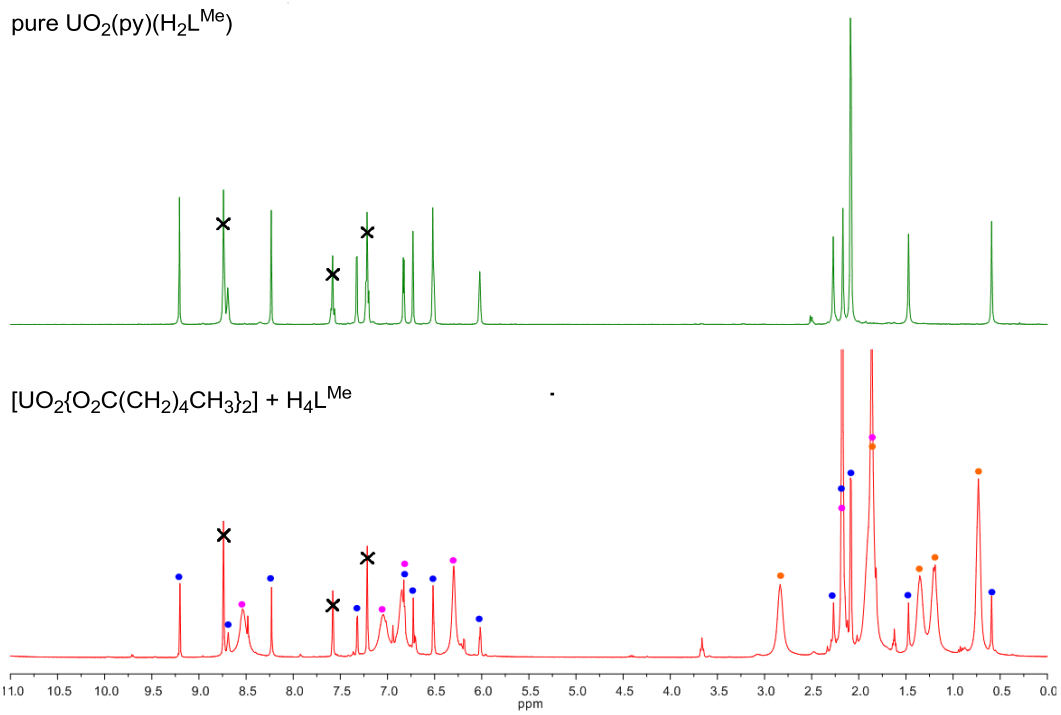

Figure 20: ^{1}H NMR spectra showing the reaction to form $[UO_2(py)(H_2L)]$ (blue markers) and $[H4L]\cdot[C_5H_{11}CO_2]_4$ (pink markers) from uranyl hexanoate (orange markers) in d_5-pyridine. Pure $[UO_2(py)(H_2L)]$ is also shown for comparison (green trace, top).

The ^{1}H NMR spectrum of the reaction mixture shows the formation of the target compound $[UO_2(py)(H_2L)]$ as well as broad resonances attributed to the formation of the protonated ligand salt $[H_4L]\cdot[C_5H_{11}CO_2]_4$. In the absence of a stronger base the hexanoic acid released upon uranyl complexation preferentially protonates the imine nitrogen on the ligand forming the hexanoate salt of the L, with the acidic proton of $[H_4L]\cdot[C_5H_{11}CO_2]_4$ presumed to have a higher pK_a value than that of pyridinium. Formation of the salt by-product renders the protonated ligand unreactive towards complexation, explaining the persistence of unreacted uranyl hexanoate that is also present in the reaction mixture after several days. When excess triethylamine was added, the broad resonances attributable to $[H_4L]\cdot[C_5H_{11}CO_2]_4$ were found to disappear, being replaced by a set of sharp, well-defined resonances corresponding to the neutral ligand. Further reaction between this newly liberated H_4L and the remaining uranyl hexanoate was not observed, with both compounds remaining unreacted in the system after several days, even at elevated temperatures.

Inspired by the reactivity of $[UO_2\{O_2C(CH_2)_4CH_3\}_2]$, the analogous reaction between H_4L and $[UO_2Cl_2(THF)_2]$ was attempted at room temperature. The formation of $[UO_2(py)(H_2L]$ was observed by ^{1}H NMR spectroscopy after 10 min, with a broad set of resonances in similar positions to those observed for $[H_4L]\cdot[C_5H_{11}CO_2]_4$, indicating

protonation of the unreacted ligand by hydrochloric acid to form the salt $[H_4L]\cdot[HCl]_4$. In contrast to the hexanoate ligand salt, $[H_4L]\cdot[HCl]_4$ is only transiently soluble in pyridine, evidenced by the disappearance of the broad resonances and the precipitation of an orange solid over 20 h. The only species remaining in solution after this period were $[UO_2(py)(H_2L)]$ and THF, the latter having been liberated from uranyl chloride at the start of the reaction. Addition of triethylamine to the reaction mixture and subsequent heating at 40 °C resulted in the dissolution of the orange solid and an increase in the ratio of $[UO_2(py)(H_2L)]$:THF from 1:3 to 1:2 after over 24 h

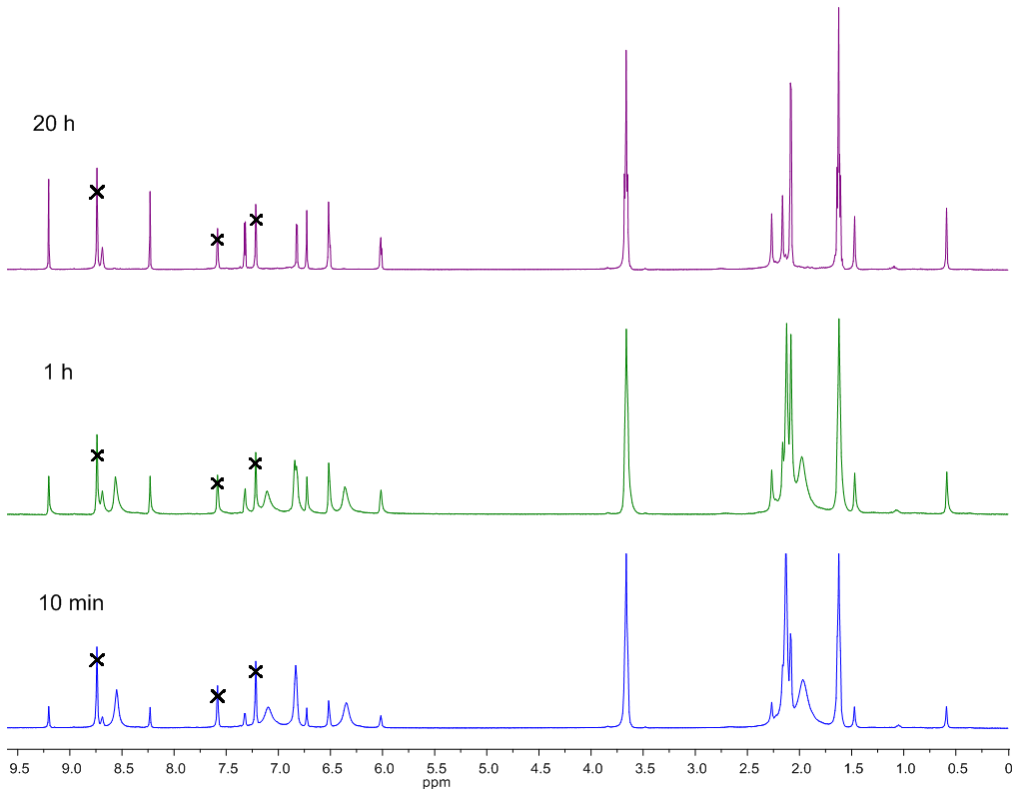

Figure 21: ^{1}H NMR spectra showing the formation of $[UO_2(py)(H_2L)]$ from $[UO_2Cl_2(THF)_2]$ and H_4L.

In summary, two new routes to the uranyl Pacman complex $[UO_2(py)(H_2L)]$ were found using either uranyl hexanoate or uranyl chloride as metal precursors. Interestingly, neither reaction proceeds to completion from a "one-pot" methodology suggesting that it is the initial formation of the ligand salt that drives the reaction, a process inhibited in presence of triethylamine. The use of refluxing conditions in these cases, intended to drive either reaction to completion, resulted in complete ligand decomposition.

For a large-scale synthesis the ideal route would allow complete conversion to the desired product and simple removal of any by-product. The reaction from $[UO_2Cl_2(THF)_2]$

proceeds with the fastest rate and in the initial step the highly-insoluble by-product $[H_4L]\cdot[HCl]_4$ precipitates out of the system cleanly. The by-product from the second step, triethylammonium chloride, is soluble in pyridine and would have to be selectively crystallised from solution to remove it from the reaction. In addition, the formation of $HNEt_3Cl$ is very slow, possibly due to the relative stability and insolubility of the salt $[H_4L]\cdot[HCl]_4$ from which it is derived.

$$[UO_2Cl_2(THF)_2] + 1.5\ H_4L \xrightarrow[RT,\ 20\ h]{py} [UO_2(py)(H_2L)] + 0.5\ [H_4L][HCl]_4$$

Scheme 13: Reaction of uranyl chloride with 1.5 equivalents of H_4L

Upon these observations, the reaction between 1.5 equivalents of H_4L, one equivalent of $[UO_2Cl_2(THF)_2]$ and no additional base was undertaken allowing complete consumption of the uranyl starting material and the simple isolation of $[UO_2(py)(H_2L)]$ in 50 % yield from a gram-scale preparation. Although the route is less efficient than the silylamide route in terms of ligand consumption, post-synthetic treatment of $[H_4L]\cdot[HCl]_4$ with triethylamine allows almost complete recovery of the sacrificial 0.5 equivalents of H_4L. The advantages of the route over the transamination method are the much simpler elimination of the by-product $[H_4L]\cdot[HCl]_4$ in comparison to KCl and the much higher yield of the reaction with respect to uranyl of 50 % in comparison to 21 % for the two step-synthesis.

5.1 Summary

The cofacial, binuclear uranyl(VI) Pacman complex $[\{UO_2(py)\}(L^A)]$ was synthesised by the reaction of the anthracenyl Pacman macrocycle H_4L^A and two equivalents of $[UO_2(N'')_2(py)_2]$ in pyridine. The reaction also produced the mono-uranyl complex $[UO_2(py)(H_2L^A)]$ that was removed by fractional crystallisation and characterised by mass spectrometry.

The reactions of the *meso*-fluorenyl substituted ligand H_4L^F with one equivalent of $[UO_2(N'')_2(py)_2]$ produced the mono-uranyl Pacman complex $[UO_2(py)(H_2L^F)]$ in high yield. The reactions with two equivalents of either $[UO_2(N'')_2(py)_2]$ or $[UO_2(N'')_2(THF)_2]$ were found to yield small quantities of the binuclear uranyl(VI) complexes $[(UO_2)_2(\mu\text{-}O)(L^F)]$ or $[(UO_2)_2\{\mu\text{-}(O\{CH_2\}_4NC_5H_5)\}(L^F)]$ respectively. Both complexes were synthesised in low yields due to potassium-impurities in the H_4L^F starting material. The use of potassium-free H_4L^F resulted in the formation of the alternative, silylated binuclear uranium(V) oxo butterfly complexes $[(Me_3SiOUO)_2(L^F)]$ and $[(PhMe_2SiOUO)_2(L^F)]$ from boiling reactions of

either $[UO_2(N'')_2(py)_2]$ or $[UO_2(N^*)_2(py)_2]$ in pyridine demonstrating that the reactivity of pure H_4L^F is the same as the octamethylated analogue H_4L.

A uranyl(VI) complex $[UO_2(H_2L^T)]$ was synthesised from the 1:1 reaction of $[UO_2(N'')_2(py)_2]$ and the tripodal, pyrrolic ligand H_3L^T. In pyridine or THF solvent the species was shown to be soluble and molecular whereas the formation of a supramolecular gel was observed in the non-polar solvents benzene and hexane. It was postulated that the gel results from aggregation of $[UO_2(H_2L^T)]$ units by coordination of the hanging ligand arm to the $[UO_2]^{2+}$ cation of an adjacent molecule.

Finally, an alternative synthesis of the mononuclear complex $[UO_2(py)(H_2L)]$ was discovered from 1.5 equivalents of the free ligand H_4L and one equivalent of $[UO_2Cl_2(THF)_2]$. The route negate the requirement for $[UO_2(N'')_2]$ and circumvents the problems associated with KCl-contamination from that starting material.

5.2 References

1 G. Givaja, M. Volpe, J. W. Leeland, M. A. Edwards, T. K. Young, S. B. Darby, S. D. Reid, A. J. Blake, C. Wilson, J. Wolowska, E. J. L. McInnes, M. Schröder, J. B. Love, *Chem. Eur. J.* **2007**, *13*, 3707-3723.

2 J. B. Love, *Chem. Commun.* **2009**, 3154-3165.

3 E. Askarizadeh, A. M. J. Devoille, D. M. Boghaei, A. M. Z. Slawin, J. B. Love, *Inorg. Chem.* **2009**, *48*, 7491-7500.

4 P. L. Arnold, D. Patel, A.-F. Pecharman, C. Wilson, J. B. Love, *Dalton Trans.* **2010**, *39*, 3501-3508.

5 P. L. Arnold, E. Hollis, F. J. White, N. Magnani, R. Caciuffo, J. B. Love, *Angew. Chem., Int. Ed. Engl.* **2011**, *50*, 887-890.

6 A. M. J. Devoille, P. Richardson, N. L. Bill, J. L. Sessler, J. B. Love, *Inorg. Chem.* **2011**, *50*, 3116-3126.

7 N. W. Alcock, *J. Chem. Soc., Dalton Trans.* **1973**, 1616-1620.

8 L. B. Serezhkina, E. V. Peresypkina, A. V. Virovets, V. V. Klepov, *Kristallografiya* **2010**, *55*, 251-253.

9 A. E. Bradley, C. Hardacre, M. Nieuwenhuyzen, W. R. Pitner, D. Sanders, K. R. Seddon, R. C. Thied, *Inorg. Chem.* **2004**, *43*, 2503-2514.

10 J. J. Berard, G. Schreckenbach, P. L. Arnold, D. Patel, J. B. Love, *Inorg. Chem.* **2008**, *47*, 11583-11592.

11 K. Takao, Y. Ikeda, *Inorg. Chem.* **2007**, *46*, 1550-1562.

12 M. Polamo, I. Mutikainen, M. Leskela, *Acta Crystallographica Section C* **1997**, *53*, 1036-1037.

13 M. Tayebani, S. Conoci, K. Feghali, S. Gambarotta, G. P. A. Yap, *Organometallics* **2000**, *19*, 4568-4574.

14 Y. Shi, C. Cao, A. L. Odom, *Inorg. Chem.* **2003**, *43*, 275-281.

15 J. M. Tanski, G. Parkin, *Inorg. Chem.* **2002**, *42*, 264-266.

16 W. H. Harman, T. D. Harris, D. E. Freedman, H. Fong, A. Chang, J. D. Rinehart, A. Ozarowski, M. T. Sougrati, F. Grandjean, G. J. Long, J. R. Long, C. J. Chang, *J. Am. Chem. Soc.* **2010**, *132*, 18115-18126.

17 P. Crewdson, S. Gambarotta, M.-C. Djoman, I. Korobkov, R. Duchateau, *Organometallics* **2005**, *24*, 5214-5216.

18 K. M. Wampler, R. R. Schrock, *Inorg. Chem.* **2007**, *46*, 8463-8465.

19 G. B. Nikiforov, P. Crewdson, S. Gambarotta, I. Korobkov, P. H. M. Budzelaar, *Organometallics* **2006**, *26*, 48-55.

20 G. T. Sazama, T. A. Betley, *Organometallics* **2011**, *30*, 4315-4319.

21 N. A. Piro, M. F. Lichterman, W. H. Harman, C. J. Chang, *J. Am. Chem. Soc.* **2011**, *133*, 2108-2111.

22 W. H. Harman, C. J. Chang, *J. Am. Chem. Soc.* **2007**, *129*, 15128-15129.

23 A. Arunachalampillai, P. Crewdson, I. Korobkov, S. Gambarotta, *Organometallics* **2006**, *25*, 3856-3866.

24 A. J. Lewis, U. J. Williams, J. M. Kikkawa, P. J. Carroll, E. J. Schelter, *Inorg. Chem.* **2011**, *51*, 37-39.

25 F. Zhou, J. Wu, M. Lin, Y. Zhao, J. Wu, Y. Zhang, W. Li, Y. Li, *Z. Anorg. Allg. Chem.* **2011**, *637*, 117-121.

26 P. D. Beer, A. G. Cheetham, M. G. B. Drew, O. D. Fox, E. J. Hayes, T. D. Rolls, *Dalton Trans.* **2003**, 603-611.

27 J. S. Hart, F. J. White, J. B. Love, *Chem. Commun.* **2011**, *47*, 5711-5713.

28 J. S. Hart, G. S. Nichol, J. B. Love, *Dalton Trans.* **2012**, *41*, 5785-5788.

29 R. E. Mulvey, *Chem. Soc. Rev.* **1991**, *20*, 167-209.

30 D. Mootz, A. Zinnius, B. Böttcher, *Angew. Chem.* **1969**, *81*, 398-399.

31 D. Barr, W. Clegg, R. E. Mulvey, R. Snaith, K. Wade, *J. Chem. Soc., Chem. Commun.* **1986**, 295-297.

32 J. L. Sessler, W.-S. Cho, V. Lynch, V. Král, *Chem. Eur. J.* **2002**, *8*, 1134-1143.

33 P. L. Arnold, R. C. White, M. G. Gardiner, **2013**, manuscript in preparation.

34 P. L. Arnold, D. Patel, C. Wilson, J. B. Love, *Nature* **2008**, *451*, 315-317.

35 R. R. Fraser, T. S. Mansour, S. Savard, *J. Org. Chem.* **1985**, *50*, 3232-3234.

36 F. G. Bordwell, G. E. Drucker, H. E. Fried, *J. Org. Chem.* **1981**, *46*, 632-635.

37 F. G. Bordwell, D. Algrim, *J. Org. Chem.* **1976**, *41*, 2507-2508.

38 G. Givaja, A. J. Blake, C. Wilson, M. Schröder, J. B. Love, *Chem. Commun.* **2003**, 2508-2509.

39 I. M. Yanachkova, M. Staevsky, *J. Mater. Sci.* **1973**, *8*, 606-610.

40 M. S. Grigor'ev, M. Y. Antipin, N. N. Krot, *Radiochemistry* **2004**, *46*, 224-231.

Conclusions

It has been shown the Pacman macrocycle can enable the single-electron reduction, *cis*/*trans* oxo group isomerisation and oxo-group silylation of two discrete $[UO_2]^{2+}$ dications when reacted with an excess of a uranyl(VI) silylamido precursor. The resulting binuclear uranium(V) complexes $[(RMe_2SiOUO)_2(L)]$ (R = Me, Ph) are the first examples containing the diamond-shaped $\{OU^V(\mu\text{-}O)_2U^VO\}$ motif, a *cis*-oxo isomer of a uranyl(V)/uranyl(V) CCI complex. The $SiMe_3$-functionalised complex displays strong magnetic exchange coupling of J_{ex} = –33 cm^{-1} between the two U^V centres and the highest temperature antiferromagnetic exchange interaction for a uranium(V) complex at 17 K. It is proposed that such strong communication between the two $5f^1$ centres is in part due to partial U–O multiple bonding, as indicated theoretical calculations, and in part due to an extremely short U···U separation of 3.36 Å. The $[(RMe_2SiOUO)_2(L)]$ complexes are the most stable uranium(V) compounds currently known, being highly inert towards oxidation, hydrolysis or disproportionation.

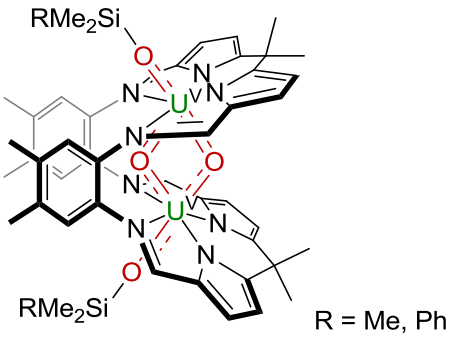

One- or two-electron reduction of $[(Me_3SiOUO)_2(L)]$ to form the $U^{IV/V}$ and $U^{IV/IV}$ salts $K[(Me_3SiOUO)_2(L)]$ and $K_2[(Me_3SiOUO)_2(L)]$ respectively was found to promote reactivity with water, with the former complex being found to yield $K[(Me_3SiOU^{IV})(\mu\text{-}OH)(OU^VO)(L)]$ complexes upon hydration which exhibit localised uranyl(V)/uranium(IV) oxidation states and singly-desilylated oxo groups. Somewhat surprisingly, these binuclear U^V complexes containing bridging hydroxides and Group 1 cations were isolated with no evidence of disproportionation even in the presence of excess H_2O. It is possible that the geometries of these particular complexes are such that electron-transfer to furnish U^{VI} and U^{IV} products is disfavoured, a postulate collaborated by the lack of electronic communication found between the two U centres. A fully desilylated butterfly complex $K_2[(OUO)_2(L)]$ was synthesised by oxidative desilylation of $K_2[(Me_3SiOUO)_2(L)]$ in pyridine with pyridine-N-oxide. In contrast to $[(Me_3SiOUO)_2(L)]$, the complex was found to be highly reactive towards hydrolysis, disproportionation and oxidation. Treatment of $K_2[(OUO)_2(L)]$ with

TMSCl re-formed the silylated complex upon which such reactivity was removed leading to the postulate that oxo-group silylation may be used as an effective strategy for protecting highly reactive U^{V} centres and that reactivity may be switched on by protecting group removal. The lithium-salt of the $[(OUO)_2(L)]^{2-}$ anion was synthesised directly from the Pacman macrocycle and a new uranyl(VI) tris-silylamido "ate" complex precursor providing the second example of a Pacman-mediated syntheses a $\{U^{V}_2O_4\}$ complex from two uranyl(VI) dications.

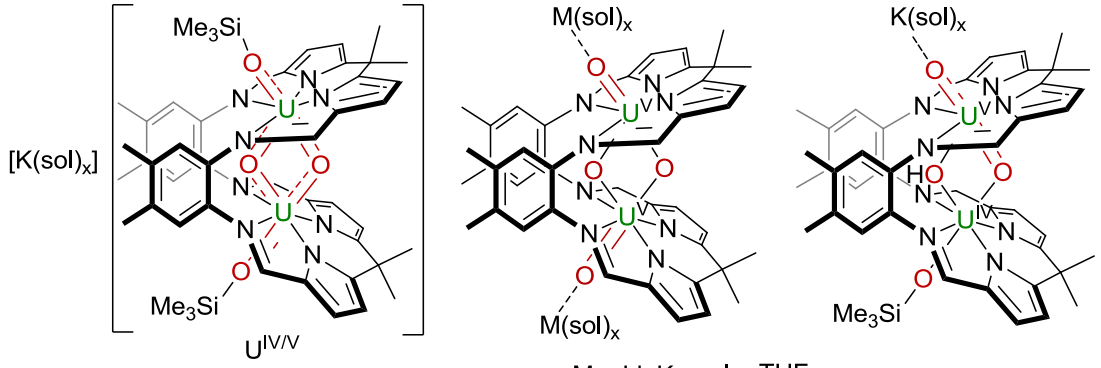

Functionalisation of the unsilylated $M_2[(OUO)_2(L)]$ complexes (M = Li, K) allowed the formation of $[\{(^{n}Bu_3Sn)OUO\}_2(L)]$, $[(PhSnOUO)_2(L)]$ and $[(^{i}PrOUO)_2(L)]$, adding to the family of binuclear oxo uranium(V) complexes featuring the $(ROU^{V}O)_2$ motif. These alkyl, silyl, and stannyl derivatives all display *cis*/*trans* arrangements of oxo ligands and extend the covalent functionalisation of uranium oxo groups to tin and carbon. The high stabilities of these compounds against oxidative decomposition provide further evidence that highly reactive uranium(V) centres can be 'protected' by functionalisation of their oxo ligands with Group 14 elements.

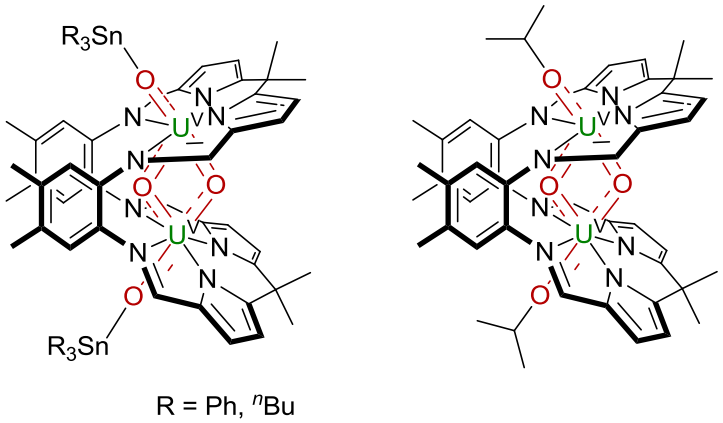

Modification of the Pacman macrocycle L by the introduction of bulky *meso* substituents did not affect the reactivity of the ligand towards the formation of binuclear uranium(V) oxo complexes. The use of the anthracene-substituted macrocycle H_4L^A was found to facilitate larger U···U separations in the resulting uranyl complexes allowing reductive functionalisation processes to be switched off. The binuclear uranyl(VI) complex $[\{UO_2(py)\}_2(L)]$ demonstrated the contrasting reactivity of L^A *vs* L and was the first example of a binuclear cofacial uranyl(VI) complex.

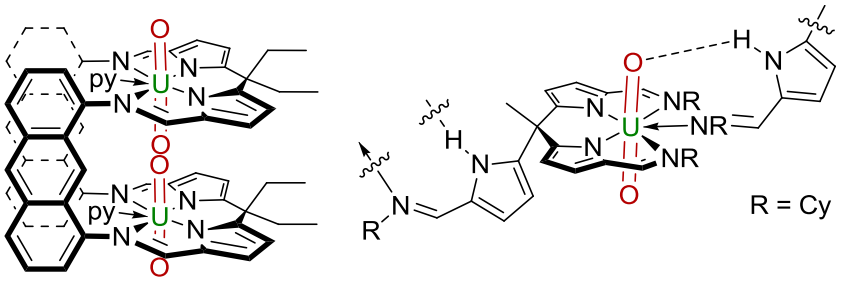

The first uranyl(VI) complex of a tripodal macrocycle $[UO_2(H_2L^T)]$ was synthesised and shown to form a supramolecular gel in non-polar solvents, a process that could be reversed by heating or by dissolution in THF or pyridine. It was postulated that $[UO_2(H_2L^T)]$ aggregates by hydrogen-bonding interactions between the $[UO_2]^{2+}$ dication and the pendent iminopyrrole ligand arm. While such weak OUO···HR hydrogen bonding interactions have been observed in the solid state, the $[UO_2(H_2L^T)]$ gel may provide an example of a material were such interactions are present in a more mobile phase.

In summary, this work has extended the reduction chemistry of uranyl Pacman complexes to include homobimetallic examples, complimenting previous on heterobimetallic uranyl(V) complexes and further emphasising the ability of the Pacman ligand to stabilise the U^V oxidation state. Many of the complexes reported in this thesis contain the $\{U^V_2O_4\}$ motif, a new structural isomer in uranium(V) oxo chemistry. In contrast to uranyl(V) complexes, the motif is highly stable with respect to U^V disproportionation when protected by covalent functionalisation. The structure of these binuclear uranium oxo complexes can be easily manipulated by both redox and ligand-exchange chemistry with the library of complexes presented in this thesis showcasing a diverse range of U–O bonding types. More importantly, the reactivity of such complexes, especially towards oxo-group functionalisation, adds to the growing evidence that high oxidation state uranyl and uranium oxo complexes exhibit greater U–O bond reactivity that previously thought. This is especially apparent for complexes in the U^V oxidation state, the rarity of which is continues to decrease as more is discovered about their structures and stability.

Experimental details and characterising data

7.1 General methods and instrumentation

All manipulations were carried out using standard Schlenk line or glovebox techniques under an atmosphere of dinitrogen unless otherwise stated. Pyridine, benzene and 1,4-dioxane were distilled from potassium under dinitrogen in a solvent still prior to use. Hexane, diethyl ether, CH_2Cl_2, toluene and THF were degassed by sparging with dinitrogen and dried by passing through a column of activated sieves in Vacuum Atmospheres solvent towers. Solvents were stored over either potassium mirrors (hexanes, benzene and toluene) or activated 4 Å molecular sieves (all others). Deuterated solvents (d_5-pyridine, d_8-THF, d_8-toluene and C_6D_6) were boiled over potassium, vacuum-transferred and freeze-pump-thaw degassed three times prior to use. Deuterated chloroform ($CDCl_3$) was dried by boiling over activated alumina before being isolated in the same manner.

^{1}H NMR, ^{29}Si NMR and ^{7}Li{^{1}H} spectra were recorded on a Bruker AVA400 spectrometer operating at 399.90, 79.4 and 155.42 MHz respectively. ^{13}C{^{1}H} NMR spectra were recorded on a Bruker AVA500 operating at 125.76 MHz. ^{1}H NMR spectra in 1:1 C_6D_6:THF were recorded with double solvent suppression on a Bruker AVA 600 spectrometer operating at 599.81 MHz. Chemical shifts are reported in parts per million and referenced to residual proton resonances calibrated against external TMS (δ = 0 ppm). All spectra were recorded at 298 K unless otherwise stated.

Matrix assisted laser desorption ionisation (MALDI) mass spectra were recorded by Dr. Logan McKay at the University of Edinburgh SICAMS facility. Elemental analyses were carried out by Mr Stephen Boyer at London Metropolitan University and by Analytische Laboratorien, Lindlar, Germany.

Infrared spectra were recorded on a Jasco 410 spectrophotometer, w = weak, m = medium, s = strong intensity. UV/Vis/NIR spectra were recorded on a Jasco V-670 spectrophotometer in a 10 mm quartz cuvette fitted with a Teflon tap. Cyclic voltammagrams were obtained using an Autolab 302 potentiostat and the data processed using GPES Manager version 4.9. Experiments were undertaken in a glovebox using a 15 mL glass vial as the cell. The working electrode consisted of a platinum wire embedded in glass, the counter electrode a platinum wire and the reference electrode silver wire. The solution employed was 1.0 mM of the compound and 0.2 M $[Bu_4N][BF_4]$ with scan rates 100–1000 mVs^{-1}. All potentials calibrated against $[Cp_2Fe]^{0/+}$ (Fc/Fc^+ = 0 V).

Variable temperature magnetic susceptibilities were measured using a Quantum Design MPMS-XL SQUID susceptometer operating at 10000 or 50000 Oe in the temperature range 2 to 300 K. The sample was loaded in a gelatine capsule in a dinitrogen-filled glovebox and suspended in a plastic straw. Diamagnetic contributions from the ligands were calculated using Pascal's constants.[1]

X-ray crystallographic data were collected at 170 K on an Oxford Diffraction Excalibur diffractometer using graphite monochromated Mo-Kα radiation equipped with an Eos CCD detector or at 100 K on an Oxford Diffraction Supernova diffractometer using mirror monochromated Cu-Kα radiation (λ = 1.5418 Å) and an Atlas CCD detector. Structures were solved using either SHEL-XS-97 direct methods,[2] SHEL-XS-97 Patterson methods,[2] or the SUPERFLIP charge-flipping program[3] and refined using a full-matrix least square refinement on $|F|^2$ using SHELXL-97.[2] All programs were used within the WinGx suite.[4] All non-hydrogen atoms refined with anisotropic displacement parameters and H-parameters were constrained to parent atoms and refined using a riding model unless otherwise stated.

H_4L,[5] H_4L^A,[6] H_4L^M,[7] $[UO_2Cl_2(THF)_2]$,[8] $[UO_2\{N(SiMe_3)_2\}_2(THF)_2]$,[9] $[UO_2(py)_2(H_2L)]$,[10] $[U\{N(SiMe_3)_2\}_2\{N(SiMe_3)SiMe_2CH_2\}]$,[11] $[UI_3(THF)_4]$,[12] $[UI_4(OEt_2)_3]$,[13] $[U(ODtbp)_3]$,[14] $KN(SiMe_3)_2$,[15] $KN(SiMe_2Ph)_2$,[16] K(TMP),[17] KN(H)Dipp,[18] $Ce(OTf)_4$,[19] $[TiCl_4(THF)_2]$[20] and (*B*-I)-9-BBN[21] were synthesised according to literature procedures. H_4L^F was prepared using a modified literature procedure employing excess NEt_3 instead of excess KOH in the final step. H_4L^F synthesised using the original literature preparation[5] is specifically denoted "KOH-derived". H_3L^T was synthesised as described in the literature[22] before being dried by melting at 120 °C under vacuum for 12 h and allowing to solidify at room temperature. $[UO_2(OAc)_2]$ was synthesised by dehydration of $[UO_2(OAc)_2(H_2O)_2]$ by at 120 °C under vacuum for 20 h. $LiN(SiMe_3)_2$ was recrystallised from hexanes and sublimed at 80 °C / 10^{-4} mbar; TMSCl, Ph_2SiHCl and were distilled from magnesium turnings and the latter stored in the absence of light. TMSOTf and $PhCH_2SiMe_3$ and were dried over 4 Å molecular sieves before use. Ph_3SnCl, $B(C_6F_5)_3$, dihydroanthracene, Ph_2NH, and $LiCH(SiMe_3)_2$ were sublimed (10^{-4} mbar, 90 °C) and Ph_2PCl, $HN(SiMe_2Ph)$, $HN(SiMe_3)_2$, MeOTf, 1,1-diemthylsiletane, H_2NDipp and $[Ti(O^iPr)_3Cl]$ were distilled under reduced pressure (10^{-1} mbar, various temperatures) prior to use. KF was dried ar 275 °C at 10^{-6} Torr for 6 h. $[FeCp_2][OTf]$ was prepared by addition of ferrocene to a solution of silver trifluoromethanesulfonate in CH_2Cl_2 followed by recrystallisation from a CH_2Cl_2/ mixture at –35 °C. TMEDA was distilled over CaH_2. Trityl chloride (Ph_3CCl) was recrystallised from

toluene and washed with hexanes. KC_8 was prepared by addition of potassium to eight molar equivalents of ground graphite at 160 °C. 18-crown-6 was purified by recrystallisation from acetonitrile before drying under vacuum for 12 h. Dry KOH was prepared by addition of degassed water to potassium in toluene under a dinitrogen atmosphere before purification by sublimation (10^{-4} mbar, 120 ºC). $AgBPh_4$ was prepared by precipitation by addition of $NaBPh_4$ to $AgNO_3$ in water followed by drying the precipitate under vacuum at 90 °C for 12 h. $[Zn\{N(SiMe_3)_2\}Cl]$ was prepared by mixing $[Zn\{N(SiMe_3)_2\}_2]$ and $ZnCl_2$ in toluene. Pyridinium chloride was synthesised by addition of 1 M HCl in Et_2O to pyridine in toluene. All other reagents were purchased and used without further purification.

7.2 Synthetic procedures described in Chapter Two

7.2.1 Synthesis of $[UO_2\{N(SiMe_3)_2\}_2(py)_2]$

a. *By donor exchange with the THF-adduct.* $[UO_2\{N(SiMe_3)_2\}_2(THF)_2]$ (1.79 g, 2.44 mmol) was dissolved in pyridine (5 mL) and stored at –35 °C. Orange crystals of $[UO_2\{N(SiMe_3)_2\}_2(py)_2]$ appeared after 24 h and were isolated by filtration, washed with hexanes (3 × 2 mL) and dried under vacuum for 1 h. The filtrate was reduced in volume to 2 mL and stored at –35 °C resulting in the precipitation of a second batch of material after 24 h which was isolated in the same manner. $[UO_2\{N(SiMe_3)_2\}_2(THF)_2]$ was isolated as an orange solid (1.32 g, 1.76 mmol, 73 %). Single crystals of the product suitable for X-ray diffraction were grown by slow evaporation of a benzene solution. ^{1}H NMR (d_5-pyridine): δ_H 0.30 (br.s, 36H, methyl). ^{1}H NMR (C_6D_6): 9.31 (br.s, 8H, pyridine), 6.91 (br.s, 4H, pyridine), 6.78 (br.s, 8H, pyridine), 0.62 (br.s, 18H, methyl), 0.46 (br.s, 54H, methyl). ^{13}C{1H} NMR (C_6D_6): δ_C 151.48 (pyridine), 139.25 (pyridine), 125.05 (pyridine), 7.46 (methyl), 7.21 (methyl). FTIR (nujol, cm^{-1}): 1637 (m), 1600 (m), 1255 (m), 1238 (m), 1224 (m), 1155 (w), 1070 (w), 1037 (w), 1010 (m), 935 (m), 887 (m), 775 (w), 755 (w). Solubility: pyridine, THF, toluene, benzene and hexane (partial).

b. *By salt elimination.* To a yellow suspension of $[UO_2Cl_2(THF)_2]$ (15.0 g, 31.0 mmol) in pyridine (15 mL) was added an orange solution of $KN(SiMe_3)_2$ (12.4 g 62.1 mmol) in pyridine (10 mL) and the mixture stirred for 9 h resulting in the dissolution of all solids to form a dark red solution. The volatiles were then evaporated under vacuum and the resultant red residue dried under vacuum for 12 h before addition of toluene (50 mL). The mixture was then stirred for 30 min with intermittent sonication (3 × 5 min, medium power) forming an orange solution and finely-suspended brown precipitate, the latter of which was allowed to settle from the solution over 2 h. The filtrate was then decanted from the solid using a

cannula, filtered through a Celite pad and reduced in volume to 10 mL under vacuum before storage at –35 °C for 12 h resulting in the precipitation of orange crystals. These were isolated by filtration and dried under vacuum for 2 h. The filtrate was reduced in volume to 5 mL and stored at –35 °C resulting in the precipitation of a second batch of material after 24 h which was isolated in the same manner. $[UO_2\{N(SiMe_3)_2\}_2(THF)_2]$ was isolated as an orange solid (13.4 g, 17.0 mmol, 58 %).

7.2.2 Synthesis of $[UO_2\{N(SiMe_2Ph)_2\}_2(py)_2]$

To a yellow suspension of $[UO_2Cl_2(THF)_2]$ (2.00 g, 4.14 mmol) in pyridine (5 mL) was added a colourless solution of $KN(SiMe_2Ph)_2$ (2.68 g, 8.28 mmol) and the resulting orange solution stirred for 3 h after which the volatiles were evaporated under vacuum and the resulting yellow oil dried under vacuum for 12 h. The product was then extracted into boiling hexanes (10 x 10 mL), filtered at 80 °C through a Celite column, and the resulting orange filtrate allowed to cool to room temperature resulting in the precipitation of yellow crystals after 12 h. The product was then isolated by filtration and dried under vacuum. $[UO_2\{N(SiMe_2Ph)_2\}_2(py)_2]$ was isolated by filtration as a yellow solid (2.89 g, 2.90 mmol, 70 %). Single crystals of the product were grown from pyridine solution at –30 °C. ^{1}H NMR (C_6D_6): δ_H 8.52 (m, 4H, pyridine), 7.50 (d, 8H, $SiMe_2$*Ph*), 7.12 (m, 12H, $SiMe_2$*Ph*) 6.95 (t, 2H, pyridine), 6.72 (m, 4H, pyridine), 0.54 (s, 24H, Si*Me*$_2$Ph). ^{13}C{^{1}H} NMR (C_6D_6) δ_C 151.76 (pyridine), 147.18 (quaternary, $SiMe_2$*Ph*) 138.65 (pyridine) 134.62 ($SiMe_2$*Ph*), 128.35 ($SiMe_2$*Ph*), 127.43 ($SiMe_2$*Ph*), 124.88 (pyridine), 6.89 (Si*Me*$_2$Ph). Analysis. Found: C, 51.85; H, 5.48; N, 5.48 %. $C_{42}H_{54}N_4O_2Si_4U$ requires: C, 50.58; H, 5.46; N, 5.62 %.FTIR (nujol, cm^{-1}): 1600 (w), 1247 (m), 1238 (w), 1222 (m) 1182 (m), 1155 (m), 1106 (m), 1066 (w), 1039 (w), 1004(w), 950 (s), 923 (w), 833 (m) , 800 (w).

7.2.3 Synthesis of $[(Me_3SiOUO)_2(L)]$

a. *From H_4L and $[UO_2\{N(SiMe_3)_2\}_2(py)_2]$ by heating only*. To a yellow solution of H_4L (1.00 g, 1.51 mmol) in pyridine (7 mL) in a Teflon-tapped ampoule was added an orange solution of $[UO_2\{N(SiMe_3)_2\}_2(py)_2]$ (2.837 g, 37.9 mmol, 2.5 equiv) in pyridine (7 mL) and the resulting brown solution heated at 120 °C for 12 h. The volatiles were then evaporated under vacuum and the resulting brown solids dried under vacuum for 12 h. Extraction into diethyl ether (50 mL) afforded a brown suspension which was filtered and the filtrate concentrated to 5 mL before being stored at –35 °C. The brown, ether-insoluble material remaining after extraction was dried for 3 h under vacuum and stored in the glovebox (**P** and intractable material, yield 1.8 g). Brown crystalline $[(Me_3SiOUO)_2(L)]$

formed after storage of the filtrate for 24 h and was isolated by filtration and dried under vacuum for 30 min. The product was collected as a brown solid (353 mg, 0.263 mmol, 17 %). Crystals of $[(Me_3SiOUO)_2L]$ suitable for single crystal X-ray diffraction were grown at –35°C from a saturated toluene solution. ^{1}H NMR (C_6D_6): δ_H 14.81 (s, 18H, $SiMe_3$), 13.21 (d, 4H, pyrrole), 8.90 (d, 4H, pyrrole), 7.73 (s, 4H, imine), 4.38 (s, 6H, *meso*-methyl), –3.15 (s, 12H, aryl-methyl), –3.78 (s, 4H, aryl), –11.08 (s, 6H, *meso*-methyl). ^{1}H NMR (1:1 C_6D_6:THF): δ_H 15.50 (s, 18H, $SiMe_3$), 12.72 (s, 4H, pyrrole), 8.64 (s, 4H, pyrrole), 7.77 (s, 4H, imine), 4.16 (s, 6H, *meso*-methyl), −2.77 (s, 12H, aryl-methyl), −3.55 (s, 4H, aryl), −11.52 (s, 6H, *meso*-methyl). ^{1}H NMR (d_5-pyridine): δ_H 14.61 (s, 18H, $SiMe_3$), 13.17 (d, 4H, pyrrole), 9.13 (d, 4H, pyrrole), 8.56 (s, 4H, imine), 4.43 (s, 6H, *meso*-methyl), –2.78 (s, 12H, aryl-methyl), –3.32 (s, 4H, aryl), –10.73 (s, 6H, *meso*-methyl). ^{29}Si NMR (C_6D_6): δ_{Si} 160.1. Analysis. Found: C, 42.83; H, 4.23; N, 8.39. $C_{42}H_{54}N_4O_2Si_4U$ requires: C, 42.92; H, 4.35; N, 8.34 %. FTIR (Nujol mull, cm^{-1}): (L = stretches assigned to the ligand) ν 1594 (s, L), 1575 (s, L), 1284 (s, L), 1269 (m, Si-CH_3), 1100 (m, Si-O), 1049 (s, L), 1018 (m, L), 906 (w, L), 862 (m, U-O), 802 (m, U-O) cm^{-1}. Vis/NIR (THF, 11.2×10^{-3} M): 1018 nm (ε = 110 L mol^{-1} cm^{-1}), 1040 (ε = 66 L mol^{-1} cm^{-1}), 1163 (ε = 78 L mol^{-1} cm^{-1}), 1592 (ε = 49 L mol^{-1} cm^{-1}), 1665 (ε = 63 L mol^{-1} cm^{-1}). μ_{eff} (Evans' method): 2.42 μ_B per molecule. SQUID: see Chapter Two, section 2.5. Cyclic Voltammetry (THF): No oxidation was observed within the limits of the solvent window (–3 to + 1 V *vs* Fc^+/Fc) irreversible reduction E_{pa} –2.40 V. Solubility: pyridine, THF, toluene, benzene, diethyl ether and hexane. Air/moisture stability: of $[(Me_3SiOUO)_2(L)]$ (10 mg, 0.007 mmol) and 1,3,5-tri-tert-butylbenzene (2 mg, 0.007 mmol) was dissolved in wet C_6D_6 (0.5 mL, used as purchased) in air. Neither precipitation nor decomposition was observed after 48 h, visually, and by ^{1}H NMR spectroscopy. 20 % decomposition to H_4L was seen after 5 d by ^{1}H NMR spectroscopy.

b. *From $[UO_2(py)(H_2L)]$ and $[UO_2\{N(SiMe_3)_2\}_2(py)_2]$*. To a brown solution of $[UO_2(py)(H_2L)]$ (285 mg, 0.283 mmol) in pyridine (2 mL) in a Teflon-tapped ampoule was added an orange solution of $[UO_2\{N(SiMe_3)_2\}_2(py)_2]$ (318 mg 0.424 mmol, 1.5 equiv) in pyridine (2 mL) and the resulting brown solution heated at 120 °C for 12 h. The volatiles were then evaporated under vacuum and the resulting brown solids dried under vacuum for 12 h. The product was then extracted into diethyl ether (20 mL) leaving a brown solid (190 mg) which comprises **P** and a small amount of intractable material. The brown filtrate was reduced in volume to 2 mL under vacuum before being stored at –35 °C. Brown crystals of the product formed from the filtrate after 24 h and the product was isolated by filtration and

dried under vacuum for 30 min. [$(Me_3SiOUO)_2$(L)] was isolated as a brown solid (95 mg, 0.071 mmol, 25 %).

c. *Optimised preparation by heating and TMSCl addition.*To a yellow solution of H_4L (1 g, 1.51 mmol) in pyridine in a Teflon-tapped ampoule (7 mL) was added an orange solution of [$UO_2\{N(SiMe_3)_2\}_2(py)_2$] (2.837 g, 3.79 mmol, 2.5 equiv) in pyridine (7 mL) and the resulting brown solution heated at 120 °C for 12 h. An excess of trimethylsilyl chloride (0.7 mL, 5.60 mmol, 3.7 equiv) was then added to the suspension and the mixture stirred for 5 min resulting in the dissolution of all residual solids. The volatiles were evaporated under reduced pressure and the resulting brown solids dried under vacuum for 12 h. Extraction into diethyl ether (50 mL) afforded a brown suspension which was filtered and the filtrate concentrated to 5 mL and cooled to –35 °C. The brown, ether-insoluble material remaining after extraction was discarded. After storage of the filtrate for 24 h, brown crystals of [$(Me_3SiOUO)_2$(L)] formed and were isolated by filtration and dried under vacuum for 30 min. The product was collected as a brown solid (1.110 g, 0.827 mmol, 55 %).

7.2.4 Synthesis of [$(PhMe_2SiOUO)_2$(L)]

To a brown solution of [UO_2(py)(H_2L)], 1 (93 mg, 0.092 mmol) in pyridine (1.5 mL) in a Teflon-tapped ampoule was added a solution of [$UO_2\{N(SiMe_2Ph)_2\}_2(py)_2$] (138 mg 0.139 mmol, 1.5 equiv) in pyridine (1.5 mL) and the resulting brown solution heated at 120 °C for 12 h. The volatiles were then evaporated under vacuum and the resulting brown solids dried under vacuum for 12 h. The product [$(PhMe_2SiOUO)_2$(L)] was then extracted into hot toluene (5 x 2 mL) leaving an intractable brown solid containing **P*** an a small amount of other material. The brown filtrate was reduced in volume under vacuum to 1 mL before being stored at –35 °C. Microcrystalline solids appeared from the filtrate after 24 h and the product was isolated by filtration and dried under vacuum for 30 min. [$(PhMe_2SiOUO)_2$(L)] was collected as a brown solid (31 mg, 0.021 mmol, 22 %). Single crystals of the product suitable for X-ray diffraction were grown by slow diffusion of hexane into a saturated benzene solution at room temperature. Characterisation for [$(PhMe_2SiOUO)_2$(L)]: ^{1}H NMR (C_6D_6): δ_H 17.35 (s, 12H, Si*Me*$_2$Ph), 14.67 (d, 4H, J = 7 Hz Si*Me*$_2$Ph), 13.09 (d, 4H, J = 3 Hz, pyrrole), 8.74 (d, 4H, J = 3 Hz, pyrrole), 8.48 (t, 4H, J = 7 Hz, SiMe$_2$*Ph*), 7.81 (t, 2H, J = 7 Hz, SiMe$_2$*Ph*), 7.58 (s, 4H, imine) 4.30 (s, 6H, *meso*-methyl), –2.89 (s, 12H, aryl-methyl), –4.00 (s, 4H, aryl), –11.20 (s, 6H, *meso*-methyl). ^{1}H NMR (d_5-pyridine): δ_H 17.23 (s, 12H, Si*Me*$_2$Ph), 15.57 (d, 4H, J = 7 Hz SiMe$_2$*Ph*), 13.11 (d, 4H, J = 3 Hz, pyrrole), 9.01 (d, 4H, J = 3 Hz, pyrrole), 8.88 (t, 4H, J = 7 Hz, SiMe$_2$*Ph*), 8.39 (s, 4H, imine), 8.15 (t, 2H, J = 7 Hz, SiMe$_2$*Ph*), 4.38 (s, 6H, *meso*-methyl), –2.72 (s, 12H, aryl-methyl), –3.74 (s, 4H, aryl), –

10.94 (s, 6H, *meso*-methyl). ^{29}Si NMR (C_6D_6): δ_{Si} 151.9. Analysis. Found: C, 49.09; H, 4.58; N, 6.87 %. $C_{58}H_{62}N_8O_4Si_2U_2.(C_6H_5CH_3)_{0.6}$ requires: C, 49.09; H, 4.42; N, 7.35 %. IR (Nujol mull, cm^{-1}): ν 1598 (s, L), 1575 (s, L), 1265 (m, Si-Me), 1114 (m, Si-O), 906 (m, L), 890–850 (s, U-O stretches). μ_{eff} (Evans' method, C_6D_6): 2.46 μ_B per molecule. Solubility: pyridine, THF, toluene and benzene.

Characterisation for compound **P*** isolated from this reaction: ^{1}H NMR (d_5-pyridine): silent. FTIR (Nujol mull, cm^{-1}) ν 1592 (m, L), 1573 (m, L), 1287 (m, L), 1051 (w, L), 1020 (w, L), 914 (w asymmetric stretch for $[UO_2]^{2+}$).

7.2.5 Reactions of $[(Me_3SiOUO)_2(L)]$ with oxidants

$[Cp_2Fe][OTf]$: To a Teflon-valved valve NMR tube containing a brown solution of $[(Me_3SiOUO)_2(L)]$ (12.3 mg, 0.009 mmol) in C_6D_6 (0.5 mL) was added a solution of ferrocenium trifluoromethanesulfonate (6.1 mg, 0.018 mmol, 2 equiv) in C_6D_6 (0.2 mL). No reaction was observed by ^{1}H NMR spectroscopy after one week.

$Ce(OTf)_4$: To a Teflon-valved valve NMR tube containing a brown solution of $[(Me_3SiOUO)_2(L)]$ (10 mg, 0.007 mmol) in C_6D_6 (0.5 mL) was added solid $Ce(OTf)_4$ (6.0 mg, 0.018 mmol, 2 equiv). No reaction was observed by ^{1}H NMR spectroscopy after one week.

$AgBPh_4$: To a Teflon-valved valve NMR tube containing a brown solution of $[(Me_3SiOUO)_2(L)]$ (8 mg, 0.005 mmol) in d_5-pyridine (0.7 mL) was added solid silver tetraphenylborate (5 mg, 0.011 mmol, 2 equiv). No reaction was observed by ^{1}H NMR spectroscopy after one week.

$[Ag][SbF_6]$: To a Teflon-valved valve NMR tube containing a brown solution of $[(Me_3SiOUO)_2(L)]$ (10 mg, 0.007 mmol) in d_5-pyridine (0.4 mL) was added a solution of $[Ag][SbF_6]$ (5 mg, 0.015 mmol, 2 equiv) in d_5-pyridine (0.3 mL). No reaction was observed by ^{1}H NMR spectroscopy after one week.

Air: An NMR tube containing a brown solution of $[(Me_3SiOUO)_2(L)]$ (10 mg, 0.007 mmol) in C_6D_6 (1 mL) was exposed to air for 48 h after which no reaction was observed by ^{1}H NMR spectroscopy.

Iodine: To a Teflon-valved valve NMR tube containing a brown solution of $[(Me_3SiOUO)_2(L)]$ (10 mg, 0.007 mmol) in C_6D_6 (1 mL) was added iodine (2.0 mg, 0.007 mmol). No reaction was observed by ^{1}H NMR spectroscopy after 24 h, with partial decomposition to afford intractable materials occurring after one week.

7.2.6 Reactivity of [(Me$_3$SiOUO)$_2$(L)] towards silyl group exchange

a. *With PhSiHCl*: To a brown solution of [(Me$_3$SiOUO)$_2$(L)] (10 mg, 0.007 mmol) in C_6D_6 (0.6 mL) in a Teflon-valved valve NMR tube was added an excess of chlorodiphenylsilane (1 drop). No reaction was observed by ^{1}H NMR spectroscopy after 24 h.

b. *With [UO$_2${N(SiMe$_3$)$_2$}$_2$(py)$_2$]*: To a brown solution of [(Me$_3$SiOUO)$_2$(L)] (10 mg, 0.007 mmol) and ^{t}Bu$_3$C$_6$H$_3$ (2 mg, 0.007 mmol) in d_5-pyridine (0.7 mL) in a Teflon-valved valve NMR tube was added an excess of solid [UO$_2${N(SiMe$_3$)$_2$}$_2$(py)$_2$] (10mg, 0.013 mmol) and the solution boiled at 120 °C for 12 h. No reaction was observed by ^{1}H NMR spectroscopy over the reaction period.

7.2.7 Reactivity of [(Me$_3$SiOUO)$_2$(L)] towards silyl-group abstraction

a. *Using TMSI:* To a brown solution of [(Me$_3$SiOUO)$_2$(L)] (17 mg, 0.012 mmol) and ^{t}Bu$_3$C$_6$H$_3$ (6 mg, 0.024 mmol, 2 equiv) in d_5-pyridine (0.6 mL) in a Teflon-valved valve NMR tube was added a colourless solution of trimethylsilyl iodide (5 mg, 0.024 mmol, 2 equiv) in d_5-pyridine (0.2 mL) and the resulting brown solution heated at 120 °C for 12 h. No reaction was observed by ^{1}H NMR spectroscopy.

b. *B-bromocatecholborane:* To a brown solution of [(Me$_3$SiOUO)$_2$(L)] (14 mg, 0.010 mmol) in d_5-pyridine (0.6 mL) in a Teflon-valved valve NMR tube was added a colourless solution of *B-bromocatecholborane* (4 mg, 0.021 mmol, 2 equiv) in d_5-pyridine (0.2 mL) and the solution boiled at 120 °C for 12 h. No reaction was observed by ^{1}H NMR spectroscopy.

7.2.8 Synthesis of [(Me$_3$SiOUO)$_2$(L)] in the dark

To a yellow solution of H_4L (10 mg, 0.015 mmol) in d_5-pyridine (0.5 mL) in an amber Teflon-valved valve NMR tube was added an orange solution of [UO$_2${N(SiMe$_3$)$_2$}$_2$(py)$_2$] (28 mg 0.038 mmol, 2.5 equiv) in d_5-pyridine (0.5 mL) and the resulting brown solution heated at 120 °C for 12 h. [(Me$_3$SiOUO)$_2$(L)] and HN(SiMe$_3$) were the only products visible by ^{1}H NMR spectroscopy after the reaction period.

7.2.9 Unnsuccesful syntheses of [(Me$_3$SiOUO)$_2$(L)]

a. *In toluene*. To a brown solution of [UO$_2$(py)(H$_2$L)], (15 mg, 0.015 mmol) in d_8-toluene (0.4 mL) in a Teflon-valved valve NMR tube was added an orange solution of [UO$_2${N(SiMe$_3$)$_2$}$_2$(py)$_2$] (17 mg 0.022 mmol, 1.5 equiv) in d_8-toluene (0.4 mL) and the

resulting brown solution heated at 110 °C in for 12 h. No reaction of was observed by ^{1}H NMR spectroscopy.

b. *In 1,4-dioxane*, To a yellow solution of H_4L (100 mg, 0.152 mmol) in 1,4-dioxane (2 mL) in a Teflon-tapped ampoule was added an orange solution of $[UO_2\{N(SiMe_3)_2\}_2(py)_2]$ (284 mg 0.379 mmol, 2.5 equiv) in 1,4-dioxane (2 mL) and the resulting brown solution heated at 100 °C in 12 h. The volatiles were then evaporated under vacuum resulting in the formation of a brown residue that was found to contain $[UO_2(py)(H_2L)]$ only by ^{1}H NMR spectroscopy.

c. *In THF:* See 7.2.16c

d. *From a uranium(IV) precursor.* To a brown solution of $[UO_2(py)(H_2L)]$ (14 mg, 0.014 mmol) in C_6D_6 (0.4 mL) in a Teflon-valved valve NMR tube was added an amber solution of $[U\{N(SiMe_3)_2\}_2\{N(SiMe_3)SiMe_2CH_2\}]$ (10 mg, 0.014 mmol, 1 equiv) in C_6D_6 (0.4 mL) and the resulting brown solution heated at 120 °C for 12 h. No reaction was observed by ^{1}H NMR spectroscopy.

e. *From excess $[UO_2\{N(SiMe_3)_2\}_2(py)_2]$*. To a brown solution of $[UO_2(py)(H_2L)]$ (10 mg, 0.009 mmol) in d_5-pyridine (0.4 mL) in a Teflon-valved valve NMR tube was added an orange solution of $[UO_2\{N(SiMe_3)_2\}_2(py)_2]$ (20 mg, 0.026 mmol, 3 equiv) in d_5-pyridine (0.3 mL) and the resulting brown solution heated at 120 °C for 12 h. After the reaction period the mixture was found to contain traces of $[(Me_3SiOUO)_2(L)]$, in addition to other unidentified products, by ^{1}H NMR spectroscopy in addition to an intractable brown solid.

7.2.10 Syntheses of $[(Me_3SiOUO)_2(L)]$ in the presence of hydrocarbylsilanes

a. *$PhCH_2SiMe_3$*. To a brown solution of $[UO_2(py)(H_2L)]$, (15 mg, 0.015 mmol) in d_5-pyridine (0.3 mL) in a Teflon-valved valve NMR tube was added an orange solution of $[UO_2\{N(SiMe_3)_2\}_2(py)_2]$ (17 mg 0.022 mmol, 1.5 equiv) and trimethylbenzylsilane (10 mg, 0.061 mmol, 4 equiv) in d_5-pyridine (0.3 mL) and the mixture heated at 120 °C for 12 h. $[(Me_3SiOUO)_2(L)]$ and $HN(SiMe_3)_2$ were the only products observed by ^{1}H NMR spectroscopy after the reaction period and no evidence for consumption of trimethylbenzylsilane was observed.

b. *1,1-Dimethylsiletane*. To a brown solution of $[UO_2(py)(H_2L)]$, (15 mg, 0.015 mmol) in d_5-pyridine (0.3 mL) in a Teflon-valved valve NMR tube was added an orange solution of $[UO_2\{N(SiMe_3)_2\}_2(py)_2]$ (17 mg 0.022 mmol, 1.5 equiv) and 1,1-dimethylsiletane (10 mg, 0.099 mmol, 7 equiv) in d_5-pyridine (0.3 mL) and the mixture heated at 120 °C for

12 h. [$(Me_3SiOUO)_2(L)$] and $HN(SiMe_3)_2$ were the only products observed by ^1H NMR spectroscopy after the reaction period and no evidence for consumption of 1,1-dimethylsiletane was observed.

7.2.11 Synthesis of [$(Me_3SiOUO)_2(L)$] in the presence of $HN(SiMe_2Ph)_2$

To a brown solution of [$UO_2(py)(H_2L)$], (15 mg, 0.015 mmol) in d_5-pyridine (0.3 mL) in a Teflon-valved valve NMR tube was added an orange solution of [$UO_2\{N(SiMe_3)_2\}_2(py)_2$] (11 mg 0.015 mmol, 1) and $HN(SiMe_2Ph)_2$ (5 mg, 0.018 mmol, 1.4 equiv) in d_5-pyridine (0.3 mL) and the mixture heated at 120 °C for 12 h. [$UO_2(py)(H_2L)$]. [$(Me_3SiOUO)_2(L)$], [$(PhMe_2SiOUO)_2(L)$] and [$(PhMe_2SiOUO)_2L(OUOSiMe_3)$] were observed in a 1:2:3 ratio by ^1H NMR spectroscopy, in addition to $HN(SiMe_3)_2$ and unreacted $HN(SiMe_2Ph)_2$. Characterisation data for [$(PhMe_2SiOUO)_2L(OUOSiMe_3)$]: ^1H NMR (C_5H_5N): δ_H 17.02 (s, 6H, Si*Me*$_2$Ph), 15.33 (d, 2H, J = 7 Hz SiMe$_2$*Ph*), 14.77 (s, 9H, $SiMe_3$), 13.15 (d, 2H, J = 3 Hz, pyrrole), 13.08 (d, 2H, J = 3 Hz, pyrrole), 9.07 (d, 3H, J = 3 Hz, pyrrole), 9.05 (d, 3H, J = 3 Hz, pyrrole), 8.87 (t, 2H, J = 7 Hz, SiMe$_2$*Ph*), 8.53 (s, 2H, imine), 8.43 (s, 2H, imine), 8.14 (t, 1H, J = 7 Hz, SiMe$_2$*Ph*), 4.47 (s, 3H, *meso*-methyl), 4.33 (s, 3H, *meso*-methyl), –2.69 (s, 6H, aryl-methyl), –2.79 (s, 6H, aryl-methyl), –3.20 (s, 2H, aryl), –3.84 (s, 2H, aryl), –10.70 (s, 3H, *meso*-methyl), –10.97 (s, 3H, *meso*-methyl).

7.2.12 Test reaction to determine amine exchange between [$UO_2\{N(SiMe_3)_2\}_2(py)_2$] and $HN(SiMe_2Ph)_2$

An orange solution of [$UO_2\{N(SiMe_3)_2\}_2(py)_2$] (10 mg, 0.0013 mmol) and $HN(SiMe_2Ph)_2$ (8 mg, 0.026 mmol, 2 equiv) was heated at 120 °C in a Teflon-valved valve NMR tube. After 10 min [$UO_2\{N(SiMe_3)_2\}_2(py)_2$], [$UO_2\{N(SiMe_2Ph)_2\}_2(py)_2$], $HN(SiMe_3)_2$ and $HN(SiMe_2Ph)_2$ were present in a 0.5:0.5:1:1 ratio by ^1H NMR spectroscopy. Heating the mixture for 12 h at 120 °C resulted in the formation of a 1:1 mixture of $HN(SiMe_3)_2$ and $HN(SiMe_2Ph)_2$ only by ^1H NMR spectroscopy.

7.2.13 Synthesis of [$(PhMe_2SiOUO)_2(L)$] in the presence of $N(SiMe_3)_3$

To a brown solution of [$UO_2(py)(H_2L)$] (10 mg, 0.0088 mmol) and $N(SiMe_3)_3$ (11 mg, 0.044 mmol) in d_5-pyridine (0.5 mL) in a Teflon-valved valve NMR tube was added an orange solution of [$UO_2\{N(SiMe_2Ph)_2\}_2(py)_2$] (13 mg 0.013 mmol) in d_5-pyridine (0.3 mL) and the resulting brown solution heated at 120 °C. After 12 h both [$UO_2(py)(H_2L)$] and [$UO_2\{N(SiMe_2Ph)_2\}_2(py)_2$] were consumed to give a solution of [$(PhMe_2SiOUO)_2(L)$] (0.0026 mmol, 0.3 eq) and $HN(SiMe_2Ph)$ (0.018 mmol, 0.7 eq) as observed by ^1H NMR

spectroscopy. No consumption of $N(SiMe_3)_3$ was observed, verified by the subsequent addition of 1eq of tBu$_3$C$_6$H$_3$ (2 mg, 0.0088 mmol) as an internal standard.

7.2.14 Synthesis of P

a: *From H_4L and [UO_2{$N(SiMe_3)_2$}$_2$($py)_2$] at 25 °C:* To a yellow solution of H_4L (100 mg, 0.151 mmol) in pyridine (2 mL) was added an orange solution of [UO_2{$N(SiMe_3)_2$}$_2$($py)_2$] (284 mg, 0.379 mmol, 2.5 equiv) in pyridine (3 mL) and the resulting brown solution stirred at room temperature for 14 d forming a brown precipitate. The solid was isolated by filtration and dried under vacuum for 2 h at 70 °C while the filtrate was reduced in volume to 2 mL under vacuum and stored at –35 °C for 24 h resulting in the precipitation of more solid. Compound **P** was isolated as brown solid (combined yield 155 mg from multiple batches). ^{1}H NMR in d_5-pyridine: Silent at 20 °C and 70 °C. Analysis. Found: C, 39.52; H, 3.37; N, 8.46. [$(HOUO)_2$(L)(UO_2){$N(SiMe_3)H$}(py)] requires C, 39.00; H, 3.45; N, 8.90. FTIR (Nujol mull, cm^{-1}): 1596 (s, L), 1573 (s, L), 1286 (m, L), 1270 (s), 1043 (s, L), 1018 (m, L), 912 (m, asymmetric stretch for $[UO_2]^{2+}$), 900 (w), 765 (w), 752 (w), 727 (m), 694 (m), 665 (m). LDI-MS: see Chapter Two, section 2.7.5. Solubility: insoluble in pyridine, THF, toluene, benzene, diethyl ether, *tert*-butanol, and hexane. Thermal stability: No change in ^{1}H NMR spectrum or solubility upon heating at 90 °C for several days in d_5-pyridine. Partial decomposition to afford intractable materials and traces of [$(Me_3SiOUO)_2$(L)] was observed upon heating at 120 ºC in d_5-pyridine for 24 h.

b: *From H_4L and [UO_2{$N(SiMe_3)_2$}$_2$($py)_2$] at 70 °C:* The same product can be made more quickly by heating the same mixture in a Teflon-tapped ampoule at 70 °C for 4 d. The attempted synthesis of **P** at temperatures above 70 °C produces quantities of [$(Me_3SiOUO)_2$(L)] in addition to **P**.

c. *From excess [UO_2{$N(SiMe_3)_2$}$_2$($py)_2$]*. To a solution of H_4L (100 mg, 0.151 mmol) in pyridine (1 mL) was added a solution of [UO_2{$N(SiMe_3)_2$}$_2$($py)_2$] (340 mg, 0.454 mmol, 3 equiv) resulting brown solution stirred at room temperature for 7 d. $HN(SiMe_3)_2$ and unreacted [UO_2{$N(SiMe_3)_2$}$_2$($py)_2$] were the only species present in solution after the reaction period by ^{1}H NMR spectroscopy.

7.2.15 Conversion of P into [$(Me_3SiOUO)_2$(L)] by treatment with Me_3SiX

a. *By treatment of in-situ generated **P** with Me_3SiCl.* To a yellow solution of H_4L (20 mg, 0.030 mmol) in d_5-pyridine (0.3 mL) in a Teflon-valved valve NMR tube was added an orange solution of [UO_2{$N(SiMe_3)_2$}$_2$($py)_2$] (57 mg, 0.076 mmol, 2.5 equiv) and ^{t}Bu$_3$C$_6$H$_3$ (8 mg, 0.030 mmol) in d_5-pyridine (0.3 mL) and the resulting brown solution allowed to stand

at room temperature. After 10 d a brown precipitate had formed and only $^{t}Bu_3C_6H_3$ and $HN(SiMe_3)_2$ were observed in the ^1H NMR spectrum. The volatiles were evaporated under vacuum and the brown residue of **P** dried for 2 h at 70 °C before being re-dissolved d_5-pyridine (0.6 mL). Trimethylsilyl chloride (drops) was then added resulting in the formation of $[(Me_3SiOUO)_2(L)]$ in 76 % total yield versus H_4L (calculated from ^1H NMR spectrum against $^{t}Bu_3C_6H_3$).

b. *Preparative scale synthesis of $[(Me_3SiOUO)_2(L)]$ using Me_3SiCl.* To a brown slurry of **P** (100 mg, 0.06 mmol based on best estimate of empirical formula) in pyridine (2 mL) was added trimethylsilyl chloride (0.1 mL) resulting in the complete dissolution of all solids to form a brown solution. The volatiles were evaporated under vacuum and the resulting brown residue dried for 2 h at 70 °C. Extraction into diethyl ether (3 x 5 mL) afforded a small quantity of yellow solid (10 mg)* and a brown filtrate which was reduced in volume to 2 mL under vacuum and stored at –35 °C. After 24 h brown crystalline $[(Me_3SiOUO)_2(L)]$ was isolated by filtration and dried under vacuum for 30 min (64 mg, 0.048 mmol, 80 % yield based on estimated empirical formula of **P**) NB: Samples of **P** formed at temperatures above 70 °C contain an amount (20 % by mass) of intractable material that is not reactive towards trimethylsilyl chloride or soluble in any common solvent. *Characterisation data of yellow solid: ^1H NMR (5 mg, d_5 pyridine): Trace quantities of $[(Me_3SiOUO)_2(L)]$ only. IR bands are attributed to residual $[(Me_3SiOUO)_2(L)]$ and other unidentified material.

c. *From TMSOTf.* To a yellow solution of H_4L (10 mg, 0.015 mmol) in d_5-pyridine (0.3 mL) in a Teflon-valved valve NMR tube was added an orange solution of $[UO_2\{N(SiMe_3)_2\}_2(py)_2]$ (29 mg, 0.038 mmol, 2.5 equiv) and $^{t}Bu_3C_6H_3$ (4 mg, 0.015 mmol) in d_5-pyridine (0.3 mL) and the resulting brown solution heated at 70 °C. After 4 d a brown precipitate had formed and only $^{t}Bu_3C_6H_3$ and $HN(SiMe_3)_2$ were observed in the ^1H NMR spectrum. The volatiles were then evaporated under vacuum and the brown residue dried for 2 h at 70 °C before being re-dissolved d_5-pyridine (0.6 mL). Trimethylsilyl trifluoromethanesulfonate (drops) was then added resulting in the formation of $[(Me_3SiOUO)_2(L)]$ in 80 % total yield by ^1H NMR spectroscopy, calibrated against $^{t}Bu_3C_6H_3$.

7.2.16 Unnsuccesful syntheses of P

a: *At –30 °C:* To a brown solution of $[UO_2(py)(H_2L)]$ (100 mg, 0.099 mmol) in pyridine (2 mL) at –30 °C was added a solution of $[UO_2\{N(SiMe_3)_2\}_2(py)_2]$ (112 mg, 0.149

mmol, 1.5 equiv) at –30 °C in pyridine (2 mL) and the resulting brown solution left at –30 °C for 30 d. No reaction was observed by ^{1}H NMR spectroscopy and the precipitation of single crystals of $[UO_2(py)(H_2L)]$ (confirmed by X-ray diffraction experiment) resulted over the reaction period.

b: *In benzene:* To a brown solution of $[UO_2(py)(H_2L)]$ (14 mg, 0.013 mmol) in C_6D_6 (0.4 mL) in a Teflon-valved valve NMR tube was added an orange solution of $[UO_2\{N(SiMe_3)_2\}_2(py)_2]$ (15 mg, 0.020 mmol, 1.5 equiv) in C_6D_6 (0.4 mL) and the mixture boiled at 80 °C for 4 d after which all the $[UO_2\{N(SiMe_3)_2\}_2(py)_2]$ and half $[UO_2(py)(H_2L)]$ had been consumed as evidenced by ^{1}H NMR spectroscopy. Addition of excess trimethylsilylchloride (0.1 mL) to the mixture resulted in the formation of $[(Me_3SiOUO)_2(L)]$ in a 1:1 ratio with the remaining $[UO_2(py)(H_2L)]$.

c: *In THF:* To a solution of H_4L (7 mg, 0.011 mmol) in d_8-THF (0.4 mL) in a Teflon-valved valve NMR tube was added a solution of $[UO_2\{N(SiMe_3)_2\}_2(py)_2]$ (20 mg, 0.027 mmol, 2.5 equiv) at in d_8-THF (0.3 mL) and the mixture heated at 80 °C for 4 d forming a brown solution. $[UO_2(THF)(H_2L)]$,[23] $[UO_2\{N(SiMe_3)_2\}_2(py)_2]$ and $HN(SiMe_3)_2$ were the only species present in solution after the reaction a 1:1.5:2 ratio by ^{1}H NMR spectroscopy.

7.2.17 Attempted deaggregation of P

a. *With Lewis acids.* To a brown slurry of **P** (10 mg 0.015 mmol based on best estimate of empirical formula) in C_6D_6 (0.5 mL) in a Teflon-valved valve NMR tube was added a solution of tris(pentafluorophenyl) borane (3 mg, 0.006 mmol, 1 equiv) in C_6D_6 (0.2 mL) and the mixture boiled at 120 °C for 12 h. No evidence of reaction was observed by visual inspection or ^{1}H NMR spectroscopy.

b. *With Lewis bases.* To a brown slurry of **P** (25 mg 0.015 mmol based on best estimate of empirical formula) in d_5-pyridine (0.5 mL) in a Teflon-valved valve NMR tube was added a solution of 4-dimethylamino-pyridine (6 mg, 0.045 mmol, 3 equiv) in d_5-pyridine (0.2 mL) and the mixture boiled at 120 °C for 12 h. No evidence of reaction was observed by visual inspection or ^{1}H NMR spectroscopy. NB: No reaction was observed between **3** and the other Lewis bases DMSO and triphenylphosphine oxide under the same conditions.

c. *With bidentate ligands.* To a brown slurry of **P** (15 mg 0.009 mmol based on best estimate of empirical formula) in d_5-pyridine (0.5 mL) in a Teflon-valved valve NMR tube was added a solution of acetylacetone (2 mg, 0.020 mmol, 2 equiv) in d_5-pyridine (0.2 mL)

and the mixture boiled at 120 °C for 12 h. No evidence of reaction was observed by visual inspection or ^{1}H NMR spectroscopy. NB. No reaction was observed between **P** and TMEDA ($Me_2NCH_2CH_2NMe_2$) under the same conditions.

7.2.18 Synthesis of [$(Ph_2HSiOUO)_2$(L)] from P

To a yellow solution of H_4L (20 mg, 0.030 mmol) in d_5-pyridine (0.3 mL) in a Teflon-valved valve NMR tube was added an orange solution of $[UO_2\{N(SiMe_3)_2\}_2(py)_2]$ **1** (57 mg, 0.076 mmol, 2.5 equiv) in d_5-pyridine (0.3 mL) and the resulting brown solution left to stand at room temperature for 10 d. After the reaction period a brown precipitate had formed and only $^{t}Bu_3C_6H_3$ and $HN(SiMe_3)_2$ were observed in the ^{1}H NMR spectrum. The volatiles were then evaporated under vacuum and the brown residue dried for 2 h at 70 °C before being re-dissolved d_5-pyridine (0.6 mL). Chlorodiphenylsilane (drops) was then added resulting in the sole formation of $[(Ph_2HSiOUO)_2(L)]$ by ^{1}H NMR spectroscopy. ^{1}H NMR (d_5-pyridine): δ_H 27.24 (s, 2H, Si*H*Ph_2), 20.03 (d, 8H, J = 7 Hz, SiH*Ph*$_2$), 12.91 (d, 4H, J = 3 Hz pyrrole), 10.84 (t, 8H, J = 7 Hz SiH*Ph*$_2$), 9.78 (t, 4H J = 7 Hz, SiH*Ph*$_2$), 9.05 (s, 4H, imine), 8.68 (d, 4H, J = 3 Hz, pyrrole), 4.15 (s, 6H, *meso*-methyl), –2.46 (s, 12H, aryl-methyl), –3.29 (s, 4H, aryl), –10.25 (s, 6H, *meso*-methyl).

7.2.19 Synthesis of P*

To a yellow solution of H_4L (10 mg, 0.015 mmol) in d_5-pyridine (0.3 mL) in a Teflon-valved valve NMR tube was added an orange solution of $[UO_2\{N(SiMe_2Ph)_2\}_2(py)_2]$ (38 mg, 0.038 mmol, 2.5 equiv) and $^{t}Bu_3C_6H_3$ (4mg, 0.015 mmol) in d_5-pyridine (0.3 mL) and the resulting brown solution heated at 70 °C. After 4 d a brown precipitate of **P*** had formed and only $^{t}Bu_3C_6H_3$ and $HN(SiMe_2Ph)_2$ were observed in the ^{1}H NMR spectrum. Addition of trimethylsilyl chloride (drops) to the reaction mixture resulted in the formation of $[(Me_3SiOUO)_2(L)]$ as the major product as well as a small quantity of mixed silylated material, supporting the prior formation of **P***.

7.2.20 Conversion of P* to [$(Me_3SiOUO)_2$(L)]

To a Teflon-valved valve NMR tube containing a brown suspension of **P*** (10 mg) in d_5-pyridine (0.6 mL) was added excess trimethylsilyl chloride (drops) resulting in the dissolution of some of the solids and the formation of $[(Me_3SiOUO)_2(L)]$ and $HN(SiMe_2Ph)(SiMe_3)$ as the only soluble products evidenced by ^{1}H NMR spectroscopy.

7.2.21 Hydrolysis of P synthesised at 120 °C to form $[(Me_3SiOUO)(OUO)(L)UO_2(\mu\text{-}OH)]_2$

A brown solution of $[UO_2(py)(H_2L)]$ (211 mg, 0.210 mmol) and $[UO_2\{N(SiMe_3)_2\}_2(py)_2]$ (235 mg, 0.315 mmol, 1.5 equiv) in pyridine (5 mL) was heated at 120 °C in a for 12 h in a Teflon-tapped ampoule resulting in the formation of a brown solution containing $[(Me_3SiOUO)_2(L)]$, as evidenced by NMR spectroscopy, and **P**. The volatiles were evaporated under vacuum and the residue suspended in THF (5 mL) which was later found to contain traces of water. The mixture was then left to stand for one week resulting in the partial dissolution of the insoluble materials and the precipitation of single crystals of the dimeric product $[(Me_3SiOUO)(OUO)(L)UO_2(\mu\text{-}OH)]_2$ suitable for X-ray diffraction.

7.2.22 Conversion of P* (made at 120 °C) to a mixture of $[(Me_3SiOUO)_2(L)]$ and $[(PhMe_2SiO)(U_2O_2)(OSiMe_3)(L)]$

To a Teflon-valved valve NMR tube containing a brown suspension of **P*** (10 mg) in d_5-pyridine (0.6 mL) was added excess trimethylsilyl chloride (drops) resulting in the dissolution of some of the solids and the formation of $[(Me_3SiOUO)_2(L)]$ and the asymmetrically-silylated compound $[(PhMe_2SiO)(U_2O_2)(OSiMe_3)(L)]$ in a 3:1 ratio as evidenced by NMR spectroscopy.

7.2.23 Oxidation of P to form $[\{(UO_2)_2(\mu\text{-}O)(L)\}(UO_2)]$

A brown solution of $[UO_2(py)(H_2L)]$ (110 mg, 0.109 mmol) and $[UO_2\{N(SiMe_3)_2\}_2(py)_2]$ (123 mg, 0.164 mmol, 1.5 equiv) in pyridine (5 mL) was heated at 70 °C in a for 4 d in a Teflon-tapped ampoule resulting in the formation of a brown suspension of **P**. The mixture was then transferred to a Schleck tube and left for one month over which air accidentally entered the vessel resulting in the precipitation of several brown crystals of $[\{(UO_2)_2(\mu\text{-}O)(L)\}(UO_2)]$ at the solvent/air interface.

7.2.24 Reactions of P with oxidants

Complex **P** shows no reactivity with $[Cp_2Fe][OTf]$, $[Ce(OTf)_4]$, trityl chloride, iodine or $[AgBPh_4]$ under analogous conditions to those employed in the reactions in section 7.2.5. For the reaction of P with O_2 see section 7.4.3b.

7.2.25 Synthesis of $[(Me_3SiOUO)_2(L)]$ in the presence of dihydroanthracene

H_4L (10 mg, 0.015 mmol), $[UO_2\{N(SiMe_3)_2\}_2(py)_2]$ (28 mg, 0.038 mmol) and DHA (27 mg, 0.15 mmol) were dissolved in d_5-pyridine (0.7 mL) and the resulting brown solution

heated at 120 °C in a Teflon-valved valve NMR tube for 12 h. Over the reaction period H_4L and $[UO_2\{N(SiMe_3)_2\}_2(py)_2]$ were completely consumed resulting in the formation of $[(Me_3SiOUO)_2(L)]$ (0.009 mmol), $HN(SiMe_3)_2$ (0.058 mmol), anthracene (0.004 mmol) and DHA (0.146 mmol) by ^1H NMR spectroscopy (calibrated against 1eq $^tBuC_6H_3$ (4 mg, 0.015 mmol). New resonances in the ^1H NMR (d_5-pyridine): δ_H 8.52 (s, anthracene), 8.09 (m, anthracene), 7.50 (m, anthracene), 0.18 (s, $HN(SiMe_3)_2$).

7.2.26 Synthesis of P in the presence of dihydroanthracene

$[UO_2(py)(H_2L)]$ (10 mg, 0.010 mmol), $[UO_2\{N(SiMe_3)_2\}_2(py)_2]$ (11 mg, 0.015 mmol, 1.5 equiv) and DHA (18 mg, 0.099 mmol, 10 equiv) were dissolved in d_5-pyridine and the resulting brown solution heated at 80 °C in a Teflon-valved NMR tube for 12 h. Over the reaction period $[UO_2(py)(H_2L)]$ and $[UO_2\{N(SiMe_3)_2\}_2(py)_2]$ were completely consumed resulting in the formation of **P** and $HN(SiMe_3)_2$ only by ^1H NMR spectroscopy. No consumption of DHA was observed. Addition of excess trimethylsilylchloride (one drop) resulted in the additional formation of $[(Me_3SiOUO)_2(L)]$ by ^1H NMR spectroscopy.

7.2.27 Thermal decomposition of $[UO_2\{N(SiMe_3)_2\}_2(py)_2]$

a. *At 50 °C.* A solution of $[UO_2\{N(SiMe_3)_2\}_2(py)_2]$ (25 mg, 0.033 mmol) and 1,3,5-*tris*-tert-butylbenzene (8 mg, 0.033 mmol) d_5-pyridine (0.6 mL) was heated at 50 °C in a Teflon-valved valve NMR tube for 24 h resulting in a 0.2 equivalents of $[UO_2\{N(SiMe_3)_2\}_2(py)_2]$ being converted to 0.4 equivalents of $HN(SiMe_3)_2$ over the reaction period (20 % decomposition) as evidenced by ^1H NMR spectroscopy. Trace amounts of dark precipitate were also formed.

b. *At 70 °C.* A solution of $[UO_2\{N(SiMe_3)_2\}_2(py)_2]$ (25 mg, 0.033 mmol) and 1,3,5-*tris*-tert-butylbenzene (8 mg, 0.033 mmol) d_5-pyridine (0.6 mL) was heated at 70 °C in a Teflon-valved valve NMR tube for 24 h resulting in a 20 % decomposition of $[UO_2\{N(SiMe_3)_2\}_2(py)_2]$ to $HN(SiMe_3)_2$ as evidenced by ^1H NMR spectroscopy. Trace amounts of dark precipitate were also formed.

c. *At 90 °C.* A solution of $[UO_2\{N(SiMe_3)_2\}_2(py)_2]$ (25 mg, 0.033 mmol) and 1,3,5-*tris*-tert-butylbenzene (8 mg, 0.033 mmol) d_5-pyridine (0.6 mL) was heated at 90 °C in a Teflon-valved valve NMR tube for 24 h resulting in a 64 % decomposition of $[UO_2\{N(SiMe_3)_2\}_2(py)_2]$ to $HN(SiMe_3)_2$ as evidenced by ^1H NMR spectroscopy. A significant amount of dark precipitate was also formed.

d. *At 120 °C.* A solution of $[UO_2\{N(SiMe_3)_2\}_2(py)_2]$ (25 mg, 0.013 mmol) and 1,3,5-*tris*-tert-butylbenzene (3 mg, 0.013 mmol) d_5-pyridine (0.6 mL) was heated at 120 °C in a

Teflon-valved valve NMR tube for 12 h resulting in the formation of a brown precipitate. Complete decomposition of $[UO_2\{N(SiMe_3)_2\}_2(py)_2]$ to 2 equivalents of $HN(SiMe_3)_2$ was observed by ^{1}H NMR spectroscopy.

e. *At 120 °C in the presence of DHA.* A solution of $[UO_2\{N(SiMe_3)_2\}_2(py)_2]$ (10 mg, 0.013 mmol), 1,3,5-*tris*-tert-butylbenzene (8 mg, 0.033 mmol) and dihydroanthracene (2 mg, 0.013 mmol) d_5-pyridine (0.6 mL) was heated at 120 °C in a Teflon-valved valve NMR tube for 12 h resulting in the formation of a brown precipitate, $HN(SiMe_3)_2$ (2 equiv) and anthracene (0.34 equiv) as evidenced by ^{1}H NMR spectroscopy. ^{1}H NMR (C_5D_5N): δ_H 8.52 (s, 0.61H, anthracene, 0.34 equiv), 8.09 (m, 1.36H, anthracene, 0.34 equiv), 7.51 (m, 1.36H, anthracene, 0.34 equiv), 7.36-7.17 (m, DHA and C_5D_5N), 3.85 (s, 2.62 H, DHA, 0.66 equiv), 1.65–1.30 (bs, 2H, *H*N(SiMe$_3$), 2 equiv), 0.18 (s, 36H, HN(Si*Me*$_3$), 2 equiv).

7.2.28 Attempted syntheses of $[UO_2(HNDipp)_2(THF)_x]$

a. *By salt elimination at room temperature*. To a yellow suspension of $[UO_2Cl_2(THF)_2]$ (150 mg, 0.310 mmol) in THF (0.5 ml) was added a colourless solution of KNH(Dipp) (Dipp = 2.6-diisopropylphenyl) (130 mg, 0.610 mmol, 2 equiv) in THF (0.5 ml) resulting in the instant formation of a brown solution and an intractable brown solid. The volatiles were then evaporated under vacuum forming a brown residue which could not be analysed by ^{1}H NMR spectroscopy.

b. *By salt elimination at 0 °C.* To a yellow suspension of $[UO_2Cl_2(THF)_2]$ (100 mg, 0.210 mmol) in THF (0.5 ml) at 0 °C was added a colourless solution of $KNH(Dipp)_2$ (Dipp = 2.6-diisopropylphenyl) (130 mg, 0.610 mmol, 2 equiv) in THF (0.5 ml) at 0 °C resulting in the instant formation of a brown solution and an intractable solid as in **a**.

7.2.29 Attempted syntheses of $[UO_2(HNDipp)_2(py)_x]$

a. *By salt elimination.* Performing the above syntheses (7.2.28a, b) in pyridine also resulted in reactant decomposition.

b. *By transamination.* To an orange solution of $[UO_2\{N(SiMe_3)\}_2(py)_2]$ (10 mg, 0.013 mmol) in d_5-pyridine (0.4 ml) in a Teflon-valved valve NMR tube was added a colourless solution of H_2NDipp (5 mg, 0.027 mmol, 2 equiv) resulting in the formation of a brown solution and an intractable brown solid. $HN(SiMe_3)_2$ and H_2NDipp were the only products obervable by ^{1}H NMR spectroscopy.

7.2.30 Attempted synthesis of $[UO_2(imidazolide)_2(py)_2]$

To a yellow suspension of $[UO_2Cl_2(THF)_2]$ (10 mg, 0.02 mmol) in d_5-pyridine (0.6 ml) in a Teflon-valved valve NMR tube was added solid potassium imidazolide (4 mg, 0.04 mmol, 2 equiv) and the mixture heated for 12 h at 120 °C after which neither starting material had dissolved.

7.2.31 Attempted synthesis of $[UO_2(TMP)_2(py)_x]$

To a yellow suspension of $[UO_2Cl_2(THF)_2]$ (20 mg, 0.04 mmol) in C_6D_6 (0.5 ml) in a Teflon-valved valve NMR tube was added a suspension of potassium 2,2,6,6-tetramethylpiperidide, K(TMP), (15 mg, 0.08 mmol, 2 equiv) in C_6D_6 (0.5 mL) and the mixture shaken for 1 min resulting in the formation of an intractable brown solid and a brown solution of HTMP as observed by ^{1}H NMR spectroscopy.

7.2.32 Attempted synthesis of $[UO_2\{N(^iPr)_2\}_2(THF)_x]$

To a yellow suspension of $[UO_2Cl_2(THF)_2]$ (15 mg, 0.031 mmol) in THF (0.4 ml) in a Teflon-valved valve NMR tube was added a colourless solution of lithium isopropylamide (7 mg, 0.062 mmol, 2 equiv) in C_6D_6 (0.2 mL) and the mixture shaken for 1 min resulting in the formation of an intractable brown solid and a brown solution of $HN(^iPr)_2$ as observed by 1H NMR spectroscopy. NB: An analogous synthesis of $[UO_2\{N(^iPr)_2\}_2(py)_2]$ was not attempted due the facile metallation of pyridine by LDA, evidenced by the formation of dark brown solutions containing $HN(^iPr)_2$ upon its dissolution in the solvent.

7.2.33 Attempted synthesis of $[UO_2\{CH(SiMe_3)_2\}_2(THF)_2]$

To a yellow suspension of $[UO_2Cl_2(THF)_2]$ (10 mg, 0.021 mmol) in C_6D_6 (0.4 ml) in a Teflon-valved valve NMR tube was added a solution of $LiCH(SiMe_3)_2$](7 mg, 0.041 mmol, 2 equiv) in C_6D_6 (0.2 mL) and the mixture shaken for 1 min resulting in the formation of an intractable brown solid and a brown solution of $H_2C(SiMe_3)_2$ as observed by ^{1}H NMR spectroscopy.

7.2.34 Synthesis of $[UO_2(NPh_2)_2(py)_x]$

To an orange solution of $[UO_2\{N(SiMe_3)\}_2(py)_2]$ (10 mg, 0.013 mmol) in d_5-pyridine (0.4 ml) in a Teflon-valved valve NMR tube was added a colourless solution of diphenylamine ($HNPh_2$) (5 mg, 0.027 mmol, 2 equiv) resulting in the formation of a brown solution of $[UO_2(NPh_2)_2(py)_x]$, and $HN(SiMe_3)_2$ by ^{1}H NMR spectroscopy. ^{1}H NMR (d_5-pyridine): δ_H 7.39 (t, J = 7 Hz, 8H, aryl), 6.93 (d, J = 7 Hz, 8H, aryl), 7.39 (t, J = 7 Hz, 4H, aryl), 0.16 (s, 36H, $HN(Si\mathit{Me}_3)_2$, 2 equiv).

7.2.35 Reaction of $[UO_2(NPh_2)_2(py)_x]$ with H_4L

To a freshly prepared brown solution of $[UO_2(NPh_2)_2(py)_x]$, (0.013 mmol) and $HN(SiMe_3)_2$ (0.026 mmol, 2 equiv) in d_5-pyridine (0.6 ml) in a Teflon-valved valve NMR tube was added a yellow solution of H_4L (98 mg, 0.013 mmol) in d_5-pyridine (0.3 ml) and the mixture left for 10 min. The resulting brown solution was then analysed by ^1H NMR spectroscopy and found to contain H_4L, $[UO_2(py)(H_2L)]$, $HNPh_2$, and $HN(SiMe_3)_2$ in 0.33:0.66:2:2 ratios respectively. The solution was then heated at 60 °C for 6 h resulting in no further reaction before being heated at 90 °C for 12 h resulting in the decomposition of the remaining $[UO_2(NPh_2)_2(py)_x]$ to form a further two equivalents of $HNPh_2$. No consumption of $[UO_2(py)(H_2L)]$ observed. Characterisation data for $HNPh_2$: ^1H NMR (C_5D_5N): δ_H 8.86 (bs, 2H, NH, 2 equiv) 7.33 (m, 16H, CH, 2 equiv), 6.94 (t, J = 2 Hz, 4H, CH, 2 equiv).

7.2.36 Synthesis of $[UO_2(NC_4H_4)_2(py)_x]$

a *NMR scale*. To a Teflon-valved valve NMR tube containing an orange solution of $[UO_2\{N(SiMe_3)\}_2(py)_2]$ (10 mg, 0.013 mmol) in d_5-pyridine (0.4 ml) was added a colourless solution of pyrrole (2 mg, 0.027 mmol, 2 equiv) resulting in the formation of a dark red brown solution of $[UO_2(NC_4H_4)_2(py)_x]$ and $HN(SiMe_3)$ (2 equiv) by ^1H NMR spectroscopy. ^1H NMR (d_5-pyridine): δ_H 8.17 (t, 4H, J = 2 Hz, pyrrolide), 6.34 (t, 4H, J = 2 Hz, pyrrolide), 0.18 (s, 36H, HN(Si*Me*$_3$), 2 equiv).

b *Attempted preparative scale*. To an orange solution of $[UO_2\{N(SiMe_3)\}_2(py)_2]$ (119 mg, 0.159 mmol) in pyridine (2 ml) at 0 °C was added a colourless solution of pyrrole (24 mg, 0.319 mmol, 2 equiv) 0 °C resulting in the formation of a dark red brown solution which was warmed to room temperature over 2 h. Removal of the volatiles under vacuum produced a dark brown, pyridine-intractable residue which was discarded.

7.2.37 Reactions of $[UO_2(NC_4H_4)_2(py)_x]$ with H_4L

NMR scale. To a Teflon-valved valve NMR tube containing a freshly-prepared red solution of $[UO_2(NC_4H_4)_2(py)_x]$ (0.053 mmol, 2 equiv) and $HN(SiMe_3)_2$ (0.126 mmol, 4 equiv) in d_5-pyridine (0.7 ml) was added a yellow solution of H_4L (18 mg, 0.027 mmol) in d_5-pyridine (0.3 ml) and the mixture left for 10 min. The resulting brown solution was then analysed by ^1H NMR spectroscopy and found to contain $[UO_2(py)(H_2L)]$, pyrrole, $[UO_2(NC_4H_4)_2(py)_x]$ and $HN(SiMe_3)_2$ in 1:2:1:2 ratios respectively. The solution was then heated at 60 °C for 6 h, causing no further reaction, before being heated at 90 °C for 12 h resulting in the decomposition of the remaining $[UO_2(NC_4H_4)_2(py)_x]$ to form a further two

equivalents of pyrrole. No consumption of $[UO_2(py)(H_2L)]$ was observed. Characterisation data for pyrrole: ^{1}H NMR (C_5D_5N): δ_H 11.66 (bs, 2H, NH, 2 equiv) 7.12 (t, J = 2 Hz, 4H, CH, 2 equiv), 6.34 (t, J = 2 Hz, 4H, CH, 2 equiv).

7.3 Synthetic procedures described in Chapter Three

7.3.1 Synthesis of $[K(THF)_x][(Me_3SiOUO)_2(L)]$

a. *By reduction of $[(Me_3SiOUO)_2(L)]$ with KC_8.* To a Teflon-valved valve NMR tube containing a brown solution of $[(Me_3SiOUO)_2(L)]$ (20 mg, 0.015 mmol) in THF (0.3 mL) was added a suspension of KC_8 (2 mg, 0.015 mmol, 1 equiv) in C_6D_6 (0.3 mL) and the mixture shaken for 1 min resulting in the formation a brown solution and a graphite precipitate. $[K(THF)_x][(Me_3SiOUO)_2(L)]$ was the only observable product by ^{1}H NMR spectroscopy after the reaction period. The species is stable in solution indefinitely under a N_2 atmosphere but all attempts to isolate solid material resulted in formation of the hydrolysed product $[K(THF)_2][(Me_3SiO)U(\mu\text{-}OH)(OUO)(L)]$. ^{1}H NMR (1:1 C_6D_6:THF): δ_H 30.98 (s, 18H, $SiMe_3$), 10.75 (s, 6H, *meso*-methyl), 6.41 (s, 4H, pyrrole), 4.09 (s, 4H, pyrrole), 0.32 (s, 4H, imine), −7.57 (s, 12H, aryl-methyl), −15.66 (s, 4H, aryl), −16.00 (s, 6H, *meso*-methyl). Vis/NIR (THF, 6.2×10^{-3} M): 924 nm (ε = 56 L mol^{-1} cm^{-1}), 1023 nm (ε = 84 L mol^{-1} cm^{-1}), 1161 nm (ε = 51.0 L mol^{-1} cm^{-1}), 1220 nm (ε = 65.0 L mol^{-1} cm^{-1}), 1382 nm (ε = 46.0 L mol^{-1} cm^{-1}), 1676 nm (ε = 61.0 L mol^{-1} cm^{-1}). Solubilty: THF and benzene.

b. *By reduction of $[(Me_3SiOUO)_2(L)]$ with potassium metal.* To a Teflon-valved valve NMR tube containing a brown solution of $[(Me_3SiOUO)_2(L)]$ (34 mg, 0.025 mmol) in 1:1 THF/C_6D_6 (0.5 mL) was added potassium metal (1 mg, 0.025 mmol, 1 equiv) and the mixture heated to 80 °C for 3 h until all the potassium was consumed forming a brown solution of $[K(THF)_x][(Me_3SiOUO)_2(L)]$ only.

c. *By oxidation of $[K(THF)_x]_2[(Me_3SiOUO)_2(L)]$ with iodine.* To a freshly prepared red-brown solution of $[K(THF)_x]_2[(Me_3SiOUO)_2(L)]$ (0.074 mmol) in THF (0.3 mL) in a Teflon-valved valve NMR tube was added a solution of iodine (1 mg, 0.037 mmol) in C_6D_6 (0.3 mL) and the mixture shaken for 1 min resulting in the formation of a brown solution of $[K(THF)_x][(Me_3SiOUO)_2(L)]$ and a white potassium iodide precipitate.

7.3.2 Synthesis of $[K(18\text{-crown-}6)(THF)_2][(Me_3SiOUO)_2(L)]$

A brown solution of $[(Me_3SiOUO)_2(L)]$ (180 mg, 0.134 mmol) in THF (2 mL) was added to stirred KC_8 (18 mg, 0.134 mmol, 1 equiv) resulting in the formation a brown solution of $[K(THF)_x][(Me_3SiOUO)_2(L)]$ and a graphite precipitate after 5 min. The mixture was left to stand for a further 5 min before the supernatant was decanted off and layered over

a solution of 18-crown-6 (35 mg, 0.134 mmol) in benzene (2 mL). Deposition of brown crystals of $[K(18\text{-crown-6})(THF)_2][(Me_3SiOUO)_2(L)]$ occurred after 2 h, some of which were suitable for single crystal X-ray diffraction. These were isolated by filtration, dried under vacuum for 30 min at 100 °C and stored in the glovebox. The filtrate was reduced in volume to 1 mL under vacuum to yield a second batch of material which was isolated in the same manner. $[K(18\text{-crown-6})(THF)_2][(Me_3SiOUO)_2(L)]$ was collected as a brown crystalline solid (190 mg from two batches, 0.106 mmol, 79 %). ^{1}H NMR (1:1 C_6D_6:THF): δ_H 31.25 (s, 18H, $SiMe_3$), 11.43 (s, 6H, *meso*-methyl), 6.56 (s, 4H, pyrrole), 4.04 (s, 4H, pyrrole), 1.40 (s, 18-crown-6, partially hidden by THF resonance) 0.66 (s, 4H, imine), −7.78 (s, 12H, aryl-methyl), –15.39 (s, 4H, aryl), −16.11 (s, 6H, *meso*-methyl). Analysis. Found: C, 46.85; H, 5.24; N, 6.50. $C_{68}H_{98}KN_8O_{12}Si_2U_2(C_4H_8O)$ requires: C, 46.69; H, 5.85; N, 5.97%. FTIR (nujol, cm^{-1}): 1595 (s, L), 1574 (s, L), 1507 (m) 1399 (w), 1351 (s), 1290 (s, L), 1276 (s, L) 1218 (m, L), 1189 (m, L), 1107 (s, O-Si), 1046 (s, L), 1018 (s, L), 963 (m, L), 928 (s), 899 (s), 836 (s), 788 (w, L), 764 (m), 727 (m, L), 646 (s), 599 (w), 585 (w), 566 (w), 517 (s), 507 (s). L = stretches attributed to the Pacman ligand. SQUID: see Chapter Three, section 3.2.2. Solubility: THF (partial)

7.3.3 Synthesis of $[K(py)_x][(Me_3SiOUO)_2(L)]$

To a brown solution of $[(Me_3SiOUO)_2(L)]$ (34 mg, 0.025 mmol) in d_5-pyridine (0.4 ml) was added potassium metal (1 mg, 0.025 mmol, 1 equiv) and the mixture heated to 80 °C in a Teflon-valved valve NMR tube for 3 h until all the potassium was consumed forming a brown solution of $[K(py)_x][(Me_3SiOUO)_2(L)]$ only. ^{1}H NMR (d_5-pyridine): δ_H 30.61 (s, 18H, $SiMe_3$), 11.59 (s, 6H, *meso*-methyl), 7.28 (s, 4H, pyrrole), 2.12 (s, 6H, *meso*-methyl), 1.06 (s, 4H, pyrrole), −7.07 (s, 12H, aryl-methyl), −14.31 (s, 4H, imine), −15.34 (s, 4H, aryl).

7.3.4 Synthesis of $[C_5H_5NH][(Me_3SiOUO)_2(L)]$

To a freshly-prepared, brown solution of $[K(py)_x][(Me_3SiOUO)_2(L)]$ (0.050 mmol) in d_5-pyridine (0.4 ml) in a Teflon-valved valve NMR tube was added a solution of pyridinium chloride (5.8 mg, 0.050 mmol) in d_5-pyridine (0.3 mL) and the solution vigorously shaken for 2 min resulting in the precipitation of red/brown solids and the formation of a pale yellow solution which was found to contain no resonances by ^{1}H NMR spectroscopy. Heating the resulting suspension at 120 °C for 2 min resulted in the dissolution of all solids to form a red solution. This was allowed to cool to room temperature slowly over 2 h resulting in the precipitation of red crystals which were isolated by filtration and dried under vacuum for 1 h. Single crystals suitable for X-ray diffraction were isolated from

the mixture prior to isolation of the bulk product. $[C_5H_5NH][(Me_3SiOUO)_2(L)]$ was isolated as a red crystalline solid (60 mg, 0.042 mmol, 84 %). ^{1}H NMR (d_5-pyridine): δ_H 31.78 (s, 18H, $SiMe_3$), 15.76 (s, 6H, *meso*-methyl), 5.08 (s, 4H, pyrrole), −0.06 (s, 6H, *meso*-methyl), −1.44 (s, 4H, pyrrole), −6.81 (s, 12H, aryl-methyl), −13.80 (s, 4H, imine), −16.73 (s, 4H, aryl). Resonances attributable to pyridinium not observed due to exchange with the solvent medium. Analysis. Found: C, 44.58; H, 4.43; N, 8.89. $C_{53}H_{64}N_9O_4Si_2U_2$ requires: C, 44.72; H, 4.53; N, 8.86 %. FTIR (nujol, cm^{-1}): 1588 (s, L), 1565 (s, L), 1505 (m) 1396 (w), 1280 (s, L), 1264 (s, L) 1186 (m, L), 1046 (s, L), 1014 (s, L), 1004 (s), 980 (m,), 904 (m), 893 (m), 872 (w), 858 (m), 835 (s) 786 (m, L), 764 (m), 727 (m, L), 688 (w) 626 (s) 595 (w), 581 (w), 565 (w), 514 (s), 500 (s). L = stretches attributed to the Pacman ligand. Solubility: boiling pyridine.

7.3.5 Synthesis of $[K(THF)_2][(Me_3SiO)U(\mu\text{-}OH)(OUO)(L)]$

a. *By hydrolysis of $[K(THF)_x][(Me_3SiOUO)_2(L)]$*. A brown solution of $[(Me_3SiOUO)_2(L)]$ (100 mg, 0.074 mmol) in THF (2 mL) was added to KC_8 (10 mg, 0.074 mmol, 1 equiv) and the mixture stirred for 5 min resulting in the formation a brown solution of $[K(THF)_x][(Me_3SiOUO)_2(L)]$) and a graphite precipitate. Water (one drop, approximately 50 µL, 3 mmol) was then added by gas-tight syringe resulting in an immediate colour change from brown to orange. The mixture was then filtered, the filtrate evaporated to dryness under vacuum, and the resulting orange residue suspended in toluene (3 mL) before the mixture was heated to boiling, resulting in the complete dissolution of all solids. Slow cooling of the resulting red solution to room temperature over 12 h caused orange microcrystalline solids to precipitate which were isolated by filtration and dried under vacuum at 100 °C for 2 h. $[K(THF)_2][(Me_3SiO)U(\mu\text{-}OH)(OUO)(L)]$ was isolated as an orange solid (45 mg, 0.033 mmol, 44 %). Crystals suitable for single crystal X-ray diffraction were grown from slow diffusion of hexanes into a 1:1 THF/C_6D_6 solution. Slow evaporation of a similar THF/C_6D_6 solution yielded crystals of an alternative dimeric polymorph. ^{1}H NMR (1:1 C_6D_6:THF): δ_H 55.15 (s, 9H, $SiMe_3$), 30.49 (s, 3H, *meso*-methyl), 19.76 (s, 2H), 15.79 (s, 3H, *meso*-methyl) 12.00 (s, 2H), −1.56 (s, 2H), −4.39 (s, 3H, *meso*-methyl), −5.37 (s, 6H, aryl-methyl), −10.34 (s, 6H, aryl-methyl), −12.79 (s, 2H), −13.47 (s, 2H), −16.15 (s, 2H) −16.26 (s, 3H, *meso*-methyl), −19.08 (s, 2H), −37.73 (s, 2H). Resonances with 2H integrations: imine, α-pyrrole, β-pyrrole and aryl. Analysis. Found: C, 44.20; H, 4.76; N, 7.18. $C_{53}H_{66}KN_8O_6SiU_2$ requires: C, 43.77; H, 4.57; N, 7.70 %. FTIR (nujol, cm^{-1}): 3643 (w, OH), 1592 (s, L), 1575 (s, L), 1510 (w), 1288 (s, L), 1276 (s, L), 1219 (w, L), 1183 (m, L), 1090 (m, Si-O), 1048 (s, L), 1018 (m, L), 964 (w ,L), 920 (s), 896 (m), 842 (m, O=U assymetric stretch), 794 (m), 780

(m, L) 724 (w, L), 624 (w), 593 (m). Vis/NIR (THF, 8.8×10^{-3} M): 634 nm (ε = 73 L mol^{-1} cm^{-1}), 1013 nm (ε = 83 L mol^{-1} cm^{-1}), 1197 nm (ε = 70 L mol^{-1} cm^{-1}), 1340 nm (ε = 46 L mol^{-1} cm^{-1}), 1401 nm (ε = 61 L mol^{-1} cm^{-1}), 1472 nm (ε = 37 L mol^{-1} cm^{-1}), 1683 (ε = 41 L mol^{-1} cm^{-1}). Solubility: THF, toluene and benzene (partial).

b. *By desilylation of [C_5H_5NH][($Me_3SiOUO)_2$(L)]*. To a red suspension of [C_5H_5NH][($Me_3SiOUO)_2$(L)] (44 mg, 0.031 mmol) in d_5-pyridine (0.7 mL) in a Teflon-valved valve NMR tube was added solid KOH (1 mg, 0.031 mmol) and the mixture left for 12 h resulting in the dissolution of all reagents and the formation of a red solution of [$K(THF)_x$][($Me_3SiOUO)_2$(L)] and one equivalent of Me_3SiOH as the only products visible by ^{1}H NMR spectroscopy.

c. *By the KOH-induced disproportionation of [($Me_3SiOUO)_2$(L)]*. To a brown solution of [($Me_3SiOUO)_2$(L)] (24 mg, 0.017 mmol) in d_8-THF (0.6 mL) in a Teflon-valved valve NMR tube was added solid KOH (1 mg, 0.017 mmol, 1 equiv) and the mixture shaken for 5 min resulting in the dissolution of all the KOH and the formation of a red solution which was found to contain [$K(THF)_2$][(Me_3SiO)U(μ-OH)(OUO)(L)] and [$K(THF)_x$[($UO_2)_2$(μ-OH)(L)] in a 2:1 ratio by ^{1}H NMR spectroscopy.

7.3.6 Synthesis of [K(18-crown-6)][(Me_3SiO)U(*μ*-OH)(OUO)(L)]

a. *By hydrolysis of [K(18-crown-6)][(Me3SiO)U(μ-OH)(OUO)(L)]*. To a brown slurry of [K(18-crown-6)][(Me_3SiO)U(μ-OH)(OUO)(L)] (50 mg, 0.028 mmol) in THF (1 mL) was added H_2O (one drop, approximately 50 μL, 3 mmol) resulting in complete dissolution of all solids to form an orange solution. The solvent was evaporated under vacuum and the remaining orange residue dried under vacuum at 100 °C for 1 h. The residue was dissolved in 1:1 THF:C_6D_6 (0.6 mL) and hexanes were allowed to slowly diffuse into the solution over one week, after which crystals suitable for X-ray diffraction were obtained. The filtrate was decanted off and the material dried under vacuum for 1 h. [K(18-crown-6)$(THF)_2$][(Me_3SiO)U(μ-OH)(OUO)(L)] was collected as a red crystalline solid (27 mg, 0017 mmol, 61 %). ^{1}H NMR (1:1 C_6D_6:THF): δ_H 55.09 (s, 9H, $SiMe_3$), 35.64 (s, 3H, *meso*-methyl), 19.91 (s, 2H), 14.41 (s, 3H, *meso*-methyl) 11.05 (s, 2H), −1.96 (s, 2H), −5.53 (s, 6H, aryl-methyl), −5.66 (s, 3H, *meso*-methyl), −9.80 (s, 6H, aryl-methyl), −12.97 (s, 2H), −14.22 (s, 2H), −16.25 (s, 2H) −16.56 (s, 3H, *meso*-methyl), −17.38 (s, 2H), −38.12 (s, 2H). Resonances with 2H integrations: imine, α-pyrrole, β-pyrrole and aryl. Analysis. Found: C, 42.48; H, 4.49; N, 6.48. $C_{57}H_{74}KN_8O_{10}SiU_2$ requires: C, 43.48; H, 4.74; N, 7.12 %. FTIR (nujol, cm^{-1}): 3645 (w, OH), 1590 (s, L), 1567 (s, L), 1503 (w), 1351 (m), 1286 (s, L), 1242

(m, L), 1217 (w, L), 1186 (m, L), 1108 (s, Si-O), 1046 (s, L), 1018 (m, L), 960 (m ,L), 926 (s), 897 (m), 833 (m, O=U assymetric stretch), 786 (m), 765 (m, L) 723 (m, L), 594 (m), 503 (m). SQUID: see Chapter Three, section 3.3.1. Solubility: THF, toluene and benzene (partial).

b. *By KF/H_2O-induced disproportionation of [$(Me_3SiOUO)_2$(L)] in the presence of 18-crown-6.* To brown solution of [$(Me_3SiOUO)_2$(L)] (20 mg, 0.015 mmol) in a 1:1 C_6D_6/THF mixture (0.6 mL) in a Teflon-valved valve NMR tube was added an excess of solid KF (5 mg, 0.086, mmol), which had been dried at 120 °C for 12 h at 10^{-1} Torr, and 18-crown-6 (10 mg, 0.038 mmol). No reaction was observed at room temperature. The mixture was then boiled at 80 °C for 4 d resulting in the formation of [K(18-crown-6)$(THF)_2$][(Me_3SiO)U(μ-OH)(OUO)(L)] and [K$(THF)_x$[$(UO_2)_2$(X)(L)] (X = OH or F) by ^{1}H NMR spectroscopy. Single crystals of the product suitable for X-ray crystallography were grown by slow diffusion of hexanes into the crude mixture. NB: Performing the same reaction in the absence of 18-crown-6 in d_5-pyrdine produced the analogous pyridine solvate as the major product. Performing the reaction with more vigorously dried KF (275 ˚C, 10^{-6} Torr, 6 h) resulted in no reaction even at elevated temperatures. Solubility: THF.

7.3.7 Attempted synthesis of [K$(THF)_x$][(Me_3SiO)U(μ-OR)(OUO)(L)]

a. *From tBuOH, R = tBu.* To a freshly-prepared, brown solution of [K$(THF)_x$][$(Me_3SiOUO)_2$(L)] (0.015 mmol) in 1:1 C_6D_6/THF (0.7 mL) in a Teflon-valved valve NMR tube was added excess *tert*-butanol (approx 10 mg) resulting in the formation of [K$(THF)_2$][(Me_3SiO)U(μ-OH)(OUO)(L)], in addition to other unidentified products, after 4 d.

7.3.8 Attempted synthesis of [K(18-crown-6)][(Me_3SiO)U(μ-OR)(OUO)(L)]

a. *From tBuOH, R = tBu.* To a brown suspension of [K(18-crown-6)][$(Me_3SiOUO)_2$(L)] (20mg, 0.011 mmol) in 1:1 C_6D_6/THF (0.7 mL) in a Teflon-valved valve NMR tube was added excess *tert*-butanol (approx 10 mg) and the mixture heated at 80 ˚C for 24 h. No dissolution of the starting material was observed.

7.3.9 Synthesis of [K$(THF)_x]_2$[$(Me_3SiOUO)_2$(L)]

a. *By reduction of [$(Me_3SiOUO)_2$(L)] with KC_8.* To a brown solution of [$(Me_3SiOUO)_2$(L)] (20 mg, 0.015 mmol) in THF (0.3 mL) in a Teflon-valved valve NMR tube was added a suspension of KC_8 (4 mg, 0.030 mmol, 2 equiv) in C_6D_6 (0.3 mL) and the mixture shaken for 1 min resulting in the formation a red-brown solution and a graphite precipitate. [K$(THF)_x]_2$[$(Me_3SiOUO)_2$(L)] was the only species present in solution after the

reaction period. ^{1}H NMR (1:1 C_6D_6:THF): δ_H 39.59 (s, 18H, $SiMe_3$), 32.57 (s, 6H, *meso*-methyl), 3.38 (s, 4H, partially obscured by THF, pyrrole), 0.79 (s, 6H, *meso*-methyl), −5.38 (s, 4H, pyrrole), −9.43 (s, 12H, aryl-methyl), −22.56 (s, 4H, imine), −33.52 (s, 4H, aryl). Vis/NIR (THF, 6.2×10^{-3} M): 785 nm (ε = 48 L mol^{-1} cm^{-1}), 926 nm (ε = 56 L mol^{-1} cm^{-1}), 1025 nm (ε = 84 L mol^{-1} cm^{-1}), 1164 nm (ε = 50 L mol^{-1} cm^{-1}), 1223 nm (ε = 64 L mol^{-1} cm^{-1}), 1383 nm (ε = 40 L mol^{-1} cm^{-1}), 1455 nm (ε = 31 L mol^{-1} cm^{-1}), 1677 nm (ε = 60 L mol^{-1} cm^{-1}). Solubility: THF, benzene (partial).

***b**: Reduction with potassium metal*.To a brown solution of $[(Me_3SiOUO)_2(L)]$ (34 mg, 0.025 mmol) in 1:1 THF/C_6D_6 (0.5 mL) in a Teflon-valved valve NMR tube was added potassium metal (2 mg, 0.050 mmol, 2 equiv) and C_6D_6 (0.3 mL) and the mixture heated to 80 °C for 12 h after which all the potassium was consumed forming a red/brown solution of $[K(THF)_x]_2[(Me_3SiOUO)_2(L)]$ as evidenced by ^{1}H NMR spectroscopy.

7.3.10 Synthesis of $[K(18\text{-crown-6})(THF)_2]_2[(Me_3SiOUO)_2(L)]$

A brown solution of $[(Me_3SiOUO)_2(L)]$ A (200 mg, 0.149 mmol) in THF (2 mL) was added to KC_8 (47 mg, 0.348 mmol, 2.3 equiv) and the mixture stirred for 5 min resulting in the formation a red-brown solution of $[K(THF)_x]_2[(Me_3SiOUO)_2(L)]$ and a graphite precipitate. The mixture was left to stand for a further 5 min before the supernatant was decanted off and layered over a solution of 18-crown-6 (50 mg, 0.298 mmol) in THF (2 mL). Deposition of $[K(18\text{-crown-6})(THF)_2]_2[(Me_3SiOUO)_2(L)]$ as a brown powder occurred at room temperature after 2 h and was isolated by filtration before being dried under vacuum for 30 min at 100 °C. The filtrate was reduced in volume to 1 mL under vacuum to yield a second batch of material which was isolated in the same manner. $[K(18\text{-crown-6})(THF)_2][(Me_3SiOUO)_2(L)]$ was isolated as a brown crystalline solid (200 mg from two batches, 0.089 mmol, 60 %). ^{1}H NMR (1:1 C_6D_6:THF): δ_H 39.81 (s, 18H, $SiMe_3$), 26.39 (s, 6H, *meso*-methyl), 5.50 (s, 48H, 18-crown-6) 2.58 (s, 4H, pyrrole), 0.65 (s, 6H, *meso*-methyl), −5.21 (s, 4H, pyrrole), −8.68 (s, 12H, aryl-methyl), −12.84 (s, 4H, imine), −32.84 (s, 4H, aryl). FTIR (nujol, cm^{-1}): 1594 (s, L), 1573 (s, L), 1506 (m) 1353 (m), 1290 (s, L), 1280 (s, L) 1221 (w, L), 1190 (m, L), 1107 (s, O-Si), 1046 (s, L), 1018 (m, L), 961 (m, L), 942 (m), 894 (m), 840 (m), 792 (w, L), 763 (w), 724 (m, L), 601 (w), 572 (w), 553 (w). L = stretches attributed to the Pacman ligand. Analysis. Found: C, 47.00; H, 6.23; N, 5.06. $C_{88}H_{138}K_2N_8O_{20}Si_2U_2$ requires: C, 47.22; H, 6.21; N, 5.01 %. Solubility: THF (partial).

7.3.11 Synthesis of $[K(py)_x]_2[(Me_3SiOUO)_2(L)]$

To a solution of $[(Me_3SiOUO)_2(L)]$ (19 mg, 0.014 mmol) in d_5-pyridine (0.4 mL) in a Teflon-valved valve NMR tube was added potassium metal (1 mg, 0.050 mmol, 2 equiv) and the mixture heated to 80 °C for 12 h after which all the potassium was consumed and a red-brown solution of $[K(py)_x]_2[(Me_3SiOUO)_2(L)]$ had formed, as evidenced by ^{1}H NMR spectroscopy. ^{1}H NMR (d_5-pyridine): δ_H 39.12 (s, 18H, $SiMe_3$), 33.18 (s, 6H, *meso*-methyl), 1.83 (s, 4H, pyrrole), 1.21 (s, 6H, *meso*-methyl), −4.91 (s, 4H, pyrrole), −9.21 (s, 12H, aryl-methyl), −21.90 (s, 4H, imine), −32.90 (s, 4H, aryl). Solubility: pyridine.

7.3.12 Synthesis of $[(Me_3SiOUO)_2(L)]$ by oxidation of $[K(THF)_x]_2[(Me_3SiOUO)_2(L)]$

To a freshly prepared red-brown solution of $[K(THF)_x]_2[(Me_3SiOUO)_2(L)]$ (0.074 mmol) in THF (0.3 mL) in a Teflon-valved valve NMR tube was added a solution of iodine (2 mg, 0.074 mmol) in C_6D_6 (0.3 mL) and the mixture shaken for 1 min resulting in the formation of a brown solution of $[(Me_3SiOUO)_2(L)]$ (By ^{1}H NMR spectroscopy) and a grey potassium iodide precipitate.

7.3.13 Synthesis of $[K(THF)_{1.5}]_2[(Me_3SiOUO)(OUO)(L)]$

a. *By oxidation of $[K(THF)_x]_2[(Me_3SiOUO)_2(L)]$ with H_2O.* A brown solution of $[(Me_3SiOUO)_2(L)]$ (100 mg, 0.074 mmol) in THF (2 mL) was added to KC_8 (24 mg, 0.178 mmol, 2.3 equiv) and the mixture stirred for 5 min resulting in the formation a brown solution of $[K(THF)_x]_2[(Me_3SiOUO)_2(L)]$ and a graphite precipitate. The mixture was then filtered into a Teflon-tapped ampoule and the filtrate treated with a H_2O/THF stock solution (0.09 ml, of a 0.405 mmol mL^{-1} stock solution, 0.67 mg, 0.037 mmol, 0.5 equiv of H_2O). The resulting brown solution was stirred for 5 min before boiling for 72 h in the absence of stirring over which red crystals where observed to precipitate and the solution became pale yellow. The product was isolated by filtration and dried under vacuum at 100 °C for 2 h. $[K(THF)_{1.5}]_2[(Me_3SiOUO)(OUO)(L)]$ was collected as a red crystalline solid (60 mg, 0.033 mmol, 52 %). Crystals suitable for single crystal X-ray diffraction were isolated from the reaction vessel immediately prior to product isolation. ^{1}H NMR *(d_5-pyridine)*: δ_H 26.97 (s, 9H, $SiMe_3$), 14.41 (s, 2H), 9.15 (2H, s), 8.66 (3H, *meso*-methyl), 3.67 (12H, m, THF) 3.47 (s, 2H), 1.64 (12H, m, THF) 0.33 (2H, s), −1.53 (2H, s) −4.28 (s, 6H, aryl-methyl), −5.53 (s, 6H, aryl-methyl), −6.68 (s, 2H), −16.26 (s, 2H), −23.61 (s, 2H) Resonances with 2H integrations: imine, α-pyrrole, β-pyrrole and aryl. One *meso*-methyl resonance was obscured by the THF solvent resonance. FTIR (nujol, cm^{-1}): 1586 (s, L), 1570 (s, L), 1280 (s, L) 1217

(w, L), 1188 (m, L), 1048 (m, L), 1013 (m, L), 953 (w, L), 890 (m), 877 (m), 837 (m) 764 (w), 720 (m, L), 595 (w), 572 (w), 525 (m). L = stretches attributed to the Pacman ligand. Analysis. Found: C, 43.69; H, 4.61; N, 7.21. $C_{114}H_{146}K_4N_{16}O_{14}Si_2U_4$ requires: C, 43.76; H, 4.70; N, 7.16 %. Vis/NIR (THF, 5.1×10^{-3} M): 712 nm (ε = 53 L mol^{-1} cm^{-1}), 783 nm (ε = 45 L mol^{-1} cm^{-1}), 852 nm (ε = 34 L mol^{-1} cm^{-1}), 927 nm (ε = 46 L mol^{-1} cm^{-1}), 1016 (ε = 86 L mol^{-1} cm^{-1}), 1167 (ε = 49 L mol^{-1} cm^{-1}), 1197 (ε = 60 L mol^{-1} cm^{-1}) 1300 (ε = 45 L mol^{-1} cm^{-1}) 1382 (ε = 38 L mol^{-1} cm^{-1}), 1410 (ε = 34 L mol^{-1} cm^{-1}). Solubility: hot THF.

b. *By oxidation of [K(THF)$_x$]$_2$[(Me$_3$SiOUO)$_2$(L)] with pyridine-N-oxide.* To a Teflon-tapped ampoule containing a brown solution of [(Me$_3$SiOUO)$_2$(L)] (213 mg, 0.159 mmol) in THF (4 mL) was added potassium (12.4 mg, 0.317 mmol, 2 equiv) and the mixture boiled at 80 °C for 16 h resulting in the formation a brown solution of [K(THF)$_x$]$_2$[(Me$_3$SiOUO)$_2$(L)]. A solution of pyridine-N-oxide (8 mg, 0.079 mmol, 0.5 equiv) in THF (1 mL) was then added and the mixture boiled for a further 36 h during which red crystals where observed to precipitate and the solution became red/brown. The product was isolated by filtration and dried under vacuum at 100 °C for two h (31 mg isolated). Concentration of the filtrate to 2 mL resulted in the precipitation of red solids which were heated back into solution. Slow cooling of the resulting red/brown solution over 24 h resulted in the precipitation of a second batch of material. [K(THF)$_{1.5}$]$_2$[(Me$_3$SiOUO)(OUO)(L)] was collected a red crystalline solid (150 mg, 0.095 mmol, 60 %).

c. *By deprotonation of [K(THF)$_2$][(Me$_3$SiO)U(μ-OH)(OUO)(L)]***.** To a Teflon-tapped ampoule containing a red-brown solution of [K(THF)$_2$][(Me$_3$SiO)U(μ-OH)(OUO)(L)] (51 mg, 0.035 mmol) in THF (4 mL) was added potassium hydride (1.4 mg, 0.035 mmol, 1 equiv) and the mixture left to stand for 4 d, with occasional shaking, resulting in the dissolution of the potassium hydride to form a brown solution. The volatiles were evaporated under vacuum and the resulting red/brown residue suspended in d_5-pyridine and heated to 120 °C resulting in the dissolution of all solids. [K(THF)$_{1.5}$]$_2$[(Me$_3$SiOUO)(OUO)(L)] was the only product observed by ^{1}H NMR spectroscopy.

7.3.14 Attempted synthesis of [K(py)$_x$][(OUO)L(OUOSiMe$_3$)]

To a red-brown suspension of [K(THF)$_{1.5}$]$_2$[(Me$_3$SiOUO)(OUO)(L)] (13 mg, 0.008 mmol) in d_5-pyridine (0.3 mL) in a Teflon-valved valve NMR tube was added a solution of iodine (1 mg, 0.0004 mmol, 0.5 equiv) in d_5-pyrdine (0.3 mL) resulting in the formation of a

red solution containing a 1:1 mixture $\{[K(py)][(OUO)_2(L)][K(py)_3]\}_2$ and $[(Me_3SiOUO)_2(L)]$ after 10 min by ^{1}H NMR spectroscopy.

7.3.15 Synthesis of $[K(THF)][K(C_5H_5NO)][(Me_3SiOUO)(OUO)(L)]$

A Teflon-valved valve NMR tube containing a brown solution of $[(Me_3SiOUO)_2(L)]$ (10 mg, 0.0074 mmol) in THF (0.3 mL) was added to a suspension of KC_8 (2 mg, 0.0171 mmol, 2.3 equiv) in C_6D_6 (0.2 mL) and the mixture shaken for 1 min resulting in the formation a brown solution of $[K(THF)_x]_2[(Me_3SiOUO)_2(L)]$ and a graphite precipitate. The solution was filtered before addition of a solution of pyridine-N-oxide (2 mg, 0.021 mmol, 2.8 equiv) in C_6D_6 (0.1 mL) and the resulting mixture boiled for 24 h during which red crystals of $[K(THF)][K(C_5H_5NO)][(Me_3SiOUO)(OUO)(L)]$ suitable for X-ray diffraction were observed to precipitate and the solution became pale yellow. ^{1}H NMR: Resonances attributable to $(Me_3Si)_2O$ and pyridine-*N*-oxide only. Solubility: Insoluble in THF.

7.3.16 Synthesis of crystals of wheel complex

To a freshly-prepared, red-brown solution of $[K(THF)_x]_2[(Me_3SiOUO)_2(L)]$ (26 mg, 0.015 mmol) in 1:1 C_6D_6:THF (0.6 mL) was added H_2O (one drop, approximately 50 µL, 3 mmol) and the mixture left for one month resulting in the precipitation of red crystals of the supramolecular wheel (5 mg, 0.0038 mol, 25 %) which were found to be suitable for single crystal X-ray diffraction.

7.3.17 Synthesis of $[K(THF)_2]_2[\{(Me_3SiO)U\}_2(\mu\text{-}O)(\mu\text{-}OH)(L)]$

To a brown solution of $[(Me_3SiOUO)_2(L)]$ (100 mg, 0.074 mmol) in THF (3 mL) in a Teflon-tapped ampoule was added K metal (6 mg, 0.149 mmol, 2 equiv) and the mixture boiled for 24 h resulting in the consumption of all potassium and the formation of a red-brown solution of $[K(THF)_x]_2[(Me_3SiOUO)_2(L)]$ as evidenced by ^{1}H NMR spectroscopy. H_2O (2.6 µL, 0.149 mmol, 2 equiv) was then added and the mixture boiled for a further 24 h resulting in the formation of a red solution and a small amount of white precipitate, which was removed by filtration. The supernatant was then reduced in volume to 1 mL under vacuum and left for 6 h resulting in the precipitation of a red/brown solid. The product was isolated by filtration and dried under vacuum for 1 h. $[\{(Me_3SiO)U\}_2(\mu\text{-}O)(\mu\text{-}OH)(L)]$ was collected as a red/brown solid (71 mg, 0.046 mmol, 60 %). ^{1}H NMR (1:1 C_6D_6:THF): δ_H 52.27 (s, 18H, $SiMe_3$), 21.72 (s, 6H, *meso*-methyl), -0.86 (s, 4H), −3.59 (s, 6H, *meso*-methyl), −8.10 (s, 4H), −13.88 (s, 12H, aryl-methyl), , −31.55 (s, 4H), and −41.34 (s, 4H). Resonances with 4H integrations: imine, α-pyrrole, β-pyrrole and aryl. Analysis. Found: C, 43.69; H, 4.61; N, 7.24. $C_{56}H_{75}KN_8O_6Si_2U_2$ requires: C, 44.03; H, 4.95; N, 7.34 %.

7.3.18 Unsuccessful synthesis of wheel molecule by desilylation of $[K(THF)_2][(Me_3SiO)U(\mu\text{-}OH)(OUO)(L)]$

a. *With $KOSiMe_3$*. To a red solution of $[K(THF)_2][(Me_3SiO)U(\mu\text{-}OH)(OUO)(L)]$ (10 mg, 0.006 mmol) in 1:1 C_6D_6:THF (0.6 mL) in Teflon-valved valve NMR tube was added an excess of solid potassium trimethylsilanoate ($KOSiMe_3$) (4 mg, 0.024 mmol, 4 equiv) and the mixture left for 30 min forming a red-brown solution. $[K(py)_x]_2[(OUO)L(OUOSiMe_3)]$, unreacted $[K(THF)_2][(Me_3SiO)U(\mu\text{-}OH)(OUO)(L)]$ and several unidentified products were present in solution by ^{1}H NMR spectroscopy.

b. *With KF*. To a red solution of $[K(THF)_2][(Me3SiO)U(\mu\text{-}OH)(OUO)(L)]$ (10 mg, 0.006 mmol) in 1:1 C_6D_6:THF (0.6 mL) in Teflon-valved valve NMR tube was added an excess of solid KF (1 mg, 0.018 mmol, 3 equiv) and the mixture boiled at 80 °C for 3 d after which there was no evidence of reaction by ^{1}H NMR spectroscopy.

7.3.19 Synthesis of $[\{(KOUO)_2(L)\}_n]$

To a brown solution of $[(Me_3SiOUO)_2(L)]$ (50 mg, 0.037 mmol) in 1:1 THF:C_6D_6 (0.7 mL) in Teflon-valved valve NMR tube was added potassium (3 mg, 0.074 mmol, 2 equiv) and the mixture boiled for 12 h resulting in the dissolution of all potassium metal and the formation of a red-brown solution of $[K(THF)_x]_2[(Me_3SiOUO)_2(L)]$. Exposure of the boiling solution to air resulted in the immediate precipitation of crystals of $[\{(KOUO)_2(L)\}_n]$, which were suitable for single crystal X-ray diffraction, in addition to other intractable brown solids. Solubility: Insoluble in THF.

7.3.20 Unsuccessful syntheses of $[\{(KOUO)_2(L)\}_n]$ by oxidative desilylation

a. *With benzoquinone*. To a freshly-prepared, red-brown solution of $[K(THF)_x]_2[(Me_3SiOUO)_2(L)]$ (0.015 mmol) in 1:1 C_6D_6/THF (0.4 mL) in Teflon-valved valve NMR tube was added a solution of benzoquinone (2 mg, 0.015 mmol, 1 equiv) in C_6D_6 (0.2 mL) forming a number of unidentified products after 24 h by ^{1}H NMR spectroscopy.

b. *With tert-butyl peroxide*. To a freshly-prepared, red-brown solution of $[K(THF)_x]_2[(Me_3SiOUO)_2(L)]$ (0.041 mmol) in 1:1 C_6D_6/THF (0.4 mL) in Teflon-valved valve NMR tube was added a solution of *t*BuO*O*t*Bu (6 mg, 0.041 mmol, 1 equiv) in C_6D_6 (0.3 mL) and the mixture boiled for 2 d at 80 °C resulting in the formation of several unidentified products by ^{1}H NMR spectroscopy.

c. *With TEMPO*. To a freshly-prepared, red-brown solution of $[K(THF)_x]_2[(Me_3SiOUO)_2(L)]$ (0.007 mmol) in 1:1 C_6D_6/THF (0.4 mL) in Teflon-valved

valve NMR tube was added a solution of 2,2-6,6-tetramethyl piperidyl oxide (TEMPO) (2 mg, 0.015 mmol, 2 equiv) in C_6D_6 (0.3 mL) forming a number of unidentified products after 24 h by ^{1}H NMR spectroscopy.

7.3.21 Unsuccessful syntheses of [{(KOUO)$_2$(L)}$_n$] by desilylation

a. *With KOSiMe$_3$*. To a brown solution of [(Me$_3$SiOUO)$_2$(L)] (10 mg, 0.007 mmol) in *d*$_5$-pyridine (0.4 mL) in Teflon-valved valve NMR tube was added a solution of KOSiMe$_3$ (1 mg, 0.007 mmol) forming [K(py)$_x$][(Me$_3$SiOUO)$_2$(L)], in addition to other unidentified products, after 24 h by ^{1}H NMR spectroscopy.

b. *From KF or KOH*. See 7.3.5 and 7.3.6 "Syntheses of [K][(Me$_3$SiO)U(μ-OH)(OUO)(L)]".

7.3.22 Attempted synthesis of [^{n}Bu$_4$N][{(OUO)$_2$(L)}] by desilylation

A brown solution of [(Me$_3$SiOUO)$_2$(L)] (10 mg, 0.007 mmol) in C_6D_6 (0.4 mL) was added to a slurry of [^{n}Bu$_4$][Ph$_3$SiF$_2$] (TBAT) (8 mg, 0.015 mmol) in C_6D_6 (0.2 mL) in a Teflon-valved valve NMR tube resulting in the immediate precipitation of a brown solid. The volatiles were evaporated under vacuum before addition of *d*$_5$-pyridine (0.6 mL) forming a red-brown solution that contained a number of unidentified products by ^{1}H NMR spectroscopy. NB: The same result was achieved by direct mixing of the reagents in *d*$_5$-pyridine.

7.3.23 Attempted syntheses of [(OUO)$_2$(L)] by oxidative desilylation

a. *With benzoquinone*. To a brown solution of [(Me$_3$SiOUO)$_2$(L)] (10 mg, 0.007 mmol) in C_6D_6 (1 mL) in a Teflon-valved valve NMR tube was added benzoquinone (1 mg, 0.007 mmol, 1 equiv) resulting in the formation of a red-brown solution after 24 h containing a number of unidentified products by ^{1}H NMR spectroscopy.

b. *From tBuOOtBu*. To a solution of [(Me$_3$SiOUO)$_2$(L)] (10 mg, 0.007 mmol) in C_6D_6 (1 mL) in a Teflon-valved valve NMR tube was added a solution a *tert*-butyl peroxide (1 mg, 0.007 mmol, 1 equiv) in C_6D_6 and the mixture boiled for 12 h resulting in the formation of a red-brown solution which contained a number of identified products by ^{1}H NMR spectroscopy.

7.3.24 Synthesis of [{K(py)}{(OUO)$_2$(L)}{K(py)$_3$}$_2$]

a. *NMR scale oxidation of [K(THF)$_{1.5}$]$_2$[(Me$_3$SiOUO)(OUO)(L)]*. To a red-brown solution [K(THF)$_{1.5}$]$_2$[(Me$_3$SiOUO)(OUO)(L)] (33 mg, 0.021 mmol) in *d*$_5$-pyridine (0.3 mL) in a Teflon-valved valve NMR tube was added a solution of pyridine-*N*-oxide (1 mg, 0.011

mmol, 0.5 equiv) in d_5-pyrdine (0.3 mL) and the resulting red-brown solution heated at 80 °C for 48 h forming a red solution of [{K(py)}{$(OUO)_2$(L)}{$K(py)_3$}$_2$], THF and 0.5 equivalents of $(Me_3Si)_2O$ as evidenced by ^{1}H NMR spectroscopy. ^{1}H NMR *(d_5*-pyridine): δ_H 11.76 (s, 4H), 8.74* (s, 4H, pyrrole) 5.15 (s, 4H, pyrrole), 4.55 (s, 6H, *meso*-methyl), 3.67 (12H, s, 3 equiv of THF liberated from [(Me_3SiOUO)(OUO)(L)]) 1.61 (12H, s, 3 equiv of THF liberated from [(Me_3SiOUO)(OUO)(L)]) 0.13 (9H, s, 0.5 equiv of $(Me_3Si)_2O$)), −2.92 (s, 12H, aryl-methyl), −3.13 (s, 4H, imine), −10.49 (s, 6H, *meso*-methyl). *Obscured by pyridine solvent and located using a 2D ^{1}H–1H correlation spectrum (COSY).

b. *Preparative scale oxidation of [K(py)$_x$]$_2$[(Me_3SiOUO)$_2$(L)]*. To a brown solution of [(Me_3SiOUO)$_2$(L)] (498 mg, 0.371 mmol) in pyridine (5 mL) in a Teflon-tapped ampoule was added potassium (7 mg, 0.177 mmol, 2 equiv) and the mixture heated at 90 °C for 12 h resulting in the consumption of all metal and the formation of a brown solution of [K(py)$_x$]$_2$[(Me_3SiOUO)$_2$(L)] to which a solution of pyridine-*N*-oxide (9 mg, 0.098 mmol, 1 equiv) in pyridine (1 mL) was added. The mixture was then heated for 6 d at 120 °C resulting in the precipitation of red crystals of [{K(py)}{$(OUO)_2$(L)}{$K(py)_3$}$_2$], several of which were removed from the mixture and found to be suitable for X-ray diffraction. The bulk product was isolated by filtration and the solids dried at 100 °C for 2 h (300 mg). The filtrate was concentrated under vacuum to 1 mL and heated to 120 °C before being allowed to cool slowly to room temperature resulting in the precipitation of a second batch of crystalline material which was isolated in the same manner. [{K(py)}{$(OUO)_2$(L)}{$K(py)_3$}$_2$] was isolated as a red crystalline solid (410 mg, 0.258 mmol, 69 %). ^{1}H NMR *(d_5*-pyridine): δ_H 11.76 (s, 4H, pyrrole), 8.74* (s, 4H, pyrrole) 5.15 (s, 4H, imine), 4.55 (s, 6H, *meso*-methyl), −2.92 (s, 12H, aryl-methyl), −3.13 (s, 4H, aryl), −10.49 (s, 6H, *meso*-methyl). *obscured by pyridine solvent and located by COSY. Analysis. Found: C, 46.78; H, 3.72; N, 10.45. $C_{62}H_{60}N_{12}O_4K_2U_2$ requires: C, 46.79; H, 3.80; N, 10.56.16 %. FTIR (nujol, cm^{-1}): 1598 (s, L), 1575 (s, L), 1508 (w), 1356 (w), 1280 (s, L) 1221 (w, L), 1190 (m, L), 1111 (w), 1046 (m, L), 1017 (m, L), 965 (w, L), 900 (m), 881 (m), 845 (w) 793 (w), 762 (s) 725 (s, L), 707 (s), 571 (s), 554 (s). L = stretches attributed to the Pacman ligand. Vis/NIR (boiling THF, 5.6 × 10^{-3} M): 897 nm (ε = 69 L mol^{-1} cm^{-1}), 1142 (ε = 55 L mol^{-1} cm^{-1}), 1191 (ε = 45 L mol^{-1} cm^{-1}), 1300 (ε = 74 L mol^{-1} cm^{-1}) 1684 (ε = 73 L mol^{-1} cm^{-1}). Solubility: Boiling pyridine, boiling THF (partial).

7.3.25 Synthesis of [(Me_3SiOUO)$_2$(L)] from [{K(py)}{$(OUO)_2$(L)}{$K(py)_3$}$_2$]

To a red solution of [{K(py)}{$(OUO)_2$(L)}{$K(py)_3$}$_2$] (14 mg, 0.009 mmol) in d_5-pyridine (0.4 mL) in a Teflon-valved valve NMR tube was added a solution of trimethylsilyl

chloride (2 mg, 0.018 mmol, 2 equiv) in d_5-pyridine and the mixture shaken for 1 min forming a brown solution in which [$(Me_3SiOUO)_2(L)$] was the only product observed in solution by ^{1}H NMR spectroscopy.

7.3.26 Stability of [{K(py)}{$(OUO)_2$(L)}{$K(py)_3$}$_2$] in protic media

a*. Acid disproportionation.* To a red solution of [{K(py)}{$(OUO)_2$(L)}{$K(py)_3$}$_2$] (10 mg, 0.006 mmol) in d_5-pyridine (0.4 mL) in a Teflon-valved valve NMR tube was added a solution of pyridinium chloride (1.5 mg, 0.012 mmol, 2 equiv) in d_5-pyridine and the mixture shaken for 1 min resulting in the formation of a brown solution and a dark precipitate in which [UO_2(py)(H_2L)] was the only product observed by ^{1}H NMR spectroscopy.

b*. Aqueous disproportionation.* To a red solution of [{K(py)}{$(OUO)_2$(L)}{$K(py)_3$}$_2$] (10 mg, 0.006 mmol) in d_5-pyridine (0.4 mL) in a Teflon-valved valve NMR tube was added an excess of deionised, N_2-degassed H_2O and the mixture shaken for 1 min resulting in the formation of a brown solution and a dark precipitate in which [UO_2(py)(H_2L)] was the only product observed in solution by ^{1}H NMR spectroscopy.

7.3.27 Synthesis of [Li(py)$_2$][UO_2{$N(SiMe_3)_2$}$_3$]

To an orange solution of [UO_2{$N(SiMe_3)_2$}$_3$(py)$_2$] (1.0139 g, 1.360 mmol) in toluene (7 mL) at –40 °C was added a colourless solution of $LiN(SiMe_3)_2$ (227 mg, 1.369 mmol, 1 equiv) in toluene (3 mL) at –40 °C and the resulting red solution allowed to warm to room temperature over 2 h. The solution was then reduced in volume to 5 mL under vacuum resulting in the precipitation of red solids. These were re-dissolved by brief immersion of the reaction vessel in boiling water before the resulting red solution was allowed to cool to room temperature over 2 h, resulting in the formation of red crystals of [Li(py)$_2$][UO_2{$N(SiMe_3)_2$}$_3$]. More material was precipitated upon storage of the vessel at –35 ˚C for 12 h after which the product was isolated by filtration and dried under vacuum for 12 h. [Li(py)$_2$][UO_2{$N(SiMe_3)_2$}$_3$] was collected as a red crystalline solid (725 mg, 0.791 mmol, 58 %). Single crystals of the product suitable for X-ray diffraction were grown from slow evaporation of a benzene solution. ^{1}H NMR (*d_5*-pyridine): δ_H 0.78 (s, 54H, Si*Me*$_3$), ^{7}Li{^{1}H} NMR (*d_5*-pyridine): δ_{Li} 3.45. ^{13}C{^{1}H} NMR (*d_5*-pyridine): δ_C 32.16 (Si*Me*$_3$). ^{1}H NMR (C_6D_6): δ_H 9.32, 8.63, 6.89, 6.79 and 6.62 (broad singlets, 10H, pyridine), 0.69, 0.63, 0.46, 0.45 (broad singlets, 54H, Si*Me*$_3$). Analysis. Found: C, 36.66; H, 7.29; N, 7.50. $C_{28}H_{64}N_5O_2LiSi_6U_2$ requires: C, 36.70; H, 7.04; N, 7.64 %. FTIR (nujol, cm^{-1}): 1601 (s), 1252 (s), 1236 (s), 1069 (w), 1040 (w), 1007 (w), 945 (s), 935 (s, uranyl assymtric stretch),

859 (s), 832 (s), 768 (m), 750 (m), 699 (m), 683 (m), 660 (m), 617 (w), 609 (s). Solubility: pyridine, THF, toluene and benzene.

7.3.28 Synthesis of [{(py)$_3$LiOUO}$_2$(L)]

To a yellow solution of H_4L (1 g, 1.51 mmol) in pyridine (10 mL) was added a red solution of $[Li(py)_2][UO_2\{N(SiMe_3)_2\}_3]$ (3.122 mg, 3.41 mmol, 2.25 equiv) in pyridine (5 mL) and the resultant red solution boiled at 125 °C in a Teflon-tapped ampoule for 12 h resulting in the formation of a brown solution. The volatiles were then evaporated under vacuum and the brown residue washed with toluene (30 mL) before being dried under vacuum at 100 °C for 2 h yielding a brown powder. Pyridine (15 ml) was then added forming a brown solution and a brown precipitate (500 mg),* the former of which was isolated by filtration before being reduced in volume to 6 ml under vacuum. Storage of the solution at –35 °C for 12 h resulted in the formation of brown, microcrystalline material which was isolated by filtration and dried under vacuum for 100 °C for 2 h. [{(py)$_3$LiOUO}$_2$(L)] was isolated as a brown microcrystalline powder (530 mg, 0.041 mmol, 21 %). Single crystals of the product suitable for X-ray diffraction were grown from a pyridine solution. ^{1}H NMR (d_5-pyridine): δ_H 11.58 (s, 4H, pyrrole), 8.40 (s, 4H, pyrrole), 4.63 (s, 4H, imine), 4.32 (s, 6H, *meso*-methyl), –3.11 (s, 12H, aryl-Me), –4.00 (s, 4H, aryl), –11.19 (s, 6H, *meso*-methyl). ^{7}Li{^{1}H} NMR (d_5-pyridine): δ_{Li} 62.01 (bs). Analysis. Found: C, 51.20; H, 4. 09; N, 11.50. $C_{72}H_{70}N_{14}O_4Li_2U_2$ requires: C, 51.31; H, 4.19; N, 11.64 %. FTIR (nujol, cm^{-1}): 1591 (s, L), 1567 (s, L), 1508 (w), 1349 (w), 1272 (s, L) 1216 (w, L), 1185 (m, L), 1105 (w), 1042 (m, L), 1015 (m, L), 960 (w, L), 900 (m), 872 (m), 836 (w) 784 (w), 758 (s) 721 (s, L), 700 (s), 566 (s), 546 (s). L = stretches attributed to the Pacman ligand. Vis/NIR (THF, 6.0 × 10–3 M): 913 nm (ε = 109 L mol^{-1} cm^{-1}), 1152 (ε = 67 L mol^{-1} cm^{-1}), 1190 (ε = 57 L mol^{-1} cm^{-1}) 1320 (ε = 70 L mol^{-1} cm^{-1}), 1684 (ε = 73 L mol^{-1} cm^{-1}). Solubility: pyridine and THF (partial).

*Addition of TMSCl to a suspension of the solid (10 mg) in d_5-pyridine (0.5 mL) resulted in partial dissolution to form a solution of [(Me$_3$SiOUO)$_2$(L)]. This observation indicates that the material is a mixture of **P** and other intractable materials analogous to that produced during the high temperature synthesis of [(Me$_3$SiOUO)$_2$(L)]. Addition of an excess of LiCl (10 mg) to a sample of the solid in d_5-pyridine (0.5 mL) did not result in reaction.

7.3.29 Synthesis of [{(py)$_3$LiOUO}$_2$(L)] from P

To a brown slurry of **P** (10 mg 0.006 mmol based on best estimate of empirical formula) in d_5-pyridine (0.5 mL) in a Teflon-valved valve NMR tube was added a solution of

$LiN(SiMe_3)_2$ (6 mg, 0.036 mmol, 6 equiv) and the mixture heated at 120 °C for at 4 d resulting in the partial dissolution of **P**. $HN(SiMe_3)_2$ and trace amounts of $[\{(py)_3LiOUO\}_2(L)]$ were the only species present by ^1H NMR spectroscopy after the reaction period.

7.3.30 Synthesis of $[\{(py)_3LiOUO\}L(OUOSiMe_3)]$

To a brown solution of $[UO_2(py)(H_2L)]$ (762 mg, 0.757 mmol) in pyridine (5 mL) was added to a red solution of $[Li(py)_2][UO_2\{N(SiMe_3)_2\}_3]$ (693 mg, 0.757 mmol, 1 equiv) in pyridine (3 mL) and the solution boiled at 125 °C in a Teflon-tapped ampoule for 12 h forming a brown solution. The volatiles were then evaporated under vacuum before the addition toluene (10 mL) yielding a brown powder and brown solution. The solution was then isolated by filtration and reduced in volume to 4 mL under vacuum before being stored at –35 °C. Brown, microcrystalline material was deposited after 12 h and was isolated by filtration before being dried under vacuum for 2 h at 100 °C. $[\{(py)_3LiOUO\}L(OUOSiMe_3)]$ was isolated as a brown microcrystalline powder (286 mg, 0.189 mmol, 25 %). Single crystals of the product suitable for X-ray diffraction were grown by slow cooling of a saturated pyridine solution. ^1H NMR (d_5-pyridine): δ_H 14.05 (s, 2H), 12.19 (s, 9H, $SiMe_3$), 9.80 (s, 2H), 9.43 (s, 2H), 6.97 (s, 2H), 6.45 (s, 2H), 5.76 (s, 3H, *meso*-methyl), 5.20 (s, 2H), 2.47 (s, 3H, *meso*-methyl), –2.13 (s, 2H), –2.44 (s, 6H, aryl-Me), –3.01 (s, 6H, aryl-Me), –4.64 (s, 2H), –7.11(s, 3H, *meso*-methyl), –11.54 (s, 3H, *meso*-methyl). Resonances with 2H integrations: imine, α-pyrrole, β-pyrrole and aryl. $^7Li\{^1H\}$ NMR (d_5-pyridine): δ_{Li} 33.16 (bs). Analysis. Found: C, 47.59; H, 4. 17; N, 10.29. $C_{60}H_{64}N_{11}O_4LiSiU_2$ requires: C, 47.59; H, 4.26; N, 10.17 %. FTIR (nujol, cm^{-1}): 1591 (s, L), 1569 (s, L), 1506 (w), 1350 (w), 1269 (s, L) 1218 (w, L), 1186 (w, L), 1105 (w), 1046 (m, L), 1015 (m, L), 967 (w, L), 883 (s, U-O), 835 (w), 821 (w), 796 (w), 765 (w) 720 (m, L), 627 (m), 593 (w), 577 (w), 564 (w), 531 (m) L = stretches attributed to the Pacman ligand. Vis/NIR (THF, 7.2×10^{-3} M): 954 nm (ε = 81 L mol^{-1} cm^{-1}), 1063 (ε = 43 L mol^{-1} cm^{-1}), 1225 (ε = 50 L mol^{-1} cm^{-1}), 1430 (ε = 67 L mol^{-1} cm^{-1}). Pyridine and THF (partial).

7.3.31 Unsuccessful synthesis of $[\{(py)_3LiOUO\}_2L(OUO)]$

To a brown solution of $[UO_2(py)(H_2L)]$ (40 mg, 0.018 mmol) in d_5-pyridine (0.4 mL) in a Teflon-valved valve NMR tube was added a solution of $LiN(SiMe_3)$ (20 mg, 0.054 mmol, 3 equiv) in d_5-pyridine (0.3 mL) forming a solution of $[\{Li(py)_3OUO\}(L)\{Li(py)\}_2]$ and 3 equivalents of $HN(SiMe_3)_2$ after 1 h by ^1H NMR spectroscopy.[24] The solution was poured onto a suspension of $[UO_2Cl_2(THF)_2]$ (20 mg, 0.018 mmol) and left for 3 d after

which only THF, $HN(SiMe_3)_2$ and trace $[UO_2(py)(H_2L)]$ were present in the ^1H NMR spectrum.

7.4 Synthetic procedures described in Chapter Four

7.4.1 Synthesis of $[\{K(py)_3K(py)(OUO)(\mu\text{-}\kappa^2\text{-}\kappa^2\text{-}O_2)(OUO)(L)\}_2]$

A brown suspension of $[\{\{K(py)\}\{(OUO)_2(L)\}\{K(py)_3\}\}_2]$ (35 mg, 0.022 mmol) in THF (4 mL) in a 10 mL quartz cuvette fitted with a Teflon-tap was freeze-pump-thaw degassed three times, exposed to a 1 atm pressure of dry dioxygen, and vigorously shaken resulting in the dissolution of all solids to form an orange solution which showed no 5*f*–5*f* transitions in the NIR spectrum. The volatiles were evaporated under vacuum, the residue dissolved in d_5-pyridine (0.4 mL) and the resulting orange solution layered with hexanes (0.4 mL). Precipitation of single crystals suitable for X-ray diffraction occurred after one week from which the solid state structure was ascertained. The bulk product was isolated by decantation of the supernatant before drying under vacuum for 2 h at 100 °C. $[K(py)_3][K(py)][(OUO)(\mu\text{-}\kappa^2\text{-}\kappa^2\text{-}O_2)(OUO)(L)]_2$ was isolated as red crystalline solid (20 mg, 0.012 mmol, 55 %). ^1H NMR *(d_5*-pyridine): δ_H 9.27 (s, 4H, imine), 7.25 (s, 4H, pyrrole) 7.06.15 (s, 4H, aryl), 6.91 (s, 4H, pyrrole), 2.52 (s, 6H, *meso*-methyl), 2.35 (s, 6H, *meso*-methyl), 1.89 (s, 12H, aryl-methyl). $^{13}C\{^1H\}$ NMR *(d_5-pyridine)*: δ_c 165.34 (aryl quarternary), 161.81 (imine), 141.77 (aryl quaternary), 133.91 (aryl quaternary), 129.22 (pyrrole), 121.73 (pyrrole), 109.60 (aryl), 41.22 (*meso*-quaternary), 37.11 (*meso*-methyl), 27.28 (*meso*-methyl), 18.97 (aryl-methyl) one aryl-quaternary carbon resonance obscured by solvent. Analysis. Found: C, 45.90; H, 3.75; N, 10.15. $C_{62}H_{60}N_{12}O_6K_2U_2$ requires: C, 45.87; H, 3.73; N, 10.35 %. FTIR (nujol, cm^{-1}): 1603 (s, L), 1581 (s, L), 1508 (w), 1360 (w), 1282 (s, L) 1226 (w, L), 1191 (m, L), 1111 (w), 1049 (m, L), 1018 (m, L), 968 (w, L), 966 (w), 924 (w, UO_2^{2+} asymmetric stretch) 900 (m), 886 (m), 842 (w), 823 (w), 766 (w) 726 (m, L), 658 (w), 599 (w). L = stretches attributed to the Pacman ligand. Vis/NIR (THF, 5.6×10^{-3} M): no NIR absorptions. Solubility: pyridine and THF (partial).

7.4.2 Synthesis of $[\{K(py)_3K(py)(UO_2)_2(\mu\text{-}O)(L)\}_2]$

To a brown suspension of $[\{\{K(py)\}\{(OUO)_2(L)\}\{K(py)_3\}\}_2]$ (17 mg, 0.011 mmol) in d_5-pyridine (0.4 mL) in a Teflon-valved valve NMR tube was added pyridine-*N*-oxide (1 mg, 0.01 mmol, one equiv) and the mixture boiled for 4 d resulting in the dissolution of all solids to form a red solution in which $[\{K(py)_3K(py)(UO_2)_2(\mu\text{-}O)(L)\}_2]$ was the only product observed by ^1H NMR spectroscopy. The solution was then layered with hexanes, resulting in precipitation of single crystals suitable for X-ray diffraction after one week. The product was

isolated by decanting the supernatant before drying under vacuum for 2 h at 100 °C. $[\{K(py)_3K(py)(UO_2)_2(\mu\text{-}O)(L)\}_2]$ was isolated as red crystalline solid (7 mg, 0.004 mmol, 36 %). ^{1}H NMR *(d_5*-pyridine): δ_H 9.32 (s, 2H, imine), 9.28 (s, 2H, imine), 7.40 (d, J = 4 Hz, 2H, pyrrole), 7.34 (s, 2H, aryl), 7.31 (s, 4H, pyrrole), 7.01 (d, J = 4 Hz, 2H, pyrrole), 6.96 (s, 2H, aryl), 6.95 (d, J = 4 Hz, 2H, pyrrole), 4.39 (s, 3H, *meso*-methyl), 2.36 (s, 3H, *meso*-methyl), 2.29 (s, 6H, aryl-methyl), 2.17 (s, 3H, *meso*-methyl), 2.15 (s, 3H, *meso*-methyl), 1.75 (s, 6H, aryl-methyl). Analysis. Found: C, 46.49; H, 3.80; N, 10.48. $C_{62}H_{60}N_{12}O_5K_2U_2$ requires: C, 46.33; H, 3.76; N, 10.46 %.

7.4.3 Synthesis of $[\{UO_2(py)_3\}\{(UO_2)_2(\mu\text{-}O)(L)\}]$

a. *By salt elimination from $[K(py)_3][K(py)](UO_2)_2(\mu\text{-}O)(L)]_2$.* To a red solution of $[K(py)_3][K(py)(UO_2)_2(\mu\text{-}O)(L)]_2$ (0.015 mmol, prepared in situ from $[\{\{K(py)\}\{(OUO)_2(L)\}\{K(py)_3\}\}_2]$ and pyridine-*N*-oxide) in d_5-pyridine (0.4 mL) in a Teflon-valved valve NMR tube was added a suspension of $[UO_2Cl_2(THF)_2]$ (7 mg, 0.015 mmol, 1 equiv) and the mixture shaken for 2 min resulting in the formation of a 70:30 mixture of the intermediated complex $K_2[\{(UO_2)_2(\mu\text{-}O)(L)\}\{UO_2Cl_2(py)_x\}]$ and $[\{UO_2(py)_3\}\{(UO_2)_2(\mu\text{-}O)(L)\}]$ as well as two equivalents of THF. The solution was then left for four weeks resulting in the quantitative conversion of the intermediate to $[\{UO_2(py)_3\}\{(UO_2)_2(\mu\text{-}O)(L)\}]$ as evidenced by ^{1}H NMR spectroscopy. ^{1}H NMR *(d_5*-pyridine): δ_H 9.30 (s, 4H, imine), 7.36 (d, J = 4 Hz, 4H, pyrrole), 7.02 (s, 4H, aryl), 6.87 (d, J = 4 Hz, 4H, pyrrole), 3.67 (m, 8H, 2·THF), 2.30 (s, 6H, *meso*-methyl), 2.18 (s, 6H, *meso*-methyl), 2.01 (s, 12H, aryl-methyl), 1.63 (m, 8H, 2HF).

7.4.4 Attempted syntheses of $[(OUO)_2(L)]$ by oxidation of $[M_2(OUO)_2(L)]$

a. *From I_2 and the potassium salt.* To a brown suspension of $[\{\{K(py)\}\{(OUO)_2(L)\}\{K(py)_3\}\}_2]$ (19 mg, 0.010 mmol) in d_5-pyridine (0.4 mL) in a Teflon-valved valve NMR tube was added a solution of iodine (3 mg, 0.010) in d_5-pyridine (0.2 mL) and the mixture left for 2 d. The volatiles were evaporated under vacuum before the addition of C_6D_6 (0.5 mL) forming a brown solution with a small amount of brown precipitate, the former was found to exhibit a large number of broad resonances in the ^{1}H NMR spectrum that could not be assigned to $[(OUO)_2(L)]$.

b. *From I_2 and the lithium salt.* To a brown suspension of $[\{(py)_3LiOUO)_2(L)]$ (29 mg, 0.017 mmol) in d_5-pyridine (0.4 mL) in a Teflon-valved valve NMR tube was added a solution of iodine (2 mg, 0.009) in d_5-pyridine (0.2 mL) and the mixture left for 2 d after which a diamagnetic product was observed by ^{1}H NMR spectroscopy. The solution was then

layered with hexanes (0.5 mL) resulting in the precipitation of brown solids which could not be redissolved.

c. *From [AgBPh$_4$] and the potassium salt.* To a brown suspension of [{{K(py)}{(OUO)$_2$(L)}{K(py)$_3$}}$_2$] (10 mg, 0.006 mmol) in d_5-pyridine (0.4 mL) in a Teflon-valved valve NMR tube was added a suspension of silver tetraphenyl borate (5 mg, 0.012 mmol, 2 equiv) in d_5-pyridine (0.2 mL) and the mixture boiled at 120 °C for 12 h resulting in the formation of a brown solution and a grey precipitate, the former of which contained a number of paramagnetic products by ^{1}H NMR spectroscopy.

d. *From [AgBPh$_4$] and the lithium salt.* To a brown suspension of [{(py)$_3$LiOUO}$_2$(L)] (9 mg, 0.005 mmol) in d_5-pyridine (0.4 mL) in a Teflon-valved valve NMR tube was added a suspension of silver tetraphenyl borate (4 mg, 0.012 mmol, 2 equiv) in d_5-pyridine (0.2 mL) and the mixture boiled for 20 h at 120 °C after which no reaction had taken place.

e. *From Ph$_3$CCl and the potassium salt.* To a brown suspension of [{{K(py)}{(OUO)$_2$(L)}{K(py)$_3$}}$_2$] (10 mg, 0.006 mmol) in d_5-pyridine (0.4 mL) in a Teflon-valved valve NMR tube was added a solution of trityl chloride (4 mg, 0.012 mmol, 2 equiv) in d_5-pyridine (0.2 mL) resulting in the formation of a red solution which contained a number of new resonances by ^{1}H NMR spectroscopy which could not be assigned.

7.4.5 Attempted synthesis of [UO$_2$(py)$_3$(UO$_2$)$_2$(O$_3$C)(L)]

A brown suspension of [{{K(py)}{(OUO)$_2$(L)}{K(py)$_3$}}$_2$] (17 mg, 0.011 mmol) in d_5-pyridine (0.6 mL) in a Teflon-valved valve NMR tube was freeze-pump-thaw degassed three times, exposed to a 1 atm pressure of dry dioxygen, and vigorously shaken, resulting in the dissolution of all solids to form a red solution after 10 min. The solution was found to contain a number of unidentified diamagnetic and paramagnetic products by ^{1}H NMR spectroscopy.

7.4.6 Attempted synthesis of [(OUO)(L)(OUOSiMe$_3$] by oxidation of [{(py)$_3$LiOUO}L(OUOSiMe$_3$)]

To a brown solution of [{(py)$_3$LiOUO}L(OUOSiMe$_3$)] (21 mg, 0.014 mmol) in d_5-pyridine (0.4 mL) in a Teflon-valved valve NMR tube was added a solution of iodine (2 mg, 0.007, one equiv) in d_5-pyridine (0.2 mL) and the mixture left for 30 min resulting in the formation of [(Me$_3$SiOUO)$_2$(L)], as well as other unidentified products, by ^{1}H NMR spectroscopy.

7.4.7 Synthesis of [(^{n}Bu$_3$SnOUO)$_2$(L)]

To brown suspension of [{{K(py)}{(OUO)$_2$(L)}{K(py)$_3$}}$_2$] (60 mg, 0.038 mmol) in pyridine (0.3 mL) was added a solution of tributyltin chloride (^{n}Bu$_3$SnCl) (35 mg, 0.105 mmol, 2.8 equiv) in pyridine (0.4 mL) and the mixture shaken for 30 s resulting in the dissolution of all solids to form an red/brown solution. The solvent was then evaporated under vacuum and the brown residue dried at 100 °C for 2 h before addition of hexanes (4 mL) forming a red solution and a white precipitate. The solution was isolated by filtration and reduced in volume to 0.3 mL under vacuum resulting in the precipitation of red solids. The crude product was recrystallized by heating the solvent to 80 °C, resulting in the dissolution of all solids, before allowing it to cool room temperature over 2 h. The resulting red crystals were isolated by decantation of the supernatant and drying the solids under vacuum for 1 h. Single crystals of the product suitable for X-ray diffraction were extracted from the mixture prior to isolation of the bulk product. [(^{n}Bu$_3$SnOUO)$_2$(L)] was isolated as a red crystalline solid (47 mg, 0.026 mmol, 70 %). ^{1}H NMR (C$_6$D$_6$): δ_H 12.57 (s, 12H, SnC*H*$_2$), 12.34 (s, 4H, pyrrole) 8.59 (s, 4H, pyrrole), 7.96 (s, 12H, SnCH$_2$C*H*$_2$) 6.47 (s, 4H, imine), 4.82 (q, J = 7 Hz, 12H, SnCH$_2$CH$_2$C*H*$_2$), 4.16 (s, 6H, *meso*-methyl), 2.46 (t, 18H, SnCH$_2$CH$_2$CH$_2$C*H*$_3$), −2.46 (s, 12H, aryl-methyl), −3.08 (s, 4H, aryl), –11.10 (s, 6H, *meso*-methyl). Specific assignment of the resonances attributable to the *n*-butyl chains was achieved by a ^{1}H–1H COSY experiment. Analysis. Found: C, 44.52; H, 5.32; N, 6.36. C$_{66}$H$_{94}$N$_8$O$_4$Sn$_2$U$_2$ requires: C, 44.61; H, 5.33; N, 6.31 %. FTIR (nujol, cm^{-1}): 1592 (s, L), 1573 (s, L), 1502 (m), 1353 (m), 1261 (s, Sn-C) 1221 (w, L), 1185 (m, L), 1042 (s, L), 1017 (s, L), 965 (w, L), 896 (m, L), 869 (m, U-O), 797 (s, U-O), 683 (m), 707 (s), 566 (s), 543 (s). L = stretches attributed to the Pacman ligand. Vis/NIR (THF, 5.6 × 10^{-3} M): 994 nm (ε = 72 L mol^{-1} cm^{-1}), 1162 (ε = 49 L mol^{-1} cm^{-1}), 1657 (ε = 78 L mol^{-1} cm^{-1}). Solubility: pyridine, THF, toluene, benzene, diethyl ether and hexanes.

7.4.8 Synthesis of [(Ph$_3$SnOUO)$_2$(L)]

To brown suspension of [{{K(py)}{(OUO)$_2$(L)}{K(py)$_3$}}$_2$] (10 mg, 0.006 mmol) in *d*$_5$-pyridine (0.3 mL) in a Teflon-valved valve NMR tube was added a solution of triphenyltin chloride (Ph$_3$SnCl) (5 mg, 0.013 mmol, 2 equiv) in pyridine (0.3 mL) and the mixture shaken for 30 s resulting in the dissolution of all solids to form an red/brown solution. The solvent was then evaporated under vacuum and the brown residue dried at 100 °C for 2 h before addition of C$_6$D$_6$ (0.4 mL) forming a red solution and an off-white precipitate. The solution was isolated by filtration and left to evaporate to dryness in a ditnitrogen atmosphere glovebox resulting in the formation of single crystals of

$[(Ph_3SnOUO)_2(L)]$, which were suitable for X-ray diffraction, after 48 h. The bulk material was dried for under vacuum for 1 h (after extraction of single crystals for analysis). $[(Ph_3SnOUO)_2(L)]$ was collected as a red crystalline solid (5 mg, 0.003 mmol, 50 %). ^{1}H NMR *(*C_6D_6): δ_H 15.39 (d, J = 7 Hz, 12H, Sn*Ph*$_3$), 11.99 (s, 4H, pyrrole) 8.95 (t, J = 7 Hz, 12H, Sn*Ph*$_3$), 8.34 (t, J = 7 Hz, 12H, Sn*Ph*$_3$), 8.18 (s, 4H, pyrrole), 6.71 (s, 4H, imine), 3.85 (s, 6H, *meso*-methyl), −2.56 (s, 12H, aryl-methyl), −3.91 (s, 4H, aryl), –10.80 (s, 6H, *meso*-methyl). Analysis. Found: C, 49.40; H, 3.62; N, 5.75. $C_{78}H_{70}N_8O_4Sn_2U_2$ requires: C, 49.39; H, 3.72; N, 5.91 %. Solubility: pyridine, THF, toluene and benzene.

7.4.9 Synthesis of [{(py)$_3$LiOUO}(L){OUO^{i}Pr}]

In a typical reaction, a red-brown solution of $[\{(py)_3LiOUO\}_2(L)]$ (10 mg, 0.006 mmol) in d_5-pyridine (0.3 mL) in a Teflon-valved valve NMR tube was added to a solution of chlorotitanium trisisopropoxide [TiCl(*i*OPr)$_3$] (3 mg, 0.006 mmol, 1 equiv) in pyridine (0.3 mL) and the mixture left for 6 h resulting in the formation of a brown solution of [{(py)$_3$LiOUO}(L){OUO^{i}Pr}] and an isopropoxide-containing by-product as the only species observed by ^{1}H NMR spectroscopy. Single crystals of the product suitable for X-ray diffraction were grown by layering hexane over the reaction mixture. Attempts to separate [{(py)$_3$LiOUO}(L){OUO^{i}Pr}] by from the by-products by removal of the pyridine solvent and extraction into benzene resulted in ligand rearrangement to form a 1:1 mixture of $[\{(py)_3LiOUO\}_2(L)]$ and $[(^iPrOUO)_2(L)]$ as evidenced by ^{1}H NMR spectroscopy. Attempts to purify the crude mixture by fractional crystallisation were unsuccessful. ^{1}H NMR *(*d_5-pyridine): δ_H 42.82 (s, 1H, OC*H*(CH$_3$)$_2$) 16.02 (s, 6H, OCH(C*H*$_3$)$_2$), 13.85 (s, 2H), 9.77 (s, 2H), 9.42 (s, 2H), 6.97 (s, 2H), 6.37 (s, 2H), 5.69 (s, 3H, *meso*-methyl), 5.03 (s, 2H), 2.41 (s, 3H, *meso*-methyl), –2.23 (s, 2H), –2.46 (s, 6H, aryl-Me), –3.00 (s, 6H, aryl-Me), –4.46 (s, 2H), –7.21(s, 3H, *meso*-methyl), –11.88 (s, 3H, *meso*-methyl). Solubility: pyridine.

7.4.10 Unsuccessful synthesis of [(^{i}PrOUO)$_2$(L)] from two equivalents of Ti(O^{i}Pr)$_3$Cl

To a brown solution of $[\{(py)_3LiOUO\}_2(L)]$ (10 mg, 0.006 mmol) in d_5-pyridine (0.3 mL) in a Teflon-valved valve NMR tube was added to a solution of chlorotitanium trisisopropoxide (3 mg, 0.012 mmol, 2 equiv) in pyridine (0.3 mL) and the mixture left for 4 d after which a 1:3 mixture of [{(py)$_3$LiOUO}(L){OUO^{i}Pr}]:[(^{i}PrOUO)$_2$(L)] was observed by ^{1}H NMR spectroscopy. Heating the mixture to accelerate the reaction resulted in the formation of intractable products.

7.4.11 Synthesis of [(^{i}PrOUO)$_2$(L)]

To a red-brown solution of [{(py)$_3$LiOUO}$_2$(L)] (200 mg, 0.119 mmol) in pyridine (5 mL) was added to a solution of chlorotitanium trisisopropoxide (150 mg, 0.593 mmol, 5 equiv) in pyridine (3 mL) and the mixture left for 4 d forming a brown solution. The volatiles were then evaporated under vacuum and the resulting brown solid dried under vacuum at 120 °C for 2 h until no further evaporation of [TiCl(*i*OPr)$_3$]was observed. Diethyl ether (15 mL) and 1,4 dioxane (1 mL) were then added forming a grey precipitate and a brown solution, the former of which was isolated by filtration before removal of the volatiles under vacuum to form a brown solid. The crude product was then dissolved in toluene (5 mL) and separated from the trace amount of remaining grey precipitate by filtration. Concentration of the filtrate to 2 mL under vacuum and storage of the solution at –35 °C for 12 h resulted in precipitation of microcrystalline brown solids which were isolated by filtration and dried at 100 ˚C for 2 h. [(^{i}PrOUO)$_2$(L)] was collected as a brown solid (170 mg, 0.101 mmol, 85 %). Single crystals of the product suitable for X-ray diffraction were grown by slow evaporation of a 1:10 THF:hexane solution at –30 °C. ^{1}H NMR (*d*$_5$-pyridine): δ_H 53.28 (s, 2H, OC*H*(CH$_3$)$_2$) 21.76 (s, 12H, OCH(C*H*$_3$)$_2$), 13.23 (s, 4H, pyrrole), 9.01 (s, 4H, pyrrole), 6.97 (s, 4H, imine), 4.66 (s, 6H, *meso*-methyl), –3.13 (s, 12H, aryl-Me), –3.95 (s, 6H, *meso*-methyl), –11.52 (s, 6H, *meso*-methyl). ^{7}Li{^{1}H} NMR (C_6D_6): No resonances. Analysis. Found: C, 45.08; H, 4.13; N, 8.67. $C_{48}H_{54}N_8O_4U_2$ requires: C, 44.93; H, 4.24; N, 8.73 %. FTIR (nujol, cm^{-1}): 1597 (s, L), 1573 (s, L), 1505 (w), 1353 (m), 1268 (s, C-C) 1221 (w, L), 1190 (m, L), 1109 (m) 1049 (s, L), 1018 (s, L), 965 (w, L), 899 (m, L), 841 (m, U-O), 766 (m, U-O), 726 (m), L = stretches attributed to the Pacman ligand. Vis/NIR (THF, 6.6×10^{-3} M): 1020 nm (ε = 96 L mol^{-1} cm^{-1}), 1177 (ε = 74 L mol^{-1} cm^{-1}), 1357 (ε = 44 L mol^{-1} cm^{-1}), 1580 (ε = 48 L mol^{-1} cm^{-1}), 1652 (ε = 68 L mol^{-1} cm^{-1}). Solubility: pyridine, THF, toluene, benzene.

7.4.12 Unsuccessful synthesis of [(^{i}PrOUO)$_2$(L)] from ^{i}PrI

To a brown suspension of [{{K(py)}{(OUO)$_2$(L)}{K(py)$_3$}}$_2$] (10 mg, 0.006 mmol) in C_6D_6 (0.4 mL) in a Teflon-valved valve NMR tube was added a solution of 2-iodopropane (^{i}PrI) (10 mg, 0.013 mmol, 2 equiv) in C_6D_6 (0.3 mL)) and the mixture shaken for 1 min resulting in the formation of a red solution containing a number of unidentified paramagnetic products in the ^{1}H NMR spectrum.

7.4.13 Oxidative Stability Tests

In a typical reaction, a Teflon-valved valve NMR tube was charged with a 10 mg solution of either [(*n*-$Bu_3SnOUO)_2$(L)] or [(^{i}PrOUO)$_2$(L)] in d_5-pyridine (0.5 mL) and freeze-pump-thaw degassed three times to remove dinitrogen. The solutions were then exposed to an atmosphere of dry oxygen at 1 atm and boiled for 4 d. The same test was performed for [$(Ph_3SnOUO)_2$(L)] from material synthesised *in situ* from [{{K(py)}{$(OUO)_2$(L)}{$K(py)_3$}}$_2$] (10 mg, 0.006 mmol) and Ph_3SnCl (5 mg, 0.013 mmol, 2 equiv) d_5-pyridine (0.5 mL). No change in the ^{1}H NMR spectra was observed of any of the compounds during the tests.

7.4.14 Attempted synthesis of [$(ClOUO)_2$(L)]

To a brown solution of [{$(py)_3LiOUO\}_2$(L)] (10 mg, 0.006 mmol) in d_5-pyridine (0.4 mL) in a Teflon-valved valve NMR tube was added a solution of [$TiCl_4(THF)_2$] (1 mg, 0.003 mmol, 0.5 equiv) in d_5-pyridine (0.2 mL) and the mixture shaken for 1 min forming a brown solution. No resonances apart from those of THF were visible in the ^{1}H NMR spectrum after the reaction period.

7.4.15 Attempted synthesis of of [$(9\text{-BBN-}OUO)_2$(L)]

To a brown suspension of [{{K(py)}{$(OUO)_2$(L)}{$K(py)_3$}}$_2$] (10 mg, 0.006 mmol) in C_6D_6 (0.4 mL) in a Teflon-valved valve NMR tube was added a solution of 9-iodo-9-borabicyclo(3.3.1)nonane (8.2 mg of a 1 mol dm^{-3} solution in hexane, 0.013 mmol, 2 equiv) in C_6D_6 (0.3 mL) and the mixture left for 2 d after which no dissolution of the starting material had occurred. Boiling the mixture at 80 °C for 24 h resulted in no change.

7.4.16 Attempted synthesis of of [$(Ph_2POUO)_2$(L)]

To a brown solution of [{$(py)_3LiOUO\}_2$(L)] (10 mg, 0.006 mmol) in d_5-pyridine (0.4 mL) in a Teflon-valved valve NMR tube was added a solution of chlorordiphenylphosphine (3 mg, 0.012 mmol, 2 equiv) in in d_5-pyridine (0.4 mL) and the mixture shaken for 30 s forming a brown solution. Chlorordiphenylphosphine was the only species present in the ^{1}H NMR spectrum after the reaction period.

7.4.17 Attempted synthesis of of [$(R_3U)OUO)_2$(L)]

b. A solution of [$U(ODtbp)_3$] (Dtbp = 2,6-ditertbutylphenyl) (20 mg, 0.023 mmol) in C_6D_6 (0.5 ml) in a Teflon-valved valve NMR tube was added a solution of iodine (3 mg, 0.0012 mmol, 0.5 equiv) in C_6D_6 (0.2 ml) forming a yellow solution of [$U(ODtbp)_3I$] by ^{1}H NMR spectroscopy.[12] A brown solution of [{$(py)_3LiOUO\}_2$(L)] (20 mg, 0.012 mmol) in

C_6D_6 (0.4 mL) was then added resulting in the immediate precipitation of intractable brown solids which could not be further characterised.

7.4.18 Attempted syntheses of [{$(UO_2)(OUO)_2(L)\}_n$]

a. *From [{{K(py)}{$(OUO)_2$(L)}{$K(py)_3$}$_2$] and [$UO_2Cl_2(THF)_2$]*. To a brown suspension of [{{K(py)}{$(OUO)_2$(L)}{$K(py)_3$}$_2$] (15 mg, 0.009 mmol) in d_5-pyridine (0.4 mL) in a Teflon-valved valve NMR tube was added a suspension of [$UO_2Cl_2(THF)_2$] (4 mg, 0.009 mmol, 1 equiv) in d_5-pyridine (0.4 mL) and the mixture left for 1 h resulting in the formation of a brown solution and a large amount of brown precipitate, the former of which exhibited no resonances in its ^{1}H NMR spectrum. Attempts to dissolve the remaining precipitate by heating the mixture at 120 °C were unsuccessful.

b. *From [{$(py)_3$LiOUO}L(OUOSiMe$_3$)] and [$UO_2Cl_2(THF)_2$]*. To a brown solution of [{$(py)_3$LiOUO}$_2$(L)] (9 mg, 0.005 mmol) in d_5-pyridine (0.4 mL) in a Teflon-valved valve NMR tube was added a suspension of [$UO_2Cl_2(THF)_2$] (5 mg, 0.010 mmol, 2 equiv) in d_5-pyridine (0.4 mL) and the mixture left for 1 h resulting in the formation of a brown solution which exhibited no resonances in its ^{1}H NMR spectrum. Attempts to crystallise the product by layering the reaction mixture with hexane were unsuccessful.

7.4.19 Attempted synthesis of [UO_2{$(OUO)_2$(L)(OUOSiMe$_3$)}$_2$]

To a brown solution of [{$(py)_3$LiOUO}L(OUOSiMe$_3$)] (10 mg, 0.006 mmol) in d_5-pyridine (0.4 mL) in a Teflon-valved valve NMR tube was added a suspension of [$UO_2Cl_2(THF)_2$] (2 mg, 0.003 mmol, 0.5 equiv) in d_5-pyridine (0.4 mL) and the mixture left for 12 h forming a brown solution and a brown precipitate. Approximately half the starting material was observed, by ^{1}H NMR spectroscopy, to have remained in solution. The mixture was then boiled at 120 °C resulting in no further consumption or dissolution or material.

7.4.20 Attempted synthesis of [{$(TiCp_2)(OUO)_2$(L)}$_n$]

To a brown suspension of [{{K(py)}{$(OUO)_2$(L)}{$K(py)_3$}$_2$] (10 mg, 0.006 mmol) in d_5-pyridine (0.4 mL) in a Teflon-valved valve NMR tube was added a solution of titanocene dichloride [Cp_2TiCl_2] (2 mg, 0.006 mmol) in d_5-pyridine (0.2 mL) and the mixture shaken for 1 min resulting in the formation of a red solution containing a number of unidentified paramagnetic products in the ^{1}H NMR spectrum.

7.4.21 Attempted syntheses of [{$Fe(CO)_2Cp)(OUO)_2$(L)}$_n$]

a. *From [$CpFe(CO)_2I$] and [{{K(py)}{$(OUO)_2$(L)}{$K(py)_3$}}$_2$]*. To a brown suspension of [{{K(py)}{$(OUO)_2$(L)}{$K(py)_3$}$_2$] (10 mg, 0.006 mmol) in d_5-pyridine (0.4

mL) in a Teflon-valved valve NMR tube was added a solution of [{$CpFe(CO)_2I$}$_2$] (2 mg, 0.006 mmol) in d_5-pyridine (0.2 mL) and the mixture shaken for 1 min resulting in the formation of an orange solution which exhibited no resonances in the ^{1}H NMR spectrum.

a. *From [$CpFe(CO)_2I$] and [{$(py)_3LiOUO\}_2$(L)]*. To a brown solution of [{$(py)_3LiOUO\}_2$(L)] (20 mg, 0.011 mmol) in d_5-pyridine (0.4 mL) in a Teflon-valved valve NMR tube was added a solution of [{$CpFe(CO)_2I\}_2$] (7 mg, 0.011 mmol) in d_5-pyridine (0.2 mL) and the mixture shaken for 1 min resulting in the formation of an orange solution which exhibited no resonances in the ^{1}H NMR spectrum.

7.4.22 Unsuccessful synthesis of [(^{n}Bu$_3$SnOUO)$_2$(L)] from P

To a brown slurry of **P** (13 mg 0.008 mmol based on best estimate of empirical formula) in d_5-pyridine (0.6 mL) in a Teflon-valved valve NMR tube was added an excess of tributyl tin chloride (0.1 mL) and the mixture heated at 120 °C for 24h. No reaction was observed by ^{1}H NMR spectroscopy. NB: A preparative synthesis of [(^{n}Bu$_3$SnOUO)$_2$(L)] may be found in section 7.4.7

7.4.23 Attempted syntheses of [(HOUO)$_2$(L)] from P

a. *From HCl*. To a brown slurry of **P** (50 mg 0.031 mmol based on best estimate of empirical formula) in pyridine (1 mL) was added a 0.25 M solution HCl in diethyl ether (0.3 mL, 0.062 mmol, 2 equiv) resulting in the dissolution of **P** to form a brown solution of [UO_2(py)(H_2L)] only as evidenced by ^{1}H NMR spectroscopy.

b. *From TfOH*. To a brown slurry of **P** (10 mg 0.006 mmol based on best estimate of empirical formula) in d_5-pyridine (0.6 mL) in a Teflon-valved valve NMR tube was added a trifluoromethanesulfonic acid (2mg, 0.012 mmol, 2 equiv) resulting in the dissolution of **P** to form a brown solution of [UO_2(py)(H_2L)], as evidenced by ^{1}H NMR spectroscopy, and a brown precipitate.

c. *From* t*BuOH*. To a brown slurry of **P** (10 mg 0.006 mmol based on best estimate of empirical formula) in d_5-pyridine (0.6 mL) in a Teflon-valved valve NMR tube was added an excess of *tert*-butanol (5 mg, 0.068 mL) and the mixture heated at 120 ˚C for 12 h over which no dissolution of **P** was observed.

7.4.24 Attempted syntheses of [(MeOUO)$_2$(L)] from P

a. *From MeI*. To a brown slurry of **P** (25 mg 0.015 mmol based on best estimate of empirical formula) in d_5-pyridine (0.7 mL) in a Teflon-valved valve NMR tube was added a solution of methyl iodide (4 mg, 0.030 mmol, 2 equiv) in d_5-pyridine (0.3 mL) and the

mixture left for 12 h after which no **P** had dissolved. Heating the mixture for 24 h at 120 °C had no effect.

b. *From MeOTf*. To a brown slurry of **P** (10 mg 0.006 mmol based on best estimate of empirical formula) in d_5-pyridine (0.5 mL) in a Teflon-valved valve NMR tube was added a solution of methyl trifluoromethanesulfonate (2 mg, 0.012 mmol, 2 equiv) in d_5-pyridine (0.2 mL) and the mixture left for 12 h after which no **P** had dissolved. Heating the mixture for 24 h at 120 °C had no effect. NB: A preparative synthesis of the related oxo-alkylated complex [(^{i}PrOUO)$_2$(L)] may be found in section 7.4.11.

7.5 Synthetic procedures described in Chapter Five

7.5.1 Synthesis of [(UO_2)(py)(H_2L^A)] and [{UO_2(py)}$_2$(L^A)]

To a yellow solution of H_4L^A (100 mg, 0.116 mmol) in pyridine (2 mL) was added an orange solution of [UO_2{N(SiMe$_3$)$_2$}$_2$(py)$_2$] (174 mg, 0.232 mmol) in pyridine (2 mL) and the resulting brown solution stirred for 4 d at room temperature causing the precipitation of brown solids which were isolated by filtration and dried under vacuum at 100 °C for 1 h (85 mg, batch A, see below). The volume of the filtrate was then reduced under vacuum to 0.5 mL and left to stand at room temperature for 24 h resulting in the precipitation of crystals of [{UO_2(py)}$_2$(L^A)]. These were isolated by filtration and dried under vacuum for 1 h at 100 ˚C. The filtrate was left to stand at room temperature for one week resulting in the precipitation of a second batch of material which was isolated in the same manner. [{UO_2(py)}$_2$(L^A)] was collected as a brown crystalline solid which contained single crystals suitable for X-ray diffraction (50 mg, 0.032 mmol, 28 %). Batch A contained a 70:30 mixture of [UO_2(py)(H_2L^A)] and [{UO_2(py)}$_2$(L^A)], equating to 0.046 mmol (40 %) and 0.019 mmol (16 %), respectively. Characterising data for [{UO_2(py)}$_2$(L^A)]: ^{1}H NMR (d_5-pyridine): δ_H 9.16 (s, 2H, aryl), 9.09 (s, 4H, imine), 8.22 (s, 2H, aryl), 7.50 (d, J = 8 Hz, 4H, aryl), 7.30 (d, J = 4 Hz, 4H, pyrrole), 7.00 (t, J = 8 Hz, 4H, aryl), 6.86 (d, J = 8 Hz, 4H, aryl), 6.78 (d, J = 4 Hz, 4H, pyrrole), 2.48 (m, 8H, CH_2) 1.09 (t, J = 7 Hz, 6H, CH_3), 0.90 (t, J = 7 Hz, 6H, CH_3). ^{13}C{^{1}H} NMR (C_5H_5N): δ_C 162.2 (quaternary), 160.3 (aryl CH), 151.5 (quaternary), 137.2 (quaternary), 132.7 (quaternary), 128.1 (quaternary), 127.7 (aryl *C*H), 125.4 (aryl *C*H), 125.2 (aryl *C*H), 125.1 (aryl *C*H) 120.4 (pyrrole *C*H) 112.2 (pyrrole *C*H) 52.1 (meso- quaternary), 39.6 (*C*H$_2$), 38.6 (*C*H$_2$), 10.8 (*C*H$_3$), 10.5 (*C*H$_3$). Analysis. Found: C, 53.70; H, 3.76; N, 8.78 %. $C_{68}H_{58}N_{10}O_4U_2$ requires: C, 52.51; H, 3.76; N, 9.01 %. FTIR (Nujol mull, cm–1): ν 1595 (s), 1551 (m), 1306 (m), 1281 (s), 1258 (m), 112 (w), 1092 (w),

1060 (m), 1015 (m), 924 (m), 912 (m, UO_2^{2+} asymmetric stretch), 878 (w), 860 (w), 761 (w), 747 (w), 718(w).

Characterisation data from Batch A: Contains 0.3 equivalents of [{UO_2(py)}$_2$(L^A)] and 0.7 equivalents of [UO_2(py)(H_2L^A)]. ^{1}H NMR (d_5-pyridine): δ_H 9.63 (s, 2H, aryl) 9.38 (s, 2H, imine), 9.01 (s, 2H, NH), 8.14 (s, 2H, aryl), 8.10 (s, 2H, imine), 7.74 (d, J = 8 Hz, 2H, aryl), 7.56 (d, J = 4 Hz, 2H, pyrrole), 7.49 (d, J = 8 Hz, 2H, aryl), 7.32 (t, 2H, J = 8 Hz, aryl), 7.26 (t, J = 8 Hz, 2H, aryl), 7.01 (d, J = 8 Hz, 2H, aryl), 6.95 (d, J = 4 Hz, 2H, pyrrole), 6.59 (d, J = 8 Hz, 2H, aryl), 6.55 (d, J = 4 Hz, 2H pyrrole), 6.15 (d, J = 4 Hz, 2H pyrrole), 2.71 (q, J = 7 Hz, 2H, CH_2), 2.54 (q, J = 7 Hz, 2H, CH_2), 2.17 (q, J = 7 Hz, 2H, CH_2), 1.60 (q, J = 7 Hz, 2H, CH_2), 1.47 (t, J = 7 Hz, 2H, CH_3), 1.05 (t, J = 7 Hz, 2H, CH_3), 0.97 (t, J = 7 Hz, 2H, CH_3), 0.54 (t, J = 7 Hz, 2H, CH_3). MALDI (α-Cyano–4-hydroxycinnamic acid matrix): Fragment A: 1126.37 (100 %), 1127.43 (80 %), 1128.46 (100 %), 1129.51 (70 %), 1130.50 (17 %). fitted to $C_{58}H_{50}N_8O_2U$ 1128.46 (100.0%), 1129.46 (63.4%), 1130.46 (21.7%), 1131.47 (4.0%), 1129.45 (3.0%). Fragment B: 1370.48 (100 %) 1371.48 (58 %) 1372.48 (6 %) 1367.54 (3 %) fitted to $C_{56}H_{46}N_8O_4U_2$: 1370.47 (100.0%), 1371.47 (61.2%), 1372.47 (20.7 %), 1373.48 (3.6 %), 1371.46 (3.0 %), 1367.46 (1.5 %), 1373.47 (1.1 %). Fragment: C 1451.53 (100 %), 1452.53180 (72 %) 1453.54224 (22 %), 1454.54682 (3 %) fitted to $C_{61}H_{53}N_9O_4U_2$ 1451.52 (100.0 %), 1452.53 (66.7 %), 1453.53 (22.8 %), 1454.53 (5.9 %), 1452.52 (3.3 %), 1453.52 (2.2 %), 1448.52 (1.5%). Fragment: D 1526.55688 (100 %), 1527.554993 (100 %), 1528.55301 (35 %), 1529.55920 (3 %) fitted to $C_{66}H_{54}N_{10}O_4U_2$ 1526.53 (100.0 %), 1527.54 (72.2 %), 1528.54 (26.5 %), 1529.54 (7.4 %), 1527.53 (3.7 %), 1528.53 (2.7 %), 1523.53 (1.5 %), 1530.55 (1.2 %), 1524.53 (1.0 %) and $C_{54}H_{38}N_8O_4U_2$ 1126.36716 (100 %), 1128.41324 (100 %).

7.5.2 Unsuccessful synthesis of pure [(UO_2)(py)(H_2L^A)]

To a yellow solution of H_4L^A (10 mg, 0.012 mmol) in d_5-pyridine (0.3 mL) in a Teflon-valved valve NMR tube was added an orange solution of [UO_2{N($SiMe_3$)$_2$}$_2$(py)$_2$] (9 mg, 0.012 mmol) in d_5-pyridine (0.3 mL) and the resulting brown solution left for 24 h at room temperature after which [(UO_2)(py)(H_2L^A)], [(UO_2)(py)(H_2L^A)] and H_4L^A, were present in a 71 : 14.5 : 14.5 molar ratio, in addition to two equivalents of HN($SiMe_3$), as observed by ^{1}H NMR spectroscopy. Heating the mixture at 120 °C resulted in no change.

7.5.3 Unsuccessful synthesis of [{UO_2(py)}$_2$(L^A)] by a salt-elimination

To a yellow solution of H_4L^A (10 mg, 0.012 mmol) in d_5-pyridine (0.3 mL) in a Teflon-valved valve NMR tube was added a colourless solution of $KN(SiMe_3)_2$ (9 mg, 0.046 mmol, 4 equiv) in d_5-pyridine (0.3 mL) forming a fluorescent orange precipitate of K_4L^A [6] after 1 h. A solution of [$UO_2Cl_2(THF)_2$] (12 mg, 0.023 mmol, 2 equiv) in d_5-pyridine (0.4 mL) was then added forming a mixture of [(UO_2)(py)(H_2L^A)] and [{UO_2(py)}$_2$(L^A)] after 24 h at room temperature as evidenced by ^{1}H NMR spectroscopy.

7.5.4 Unsuccessful reductions of [{UO_2(py)}$_2$(L^A)]

a. *[$CoCp_2$]*. To a brown solution of [{UO_2(py)}$_2$(L^A)] (10 mg, 0.006 mmol) in d_5-pyridine (0.3 mL) in a Teflon-valved valve NMR tube was added a solution of [$CoCp_2$] (2 mg, 0.012 mmol, 2 equiv) in d_5-pyridine (0.3 mL). No reaction was observed even at elevated temperatures.

b. *[$UI_3(THF)_4$]*. To a brown solution of [{UO_2(py)}$_2$(L^A)] (15 mg, 0.01 mmol) in 1:1 THF:C_6D_6 (0.3 mL) in a Teflon-valved valve NMR tube was added a solution of [$UI_3(THF)_4$] (9 mg, 0.01 mmol) in 1:1 THF:C_6D_6 (0.3 mL) resulting in the immediate precipitation of intractable brown solids which could not be characterised.

c. *KC_8*. A brown solution of [{UO_2(py)}$_2$(L^A)] (13 mg, 0.008 mmol) in d_5-pyridine (0.5 mL) was poured onto solid KC_8 (2 mg, 0.017 mmol) resulting in the immediate formation of intractable brown solids which could not be characterised.

7.5.5 Synthesis of [UO_2(THF)(H_2L^F)]

To a yellow suspension of H_4L^F (1.90 g, 2.10 mmol) in THF (10 ml) was added an orange solution of [UO_2{$N(SiMe_3)_2$}$_2$($THF)_2$] (1.52 g, 2.10 mmol) in THF (10 ml) and the resulting orange suspension stirred for 12 h resulting in the formation of a brown solid suspended in a pale yellow solution. The supernatant liquors were decanted off and the remaining solid washed with THF (3 × 5 mL) and hexanes (5 mL) before drying under vacuum for 1 h. [$UO_2(THF)_2(H_2L^F)$] was collected as a brown solid (1.65 g, 1.32 mmol, 63 %) and was found to be completely insoluble in THF. Dissolution in d_5-pyridine results in conversion to the pyridine adduct and one equivalent of THF as evidenced by ^{1}H NMR spectroscopy.

7.5.6 Synthesis of [UO_2(py)(H_2L^F)]

To a yellow suspension of H_4L^F (2.00 g, 2.21 mmol) in pyridine (10 ml) was added an orange solution of [UO_2{$N(SiMe_3)_2$}$_2$($py)_2$] (1.66 g, 2.21 mmol) in pyridine (10 ml) and

the resulting orange suspension stirred for 12 h resulting in the dissolution of all solids to form a brown solution. The volume of the solution was then reduced under vacuum to 5 mL before addition of hexanes (40 ml) which resulted in the precipitation of brown solids which were isolated by filtration, washed hexanes (3 × 10 ml) and dried under vacuum for 1 h. $[UO_2(py)(H_2L^F)]$ was collected as a brown solid (1.99 g, 1.59 mmol, 72 %). Single crystals of the product suitable for X-Ray diffraction were grown by layering of hexane over a saturated pyridine solution. ^{1}H NMR (d_5-pyridine): δ_H 10.46 (bs, 2H, NH), 9.20 (s, 2H, imine), 8.46 (s, 2H, imine), 8.26 (d, 1H, J = 7.5 Hz, fluorenyl), 8.10 (d, 1H, J = 7.5 Hz, fluorenyl), 8.04 (d, 1H, J = 7.5 Hz, fluorenyl), 7.93 (d, 1H, J = 7.5 Hz, fluorenyl), 7.82 (d, 1H, J = 7.5 Hz, fluorenyl), 7.78 (d, 1H, J = 7.5 Hz, fluorenyl), 7.55 (d, 1H, J = 7.5 Hz, fluorenyl), 7.47 (d, 1H, J = 7.5 Hz, fluorenyl) 7.41 – 7.26 (m, 4H, J = 7.5 Hz, fluorenyl) 7.21 (1H, fluorenyl, hidden by solvent peak, assigned by COSY), 7.19 (d, 2H, J = 4 Hz, pyrrole), 7.11 (t, 1H, J = 7.5 Hz, fluorenyl), 6.94 (t, 1H, J = 7.5 Hz, fluorenyl), 6.80 (s, 2H, aryl), 6.66 (s, 2H, aryl), 6.58 (t, 1H, J = 7.5 Hz, fluorenyl), 6.35 (d, 2H, J = 4 Hz, pyrrole), 6.21 (d, 2H, J = 4 Hz, pyrrole), 5.62 (d, 2H, J = 4 Hz, pyrrole), 2.11 (s, 6H, CH_3), 2.07 ppm (s, 6H, CH_3). ^{13}C{^{1}H} NMR (C_5D_5N): δ_C 162.43 (imine), 157.68 (quaternary), 154.45 (quaternary), 153.49 (quaternary), 150.31 (imine), 150.10 (quaternary), 145.92 (quaternary), 142.85 (quaternary), 141.82 (quaternary), 140.31 (quaternary) 140.07 (quaternary), 139.73 (quaternary), 139.37 (quaternary), 138.08 (quaternary), 134.28 (quaternary), 133.34 (quaternary), 132.75 (quaternary), 129.14 (fluorenyl *C*H), 128.66 (fluorenyl *C*H), 128.47 (fluorenyl *C*H), 128.28 (fluorenyl *C*H), 128.15 (fluorenyl *C*H), 127.98 (fluorenyl *C*H), 127.93 (fluorenyl *C*H), 127.80 (fluorenyl *C*H), 127.29 (fluorenyl *C*H), 126.66 (fluorenyl *C*H), 126.11 (fluorenyl *C*H), 125.85 (fluorenyl *C*H), 125.18 (aryl *C*H), 123.06 (aryl *C*H), 121.19 (pyrrole *C*H), 120.70 (fluorenyl *C*H), 120.57 (fluorenyl *C*H), 120.53 (fluorenyl *C*H), 120.45 (fluorenyl *C*H), 117.38 (pyrrole *C*H), 112.35 (pyrrole *C*H), 109.57 (pyrrole *C*H), 62.56 (sp^3 quaternary), 56.33 (sp^3 quaternary), 18.98 (CH_3), 18.89 ppm (CH_3). One quaternary carbon is masked by the broad resonances attributed to the solvent. Analysis. Found: C, 63.06; H, 4.34; N, 9.94 %. $C_{67}H_{51}N_9O_2U$ requires: C: 64.26; H: 4.10; N: 10.07. FTIR (nujol, cm^{-1}): 3411 (w, NH), 1623 (w), 1577 (s), 1496 (w), 1297 (m), 1267 (m), 1218 (w), 1191 (w), 1160 (w), 1147 (w), 1080 (w), 1044 (m), 1004 (w), 912 (w, assym. UO_2^{2+}), 895 (s), 872 (w), 775 (m), 744 (s) 705 (w). Solubility: pyridine.

7.5.7 Synthesis of $[\{K(py)_2\}\{(UO_2)_2(\mu\text{-}O)(L^F)\}\{K(py)_3\}]$

To a yellow suspension of KOH-derived H_4L^F (208 mg, 0.23 mmol) in pyridine (2 ml) was added an orange solution of $[UO_2\{N(SiMe_3)_2\}_2(py)_2]$ (345 mg, 0.46 mmol, 2 equiv)

in pyridine (4 ml) and the resulting orange suspension boiled at 120 °C in a Teflon-tapped ampoule for 12 h resulting in the formation of a brown solution as well as a brown, intractable solid. The solution was isolated by filtration and reduced in volume to 2 mL under vacuum resulting in the precipitation of a red-brown solid. The first solid was found to be completely insoluble in pyridine, THF and CH_2Cl_2 and was discarded. The second solid was isolated by filtration, washed with hexanes (2 × 1 mL) and dried under vacuum for 1 h. [{K(py)$_2$}{(UO$_2$)$_2$(μ-O)(L^F)}{K(py)$_3$}] was isolated as red-brown solid (65 mg, 0.03 mmol, 15 %). Single crystals of the product suitable for analysis by X-ray diffraction were grown from a pyridine solution at room temperature. ^{1}H NMR (d_5-pyridine) δ_H 9.37 (s, 4H, imine), 8.77 (s, 2H, fluorenyl), 8.07 (d, 2H, J = 7.5 Hz, fluorenyl), 7.90 (d, 2H, J = 7.5 Hz, fluorenyl), 7.53 (m, 4H, J = 7.5 Hz, 2 × fluorenyl), 7.16 (t, 2H, J = 7.5 Hz, fluorenyl), 7.13 (s, 4H, aryl), 6.86 (t, 2H, J = 7.5 Hz, fluorenyl), 6.17 (d, 2H, J = 3.0 Hz, pyrrole), 2.01 (s, 2H, CH_2) 2.09. One resonance attributed to the fluorenyl fragment and one to the pyrrole protons are obscured by the pyridine solvent. Analysis. Found: C, 54.86; H, 3.61; N, 9.77 %. $C_{92}H_{74}N_{14}O_5K_2U_2$ requires: C, 54.98; H, 3.71; N, 9.76 %.FTIR (nujol, cm^{-1}): 1567 (s), 1500 (w), 1288 (s), 1275 (s), 1191 (w), 1160 (w), 1086 (w), 1051 (m), 1021 (w), 1006 (w), 960 (w), 922 (w, assym. UO_2^{2+}), 896 (m), 880 (m), 839 (m), 745 (m), 724 (s), 707 (w).

7.5.8 Attempted synthesis of [{K(py)$_x$}{(UO$_2$)$_2$(μ-OH)(L^F)}]

To a brown solution of [UO$_2$(py)(H$_2$L^F)] (100 mg, 0.079 mmol) and KOH (5 mg, 0.079 mmol) in pyridine (2 ml) was added an orange solution of [UO$_2${N(SiMe$_3$)$_2$}$_2$(py)$_2$] (60 mg, 0.079 mmol) in pyridine (2 ml) and the resulting brown solution stirred at room temperature for 12 h forming at least three unidentified products after the reaction period of which separation was not possible.

7.5.9 Attempted synthesis of [{K(py)$_x$}{(UO$_2$)$_2$(μ-OH)(L)}]

To a brown solution of [UO$_2$(py)(H$_2$L)] (20 mg, 0.027 mmol) in d_5-pyridine (0.3 mL) in a Teflon-valved valve NMR tube was added solid KOH (2 mg, 0.027 mmol) resulting in the formation of a red solution of [{K(py)$_x$}{UO$_2$(OH)(H$_2$L)}] as evidenced by ^{1}H NMR spectroscopy. A solution of [UO$_2${N(SiMe$_3$)$_2$}$_2$(py)$_2$] (15 mg, 0.027 mmol) in d_5-pyridine (0.3 mL) was then added resulting in the formation of several unidentified products after the reaction period of which separation was not possible.

7.5.10 Attempted synthesis of [{K(py)$_x$}{(UO$_2$)$_2$(μ-Cl)(L^F)}]

To a yellow solution of H$_4$L^F (15 mg, 0.017 mmol) in d_5-pyridine (0.3 mL) in a Teflon-valved valve NMR tube was added a colourless solution of K{N(SiMe$_3$)$_2$} (13 mg,

0.067 mmol, 4 equiv) in d_5-pyridine (0.3 mL) resulting in the formation of $[K_4(L^F)]^6$ and 4 equivalents of $HN(SiMe_3)_2$ after 12 h. The mixture was poured onto a suspension of $[UO_2Cl_2(THF)_2]$ (16 mg, 0.017 mmol) in d_5-pyridine (0.3 mL) and left for 12 h resulting in the formation of $[UO_2(py)(H_2L^F)]$ as well as other identified products by ^{1}H NMR spectroscopy. Boiling the mixture at 120 °C for 12 h resulted in no further change.

7.5.11 Attempted synthesis of $[\{K(py)_x\}\{(UO_2)_2(\mu\text{-}F)(L)\}]$

To a brown solution of $[UO_2(py)(H_2L)]$ (20 mg, 0.019 mmol) and KF (1mg, 0.019 mmol) in d_5-pyridine (0.3 mL) in a Teflon-valved valve NMR tube was added a solution of $[UO_2\{N(SiMe_3)_2\}_2(py)_2]$ (15 mg, 0.019 mmol) in d_5-pyridine (0.3 mL) resulting in the slow formation of intractable brown solids as well as unreacted $[UO_2(py)(H_2L)]$ after one week at room temperature.

7.5.12 Synthesis of $[(UO_2)_2\{\mu\text{-}O(CH_2)_4(C_5H_5N)\}(L^F)\}]$

To a a yellow suspension of KOH-derived H_4L^F (132 mg, 0.15 mmol) in pyridine (2 ml) was added an orange solution of $[UO_2\{N(SiMe_3)_2\}_2(THF)_2]$ (215 mg, 0.29 mmol) in pyridine (2 mL) and the mixture boiled at 120 °C in a Teflon-tapped ampoule for 24 h resulting in the precipitation of a brown solids. These was isolated by filtration, washed with hexane (3 × 2 mL) and dried under vacuum for 1 h (170 mg). Analysis of the bulk solid by ^{1}H NMR spectroscopy showed it to be composed of THF, $[UO_2(THF)(H_2L^F)]$, $[(Me_3OUO)_2L^F)]$ and $[(UO_2)_2\{\mu\text{-}O(CH_2)_4(C_5H_5N)\}(L^F)\}]$ as well as intractable material. Single crystals of $[(UO_2)_2\{\mu\text{-}O(CH_2)_4(C_5H_5N)\}(L^F)\}]$ suitable for analysis by X-ray diffraction were grown at room temperature from the pyridine supernatant which was layered with the hexane washings during workup and left for one week. These were isolated by filtration, after extraction of single crystals for diffraction studies, and dried under vacuum for 1 h. $[(UO_2)_2\{\mu\text{-}O(CH_2)_4(C_5H_5N)\}(L^F)\}]$ was isolated as a brown solid (20 mg, 0.01 mmol, 9 %). ^{1}H NMR (d_5-pyridine): δ_H 9.34 (s, 4H, imine), 8.73 (s, 2H, fluorenyl), 8.05 (d, 2H, J = 7.5 Hz, fluorenyl), 7.92 (d, 2H, J = 7.5 Hz, fluorenyl), 7.56 (t, 2H, J = 7.5 Hz, fluorenyl), 7.23 (d, 4H, pyrrole), 7.18 (t, 2H, J = 7.5 Hz, fluorenyl),7.13 (t, 2H, J = 7.5 Hz, fluorenyl), (6.87 (t, 2H, J = 7.5 Hz, fluorenyl), 6.20 (d, 2H, J = 3.0 Hz, pyrrole), 2.12 (s, 2H, CH_2) 2.09 (s, 2H, CH_2), 2.03 ppm (s, 2H, CH_2) and 2.01 ppm (s, 12H, CH_3). One resonance attributed to the fluorenyl fragment and one to the aryl ring are obscured by the pyridine solvent and resonances attributed to the asymmetric $C_5H_5N(CH_2)_4O$ species are too small to discern. Trace amounts of $[UO_2(py)(H_2L^F)]$ are also present in the isolated material.

7.5.13 Synthesis of [(Me$_3$SiOUO)$_2$(L^F)]

To a yellow slurry of H_4L^F (20 mg, 0.022 mmol) in d_5-pyridine (0.4 ml) in a Teflon-valved valve NMR tube was added an orange solution of $[UO_2\{N(SiMe_3)_2\}_2(py)_2]$ (41.4 mg, 0.055 mmol, 2.5 equiv) in d_5-pyridine (0.4 ml) and the resulting orange slurry boiled for 12 h at 120 °C. The volatiles were then evaporated under vacuum and the resulting brown residue dried at 90 °C for 2 h before addition of d_5-pyridine (0.7 ml) which resulted in partial dissolution of the brown residue to form a brown solution and insoluble brown precipitate. $[(Me_3SiOUO)_2(L^F)]$ was the only product present in solution by ^{1}H NMR spectroscopy. ^{1}H NMR (d_5-pyridine): δ_H 21.09 (s, 2H, fluorenyl), 14.36 (s, 18H, Si*Me*$_3$), 12.63 (s, 4H, pyrrole), 12.15 (s, 2H, fluorenyl), 9.49 (s, 2H, fluorenyl), 8.49 (s, 2H, fluorenyl), 8.28 (s, 4H, pyrrole), 7.92 (s, 4H, imine), 6.24 (s, 2H, fluorenyl), 3.83 (s, 2H, fluorenyl), -0.25 (s, 2H, fluorenyl), –2.75 (s, 12H, methyl), –3.24 (s, 4H, aryl), –11.43 (s, 2H, fluorenyl). Solubility: pyridine, THF, toluene (partial).

7.5.14 Synthesis of [(PhMe$_2$SiOUO)$_2$(L^F)]

To a brown solution of $[UO_2(py)(H_2L^F)]$ (15 mg, 0.012 mmol) in d_5-pyridine (0.4 ml) in a Teflon-valved valve NMR tube was added an orange solution of $[UO_2\{N(SiMe_2Ph)_2\}_2(py)_2]$ (17.9 mg, 0.018 mmol, 1.5 equiv) in d_5-pyridine (0.3 ml) and the mixture heated for 12 h at 120 °C resulting in the formation of a brown solution and a brown precipitate. $[(Me_3SiOUO)_2(L^F)]$ and $HN(SiMe_2Ph)_2$ were the only products present in solution by ^{1}H NMR spectroscopy after the reaction period. ^{1}H NMR (d_5-pyridine): δ_H 21.24 (d, 2H, J = 7 Hz, fluorenyl), 16.18 (s, 12H, Si*Me*$_2$Ph), 15.87 (d, J = 7 Hz, 4H, SiMe$_2$*Ph*), 12.48 (s, 4H, pyrrole), 12.17 (t, 2H, J = 7 Hz, fluorenyl), 9.50 (t, 2H, J = 7 Hz, fluorenyl), 8.87 (t, 4H, J = 7 Hz, SiMe$_2$*Ph*), 8.47 (d, 2H, J = 7 Hz, fluorenyl), 8.12 (t, 2H, J = 7 Hz, SiMe$_2$*Ph*), 8.06 (s, 4H, pyrrole), 7.78 (m, HN(Si*Me*$_2$Ph + imine), 7.45 (m, HN(Si*Me*$_2$Ph), 6.24 (d, 2H, J = 7 Hz, fluorenyl), 3.86 (t, 2H, J = 7 Hz, fluorenyl), 0.42 (s, *H*N(SiM*e*$_2$Ph), -0.21 (t, 2H, J = 7 Hz, fluorenyl), –2.64 (s, 12H, methyl), –3.57 (s, 4H, aryl), –11.30 (d, 2H, J = 7 Hz, fluorenyl).

7.5.15 Synthesis of soluble [UO$_2$(HL^T)]

To a pale pink solution of H_3L (62 mg, 0.112 mmol) in d_5-pyridine (0.3 mL) in a Teflon-valved valve NMR tube was added an orange solution of $[UO_2\{N(SiMe_3)_2\}_2(py)_2]$ (84 mg, 0.112 mmol) in d_5-pyridine (0.3 mL) forming a brown solution of $(UO_2(HL^T)]$ and two equivalents of $HN(SiMe_3)_2$ as the only products observed by ^{1}H NMR spectroscopy after 12 h. ^{1}H NMR (d_5-pyridine): δ_H 11.78 (s, 1H, N*H*), 9.44 (s, 2H, imine), 8.25 (s, 1H, imine),

7.09 (d, 2H, J = 3 Hz, pyrrole), 6.81 (bs, 1H, J pyrrole), 6.70 (bs, 1H, J pyrrole), 6.51 (d, 2H, J = 3 Hz, pyrrole), 3.27 (t, 2H, J = 12 Hz, cyclohexyl), 3.08 (t, 1H, J = 12 Hz, cyclohexyl), 2.53 (s, 3H, CH_3), 2.08 (d, 2H, cyclohexyl), 1.97 (d, 2H, cyclohexyl), 1.70 (m, 8H, cyclohexyl), 1.60 – 1.00 (m, cyclohexyl) 14H, 0.81 (m, 4H, cyclohexyl), 0.20 (s, 36H, HN{Si(CH_3)$_3$}$_2$. Analysis. Found: C, 51.15; H, 5.72; N, 10.25 %. $C_{35}H_{45}N_6O_2U_2$ requires: C, 51.28; H, 5.53; N, 10.25 %. FTIR (nujol, cm^{-1}): 3462 (w, NH), 3370 (w, NH), 1634 (m, imine), 1603 (s, imine), 1562 (w) 1489 (w), 1448 (s), 1207 (w) 1118 (w), 1007 (w), 1043 (w), 1014 (w), 964 (w), 916 (s, assym UO_2^{2+} stretch) 891 (w), 849 (w), 761 (m), 726 (w), 707 (w), 685 (w).

7.5.16 Synthesis of [(UO$_2$)(L^T)] gel

a. A brown solution of [(UO$_2$)(HL^T)] (0.030 mmol) in d_5-pyridine (0.6 mL) was prepared as above in a Teflon-valved valve NMR tube and the volatiles evaporated under vacuum before C_6D_6 (0.5 ml) was added to the resulting brown residue forming a brown solution which, after shaking for 10 s, formed an immobile gel. Removal of the solvent under vacuum and redissolution in d_5-pyridine (0.5 mL) or THF (0.5 ml) resulted in the reformation of a soluble phase with addition of an equal volume toluene, benzene or hexanes to the solution instigating gelation. Heating of the gel to 67 °C in pure benzene resulted in the formation of a soluble phase which reverted back to a gel upon slow cooling over 12 h.

b. To a pale pink solution of H_3L (10 mg, 0.018 mmol) in C_6D_6 (0.3 mL) in a Teflon-valved valve NMR tube was added a solution of [UO$_2${N(SiMe$_3$)$_2$}$_2$(py)$_2$] (14 mg, 0.018 mmol) in C_6D_6 (0.3 mL) resulting in the immediate formation of a brown solution. Shaking of the solution for 10 s resulted in the formation of an immobile gel. Removal of the solvent under vacuum, drying the resultant brown residue for 12 h before addition of d_5-pyridine (0.5 mL) resulted in the full dissolution of all material and [UO$_2$(HL^T)] and trace H_3L^T being the only products observed by ^{1}H NMR spectroscopy.

7.5.17 Attempted de-aggregations of [(UO$_2$)(L^T)] gel

a. *With Me$_4$NCl.* To a freshly prepared sample of the [(UO$_2$)(HL^T)] gel (0.030 mmol) in C_6D_6 (0.7 mL) in a Teflon-valved valve NMR tube was added excess solid tetramethyl ammonium chloride (Me_4NCl) (10 mg, 0.091 mmol) and the mixture heated to 67 °C resulting in the dissolution of all solids to form a brown solution. No gelation was observed upon cooling to room temperature, however no evidence for the formation [Me$_3$N][(UO$_2$)(Cl)(HL^T)] was observed with H_3L^T and HN(SiMe$_3$)$_2$ the only products visible by ^{1}H NMR spectroscopy.

b. *With KCl.* To a freshly prepared sample of the [$(UO_2)(HL^T)$] gel (0.030 mmol) in C_6D_6 (0.7 mL) in a Teflon-valved valve NMR tube was added excess KCl (10 mg, 0.134 mmol) and the mixture heated to 67 °C resulting in the dissolution of all solids to form a brown solution. No gelation was observed upon cooling to room temperature, however no evidence for the formation K[$(UO_2)(Cl)(HL^T)$] was observed with H_3L^T and $HN(SiMe_3)_2$ the only products visible by ^{1}H NMR spectroscopy.

c. *With KF*. To a freshly prepared sample of the [$(UO_2)(HL^T)$] gel (0.030 mmol) in C_6D_6 (0.7 mL) in a Teflon-valved valve NMR tube was added excess KCl (5 mg, 0.086 mmol) and the mixture heated to 67 °C resulting in the dissolution of all solids to form a brown solution. No gelation was observed upon cooling to room temperature, however no evidence for the formation K[$(UO_2)(F)(HL^T)$] was observed with H_3L^T and $HN(SiMe_3)_2$ the only products visible by ^{1}H NMR spectroscopy.

d. *With pyridine-N-oxide.* To a freshly prepared sample of the [$(UO_2)(HL^T)$] gel (0.018 mmol) in C_6D_6 (0.6 mL) in a Teflon-valved valve NMR tube was added a solution of pyridine-*N*-oxide (2 mg, 0.018) mmol) in C_6D_6 (0.3 mL) resulting in the dissolution of all solids to form a brown solution after 30 min. No evidence for the formation [$(UO_2)(C_5H_5NO)(HL^T)$] was observed with H_3L^T, $HN(SiMe_3)$, and pyridine-N-oxide being the only products visible by ^{1}H NMR spectroscopy.

e. *With Ph_3PO.* To a freshly prepared sample of the [$(UO_2)(HL^T)$] gel (0.036 mmol) in C_6D_6 (0.6 mL) in a Teflon-valved valve NMR tube was added a solution of triphenyl phosphine oxide (20 mg, 0.072 mmol, 2 equiv) in C_6D_6 (0.3 mL) resulting in the dissolution of all solids to form a brown solution after 1 d. No evidence for the formation [$(UO_2)(Ph_3PO)(HL^T)$] was observed with the formation of a number of unidentified products visible by ^{1}H NMR spectroscopy.

f. *With $LiN(SiMe_3)_2$.* To a freshly prepared sample of the [$(UO_2)(HL^T)$] gel (0.018 mmol) in C_6D_6 (0.6 mL) in a Teflon-valved valve NMR tube was added a solution of $LiN(SiMe_3)_2$ (4 mg, 0.018 mmol, 1 equiv) in C_6D_6 (0.3 mL) resulting in the dissolution of all solids to form a red-brown solution after 2 h. No evidence for the formation [$Li(py)_x$][$(UO_2)\{N(SiMe_3)_2\}(HL^T)$] was observed with the formation of a number of unidentified products instead observed by ^{1}H NMR spectroscopy. Single crystals of [$Li_6(L^T)_2$] were grown from the mixture after one week.

7.5.18 Synthesis of $[Li_6(L^T)_2]$

To a pale pink solution of H_3L (100 mg, 0.181 mmol) in benzene (3 mL) was added a solution of $LiN(SiMe_3)_2$ (108 mg, 0.543 mmol) in benzene (3 mL) forming a pale pink solution which was reduced in volume to 2 mL under vacuum resulting in the precipitation of a pink solid. Immersion of the reaction vessel in a boiling water bath caused the solid to redissolve and colourless crystals of pure $[Li_6(L^T)_2]$ were formed upon slow cooling. These were isolated by filtration and dried for under vacuum for 1 h with the product isolated as a white crystalline solid. ^{1}H NMR (C_6D_6): δ_H 7.55 (s, 3H, imine), 6.86 (d, 3H, J = 3 Hz, pyrrole), 6.66 (bs, 3H, J = 3 Hz pyrrole), 2.78 (s, 3H, CH_3), 2.32 (m, 3H, cyclohexyl), 1.60 (m, 6H, cyclohexyl), 1.47 (m, 3H, cyclohexyl), 1.2–0.9 (m, 16H, cyclohexyl), 0.41 (m, 6H, cyclohexyl). All other data reported previously.[22]

7.5.19 Attempted synthesis of $[UO_2(py)\{Li(py)_x\}(L^T)]$

a. To a colourless solution of $[Li_6(L^T)_2]$ (10 mg, 0.009 mmol) in C_6D_6 (0.3 mL) in a Teflon-valved valve NMR tube was added a yellow suspension of $[UO_2Cl_2(THF)_2]$ (9 mg, 0.018 mmol) in C_6D_6 (0.3 mL) resulting in the formation of intractable brown solid. The volatiles were then evaporated under vacuum and the resultant brown residue dissolved in d_5-pyrdine (0.6 mL) and was found to contain $[UO_2(HL^T)]$ and H_3L by ^{1}H NMR spectroscopy.

b. To a pale pink solution of H_3L^T (10 mg, 0.018 mmol) in C_6D_6 (0.3 mL) in a Teflon-valved valve NMR tube was added a red solution of $[Li(py)_2][UO_2\{N(SiMe_3)_2\}_2(py)_2]$ (17 mg, 0.018 mmol) in C_6D_6 forming a brown intractable solid which was not characterised further.

7.5.20 Attempted synthesis of $[U(L^T)]$

a. *From $[Li_6(L^T)_2]$and $UI_3(THF)_4$.* To a colourless solution of $[Li_6(L^T)_2]$ (10 mg, 0.009 mmol) in C_6D_6 (0.3 mL) in a Teflon-valved valve NMR tube was added a blue suspension of $[UI_3(THF)_4]$ (16 mg, 0.018 mmol) in benzene (0.3 mL) inducing the precipitation of dark solids. Heating the mixture to 80 °C resulted in the dissolution of the majority of the solid after which it was determined by ^{1}H NMR spectroscopy that no reaction had occurred. Heating the mixture at 80 °C for 12 h resulted in no change.

b. *From $[K_3(L^T)]$ and $UI_3(THF)_4$.* To a pale pink solution of H_3L^T (10 mg, 0.018 mmol) in C_6D_6 (0.3 mL) in a Teflon-valved valve NMR tube was added a colourless solution of $KN(SiMe_3)_2$ (11 mg, 0.054 mmol, 3 equiv) in C_6D_6 (0.3 mL) resulting in the immediate

precipitation of pink [$K_3(L^T)$] to which was added a blue suspension of [$UI_3(THF)_4$] (16 mg, 0.018 mmol) in C_6D_6 (0.4 mL). No dissolution of the potassium salt was observed upon heating the mixture to 80 °C. Removal of the solvent under vacuum before addition of THF (0.6 mL) did not dissolve the mixture.

7.5.21 Attempted synthesis of [UI(L^T)]

To a partial suspension of [$Li_6(L^T)_2$] (14 mg, 0.013 mmol) in C_6D_6 (0.3 mL)) in a Teflon-valved valve NMR tube was added a red solution of $UI_4(OEt_2)_4$ (23 mg, 0.026 mmol) in benzene (0.3 mL) with no colour change or dissolution of the residual lithium salt observed after 12 h. Heating the mixture at 80 °C for 12 h resulted in the full dissolution of all materials although no reaction was observed by ^{1}H NMR spectroscopy.

7.5.22 Attempted synthesis of [$UO_2(L^M)$]

a. *By transamination between H_2L^M and [UO_2{$N(SiMe_3)_2$}$_2(py)_2$]*. To a colourless solution of H_2L^M (12 mg, 0.026 mmol) in C_6D_6 (0.3 mL) in a Teflon-valved valve NMR tube was added an orange solution of [UO_2{$N(SiMe_3)_2$}$_2(py)_2$] (19 mg, 0.026 mmol) in C_6D_6 (0.3 mL) with no reaction observed by ^{1}H NMR spectroscopy after one week. Heating the mixture to 60 °C resulted in the decomposition of the [UO_2{$N(SiMe_3)_2$}$_2(py)_2$] to form a brown solution of $HN(SiMe_3)_2$ and a brown solid.

b. *By salt elimination from [$Li_2(L^M)$] and [$UO_2Cl_2(THF)_2$]*. To a colourless solution of H_2L^M (10 mg, 0.022 mmol) in C_6D_6 (0.3 mL) in a Teflon-valved valve NMR tube was added a colourless solution of $LiN(SiMe_3)_2$ (7 mg, 0.044 mmol, 2 equiv) in C_6D_6 (0.3 mL) resulting in the formation of a solution of [$Li_2(L^M)$] after 30 min by ^{1}H NMR spectroscopy. The mixture was poured onto a suspension of [$UO_2Cl_2(THF)_2$] in C_6D_6 (0.3 mL) resulting in the formation of a brown intractable solid that could not be characterised further.

7.5.23 Attempted synthesis of [$UO_2(L^M)(py)_x$]

To a colourless solution of H_2L^M (100 mg, 0.222 mmol) in pyridine (2 mL) was added $LiN(SiMe_3)_2$ (74 mg, 0.544 mmol, 2 equiv) in pyridine (2 mL) and the resulting colourless solution stirred for 12 h. The solution was then added, drop-wise, to a yellow suspension of [$UO_2Cl_2(THF)_2$] (108 mg, 0.222 mmol) in pyridine (2 mL) forming a brown solution after stirring for 12 h. The volatiles were then removed under vacuum and the ensuing brown residue dried for 1 h under vacuum. Analysis of the material by ^{1}H NMR spectroscopy (2 × 10 mg samples in 0.5 mL C_6D_6 or C_5D_5N) revealed a mixture of several unidentified compounds and not the formation of the target product.

7.5.24 Unsuccessful synthesis of $[UO_2(py)_2(H_2L)]$ from $[UO_2(OAc)_2]$

To a yellow suspension of $[UO_2(OAc)_2]$ (1.50 g, 3.57 mmol) in pyridine (5 mL) was a yellow solution of H_4L (2.55 g, 3.57 mmol) in pyridine (5 mL) and the mixture boiled for 12 h over which no dissolution of $[UO_2(OAc)_2]$ was observed.

7.5.25 Synthesis of $[UO_2\{OOC(CH_2)_4CH_3\}_2]$

To a yellow suspension of $[UO_2(OAc)(H_2O)_2]$ (1.50 g, 3.54 mmol) in THF (10 mL) was added hexanoic acid (1.2 mL, 8.9 mmol, 2.5 equiv) and the mixture stirred for 30 min resulting in the complete dissolution of starting material to form a yellow solution. The volatiles were then evaporated under vacuum and the resulting solid dried at 120 °C for 24 h. The crude product was washed with dry hexane (3 × 5 mL) under an atmosphere of dinitrogen before drying under vacuum for 30 min. $[UO_2\{OOC(CH_2)_4CH_3\}_2]$ was collected as a bright yellow solid (1.60 g, 3.21 mmol, 91 %). ^{1}H NMR (C_6D_6): δ_H 3.55 (br, 4H, CH_2), 2.26 (br, 4H, CH_2), 1.47 (br, 4H, CH_2), 1.34 (q, 4H, J = 7 Hz, CH_2), 0.86 ppm (t, 6H, J = 7 Hz, CH_3). $^{13}C\{^1H\}$ NMR (C_6D_6): δ_C 39.56 (CH_2), 31.98 (CH_2), 25.38 (CH_2), 22.89, (CH_2), 14.17 ppm (CH_3). Analysis. Found: C, 28.81; H, 4.43; %. $C_{12}H_{22}O_4U_2$ requires: C, 27.50; H, 4.48; N, < 0.1 %.FTIR (nujol, cm^{-1}): 1596 (m), 1538 (s, CO_2^-), 1399 (s), 1340 (m), 1286 (m), 1261 (w), 1226 (m), 1218 (w), 1112 (m), 945 (s, UO_2^{2+} assym. stretch) 729 (m), 649 (w). Solubility: pyridine, THF, toluene, benzene and hexane.

7.5.26 Synthesis of $[UO_2(py)_2(H_2L)]$ from $[UO_2\{OOC(CH_2)_4CH_3\}_2]$

To a solution of H_4L (20.0 mg, 0.03 mmol) in d_5-pyridine (0.3 mL) was added a solution of $[UO_2\{OOC(CH_2)_4CH_3\}_2]$ (15.1 mg, 0.03 mmol) in d_5 pyridine (0.3 mL) resulting in the formation of $[UO_2(py)_2(H_2L)]$ and $[H_8L][C_5H_{11}COO]$ as the only observable products by ^{1}H NMR spectroscopy after 20 h.

7.5.27 Synthesis of $[UO_2(py)_2(H_2L)]$ from $[UO_2Cl_2(THF)_2]$

To a yellow solution of H_4L (2.05 g, 3.10 mmol) in pyridine (5 mL) was added a yellow suspension of $[UO_2Cl_2(THF)_2]$ (1.00 g, 2.07 mmol) in pyridine (5 mL) resulting in the formation of a brown solution and the bright orange precipitate $[H_4L]\cdot 4[HCl]$. The resulting mixture was then stirred for 12 h before filtration through a Celite pad and removal of half the solvent under vacuum. Hexanes (20 mL) were then added resulting in the precipitation of a brown solid which was isolated by filtration and washed with hexane (3 × 5 mL). $[UO_2(py)(H_2L)]$ was collected as a brown solid yield 1.41g, 1.40 mol, 68 %. All characterisation data has been reported previously.

7.6 References

1 G. A. Bain, J. F. Berry, *J. Chem. Educ.* **2008**, *85*, 532.

2 G. Sheldrick, *Acta Crystallogr., Sect. A* **2008**, *64*, 112-122.

3 L. Palatinus, G. Chapuis, *J. Appl. Crystallogr.* **2007**, *40*, 786-790.

4 L. Farrugia, *J. Appl. Crystallogr.* **1999**, *32*, 837-838.

5 G. Givaja, M. Volpe, J. W. Leeland, M. A. Edwards, T. K. Young, S. B. Darby, S. D. Reid, A. J. Blake, C. Wilson, J. Wolowska, E. J. L. McInnes, M. Schröder, J. B. Love, *Chem. Eur. J.* **2007**, *13*, 3707-3723.

6 E. Askarizadeh, A. M. J. Devoille, D. M. Boghaei, A. M. Z. Slawin, J. B. Love, *Inorg. Chem.* **2009**, *48*, 7491-7500.

7 J. L. Sessler, W.-S. Cho, V. Lynch, V. Král, *Chem. Eur. J.* **2002**, *8*, 1134-1143.

8 M. P. Wilkerson, C. J. Burns, R. T. Paine, B. L. Scott, *Inorg. Chem.* **1999**, *38*, 4156-4158.

9 D. M. Barnhart, C. J. Burns, N. N. Sauer, J. G. Watkin, *Inorg. Chem.* **1995**, *34*, 4079-4084.

10 P. L. Arnold, E. Hollis, F. J. White, N. Magnani, R. Caciuffo, J. B. Love, *Angew. Chem., Int. Ed. Engl.* **2011**, *50*, 887-890.

11 M. J. Monreal, R. K. Thomson, T. Cantat, N. E. Travia, B. L. Scott, J. L. Kiplinger, *Organometallics* **2011**, *30*, 2031-2038.

12 L. R. Avens, D. M. Barnhart, C. J. Burns, S. D. McKee, W. H. Smith, *Inorg. Chem.* **1994**, *33*, 4245-4254.

13 C. D. Carmichael, N. A. Jones, P. L. Arnold, *Inorg. Chem.* **2008**, *47*, 8577-8579.

14 W. G. Van der Sluys, C. J. Burns, J. C. Huffman, A. P. Sattelberger, *J. Am. Chem. Soc.* **1988**, *110*, 5924-5925.

15 S. M. Mansell, B. F. Perandones, P. L. Arnold, *J. Organomet. Chem.* **2010**, *695*, 2814-2821.

16 W. J. Evans, D. B. Rego, J. W. Ziller, *Inorg. Chem.* **2006**, *45*, 3437-3443.

17 D. R. Armstrong, D. V. Graham, A. R. Kennedy, R. E. Mulvey, C. T. O'Hara, *Chem. Eur. J.* **2008**, *14*, 8025-8034.

18 W. J. Evans, M. A. Ansari, J. W. Ziller, S. I. Khan, *Inorg. Chem.* **1996**, *35*, 5435-5444.

19 Jean C. Berthet, M. Lance, M. Nierlich, M. Ephritikhine, *Eur. J. Inorg. Chem.* **2000**, *2000*, 1969-1973.

20 L. E. Manzer, *Inorg. Synth.* **1982**, *21*, 135-140.

21 H. C. Brown, S. U. Kulkarni, *J. Organomet. Chem.* **1979**, *168*, 281-293.

22 J. S. Hart, F. J. White, J. B. Love, *Chem. Commun.* **2011**, *47*, 5711-5713.

23 P. L. Arnold, D. Patel, C. Wilson, J. B. Love, *Nature* **2008**, *451*, 315-317.

24 P. L. Arnold, A.-F. Pécharman, E. Hollis, A. Yahia, L. Maron, S. Parsons, J. B. Love, *Nature Chem.* **2010**, *2*, 1056-1061.

Appendix 1: Published papers

nature chemistry

ARTICLES

PUBLISHED ONLINE: 21 FEBRUARY 2012 | DOI: 10.1038/NCHEM.1270

Strongly coupled binuclear uranium–oxo complexes from uranyl oxo rearrangement and reductive silylation

Polly L. Arnold[1†]*, Guy M. Jones[1], Samuel O. Odoh[2], Georg Schreckenbach[2], Nicola Magnani[3,4] and Jason B. Love[1†]*

The most common motif in uranium chemistry is the d^0f^0 uranyl ion $[UO_2]^{2+}$ in which the oxo groups are rigorously linear and inert. Alternative geometries, such as the *cis*-uranyl, have been identified theoretically and implicated in oxo-atom transfer reactions that are relevant to environmental speciation and nuclear waste remediation. Single electron reduction is now known to impart greater oxo-group reactivity, but with retention of the linear OUO motif, and reactions of the oxo groups to form new covalent bonds remain rare. Here, we describe the synthesis, structure, reactivity and magnetic properties of a binuclear uranium–oxo complex. Formed through a combination of reduction and oxo-silylation and migration from a *trans* to a *cis* position, the new butterfly-shaped Si–OUO_2UO–Si molecule shows remarkably strong U^V–U^V coupling and chemical inertness, suggesting that this rearranged uranium oxo motif might exist for other actinide species in the environment, and have relevance to the aggregation of actinide oxide clusters.

The linear uranyl dication $[O{=}U{=}O]^{2+}$ is present in the majority of known uranium compounds. It contains strongly covalently bound, rigorously axial oxo groups that exhibit almost no chemistry[1]. Like its heavier, highly radioactive neptunyl and plutonyl congeners, the singly reduced pentavalent uranyl cation $[O{=}U{=}O]^{+}$ retains the linear, strongly covalent metal dioxo core, but exhibits an enhanced oxo basicity[2–4]. This results in the formation of cation–cation clusters through coordination of the oxo groups to other uranyl centres[5] and causes unwanted precipitation in nuclear waste processing streams[6]. The enhanced oxo-basicity also facilitates electron transfer between U^V cations in disproportionation reactions, allowing the desirable removal of uranium from groundwater as insoluble U^{IV} salts[7]. The pentavalent uranyl cation, $[UO_2]^+$ (refs 2,8), is unstable in water and has therefore been difficult to study, but recent investigations under anaerobic conditions have allowed both T-shaped and diamond-shaped cation–cation interactions (CCIs) in $[UO_2]^+$ complexes to be stabilized[9,10], and have also allowed coordination of other metal cations by the uranyl oxo groups.

We previously reported the syntheses of Pacman-shaped mono-uranyl complexes of the Schiff-base polypyrrolic macrocycle L, $[UO_2(S)(H_2L)]$ **1** (Fig. 1, S = tetrahydrofuran (THF) or pyridine (py)), from transamination reactions of H_4L and the uranyl silylamide $[UO_2\{N(SiMe_3)_2\}_2(THF)_2]$. We attributed our inability to coordinate a second uranyl group in the vacant N_4-donor pocket to the lack of space remaining in the macrocyclic cleft for another *trans*-dioxo group[11]. However, the presence of this compartment allowed us to make a variety of heterobimetallic complexes by substitution of the remaining two acidic hydrogens with *d* and 4*f* metals with no axial ligand requirements[12,13]. Furthermore, we demonstrated that potassium or lithium base activation of the uranyl oxo groups promoted unprecedented UO–Si and UO–H bond-forming reactions[14–16]. Other than these examples, the formation of covalent oxygen-element bonds in uranyl chemistry remains restricted to a few discrete silyl complexes[17,18].

In contrast to the ubiquitous *trans* arrangement of the uranyl oxo groups, the *cis* motif presents a fascinating synthetic target that is as yet unseen in any experimental uranium chemistry[19,20]. The *cis* isomer appears to play a particularly important role in ligand exchange processes between uranium centres in uranyl hydroxides and aquo complexes[21–25], species that are prevalent in high-pH nuclear wastes[26–28]. In acid solutions, both T-shaped tris(oxo) and *cis*-uranyl geometries have been invoked as intermediates in proton transfer reactions that lead to uranyl oxo-group exchange, a process that remains poorly understood[29–32]. Also, uranium lies directly below the group 6 transition metals, the dioxo complexes of which are widespread in both enzymatic and industrial oxidation catalysis[33] and can adopt either the *cis*- or *trans*-dioxo geometry, depending on *d*-electron configuration. Regardless of electron count, all actinyl structures reported to date have linear AnO_2^{n+} geometries. However, theoretical work has shown that the *cis*-uranyl should be energetically accessible at 18 kcal mol^{-1} above the *trans* isomer.

Here, we show that mixing solutions of the binucleating macrocycle H_4L and excess quantities of uranyl silylamide complexes results in an unprecedented butterfly-shaped U^V oxo dimer. This compound displays a new structural motif for high-valent uranium in which one of the four traditionally inert uranyl oxo groups in the reagents has moved into a *cis* site, affording a tightly bound U_2O_2 core. Also, the two exogenous oxo groups of this molecule are silylated during the synthesis to form a bis(U^VU^V)dioxo core of remarkable air stability and with an extremely strong U–U electronic interaction.

Results and discussion

Synthesis of reductively silylated binuclear uranium–oxo complexes. Reactions between pyridine solutions of the mono(uranyl) Pacman

[1]EaStCHEM School of Chemistry, University of Edinburgh, Edinburgh EH9 3JJ, UK, [2]Department of Chemistry, University of Manitoba, Winnipeg, Manitoba, Canada R3T 2N2, [3]Chemical Sciences Division, Lawrence Berkeley National Laboratory, 1 Cyclotron Road, Stop 70A1150, Berkeley, California 94720-8175, USA, [4]European Commission, Joint Research Centre, Institute for Transuranium Elements, Postfach 2340, D-76125 Karlsruhe, Germany; †These authors contributed equally to this work. *e-mail: polly.arnold@ed.ac.uk; jason.love@ed.ac.uk

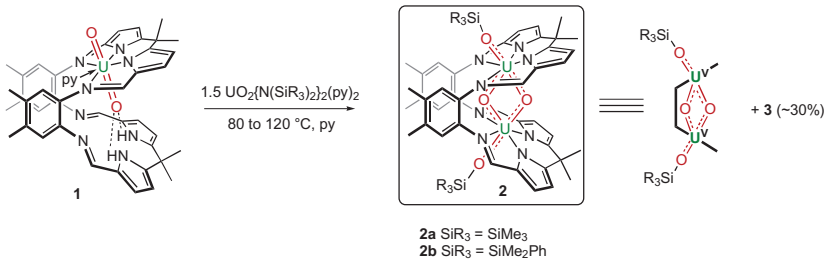

Figure 1 | The new butterfly-shaped binuclear U^V complexes are formed from the addition of excess uranyl amide salts to the wedge-shaped uranyl macrocyclic complex as a result of oxo-silylation and oxo-migration from a *trans* to a *cis* position. The reactions between $[UO_2(py)(H_2L)]$ **1** and $[UO_2\{N(SiR_3)_2\}_2(py)_2]$ (py = pyridine) result in the new binuclear U^V complexes **2** (SiR_3 = $SiMe_3$ **2a**, $SiMe_2Ph$ **2b**), which incorporate two closely bound uranium oxo groups in the Schiff-base macrocyclic framework resulting from oxo-group rearrangement, reduction and silylation.

complex **1** and 1.5 molar equivalents of the uranyl silylamides $[UO_2\{N(SiR_3)_2\}_2(py)_2]$ (SiR_3 = $SiMe_3$, $SiMe_2Ph$; py = pyridine) at 120 °C for 12 h afford the brown, toluene-soluble, paramagnetic binuclear pentavalent uranium complexes $[(R_3SiOUO)_2(L)]$ **2** (SiR_3 = $SiMe_3$ **2a**, 25%; $SiMe_2Ph$ **2b**, 22%) and the poorly soluble material **3** (SiR_3 = $SiMe_3$ **3a**; $SiMe_2Ph$ **3b**, ~30%, Fig. 1). A similar reaction between the macrocycle H_4L and 2.5 equiv. of $[UO_2\{N(SiMe_3)_2\}_2(py)_2]$ also generated **2a** (37%), and reactions in the absence of pyridine (THF solvent) also generated **2a**, albeit at a much slower rate.

The ^{1}H NMR spectrum of **2a** is consistent with its high symmetry and paramagnetism, displaying eight resonances between +14.8 and −11 ppm. Furthermore, a resonance at 160 ppm in the ^{29}Si NMR spectrum can be tentatively assigned to the $SiMe_3$ group of the newly silylated oxo group. The Fourier-transform infrared (FTIR) spectrum of **2a** contains bands at 862 and 802 cm^{-1} assigned to U–O stretches that are weakened and desymmetrized with respect to **1** (ν U=O, 908 cm^{-1}), and a Si–O stretch at 1,100 cm^{-1}; these data support the assignment of the pentavalent oxidation state.

A single-crystal X-ray diffraction study on **2a** (crystals grown from toluene solution) shows a new structural type in uranium oxo chemistry with a butterfly-type core geometry (Fig. 2; see Supplementary Fig. S23 for **2b**). Interestingly, it is similar to that predicted by Schreckenbach and co-workers in a recent computational study as being energetically accessible for two U^{VI} uranyl ions in the Pacman macrocycle[34,35], and is notable in that the normally robust *trans*-uranyl geometry has been lost following the formation of the U_2O_4 core. Although the majority of singly reduced uranyl complexes show the interaction of one or both oxo groups with another metal cation, this is the first case in which the same yl-derived-oxo group is shared by two uranium centres in a mutually *trans* geometry, as a result of the migration of one oxo group to a mutually *cis* position.

In the structure of **2a** the U_2O_2 core is a C_{2v}-symmetrical diamond shape with an average U–O distance of 2.094 Å (range, 0.012 Å). The related phenyldimethylsilylated complex **2b** has an average U–O distance of 2.081 Å. This diamond-shaped core has precedence in a few lower-oxidation-state uranium complexes, notably in pentavalent uranyl complexes, but also in the oxo-bridged U^{IV} dimer $[(Cp^{\ddagger})_2U(\mu\text{-}O)]_2$($Cp^{\ddagger}$ = $C_5H_3^tBu_2$) in which one U–O bond distance of 2.096(6) Å is similar to that of the two *endo*-oxo atoms in **2**. The butterfly shape, however, has not previously been observed in uranyl or uranium chemistry. The silylated *exo*-oxygen atoms, now formally siloxides, retain evidence of U–O multiple bonding with U1–O1 and U2–O4 distances of 2.034(4) and 2.040(4) Å, respectively[10,12,36]. Each uranium cation adopts a pentagonal bipyramidal geometry with axial oxo/siloxide ligands and the N_4-donor set of the macrocycle equatorial. The fifth equatorial site, in which a solvent donor atom is usually seen, is occupied instead by an oxo group that was originally bound in an axial position of the adjacent uranyl. The other notable feature is that both *exo*-oxo groups have undergone spontaneous silylation, affording a U^VU^V dimer with a very short U···U separation of 3.3557(5) Å. Similarly short U···U separations have been seen in the $U^{III}U^{III}$ amido-bridged complex $[U(\eta\text{-}C_8H_8)]_2[\mu\text{-}\kappa^4\text{:}\kappa^4\text{-}HN(CH_2)_3N(CH_2)_2N(CH_2)_3NH]$ (ref. 37) and also the $U^{IV}U^V$ complex $[K(dme)_4][\{(\mu_3\text{-}N)K(dme)_2U\}_2(\mu_4\text{-}\eta^5\text{:}\eta^3\text{:}\eta^2\text{-}$octamethylcalix(4)pyrrole)$]_2$ (ref. 38), although the uranium centres in these complexes are more reduced (that is, larger) than in **2**. Pentavalent uranyl complexes that dimerise to form asymmetric U_2O_2 diamond cores of C_{2h}-symmetry have longer U···U separations, for example, ~3.43 Å in $[(\{(^{Ad}ArO)_3\text{-}TACN\}U)_2(\mu\text{-}O)_2]$ (TACN = triazacyclononane)[39], 3.47 Å in $[U^VO_2Sm(py)_2(L)]_2$ and 3.55 Å in $[U_2^V(\mu\text{-}OPr^i)_2(OPr^i)_8]$ (refs 10,12,36).

Electronic structure analysis of 2a. Analysis of the bonding in the U_2O_4 core of **2a** was undertaken using density functional theory (DFT) and natural bond order (NBO) calculations. Single point calculations in a pyridine solvent continuum were carried out on a molecule of **2a** for which the geometry had been optimized in the gas phase (see Supplementary Information). Three possible arrangements of the two uranium-centred *f*-electrons were considered: triplet (ferromagnetically coupled, $f^{\alpha}f^{\alpha}$), antiferromagnetic unrestricted broken-symmetry singlet ($f^{\alpha}f^{\beta}$ independently localized orbitals) and restricted singlet ($f^{\alpha\beta}$ delocalized orbital over both uranium centres). The unrestricted singlet state was calculated to be more stable than the triplet and restricted singlet states by 1.4 and 42.7 kcal mol^{-1}, respectively, in pyridine when the B3LYP functional was used with relativistic pseudopotentials. This is also the case when larger basis sets were employed.

For the unrestricted singlet state of **2a**, the bonds between the uranium and the *endo*- and *cis*-oxo atoms were calculated to be between 2.092 and 2.099 Å, and the U–O_{exo} bond lengths were calculated to be 2.053 Å, within 0.01 Å of those obtained experimentally. The U···U separation was calculated as 3.366 and 3.379 Å in the unrestricted broken-symmetry singlet and triplet states, respectively. The calculated Mayer and Wiberg (in parentheses) bond orders for the O_{exo}–Si, U–O_{exo}, U–O_{endo} and U–O_{cis} were calculated as 1.04 (0.57), 1.27 (0.79), 1.20 (0.79) and 1.19 (0.79), respectively. The bonds within the U_2O_4 core can therefore be considered formally as single bonds with some double-bond character, although the U–O_{exo} bonds are slightly stronger. This is also the case for both the electronic triplet and unrestricted singlet states.

The α-(HOMO-27) and β-(HOMO-27) orbitals obtained with the B3LYP functional for the unrestricted singlet state are depicted in Fig. 3a,b and describe the primary σ-bonding interaction in the U_2O_4 core. The contributions from the *trans-endo*-oxo atom to

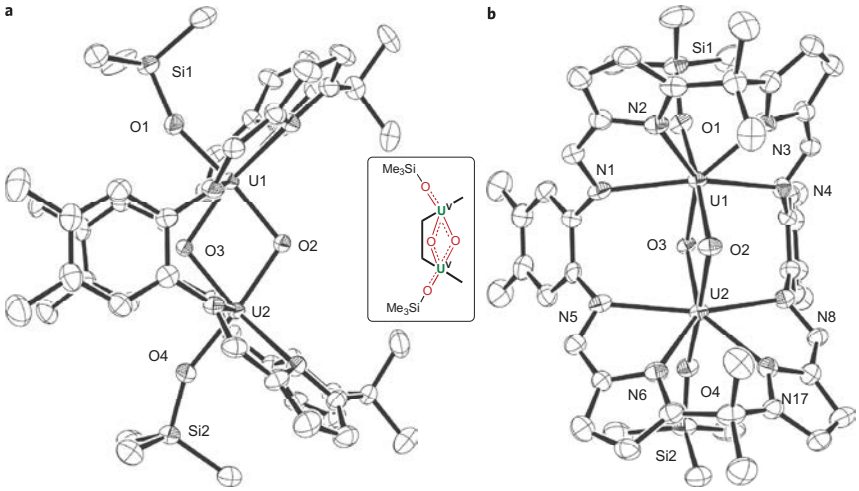

Figure 2 | Solid-state structure of the binuclear silylated uranium oxo complex [$(Me_3SiOUO)_2(L)$] 2a. a,**b**, Side-on (**a**) and face-on (**b**) views. The butterfly shape has not been observed before in uranyl or uranium chemistry, and both *exo*-oxo groups have undergone spontaneous silylation, affording a dinuclear U^VU^V complex with a very short U···U separation, and a symmetrical, tightly bound U_2O_2 diamond core. For clarity, all hydrogen atoms and solvent of crystallization are omitted (displacement ellipsoids are drawn at 50% probability). Selected distances (Å): U1···U2, 3.3557(5); U1–O1, 2.034(4); U1–O2, 2.099(4); U1–O3, 2.098(4); O1–Si1, 1.666(4). Selected angles (deg): U1–O2–U2, 106.6(2); U1–O3–U2, 106.3(2); O2–U1–O3, 73.3(2); O1–U1–O2, 173.4(2); Si1–O1–U1, 157.7(3).

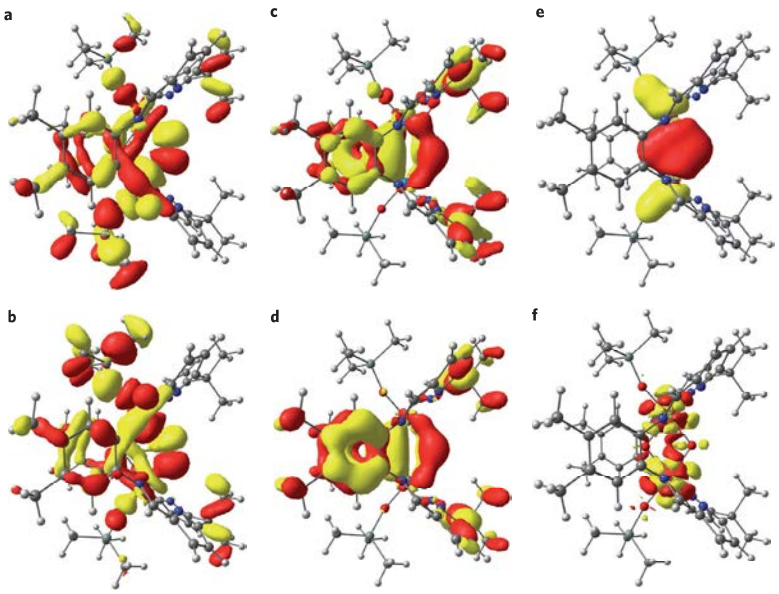

Figure 3 | Molecular orbitals of primary σ and π character in the unrestricted singlet state of 2a. a, α-(HOMO-27), with energy of −0.333 a.u. and contributions of 27% *endo*-oxo 2*p*, 13% *exo*-oxo 2*p*, 3% *cis*-oxo 2*p* and 13% U-5*f*. **b**, β-(HOMO-27), with energy of −0.333 a.u. and contributions of 25% *endo*-oxo 2*p*, 11% *exo*-oxo 2*p*, 3% *cis*-oxo 2*p* and 13% U-5*f*. These σ-type orbitals extend across the U_2O_2 core. **c**, α-(HOMO-28) with energy of −0.334 a.u. and contributions of 34% *cis*-oxo 2*p* and 9% *endo*-oxo 2*p*, 5% U-5*f* and 6% U-6*d*. **d**, β-(HOMO-28), with energy of −0.334 a.u. and contributions of 37% *cis*-oxo 2*p*, 9% *endo*-oxo 2*p*, 5% U-5*f* and 5% U-6*d*. These orbitals depict the weaker π-type interaction across the U_2O_2 core. **e**, HOMO-145 (bonding with respect to the two U atoms) with an energy of −1.094 a.u. and **f**, the antibonding counterpart to HOMO-145, both predominantly U-5*f*, with very minor components from the O2*s* orbitals.

these orbitals are significantly larger than those from the *cis*-oxo atom, although the calculated Mulliken charges and spin densities on both atoms are essentially identical. There is another set of σ-type orbitals at slightly higher energy with greater contributions from the *cis*-oxo atom. Thus, although the σ-framework is weaker in **2a** than in the calculated structure of the hexavalent uranyl analogue[34], a strongly bound *cis*-oxo component can be identified in **2a**. In addition, there is a weaker π-type bonding interaction in the U_2O_2 core. The π-type orbitals (Fig. 3c,d) are dominated by 2*p*-contributions from the *cis*-oxo atom and appear to be the only remnants of more prominent and stable π-interactions in the calculated structure of the hexavalent, non-silylated counterpart[34].

The combined structural and computational data show that the butterfly $U_2O_4Si_2$ motif can be formulated as singly bonded uranium oxo and siloxide groups combined with a significant π-bonding contribution from the *cis*-oxo group. Formally, this has resulted from the rearrangement of two linear pentavalent actinyls into a new bonding mode for uranium in which one oxo group is shared and *trans*, and one has adopted a *cis* position.

The diamond U_2O_2 geometry adopted in **2a** has been observed in related group 6 chemistry. For example, oxidation reactions of the quadruply metal–metal bonded Mo acetate dimer in the presence of good π-accepting ligands form $Mo^{V}(\mu\text{-}O)_2Mo^{V}$ complexes that have single M–M bonds[40]. It is therefore tempting to look for a direct metal–metal interaction in **2a**, as no *f*-block metal–metal bonded complex has been reported. The calculated U···U separation of 3.366 Å is much shorter than twice the covalent radius of the uranium atom (3.92 Å), which may indicate some bonding interaction. This is reflected in the non-trivial calculated Mayer bond order of 0.34 between the uranium atoms, which is only slightly lower than those calculated for some of the U–N bonds in **2a** (range 0.38–0.55). NBO analysis allows the identification of a set of bonding and antibonding orbitals (Fig. 3e,f, respectively) with almost exclusively *f*-orbital based overlap between the uranium centres. However, **2a** is clearly paramagnetic at room temperature, with spin-pairing occurring only at 17 K (see below). Although there are no reported examples of molecular bonds between two *f*-block elements, multiple U–U bonds with distinctly different interactions compared to transition metals have been predicted by theory[41].

Allied with the proximate uranium cations in **2a**, the unusual properties of the 5*f* orbitals make actinide ions attractive building blocks for new nanomagnetic materials, but the fundamental understanding of the factors that govern the exchange interactions and electron delocalization are poorly understood, a factor exacerbated by the rarity of $5f^1$ dimers, which are the easiest to study[42]. A variable-temperature study of the magnetism of **2a** (Fig. 4) shows Curie–Weiss behaviour down to 25 K with an effective moment of $1.53\mu_B$/U ion at 300 K. This value is lower than would be expected for a single U f^1 ion ($\mu_{eff} = 2.54\mu_B$/U ion in the L-S coupling scheme). This reduction can be attributed neither to room-temperature antiferromagnetic coupling nor to an orbital contribution from metal–ligand covalency (the latter argument for this observation having been disputed previously[43]), but instead arises from the strong ligand field typical of the uranyl-type geometry. Below these temperatures, a clear signature of antiferromagnetic coupling between the f^1 centres occurs, with the $\chi(T)$ curve peaking at a Néel temperature of 17 K, much higher than in other O-bridged di-uranium molecules for which the maximum observed was 5 K (ref. 10), but similar to that seen for the singly oxo-bridged U^{IV} complex $[(\{(^{Ad}ArO)_3\text{-}TACN\}U)_2(\mu\text{-}O)]$ at 20 K (ref. 39). For the latter example, it was postulated that the geometry of the oxo-group interaction and not the shortened U···U separation was the primary mediator of superexchange. The magnetic coupling due to superexchange across the two oxo groups was modelled by a spin Hamiltonian containing the Zeeman terms (one for each magnetic site) and the exchange interaction (see Supplementary Information). The resulting exchange interaction, $J_{ex} = -33\ cm^{-1}$, is particularly large, suggesting that the butterfly geometry could be of use in building more complex magnetic architectures through replacement of the silyl groups with further metal ions.

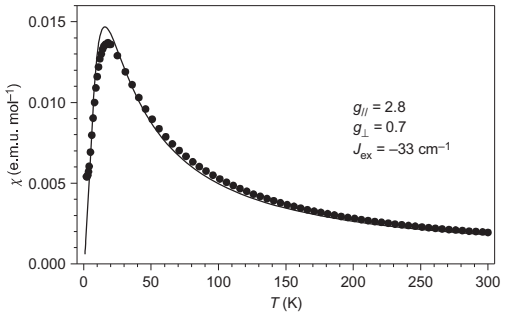

Figure 4 | Solid-state magnetic behaviour of 2a between 2 and 300 K. Spin pairing can be observed as high as 17 K. Symbols are the experimentally measured temperature dependence of the magnetic susceptibility (χ versus T) and the line shows the calculated fit to the data, using a spin model based on superexchange across the two bridging oxo groups.

Mechanistic insight into the formation of 2. The low yields of **2** and lack of obvious reducing agent in the synthetic procedure led us to investigate reactions at lower temperatures (Fig. 5). It is clear from these investigations that two competing reactions occur, one at a lower temperature that involves metallation of the uranyl oxo, and one at an elevated temperature that results in reductive silylation. Reaction of H_4L and 2.5 equiv. of $[UO_2\{N(SiMe_3)_2\}_2(py)_2]$ for two weeks at 20 °C formed the insoluble paramagnetic product **3a** and $HN(SiMe_3)_2$. Compound **3** forms more quickly and equally cleanly at temperatures up to 80 °C, but above 80 °C both **2** and **3** are formed, as well as a small quantity of decomposition products. Significantly, **3** was found to react with $ClSiR_3$ to form **2** in high yields. This secondary treatment of **3a** thus allows for the two-step synthesis of **2a** directly from the macrocyclic ligand in overall 73% yield in gram quantities.

We have been unable to determine crystallographically the structure of **3**. However, calibrated NMR-scale reactions show that 4 equiv. of by-product $HN(SiR_3)_2$ are generated during the reaction between H_4L and $[UO_2\{N(SiR_3)_2\}_2(py)_2]$ and that 2.5 equiv. of UO_2^{2+} are consumed per Pacman ligand. A further 1 equiv. of $HN(SiR_3)_2$ is liberated on reaction of **3** with $ClSiMe_3$ (Fig. 5). This therefore suggests that **3** has an aggregated structure based on $[(UO_2)_{2.5}(L)\{NH(SiR_3)\}(py)]$, an empirical formula supported by elemental analysis. Furthermore, a reaction between **3b** and an excess of Me_3SiCl generated a mixture of **2a** (75%) and the mixed silylated $[(Me_3SiOUO)(Me_2PhSiOUO)(L)]$ (25%), but no **2b**. Knowing that the silyl groups do not rearrange in these conditions, this suggests that only some of the oxo groups in **3** are silylated.

The laser desorption ionization (LDI) mass spectrum of **3** (Supplementary Fig. S15) contains a number of peaks that support an oligomeric structure. The highest ion visible is at 3,173 AMU and is assigned as a hexakis uranium dioxo complex of two Pacman ligands that incorporates silylamide. In turn, the series of ions in the range 2,300–3,200 AMU are related to one another by the loss of silylamide, UO_2 or UO_3 groups. More intense features occur at 2,096 AMU for a combination of two uranium oxo

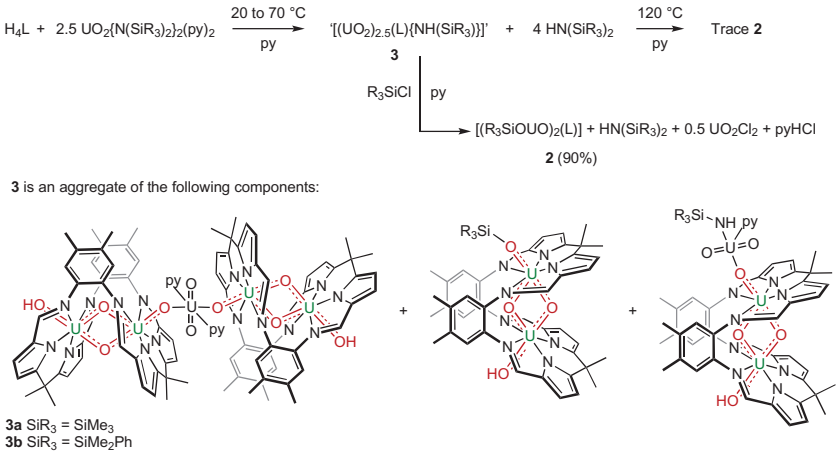

Figure 5 | Reactions between uranyl silylamides and H_4L to afford butterfly-uranyl complexes 2 and 3 and probable structures of the constituent parts of 3. At low temperatures, the same ratio of 2.5 UO_2^{2+} to one macrocycle ligand is observed, and although reduction processes are occurring, the product precipitates. Addition of trialkylchlorosilane generates **2** from the precipitate, releasing other fragments that made up the complex structure of **3**, including silylamine and the remaining 0.5 equiv. of UO_2^{2+}.

Pacman compounds and at 1,239 AMU for a mono(silylated) complex, and the base peak at 1,167 AMU is due to a bis(uranium oxo)Pacman complex. No assignable parent or daughter ions were observed in the electron impact or electrospray ionization mass spectra of **3**. From these data it is clear that **2** and **3** have related butterfly uranium oxo core structures, as is also supported by the reaction of **3** with R_3SiCl to form **2**. Further support for an aggregated structure for **3** was suggested from the X-ray structure of $[\{(Me_3SiOUO)(UO_2)(L)\}UO_2(thf)_2(\mu\text{-}OH)_2]_2$ **4** (Supplementary Fig. S24), isolated as a result of adventitious air ingress to a solution of **3a**. This compound contains the core U_2O_4 butterfly unit of **2a** already installed, with one *exo*-oxo group silylated, and the other oxo participating in a CCI with a uranyl hydroxide dimer.

The source of the silyl group in **2** can be traced to the uranyl silylamide, and not the by-product silazane $HN(SiR_3)_2$. The reaction between **1** and $[UO_2\{N(SiMe_2Ph)_2\}_2(py)_2]$ to form **2b** was carried out in the presence of the silylamine $N(SiMe_3)_3$. No evidence for **2a** or the mixed silyl complex $[(Me_3SiOUO)(Me_2PhSiOUO)(L)]$ was found in the ^{1}H NMR spectrum, confirming that the oxo-silyl groups derive from a metal-bound silylamido or amino group. This observation contrasts with the DFT calculations pertaining to our previous reductive silylation chemistry of Pacman uranyl complexes in which it was shown that model compounds with K cations bound to a uranyl oxo group can undergo S_N2-type homolytic bond cleavage reactions with aminosilanes[44,45]. Although a detailed evaluation of the mechanism of formation of **2** is ongoing, the observations described above suggest that two competing, reductive pathways occur that involve either U–N or N–Si bond homolysis (for a speculative mechanism see Supplementary Fig. S19). The nature of the bridging groups that form **3** is unclear, although the presence of OH groups is implicit to this mechanism and would facilitate aggregation[16]. It is likely that initial single-electron reduction of **1** occurs on addition of uranyl silylamide, with a concomitant loss of aminyl radical (that is, homolytic U–N scission), and that further uranyl silylamide is required to promote subsequent reduction and silylation reactions (that is, N–Si homolysis). We have seen similar reduction chemistry during the formation of lanthanide-incorporated pentavalent uranyl complexes[12], and coordination of a Lewis acid to the uranyl oxo group can facilitate reduction[15,46]. Unfortunately, our efforts to probe the nature of the radical species in these reactions have as yet proved inconclusive.

Reactivity of 2. Almost all of the recently isolated $[U^VO_2]^+$ complexes are relatively unstable towards redox decomposition, so it is remarkable that, on exposure to air for 48 h, a wet benzene solution of **2a** shows virtually no change in its ^{1}H NMR spectrum. Furthermore, after five days, only 20% decomposition of **2a** cleanly to free ligand H_4L is observed. Solution cyclic voltammetry experiments display no oxidation processes within the window of study afforded by the THF solvent. In accordance with this, no reactions are observed between **2a** (or **3a**) and chemical oxidants such as iodine or cerium(IV) triflate. Complex **2a** is also very thermally robust and unreactive towards exchange of the O–SiR_3 group. For example, **2a** can be recovered unchanged after 12 h in boiling pyridine, and the addition of excess quantities of Me_3SiCl, Ph_2SiHCl or $[UO_2\{N(SiMe_3)_2\}_2(py)_2]$ gave no reaction, even at elevated temperatures.

Conclusions

We have shown that the facile rearrangement of a *trans*-uranyl oxo into a mutually *cis* position between two high-oxidation-state uranium ions occurs on reduction, thereby forming a new butterfly-shaped uranium oxo motif with remarkable stability and strong U–U electronic coupling. The formation of this f^1–f^1 motif is possibly facilitated by the rigid constraints of the macrocyclic framework that disfavour the complexation of two linear uranyl cations. However, due to the redox stability exhibited by this compound, it is of interest to consider whether this motif has been perhaps overlooked in favour of its linear congener in actinyl chemistry outside the laboratory.

The mechanisms of the two competing pathways to **2** and **3** are as yet unknown. It remains unclear how the reduction and silylation processes occur, although the reactions of **3** and the isolation of **4** imply that the interaction of the extra half equivalent of uranyl silylamide with the $U_2O_4(L)$ core is requisite. Further investigation into the mechanism is required to determine to what extent this work bears relevance to the proton, electron transfer and oxo group exchange reactions that occur in aqueous uranyl systems, and if it is possible to draw analogies to transition-metal oxo chemistry.

The extremely short U–U separation, magnetic coupling and broken-symmetry singlet ground state exhibited by **2a** indicate strong communication between the two f^1 centres and suggest that the precise details of the electronic and magnetic structure will be of widespread interest.

Methods

Experiments were carried out under a dry, oxygen-free dinitrogen atmosphere, with reagents dissolved or suspended in aprotic solvents, and combined or isolated using cannula and glovebox techniques. We heated pyridine solutions of the hinged macrocyclic complex $[UO_2(py)(H_2L)]$ (py = pyridine), in which one compartment bound the uranyl dication and the other still contained two pyrrolic H atoms, with 1.5 equiv. of the uranyl bis(silylamide) complex $[UO_2\{N(SiR_3)_2\}_2(py)_2]$ at 120 °C for 12 h. This afforded the new, reduced and silylated bimetallic uranium oxo complexes $[(R_3SiOUO)_2(L)]$ for two different SiR_3 derivatives. The poorly soluble by-product could be converted into the target compound by treatment with R_3SiCl, with presumed elimination of a uranyl-containing material. At temperatures below 70 °C, the poorly soluble by-product was now the dominant product, and could be converted very cleanly, in high yield, to the same bimetallic $[(R_3SiOUO)_2(L)]$. Repetitions of the reaction with different silylamides and silylamines were carried out to confirm that the reducing electron derived from cleavage of a U–$N(SiR_3)_2$ bond, and the silyl group from a metal-bound UN–SiR_3 group. All compounds were characterized by a variety of methods, including elemental analysis, FTIR spectroscopy, magnetic moment measurements, mass spectrometry, NMR spectroscopy and single-crystal X-ray diffraction studies.

The geometry of **2a** was optimized in the gas phase using DFT calculations in three different spin states: antiferromagnetic broken-symmetry singlet, restricted singlet and ferromagnetic triplet states. Single-point DFT calculations in a model pyridine solvent were carried out on the optimized structures using a polarizable continuum solvation model. The uranium atom was described with the Stuttgart relativistic pseudopotential[47,48] and all other atoms were described with the 6-31G** basis set. Single-point calculations were carried out with the 6-311 ++G** basis to check for the basis set dependency of the relative energies of the three electronic states considered. These calculations were performed with the Gaussian 03 suite of programs[49]. The molecular orbitals obtained were plotted with isosurface contours of 0.02. Scalar relativistic calculations with all-electron basis sets using a four-component approach were also carried out with the Priroda program[50]. The PBE functional was used in these calculations while using a triple-ζ (cc-pVTZ) basis set. The small-component portion was described using appropriate kinetically balanced basis sets. Mayer bond orders were calculated after geometry optimization.

Received 5 October 2011; accepted 13 January 2012; published online 21 February 2012

References

1. Denning, R. G. Electronic structure and bonding in actinyl ions and their analogs. *J. Phys. Chem. A* **111,** 4125–4143 (2007).
2. Arnold, P. L., Love, J. B. & Patel, D. Pentavalent uranyl complexes. *Coord. Chem. Rev.* **253,** 1973–1978 (2009).
3. Schettini, M. F., Wu, G. & Hayton, T. W. Coordination of N-donor ligands to a uranyl(V) beta-diketiminate complex. *Inorg. Chem.* **48,** 11799–11808 (2009).
4. Berthet, J-C., Siffredi, G., Thuéry, P. & Ephritikhine, M. Easy access to stable pentavalent uranyl complexes. *Chem. Commun.* 3184–3185 (2006).
5. Nocton, G. *et al.* Synthesis, structure, and bonding of stable complexes of pentavalent uranyl. *J. Am. Chem. Soc.* **132,** 495–508 (2010).
6. Steele, H. & Taylor, R. J. A theoretical study of the inner-sphere disproportionation reaction mechanism of the pentavalent actinyl ions. *Inorg. Chem.* **46,** 6311–6318 (2007).
7. Suzuki, Y., Kelly, S. D., Kemner, K. M. & Banfield, J. F. Radionuclide contamination: nanometre-size products of uranium bioreduction. *Nature* **419,** 134 (2002).
8. Ikeda, A. *et al.* Comparative study of uranyl(VI) and -(V) carbonato complexes in an aqueous solution. *Inorg. Chem.* **46,** 4212–4219 (2007).
9. Burdet, F., Pecaut, J. & Mazzanti, M. Isolation of a tetrameric cation–cation complex of pentavalent uranyl. *J. Am. Chem. Soc.* **128,** 16512–16513 (2006).
10. Nocton, G., Horeglad, P., Pecaut, J. & Mazzanti, M. Polynuclear cation–cation complexes of pentavalent uranyl: relating stability and magnetic properties to structure. *J. Am. Chem. Soc.* **130,** 16633–16645 (2008).
11. Arnold, P. L., Blake, A. J., Wilson, C. & Love, J. B. Uranyl complexation by a schiff-base, polypyrrolic macrocycle. *Inorg. Chem.* **43,** 8206–8208 (2004).
12. Arnold, P. L. *et al.* Single-electron uranyl reduction by a rare-earth cation. *Angew. Chem. Int. Ed.* **50,** 887–890 (2011).
13. Arnold, P. L., Patel, D., Blake, A. J., Wilson, C. & Love, J. B. Selective oxo functionalization of the uranyl ion with 3*d* metal cations. *J. Am. Chem. Soc.* **128,** 9610–9611 (2006).
14. Arnold, P. L., Patel, D., Wilson, C. & Love, J. B. Reduction and selective oxo group silylation of the uranyl dication. *Nature* **451,** 315–317 (2008).
15. Arnold, P. L. *et al.* Uranyl oxo activation and functionalisation by metal cation coordination. *Nature Chem.* **2,** 1056–1061 (2010).
16. Arnold, P. L., Pecharman, A. F. & Love, J. B. Oxo-group protonation and silylation of pentavalent uranyl Pacman complexes. *Angew. Chem. Int. Ed.* **50,** 9456–9458 (2011).
17. Brown, J. L., Wu, G. & Hayton, T. W. Oxo ligand silylation in a uranyl beta-ketoiminate complex. *J. Am. Chem. Soc.* **132,** 7248–7249 (2010).
18. Berthet, J. C., Siffredi, G., Thuéry, P. & Ephritikhine, M. Controlled chemical reduction of uranyl salts into $UX_4(MeCN)_4$ (X= Cl, Br, I) with Me_3SiX reagents. *Eur. J. Inorg. Chem.* 4017–4020 (2007).
19. Schreckenbach, G., Hay, P. J. & Martin, R. L. Theoretical study of stable *trans* and *cis* isomers in $[UO_2(OH)_4]^{2-}$ using relativistic density functional theory. *Inorg. Chem.* **37,** 4442–4451 (1998).
20. Villiers, C., Thuéry, P. & Ephritikhine, M. The first *cis*-dioxido uranyl compound under scrutiny. *Angew. Chem. Int. Ed.* **47,** 5892–5893 (2008).
21. Fortier, S. & Hayton, T. W. Oxo ligand functionalization in the uranyl ion ($[UO_2]^{2+}$). *Coord. Chem. Rev.* **254,** 197–214 (2010).
22. Shamov, G. A. & Schreckenbach, G. Theoretical study of the oxygen exchange in uranyl hydroxide. An old riddle solved? *J. Am. Chem. Soc.* **130,** 13735–13744 (2008).
23. Muller, K., Brendler, V. & Foerstendorf, H. Aqueous uranium(VI) hydrolysis species characterized by attenuated total reflection Fourier-transform infrared spectroscopy. *Inorg. Chem.* **47,** 10127–10134 (2008).
24. Clark, D. L. *et al.* Chemical speciation of the uranyl ion under highly alkaline conditions. Synthesis, structures, and oxo ligand exchange dynamics. *Inorg. Chem.* **38,** 1456–1466 (1999).
25. Watson, L. A. & Hay, B. P. Role of the uranyl oxo group as a hydrogen bond acceptor. *Inorg. Chem.* **50,** 2599–2605 (2011).
26. Biswas, B., Mougel, V., Pecaut, J. & Mazzanti, M. Base-driven assembly of large uranium oxo/hydroxo clusters. *Angew. Chem. Int. Ed.* **50,** 5744–5747 (2011).
27. Konze, W. V. *et al*, in . *Plutonium Futures—The Science* Vol. 532, Conference Proceedings (eds Pillay, K. K. S. & Kim, K. C.) 261–262 (AIP, 2000).
28. Wilkerson, M. P. *et al.* Basicity of uranyl oxo ligands upon coordination of alkoxides. *Inorg. Chem.* **39,** 5277–5285 (2000).
29. Bühl, M. & Schreckenbach, G. Oxygen exchange in uranyl hydroxide via two non-classical ions. *Inorg. Chem.* **49,** 3821–3827 (2010).
30. Szabo, Z. & Grenthe, I. On the mechanism of oxygen exchange between uranyl(VI) oxygen and water in strongly alkaline solution as studied by ^{17}O NMR magnetization transfer. *Inorg. Chem.* **49,** 4928–4933 (2010).
31. Tsushima, S., Rossberg, A., Ikeda, A., Muller, K. & Scheinost, A. C. Stoichiometry and structure of uranyl(VI) hydroxo dimer and trimer complexes in aqueous solution. *Inorg. Chem.* **46,** 10819–10826 (2007).
32. Hratchian, H. P. *et al.* Theoretical investigation of uranyl dihydroxide: oxo ligand exchange, water catalysis, and vibrational spectra. *J. Phys. Chem. A* **109,** 8579–8586 (2005).
33. Anderson, T. M. *et al.* A late-transition metal oxo complex: $K_7Na_9[O{=}Pt^{IV}(H_2O)L_2]$, $L{=}[PW_9O_{34}]_9$. *Science* **306,** 2074–2077 (2004).
34. Pan, Q-J., Shamov, G. A. & Schreckenbach, G. Binuclear uranium(VI) complexes with a 'Pacman' expanded porphyrin: computational evidence for highly unusual bis-actinyl structures. *Chem. Eur. J.* **16,** 2282–2290 (2010).
35. Pan, Q-J. & Schreckenbach, G. Binuclear hexa- and pentavalent uranium complexes with a polypyrrolic ligand: A density functional study of water- and hydronium-induced reactions. *Inorg. Chem.* **49,** 6509–6517 (2010).
36. Cotton, F. A., Marler, D. O. & Schwotzer, W. Dinuclear uranium alkoxides. Preparation and structures of $KU_2(OCMe_3)_9$, $U_2(OCMe_3)_9$, and $U_2(OCHMe_2)_{10}$, containing [uranium(IV), uranium(IV)], [uranium(IV), uranium(V)], and [uranium(V), uranium(V)], respectively. *Inorg. Chem.* **23,** 4211–4215 (1984).
37. Le Borgne, T., Lance, M., Nierlich, M. & Ephritikhine, M. Synthesis and crystal structure of $[U(\eta\text{-}C_8H_8)]_2[\mu\text{-}\eta^4\text{:}\eta^4\text{-}HN(CH_2)_3N(CH_2)_3N(CH_2)_3NH]$, a dinuclear compound with a bridging tetra-amide ligand. *J. Organomet. Chem.* **598,** 313–317 (2000).
38. Korobkov, I., Gambarotta, S. & Yap, G. P. A. A highly reactive uranium complex supported by the calix[4]tetrapyrrole tetraanion affording dinitrogen cleavage, solvent deoxygenation, and polysilanol depolymerization. *Angew. Chem. Int. Ed.* **41,** 3433–3436 (2002).
39. Lam, O. P., Heinemann, F. W. & Meyer, K. Activation of elemental S, Se and Te with uranium(III): bridging U–E–U (E=S, Se) and diamond-core complexes $U\text{–}E_2\text{–}U$ (E=O, S, Se, Te). *Chem. Sci.* **2,** 1538–1547 (2011).
40. Dulebohn, J. I., Stamatakos, T. C., Ward, D. L. & Nocera, D. G. The preparation of dimolybdenum(V,V) complexes from molybdenum quadruply bonded metal–metal dimers. *Polyhedron* **10,** 2813–2820 (1991).
41. Gagliardi, L. & Roos, B. O. Quantum chemical calculations show that the uranium molecule U_2 has a quintuple bond. *Nature* **433,** 848–851 (2005).
42. Rinehart, J. D., Harris, T. D., Kozimor, S. A., Bartlett, B. M. & Long, J. R. Magnetic exchange coupling in actinide-containing molecules. *Inorg. Chem.* **48,** 3382–3395 (2009).
43. Graves, C. R. *et al.* Organometallic uranium(V) imido halide complexes: from synthesis to electronic structure and bonding. *J. Am. Chem. Soc.* **130,** 5272–5285 (2008).

44. Yahia, A., Arnold, P. L., Love, J. B. & Maron, L. A DFT study of the single electron reduction and silylation of the U–O bond of the uranyl dication in a macrocyclic environment. *Chem. Commun.* 2402–2404 (2009).
45. Yahia, A., Arnold, P. L., Love, J. B. & Maron, L. The effect of the equatorial environment on oxo-group silylation of the uranyl dication: a computational study. *Chem. Eur. J.* **16,** 4881–4888 (2010).
46. Hayton, T. W. & Wu, G. Exploring the effects of reduction or Lewis acid coordination on the U=O bond of the uranyl moiety. *Inorg. Chem.* **48,** 3065–3072 (2009).
47. Kuchle, W., Dolg, M., Stoll, H. & Preuss, H. *Ab initio* pseudopotentials for Hg through Rn .1. Parameter sets and atomic calculations. *Mol. Phys.* **74,** 1245–1263 (1991).
48. Kuchle, W., Dolg, M., Stoll, H. & Preuss, H. Energy-adjusted pseudopotentials for the actinides—parameter sets and test calculations for thorium and thorium monoxide. *J. Chem. Phys.* **100,** 7535–7542 (1994).
49. Gaussian 09, Revision A.2 (Gaussian, Inc., 2009).
50. Laikov, D. N. & Ustynyuk, Y. A. PRIRODA-04: A quantum-chemical program suite. New possibilities in the study of molecular systems with the application of parallel computing. *Russ. Chem. Bull.* **54,** 820–826 (2005).

Acknowledgements
P.L.A. and J.B.L. acknowledge support from the Engineering and Physical Sciences Research Council EPSRC (UK), EaStCHEM and the University of Edinburgh. G.S. acknowledges financial support from the Natural Sciences and Engineering Research Council of Canada (NSERC).

Author contributions
G.M.J. synthesized and characterized the compounds. P.L.A. and J.B.L. generated and managed the project, helped characterize the complexes, analysed the data and wrote the manuscript. G.S. and S.O.O. carried out and interpreted the computational analyses of bonding. N.M. performed the ligand-field and magnetic superexchange calculations.

Additional information
The authors declare no competing financial interests. Supplementary information accompanies this paper at www.nature.com/naturechemistry. Reprints and permission information is available online at http://www.nature.com/reprints. Correspondence and requests for materials should be addressed to P.L.A. and J.B.L.

Uranyl Complexes

DOI: 10.1002/anie.201207609

Controlled Deprotection and Reorganization of Uranyl Oxo Groups in a Binuclear Macrocyclic Environment**

Guy M. Jones, Polly L. Arnold, and Jason B. Love**

The two, strongly covalently bound, mutually *trans* oxo ligands of uranyl compounds are highly inert towards yl group reactions or exchange,[1] even upon single-electron reduction to $[UO_2]^+$. However, these latter f^1 compounds show enhanced Lewis basicity, resulting in recent studies on oxo coordination to alkali metals,[2,3] lanthanides,[4] actinides,[5] and other uranyl cations[3,6,7] through so-called cation–cation interactions (CCIs), as well as coordination to Lewis acidic boranes.[8] Although kinetically inert under anaerobic conditions, the vast majority of uranyl(V) complexes decompose upon exposure to air, either by oxidation or, more frequently, proton-coupled disproportionation reactions.[9,10]

In 2008 we reported a new reaction for the uranyl dication in which concurrent single-electron reduction and oxo-group silylation occurred, providing the first example of covalent bond formation for the uranyl oxo group.[11] In this case, a single uranyl cation was complexed by the Schiff base polypyrrolic macrocycle L in a Pacman-shaped cleft structure, a design that facilitates this chemistry. Since this discovery, the reductive silylation of uranyl β-ketoiminate complexes[12] and their perfluoroborane adducts has been reported, but overall oxo functionalization reactions remain rare.[8,13] These oxo-silylated complexes are stable indefinitely under anaerobic conditions, although little is known of their stability in air.

We reported recently the synthesis of the binuclear uranium(V) dioxo complex **A** of L (Scheme 1).[14] This complex is unique in that it is derived from two *trans*-uranyl dications, but features one mutually *trans* and one mutually *cis* oxo ligand within a multiply bonded U_2O_2 core, as well as two silylated *exo*-oxo groups; **A** can be considered as an oxo-rearranged, silylated analogue of the dimeric CCI complex **B**. The ready availability of **A** and its surprising inertness towards disproportionation, hydrolysis, and oxidation led us to investigate the origin of its unique stability. Herein, we describe for the first time a method that allows the removal of the silyl groups, reinstating oxo yl character, and show that this deprotection step is key to the rearrangement of the *cis*/*trans*-oxo motif back to the traditional linear uranyl geometry. We also show that the $U^{VI/V}$ redox couple can be exploited to carry out the two-electron reduction of dioxygen to peroxide.

[*] G. M. Jones, Prof. P. L. Arnold, Dr. J. B. Love
EaStCHEM School of Chemistry, University of Edinburgh
West Mains Road, Edinburgh, EH9 3JJ (UK)
E-mail: polly.arnold@ed.ac.uk
jason.love@ed.ac.uk

[**] We thank the University of Edinburgh and EPSRC (UK) for funding.
Supporting information for this article is available on the WWW under http://dx.doi.org/10.1002/anie.201207609.

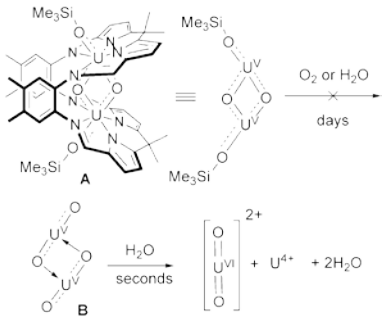

Scheme 1. Aerobic and aqueous stability of the uranium siloxydioxo complex $[(Me_3SiOUO)_2(L)]$ **A** and the contrasting spontaneous disproportionation of structurally related CCI complexes **B**.

The reaction between **A** and two equivalents of potassium graphite or potassium metal in THF cleanly generates the U^{IV}/U^{IV} salt $K_2[(Me_3SiOUO)_2(L)]$ (**1a**) in solution (Scheme 2). The complex retains its C_{2v} symmetry upon reduction, with seven ligand resonances displayed between +35 and −35 ppm in the ^1H NMR spectrum. The additional resonance at 39.6 ppm, integrating to 18 protons, demonstrates that both of the $SiMe_3$ groups are retained upon reduction of the uranium centers. Although highly soluble, **1** can be isolated as a solid by treating a solution of the THF

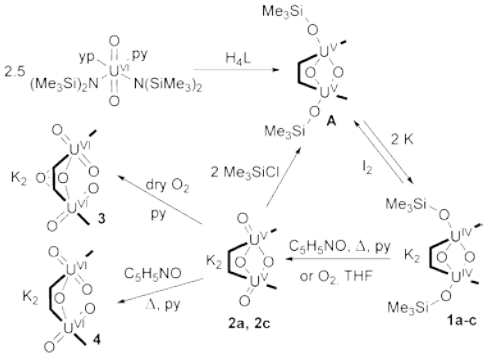

Scheme 2. Synthesis of complexes **1**–**4**: **a** = THF solvate, **b** = THF/[18]crown-6 solvate, **c** = pyridine solvate. **3** and **4** are solvated by pyridine. The bonding of potassium and the resulting nuclearities of the complexes are not shown.

solvate **1a** with two equivalents of [18]crown-6, precipitating $[K(thf)_2([18]crown\text{-}6)]_2[(Me_3SiOUO)_2(L)]$ (**1b**) in 60% yield.

While the growth of single crystals suitable for X-ray diffraction was not possible owing to the poor solubility of this material in THF, its composition is supported by ^{1}H NMR, IR, and UV/Vis spectroscopy and elemental analysis (see the Supporting Information). As expected, reoxidation of either **1a** or **1b** with single equivalents of iodine leads to the clean reformation of **A** with elimination of potassium iodide. To our surprise however, carrying out the analogous two-electron oxidation with pyridine-*N*-oxide results in the formation of the doubly desilylated, binuclear U^V compound $K_2[(OUO)_2(L)]$ (**2**) and half an equivalent of $(Me_3Si)_2O$ as the only products observable by ^{1}H NMR spectroscopy (Scheme 2). The ^{1}H NMR spectrum of **2** is similar to **A**, albeit with the notable absence of a $SiMe_3$ resonance at 15 ppm. Isolation of the pyridine solvate **2c** in the bulk is achieved using a one-pot strategy in which **A** is reduced to the U^{IV}/U^{IV} salt **1c** and then oxidized by the addition of one equivalent of pyridine-*N*-oxide; boiling the resulting mixture for 6 days results in the precipitation of crystalline **2c** in 69% yield.

Analysis of the crystal structure of **2c** (Figure 1) confirmed the absence of the silyl substituents and the presence of U^V oxidation states in which the average U–O bond length

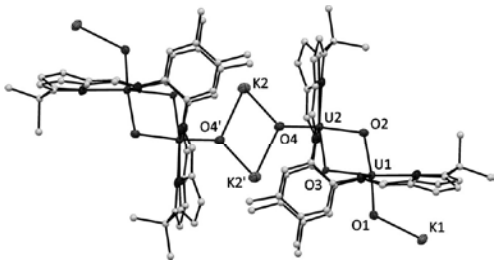

Figure 1. X-ray crystal structure of **2c**. For clarity, all of the hydrogen atoms and pyridine donors to potassium are omitted; where shown, ellipsoids are set at 50% probability.

of 2.03 Å is comparable to that seen in the silylated analogue **A** (2.09 Å). In contrast to **A**, which exhibits six almost identical U–O bond distances of between 2.03 to 2.10 Å, those in **2c** show significant variation between the four U–O_{endo} bonds (2.090(6), 2.101(5), 2.105(6), and 2.168(5) Å) and the two U–O_{exo} bonds (1.871(5) and 1.851(6) Å), with the latter being much more indicative of yl-type U–O multiple bonding. The U1···U2 separation of 3.3795(5) Å is short but elongated slightly compared to that of 3.3557(5) Å seen in **A**. The contrast in bonding in **2c** to its silylated analogue **A** is further represented in their UV/Vis-NIR spectra, which are very different despite their common oxidation states (see the Supporting Information). The alternative, unsolvated analogue **2a** was synthesized by direct exposure of a THF solution of **1a** to air, resulting in the immediate precipitation of crystals of **2a** along with other intractable materials. In contrast to **2c**, in which pyridine solvation of the external potassium cations truncates the structure as a crystallographic dimer, **2a** has a polymeric structure in which each potassium bridges two Pacman molecules in a K_2O_2 diamond motif (see the Supporting Information). These desilylated compounds are best classified as displaying bimetallic *endo*-oxo-bridged U^V motifs with terminal *exo*-oxo groups. Although the former presents a very common bonding motif in uranium chemistry, U^V complexes exhibiting terminal oxo groups are still rare,[15] with $[U(O)\{N(SiMe_3)_2\}_2]$ having a similar U=O bond length (1.817(1) Å) to those in **2c**.[16] Furthermore, the terminal U^V oxo complexes $[\{(RArO)_3tacn\}U(O)]$ (R = *t*Bu or 1-adamantyl, tacn = 1,4,7-triazacyclononane)[17] can be oxidized to their U^{VI} analogues.[18]

The differences in structure and bonding between oxo-silylated **A** and oxo-unfunctionalized **2c** are mirrored by differences in their stability towards oxidation. While boiling solutions of **A** are stable indefinitely under an atmosphere of dry dioxygen, the exposure of a THF or pyridine solution of **2c** to dioxygen results in instantaneous oxidation and the sole formation of the binuclear U^{VI} peroxide $K_2[(\mu\text{-}\kappa^2\text{-}\kappa^2\text{-}O_2)(UO_2)_2(L)]$ (**3**), isolated in 55% yield (Scheme 2). The ^{1}H NMR spectrum of **3** shows seven resonances indicating that the C_{2v} symmetry seen for **2**, and the silylated complexes **A** and **1**, is retained. In contrast however, all of these resonances are within the 0–10 ppm range, supporting the formation of a diamagnetic complex. The absence of f–f absorptions in the NIR spectrum supports the assignment of formal U^{VI} oxidation states, along with the presence of the asymmetric $[UO_2]^{2+}$ stretch in the IR spectrum at 924 cm^{-1}.

The solid-state structure of **3** (Figure 2) depicts a wedge-shaped, Pacman macrocycle, with symmetrical occupation of each of the N_4-donor pockets by uranyl dications. The $\{OU(\mu\text{-}O)_2UO\}$ *cis*/*trans* oxo-group bonding motif seen in **A** is replaced by two discrete, linear $[UO_2]^{2+}$ units in which the four U–O bond distances (1.781(6) to 1.788(6) Å) are characteristic of uranyl(VI). The accommodation of both $[UO_2]^{2+}$ dications by the macrocycle is facilitated by significant structural distortion away from the usual Pacman geometry, resulting in an inter-cleft bite angle of 90.1° for **3**

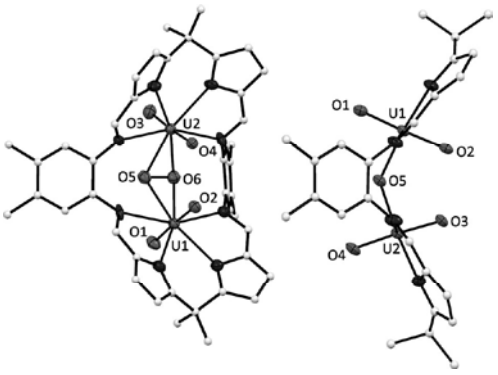

Figure 2. X-ray crystal structures of **3** (left) and **4** (right, side-on view). For clarity, all of the hydrogen atoms, K atoms, and solvent donors are omitted. Where shown, ellipsoids are set at 50% probability.

compared to 61.3° and 65.1° for **A** and **2c**, respectively; this widening of the cleft presumably prevents clashing of the *endo*-oxo groups. In **3**, each uranium center has approximate hexagonal bipyramidal geometry, with the two axially bound oxo ligands sited perpendicular to the four equatorial nitrogen donors of the Pacman macrocycle. The fifth and sixth equatorial donors to each metal center are provided by the bridging peroxide ligand, which lies sandwiched between the two aryl spacers of the wedge-shaped ligand in a μ-κ^2-κ^2 motif. The O5–O6 bond length is 1.433(7) Å and is characteristic of peroxide; charge balance is maintained by retention of the two potassium cations which coordinate to the *exo*-uranyl oxo atom O1, the bridging peroxide atoms O5 and O6, and the O2 and O4 atoms of separate Pacman molecules (see the Supporting Information). Although numerous uranyl peroxide complexes are known, they are formed exclusively by ligand exchange between uranyl(VI) precursors.[19] In contrast, compound **3** is the first uranyl peroxide complex formed by a redox reaction, adding to the wealth of small molecule activation chemistry known for uranium complexes.[20] Recently a uranyl(V) complex was shown to react with dioxygen, but in this case it formed an oxo-bridged uranyl(VI) complex.[7]

Oxidation of the U^V complex **2c** with pyridine-*N*-oxide instead of dioxygen yields the mono-oxo-bridged complex $K_2[(UO_2)(\mu\text{-}O)(UO_2)(L)]$ **4** in moderate yield (Scheme 2). The solid-state structure of **4** (Figure 2) is similar to that of **3**, with occupation of the Pacman ligand by two uranyl(VI) dications in adjacent N_4 donor pockets. In contrast to **3** however, the single oxide ligand O5, rather than peroxide, bridges U1 and U2 at the obtuse U1-O5-U2 angle of 136.4(3)°, resulting in pentagonal bipyramidal uranium geometries. In analogy with **3**, the mono-oxo structure exists as a crystallographic dimer maintained by uranyl/potassium CCIs (see the Supporting Information). In contrast to **3** however, the ^{1}H NMR spectrum of **4** displays 14 resonances for the Pacman ligand, indicating that the asymmetry in the solid-state structure due to K-coordination is retained in solution.

The uranyl(VI) complexes **3** and **4** form only the second and third examples of cofacial, binuclear uranyl Pacman complexes, the first reported by us using an expanded, anthracene-derived Pacman macrocycle.[21] More importantly however, the isolation of both complexes provides further insight into the nature and stability of the binuclear U^V precursors **A** and **2c**. While **A** is a highly unusual example of an air-stable U^V complex, desilylation of the oxo ligands to form **2c** uncovers underlying reactivity. Furthermore, oxidation of the desilylated complex **2c** causes oxo-group rearrangement to occur, re-forming the traditional uranyl(VI) bonding motif from which **A** was originally derived. Treatment of **2c** with chlorotrimethylsilane allows the clean transformation back to **A**, upon which its stability against oxidation is restored, suggesting that the oxo-bound SiR_3 groups in **A** are responsible for its remarkable redox stability. As such, the trialkylsilyl group may be viewed as an effective protecting group for the uranyl oxo and therefore analogous to the well-documented silyl-group protection of functional groups in organic synthesis. Unlike the latter, we have been unable to deprotect **A** using common reagents such as fluoride.

The desilylated complex $[(OUO)_2(L)]^{2-}$ **2**, is highly reactive towards oxidation, resulting in preferential formation of compounds that contain two discrete uranyl dications and not the elusive *cis*-uranyl. This is surprising, as DFT calculations show only a circa 16 kcal mol^{-1} difference in energy between the two forms,[22] and the macrocyclic framework has distorted appreciably to accommodate the two *trans*-uranyl motifs. Even so, the more yl-like nature of the desilylated complex **2** than **A** means that it is a more realistic model of the actinyl(V) CCI complexes that are proposed to exist in nuclear waste mixtures and which participate in redox processes and are disruptive to fuel reprocessing. Overall, the synthesis and characterization of these complexes demonstrate our ability to exploit the Pacman macrocyclic framework to manipulate uranyl oxo group bonding and reactivity through control of the uranium oxidation state and oxo-group functionalization.

Received: September 19, 2012
Published online: November 6, 2012

Keywords: actinides · Schiff base macrocycles · silylation · uranium · uranyl complexes

[1] R. G. Denning, *J. Phys. Chem. A* **2007**, *111*, 4125 – 4143.
[2] P. L. Arnold, A.-F. Pécharman, E. Hollis, A. Yahia, L. Maron, S. Parsons, J. B. Love, *Nat. Chem.* **2010**, *2*, 1056 – 1061; J.-C. Berthet, G. Siffredi, P. Thuéry, M. Ephritikhine, *Chem. Commun.* **2006**, 3184 – 3186; J.-C. Berthet, G. Siffredi, P. Thuéry, M. Ephritikhine, *Dalton Trans.* **2009**, 3478 – 3494; L. Natrajan, F. Burdet, J. Pécaut, M. Mazzanti, *J. Am. Chem. Soc.* **2006**, *128*, 7152 – 7153; G. Nocton, P. Horeglad, V. Vetere, J. Pécaut, L. Dubois, P. Maldivi, N. M. Edelstein, M. Mazzanti, *J. Am. Chem. Soc.* **2010**, *132*, 495 – 508.
[3] F. Burdet, J. Pécaut, M. Mazzanti, *J. Am. Chem. Soc.* **2006**, *128*, 16512 – 16513.
[4] P. L. Arnold, E. Hollis, F. J. White, N. Magnani, R. Caciuffo, J. B. Love, *Angew. Chem.* **2011**, *123*, 917 – 920; *Angew. Chem. Int. Ed.* **2011**, *50*, 887 – 890.
[5] V. Mougel, J. Pecaut, M. Mazzanti, *Chem. Commun.* **2012**, *48*, 868 – 870.
[6] G. Nocton, P. Horeglad, J. Pécaut, M. Mazzanti, *J. Am. Chem. Soc.* **2008**, *130*, 16633 – 16645; V. Mougel, P. Horeglad, G. Nocton, J. Pécaut, M. Mazzanti, *Angew. Chem.* **2009**, *121*, 8629 – 8632; *Angew. Chem. Int. Ed.* **2009**, *48*, 8477 – 8480.
[7] L. Chatelain, V. Mougel, J. Pecaut, M. Mazzanti, *Chem. Sci.* **2012**, *3*, 1075 – 1079.
[8] D. D. Schnaars, G. Wu, T. W. Hayton, *Inorg. Chem.* **2011**, *50*, 4695 – 4697; D. D. Schnaars, G. Wu, T. W. Hayton, *Inorg. Chem.* **2011**, *50*, 9642 – 9649.
[9] A. Ekstrom, *Inorg. Chem.* **1974**, *13*, 2237 – 2241; H. Steele, R. J. Taylor, *Inorg. Chem.* **2007**, *46*, 6311 – 6318.
[10] S. Tsushima, *Inorg. Chem.* **2012**, *51*, 1434 – 1439.
[11] P. L. Arnold, D. Patel, C. Wilson, J. B. Love, *Nature* **2008**, *451*, 315 – 317.
[12] J. L. Brown, G. Wu, T. W. Hayton, *J. Am. Chem. Soc.* **2010**, *132*, 7248 – 7249.
[13] P. L. Arnold, A.-F. Pécharman, J. B. Love, *Angew. Chem.* **2011**, *123*, 9628 – 9630; *Angew. Chem. Int. Ed.* **2011**, *50*, 9456 – 9458.
[14] P. L. Arnold, G. M. Jones, S. O. Odoh, G. Schreckenbach, N. Magnani, J. B. Love, *Nat. Chem.* **2012**, *4*, 221 – 227.

[15] D. S. J. Arney, C. J. Burns, *J. Am. Chem. Soc.* **1993**, *115*, 9840 – 9841.
[16] S. Fortier, J. L. Brown, N. Kaltsoyannis, G. Wu, T. W. Hayton, *Inorg. Chem.* **2012**, *51*, 1625 – 1633.
[17] S. C. Bart, C. Anthon, F. W. Heinemann, E. Bill, N. M. Edelstein, K. Meyer, *J. Am. Chem. Soc.* **2008**, *130*, 12536 – 12546.
[18] B. Kosog, H. S. La Pierre, F. W. Heinemann, S. T. Liddle, K. Meyer, *J. Am. Chem. Soc.* **2012**, *134*, 5284 – 5289.
[19] I. M. Aladzheva, O. V. Bykhovskaya, Y. V. Nelyubina, Z. S. Klemenkova, P. V. Petrovskii, I. L. Odinets, *Inorg. Chim. Acta* **2011**, *373*, 130 – 136; R. Haegele, J. C. A. Boeyens, *J. Chem. Soc. Dalton Trans.* **1977**, 648 – 650; P. Thuéry, M. Nierlich, B. W. Baldwin, N. Komatsuzaki, T. Hirose, *J. Chem. Soc. Dalton Trans.* **1999**, 1047 – 1048; G. E. Sigmon, J. Ling, D. K. Unruh, L. Moore-Shay, M. Ward, B. Weaver, P. C. Burns, *J. Am. Chem. Soc.* **2009**, *131*, 16648 – 16649; G. H. John, I. May, M. J. Sarsfield, H. M. Steele, D. Collison, M. Helliwell, J. D. McKinney, *Dalton Trans.* **2004**, 734 – 740; A. R. de Aquino, P. C. Isolani, J. Zukerman-Schpector, L. B. Zinner, G. Vicentini, *J. Alloys Compd.* **2001**, *323 – 324*, 18 – 21; B. Masci, P. Thuéry, *Polyhedron* **2005**, *24*, 229 – 237; J. Ling, J. Qiu, G. E. Sigmon, M. Ward, J. E. S. Szymanowski, P. C. Burns, *J. Am. Chem. Soc.* **2010**, *132*, 13395 – 13402; P. Thuéry, B. Masci, *Supramol. Chem.* **2003**, *15*, 95 – 99; J. Ling, C. M. Wallace, J. E. S. Szymanowski, P. C. Burns, *Angew. Chem.* **2010**, *122*, 7429 – 7431; *Angew. Chem. Int. Ed.* **2010**, *49*, 7271 – 7273; G. A. Doyle, D. M. L. Goodgame, A. Sinden, D. J. Williams, *J. Chem. Soc. Chem. Commun.* **1993**, 1170 – 1172; D. Rose, Y.-D. Chang, Q. Chen, J. Zubieta, *Inorg. Chem.* **1994**, *33*, 5167 – 5168.
[20] P. L. Arnold, *Chem. Commun.* **2011**, *47*, 9005 – 9010.
[21] P. L. Arnold, G. M. Jones, Q.-J. Pan, G. Schreckenbach, J. B. Love, *Dalton Trans.* **2012**, *41*, 6595 – 6597.
[22] M. Bühl, G. Schreckenbach, *Inorg. Chem.* **2010**, *49*, 3821 – 3827.

Dalton Transactions

Cite this: *Dalton Trans.*, 2012, **41**, 6595

www.rsc.org/dalton

COMMUNICATION

Co-linear, double-uranyl coordination by an expanded Schiff-base polypyrrole macrocycle†

Polly L. Arnold,*[a] Guy M. Jones,[a] Qing-Jiang Pan,[b,c] Georg Schreckenbach[b] and Jason B. Love*[a]

Received 22nd February 2012, Accepted 27th March 2012
DOI: 10.1039/c2dt30658a

Expansion of a Schiff-base polypyrrolic macrocycle allows the formation of a binuclear uranyl complex with co-linear uranyl ions and a very short oxo–oxo distance.

The actinyl ions, $[AnO_2]^{n+}$, (An = U, Np, Pu, n = 1,2) have metal dioxo motifs in which linear MO_2 geometries are dominant due to strong covalent multiple M–O bonding and relativistic effects.[1] Of these, the hexavalent uranyl is the best-known and arguably the most important, due to its natural occurrence in the environment and the fact that it makes up approximately 95% of the dissolved metal ions in standard civil nuclear waste.[2,3] The uranyl dication has the least basic oxo groups compared to the other actinyl ions—including the reduced, pentavalent uranyl mono-cation—and exhibits little chemistry.[4] This is a significant property as the interaction of actinyl ions through oxo-bridge formation to other cations, known as cation–cation interactions (CCIs),[5] is important to nuclear waste processing since it can lead to undesirable precipitation of clusters. Furthermore, proton and oxo group exchange reactions that occur during the reductive precipitation of uranyl under anaerobic conditions are facilitated by oxo-bridging between the actinyl centres.[6–9] Well understood cluster formation reactions have also been used in recent years to direct the formation of actinide dimers and oligomers that display interesting electronic coupling, and that help elucidate the fundamental bonding behaviour of f-electrons.[10] This is still a poorly understood area, and one made difficult for theoretical studies by relativistic effects.

We have been studying uranyl $[UO_2]^{2+}$ oxo-group hydrogen-bonding,[11] transition-metal coordination,[12] and reduction through the formation of covalent O–Si and O–H bonds,[13–15] or lanthanide metallation,[16] in a Pacman-shaped, polypyrrolic macrocyclic framework, which both equatorially coordinates, and desymmetrises the uranyl ion (Chart 1, **A**). While under normal conditions only one uranyl cation can fit into the cavity of H_4L, we have shown recently that a new binuclear diuranium dioxo geometry can occur in which both reductive silylation and the migration of one oxo group to a mutually *cis* position are apparent (Chart 1, **B**).[17] In related work we have shown that binuclear transition metal complexes of the expanded Pacman ligand H_4L^A exhibit greater metal–metal separation and afford superior performance in oxygen reduction catalysis (Chart 1, **C**).[18–20] Computational studies by us suggested that this latter ligand should allow the coordination of two actinyl ions, albeit with close oxo–oxo distances.[21] Herein, we report experimental evidence for the formation of binuclear uranyl complexes of H_4L^A and confirm the theoretical predictions.

The reaction between the free base anthracenyl macrocycle H_4L^A and one equivalent of the uranyl bis(silylamido) complex $[UO_2\{N(SiMe_3)_2\}_2(py)_2]$ (py = pyridine) in pyridine solution was not as straightforward as that of the analogous ligand H_4L, affording a mixture of the brown mono- and bi-nuclear uranyl complexes $[UO_2(py)(H_2L^A)]$ **1** and $[\{UO_2(py)\}_2(L^A)]$ **2** in addition to unreacted ligand in 70 : 15 : 15 ratio respectively, even at elevated temperatures. Although the reaction between H_4L^A and two equivalents of $[UO_2\{N(SiMe_3)_2\}_2(py)_2]$ also yields a mixture of **1** and **2**, the latter is formed in much greater yield of 50%, alongside nearly the same amount (46%) of

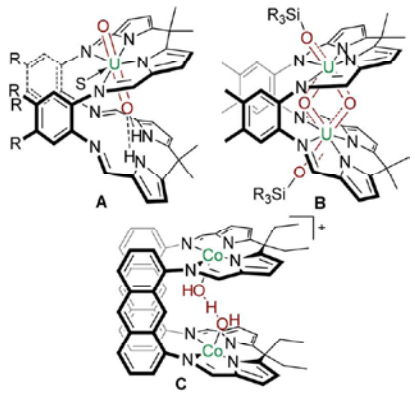

Chart 1 The desymmetrisation of the uranyl ion upon coordination in the Pacman macrocycle (H_4L) **A**, the oxo-rearranged product **B** that allows two uranyl ions to coordinate, and the dicobalt catalyst for O_2 reduction of the expanded polypyrrolic macrocycle with anthracenyl (H_4L^A) hinge **C**. S = donor solvent molecule.

[a]*EaStCHEM School of Chemistry, University of Edinburgh, The King's Buildings, Edinburgh, UK, EH9 3JJ. E-mail: polly.arnold@ed.ac.uk, jason.love@ed.ac.uk*
[b]*Department of Chemistry, University of Manitoba, Winnipeg, Manitoba, Canada, R3T 2N2*
[c]*Key Laboratory of Functional Inorganic Material Chemistry of Education Ministry, School of Chemistry and Materials Science, Heilongjiang University, Harbin, China 150080*

†Electronic supplementary information (ESI) available: full experimental and crystallographic details. CCDC reference number 867432. For ESI and crystallographic data in CIF or other electronic format see DOI: 10.1039/c2dt30658a

compound **1**. Both **1** and **2** have similar solubilities, being insoluble in non-polar organic solvents and poorly soluble in pyridine, a property which causes unwanted precipitation of both products over the course of the reaction inhibiting the formation of **2** as a single product. Despite this, fractional crystallisation from the crude mixture did allow isolation of pure samples of **2**, albeit in low yields (Scheme 1). The binuclear complex **2** represents the first example of a simple bis-uranyl Pacman molecular compound and incorporates a highly unusual co-facial coordination environment for two uranyl ions (see later). In the ^{1}H NMR spectrum of **1**, an asymmetric ligand arrangement is seen, consistent with only one of the two N_4 donor sets being occupied by the uranyl cation. This is evidenced by the presence of two sets of four resonances each for the CH_2 (2.71, 2.54, 2.17 and 1.60 ppm) and CH_3 protons (1.47, 1.05, 0.97 and 0.54 ppm) of the ethyl *meso*-groups. The magnetic non-equivalence of all four alkyl groups reinforces the assignment of an asymmetric Pacman geometry to the molecule in solution, with the four sets of resonances due to distinct inner- and outer-cleft ethyl groups. In contrast, the ^{1}H NMR spectrum of **2** displays a symmetrical set of ligand resonances consistent with both N_4 donor sets being occupied, with four, as opposed to eight, *meso*-ethyl resonances at 0.90, 1.09, (CH_3) and 2.48 (two overlapping CH_2 resonances) ppm (see SI†).

The difficulty experienced in the synthesis and isolation of **1** and **2** contrasts with the calculated relative thermodynamic stabilities of the products. In the gas-phase calculations, the mono (actinyl) complexes $[AnO_2(H_2L^A)]$ An = U, Np, Pu were found to be more stable than the binuclear complexes $[\{AnO_2\}_2(L^A)]$ by 40–50 kcal mol^{-1}, a considerable margin presumably arising from the steric clash between the oxo-groups resulting upon complexation of a second uranyl cation. However, the calculated structures omitted the donor solvent molecule in the fifth equatorial site, and calculations that incorporated a continuum solvent model were found to stabilise the formation energy of the binuclear complex by 11 kcal mol^{-1}, so reducing the barrier to its formation.[21]

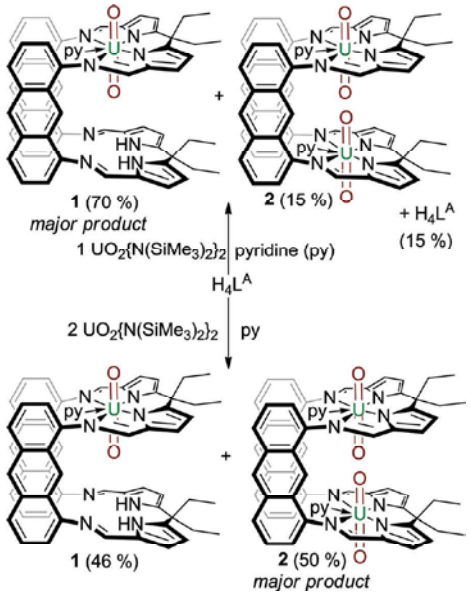

Scheme 1 Synthesis of mono and di(uranyl) Pacman complexes of L^A.

Single crystals suitable for an X-ray structure determination of **2**‡ were grown from pyridine and the solid state structure is shown in Fig. 1, along with selected distances and angles. Both uranyl cations display pentagonal bipyramidal geometries with the macrocyclic N_4-donor set and the pyridine N-donor atom comprising the equatorial donor ligands and the two oxo atoms, which are mutually *trans* (O–U–O angles 174.0(2) and 176.0(2)°) comprising the axial ligands. The U–O bond distances are short (range = 1.747(4) to 1.779(4) Å) and support the presence of the U(VI) oxidation state; the absorption at 912 cm^{-1} in the IR spectrum of **2** is also consistent with $[UO_2]^{2+}$. The most notable feature is the short separation of the two oxo groups, O1···O3 2.709(6) Å within the molecular cleft. The two uranyl cations are evidently coordinated with ease in the macrocyclic cavity generated by the anthracenyl groups of L^A; the N_4-donor sets remain approximately co-planar, subtending an angle of 16.8° due to the steric demand of the *meso*-ethyl groups. However, the two N_4 donor planes are slipped laterally relative to the *meso*-carbons, by rotation around all four N–C

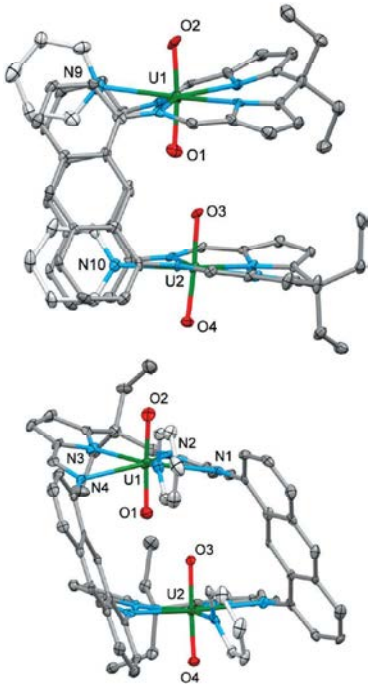

Fig. 1 Solid state structure of **2**. For clarity, all hydrogen atoms are omitted (displacement ellipsoids are drawn at 50% probability). Selected distances (Å) and angles (°): U1–O1 1.747(4), U1–O2 1.779(4), U1–O3 1.764(4), U1–O4 1.778(4), U1–N1 2.558(6), U1–N2 2.417(6), U1–N3 2.430(6), U1–N4 2.595(6), O1–U1-O2 174.0(2), 176.0(2).

anthracenyl bonds. Thus, the perpendicular distance between U1 and the plane described by U2, O3, O4, and the pyridine nitrogen N10 is 1.957 Å. This lateral twist also allows for favourable π-stacking interactions between the pyridine molecules located in the fifth equatorial coordination site and anthracenyl hinge groups. This contrasts to the complexes of the parent phenylenediamine-derived macrocycle L, in which the inhibition of lateral twisting does not allow favourable aromatic π-stacking interactions.

Attempts to crystallise the mono-uranyl complex **1** from mixtures of **1** and **2** were unsuccessful. However, its structure was verified by analysis of the crude mixture by MALDI-MS in which the ion at 1128 amu was attributed to $[UO_2(H_2L^A)]^+$, a fragment resulting from desolvation of **1** upon ionisation. Also, a peak at 1528 amu was ascribed to the loss of a single ethyl group from the binuclear complex **2**, with further ions at 1452 and 1370 corresponding to mono- and un-solvated fragments.

Examples of complexes which contain a similarly close uranyl oxo contact in the solid state are relatively rare. The uranyl oxalates $[NH_4]_2[(U^{VI}O_2)_2(\mu_4\text{-}C_2O_4)_3]$,[22] $[Rb]_2[(U^{VI}O_2)_2(\mu_4\text{-}C_2O_4)_3]$,[23] and $[alkyl\text{-}imidazolium]_2[(U^{VI}O_2)_2(\mu_4\text{-}C_2O_4)(NO_3)_4]$,[24] have similarly short oxo–oxo distances of 2.434, 2.702, and 2.703 Å, respectively; all other close O···O separations are >2.8 Å and result from crystal packing in the solid state (39 examples up to 3.0 Å).[25] To our knowledge, none of these contacts persist in solution, whereas a solution of **2** survives unchanged in boiling pyridine over 24 h.

The proximity of the two hexavalent uranyl oxo groups suggests that (electro)chemical reduction by one or more electrons might yield a bimetallic complex with an interesting electronic structure. We have shown previously that magnetic super-exchange is facilitated in the binuclear uranium dioxo complex **B**,[17] and single-electron reduction has been shown to enhance significantly the magnetic properties of lanthanide dinitrogen complexes.[26] Preliminary cyclic voltammetry of **2** in THF (0.2 M Bu_4NBF_4, Fc^+/Fc)† displayed only an irreversible reduction at Ep^c −2.46 V. If this is assigned to a reduction of the two non-communicating U^{VI} centres, it represents a significantly more difficult reduction than that of the mononuclear complex $[UO_2(THF)(H_2L)]$ **A** which shows a clear, quasi-reversible U^{VI}/U^V couple at −1.17 V and an irreversible feature, presumed to be U^V to U^{IV} at −2.88 V.[27] On first inspection, it is a surprise that the redox chemistry of these complexes should be so different, as each uranyl centre contains the same macrocyclic donor set in the equatorial plane. However, the proximity of the oxo atoms within the macrocyclic cleft may be destabilising the reduced states as the Lewis basicity of the oxo groups would be expected to increase considerably on reduction from $[UO_2]^{2+}$ to $[UO_2]^+$. Also, the parallel orientation of the uranyl groups within the macrocyclic cleft hinders the formation of diamond or T-shaped CCIs. In support of this, the CV of the mixture of **1** and **2** (since **1** cannot be isolated pure) showed extra, irreversible reductions at Ep^c −1.45 and −2.6 V, potentials similar to those seen for the U^{VI}/U^V and U^V/U^{IV} couples respectively in **A**, indicating that the pentavalent oxidation state should be almost as readily accessible for mononuclear **1** as it is for **A**. Furthermore, binuclear complexes of L^A without ancillary ligands in the molecular cleft such as the Co complex $[Co_2(L^A)]$ display more straightforward reduction chemistry, with a quasi-reversible reduction at Ep^c −2.32 V (Fc^+/Fc, PhCN, PT WE) for the Co^{II}/Co^I couple.[18]

We have shown that the computationally-predicted binuclear uranyl complex of L^A, **2**, can be synthesised, albeit in low yield due to the difficulties in its isolation from the mononuclear complex **1**. The structure of **2** reveals a close oxo–oxo distance within the molecular cleft which considerably affects the reduction chemistry exhibited by these complexes. The computational work also predicted the existence and stability of mixed uranyl–transition metal complexes, so it will be of interest to determine whether these mixed-metal compounds can be prepared and their oxo group chemistry evaluated.

References

‡ Crystallographic details for **2**: Single crystals were grown from pyridine solution, $C_{68}H_{58}N_{10}O_4U_2$, M 1555.3, monoclinic, $P2_1/n$, a = 13.5141 (2), b = 17.9909 (4), c = 23.4778 (5) Å, β = 92.443 (3), V = 5702.99(19) Å^3, Temp 100 K, Z = 4, 12 703 independent reflections, R(int) 0.074, $R[F^2 > 2\sigma(F^2)]$0.051, CCDC 867432.

1 R. G. Denning, *J. Phys. Chem. A*, 2007, **111**, 4125–4143.
2 K. L. Nash and G. J. Lumetta, *Advanced Separation Techniques for Nuclear Waste Reprocessing and Radioactive Waste Treatment*, Woodhead Publishing, Cambridge, 2011, pp. 1–512.
3 Z. Szabó and I. Grenthe, *Inorg. Chem.*, 2007, **46**, 9372–9378.
4 P. L. Arnold, J. B. Love and D. Patel, *Coord. Chem. Rev.*, 2009, **253**, 1973–1978.
5 J. C. Sullivan, J. C. Hindman and A. J. Zielen, *J. Am. Chem. Soc.*, 1961, **83**, 3373–3378.
6 K. S. Boland, S. D. Conradson, A. L. Costello, A. J. Gaunt, S. A. Kozimor, I. May, S. D. Reilly and D. D. Schnaars, *Dalton Trans.*, 2012, **41**, 2003–2010.
7 E. S. Ilton, J.-F. Boily, E. C. Buck, F. N. Skomurski, K. M. Rosso, C. L. Cahill, J. R. Bargar and A. R. Felmy, *Environ. Sci. Technol.*, 2009, **44**, 170–176.
8 H. Steele and R. J. Taylor, *Inorg. Chem.*, 2007, **46**, 6311–6318.
9 E. S. Ilton, A. Haiduc, C. L. Cahill and A. R. Felmy, *Inorg. Chem.*, 2005, **44**, 2986–2988.
10 L. Chatelain, V. Mougel, J. Pecaut and M. Mazzanti, *Chem. Sci.*, 2012, **3**, 1075.
11 P. L. Arnold, A. J. Blake, C. Wilson and J. B. Love, *Inorg. Chem.*, 2004, **43**, 8206–8208.
12 P. L. Arnold, D. Patel, A. J. Blake, C. Wilson and J. B. Love, *J. Am. Chem. Soc.*, 2006, **128**, 9610–9611.
13 P. L. Arnold, E. Hollis, F. J. White, N. Magnani, R. Caciuffo and J. B. Love, *Angew. Chem., Int. Ed.*, 2011, **50**, 887–890.
14 P. L. Arnold, A.-F. Pecharman, E. Hollis, A. Yahia, L. Maron, S. Parsons and J. B. Love, *Nat. Chem.*, 2010, **2**, 1056–1061.
15 P. L. Arnold, D. Patel, C. Wilson and J. B. Love, *Nature*, 2008, **451**, 315–317.
16 P. L. Arnold, E. Hollis, F. J. White, N. Magnani, R. Caciuffo and J. B. Love, *Angew. Chem., Int. Ed.*, 2011, **50**, 887–890.
17 P. L. Arnold, G. M. Jones, S. O. Odoh, G. Schreckenbach, N. Magnani and J. B. Love, *Nat. Chem.*, 2012, **4**, 221–227.
18 A. M. J. Devoille and J. B. Love, *Dalton Trans.*, 2012, **41**, 65–72.
19 A. M. J. Devoille, P. Richardson, N. L. Bill, J. L. Sessler and J. B. Love, *Inorg. Chem.*, 2011, **50**, 3116–3126.
20 E. Askarizadeh, A. M. J. Devoille, D. M. Boghaei, A. M. Z. Slawin and J. B. Love, *Inorg. Chem.*, 2009, **48**, 7491–7500.
21 Q.-J. Pan, G. Schreckenbach, P. L. Arnold and J. B. Love, *Chem. Commun.*, 2011, **47**, 5720–5722.
22 N. W. Alcock, *J. Chem. Soc., Dalton Trans.*, 1973, 1616–1620.
23 L. Serezhkina, E. Peresypkina, A. Virovets and V. Klepov, *Crystallogr. Rep.*, 2010, **55**, 221–223.
24 A. E. Bradley, C. Hardacre, M. Nieuwenhuyzen, W. R. Pitner, D. Sanders, K. R. Seddon and R. C. Thied, *Inorg. Chem.*, 2004, **43**, 2503–2514.
25 D. A. Fletcher, R. F. McMeeking and D. Parkin, *J. Chem. Inf. Model.*, 1996, **36**, 746.
26 J. D. Rinehart, M. Fang, W. J. Evans and J. R. Long, *Nat. Chem.*, 2011, **3**, 538–542.
27 J. J. Berard, G. Schreckenbach, P. L. Arnold, D. Patel and J. B. Love, *Inorg. Chem.*, 2008, **47**, 11583–11592.